Structures et interactions des enzymes du cycle de Calvin-Benson-Bassham

Théo Le Moigne

université PARIS-SACLAY

Structures et interactions des enzymes du cycle de Calvin-Benson-Bassham

Structures and interactions of Calvin-Benson-Bassham cycle enzymes

Thèse de doctorat de l'université Paris-Saclay

École doctorale n° 567 : Sciences du végétal : du gène à l'écosystème (SEVE)
Spécialité de doctorat : Biologie
Graduate School : BioSphERA Référent : Faculté des sciences d'Orsay

Thèse préparée dans les unités de recherche **Laboratoire de Biologie Moléculaire et Cellulaire des Eucaryotes (Institut de Biologie Physico-Chimique, CNRS et Sorbonne Université) et Laboratoire de Biologie Computationnelle et Quantitative (Institut de Biologie Paris-Seine, Sorbonne Université et CNRS)**, sous la direction de **Julien HENRI**, Maître de conférences, et le co-encadrement de **Stéphane LEMAIRE**, Directeur de recherches CNRS

Thèse soutenue à Paris, le 04 octobre 2022, par

Théo LE MOIGNE

Composition du Jury

Sylvie NESSLER Professeur, Université Paris-Saclay	Présidente
Mirjam CZJZEK Directrice de recherche, CNRS, Sorbonne Université	Rapporteure et Examinatrice
Nicolas ROUHIER Professeur, Université de Lorraine	Rapporteur et examinateur
Alix BOULOUIS Maîtresse de conférences, Sorbonne Université	Examinatrice
Hélène LAUNAY Chargée de recherche, CNRS, Aix-Marseille université	Examinatrice
Julien HENRI Maître de conférences, Sorbonne Université	Directeur de thèse

THESE DE DOCTORAT

NNT : 2022UPASB056

université PARIS-SACLAY | ÉCOLE DOCTORALE Sciences du végétal : du gène à l'écosystème (SEVE)

Titre : Structures et interactions des enzymes du cycle de Calvin-Benson-Bassham

Mots clés : photosynthèse, fixation de carbone, microalgue, biologie structurale

Résumé : La photosynthèse est l'un des principaux processus permettant la vie sur Terre. Elle se déroule en deux phases, la conversion de l'énergie lumineuse et de l'eau en pouvoir réducteur et en énergie chimique et le cycle de Calvin-Benson-Bassham (CBBC) qui fixe le CO_2 atmosphérique en molécules organiques.

Le CBBC est catalysé par onze enzymes, essentielles à la photosynthèse et conservées dans la lignée verte des plantes et des microalgues. Les enzymes du CBBC sont régulées par de multiples modes, dont des modifications post-traductionnelles et des interactions protéine-protéine.

Afin de décrire le système CBBC au niveau moléculaire, nous avons cherché à déterminer la structure tridimensionnelle de ces enzymes à haute résolution.

J'ai purifié, cristallisé, résolu et analysé les structures cristallines de la ribose-5-phosphate isomérase (RPI), de la fructose bisphosphate aldolase (FBA), de la sédoheptulose-1,7-bisphosphatase (SBPase) et de la phosphoglycérate kinase (PGK) de la microalgue verte modèle *Chlamydomonas reinhardtii*. J'ai également recherché des complexes multi-enzymatiques entre les enzymes du CBBC *in vitro*.

Title : Structures and interactions of Calvin-Benson-Bassham cycle enzymes

Keywords : photosynthesis, carbon fixation, microalgae, structural biology

Abstract : Photosynthesis is one of the main processes supporting life. It is composed of two phases, the conversion of light energy and water into reductive power and chemical energy, and the Calvin-Benson-Bassham cycle (CBBC) that fixes atmospheric CO_2 into organic molecules.

The CBBC is catalyzed by eleven enzymes, essential for photosynthesis and conserved in the green lineage of plants and microalgae. CBBC enzymes are regulated by multiple modes, including post-translational modifications and protein-protein interactions.

In order to describe the CBBC system at the molecular level, we aimed at determining the tridimensional structure of these enzymes at high resolution.

I purified, crystallized, solved and analyzed the crystal structures of the ribose-5-phosphate isomerase (RPI), the fructose bisphosphate aldolase (FBA), the sedoheptulose-1,7-bisphosphatase (SBPase), and the phosphoglycerate kinase (PGK) from the model green microalga *Chlamydomonas reinhardtii*, and searched for multi-enzymatic complexes formed by CBBC enzymes *in vitro*.

REMERCIEMENTS

La science est un travail d'équipe avant tout, et c'est également le cas pour un doctorat c'est pourquoi, je tiens à remercier toutes les personnes m'ayant aidé de près ou de loin à l'élaboration et à la réalisation de celui-ci.

Je tiens tout d'abord à remercier les rapporteurs de ce manuscrit, Dr. Mirjam Czjzek et Pr. Nicolas Rouhier pour avoir accepté d'évaluer mon travail. Merci également aux examinatrices Dr. Alix Boulouis, Dr. Hélène Launay et Pr. Sylvie Nessler d'avoir pris le temps de faire partie de mon jury. Merci également aux membres de mon comité de thèse, Dr. Catherine de Vitry, Dr. Sandrine Lanfranchi et Pr. Herman van Tilbeurgh pour avoir suivi l'évolution de mon projet.

Un immense merci au Dr. Julien Henri, mon directeur de thèse qui n'a pas hésité à me proposer de me prendre en tant que son premier étudiant de thèse tout en sachant que je ne souhaitais pas, à l'époque, faire de thèse. Je ne regrette absolument pas ma décision et me réjouis même que tu ais réussi à me convaincre d'entreprendre celle-ci. Merci d'avoir pris le temps de répondre à toutes mes questions scientifiques ou non, de m'avoir expliqué la biologie structurale de nuit au synchrotron et pour tout le reste. Ta gentillesse, ta patience et ta vision des choses positive même en cas de résultat décevant sont des qualités idéales pour tout étudiant et je n'aurai pas pu tomber mieux.

Un grand merci au Dr. Stéphane Lemaire de m'avoir fait confiance pour intégrer son équipe sans douter de mes capacités à mener à bien ce doctorat dès le départ quand je n'en étais pas sûr moi-même et pour avoir pris le temps de corriger mes travaux et présentations importantes tout au long de mon doctorat. Merci aux Drs. Pierre Crozet, Antoine Danon et Christophe Marchand de cette même équipe. Des discussions sérieuses à propos des modifications redox, de la fameuse structure de FBPase impossible à obtenir aux dégustation de vins/bières à l'aveugle et désaccords musicaux ou d'opinions à propos de films, ce ne furent que des bons moments.

Par ordre chronologique de ces trois années, merci à tous ceux que j'ai rencontré à l'IBPC et en premier lieu au Dr. Teresa Teixeira pour m'avoir accueilli au sein de son unité. Ensuite, évidement, Félix de Carpentier et Nicolas Boisset, ce minuscule bureau où je me cognais dans vos chaises pour accéder à la mienne n'était finalement pas si mal en votre compagnie. Les discussions et cafés partagés avec vous n'ont pas forcément fait avancer la science mais étaient néanmoins nécessaires selon moi. Un merci ensuite à tous ceux avec lesquels j'ai pu discuter durant les « drinking thursdays », dans l'UMR 8226 et le reste de l'institut et qui sont trop nombreux pour être tous cités ici. Mais, un merci particulier à Alejandro, Antonin C., Antonin N., Bechara, Cyrielle, Cynthia, Ferdinand, Jeanne LP., Oznur et Prisca, vous avoir rencontrés est une chance et m'a permis de passer de très bons moments en votre compagnie !

Si l'IBPC fut la première « maison » scientifique de mon doctorat, la seconde fut l'IBPS et le LCQB dirigé par Pr. Alessandra Carbone que je remercie pour m'avoir également accueilli au sein de celui-ci. Un nouveau lieu impliquant de nouvelles rencontres, Nicolas Cornille, Giusi Favoino et Achille Julienne font notamment partie de celles-ci. Les moments de convivialités partagés dans des conditions sanitaires des plus contraignantes furent une sorte de bouée de sauvetage sociale dans une période difficile. Mes voyages au C3 furent tous dignes d'intérêt bien que parfois énervants. L'agrandissement de l'équipe me permet également de remercier tous ceux qui sont venus renforcer celle-ci, temporairement ou non. Merci, donc, à Clémence, Esther, Fabio, Guillaume, Hugo, Jeanne G., Lou, Lucile, Maria, Mariette, Martina, Phuc, Pietro pour toutes ces interactions, cafés, gâteaux, raclette et spécialités italiennes partagés.

Merci à tous les « malakoffiots » et « malakoffiotes » ou non qui se reconnaitront sans besoin de les citer ! Merci à ma famille, mes parents Agnès et Dominique qui m'ont soutenu sans toujours comprendre ce que je fais dans les détails mais en étant tout de même intéressés. A ma grande sœur Alice, si nos caractères sont différents, ça ne m'empêche pas de t'apprécier énormément ! Et enfin, merci à ceux qui font partie de la famille, même de manière pas vraiment officielle, Briac, Elisabeth, Guilhem et bien évidement Thierry, même si tu n'es plus là.

Sommaire

ABREVIATIONS

1,3-bPGA : 1,3-bisphosphoglycérate

3-PGA : 3-phosphoglycérate

CATH classification : *Class, Architecture, Topology/fold, Homologous superfamily classification* (http://www.cathdb.info/)

CBBC : cycle de Calvin-Benson-Bassham

Chlamydomonas : *Chlamydomonas reinhardtii*

CP12 : *chloroplast protein of 12 kDa*

DHAP : dihydroxyacétone phosphate

E4P : érythrose-4-phosphate

EC : *enzyme commission number*

EPYC1 : *Essential Pyrenoid Component* 1

FBP : fructose-1,6-bisphosphate

F6P : fructose-6-phosphate

FBA : fructose-1,6-bisphosphate aldolase

FBPase : fructose-1,6-bisphosphatase

G3P : glycéraldéhyde-3-phosphate

GAPDH : glycéraldéhyde-3-phosphate déshydrogénase

PDB : *protein data bank* (https://www.rcsb.org/)

PGK : phosphoglycérate kinase

PRK : phosphoribulokinase

R5P : ribose-5-phosphate

RPE : ribulose-5-phosphate-3-épimérase

RPI : ribose-5-phosphate isomérase

Rubisco : ribulose-1,5-bisphosphate carboxylase/oxygénase

Ru5P : ribulose-5-phosphate

RuBP : ribulose-1,5-bisphosphate

TPI : triose phosphate isomérase

TRK : transkétolase

SBP : sédoheptulose-1,7-bisphosphate

S7P : sédoheptulose-7-phosphate

SBPase : sédoheptulose-1,7-bisphosphatase

X5P : xylulose-5-phosphate

1 INTRODUCTION

1.1 PHOTOSYNTHESE

La photosynthèse est le processus biologique convertissant l'énergie lumineuse en énergie chimique, permettant la conversion du carbone inorganique présent dans l'atmosphère en carbone organique pouvant être utilisé dans l'ensemble des processus métaboliques de la biosphère (Pfannschmidt and Yang 2012). C'est l'un des processus les plus important pour la vie terrestre car il est à la base de toutes les chaînes et réseaux trophiques. L'étude de la photosynthèse se répartit à de vastes échelles de mesures, depuis l'espace via des satellites pour mesurer des taux d'absorption de CO_2 de zones entières de la planète jusqu'à l'échelle atomique à laquelle les flux d'électrons à travers les membranes des thylakoïdes peuvent être mesurés. Malgré tous ces efforts et de nombreux succès, il reste encore des zones d'ombres dans la compréhension de la photosynthèse.

La photosynthèse dans les chloroplastes se divise en deux grandes phases respectivement localisées à la membrane des thylakoïdes (phase photochimique) et dans le stroma (phase biosynthétique). Ces deux phases ont pour fonctions successives d'absorber l'énergie lumineuse, de la convertir en énergie chimique (ATP) et pouvoir réducteur (NADPH), qui seront utilisés dans la seconde phase qui permet la fixation du CO_2 atmosphérique en oses (sucres) employés comme sources d'énergie, de biosynthèse, ou mis en réserve (Johnson 2016).

La première phase de conversion de l'énergie lumineuse peut être résumée sous la forme de l'équation :

$$2\ H_2O + h\eta \rightarrow O_2 + 4\ H^+ + 4\ e^-$$

Cette réaction implique une succession de réductions et d'oxydations de différents composants à travers des complexes de protéines permettant un transfert d'électrons (Figure 1) (Johnson 2016).

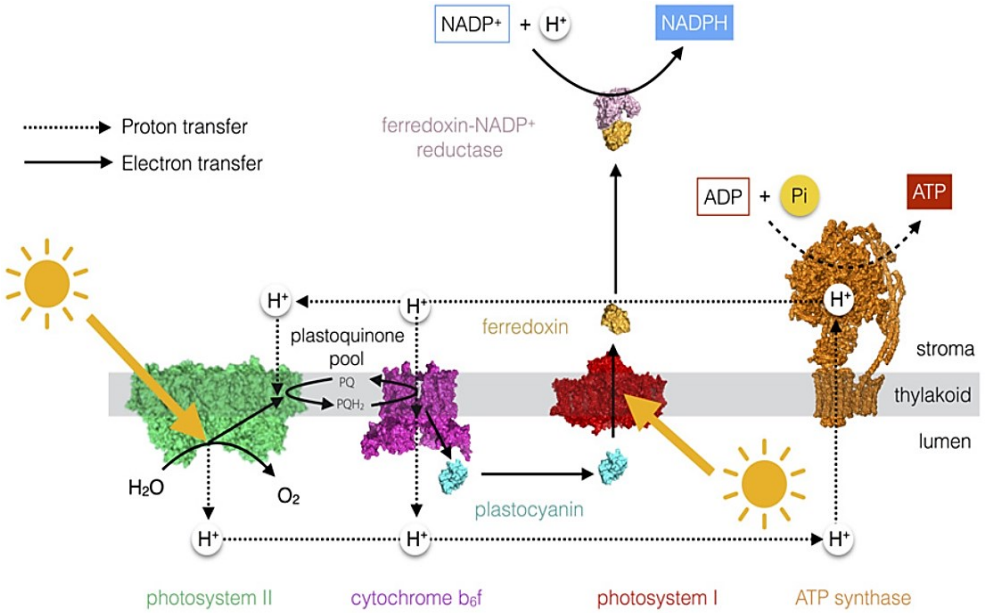

Figure 1 : Schéma reproduit de Johnson (2016) de la chaîne linéaire de transfert d'électrons depuis les molécules d'eau jusqu'au NADPH et à la synthèse d'ATP.

Ce flux linéaire d'électrons traverse le photosystème II, le cytochrome b_6f, le photosystème I, l'ATP synthase et la ferrédoxine $NADP^+$ réductase, accumulant dans le stroma NADPH et ATP.

L'ATP et le NADPH vont ensuite être utilisés dans la seconde phase de la photosynthèse pour la fixation du CO_2 atmosphérique en oses qui peut être résumée par l'équation :

$$CO_2 + 4H^+ + 4\,e^- \rightarrow CH_2O + H_2O$$

Cette seconde phase est catalysée par onze enzymes au cours d'un cycle métabolique en treize étapes découvert par Bassham, Benson, et Calvin (ci-après nommé CBBC).

En résumé, on peut réunir les deux équations en une seule :

$$H_2O + h\eta + CO_2 \rightarrow CH_2O + O_2$$

Cette réaction a une énergie libre positive de 479 $kJ.mol^{-1}$ ce qui en fait une réaction endergonique requérant l'énergie accumulée par la phase photochimique pour sa réalisation. La photosynthèse est

essentielle à la biosphère, en fournissant de l'énergie via la conversion de 200 milliards de tonnes de CO_2 en molécules organiques tout en relarguant 140 milliards de tonnes de dioxygène dans l'atmosphère par an (Johnson 2016). Son importance en tant qu'objet d'étude repose sur son rôle en tant que fournisseur primaire de molécules organiques mais également sur son rôle dans les échanges gazeux entre atmosphère et biosphère.

1.2 *CHLAMYDOMONAS REINHARDTII*

Si les plantes terrestres sont les modèles usuels de biologie végétale, elles ne représentent pas les seuls organismes capables de photosynthèse. Les microalgues vertes eucaryotes et les cyanobactéries sont pourvues de systèmes photosynthétiques similaires, réalisant les deux phases de la photosynthèse de manière essentiellement identique. Les algues sont également responsables de 50% de la fixation de carbone inorganique global et sont donc des producteurs primaires important (Field et al. 1998). Ainsi, le travail que j'ai réalisé pendant ma thèse sur la microalgue photosynthétique *Chlamydomonas reinhardtii* (ci-après Chlamydomonas) cible des protéines communes à toutes les espèces du groupe des *Viridiplantae*.

1.2.1 Un organisme modèle

Chlamydomonas est un organisme modèle d'étude moléculaire et cellulaire de la photosynthèse utilisé comme tel depuis 1960 et la création des premiers mutants de gènes photosynthétiques par R. P. Levine (Salomé and Merchant 2019; Levine 1960). Cette microalgue a ensuite continué à être utilisée pour la recherche fondamentale et certaines applications biotechnologiques en raison de propriétés intéressantes.

La première de ces caractéristiques que j'ai évoquée dans la section précédente est la conservation globale des réactions, enzymes et mécanismes de la photosynthèse. Les séquences de la grande sous-unité de la Rubisco entre Chlamydomonas et *Arabidopsis thaliana* présentent ainsi 88% d'identité, 89% avec celle du soja (*Glycine max*) et 84% avec celle de *Synechocystis sp*., une cyanobactérie photosynthétique. Ainsi, les découvertes et informations identifiées

chez Chlamydomonas peuvent généralement être transposées ou extrapolées chez d'autres organismes photosynthétiques comme les modèles de plantes terrestres *Arabidopsis thaliana*, *Spinacia oleracea*, *Pisum sativum*. Chlamydomonas est également un autotrophe facultatif permettant à l'algue de survivre et se développer par hétérotrophie en présence d'une source externe de carbone autre que le CO_2. L'existence de ces deux modes de développement est un avantage considérable pour l'étude des gènes de la photosynthèse permettant l'obtention de souches viables mutées pour les gènes de facteurs de la photosynthèse. Ainsi de nombreux mutants de Chlamydomonas sont rassemblés et disponibles à l'utilisation dans des banques référencées (ChlamyStation, CLiP). Les génomes nucléaire, mitochondrial et chloroplastique de Chlamydomonas ont été séquencés et annotés (Craig et al. 2022; Merchant et al. 2007). Des transcriptomes ont été établis dans diverses conditions de culture, par exemple au cours d'alternances de cycles circadiens (Strenkert et al. 2019). Des protéomes de différents compartiments cellulaires de Chlamydomonas dans plusieurs conditions sont également disponibles (Wang et al. 2022; Küken et al. 2018; Mettler et al. 2014). De même, les modifications post-traductionnelles de ces protéines font l'objet d'analyses chez Chlamydomonas (Pérez-Pérez et al. 2017; Morisse et al. 2014b; Wang et al. 2014; Zaffagnini et al. 2012a).

Chlamydomonas se cultive en milieux liquide ou solide, avec un temps de développement rapide comparé aux plantes (Salomé and Merchant 2019). Dans un milieu supplémenté en acétate et à température optimale, *Chlamydomonas reinhardtii* a un temps de doublement de 8h permettant d'obtenir des quantités de cellules suffisantes pour une majorité d'analyses biochimiques dans un délai d'une semaine. Il est possible de transformer le génome nucléaire par électroporation et les génomes chloroplastique et mitochondrial par biolistique. L'éditeur génétique CRISPR-Cas9 a été adapté pour Chlamydomonas (Shin et al. 2016).

1.2.2 Utilisations de *Chlamydomonas reinhardtii*

Chlamydomonas est utilisée dans la recherche fondamentale, mais également dans l'industrie pour des applications biotechnologiques. Les outils génétiques couplés à sa capacité à

produire des molécules organiques à partir de lumière en font un bon organisme pour la production de biocarburants ou de molécules à haute valeur ajoutée (Lam et al. 2018; Burgess et al. 2011). Si aujourd'hui la production de biocarburant n'est pas rentable en termes de coûts de production, des recherches sont en cours pour optimiser ou améliorer ceux-ci. De la même manière, grâce aux nombreux outils déjà disponibles et accessibles et du fait de sa facilité d'utilisation en laboratoire, Chlamydomonas est un châssis pour la biologie synthétique (Vavitsas et al. 2019).

Une piste possible d'amélioration des coûts de production de biocarburants dérivés de microalgues pourrait notamment passer par une modification de la phase biosynthétique pour améliorer l'efficacité du CBBC. Des taux de fixation de CO_2 plus élevés pourraient ainsi mener à de meilleurs rendements de molécules produites par nombre de cellules ce qui rendrait la production par microalgue plus compétitive. Dans cette optique d'amélioration du rendement de la photosynthèse, une compréhension du fonctionnement des enzymes du CBBC chez Chlamydomonas est donc souhaitable.

Réunissant tous ces avantages, *Chlamydomonas reinhardtii* a donc été sélectionnée comme organisme modèle pour nos recherches. Toute la suite de ce manuscrit concernera donc, sauf mention contraire des protéines, organites, cellules et mécanismes de *Chlamydomonas reinhardtii*.

1.3 CYCLE DE CALVIN-BENSON-BASSHAM

La seconde phase de la photosynthèse est appelée cycle de Calvin-Benson-Bassham. Sa découverte et les descriptions des réactions et métabolites le composant ont été publiés dans une série d'articles entre 1950 et 1954 par les trois chercheurs dont le cycle porte le nom (Bassham et al. 1954). Cette découverte a donné lieu à l'attribution du prix Nobel de Chimie à Melvin Calvin en 1961 pour ces travaux.

1.3.1 Les enzymes du cycle

Le cycle de Calvin-Benson-Bassham permet la fixation du CO_2 en triose suivant treize réactions catalysées par onze enzymes (Figure 2).

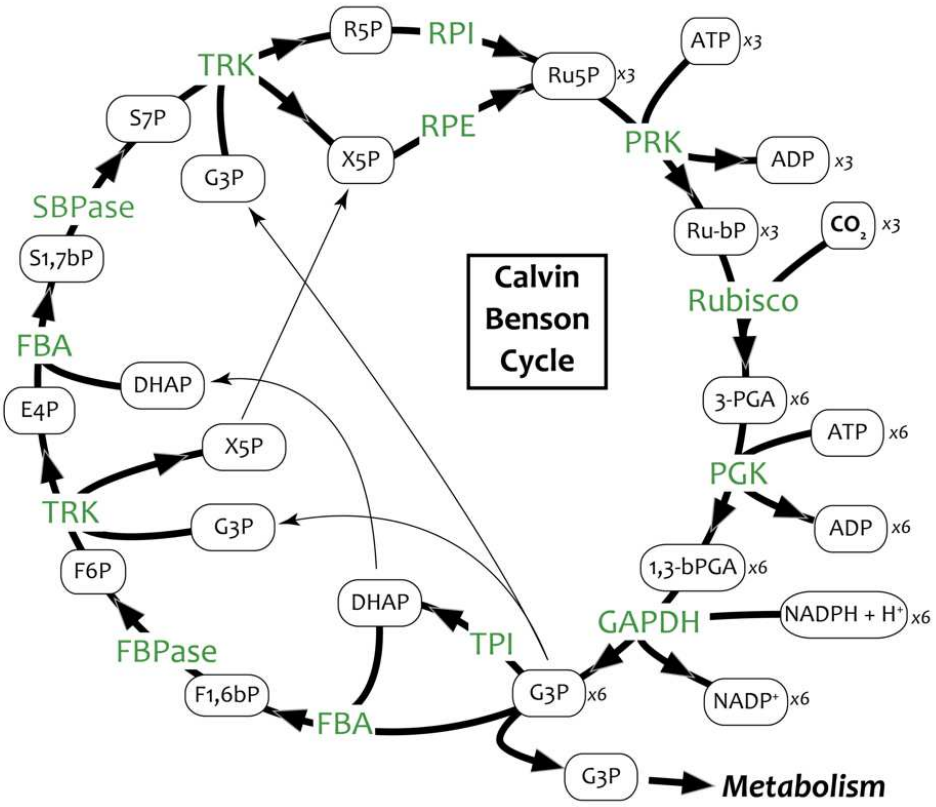

Figure 2 : Le cycle de Calvin-Benson-Bassham (Le Moigne et al. 2022a). Les noms des enzymes sont colorés en verts, ceux des métabolites en noirs. Les ratios stœchiométriques correspondent à la production d'un triose à partir de trois CO_2. La signification des acronymes est indiquée dans la liste des abréviations (*cf.* p. 7)

L'enzyme qui catalyse la fixation du CO_2 en deux molécules de 3-phosphoglycérate (3-PGA) en utilisant le ribulose-1,5-bisphosphate (RuBP) comme co-substrat est la ribulose-1,5-bisphosphate carboxylase/oxygénase (Rubisco) (Andersson and Backlund 2008). Cette enzyme est, sans doute, la plus étudiée du CBBC et la protéine la plus abondante sur terre (Bar-On and Milo 2019). La phosphoglycérate kinase (PGK) catalyse ensuite le transfert d'un groupement phosphate

de l'ATP au 3-phosphosphoglycérate (3-PGA). Le 1,3-bisphosphoglycérate (1,3-PGA) produit est déphosphorylé et réduit en glycéraldéhyde-3-phosphate (G3P) par la glycéraldéhyde-3-phosphate-déshydrogénase (GAPDH) qui utilise le pouvoir réducteur d'une molécule de NADPH. Le G3P représente un carrefour métabolique car il peut être dirigé vers les autres voies métaboliques de la cellule ou contribuer à régénérer le RuBP pour entretenir l'équilibre du cycle. Pour cette régénération, le G3P est alors substrat d'une série de trois réactions. La transkétolase (TRK) qui convertit le G3P et le fructose-6-phosphate (F6P) en xylulose-5-phosphate (X5P) et érythrose-4-phosphate (E4P) ; la transkétolase convertit le G3P et le sédoheptulose-7-phosphate (S7P) en X5P et ribose-5-phosphate (R5P). Enfin, le G3P est substrat de la triose phosphate isomérase (TPI) qui l'isomérise en dihydroxyacétone phosphate (DHAP). Le DHAP est alors substrat de la fructose-1,6-bisphosphate aldolase (FBA) qui le lie au G3P pour former du fructose-1,6-bisphosphate (FBP) ou à l'érythrose-4-phosphate (E4P) pour former du sédoheptulose-1,7-bisphosphate (SBP). La fructose-1,6-bisphosphatase (FBPase) et la sédoheptulose-1,7-bisphosphatase (SBPase) vont respectivement hydrolyser le FBP et le SBP en F6P et en S7P. Enfin, la régénération du RuBP substrat de la Rubisco se fait via trois enzymes, la phosphoribulokinase (PRK), la ribose-5-phosphate isomérase (RPI), la ribulose-5-phosphate-3-épimérase (RPE), ces deux dernières isomérisant respectivement le R5P et le X5P en ribulose-5-phosphate (RuP). La PRK va phosphoryler le RuP en RuBP en utilisant un ATP comme co-substrat. Les onze enzymes sont nécessaires au CBBC dans le chloroplaste mais ne sont pas toutes exclusives à celui-ci.

1.3.2 Fonctions enzymatiques communes à d'autres voies métaboliques

Trois des onze enzymes du cycle ont une unique fonction métabolique connue, telle que décrite ci-dessus dans le CBBC : la Rubisco, la PRK, et la SBPase. Cette dernière est remplacée chez les cyanobactéries par une enzyme assurant la double fonction FBPase/SBPase (Tamoi et al. 1996). Au contraire, des enzymes homologues à huit enzymes du CBBC ont des fonctions attribuées à d'autres voies métaboliques.

Les enzymes GAPDH, TPI, PGK et FBA contribuent toutes à la glycolyse (Figure 3). Cette voie métabolique commence par la dissociation d'oses à six carbones (le D-glucose) en deux oses à trois carbones (le G3P et le DHAP). Dans le cadre de cette voie métabolique elles catalysent les réactions inverses à celles catalysées dans le CBBC. La glycolyse a lieu dans le cytosol des organismes non photosynthétiques. Chez Chlamydomonas sa localisation se répartit entre le cytosol et le chloroplaste (Johnson and Alric 2013; Klein 1986), la première partie du glucose au G3P se situant dans le chloroplaste et la seconde partie du 3-PGA au pyruvate dans le cytosol.

De la même manière, la néoglucogénèse ou gluconéogenèse est une voie métabolique permettant la synthèse de glucose à partir de précurseurs ayant moins de carbones comme le DHAP ou le G3P. Cette voie métabolique se déroule dans le chloroplaste chez Chlamydomonas. Elle fait intervenir la FBPase et la FBA (Figure 3) (Johnson and Alric 2013).

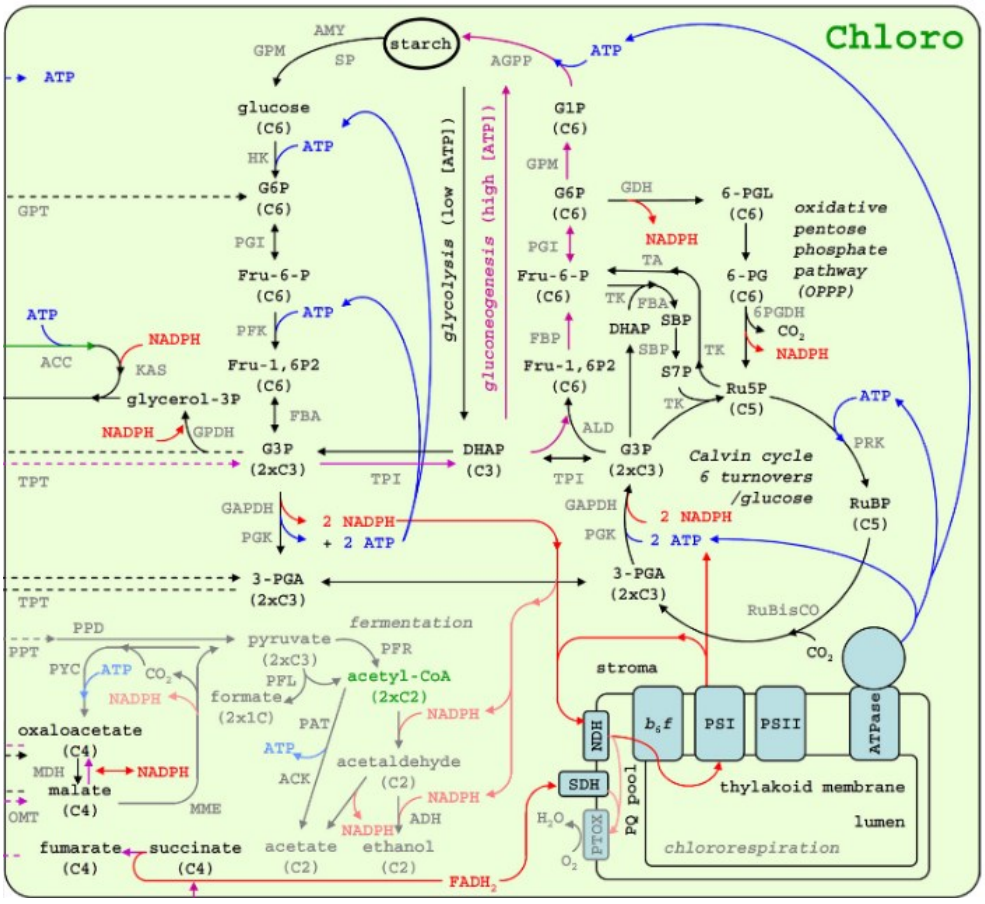

Figure 3 : Schéma du métabolisme du carbone dans le chloroplaste de *Chlamydomonas reinhardtii* (adapté de Johnson and Alric (2013)).

Les trois dernières enzymes ayant une fonction à la fois dans le CBBC et dans une autre voie métabolique sont RPI, RPE et TRK. Celles-ci sont impliquées dans la voie des pentoses phosphates. Cette voie métabolique permet la production de pouvoir réducteur sous la forme de NADPH mais aussi de composés carbonés impliqués dans la synthèse de nucléotides, des acides aminés aromatiques et d'autres voies de biosynthèses. Si la répartition quantitative de ces enzymes entre le cytosol et le chloroplaste a été étudiée chez les plantes (Kruger and von Schaewen 2003), chez Chlamydomonas seule la répartition de la glucose-6-phosphate déshydrogénase et de la 6-phosphogluconate déshydrogénase a été étudiée (Klein 1986). En revanche, la localisation de ces enzymes est connue. Il est possible de prédire de manière fiable l'adressage des protéines à un compartiment en utilisant des prédicteurs informatiques de peptides d'adressage (Almagro

Armenteros et al. 2019; Tardif et al. 2012). Les enzymes du CBBC sont toutes codées par des gènes dans le noyau puis traduites dans le cytosol avant d'être importées vers le chloroplaste via ces peptides d'adressage, la seule exception étant la grande sous-unité de la Rubisco qui est codée par un gène du génome chloroplastique. En utilisant des étiquettes fluorescentes la localisation expérimentale intra-cellulaire des protéines du cycle de Calvin-Benson-Bassham a été rendue disponible il y a peu de temps via une prépublication (Wang et al. 2022). Cette analyse permet non seulement de confirmer la présence des enzymes du CBBC dans le chloroplaste mais aussi leurs localisations de manière 1,85 fois plus importante à proximité du pyrénoïde contenant la majorité de la Rubisco de la cellule (détaillé ci-après section 1.3.3.1).

La plupart de ces types d'enzymes ont donc une fonction à la fois dans le chloroplaste et dans le cytosol. Il existe chez Chlamydomonas plusieurs gènes codant pour différents paralogues de ces protéines, certaines étant prédites adressées au chloroplaste et d'autres adressées au cytosol. Sauf précision contraire les paralogues étudiés ici sont ceux participant au cycle de Calvin-Benson-Bassham. Si le CBBC a été établi en tant que voie métabolique en 1950, les enzymes catalysant ses réactions ont été isolées et leurs propriétés catalytiques caractérisées au cours des décennies suivantes. Les structures tridimensionnelles ne sont connues que pour certaines de ces enzymes, souvent pour des homologues non photosynthétiques et en aucun cas toutes disponibles chez un organisme photosynthétique modèle unique.

1.3.3 Enzymes de structures connues

1.3.3.1 Rubisco

La Rubisco (EC 4.1.1.39) est l'enzyme la plus abondante sur terre (Bar-On and Milo 2019). Elle catalyse l'étape cruciale de fixation du carbone inorganique en oses. Malgré son importance, la Rubisco est relativement inefficace tant du point de vue de sa constante catalytique (k_{cat}= 5,8 sec^{-1}) que du point de vue de son affinité pour le substrat CO_2 ($K_M(CO_2)$ = 29 $\mu mol.L^{-1}$) (Tcherkez et al. 2006). En outre, la Rubisco se lie de manière concurrentielle au CO_2 ou au dioxygène

($K_M(O_2)$ = 529 µmol.L^{-1}) (Genkov and Spreitzer 2009). Cette double affinité conduit à la fréquente oxygénation du RuBP aux concentrations effectives de ces ligands. Or, l'oxygénation du RuBP produit du 2-phosphoglycolate, un inhibiteur de TPI et SBPase, dont l'élimination passe par la voie de photorespiration, coûteuse en énergie.

La Rubisco est composée de deux types de sous-unités : la grande sous-unité (RbcL) d'une masse de 55 kDa, et la petite sous-unité (RbcS) de 15 kDa. Huit RbcL et huit RbcS s'associent en un complexe hexa-décamérique (Figure 4) (Andersson and Backlund 2008). La grande sous-unité de celle-ci se compose de deux domaines, un N-terminal composé d'un feuillet β antiparallèle de quatre brins, entouré de cinq hélices α (CATH classification 3.30.70.150) et un domaine C-terminal catalytique en tonneau TIM (CATH classification 3.20.20.110). La petite sous-unité est composée d'un seul domaine comportant un feuillet β antiparallèle de quatre brins, accolé à deux hélices α (CATH classification 3.30.190.10).

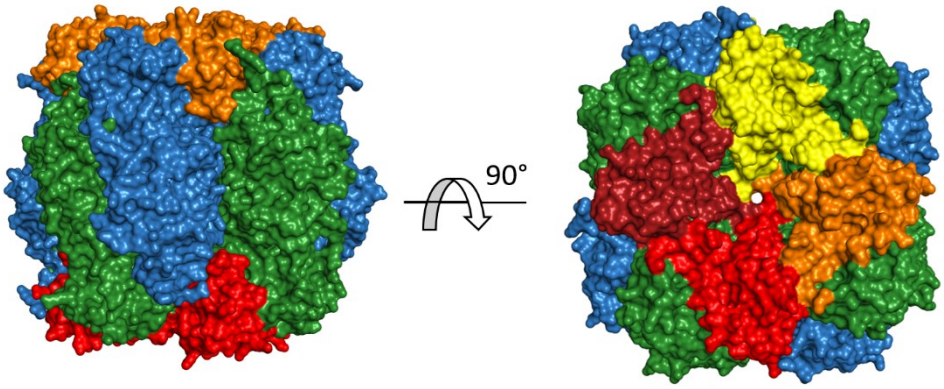

Figure 4 : Représentation de la surface d'exclusion du solvant de Connolly d'un hexa-décamère de CrRubisco (Code PDB : 1GK8) dans deux orientations différentes. Les huit grandes sous-unités sont colorées alternativement en bleues et vertes. Les huit petites sous-unités sont colorées à gauche en rouge et orange, à droite en rouge, orange et jaune.

Dans la structure de la Rubisco de Chlamydomonas résolue par Taylor et al. (2001), les auteurs confirment une conservation importante des résidus du site actif avec les Rubisco d'autres espèces

(Jordan and Ogren 1981). Chez Chlamydomonas, la Rubisco est localisée dans un compartiment spécialisé du stroma du chloroplaste, le pyrénoïde, qui assure la même fonction que les carboxysomes des cyanobactéries (Bracher et al. 2017). Cette fonction est de pallier l'inefficacité catalytique et d'affinité de la Rubisco pour le CO_2 en concentrant celui-ci, ainsi que l'enzyme, dans ce compartiment. Ce compartiment concentre la majorité de la Rubisco de la cellule en une matrice pseudo-cristalline qui comporte également les protéines essentielles au fonctionnement de la Rubisco comme des protéines chaperons et la Rubisco activase (Wang and Jonikas 2020; Zhan et al. 2018; Mackinder et al. 2017; Meyer et al. 2017).

1.3.3.2 Transkétolase

La transkétolase (TRK) (E.C. 2.2.1.1) de Chlamydomonas est un homo-dimère dont la structure et la fonction ont été caractérisées en 2017 (Pasquini et al. 2017). L'état homo-dimérique de 150 kDa observé dans l'unité asymétrique est confirmé par des expériences de diffusion des rayons X aux petits angles (SAXS). Ces dimères de forme triangulaire se superposent aux deux autres structures de TRK issus d'autres organismes de la PDB (respectivement le maïs *Zea mays* et la levure *Saccharomyces cerevisiae* avec pour codes PDB : 1ITZ et 1TRK) avec moins de 1.5 Å de distance moyenne entre carbones équivalents (RMSD). Chaque monomère est composé de 670 résidus formant trois domaines α/β chacun contenant un feuillet β central entouré par des hélices α. Le domaine en N-terminal peut fixer un ion Mg^{2+} et un pyrophosphate de thiamine (PPT) qui sont deux cofacteurs indispensables à l'activité catalytique de la TRK. Le domaine central de la protéine permet la fixation du noyau pyrimidine du PPT et le domaine C-terminal est le plus petit et n'est impliqué ni dans la fixation de cofacteur, ni du substrat, ni dans l'interface de dimérisation de la TRK (Figure 5).

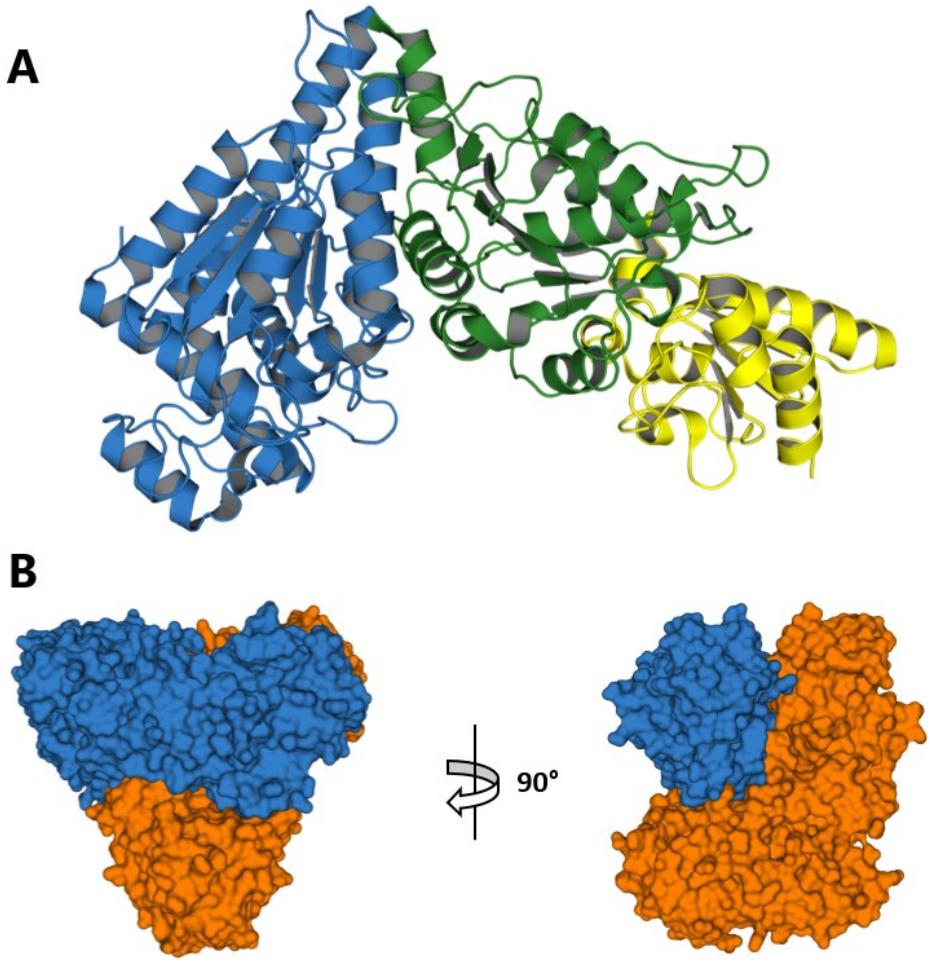

Figure 5 : A. Représentation en ruban d'un monomère de CrTRK (Code PDB : 5ND6) coloré respectivement en bleu, vert et jaune pour les domaines N-terminal, central et C-terminal. **B.** Représentation de la surface accessible au solvant d'un homo-dimère de CrTRK aux sous-unités colorées en bleu et orange dans deux orientations différentes.

1.3.3.3 Triose phosphate isomérase

Il existe en général chez les organismes photosynthétiques deux paralogues de TPI (E.C. 5.3.1.1) l'un étant cytoplasmique et impliqué dans la glycolyse, l'autre étant localisé dans le chloroplaste et participant au CBBC. Chez Chlamydomonas, seul le paralogue chloroplastique est présent et réalise les deux fonctions dans le chloroplaste, la glycolyse étant répartie entre le chloroplaste et le

cytosol (Johnson and Alric 2013). Ce paralogue chloroplastique a sa structure et sa fonction décrites chez Chlamydomonas (Zaffagnini et al. 2014). La structure quaternaire de TPI s'organise en homo-dimère de 60 kDa chez tous les organismes où elle a été étudiée à deux exceptions, où elle s'organise en homo-tétramère : *Thermogata maritima* (Maes et al. 1999) et *Pyrococcus woesei* (Walden et al. 2001). TPI est replié en tonneau TIM (CATH classification 3.20.20.110) composé de huit brins β parallèles entourés de huit hélices α (Figure 6). Les superpositions entre la structure de TPI chloroplastique et les structures de TPI cytoplasmiques ne montrent pas de différences significatives de structure en dehors de la conformation d'une boucle du site actif en conformation fermée dans la structure de TPI de lapin *Oryctolagus cuniculus* (code PDB : 1R2R). Le site actif de CrTPI ne présente pas davantage de différence avec ceux déjà décrits chez d'autres organismes. Il est également intéressant de mentionner que la TPI chloroplastique est décrite comme une enzyme ayant des propriétés catalytiques parfaites car elle n'est limitée que par la constante de diffusion limite des substrats dans le site actif (10^8 $M^{-1}.s^{-1}$). Cependant il semblerait que des différences soit présentes entre les espèces puisque le ratio k_{cat}/K_M de la TPI d'Arabidopsis est de $5,84*10^6$ $M^{-1}.s^{-1}$, celui de l'épinard $6,63*10^6$ $M^{-1}.s^{-1}$, celui de *Plasmodium falciparum* $1,23*10^7$ $M^{-1}.s^{-1}$, et celui de *Saccharomyces cerevisiae* $4,27*10^6$ $M^{-1}.s^{-1}$ (López-Castillo et al. 2016; Samanta et al. 2011; González-Mondragón et al. 2004; Tang et al. 1999). En comparaison, le rapport k_{cat}/K_M de la TPI de *Chlamydomonas reinhardtii* est de $1,12*10^5$ $M^{-1}.s^{-1}$, ce qui est parmi les valeurs les plus faibles parmi celles connues (Zaffagnini et al. 2014).

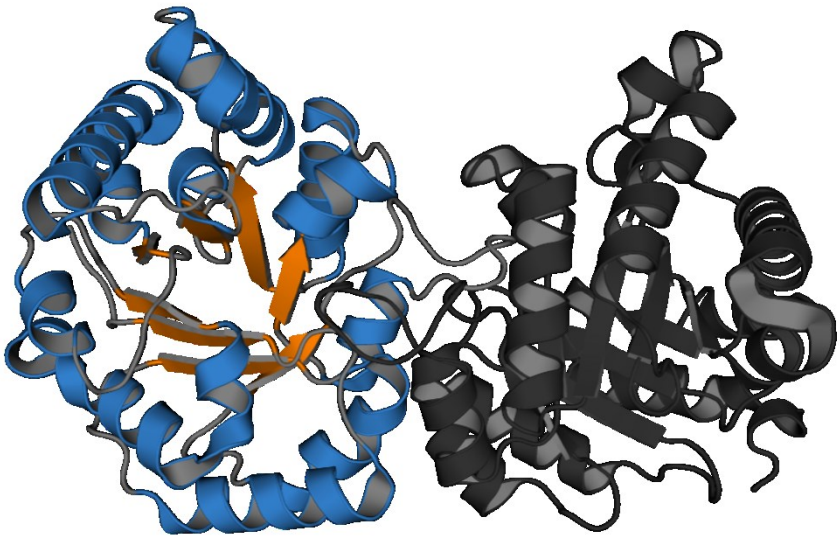

Figure 6 : Représentation en ruban d'un dimère de CrTPI (Code PDB : 4MKN) un monomère est coloré en noir. Le second monomère est coloré en gris pour les boucles, en orange pour ses brins β et en bleu pour ses hélices α.

1.3.3.4 Ribose phosphate épimérase

La structure de RPE a été résolue au sein de mon équipe en 2019 et l'enzyme a fait l'objet d'analyses fonctionnelles en collaboration avec l'Université de Bologne (Laboratory of Molecular Plant Physiology, Department of Pharmacy and Biotechnology, University of Bologna).

RPE (E.C. 5.1.3.1) est une enzyme ayant deux paralogues identifiés chez Chlamydomonas, l'un adressé au chloroplaste et l'autre au cytosol, respectivement nommés RPE1 et RPE2. RPE1 est active dans la voie oxydative des pentoses phosphates et dans le CBBC au sein du chloroplaste tandis que RPE2 est active seulement dans la voie oxydative des pentoses phosphates du cytosol (Merchant et al. 2007). RPE1 possède un repliement en tonneau TIM composé de huit feuillets β formant un cylindre central (Figure 7 A.). A une échelle plus grande RPE1 s'organise en un homo-hexamère de 160 kDa (Figure 7 B).

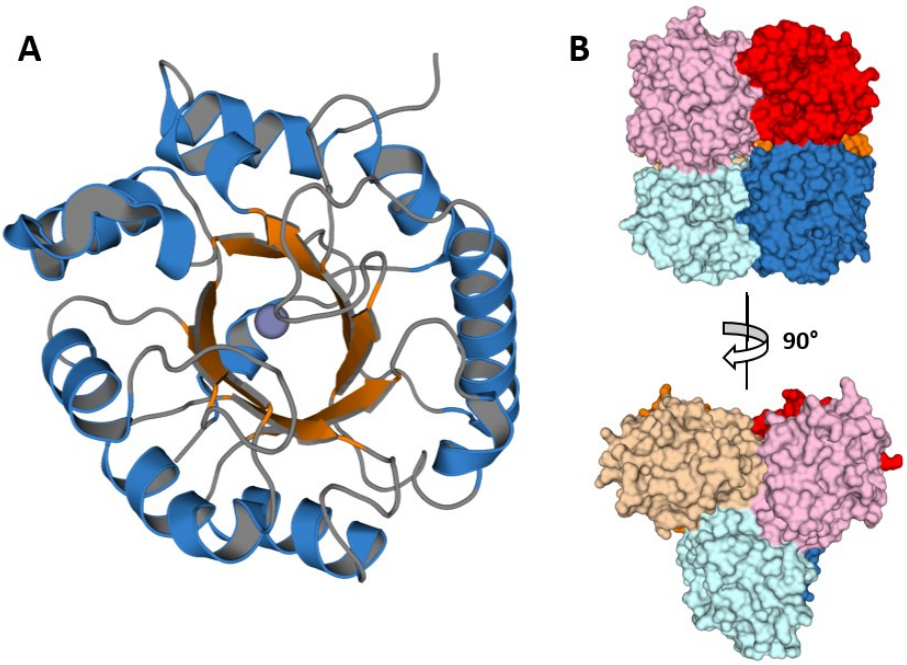

Figure 7 : A. Représentation en ruban de CrRPE (Code PDB : 7B1W), les brins β sont colorés en orange, les hélices α en bleue et l'atome de zinc du site catalytique en gris. **B.** Représentation de la surface accessible au solvant de deux orientations d'un homo-hexamère de CrRPE ; les six sous-unités sont colorées en deux teintes de rouge, bleu et orange.

Il existe actuellement vingt-trois structures de RPE disponibles dans la PDB, dont trois structures de protéines issues d'organismes photosynthétiques, permettant une analyse comparative avec Chlamydomonas. Ces différentes structures ont toutes le même repliement en tonneau TIM, mais présentent certaines particularités qui les distinguent. Par exemple, RPE étant une métalloenzyme elle a besoin d'un ion métallique pour son activité catalytique. La nature de cet ion métallique semble différer en fonction de l'espèce de laquelle la séquence protéique est issue. Dans la structure de RPE d'*Escherichia coli*, des études mettent en évidence un ion fer II (Fe^{2+}) (Sobota and Imlay 2011) tandis que chez le riz il semblerait que cet ion soit un ion Zn^{2+} (Jelakovic et al. 2003). Chez Chlamydomonas, un ion Zn^{2+} semble mieux correspondre à la densité électronique obtenue dans le jeu de données, comme confirmé ultérieurement par mesure de la fluorescence aux rayons X du Zinc des cristaux.

1.3.3.5 Phosphoribulokinase

La PRK (E.C. 2.7.1.19) est l'enzyme précédant la Rubisco dans le CBBC, sa seule fonction connue est sa contribution à la photosynthèse. Chez Chlamydomonas, elle se présente sous la forme d'un homo-dimère de 70 kDa. La structure tridimensionnelle de l'enzyme a été résolue en même temps que celle de PRK d'*Arabidopsis thaliana* en 2019 (Gurrieri et al. 2019). Cette structure consiste en un long feuillet β mixte de neuf brins entouré par neuf hélices αet de quatre autres petits brins β. Ce grand feuillet est symétrique à celui du second monomère. L'interface d'homo-dimérisation est un motif à deux brins β antiparallèles (Figure 8). Le site actif de cette enzyme est situé dans le sillon à l'opposé de l'interface de dimérisation. La surface de cette poche catalytique est chargée positivement ce qui facilite une fixation du RuP ainsi que de l'ATP qui fournit le phosphate nécessaire à la phosphorylation. Cette molécule d'ATP est notamment coordonnée par des résidus se situant sur une boucle qui contient une cystéine connue pour faire partie des mécanismes de régulation par oxydo-réduction (nommés ci-après mécanismes redox) chez les organismes photosynthétiques.

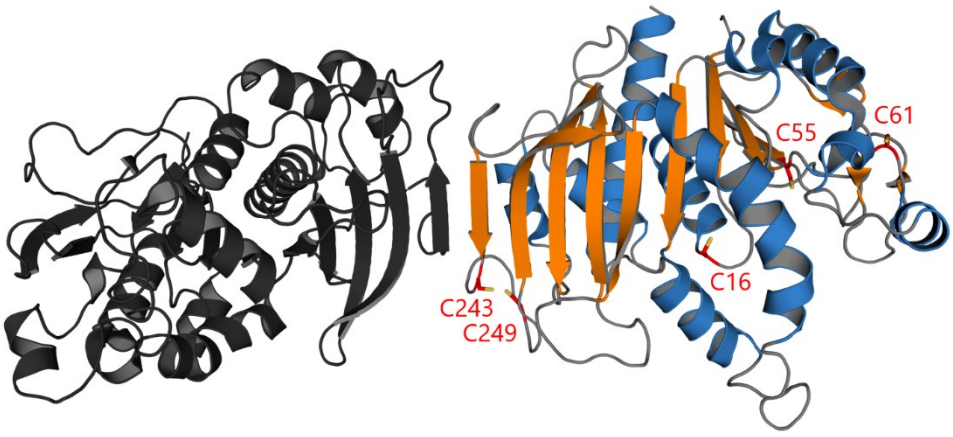

Figure 8 : Dimère de CrPRK (Code PDB : 6H7G) représenté en ruban. L'un des monomères est coloré en noir, le second est coloré en fonction de ses structures secondaires avec les hélices α en bleu, les brins β en orange et les boucles en gris. Les cystéines de ce monomère sont colorées en rouge et annotées.

1.3.3.6 Glycéraldéhyde-3-phosphate déshydrogénase (GAPDH)

GAPDH (E.C. 1.2.1.13) est l'enzyme qui suit la PGK dans le CBBC. La structure de cette enzyme chez Chlamydomonas fait l'objet d'une récente publication (Mattioli et al. 2022). Si différentes isoformes de GAPDH (GAPA et GAPA/B) existent chez les plantes, il n'existe qu'une GAPDH chloroplastique chez Chlamydomonas (isoforme GAPA). Cette enzyme est décrite comme ayant une organisation homo-tétramérique (Figure 9 B) avec deux domaines par monomère et une boucle « S ». Ces deux domaines ont pour fonctions de fixer le cofacteur de l'enzyme en N-terminal et de catalyser la réaction en C-terminal, la boucle « S » permettant l'assemblage de l'homo-tétramère. Trois structures de CrGAPA ont été déterminées respectivement en présence de $NADP^+$, de NAD^+, et de $NADP^+$ avec la cystéine catalytique oxydée en sulfinate/sulfonate ($-SO_2^-$/$-SO_3^-$) (Codes PDB : 7ZQ3, 7ZQ4, 7ZQK). Le domaine catalytique contient une diade catalytique composée des résidus Cys149/His176 (Figure 9 A) et de deux sites de liaisons des phosphates du substrat dont les résidus, respectivement S148, T208, G209, A210 et T179, R195, R231, sont conservés dans les séquences de GAPDH photosynthétiques. La diade catalytique permet à la cystéine 149 d'être sous forme déprotonée $-S^-$ et donc réactive, l'histidine 176 captant le proton. Cet article décrit également la régulation de GAPDH de cette protéine via des modifications post-traductionnelles. La cystéine 149 est susceptible d'être nitrosylée (détaillé dans la section 1.4.1.3) et d'inactiver l'activité catalytique de GAPDH (Mattioli et al. 2022).

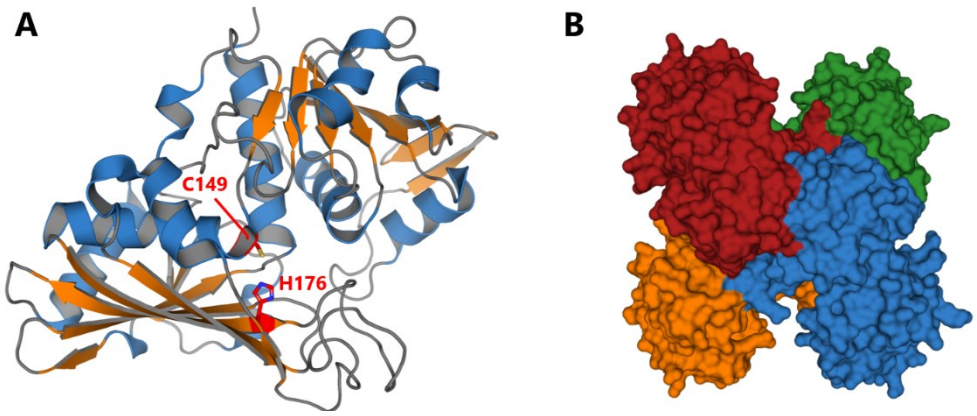

Figure 9 : A. Monomère de CrGAPDH (code PDB : 7ZQK) représenté en ruban, coloré en fonction de ses structures secondaires avec les hélices α en bleues, les brins β en oranges et les boucles en grises. La diade catalytique C149/H176 est colorée en rouge et annotée. **B.** Représentation de la surface accessible au solvant d'un homo-tétramère de CrGAPDH avec les différents monomères colorés en rouge, orange, bleu et vert.

Les différentes structures disponibles des enzymes du CBBC de Chlamydomonas passées en revue ne semblent pas différer fondamentalement de leurs paralogues non photosynthétiques. En revanche, un point de différence de ces structures est la régulation de leurs activités catalytiques en fonction de paramètres spécifiques à la photosynthèse. Les modifications post-traductionnelles ciblant les enzymes du CBBC font ainsi l'objet de la section suivante de ce manuscrit.

1.4 Regulations des enzymes du cycle de Calvin-Benson-Bassham

Toutes les enzymes du CBBC sont soumises à de multiples régulations de leurs activités catalytiques. La nécessité d'une régulation de ces activités provient de l'organisation même de la photosynthèse. En effet, le CBBC dépend de l'apport d'ATP et de NADPH pour pouvoir fonctionner et régénérer son substrat, or ces deux métabolites sont principalement synthétisés durant la phase photochimique en présence de lumière, par les complexes photosynthétiques localisés aux thylakoïdes. Pour éviter un déséquilibre dans la concentration de ces métabolites durant les

périodes d'obscurité, le CBBC est inactivé de manière réversible par plusieurs mécanismes de régulation que nous allons détailler ici.

1.4.1 Régulations par oxydo-réduction

La régulation des enzymes du CBBC par des modifications post-traductionnelles d'oxydo-réduction (redox) réversibles peut se dérouler de plusieurs manières, notamment par la réduction de ponts disulfures établis entre paires de cystéines d'une même chaîne peptidique, de deux chaînes peptidiques indépendantes, ou par glutathionylation ou nitrosylation de cystéines. Si toutes les enzymes et mécanismes de régulations ne sont pas décrits pour les enzymes du CBBC, elles sont toutes retrouvées dans des études de protéomique réalisées sur Chlamydomonas portant sur la S-nitrosylation, la S-glutathionylation ou bien le ciblage par les thiorédoxines (Zaffagnini et al. 2019; Morisse et al. 2014b; Zaffagnini et al. 2012a; Lemaire et al. 2004). Ces modifications peuvent servir à modifier l'activité des enzymes, leurs assemblages supramoléculaires ou bien protéger de l'oxydation irréversible des cystéines en acides sulfénique, sulfinique et sulfonique. Ainsi, la Rubisco possède des cystéines qui ont un rôle protecteur, et dont la fonction est de servir de bouclier contre l'oxydation d'autre cystéines ayant une fonction essentielle (García-Murria et al. 2018). Ici je me focaliserai seulement sur les trois types de modifications les mieux étudiées chez Chlamydomonas qui sont la formation de ponts disulfures, la glutathionylation et la nitrosylation des cystéines.

1.4.1.1 Ponts disulfures

La formation de ponts disulfures dans les protéines consiste en l'établissement d'une liaison covalente de deux résidus cystéine possédant un atome de soufre dans les groupements thiols de leurs chaînes latérales. Les deux chaînes latérales se lient pour former un pont disulfure de structure R-S-S-R. Réciproquement, la réduction de ce pont disulfure consiste à passer de R-S-S-R à la forme R-SH. Ces liaisons covalentes possèdent des fonctions importantes pour la structure et la stabilité des protéines, mais peuvent également être impliquées dans des mécanismes de changement de conformation des protéines pour en modifier la fonction ou l'activité.

La réduction de ponts disulfures entraînant une modification de l'activité enzymatique de cinq enzymes du CBBC en fonction de la luminosité a été l'un des premiers sujets à être étudié (Gurrieri et al. 2021; Balsera and Buchanan 2019; Cejudo et al. 2019; Zaffagnini et al. 2019; Michelet et al. 2013; Schürmann and Buchanan 2008; Schürmann and Jacquot 2000; Huppe and Buchanan 1989). Cette régulation est directement liée à la luminosité et au flux d'électrons dans la membrane du chloroplaste. En effet, la réduction des ponts disulfures des enzymes du CBBC est l'aboutissement d'une chaîne de transfert de pouvoir réducteur appelé le système ferrédoxine/thiorédoxine détaillé dans une revue de 2013 (Michelet et al. 2013) ainsi que dans un chapitre d'ouvrage paru en 2022 (Le Moigne et al. 2022a). Dans les organismes photosynthétiques, cinq enzymes du CBBC sont décrites comme pouvant être régulées par la réduction d'un pont disulfure pour augmenter leurs activités : la SBPase, la FBPase, la GAPDH, la PRK et la PGK (Gurrieri et al. 2019; Gütle et al. 2016; Morisse et al. 2014a; Michelet et al. 2013). Chez Chlamydomonas, SBPase et FBPase ne font pas l'objet de publication explicitant ce mécanisme mais sont actuellement à l'étude dans l'équipe.

En revanche, des études de protéomique ayant pour objectifs d'identifier les différentes cibles des thiorédoxines existent, indiquant que toutes les enzymes du CBBC sont cibles des thiorédoxines (Pérez-Pérez et al. 2017; Lemaire et al. 2004). De plus, PRK et PGK font l'objet de publications chez Chlamydomonas qui décrivent quelles cystéines sont impliquées dans ces ponts disulfures régulateurs.

La régulation par réduction de pont disulfure de PGK s'effectue via la paire de cystéine C227/C361. CrPGK en présence de l'agent réducteur DTT (dithiothréitol) présente une augmentation significative de son activité comparée à l'absence de DTT ou la présence de DTTox. L'activité de celle-ci présente également une augmentation en présence de thiorédoxine de type f qui est le type de thiorédoxine affecté à la régulation des enzymes du CBBC. L'analyse de mutants de substitution des cystéines 108, 227 et 361 par des sérines montre également une perte de sensibilité au DTT pour les deux derniers mutants ce qui n'est pas le cas du mutant C108S, permettant l'identification des cystéines régulatrices (Morisse et al. 2014a).

Le cas de la régulation redox de GAPDH est particulier. Sa régulation possède des caractéristiques différentes chez les Streptophytes (plantes terrestres entre autres) par rapport aux autres organismes photosynthétiques comme les Chlorophytes dont fait partie Chlamydomonas. L'activité de GAPDH *in vivo* est dépendante de la présence du flux d'électron menant à l'activation du système ferrédoxine/thiorédoxine. Ce comportement est confirmé *in vitro* en présence de DTT et chez plusieurs espèces (passé en revue dans Michelet et al. (2013)). La GAPDH photosynthétique est codée par deux gènes (gapA et gapB) qui se différencient par la présence au niveau protéique d'une extension C-terminale de trente acides aminés qui contient la paire de cystéines régulatrices réduites par les thiorédoxines chez GAPB. Cette extension est absente chez GAPA. Ces deux isoformes peuvent s'associer en homo-tétramères composés de deux GAPA et deux GAPB ou bien de quatre GAPA. Chez Chlamydomonas, seul le gène gapA est présent, on ne retrouve donc que la protéine GAPA dépourvue de l'extension C-terminale régulatrice. En revanche, CrGAPDH est, chez Chlamydomonas, bien soumise à d'autres types de régulations redox détaillés ci-après (*cf.* section 1.4.1.3).

CrPRK peut former deux ponts disulfures grâce à quatre cystéines : les paires C16/C55 et C243/C249 (Gurrieri et al. 2019; Thieulin-Pardo et al. 2015). La cystéine 55 est localisée sur la boucle permettant la fixation de l'ATP proche du site actif (*cf.* partie 1.3.3.5). En se liant à la cystéine 16 cette boucle change de conformation et empêche la fixation de cette molécule d'ATP au site actif. Sous forme réduite, la boucle est en conformation ouverte et peut lier l'ATP. La seconde paire de cystéines est située à l'opposé du site actif et possède une fonction dans le relâchement de la structure globale de l'enzyme ainsi que dans son association en complexe qui sera détaillée ci-après.

Si la réduction d'un pont disulfure menant à l'augmentation des activités de SBPase et FBPase a été décrite chez le pois (*Pisum sativum*) et chez une mousse photosynthétique *Physcomitrella patens* (Gütle et al. 2016; Chiadmi 1999; Jacquot et al. 1997; Jacquot et al. 1995), ce n'est pas le cas chez Chlamydomonas. De même, les autres enzymes du CBBC semblent interagir avec les thiorédoxines mais l'importance et le rôle fonctionnel de ces régulations potentielles restent inexplorés. Les

thiorédoxines étant capable non seulement de réduire des ponts disulfures entres deux cystéines mais aussi entre une cystéine et un autre composant, il n'est pas exclu que certaines enzymes du CBBC soit seulement la cible de modifications post traductionnelles sur leurs cystéines plutôt que de la formation de pont disulfures.

1.4.1.2 S-glutathionylation

Le glutathion est un tripeptide de séquence γ-L-glutamyl-L-cystéinyl-L-glycine. Cette molécule existe sous deux formes, une forme réduite (GSH) et une forme oxydée (GSSG). Ces deux formes ne sont pas présentes en concentration égale dans la cellule, la forme GSSG étant réduite par la glutathion réductase pour permettre à la forme GSH de jouer son rôle principal de tampon réducteur et d'antioxydant de la cellule aidant à la détoxification des espèces réactives de l'oxygène (ROS) notamment produites durant la photosynthèse (Keech et al. 2017; Rouhier et al. 2015). La S-glutathionylation consiste en une modification post-traductionnelle consistant à la greffe d'un GSH à un atome de soufre d'une cystéine. Cette modification post-traductionnelle peut avoir pour fonction de protéger les cystéines d'une oxydation irréversible par un ROS, mais également de moduler les activités enzymatiques de certaines enzymes (Zaffagnini et al. 2012b; Michelet et al. 2008).

Chez Chlamydomonas, toutes les enzymes du CBBC sont la cible de S-glutathionylation (Zaffagnini et al. 2014; Zaffagnini et al. 2012a). Si l'identification des cystéines glutathionylées n'est pas disponible pour toutes les enzymes, elle l'est néanmoins pour certaines d'entre elles. Ainsi, les cystéines C172, C247, C427 de la grande sous-unité de la Rubisco, C159 et C412 de PGK, C58, C256 et C405 de FBA, C109 de FBPase, C84 de TRK C47 et C274 de PRK ont formellement été identifiées comme glutathionylées. La même étude montre également une modification de l'activité de PRK qui perd 85% de son activité en présence de GSSG, cette inhibition étant réversible par l'ajout de DTT. De la même manière, GAPDH réagit à la présence de GSH par une baisse de son activité chez Chlamydomonas ainsi que par une protection contre l'oxydation irréversible et a été trouvée comme glutathionylée chez Arabidopsis (Zaffagnini et al. 2007).

La S-glutathionylation semble donc avoir une fonction soit régulatrice, soit protectrice des thiols des enzymes du CBBC. Mais cette modification n'est pas la seule à être possible ou démontrée sur ces mêmes thiols. En effet, si le glutathion est une molécule abondante dans la cellule, celui-ci peut aussi réagir avec un oxide nitrique pour aboutir à la molécule de nitrosoglutathion (GSNO). Ce GSNO a lui-même des fonctions dans les mécanismes de régulation et de disponibilité de l'oxide nitrique dans les cellules, et participe notamment la S-nitrosylation.

1.4.1.3 S-nitrosylation

La S-nitrosylation est une autre modification post-traductionnelle, qui consiste en l'ajout covalent d'un oxide nitrique (NO) à l'atome de soufre d'une cystéine, transformant la chaîne latérale -SH de celle-ci en -SNO. Cette modification est impliquée dans de nombreux mécanismes physiologiques et localisée dans différents compartiments cellulaires notamment le chloroplaste chez les plantes. Si cette modification est moins stable que la S-glutathionylation, elle reste importante dans les modifications redox, le transfert d'un NO pouvant se faire d'un thiol modifié -SNO vers un glutathion créant un nitrosoglutathion lui-même capable de nitrosyler un autre thiol. Il a également été montré chez la drosophile (*Drosophila melanogaste*r) la possibilité de transfert d'un NO d'une protéine vers une autre protéine, soit une trans-nitrosylation, celle-ci étant notamment induite par GAPDH (Kornberg et al. 2010).

Chez *Chlamydomonas reinhardtii* une étude de protéomique a identifié l'existence de 492 protéines sujettes à une S-nitrosylation. Parmi ces protéines, les onze enzymes du CBBC sont présentes. Les résidus étant la cible de ces modifications ont également pu être identifiés pour certaines de ces enzymes. Il s'agit des cystéines C172, C247, C427, C459 de la grande sous-unité de la Rubisco, C110 de la petite sous-unité de la Rubisco, C412 de PGK, C245, 273 de TPI, C58, C142 et C256 de FBA, C233 de FBPase, C582 de TRK, C351 et C358 de SBPase, C47 de PRK (Morisse et al. 2014b). Comme mentionné précédemment (*cf.* section 1.3.3.6) GAPDH peut également être nitrosylée sur sa cystéine de sa diade catalytique en présence de GSNO. Cette nitrosylation provoque une baisse de 90% de son activité

après 30 minutes en présence de 2 mmol.L^{-1} de GSNO (Mattioli et al. 2022).

Contrairement à la S-glutathionylation, la fonction des S-nitrosylations n'a pas été décrite pour les enzymes du CBBC chez Chlamydomonas. Ces modifications pourraient tout à fait avoir un rôle important ou au contraire aucun effet physiologique.

Si les cystéines sont la cible de modifications post-traductionnelles du fait de leurs réactivités, ce ne sont pas les seuls acides aminés à posséder une réactivité importante. Ainsi d'autre modifications existent également dans les cellules et sur les enzymes du CBBC.

1.4.2 Autres modifications post-traductionnelles et mécanismes de régulations

Le cycle de Calvin-Benson-Bassham est sujet à une régulation via des mécanismes d'oxydo-réduction, mais ce ne sont pas les seuls mécanismes à pouvoir influer sur son activité. En effet, il existe plusieurs niveaux de régulations via d'autres modifications post-traductionnelles ou via d'autres molécules.

1.4.2.1 Phosphorylation

La phosphorylation est l'une des modifications post-traductionnelles les plus connues. Elle consiste en l'ajout d'un groupement phosphate (PO_3^-) sur une chaine latérale, le plus souvent d'une sérine, d'une thréonine ou d'une tyrosine. Ces phosphorylations sont impliquées dans le contrôle de chaînes de signalisation, ainsi que dans la stabilité, la fonction, l'activité, la localisation et les interactions entres protéines. De ce fait, plusieurs études du phosphoprotéome de Chlamydomonas ont été effectuées par plusieurs méthodes (McConnell et al. 2018; Roustan and Weckwerth 2018; Roustan et al. 2017; Wang et al. 2014). En fonction de l'approche expérimentale, toutes ou une partie des enzymes du CBBC possèdent des sites de phosphorylation sur des résidus sérine ou thréonine à la seule exception de FBPase qui n'est retrouvée dans aucune étude. Ces sites de modifications et la numérotation des résidus sont disponibles dans le tableau 3 du chapitre 8 du Chlamydomonas Sourcebook (Le Moigne

et al. 2022a). En revanche, ces études de phosphoprotéomique n'identifient pas formellement la potentielle fonction des phosphorylations sur les enzymes du CBBC chez Chlamydomonas.

1.4.2.2 Autres modifications post-traductionnelles

En plus des modifications redox et des phosphorylations les enzymes du CBBC font l'objet de diverses autres modifications. Ainsi, il a été rapporté que la Rubisco est sujette à la méthylation de sa lysine 14 de fonction inconnue et dépendante de l'organisme, ainsi que de nombreuses autres modifications (Houtz et al. 2007). Chez le pois (*Pisum sativum*) FBA est également décrite comme sujette à une triple méthylation de fonction inconnue (Mininno et al. 2012). Chez *Arabidopsis thaliana*, une étude sur l'acétylation des lysines retrouve la grande et la petite sous-unité de la Rubisco, PGK et GAPDH (Finkemeier et al. 2011). Il existe ainsi d'autres modifications des enzymes du CBBC chez d'autres organismes photosynthétiques qui pourraient également être présentes chez Chlamydomonas.

1.4.2.3 Concentration en magnésium et calcium

Les modifications post-traductionnelles sont l'un des moyens de réguler les activités des enzymes, mais celles-ci sont également affectées par la concentration en certains ions divalents. En effet, chez plusieurs espèces photosynthétiques dont Chlamydomonas la présence d'ions divalents et plus précisément de Mg^{2+} augmente l'activité de la FBPase (Chardot and Meunier 1991; Huppe and Buchanan 1989; Udvardy et al. 1982). C'est également le cas pour la TRK de Chlamydomonas qui nécessite une concentration d'ion Mg^{2+} de l'ordre du millimolaire pour être active (Pasquini et al. 2017). Cette dépendance des enzymes à une quantité de magnésium semble être reliée à leur régulation en fonction de la présence ou l'absence de lumière, la concentration d'ion Mg^{2+} dans le stroma étant modulée par la lumière, passant de 0.5 $mmol.L^{-1}$ à l'obscurité à 2 $mmol.L^{-1}$ après 10 minute d'illumination (Ishijima et al. 2003; Portis and Heldt 1976). De la même manière, la concentration d'ion calcium Ca^{2+} a plusieurs effets au sein de la photosynthèse et peut notamment réguler l'activité des SBPase et FBPase d'épinard ou être indispensable à l'activité de la TRK d'*Arabidopsis thaliana* (Wang et al. 2019).

Cette activation par une concentration de magnésium est également dépendante du pH du stroma, le pH optimal de la FBPase variant en fonction de la concentration de magnésium (Huppe and Buchanan 1989).

1.4.2.3. Equilibres acido-basiques (pH)

Le décalage dans le pH optimum d'une enzyme peut également être relié à la régulation des enzymes du CBBC en fonction de la transition lumière/obscurité. Lors d'une exposition à la lumière, le pH du stroma va augmenter ce qui va alors provoquer l'activation de la FBPase et de la Rubisco. Ces changements de pH provoquent également beaucoup d'autres modulations passées en revue en 2022 (Trinh and Masuda 2022), et que l'on peut attribuer aux changements d'états de protonation de groupements acido-basiques exposés au solvant.

1.4.3 Associations en complexes protéiques

1.4.3.1 Complexes homo-multimériques

Comme synthétisé dans les descriptions des enzymes du CBBC dont la structure est disponible chez Chlamydomonas, ces enzymes ne sont rarement des monomères, mais sont souvent associées en assemblage homo-multimériques. Ces assemblages homo-multimériques peuvent être relativement simple comme un homo-dimère de TRK, ou plus complexes comme la Rubisco qui chez Chlamydomonas est un assemblage de huit petites et huit grandes sous-unités (Pasquini et al. 2017; Andersson and Backlund 2008). Ainsi pour les enzymes décrites précédemment, PRK et TPI sont des homo-dimères, RPE un homo-hexamère et GAPDH un homo-tétramère de GAPA (A_4 GAPDH) chez Chlamydomonas mais peut également être trouvée sous la forme d'un tétramère composé de deux sous-unités GAPA et deux sous-unités GAPB (A_2B_2 GAPDH) chez les plantes (Mattioli et al. 2022; Gurrieri et al. 2019; Zaffagnini et al. 2014).

Ces assemblages peuvent varier en fonction de l'espèce, la Rubisco étant retrouvée sous forme dimérique de grandes sous-unités chez *Rhodospirullum rubrum* (Schneider et al. 1986) ou encore sous la forme de pentamères de dimères de grandes sous-unités chez une

archée thermophile (*Thermococcus kodakaraensis*) (Kitano et al. 2001). Cette existence de plusieurs possibilités d'assemblages ainsi que le positionnement des sites catalytiques dans les structures enzymatiques permettent d'émettre l'hypothèse d'une ou plusieurs fonctions biologiques à ces assemblages homo-oligomériques. Certaines études mentionnent par exemple un caractère allostérique de la FBPase d'épinard (Giudici-Orticoni et al. 1990). Si peu d'études sont disponibles sur ces assemblages homo-oligomériques, l'effet régulateur d'assemblages en complexes hétéro-multimériques est lui mieux caractérisé.

1.4.3.2 Complexes hétéro-multimériques

Chez les organismes photosynthétiques, dont Chlamydomonas, les enzymes du CBBC sont retrouvées associées dans des assemblages hétéro-multimériques. Ces assemblages possèdent des fonctions différentes et peuvent participer à la régulation des activités des enzymes du CBBC.

1.4.3.2.1 Rubisco/EPYC1

Comme précisé dans la partie 1.3.3.1, *Chlamydomonas reinhardtii* possède un mécanisme de concentration du carbone lui permettant de pallier la relative inefficacité de l'enzyme et sa double spécificité vis-à-vis du CO_2 et de l'O_2. Ce mécanisme consiste en une sous-compartimentation appelée pyrénoïde au sein du stroma du chloroplaste. Celui-ci a été décrit comme pseudo-cristallin, ou comme une séparation de phase liquide-liquide entre le pyrénoïde et le reste du stroma (Barrett et al. 2021; He et al. 2020; Wunder et al. 2019). Les quatre protéines les plus abondantes qui le composent sont par ordre d'abondance la grande sous-unité de la Rubisco, la petite sous-unité de la Rubisco, la Rubisco activase et la petite protéine intrinsèquement désordonnée EPYC1 (*Essential Pyrenoïd Component 1*) en plus de dizaines d'autres protéines (Zhan et al. 2018; Mackinder et al. 2016). Cette protéine EPYC1 est essentielle à la formation du pyrénoïde chez Chlamydomonas car elle permet un pontage entre plusieurs petites sous-unités de Rubisco hexa-décamériques pour les lier en un ensemble continu. EPYC1 contient 5 sites d'interaction avec la Rubisco (He et al. 2020) et permet la formation d'un assemblage de taille

comparable à celle d'un compartiment cellulaire, observable en microscopie optique.

1.4.3.2.2 GAPDH-CP12-PRK

La présence de protéines désordonnées ayant une fonction dans les assemblages des enzymes du CBBC n'est pas une exclusivité d'EPYC1. La protéine CP12 retrouvée dans divers organismes photosynthétiques est décrite comme pouvant s'associer à GAPDH et PRK pour former un complexe inhibiteur de leurs activités enzymatiques (Gurrieri et al. 2021). Cette protéine est composée d'environ 80 acides aminés et est intrinsèquement désordonnée dans son état réduit (Launay et al. 2016). Elle possède deux paires de cystéines conservées (Groben et al. 2010) qui sont situées dans les domaines C et N terminaux qui servent respectivement aux interactions avec GAPDH et PRK. Ces paires de cystéines peuvent être oxydées pour former des ponts disulfures, ce qui provoque un changement d'organisation de la protéine qui s'organise partiellement en hélices α permettant une interaction avec GAPDH et le début de l'assemblage du complexe GAPDH-CP12-PRK (Launay et al. 2018; Fermani et al. 2012).

Ce complexe, formé par deux tétramères de GAPDH et deux dimères de PRK reliés par quatre CP12 possède deux structures expérimentalement résolues chez *Arabidopsis thaliana* (Yu et al. 2020) et la cyanobactérie *Thermosynechococcus elongatus* (McFarlane et al. 2019). L'analyse de ces structures et de celles du complexe antérieur entre CP12 et GAPDH permettent d'observer que CP12 se loge dans la crevasse catalytique de GAPDH et sous condition de pouvoir former un pont disulfure va inhiber l'activité de celle-ci (Erales et al. 2011). De la même manière, CP12 se loge dans le site actif de PRK et utilise l'arginine 64 pour interagir avec celle-ci en empêchant cette arginine d'effectuer son action catalytique (Figure 10) (Avilan et al. 1997). Pour restaurer l'activité des enzymes, le complexe doit se dissocier. Une thiorédoxine assure la réduction des ponts disulfure de CP12, prérequis à la dissociation de GAPDH et PRK (Yu et al. 2020; Marri et al. 2009).

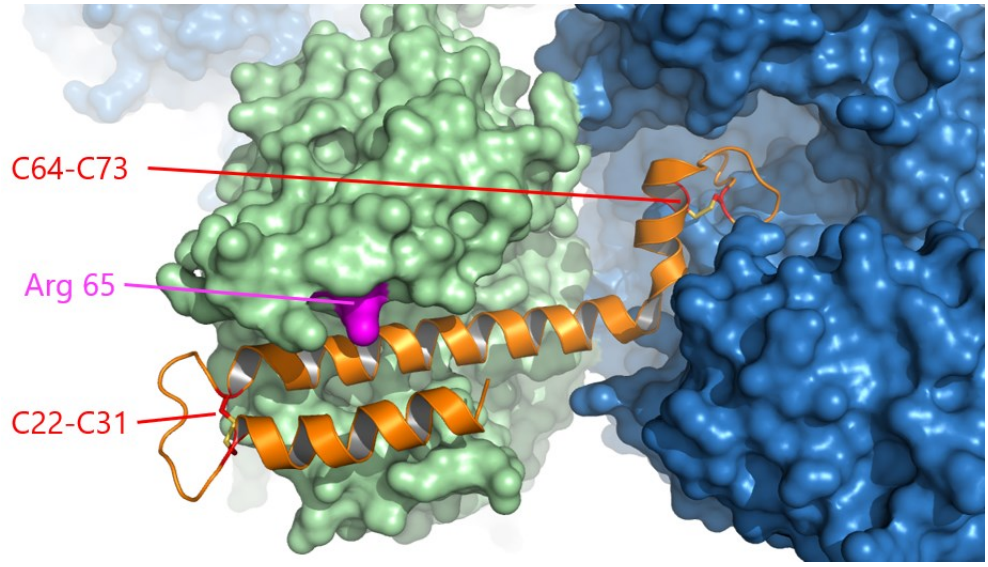

Figure 10 : CP12 d'*Arabidopsis thaliana* dans le complexe GAPDH-CP12-PRK (Code PDB : 6KEZ). CP12 est représentée en ruban et colorée en orange à l'exception des cystéines colorées en rouges et annotées. Les surfaces d'exclusion de Connolly de GAPDH et PRK sont colorées respectivement en bleu et en vert. L'arginine 65, correspondant à l'arginine 64 de Chlamydomonas, est colorée en rose.

1.4.3.2.3 Complexes hypothétiques

Le complexe GAPDH-CP12-PRK n'est pas le seul complexe d'enzymes du cycle de Calvin-Benson-Bassham à être décrit. Commençant en 1964 jusqu'en 1998, il existe des articles décrivant des co-localisations, des co-purifications ou des associations d'enzymes du CBBC chez plusieurs organismes photosynthétiques. Ainsi, l'existence d'un complexe entre RPI, PRK, Rubisco et PGK est décrit chez l'épinard (*Spinacia oleracea*) via des co-élutions de chromatographie associés à des mesures d'activités enzymatiques de plusieurs de ces enzymes et par des détections par immuno-blots (Ricard et al. 1994; Rault et al. 1993; Gontero et al. 1988). D'autres articles mentionnent l'association de la Rubisco avec PRK et RPI chez le riz (*Oryza sativa*) (Mendiola and Akazawa 1964) et dans le tabac (*Nicotiana tabacum*) (Van Noort and Wildman 1964). Chez *Rhodospirullum rubrum*, une co-purification de protéines ayant les activités de PRK et FBPase dépendant de la présence de magnésium a été décrite (Joint et al. 1972b, a). La Rubisco d'épinard est également retrouvée dans une association avec PRK et une enzyme non identifiée (Hosur et al. 1993; Sainis et al. 1989).

GAPDH et PRK sont retrouvées associées chez l'épinard (Clasper et al. 1991) et chez *Scenedesnus obliquus* (Nicholson et al. 1987). Ces même GAPDH et PRK sont également présentes dans de plus larges assemblages comprenant RPI, Rubisco et SBPase chez l'épinard (Suss et al. 1993). Toujours chez l'épinard, RPI, PRK et la Rubisco sont décrites associées dans un complexe aidant au transfert des métabolites d'un site actif vers le suivant dans le cycle pour augmenter l'efficacité globale des enzymes en augmentant la concentration locale de substrats (Sainis and Jawali 1994). Cette fonction biologique de canalisation métabolique (*channeling*) est régulièrement mentionnée dans plusieurs des articles précédemment cités et en parallèle des complexes enzymatiques de la glycolyse ayant cette même fonction (Gontero et al. 1993; Gontero et al. 1988).

Chez Chlamydomonas, il n'existe pas de preuves formelles à propos de ces potentiels complexes d'enzymes du CBBC, en dehors d'études de co-localisations (Wang et al. 2022; Suss et al. 1995). Ces co-localisations d'enzymes du CBBC placent la majorité de la Rubisco dans le pyrénoïde et les autres enzymes du cycle autour de celui-ci (Wang et al. 2022). La formation hypothétique de complexes multi-enzymatiques du CBBC reste à évaluer *in vitro*.

1.5 PHOTOPRODUCTION OF REDUCING POWER AND THE CALVIN-BENSON CYCLE

1.5.1 Résumé du chapitre

J'ai eu l'occasion de participer à la rédaction du « Chlamy Sourcebook 2022 », un livre de référence pour la communauté de biologie moléculaire et cellulaire de cet organisme modèle de la photosynthèse. Dans le chapitre 8, notre équipe traite des structures et des régulations redox du CBBC. Nous décrivons le transfert d'électrons depuis les molécules d'eau jusqu'au NADPH, la chaîne de transfert de ce pouvoir réducteur entres les ferrédoxines, ferrédoxine-thiorédoxine réductases et thiorédoxines. Ces mêmes thiorédoxines étant actrices de la régulation du CBBC, une description de celui-ci, de sa régulation notamment par les thiorédoxines, des structures connues et des assemblages supramoléculaires connus constituent la seconde partie de ce chapitre. Il se termine ensuite par une description des

nombreux rôles du NADPH dans la cellule, puis par une description des outils d'ingénierie biotechnologiques pour utiliser Chlamydomonas comme châssis de biologie synthétique, en vue par exemple d'en modifier les capacités métaboliques.

Mon travail de doctorat s'inscrit principalement dans le sous-chapitre V de cette revue : les structures des enzymes du cycle dont quatre que j'ai personnellement résolues par cristallographie aux rayons-X, tandis que j'ai en parallèle résolu la structure cristallographique d'une thiorédoxine z, la première déterminée pour ce type distinct, et qui s'avère régulatrice de PRK (*cf*. annexe 1).

1.5.2 Photoproduction of reducing power and the Calvin-Benson Cycle

Chapter 8

Photoproduction of reducing power and the Calvin-Benson Cycle (WC_{FAW}: 14074)

Théo Le Moigne[1,2,3,*], Nicolas D. Boisset[1,2,3,*], Félix de Carpentier[1,2,3], Pierre Crozet[1,2,4], Antoine Danon[1,2], Julien Henri[1,2], Christophe H. Marchand[1,2], Stéphane D. Lemaire[1,2,#], Xenie Johnson[5,#]

1. Sorbonne Université, CNRS, UMR7238, Institut de Biologie Paris-Seine, Laboratoire de Biologie Computationnelle et Quantitative, Paris, France

2. Sorbonne Université, CNRS, UMR8226, Institut de Biologie Physico-Chimique, Laboratoire de Biologie Moléculaire et Cellulaire des Eucaryotes, Paris, France

3. Faculty of Sciences, Doctoral School of Plant Sciences, Université Paris-Saclay, Saint-Aubin, France

4. Sorbonne Université, Polytech-Sorbonne, Paris France

5. Aix Marseille Univ., CEA, CNRS, Biosciences and Biotechnology Institute Aix-Marseille, Saint Paul-Lez-Durance, France F-13108

*** =** These authors contributed equally

\# corresponding authors

Abstract:

This chapter provides detailed overview of our current knowledge about the production and distribution of reducing power within the chloroplast of *Chlamydomonas* and about the structural and functional properties of the Calvin-Benson Cycle (CBC), which provides the cell with fixed carbon. Photosynthesis proceeds from the capture of light energy to the conversion of this energy into high-energy bonds (ATP) and reducing power (NADPH), both of which are mainly directed to the CBC to fuel carbon fixation and are also used for other anabolic processes. We describe how ferredoxins (FDX) orchestrate electron distribution downstream of photosystem I for both NADPH production and the reduction of thioredoxins (TRXs). The FDX-TRX system, which provides electrons for antioxidant and signaling functions, has been extensively studied in *Chlamydomonas*, and especially its role in light-dependent activation of the CBC. We detail the function of the CBC in *Chlamydomonas*, highlight its differences with other photosynthetic organisms and discuss what is known about its regulation and structural organization. We also consider the energetics and dual purpose of NADPH turnover in providing the assimilatory power that fuels the CBC and in maintaining linear electron flow, and emphasize the various pathways that contribute to the maintenance of optimal NADPH/NADP+ pools in the light. Finally, we discuss possibilities for using *Chlamydomonas* as a chassis for engineering and improving carbon fixation through synthetic biology approaches.

Key Words:

Calvin-Benson cycle, carbon fixation, ferredoxin, NADPH, reducing power, redox control, thioredoxin

I. Introduction to linear electron flow, water to NADPH

Photosynthesis proceeds from the capture of light energy to the conversion of this energy into high-energy chemical bonds (ATP) and reducing power (NADPH). *Chlamydomonas* grown in the absence of acetate relies on photosynthesis as the only source of ATP and NADPH, and the majority of this goes towards the Calvin-Benson Cycle (CBC) and thus CO_2 fixation. Linear photosynthetic electron flow denotes the transfer of electrons from H_2O, the primary electron donor that is oxidized at the level of Photosystem II (PSII), to a terminal electron acceptor $NADP^+$ that is reduced at the acceptor side of Photosystem I (PSI). Plastoquinones, the cytochrome b_6f complex and plastocyanin act as intersystem electron carriers between PSII and PSI in the thylakoid membrane. The stromal electron carriers, including flavodiiron proteins, thioredoxins and ferredoxins, exert control on intersystem electron transport, which helps optimize electron transfer in relation to inputs (light) and outputs (metabolites). This assures a tight integration of the electron transfer reactions with downstream metabolic processes, principally the CBC, in the chloroplast (see Vol2, Chapter 18 for details).

II. Ferredoxins orchestrate electron transfer downstream of PSI

After the light reactions, carried out at the level of the thylakoid membranes, electrons from the stromal ridge of PSI (constituted by PsaC, PSAD and PsaE, which harbor the Fe-S redox clusters F_X, F_A and F_B; see Chapter 16), are transferred to Ferredoxin (FDX) in the chloroplast stroma. Marco and co-workers reported on a PsaC K35D mutant in which FDX binding to PSI was abolished (Marco, Elman, & Yacoby, 2019; Marco et al., 2018). Numerous biological processes are based on redox reactions that use electron carriers such as the FDXs, which are small (10-11 Da), soluble Fe-S cluster proteins that are widely distributed in microorganisms, plants and animals. Indeed, they serve as low potential, single electron carriers with E_m values ranging from -310 mV to -455 mV. These electrochemical properties allow them to operate as electron donors in a multitude of metabolic and signaling pathways (Hanke & Mulo, 2013). FDXs play a central role in chloroplast metabolism. Once reduced, FDX can transfer electrons to proteins involved in diverse pathways including Ferredoxin-$NADP^+$ Reductase (FNR) for $NADP^+$ reduction, Ferredoxin-Thioredoxin Reductase (FTR) for the reduction of thioredoxins (TRXs), which provide electrons for antioxidant and signaling functions, Sulfite Reductase (SiR) for sulfur assimilation, Nitrite Reductase (NiR) and Ferredoxin-dependent Glutamate Synthetase (GOGAT) for nitrogen assimilation, hydrogenase for hydrogen production under anaerobic conditions (Winkler, Hemschemeier, Jacobs, Stripp, & Happe, 2010), fatty acid desaturases for the biosynthesis of lipids (Yang et al., 2015) and photosynthetic cyclic electron flow via ferredoxin-plastoquinone reductase (Hertle et al., 2013).

The *Chlamydomonas* genome encodes at least thirteen *FDX* genes (Yang et al., 2015), mostly chloroplastic (Table 1), among which six FDXs (FDX1-FDX6) have been studied in more detail. The major FDX in *Chlamydomonas* (FDX1, previously named PETF) was initially purified by Paul Levine (Gorman & Levine, 1966). The function of FDXs can be inferred from their expression patterns and their substrate specificities. Under standard growth in the presence of acetate, FDX1 contributes 98% of the total ferredoxin-encoding transcript pool. *FDX1* expression is regulated by light and the circadian clock and the encoded protein is the most efficient electron donor to FNR and FTR. FDX1 is therefore likely the main electron donor for carbon fixation and redox homeostasis (S. D. Lemaire et al., 1999; Terauchi et al., 2009). In contrast, FDX2 is not regulated by light but by nitrogen sources and is an efficient electron donor to NiR (Hirasawa et al., 2010; Strenkert et al., 2019; Terauchi et al., 2009). FDX2 can also transfer electrons to FNR, however there is a significant preference for FDX1 (Mosebach et al., 2017), while mutating two residues from the kinetically slower FDX2 confers it with redox properties similar to FDX1 (Boehm et al., 2016). FDX3-6 are reduced in the light but are unable to supply FNR with electrons for the reduction of $NADP^+$ (Boehm et al., 2016). Therefore, FDX1-6 exhibit distinct substrate specificities suggesting specialization for allocation of reducing power to specific metabolic pathways. FDX substrate specificities are likely mediated by key residues controlling electrostatic interactions with partner proteins (Boehm et al., 2016; Garcia-Sanchez et al., 1997; Jacquot, Stein, et al., 1997).

FDX5 is specifically expressed under dark-hypoxic conditions and copper or sulfur deprivation but it is not able to reduce hydrogenase, which is preferentially reduced by FDX1 (Jacobs, Pudollek, Hemschemeier, & Happe, 2009; Yacoby et al., 2011). FDX5 appears to be important for hydrogenase maturation, fatty acid desaturation, dark metabolism, maintenance of the thylakoid membrane and responses to sulfur depletion (Subramanian et al., 2019; Yang et al., 2015). The FDX9 gene is only expressed in the dark and was recently identified as co-regulated with hydrogenase genes and may also play some role in hydrogen production (Strenkert et al., 2019). A ferredoxin interactome identified more than 200 putative partner proteins in *Chlamydomonas* (Peden et al., 2013), with 43 potential partners of FDX5 (Subramanian et al., 2019). For a more complete overview of *Chlamydomonas* FDXs we refer the reader to dedicated reviews (Sawyer & Winkler, 2017; Terashima, Specht, & Hippler, 2011; Winkler et al., 2010). In the present chapter we will further detail the functions of FDX1 linked to carbon fixation and redox homeostasis that is mediated by FNR and FTR.

III. Ferredoxin $NADP^+$ reductase and the $NADPH/NADP^+$ couple

In the light, FDX reduces the FAD containing Ferredoxin-$NADP^+$ Reductase (FNR) in two single-electron steps; FNR then transfers the 2 electrons to $NADP^+$ completing linear electron flow. Under aerobic conditions, the abundance of FNR is equal to that of plastocyanin in *Chlamydomonas*, providing an electron pathway for the reduction of $NADP^+$ (Nikolova, Heilmann, Hawat, Gabelein, & Hippler, 2018). The *Chlamydomonas* genome does not have orthologues of the conserved tethering proteins that allow close interaction of FNR with the thylakoid membranes as found in higher plants. However, a PSI-LHCI-FNR-LHCSR3 complex in cells in state I has been identified (Bergner et al., 2015), and this complex appears to be destabilised in the absence of PGR5/PGRL1 proteins (Mosebach et al., 2017). To facilitate this very close interaction between FNR and PSI, FNR (like FDX) localizes to the PSI stromal ridge, with possible interactions with PsaE, B, F and at least 1 LHC1 (Marco et al., 2019).

$NADP^+$ (Nicotinamide Adenine Dinucleotide Phosphate) is the major pyridine nucleotide found in the plastid and is considered the final acceptor of electrons issued from H_2O oxidation in oxygenic photosynthesis. Apart from CO_2 fixation, NADPH is required for other plastid-localized processes including tetrapyrrole synthesis, lipid biosynthesis and detoxification of reactive oxygen species (ROS). As NADPH is the universal electron carrier for photosynthesis and chloroplast metabolism, both the flux and the directionality along these pathways are highly dependent upon the relative concentrations of NADPH and $NADP^+$. However, NADPH rarely accumulates in the light because it is rapidly utilized by these same metabolic reactions. The $NADP^+$/NADPH couple has a low oxidation-reduction potential (E'_0 at pH 7.0 = - 320 mV), which makes NADPH a powerful reductant.

$NADP^+ + H^+ + 2e^- <-> NADPH$

This can also be written as:

$NADP^+ + 2H^+ + 2e^- <-> NADPH + H^+$

because it shows the 2 hydrogen ions generated as a consequence of water oxidation as well as the electrons that will serve as reductant.

IV. The ferredoxin-thioredoxin system

1. Components and function of the ferredoxin-thioredoxin system

The ferredoxin-thioredoxin system, located in chloroplasts, is composed of ferredoxins (FDXs), Ferredoxin-Thioredoxin Reductase (FTR) and thioredoxins (TRXs) (Figure 1, Table 1) (L. Michelet et al., 2013; Zaffagnini et al., 2019). This system converts a light-driven electron signal (photoreduced FDX1) into a thiol signal transmitted by FTR to different isoforms of TRXs. FTR is a thin, flat enzyme that allows docking of FDX on one side and TRX on the other side. It contains a [4Fe-4S] cluster functionally and physically connected with a redox active disulfide (Dai et al., 2007). FTR is heterodimeric, with a highly conserved catalytic subunit of 13 kDa (FTRC) and a variable subunit (FTRV) exhibiting different molecular masses among organisms (Dai, Johansson, Miginiac-Maslow, Schurmann, & Eklund, 2004;

Schurmann, 2002). The coexpression of both subunits is required to produce a functional FTR, although the exact function of FTRV remains unknown (Keryer, Collin, Lavergne, Lemaire, & Issakidis-Bourguet, 2004). *Chlamydomonas* FTR, purified in 1990 (Huppe, de Lamotte-Guery, Jacquot, & Buchanan, 1990), is a typical FTRC/FTRV heterodimer with an FTRC of 13 kDa and an FTRV of 10 kDa. The nuclear genome of *Chlamydomonas* contains a single gene encoding each subunit (Table 1). The formation of the FDX-FTR complex requires the presence of the negatively charged Glu91 in FDX1 (Jacquot, Stein, et al., 1997).

Thioredoxins (TRXs) are ubiquitous disulfide bond oxidoreductases found in all free-living organisms. They contain a canonical disulfide active site (W-C-G/P-P-C) responsible for disulfide oxidoreductase activity and a redox midpoint potential of between -270 and -300 mV at pH 7.0 (Aslund, Berndt, & Holmgren, 1997; Collin et al., 2003; Collin et al., 2004; Hirasawa et al., 1999). Since its discovery as a hydrogen donor for ribonucleotide reductase in *Escherichia coli* (Laurent, Moore, & Reichard, 1964; Sengupta & Holmgren, 2014), the TRX system has been extensively studied and recognized as having multiple roles in a myriad of cellular processes and human diseases (Buchanan, Holmgren, Jacquot, & Scheibe, 2012; Hanschmann, Godoy, Berndt, Hudemann, & Lillig, 2013; Lee, Kim, & Lee, 2013; Toledano, Delaunay-Moisan, Outten, & Igbaria, 2013).

In photosynthetic organisms, TRXs constitute multigenic families and phylogenetic analyses have revealed the existence of different types of TRX proteins localized in diverse subcellular compartments: 2 TRXf, TRXm, TRXx, TRXy and TRXz are in chloroplasts while TRXo and TRXh are in mitochondria and the cytosol (Lemaire, Michelet, Zaffagnini, Massot, & Issakidis-Bourguet, 2007; Meyer, Belin, Delorme-Hinoux, Reichheld, & Riondet, 2012; Serrato, Fernandez-Trijueque, Barajas-Lopez, Chueca, & Sahrawy, 2013). Cytosolic and mitochondrial TRXs are reduced by NADPH-dependent thioredoxin reductases (NTRs) like TRXs in non-photosynthetic organisms. By contrast, chloroplast TRXs are specifically reduced by FTR (Balsera, Uberegui, Schurmann, & Buchanan, 2014; Chibani, Wingsle, Jacquot, Gelhaye, & Rouhier, 2009; Jacquot, Eklund, Rouhier, & Schurmann, 2009; L. Michelet et al., 2013; Schurmann & Buchanan, 2008; Yoshida & Hisabori, 2017). Once reduced, TRXs can specifically reduce disulfide bonds on their target proteins.

The FDX-TRX system was initially identified as a light signaling mechanism controlling the activity of several CBC enzymes (Buchanan, 2016; L. Michelet et al., 2013). These enzymes have low activity in the dark and become activated in the light through reduction of one or several regulatory disulfide bonds. This reduction triggers a slow conformational change, shifting the target enzyme from a low to a high activity state. The FDX-TRX system ensures coupling of metabolism with the redox state of the PET chain and the availability of reducing equivalents. In addition to CBC enzymes, many other enzymes involved in diverse pathways are regulated by light through TRX-dependent reduction of disulfide bonds (Lemaire et al., 2007; Montrichard et al., 2009; Schurmann & Buchanan, 2008). This includes ATP synthase, which is responsible for the light-driven ATP production required for the functioning of the CBC (Buchert, Bailleul, & Hisabori, 2017; Sekiguchi et al., 2020), acetyl-CoA carboxylase, which catalyzes the first committed step of fatty acid biosynthesis (Sasaki, Kozaki, & Hatano, 1997), ADP-glucose pyrophosphorylase, glucan:water dikinase and beta-amylase BAM1, which are involved in starch metabolism (Ballicora, Frueauf, Fu, Schurmann, & Preiss, 2000; Geigenberger, Kolbe, & Tiessen, 2005; Mikkelsen, Mutenda, Mant, Schurmann, & Blennow, 2005; Sparla, Costa, Lo Schiavo, Pupillo, & Trost, 2006), and the oxidative pentose phosphate pathway (OPPP) enzyme glucose-6-phosphate dehydrogenase, which is inactivated by TRX-dependent reduction in the light (Farr, Huppe, & Turpin, 1994; Nee, Zaffagnini, Trost, & Issakidis-Bourguet, 2009; Wenderoth, Scheibe, & von Schaewen, 1997). The mechanisms associated with TRX regulation are the best characterized redox signaling pathways in photosynthetic organisms (Foyer & Noctor, 2005); they have been investigated in detail at the molecular and structural levels in different model systems, including *Chlamydomonas*.

In addition to their role in the control of metabolic enzymes through reduction of regulatory disulfides where the electrons and protons provided by TRX are not used in the reaction catalyzed by the enzyme,

TRXs can also reduce catalytic disulfides and thereby play a major role in detoxification of reactive oxygen species (ROS) and maintenance of redox homeostasis in the chloroplast. Indeed, TRXs serve as substrates, providing electrons for the regeneration of different types of antioxidant chloroplast enzymes including peroxiredoxins (PRXs) (Dietz, 2011), glutathione peroxidases (GPXs) (Navrot, Gelhaye, Jacquot, & Rouhier, 2006) and methionine sulfoxide reductases (MSRs) (Tarrago et al., 2009). In these cases, TRXs function as a substrate since the target enzymes use the electrons and protons in the reaction that they catalyze. A TRX-related system named NADPH-TRX reductase C (NTRC) consists of a fusion protein containing a TRX domain and an NTR domain. NTRC plays an important role in the maintenance of chloroplast redox homeostasis by providing electrons to antioxidant enzymes such as PRXs (Perez-Ruiz, Naranjo, Ojeda, Guinea, & Cejudo, 2017; Yoshida & Hisabori, 2016).

The TRX isoforms of the chloroplast (f, m, x, y, z) are each generally encoded by multiple nuclear genes (Chibani et al., 2009; Lemaire et al., 2007). This multiplicity is more limited in microorganisms, which make them, for these reasons among others, potentially simpler models to study TRXs. For example, *Synechocystis* sp. PCC 6803 has four TRXs (1 TRXm, 1 TRXx, 1 TRXy and one that is atypical), *Ostreococcus lucimarinus* has five chloroplastic TRXs (2 TRXf, 1 TRXm, 1 TRXx, no TRXy, 1 TRXz) and *Chlamydomonas* has 6 chloroplastic TRXs (2 TRXf, 1 TRXm, 1 TRXx, 1 TRXy, 1 TRXz) (while Arabidopsis has 10 and poplar 13) (Chibani et al., 2009; Lemaire et al., 2007; Perez-Perez, Martin-Figueroa, & Florencio, 2009; Zaffagnini et al., 2019). All chloroplastic TRXs are reduced by FTR (Chibani et al., 2009; Yoshida & Hisabori, 2017) and some of them, such as TRX*z*, may be reduced by NTRC as well (Yoshida & Hisabori, 2016). Biochemical analyses suggest that CBC enzymes are preferentially regulated by f-type TRXs (Chibani, Couturier, Selles, Jacquot, & Rouhier, 2010; Lemaire et al., 2007; L. Michelet et al., 2013; Nee et al., 2009). TRXx and TRXy are the most efficient TRXs for the reduction of PRXs, GPXs and MSRs (Chibani, Tarrago, Schurmann, Jacquot, & Rouhier, 2011; Collin et al., 2003; Collin et al., 2004). TRXz has been characterized as a subunit and regulator of the plastid encoded RNA polymerase (Arsova et al., 2010; Schroter, Steiner, Matthai, & Pfannschmidt, 2010) and thereby it plays an important role in chloroplast transcription and chloroplast development (Arsova et al., 2010; Diaz et al., 2018; Huang et al., 2013). The specificity of TRXm is less clear: it can replace TRXf for activation of metabolic enzymes, though less efficiently, and it was suggested to play a role in the transfer of reducing equivalents from the stroma to the thylakoid lumen or in the regulation of chloroplastic proteins involved in electron transfer pathways (Courteille et al., 2013).

Beyond established targets for which TRX reduction was confirmed biochemically, proteomic analyses based on TRX-affinity columns or *in vitro* TRX reduction revealed hundreds of putative TRX targets in diverse organisms ((Perez-Perez et al., 2017) and references therein).

2. The ferredoxin-thioredoxin system in Chlamydomonas

The FDX-TRX system has been extensively studied in *Chlamydomonas*. Several components of the system including FTR and TRXh, TRXf and TRXm were identified in the early 90's (Huppe et al., 1990; Huppe, Picaud, Buchanan, & Miginiac-Maslow, 1991). After purification from *Chlamydomonas* cultures, the primary sequence of TRXm and TRXh1 were determined by Edman sequencing (Decottignies, Schmitter, Dutka, Jacquot, & Miginiac-Maslow, 1991; Decottignies et al., 1990), allowing cloning of the corresponding cDNA and genomic sequences, and initial characterizations of the proteins after purification of the TRXs expressed in *E. coli* (Jacquot, Stein, Hodges, & Miginiac-Maslow, 1992; Stein et al., 1995). Numerous structures of these two TRXs were solved by NMR or X-ray crystallography (Krimm et al., 1998; Lancelin et al., 2000; Lancelin, Stein, & Jacquot, 1993; Marchand et al., 2019; Menchise et al., 2000; Menchise et al., 2001; Mittard et al., 1997; Mittard et al., 1995). The biochemical and physico-chemical properties of these two TRXs were investigated extensively, primarily because they served as model proteins to study one-electron oxidation and protein stability and folding (Hirasawa et al., 1999; Lemaire et al., 2000; Lemaire et al., 2018; Lmoumene, Conte,

Jacquot, & Houee-Levin, 2000; Richardson, Lemaire, Jacquot, & Makhatadze, 2000; Setterdahl et al., 2003; Sicard-Roselli et al., 2004).

The availability of genomic sequences led to the identification of new chloroplast thioredoxin isoforms, including a second TRXf and 4 new types of TRX proteins: 1 TRXo, 1 TRXx, 1 TRXy and 1 TRXz (Le Moigne, Gurrieri, et al., 2021; Lemaire, Collin, Keryer, Issakidis-Bourguet, et al., 2003; Lemaire, Collin, Keryer, Quesada, & Miginiac-Maslow, 2003; Lemaire & Miginiac-Maslow, 2004). These TRXs exhibit properties and specificities comparable to those of land plant. While CBC enzymes are preferentially activated by TRXf and to a lesser extent by TRXm, TRXx and TRXy are more efficient for reducing antioxidant enzymes such as PRXs. The recently solved structures of *Chlamydomonas* TRXf2 (Lemaire et al., 2018) and TRXz (Le Moigne, Gurrieri, et al., 2021) indicate that the surface electrostatic charge distribution is a major determinant of TRX specificity. The role of TRX in regulating CBC enzymes, extensively studied in land plants and *Chlamydomonas*, is detailed in a section of this chapter, "The Calvin-Benson cycle in *Chlamydomonas reinhardtii*".

Besides CBC regulation, *Chlamydomonas* TRXs participate in the maintenance of ROS homeostasis through reduction of PRXs and GPXs (Charoenwattanasatien et al., 2020; Dayer, Fischer, Eggen, & Lemaire, 2008; Goyer et al., 2002), and may also play a role in hydrogen peroxide signaling through regulation of catalase (Shao, Beck, Lemaire, & Krieger-Liszkay, 2008). In addition, TRXs regulate chloroplast redox homeostasis through redox-dependent activation of NADP-malate dehydrogenase (NADP-MDH). This enzyme is involved in the export of reducing power from the chloroplast to the cytosol through the malate shuttle (Selinski & Scheibe, 2019). Chloroplastic NADP-MDHs from land plants are redox regulated through two disulfide bonds present in N- and C-terminal extensions (Issakidis, Lemaire, Decottignies, Jacquot, & Miginiac-Maslow, 1996). By contrast, *Chlamydomonas* NADP-MDH (MDH5) contains a single C-terminal TRX-regulated disulfide bond (Lemaire et al., 2005). The recently identified calredoxin (CRX) is a chloroplast-localized protein from *Chlamydomonas* that is able to integrate calcium and redox signals as it comprises a Ca^{2+}-binding CaM domain with four EF-hands, which controls a thioredoxin domain that exhibits a typical thioredoxin-fold and Ca^{2+}-dependent thioredoxin activity (Hochmal et al., 2016). The structural determinants of CRX underlying this calcium-dependent control of TRX activity were recently unraveled as well as the interaction and reduction of CRX with PRX1, a major chloroplastic PRX (Charoenwattanasatien et al., 2020). The *Chlamydomonas* genome also contains a gene encoding NTRC, which has not yet been studied (Table 1).

Many genes encoding components of the FDX-TRX system were shown to be regulated by light and the circadian clock (S. D. Lemaire et al., 1999; Strenkert et al., 2019), oxidative stress (Blaby et al., 2015; Terauchi et al., 2009) and heavy metals (S. Lemaire et al., 1999). *Chlamydomonas* is well-adapted for genome-wide proteomic analyses (Rolland et al., 2009) (see Chapter 12), making it ideal for developing redox proteomic approaches aimed at identifying new TRX targets (Lemaire et al., 2004). The most comprehensive thioredoxome (thioredoxin interacting proteome) was established in *Chlamydomonas* and identified 1188 proteins and 1052 cysteines regulated by TRX (Perez-Perez et al., 2017). Considering the multiplicity of TRX isoforms and their multiple targets, dissecting their functions *in vivo* is a highly challenging task since alteration of the TRX system through genetic engineering will likely impact a multitude of cellular processes and pathways. Therefore, *in vivo* engineering of TRX-regulation should rather focus on altering the redox properties of target enzymes (*e.g.* engineering of disulfide bonds through mutagenesis). This strategy was recently applied to show that autophagy is regulated by TRX in *Saccharomyces cerevisiae* and *Chlamydomonas* through oxidoreduction of a regulatory disulfide bond of the ATG4 cysteine protease (Perez-Perez, Lemaire, & Crespo, 2016; Perez-Perez, Zaffagnini, Marchand, Crespo, & Lemaire, 2014). The *Chlamydomonas* thioredoxome contains more than 350 chloroplastic proteins, showing again the multiple roles of TRXs for electron distribution in the stroma.

V. The Calvin-Benson cycle in *Chlamydomonas reinhardtii*

This section will focus on the CBC. We describe the functioning of this cardinal metabolic pathway in *Chlamydomonas*, highlight differences in the pathway among photosynthetic organisms and detail what is known in *Chlamydomonas* about its regulation and structural organization.

1. Components and functioning of the Calvin-Benson cycle in Chlamydomonas

The CBC is a conserved cyclic loop of 13 chemical reactions that ensures the process of carbon fixation (Melvin Calvin and collaborators, Nobel Prize in Chemistry 1961). The fixation of CO_2 occurs by carboxylation of the acceptor pentose, ribulose-1,5-bisphosphate (RuBP), that is subsequently recycled through 12 reaction steps (Benson et al., 1952). The 13 CBC reactions are catalyzed by 11 enzymes that group into 3 phases: (i) ribulose-5-phosphate is phosphorylated by phosphoribulokinase (PRK) (Hurwitz, Weissbach, Horecker, & Smyrniotis, 1956; Moll & Levine, 1970), generating ribulose-1,5-bisphosphate (RuBP), which serves as the acceptor for CO_2 fixation in a reacton catalyzed by ribulose-1,5-bisphosphate carboxylase/oxygenase (Rubisco); (ii) the 3-phosphoglycerate produced enters the reduction phase, which is catalyzed by phosphoglycerate kinase (PGK) and glyceraldehyde-3-phosphate dehydrogenase (GAPDH) to form glyceraldehyde-3-phosphate; (iii) ribulose-5-phosphate is then regenerated by the collective activities of triose-phosphate isomerase (TPI), fructose-6-phosphate aldolase (FBA), fructose-1,6-bisphosphatase (FBPase), transketolase (TRK), sedoheptulose-1,7-bisphosphatase (SBPase), ribulose-5-phosphate epimerase (RPE) and ribose-5-phosphate isomerase (RPI). Three CO_2 molecules eventually yield one triose while the pool of ribulose-1,5-bisphosphate acceptors is regenerated at each iteration of the cycle. For each fixed CO_2, the CBC consumes 3 ATP molecules (one by PRK and two by PGK) and oxidizes two NADPH molecules (GAPDH).

The CBC is present in all oxygenic photosynthetic eukaryotes and is highly conserved. All enzymes are present in *Chlamydomonas* and exhibit sequences and structures that are conserved with those of land plants (Table 2). CBC enzymes are highly abundant as determined by global or targeted proteomic approaches (Hammel et al., 2020; Mettler et al., 2014; Schroda, Hemme, & Muhlhaus, 2015; Wienkoop et al., 2010); Rubisco is the most abundant protein on Earth with 90% found in the leaves of land plants (Bar-On & Milo, 2019). In *Chlamydomonas* the CBC enzymes were shown to collectively represent 11.9% of total cell proteins, with a 128-fold difference between the most abundant (RbcL, 268 µM) and the least abundant (TPI, 2 µM) (Hammel et al., 2020). This abundance combined with the measurements of CBC metabolites suggest that some CBC enzymes are near-saturated *in vivo* (Rubisco, PGK, FBPase, SBPase) whilst the remainder operate at low substrate saturation (Mettler et al., 2014). In *Chlamydomonas*, RbcS is less abundant (182 µM) than RbcL, suggesting that the Rubisco holoenzyme represents less than 2% of total proteins (see Chapter 7). Indeed, Rubisco is much less abundant in *Chlamydomonas* than in land plants where it can account for several tens of percent of the proteome. The higher abundance of RbcL compared to RbcS in *Chlamydomonas* may be linked to its independent moonlighting functions in the control of mRNA homeostasis and gene expression (Zhan et al., 2015).

The expression of CBC genes (mRNA accumulation) is regulated by light and the circadian clock with maximal expression during the light phase and minimal during the dark phase of the diel cycle, while the protein abundances also show some oscillations, although less pronounced (Lemaire, Miginiac-Maslow, & Jacquot, 2002; S. D. Lemaire et al., 1999; Schmollinger et al., 2014; Strenkert et al., 2019). RbcS in plants and green algae is encoded in the nucleus and translated by cytosolic ribosomes before being imported into the chloroplast where it is processed to its mature form. In contrast, RbcL is the only CBC protein in these organisms encoded by the chloroplast genome.

One major difference in many algae and cyanobacteria compared to land plants is the presence of carbon concentration mechanisms (CCMs), which increases the CO_2 concentration in the vicinity of Rubisco to favor its carboxylation rate over its oxygenase activity (Lin, Occhialini, Andralojc, Parry, & Hanson, 2014; Rae et al., 2013; J. A. Raven, Giordano, Beardall, & Maberly, 2012). One feature of the CCM is the pyrenoid, a liquid-like microcompartment present in the chloroplasts of algae and

hornworts which contains densely packed Rubisco (see Chapter 7). The pyrenoid is therefore functionally analogous to, though structurally different from, the carboxysomes of cyanobacteria (Kerfeld & Melnicki, 2016). The pyrenoid in conjunction with other components of the CCM mitigates the low catalytic efficiency of Rubisco and the dual substrate specificity of its active site for CO_2 and O_2 (Spreitzer & Salvucci, 2002). CO_2 is the substrate for the productive carbon-fixing step of the CBC, but the oxygenase activity of Rubisco leads to the production of glycolate, which is recycled by the non-productive and energetically-costly photorespiratory pathway (Foyer, Bloom, Queval, & Noctor, 2009; South, Cavanagh, Liu, & Ort, 2019). The CCM also mitigates the limited availability of CO_2 in aquatic environments where uptake is hampered by slower diffusion rates and the conversion of most CO_2 to the bicarbonate anion, which cannot diffuse across the lipid bilayers of the plasma membrane and chloroplast envelope (Y. Wang, Stessman, & Spalding, 2015). Rubisco is the only CBC enzyme present in the pyrenoid as revealed by proteomic studies, activity assays and fluorescence microscopy (Kuken et al., 2018; L. C. M. Mackinder et al., 2017; L. C. Mackinder et al., 2016; Zhan et al., 2018). Therefore, a high flux of RuBP and 3PGA between the pyrenoid interior or "matrix" containing Rubisco and the stroma containing all other CBC enzymes must occur. Computational modeling of *Chlamydomonas* CBC suggested that there is no major diffusional barrier to this cellular metabolic trafficking of RuBP and 3PGA, which might involve pyrenoid minitubules that connect the stroma to the interior of the pyrenoid (Engel et al., 2015; Kuken et al., 2018; Syeda et al., 2015). Due to the presence of the CCM, *Chlamydomonas* and most other photosynthetic aquatic microorganisms are efficient energy converters; their photorespiration is low, and they require less Rubisco (J. A. Raven, Beardall, & Sanchez-Baracaldo, 2017).

2. Regulation mediated by post-translational modifications

a. Thioredoxin dependent regulation of CBC enzymes

In land plants four enzymes of the CBC (FBPase, SBPase, PRK and A_2B_2-GAPDH) are activated by the FDX-TRX system, enabling light-dependent modulation of CBC activity. The light-dependent activation of SBPase, FBPase and PRK was initially reported in the unicellular green alga Chlorella (Bassham, 1971; Pedersen, Kirk, & Bassham, 1966). Each of these four enzymes contains a regulatory disulfide reduced specifically or preferentially by TRXf and which upon reduction triggers a conformational change of the enzyme from a low to a high activity state (L. Michelet et al., 2013). Comparisons of the redox regulatory properties of enzymes from cyanobacteria, diatoms, algae and higher plants suggest that the light-dependent regulation mediated by TRX has been progressively introduced during evolution by the addition of regulatory disulfides (Lemaire et al., 2007; L. Michelet et al., 2013; Ruelland & Miginiac-Maslow, 1999). The Synechocystis CBC enzymes are generally not regulated through TRX-dependent regulatory disulfides (Balsera et al., 2014; Tamoi, Murakami, Takeda, & Shigeoka, 1998) unlike their *Chlamydomonas* counterparts (Farr et al., 1994; Huppe & Buchanan, 1989; Huppe, Farr, & Turpin, 1994). By contrast with land plants that contain a TRX-dependent isoform of GAPDH (A_2B_2-GAPDH), this control is absent in *Chlamydomonas* where another enzyme, PGK, is instead regulated by TRX (Morisse, Michelet, et al., 2014). *Chlamydomonas* CBC contains 4 established targets of TRX: SBPase, FBPase, PRK and PGK.

Glyceraldehyde-3-phosphate dehydrogenase (GAPDH)

Land plants contain several isoforms of GAPDH encoded by the *GAPA*, *GAPB* and *GAPC* genes. GAPC corresponds to the glycolytic type while GAPA and GAPB encode nearly identical photosynthetic GAPDH subunits, but GAPB contains a specific C-terminal extension containing the TRX dependent regulatory disulfide responsible for the light/dark regulation of the enzyme (Baalmann, Scheibe, Cerff, & Martin, 1996; Sparla, Pupillo, & Trost, 2002). Two isoforms participate in the CBC: the major form is heterotetrameric A_2B_2-GAPDH and the minor form is homotetrameric A_4-GAPDH (Trost et al., 2006). By contrast with NAD(H)-specific glycolytic GAPDH (GAPC) (Zaffagnini, Fermani, Costa, Lemaire, & Trost, 2013), photosynthetic GAPDH uses both NAD(H) and NADP(H) as coenzymes (Melandri, Baccarini, & Pupillo, 1968). The NADPH dependent activity of A_2B_2-GAPDH is specifically light regulated

by TRXf while the A_4 isoform is not (Marri et al., 2009). Structural and kinetic analyses demonstrated that the C-terminal extension of GAPB acts as a redox-sensitive auto-inhibitory domain forming a bulky hairpin structure in the proximity of the NADP-binding site (Fermani et al., 2007; Sparla et al., 2005). The *GAPB* gene is only found in the genomes of Streptophytes (land plants and Charophytes (Petersen, Teich, Becker, Cerff, & Brinkmann, 2006)), and the Prasinophycean green algae (*e.g.* Ostreococcus, (Robbens, Petersen, Brinkmann, Rouze, & Van de Peer, 2007)). It is absent in all other oxygenic phototrophs, which usually contain a single *GAPA* gene, except for the cryptomonads, diatoms and chromalveolates in which chloroplast GAPDH is generally encoded by *GAPC*-type genes (Liaud, Brandt, Scherzinger, & Cerff, 1997). A_4-GAPDH is a minor GAPDH isoform in land plants (Howard, Lloyd, & Raines, 2011; Scagliarini, Trost, Pupillo, & Valenti, 1993), but is the only isoform of photosynthetic GAPDH in green algae, red algae and cyanobacteria (Petersen et al., 2006). The *Chlamydomonas* genome contains a single *GAPA* gene (Table 2) and the CBC operates only with A_4-GAPDH, which lacks regulatory cysteines and is therefore not directly regulated by TRX. In all organisms, including *Chlamydomonas*, GAPDH is indirectly regulated by TRX through the formation of a complex with two TRX-regulated proteins, PRK and CP12 (Graciet, Lebreton, & Gontero, 2004; Trost et al., 2006; Wedel & Soll, 1998). This is the only known mechanism of light/dark regulation of GAPDH in *Chlamydomonas* and all other GAPB-deficient species. This will be discussed further below in the section on the supramolecular organization of the CBC.

Phosphoglycerate kinase (PGK)

PGK, a CBC enzyme that converts 3-PGA produced by the Rubisco reaction to 1,3-bisphosphoglycerate, the substrate of GAPDH, is not known to be redox regulated in land plants. By contrast, a TRX-dependent redox activation was reported in *Chlamydomonas*, *Synechocystis* and *Phaeodactylum tricornutum* (Bosco, Aleanzi, & Iglesias, 2012; Morisse, Michelet, et al., 2014; Tsukamoto, Fukushima, Hara, & Hisabori, 2013). This may suggest that this regulatory mechanism has been lost in land plants after the invention of GAPB or that it is a recent innovation of some aquatic phototrophs. In *Chlamydomonas* chloroplastic PGK, the regulatory disulfide bond involves the two C-terminal cysteines, has a midpoint redox potential of -335 mV at pH 7.0 and its reduction, preferentially performed by TRXf increases the enzyme turnover number but does not affect the enzyme affinities for its substrates (Morisse, Michelet, et al., 2014).

Phosphoribulokinase (PRK)

PRK is a homodimer in eukaryotes (Gurrieri et al., 2019; Porter, Milanez, Stringer, & Hartman, 1986) and each monomer contains 4 strictly conserved cysteines. PRK is unique to the CBC and has therefore no cytosolic counterpart. It has a low activity in the oxidized form and is activated by TRX-dependent reduction of the N-terminal Cys16-Cys55 regulatory disulfide (Brandes, Larimer, & Hartman, 1996). Formation of the Cys16-Cys55 disulfide efficiently blocks the activity because Cys55 likely plays a role in catalysis through binding of the sugar phosphate substrate (Milanez, Mural, & Hartman, 1991; Porter & Hartman, 1990). As in the case of other CBC enzymes, TRXf is more efficient for activation of PRK compared to TRXm while no activation by TRXx and TRXy was observed in Arabidopsis (Marri et al., 2009). PRK was purified from *Chlamydomonas* and shown to be activated by TRXf through reduction of the conserved N-terminal disulfide (Farr et al., 1994; Lebreton, Graciet, & Gontero, 2003). Two C-terminal cysteines were shown to participate in a disulfide formation, which might alter the physical interaction of PRK with GAPDH and CP12 (Thieulin-Pardo, Remy, Lignon, Lebrun, & Gontero, 2015). Proteomic approaches also identified this disulfide as a target of TRX (Perez-Perez et al., 2017). *Chlamydomonas* PRK is preferentially activated by TRXf (Gurrieri et al., 2019) but can also be activated, to a lesser extent, by TRXz (Le Moigne, Gurrieri, et al., 2021).

Fructose-1,6-bisphosphatase (FBPase)

Oxidized land plant FBPase has a basal activity (20-30%) and becomes fully activated upon disulfide reduction, which is strictly dependent on TRXf; all other TRX types are inefficient. The molecular mechanism of TRX dependent activation of FBPase was initially unraveled for pea FBPase. Compared

to cytosolic FBPase, which participates in gluconeogenesis and is not redox regulated by TRX, pea chloroplast FBPase contains two insertions containing cysteines that form the regulatory disulfide bond (Cys153-Cys178) (Chiadmi, Navaza, Miginiac-Maslow, Jacquot, & Cherfils, 1999; Jacquot et al., 1995; Jacquot, Lopez-Jaramillo, et al., 1997; Rodriguez-Suarez, Mora-Garcia, & Wolosiuk, 1997). The conformational changes linking the redox state of the regulatory cysteines and the level of activation of the enzyme have been established by comparing the structure of oxidized and reduced FBPase (Chiadmi et al., 1999; Jacquot et al., 1995; Jacquot, Lopez-Jaramillo, et al., 1997; Rodriguez-Suarez et al., 1997). Formation of the disulfide forces the sliding of a loop by 8-9 Å towards the active site, thereby disrupting the binding sites for the catalytic Mg^{2+} cations (Chiadmi et al., 1999). Therefore, in contrast to other CBC enzymes, the conformational changes induced by the oxidation of the regulatory disulfide do not impact the active site or its proximity but stabilizes a general conformation in which the active site is almost non-functional. Chloroplastic FBPase was the first TRX (TRXf) target purified from *Chlamydomonas* (Chiadmi et al., 1999; Jacquot et al., 1995; Jacquot, Lopez-Jaramillo, et al., 1997; Rodriguez-Suarez et al., 1997).

Sedoheptulose-1,7-bisphosphatase (SBPase)

SBPase is a homodimeric enzyme that is unique to the CBC and has no cytosolic counterpart. SBPase contains a single regulatory disulfide that is preferentially reduced by TRXf (Dunford, Durrant, Catley, & Dyer, 1998; Gutle et al., 2016; Nishizawa & Buchanan, 1981). The regulatory cysteines are conserved in all photosynthetic eukaryotes including *Chlamydomonas*, but the algal enzyme has not been characterized biochemically.

Rubisco and Rubisco activase (see also Chapter 7)

Despite the finding that Rubisco was systematically identified among putative TRX targets in redox proteomic studies performed in photosynthetic cells (L. Michelet et al., 2013; Perez-Perez et al., 2017), a direct effect of TRX on Rubisco has not yet been reported. In the large subunit of *Chlamydomonas* Rubisco, seven of the twelve cysteines are highly conserved among photosynthetic eukaryotes (Moreno, Garcia-Murria, & Marin-Navarro, 2008) and among them, oxidation of Cys172, Cys192, Cys449 and Cys459 was reported to play a prominent role either in Rubisco inactivation and degradation through conformational modulation (Garcia-Murria et al., 2008; Garcia-Murria, Sudhani, Marin-Navarro, Sanchez Del Pino, & Moreno, 2018; Marin-Navarro & Moreno, 2006) or chloroplastic mRNA binding (Uniacke & Zerges, 2008; Yosef et al., 2004; Zhan et al., 2015). The Cys449-Cys459 pair was proposed to function as a redox sensor (Garcia-Murria et al., 2008) and Cys459 is reduced in the presence of TRX (Perez-Perez et al., 2017), but an experimental demonstration of a direct TRX-dependent regulation of Rubisco remains to be established. In some species, Rubisco may be indirectly regulated by TRX through Rubisco activase (RCA), an ATP-dependent molecular chaperone of the AAA+ family required to release tight binding inhibitors from the active site of Rubisco (Portis, 2003; Portis, Li, Wang, & Salvucci, 2008). The ATPase activity of RCA is controlled by the ADP/ATP ratio and/or by the FDX-TRX system. Two types of RCA have been identified: the short form (beta isoform), not regulated by TRX, and the long form (alpha isoform) which contains a TRXf-dependent regulatory disulfide (Zhang, Schurmann, & Portis, 2001). The extension contains negative charges that, upon oxidation of the disulfide, interact with the ATP binding site and inhibits the enzyme while reduction by TRXf alleviates this inhibition (Portis et al., 2008; D. Wang & Portis, 2006). Some species, such as Arabidopsis, contain both alpha and beta isoforms while others such as tobacco, maize and green algae only contain the short beta isoform, but they still exhibit light dependent regulation of RCA activity due to a unique sensitivity to ADP/ATP ratios (Carmo-Silva & Salvucci, 2013; Salvucci, Werneke, Ogren, & Portis, 1987) and to light-dependent fluctuations of magnesium ions (Hazra, Henderson, Liles, Hilton, & Wachter, 2015).

b. A diversity of post-translational modifications in Chlamydomonas CBC

Proteome-wide analysis of post-translationally modified proteins have considerably challenged our current models of CBC regulation, which has been focused on the activation by TRXf of 4 CBC enzymes

plus CP12. In addition to TRX-regulation, two other types of redox modifications have been investigated in *Chlamydomonas* using proteomics: glutathionylation and nitrosylation. Glutathionylation results in the formation of a mixed disulfide bond between a protein cysteine and the thiol group of glutathione, the major non-protein thiol in most organisms (Rouhier, Lemaire, & Jacquot, 2008; Zaffagnini, Bedhomme, Marchand, et al., 2012; Zaffagnini et al., 2019). Glutathionylation is a widespread oxidative modification involved in the modulation of protein function but also in the protection of protein Cys from irreversible oxidation. Nitrosylation results in the formation of nitrosothiols by the reaction of protein thiols with a nitric oxide (NO) moiety. It can be triggered chemically by reactive nitrogen species (RNS) such as NO and related species, but also by transnitrosylation reactions mediated by small nitrosothiols (*e.g.* nitrosoglutathione, GSNO) or other nitrosylated proteins (Benhar, Forrester, & Stamler, 2009; Chen et al., 2020; Hess, Matsumoto, Kim, Marshall, & Stamler, 2005; Hogg, 2002; Zaffagnini et al., 2014). In *Chlamydomonas,* NO signaling participates in the regulation of nutrient acquisition, photosynthetic efficiency, and other processes including autophagy and programmed cell death (Calatrava et al., 2017; De Mia, Lemaire, Choquet, & Wollman, 2019; Kuo, Chang, Lin, & Lee, 2020; Sanz-Luque, Ocana-Calahorro, Llamas, Galvan, & Fernandez, 2013; Wei et al., 2014; Zalutskaya, Kochemasova, & Ermilova, 2018). Both nitrosylation and glutathionylation can be reversed by TRX and/or glutathione/glutaredoxins (GRXs) (Bedhomme et al., 2012; Zaffagnini, Bedhomme, Marchand, et al., 2012; Zaffagnini et al., 2016). As GSNO has been proposed to trigger both nitrosylation and glutathionylation, these two modifications could be dependent on GSNO homeostasis, which is under the control of a GSNO reductase that was recently characterized biochemically and structurally in *Chlamydomonas* (Tagliani et al., 2021).

In *Chlamydomonas*, proteomic studies identified 225 proteins regulated by glutathionylation (Michelet et al., 2008; Zaffagnini, Bedhomme, Groni, et al., 2012) and nearly 400 nitrosylated cysteines in 492 nitrosylated proteins (Morisse, Zaffagnini, Gao, Lemaire, & Marchand, 2014). The thioredoxome (TRX-interacting proteome) has also been investigated in *Chlamydomonas* and allowed the identification of 1188 proteins and 1052 cysteines regulated by TRX (Perez-Perez et al., 2017). Comparison of these datasets suggests the existence of a complex redox regulation network in *Chlamydomonas* and provides evidence of a tremendous selectivity of post-translational redox modifications for specific cysteine residues, even within the same protein. These results indicate that the Cys proteome does not represent a small subset of highly reactive Cys residues that are modified through indiscriminate interaction with the molecules they encounter, but represents a complex system of post-translational modifications (PTMs) associated with redox conditions that are specific for distinct interconnected protein networks (Perez-Perez et al., 2017). The CBC is a major target pathway within this complex network since all *Chlamydomonas* CBC enzymes were identified as potential targets of nitrosylation (Morisse, Zaffagnini, et al., 2014), glutathionylation (Michelet et al., 2008; Zaffagnini, Bedhomme, Groni, et al., 2012; Zaffagnini et al., 2014) and thioredoxin mediated redox regulation (Lemaire et al., 2004; Morisse, Michelet, et al., 2014; Perez-Perez et al., 2017) (Table 3). Most of these modifications have been confirmed on the corresponding purified enzyme, with the modified cysteines mapped. However, the effect of the modification varies considerably between enzymes (Bedhomme et al., 2012; Zaffagnini, Bedhomme, Groni, et al., 2012; Zaffagnini, Fermani, et al., 2013; Zaffagnini et al., 2007; Zaffagnini et al., 2014; Zaffagnini, Morisse, et al., 2013). For example, TPI and A_4-GAPDH were both confirmed to undergo glutathionylation and nitrosylation, with PTMs fully inhibiting GAPDH activity but barely affecting TPI activity (Zaffagnini et al., 2014). Some modified enzymes may represent moonlighting proteins that, upon redox PTMs, are diverted to new functions unrelated to their metabolic role in carbon metabolism, as shown for cytosolic GAPDH in mammals (Zaffagnini, Fermani, et al., 2013). Among CBC enzymes, a moonlighting function has been reported for *Chlamydomonas* RbcL (see Vol 2, Chapter 7). It binds chloroplast mRNAs and accumulates in chloroplast stress granules under oxidative stress conditions (Cohen, Sapir, & Shapira, 2006; Knopf & Shapira, 2005; Uniacke & Zerges, 2008; Yosef et al., 2004). RbcL undergoes numerous redox modifications that may participate in the regulation of this moonlighting function (**Table 3**).

Interestingly, all CBC enzymes except FBPase were also identified in the phosphoproteome of *Chlamydomonas* with multiple modified residues for most enzymes (McConnell, Werth, & Hicks, 2018; H. Wang et al., 2014). *Chlamydomonas* CBC enzymes likely undergo multiple other modifications that remain to be investigated in detail. For example, recent proteomic data showed that most if not all CBC enzymes of land plants can be crotonylated on multiple lysine residues (Liu et al., 2018; Sun et al., 2017; J. Sun et al., 2019; Xu et al., 2021). The functional role of all these modifications is still unknown. Therefore, it appears that CBC enzymes are regulated by an intricate network of PTMs, with different modifications that may not occur at the same time, at the same site, to the same extent or under the same physiological/cellular conditions (see Chapter 1 for details). Regulation by PTM may allow a tight coupling between the activity and function of CBC enzymes and environmental conditions.

3. Structure and supramolecular organization

- Structural features of Calvin-Benson Cycle enzymes

The CBC enzymes have been studied by biochemical and proteomic approaches, which have unraveled some of their functions, specificities, and mechanisms of regulation. To go further into the characterization of these enzymes, their structures were determined by X-ray crystallography. We will inventory the current knowledge on the structures of the eleven CBC enzymes and the small interacting protein CP12 (Erales, Lignon, & Gontero, 2009) from *Chlamydomonas* (Table 2). We focus on solvent-exposed regulatory cysteines that are susceptible to redox modification in the folded state of the protein, since they elucidate how CBC functioning is coupled to the redox state of the PET chain, and thus to light. Structural information on *Chlamydomonas* CBC proteins is described and referenced using the Protein Data Bank (PDB) 4-character codes. Unless otherwise stated residues are numbered according to the mature protein, after cleavage of the transit peptide. The structure of each enzyme is represented in Figure 3.

Rubisco

Rubisco is a heteromultimeric assembly of two gene products: a large subunit (LSU) and a small subunit (SSU). A complex set of chaperones (Aigner et al., 2017) guide eight LSU and eight SSU into a hexadecameric (LSU_8:SSU_8) working assembly (Andersson & Backlund, 2008) (see Vol 2, Chapter 7). Rubisco is classified as a lyase because it catalyzes the formation of carbon-carbon bonds between RuBP and carbon dioxide (CO_2). When utilizing dioxygen (O_2) instead of CO_2, Rubisco will form 3-PGA and 2-phosphoglycolate; the latter is toxic and is detoxified at a energetic cost to the cell. *Chlamydomonas* Rubisco is a major constituent of the pyrenoid, which is a component of the CCM. This subcellular compartment becomes especially prominent under low CO_2 conditions and is the site at which CO_2 is concentrated in the vicinity of Rubisco; this organization allows for the more efficient fixation of CO_2. Additionally, the pyrenoid has interesting physical properties and undergoes liquid-liquid phase separation during cell division (see Vol 2, Chapter 7).

Rubisco SSU folds as a two-layer α/β sandwich. Rubisco LSU is composed of two domains, the B domain is an α/β TIM barrel and the N domain is a ferredoxin-like α+β sandwich (M. S. Chapman et al., 1988). The structure, 1GK8 for *Chlamydomonas* Rubisco, was determined at atomic resolution by X-ray crystallography of the protein complexed with the RuBP analog 2-carboxyarabinitol-1,5-diphosphate (CAP) and magnesium (Taylor, Backlund, Bjorhall, Spreitzer, & Andersson, 2001). CAP is bound by the B domain of one LSU through residues Lys175, Lys177, His294, Arg295, His327, Lys334, Leu335, Ser379, Gly380, Gly381, Gly403, and Gly404, and by the N domain of a neighboring LSU through residues Glu60, Thr65, Trp66, and Asn123. Thr173, carbamylated Lys201, Asp203, and Glu204 interact with magnesium. The betaA-betaB loop is different in the algal structure compared to its spinach ortholog (1RCX), and the residues of the loop are important for the holoenzyme function.

Phosphoglycerate kinase (PGK)

An *in silico* three-dimensional model of reduced *Chlamydomonas* PGK1 was built from the ortholog crystal structure from *Bacillus stearothermophilus*, which has the highest sequence identity in the

structural database (Morisse, Michelet, et al., 2014). PGK is composed of two domains adopting the Rossman fold and connected by a hinge containing a long α-helix. Consistent with most reported PGK structures, *Chlamydomonas* PGK is a monomer in solution. Its oxidation was evaluated by energy minimization. Molecular dynamics suggested that redox control of *Chlamydomonas* PGK is exerted by the modulation of domain-domain contacts through the hinge dynamics. The Cys227-Cys361 disulfide bridge of oxidized PGK rigidifies the enzyme, preventing it from attaining the optimal closed conformation.

Glyceraldehyde-3-phosphate dehydrogenase (GAPDH)

No experimental structure is yet available for *Chlamydomonas* A_4-GAPDH, but the ortholog from Arabidopsis is a proxy of high sequence identity (>80 %). *Chlamydomonas* A_4-GAPDH is most probably folded as Arabidopsis 3K2B (Fermani et al., 2010), that is itself highly similar to spinach 1JN0 (Fermani et al., 2001) and 1RM4 (Sparla et al., 2004). The GAPDH monomer is composed of two domains: an amino-terminal NADP-coenzyme binding domain with an α/β Rossman fold into which is inserted a catalytic domain folded as an eight-stranded anti-parallel β-sheet and two α-helices. An S-loop protrudes from the β-sheet and contacts NADP nicotinamide. GAPDH monomers assemble into a tetrameric dimer of dimers. The structure of the higher-order redox-controlled assemblies of GAPDH with PRK will be discussed in the next section.

Triose phosphate isomerase (TPI)

The crystal structure 4MKN of *Chlamydomonas* TPI was determined at 1.1 Å resolution (Zaffagnini et al., 2014). TPI folds as an α/β barrel typical of the TIM topology. The alternance of eight α-helices and eight β-strands defines a core parallel β-barrel surrounded by α-helices. TIM barrels are among the most abundant folds in proteins (Jansen & Gerstein, 2000). *Chlamydomonas* TPI is homodimeric, with the enzymatic site located near the dimer interface and the catalytic residues at the carboxy-pole of the β-barrel from each protomer. Because it is the most exposed to solvent among the five cysteines of TPI, Cys219 is the most probable site of glutathionylation and nitrosylation, although these modifications barely affected catalytic properties *in vitro* (Zaffagnini et al., 2014).

Fructose-1,6-bisphosphate aldolase (FBA)

The crystal structure 7B2N of *Chlamydomonas* FBA was recently determined by the authors(Le Moigne, Sarti, et al., 2021). FBA folds as an α/β TIM barrel supplemented by a β-sheet of two antiparallel strands and a pair of carboxy-terminal α-helices. The active site residues sit at the carboxy-pole of the β-barrel where they contribute an electropositive cleft adapted to the binding of the phosphates of the substrates. *Chlamydomonas* FBA is a homotetramer with one dimer interface at the opposite side of the active site and the other dimer interface involving the additional two-strand β-sheet. The contacting subunit is located 18 Å away from the active site, with the additional β-sheet likely controlling accessibility to the catalytic pocket. All six cysteine residues of FBA have been reported to be redox modified (Table 3). Cys256 is the most exposed to solvent, in comparison to Cys58 and Cys142 whose reported susceptibility to nitrosylation may result from conformational changes or local unfolding. Arabidopsis cytosolic Ald2 is irreversibly inactivated by the cysteine nitrosylating agent GSNO, while GSSG partially and reversibly inactivated the enzyme (van der Linde et al., 2011). Disulfide bridge formation rearranges the active site of a metazoan aldolase into an inactive conformation (Heyduk, Michalczyk, & Kochman, 1991).

Fructose-1,6-bisphosphatase (FBPase)

No experimental crystal structure is available for *Chlamydomonas* FBPase, but a faithful homology model can be assumed from spinach or pea photosynthetic orthologs, 1SPI and 1D9Q, respectively (Chiadmi et al., 1999; Villeret, Huang, Zhang, Xue, & Lipscomb, 1995). FBPases fold into two domains, each composed of an antiparallel β-sheet surrounded by α-helices; these monomers assemble into a dimer of dimers. As mentioned in the previous section, a regulatory disulfide bridge between Cys153

and Cys173 of pea FBPase stabilizes a disordered 20-amino acid peptide segment into an ordered α-helix, displacing two β-strands that eventually disrupt the binding of the catalytic Mg^{2+} in the catalytic pocket located 20 Å away. Reduction of the regulatory disulfide bridge restores the disordered character of the peptidic segment and Mg^{2+} binding. FBPase is exclusively reduced by TRXf due to complementary FBPase-TRXf interaction surfaces. Electrostatic potential appears to be the main driver of this selectivity, with a marked electropositive potential around the TRXf redox site that mirrors an electronegative potential around the FBPase redox regulatory site (Lemaire et al., 2018).

Sedoheptulose-1,7-bisphosphatase (SBPase)

A photosynthetic SBPase structure 5IZ3 was first reported for the moss Physcomitrella (Gutle et al., 2016). We recently solved the crystal structure 7B2O of the *Chlamydomonas* ortholog. SBPase shares the same fold and has high structural similarity to FBPase, with an average distance of 1.241 Å between equivalent residues for the alignment of *Chlamydomonas* SBPase with pea FBPase. Meanwhile, the peptidic extension bearing the regulatory disulfide Cys153-Cys173 in the pea FBPase is shorter and devoid of cysteine in SBPase. Conversely, disulfide bridged Cys115 and Cys120 are located in a distinct β-hairpin motif in *Chlamydomonas* FBPase. The unique structural features of the redox regulatory disulfides in each enzyme argues in favor of a distinct phylogenetic origin between SBPase (archeal ancestry) and FBPase (bacterial ancestry) (Gutle et al., 2016).

Transketolase (TRK)

The crystal structures 5ND6 and 5ND5 of *Chlamydomonas* TRK were respectively determined in the apo state or bound to the cofactor thiamine pyrophosphate (TPP) and Mg^{2+} (Pasquini et al., 2017). TRK is composed of three α/β domains, each centered on a five stranded β-sheet interspersed by α-helices; the monomer assembles into an intricate homodimer. The amino-terminal domain binds Mg^{2+} and the TPP pyrophosphate (PP) moiety. The middle domain binds the TPP pyrimidine (Pyr) moiety. The PP domain of one dimer subunit and the Pyr domain of the other subunit both participate in the formation of one active site. By comparison with the apoprotein structure, the binding of TPP-Mg^{2+} appears to stabilize an ordered conformation on two peptidic segments of the active site. The C-terminal domain is neither involved in cofactor interaction nor dimerization. Oxidation of TRK-TPP-Mg^{2+} bears no catalytic consequence even though the cysteine pairs Cys173-Cys220, Cys204-Cys210, and Cys470-Cys484 are within disulfide bonding distance. However, TRK-TPP is reversibly inactivated by oxidized dithiothreitol (DTTox) treatment with a sensitivity that depends on the Mg^{2+} concentration. Indeed, >80% TRK activity is preserved from DTTox-mediated inactivation in the presence of 2 $mmol.L^{-1}$ Mg^{2+} while the same oxidative treatment inactivates >50% of the enzyme at Mg^{2+} concentrations lower than 0.05 $mmol.L^{-1}$ (Pasquini et al., 2017). Illumination of chloroplasts causes an increase in the stroma Mg^{2+} concentration above the TRK-protection threshold value of 1–3 $mmol.L^{-1}$ (Portis & Heldt, 1976), which helps coordinate photosystem activity with the activity of the CBC.

Ribose-5-phosphate isomerase (RPI)

The crystal structure 6ZXT of *Chlamydomonas* RPI was determined at 1.40 Å resolution (Le Moigne, Crozet, Lemaire, & Henri, 2020). RPI is a homodimer and each subunit folds as two domains: a Rossman fold at the amino-terminus and an ACT domain at the carboxy-terminus. The ACT (**A**spartate kinase, **C**horismate mutase and **T**yrA) domain is composed of a four-stranded antiparallel β-sheet and two α-helices and determines the dimeric quaternary state. The active site is remote from the dimerization interface and 13 residues contribute to an electropositive pocket of ideal dimensions to accommodate the ribose-5-phosphate substrate. At the opposite side of the protein, an extended electronegative surface runs along both protomers and is a candidate platform to interact with electropositive partner proteins. Among four cysteines of *Chlamydomonas* RPI, the most solvent-exposed is Cys175, located near the dimer interface. Moreover, Thr61 and Ser87 were suggested to be phosphorylated in *Chlamydomonas* protein extracts (McConnell et al., 2018; H. Wang et al., 2014). The Thr61 side chain

hydroxyl sits inside the enzymatic pocket and phosphorylation of this residue would prevent substrate binding.

Ribulose-5-phosphate 3-epimerase (RPE)

The authors recently determined the high-resolution crystal structure 7B1W of *Chlamydomonas* RPE. RPE folds as an α/β TIM barrel with a metal ion at the carboxy-pole of the barrel. His72, Asp74, His105, and Asp216 (full-length sequence numbering) coordinate the metal that was identified as Zn^{2+} in the ortholog structures 1H1Z and 2FLI. Three loops, A, B, and C, project from strands 1, 2, and 6 and delimit the active site cavity around the Zn^{2+}. Ser50, Ser239, and Thr220 were reported to be phosphorylated (McConnell et al., 2018; H. Wang et al., 2014). Their side chains are located at 10-17 Å from the Zn^{2+}, at the entrance of the catalytic pocket where their phosphorylation would decrease the affinity for ribulose-5-phosphate by steric and charge repulsion effects. RPE assembles as a homohexamer composed of a trimer of dimers. The trimer neighbor of each protomer pushes the aforementioned loop C towards the catalytic site, reducing its accessibility for substrate. Hence, homohexamerization is likely to increase the Michaelis constant of *Chlamydomonas* RPE. An extra α-helix caps the amino-pole of the barrel. This cap, bearing the *Chlamydomonas*-specific Cys37 residue, is in a solvent-exposed environment. Cys68, Cys150, and Cys204 are each located 10-18 Å from Cys37 and may form disulfide bridges if Cys37 is given enough flexibility. All four of these cysteines may also be modified, *e.g.* by nitrosylation or glutathionylation, given their accessibility in the model. The effect of such redox modifications is however hard to rationalize because all cysteines are >18 Å from the active site, separated from it by the depth of the barrel.

Phosphoribulokinase (PRK)

Experimental structures of oxygenic photosynthetic PRKs were reported for *Chlamydomonas* (6H7G), Arabidopsis (6H7H, 6KEW, 6KEX), and Synechococcus (6KEV, 6HZK, 6HZL) (Gurrieri et al., 2019; Wilson, Hayer-Hartl, & Bracher, 2019; A. Yu et al., 2020). PRK is an elongated homodimer with a subunit-to-subunit continuous mixed β-sheet of 20 strands (10 strands per subunit), defining a rod-like molecular shape. The active site lies at the extremities of the rod in a shallow cleft. The phosphate group of the substrate is expected to bind Arg64, Arg67, Tyr103, and His105 that bind a sulfate in the crystal structure. Two cysteine pairs are amenable to disulfide bonding: Cys16-Cys55 in the catalytic cleft, and Cys243-Cys249 near the dimerization surface. The formation of the Cys16-Cys55 disulfide would reduce catalytic efficiency (A. Yu et al., 2020) while the redox effect of the disulfide near the dimer interface may modify the flexibility of the assembly.

No experimental structures of PGK, GAPDH, FBPase, CP12, and RCA from *Chlamydomonas reinhardtii* have been reported at the date of this review. Although computational homology models predict the structure of globular proteins aligned onto models from other organisms or cytosolic pathways, these predictions may contain local erroneous predictions that are hard to discriminate. A complete understanding of photosynthetic carbon fixation thus requires a description of the remaining structures at high resolution. When X-ray crystallography proves difficult for disordered, dynamic or generally hard to crystallize objects, the other structural tools such as single-particle cryo-electron microscopy (cryo-EM) or nuclear magnetic resonance (NMR) will likely provide solutions. To achieve complete modeling of the carbon flow in the cycle, the exact catalytic mechanisms of each step of the CBC will need to be investigated. This includes but is not limited to; the type of catalysis, multiple substrate/product reaction orders, allosteric effects, affinity constants and catalytic constants. Supplementary controls over enzymes such as excess product or excess substrate inhibition, are likely to occur. Sub-organellar protein localization in the pyrenoid, in translational T-zones (Y. Sun et al., 2019) or at the thylakoid membranes (Zerges, Wang, & Rochaix, 2002) may be analyzed by *in situ* cryogenic electron tomography. Nevertheless, supramolecular assembly of CBC enzymes is likely an important determinant of the rate of carbon fixation, as reviewed in the next section.

- Supramolecular organization of the Calvin-Benson cycle

Past work *in vivo* and *in vitro* repeatedly suggested that CBC enzymes form higher-order complexes (Anderson et al., 1995; Gontero, Mulliert, Rault, Giudici-Orticoni, & Ricard, 1993; Jebanathirajah & Coleman, 1998; Rault, Giudici-Orticoni, Gontero, & Ricard, 1993; Romanova, Semenova, Ignat'ev, Novichkova, & Fomina, 2016; Sainis & Harris, 1986; Suss, Arkona, Manteuffel, & Adler, 1993; Teige, Melzer, & Suss, 1998), either for allosteric control of reaction rates (Ricard, Giudici-Orticoni, & Buc, 1990; Ricard, Giudici-Orticoni, & Gontero, 1994), for controlling the geometry of active sites (Avilan, Gontero, Lebreton, & Ricard, 1997b; Graciet, Lebreton, Camadro, & Gontero, 2002; Graciet et al., 2004; Lebreton et al., 2003) or for partitioning the enzymes into catalytically optimized assemblies (H. Wang et al., 2019; Wunder, Cheng, Lai, Li, & Mueller-Cajar, 2018). However, only the structures of PRK-CP12-GAPDH complex (6GVE and 6KEZ) and Rubisco condensates (6HBC, 7JFO, and 7JSX) are available as samples of the supramolecular organization of the CBC (McFarlane et al., 2019; H. Wang et al., 2019; A. Yu et al., 2020).

In the pyrenoid, Rubisco-Rubisco interaction is mediated by the intrinsically disordered protein EPYC1, which contains five Rubisco small-subunit (RbcS) sequence-repeated binding regions (He et al., 2020; L. C. Mackinder et al., 2016) (Chapter 7). In the 7JFO complex, EPYC1 repeat 1, folds as an α-helix that binds RbcS via three salt bridges (EPYC1-RbcS) Arg64-Glu24, Glu66-Arg91, Arg71-Asp23, and a hydrophobic interface composed of EPYC1 residues Trp63, Leu67, and Leu70 and RbcS residues Met87, Leu90, and Val94. Each EPYC1 region has a millimolar affinity for Rubisco along with a high dissociation constant, accounting for the dynamic character of the pyrenoid matrix.

PRK homodimers and GAPDH homotetramers form a supramolecular complex with the small, intrinsically disordered proteins CP12, which act as connectors (Avilan et al., 2012; Gontero & Avilan, 2011; Graciet et al., 2003; Graciet et al., 2004; Launay et al., 2016; Lebreton, Andreescu, Graciet, & Gontero, 2006). The formation of the PRK-CP12-GAPDH complex allows for fine regulation of PRK and A_4-GAPDH activities (reviewed in (Trost et al., 2006). CP12 is an intrinsically disordered protein, especially when fully reduced, and upon oxidation the formation of two disulfide bonds within the polypeptide decreases this disorder (Graciet et al., 2003; Marri et al., 2010; Marri et al., 2008). In Arabidopsis, the C-terminal disulfide has a redox potential comparable to GAPB (E_m = -352 mV at pH 7.9, (Marri et al., 2008)) allowing reduction of CP12 disulfides by TRXs, although with no strict specificity (Marri et al., 2009). In both Arabidopsis (Fermani et al., 2012; Marri et al., 2008) and *Chlamydomonas* (Kaaki, Woudstra, Gontero, & Halgand, 2013), A_4-GAPDH binds two CP12 molecules. However, while this binding is very strong in *Chlamydomonas* (K_D 0.4 nM) and leads to inhibition of GAPDH activity (Erales, Mekhalfi, Woudstra, & Gontero, 2011), it is much weaker in Arabidopsis (K_D 0.2 µM, (Marri et al., 2008)) and barely affects GAPDH activity (Marri, Trost, Pupillo, & Sparla, 2005; Marri et al., 2008). Nevertheless, binding of two PRK molecules to the GAPDH/CP12 complex results in strong inhibition of both enzymes (Marri et al., 2005). PRK is also inhibited in the supercomplex because catalytic Arg64 residue is mobilized for CP12-GAPDH interaction (Avilan, Gontero, Lebreton, & Ricard, 1997a). Therefore, PRK-CP12-GAPDH complexes accumulate in the dark and lead to inhibition of PRK and GAPDH activities, while upon illumination TRX reduction causes rapid dissociation of the complex, and recovery of enzyme activities (Marri et al., 2009). Experimental structures of GAPDH-CP12-PRK were determined from Thermosynechococcus (6GVE) and Arabidopsis (6KEZ) (McFarlane et al., 2019; A. Yu et al., 2020); the Arabidopsis structure is likely to resemble that of *Chlamydomonas*. In the crystal asymmetric unit, GAPDH-CP12-PRK is modelled with two oxidized PRK dimers, four oxidized CP12 and two GAPDH tetramers. In this complex, CP12 bears two TRX-dependent disulfides at Cys22-Cys31 and Cys64-Cys73 and is folded into three α-helices. CP12 is inserted in the PRK catalytic cleft on one side and in between two GAPDH subunits on the other side (Figure 4). In GAPDH, five residues from helix 254-269, two loop residues at positions 252-253 and one at position 305 come into contact with seven residues of PRK at positions 248, 283, 286, 299-301, and 308. They reinforce the stability of the ensemble.

VI. Energetic considerations and the dual purpose of NADPH turnover

1. NADPH and ATP: the assimilatory power duo

Photoreduction of $NADP^+$ to generate NADPH serves an important dual purpose, firstly, to provide assimilatory power for the CBC and secondly, to maintain linear electron flow. With 3 rounds of the CBC, NADPH donates 12 hydrogens of "reducing power" during the reductive phase to produce 6 glyceraldehyde-3-phosphate (GAP) from the 6 3-phosphoglyceric acid (3-PGA) molecules generated by the carboxylation reaction. $NADP^+$ regenerated as a consequence of the use of reductant in CO_2 assimilation is required to maintain linear electron flow because photosynthetic electron transfer and water oxidation cannot proceed without a terminal electron acceptor. Thus, oxidation of the primary electron donor for photosynthesis, water, renews the NADPH pool, while the CBC consumes the NADPH produced by electron transport, re-establishing the $NADP^+$ pool. A limitation in $NADP^+$ can be observed at the onset of illumination, in high light, in fluctuating light, in a transition from dark to light under anaerobic conditions and under nutrient deprivation (see references in the rest of this section). This situation creates a high NADPH/$NADP^+$ ratio and ultimately results in the production of reactive oxygen species and damage to PSI. However, in contrast to PSII photoinhibition, this is rarely witnessed for *Chlamydomonas* under physiological conditions (Chaux, Peltier, & Johnson, 2015). Pathways that contribute to the NADPH/$NADP^+$ balance have been identified using forward and reverse genetics combined with photosynthetic physiology and metabolite measurements. In recent years this knowledge has been enhanced by transcriptomic, proteomic and metabolomic studies.

ATP is the other component of the electron transport-derived, assimilatory 'power duo'. Three cycles of the CBC requires the high energy injection of 18 phosphates (from ATP), into two separate reactions of the reductive phase. ATP limitation induces a different set of regulatory pathways in the light than that of an elevated NADPH/$NADP^+$ ratio, including photoprotective heat dissipation at the level of PSII (nonphotochemical quenching). ATP production is not a redox reaction; its synthesis is fueled by the proton gradient generated by both linear and cyclic electron flows and is also strongly dependent on the levels of its substrates, ADP and Pi (for a comprehensive discussion see (Walker, 1992)). Furthermore, although NADPH regeneration is often treated separately from ATP production and limitation, the two are intertwined. NADPH in balance with $NADP^+$ facilitates cyclic electron flow that produces a proton gradient and ATP synthesis (Alric, 2010). Additionally, ATP and NADPH are required in stoichiometric quantities (3 ATP for 2 NADPH) for CO_2 assimilation by the CBC, with more ATP required under CO_2 limiting conditions (Allen, 2003; Lucker & Kramer, 2013), which means that an ATP deficiency will have a direct effect on the consumption and turnover of NADPH. Thus, it can be difficult to separate the outcome of ATP limitation from those of NADPH over-production in a "chicken-and-egg" scenario.

2. Pathways that contribute to maintenance of optimal NADPH/$NADP^+$ pools in the light

a. Detoxification Pathways

A sustained increase in the NADPH/$NADP^+$ ratio leads to over-reduction of PSI donor side electron carriers. Oxygen radicals, principally hydrogen peroxide (H_2O_2) and the super oxide anion ($O_2^{\bullet -}$), are formed in the iron-sulfur centers of PSI, FDX and stromal flavodehydrogenases via non-enzymatic O_2 photoreduction. These reactions occur at all light intensities but increase with elevated light intensity; water-water pathways (considering the first H_2O to be the primary electron donor to PSII and oxygen the electron acceptor to regenerate H_2O) have evolved for detoxification of the reactive oxygen species hydrogen peroxide and superoxide anion radical that may be formed by the Mehler (O_2 to H_2O_2 to H_2O) or Asada (O_2 to $O_2^{\bullet -}$ to H_2O_2 to H_2O) reactions (Figure 5). These pathways are highly conserved in oxygenic phototrophs and the major detoxification enzymes for these reactions have been characterized in *Chlamydomonas* chloroplast: Fe-superoxide dismutase (Fe-SOD1 of 3 isoforms) (Kitayama, Kitayama, Osafune, & Togasaki, 1999), Mn-SOD3 (of 5 isoforms) under Fe limiting conditions (Page et al., 2012), catalase (CAT1 of 2 isoforms) (Laure Michelet et al., 2013) and ascorbate peroxidase 4 (APX4 of 5 isoforms) (Kuo, Cai, & Lee, 2020), which uses an iron and an ascorbate to

reduce H_2O_2 to H_2O. Mono-dehydroascorbate reductase (MDAR1) (Yeh et al., 2019) recycles oxidized ascorbate back to its reduced form at the expense of NADPH. In the *Chlamydomonas* genome, homologues for both Dehydroascorbate Reductase (1 isoform) and Gluthathione Reductase (2 isoforms) are found but remain uncharacterised. H_2O_2 can block redox activation of CBC enzymes, so its detoxification is vital to maintain CO_2 fixation (Charles & Halliwell, 1981). However, in *Chlamydomonas*, Catalase is down-regulated by light and is only activated after APX4, allowing for a threshold level of H_20_2 accumulation which is required to activate retrograde protection pathways (Shao et al., 2008). The deletion of the aforementioned genes results in high light photosensitive phenotypes in *Chlamydomonas*.

b. Interactions between Photosynthesis and Respiration

In steady state mixotrophic or phototrophic conditions, O_2 photoreduction by mitochondrial respiration due to the exchange of reductant and photosynthate between the chloroplast and mitochondria is observed. The relationship between photosynthesis and respiration is dependent on light intensity; at low light intensities there is a break in the net O_2 exchange rate that has been confirmed as an inhibition of respiration by photosynthesis in the light known as the Kok effect (Kok, 1949). In different algal species, the Kok effect is enhanced by preferential excitation of of Photosystem I at 695 nm (Hoch, Owens, & Kok, 1963; Jones & Myers, 1963). The implications of the control of the Kok effect by PSI activity have not yet been fully understood, but the ADP:ATP ratio and cyclic electron flow were ruled out as the controlling factors (Healey & Myers, 1971; Peltier & Thibault, 1985). The preferred hypothesis to explain the inhibition of respiration at low light intensities is that there is an import of reductant towards the chloroplast and photosynthetic electron transport and away from mitochondrial reactions. This would occur through an exchange of NADH for NADPH via a metabolite transport mechanism, such as the malate shuttle (see section below).

As light intensities increase and in the presence of an active CBC, respiration increases in accord with the light, which is known as Light Enhanced Dark Respiration (LEDR). Measures of respiration after a light treatment show a good correlation with CO_2 uptake in the light (Peltier & Thibault, 1985; Xue, Gauthier, Turpin, & Weger, 1996). This increase in respiration is due to the export of photosynthate in the form of triose phosphate to the mitochondria as well as an increase in alternative oxidase (AOX) activity. The minimum rate of respiration in the light is set by the requirement for carbon skeletons for amino acid biosynthesis (John A. Raven & Beardall, 2003). A respiratory-defective mutant cannot grow in the dark on acetate, but is however viable in the light, just as the inverse is true for non-photosynthetic mutants, which are able to grow on acetate in the dark but not in the light with CO_2 (Levine, 1960; Matagne, Michel-Wolwertz, Munaut, Duyckaerts, & Sluse, 1989). The interdependence between these two energetic organelles is not critical for survival but serves to optimize and conserve energy in *Chlamydomonas*.

Inhibiting mitochondrial activity affects the chloroplast redox poise. This is observed under anaerobic light conditions (Kessler, 1973) or via the addition of mitochondrial electron transport inhibitors. Myxothiazole and Antimycin A inhibit the cytochrome *bc1* complex and salicylhydroxamic acid (SHAM) inhibits the Alternative Oxidase in *Chlamydomonas* (Gans & Rebeille, 1990; Rebeille & Gans, 1988). AOX (2 mitochondrial isoforms) has a strong activity in *Chlamydomonas* (Weger, Guy, & Turpin, 1990) and its uncoupling effect in mitochondrial respiration has been shown to modulate the redox state of both plastoquinone and ubiquinone under high light conditions (Kaye et al., 2019; Mathy et al., 2010). The reducing effect on the PQ pool when mitochondrial respiration is inhibited is due to ATP depletion in the cell, which results in the stimulation of the upper half of glycolysis and the loss of consumption of NADH by oxidative phosphorylation. A reduced PQ pool results in a photo-protective shift towards State 2 (LHCII antennae attach to PSI) (Allen, Bennett, Steinback, & Arntzen, 1981), while, interestingly, cells trapped in state I cannot evolve oxygen when respiration is inhibited by low oxygen concentrations (Forti, 2008). Numerous studies have shown that state transitions modulate the capacity for NADPH and ATP production in the chloroplast in response to both respiratory status and nitrogen metabolism (Bulté, Gans, Rebéillé, & Wollman, 1990; Cardol et al., 2009; Forti, Furia,

Bombelli, & Finazzi, 2003; Turpin, 1991). Active NH_4 metabolism increases the NADPH/$NADP^+$ ratio and the cells are maintained in State 2; under these conditions the ATP/NADPH ratio in the chloroplast increases dramatically, with a resulting decrease in CO_2 fixation and an increase in AOX activity (Franck, Dinant, Cardol, Remacle, & Matagne, 2008; Gauthier & Turpin, 1997).

c. *Starch, OPPP and glycolysis in plastid metabolism*

In *Chlamydomonas* chloroplasts, proteomic studies confirm that the upper half of glycolysis is compartmentalized to the plastid (Terashima et al., 2011). In conditions where NADPH is forcibly depleted from the plastid using inhibitors of photosynthesis and anaerobic incubation, measurements of PSI P_{700} oxidation prove that NADPH can be provided by the conversion of G3P to 3PGA in glycolysis (Johnson & Alric, 2012). The chloroplast-localized OPPP can be considered an alternative pathway to this "upper half" of glycolysis: G6P can be converted to F6P by phosphoglucose isomerase in the case of glycolysis or oxidized to 6-phosphoglucolactone by G6P-dehydrogenase as a part of the OPPP, yielding 2 molecules of NADPH. The activity of glycolysis under phototrophic or mixotrophic conditions was found to be 7 times greater than that of the OPPP (Klein, 1986). G6P-dehydrogenase activity is inhibited by high levels of NADPH and ribulose-1,5-bisphosphate (RuBP) (Lendzian & Bassham, 1975), and subject to light-driven redox modulation in *Chlamydomonas* (Farr et al., 1994). In Arabidopsis, reduction of the Cys99-Cys107 disulfide bond of chloroplastic G6PDH isoform P1, mediated by TRXf, causes inactivation of the enzyme (Nee et al., 2009). The cysteine pair is conserved in the *Chlamydomonas* G6PDH sequence, supporting a similar mechanism for redox regulation.

Starch accumulation provides another means to favorably adjust the NADPH/$NADP^+$ to avoid oxidative stress and maintain metabolites for the CBC. The *sta6* mutant that lacks ADP-glucose pyrophosphorylase activity (Zabawinski et al., 2001) and thus is unable to accumulate starch, has been extensively used to understand NADPH turnover in a genetic background devoid of the starch sink (see Chapter 1). In *sta6* grown phototrophically, CO_2 assimilation rates are gradually attenuated and an elevated NADPH / $NADP^+$ results in redirection of reducing equivalents that favors mitochondrial respiration (myxothiazole sensitive pathway) over carbon fixation and eventually leads to photoinhibition (Krishnan et al., 2015). In *sta6* under N-deficient mixotrophic conditions, NADPH imbalance is further accentuated and results in shunting fixed carbon towards the accumulation of soluble lipid as a reserve material (Li et al., 2010; Z. T. Wang, Ullrich, Joo, Waffenschmidt, & Goodenough, 2009). As linear electron flow is downregulated, the source of NADPH for lipid synthesis is derived from the activity of the OPPP, for example transaldolase is significantly transcriptionally upregulated (Goodenough et al., 2014). Under N-deficient conditions, upregulated enzymes outside of the chloroplast include the glyoxylate cycle enzymes, Malate Synthase 1 and Isocitrate Lyase 1 for sustained acetate uptake as the cell transitions from mixotrophic to heterotrophic metabolism, as well as Phosphoenolpyruvate Carboxykinase 1 and Fructose Bisphosphatase1 (chloroplastic), which are implicated in the gluconeogenic flow of carbon towards starch; in the *sta6* mutant, carbon is shunted towards OPPP, presumably for NADPH generation in the light when linear electron flow and CBC cycle are down-regulated (Blaby et al., 2013).

d. *NADP Malate dehydrogenase (MDY)*

A high NADPH/$NADP^+$ ratio is linked to thioredoxin activation and redox regulation (see section 4b of this chapter). A reduced stromal redox poise can be balanced by the transfer of reducing equivalents between compartments (Selinski & Scheibe, 2019) through the activities of enzymes like the chloroplast MDY, which is only found in the green lineage. The malate shunt operates in two directions, excess NADPH is consumed by the mitochondria to re-equilibrate the NADPH/$NADP^+$ ratio in phototrophic conditions or reductant is supplied to the chloroplast by the mitochondria in mixotrophic conditions (Boyle & Morgan, 2009; S. P. Chapman, Paget, Johnson, & Schwartz, 2015; Xue et al., 1996). The *Chlamydomonas* NADP-Malate Dehydrogenase 1 and 5 (MDY1 and MDY5 of 5 isoforms) are plastidial isoforms that reversibly reduces oxaloacetate to malate and oxidizes NADPH. The chloroplast MDY5 of *Chlamydomonas* is more rapidly activated than the analogous enzyme in higher plants, and

this property is conserved in other green algal homologues of MDY5 (Lemaire et al., 2005). Malate is then transported via chloroplast envelope localized transporters to shunt reducing power to the cytosol / mitochondria (MDY3 cytosolic and MDY4 mitochondrial). *Chlamydomonas* has three homologues of Arabidopsis 2-oxoglutarate/malate transporter (Weber et al., 1995): one of them, the LCI20 (low-CO_2-inducible) protein, occurs in the chloroplast proteome (Terashima et al., 2011) and is significantly upregulated under mixotrophic conditions (Puzanskiy, Romanyuk, Kirpichnikova, & Shishova, 2020). In glyoxysomes, NAD-Malate Dehydrogenase (MDY2), has a secondary effect on NADPH consumption in the chloroplast under nitrogen deprivation conditions in the light (Kong et al., 2018).

e. Chloroplastic NAD(P)H dehydrogenase, NDA-2

This monomeric type-2 NAD(P)H dehydrogenase enzyme is anchored to the thylakoid membrane and reduces plastoquinone at the expense of NAD(P)H (Desplats et al., 2009). Of the 6 NDA isoforms in *Chlamydomonas*, only NDA-2 and NDA-3 are found in chloroplasts (Terashima et al., 2011), the others all have predicted or characterized (NDA-1) localization to mitochondria (Lecler, Vigeolas, Emonds-Alt, Cardol, & Remacle, 2012). NDA-2 has a significantly higher affinity for NADH than NADPH and it is hypothesized that a transhydrogenase may be required for its activity (Peltier, Aro, & Shikanai, 2016). NDA-2 is also considered the most probable enzyme for cycling electrons around PSI under mixotrophic or phototrophic aerobic light conditions, where PSII photochemistry is active and PGR5/PGRL1 are not activated (Alric, 2010). NDA-2 is considered non-photochemical and non-electrogenic, active in the dark in chlororespiration (in tandem with the plastid terminal oxidase 2) (Jans et al., 2008) and in the light under sulfur and nitrogen deprivation to modulate the redox poise of the plastoquinone pool (Mignolet, Lecler, Ghysels, Remacle, & Franck, 2012; Saroussi, Wittkopp, & Grossman, 2016). Under N-deficient phototrophic conditions, a condition in which the plastid must receive reducing power from the mitochondria, NADPH recycling via NDA-2 is the main pathway to increase cyclic electron transfer around PSI to generate housekeeping ATP and maintain PSII quenching. Here, NADPH would be primarily generated by metabolic reactions, plastidial glycolysis as well as triose-phosphate and malate import, rather than generated by linear electron flow (Saroussi et al., 2016).

f. Flavodiiron Proteins and Mehler reaction

A rapid change in light conditions produces the chlorophyll fluorescence signature called the Kautsky effect that attests to a rapid accumulation followed by a consumption of reductant that feeds back along the whole of the electron transport chain. Mutants devoid of Flavodiiron (FLV) proteins lose this transient kinetic and chlorophyll fluorescence proceeds directly to F_{max} (Chaux et al., 2017). This is driven by a light intensity starting around 100 µmol m^{-2} sec^{-1}, suggesting that the process relies on a threshold of substrate to be activated. FLV proteins in a number of species function in oxygen photoreduction at the acceptor side of PSI to oxidize NADPH and donate the hydrogens to oxygen to yield water (Allahverdiyeva et al., 2013). FLVA/B are soluble proteins that form heterodimers and bind flavin and non-heme Fe co-factors, and their activity is transiently observed during an initial shift from the dark to the light but is no longer measurable after 5 minutes in the light (Chaux et al., 2017). The physiological relevance of this transient expression, in agreement with work in cyanobacteria, *Marchantia* and *Physcomitrella*, is to prime or oxidize the electron transfer carriers of the photosynthetic electron transfer chain until CBC enzymes are redox activated, creating a proton motive force (*pmf*) for ATP synthesis and rapidly providing a renewed source of $NADP^+$ (Allahverdiyeva et al., 2013; Chaux et al., 2017; Gerotto et al., 2016; Shimakawa et al., 2017). The deactivation of this process remains to be understood but may be associated with differences in affinity for NADPH between FLV and CBC enzymes (Yamamoto, Takahashi, Badger, & Shikanai, 2016). FLV proteins gradually replace hydrogenases (H^+ reduction) during a dark to light transition in anaerobic conditions and both enable *Chlamydomonas* cells to reoxidize the electron transport chain in the light (Burlacot et al., 2018; Ghysels, Godaux, Matagne, Cardol, & Franck, 2013).

In an absence of the FLV pathway, over the course of a fluctuating light treatment, an alternative O_2 photoreduction pathway is stimulated to a much greater extent than in wild type cells. The Mehler/Asada reactions are highly stimulated in an *flv* mutant, but their associated detoxification reactions must be exceeded because destruction of oxidizable P_{700} and a loss of PSI complex proteins are observed (Chaux et al., 2017). A second function of the FLV proteins is to reduce the amplitude of Mehler/Asada type reactions in fluctuating light in *Chlamydomonas*. In prolonged high light, $O_2^{\bullet-}$ to H_2O_2 production is constitutive and catalase, FE-SOD, APX and MDAR (consumer of NADPH) are required for cell survival via ROS detoxification (Ledford & Niyogi, 2005). In the regulation of NADPH photoproduction, these prolonged water-water cycles should not be ignored and would replace NADP+ photo-reduction and act as terminal electron acceptors, so their activity contributes to maintenance of *pmf* (Forti & Elli, 1996) and recycling NADPH to $NADP^+$ (Figure 5).

g. NADPH-controlled interplay between cyclic electron flow and oxygen photoreduction

Photosynthetic O_2 uptake in algae is stimulated by light exciting photosystem II, and diminished when most of the light light excites photosystem I (Setlik, Ried, & Berkova, 1973). Mutants without the *pgr5/pgrl1* pathway mimic the PSII stimulation experiment, with both linear electron flow and O_2 photoreduction being highly induced (Dang et al., 2014; Johnson et al., 2014). A strong O_2 uptake is due to reoxidation of NADPH via FLV proteins as well as activation of respiratory pathways. When NADPH accumulates, for instance in PSI light or in a mutant lacking Rubisco, it causes inhibition of linear electron transport, observed by a marked increase in cyclic electron flow and less O_2 photoreduction (Alric, Lavergne, & Rappaport, 2010; Johnson et al., 2014). Increased light-induced O_2 uptake is associated with a state of increased demand for ATP in the chloroplast (Setlik et al., 1973) and O_2 photoreduction pathways release the restriction on linear electron transport / water-water pathways. Conversely, Photosystem I-mediated cyclic electron transport, by raising the ATP level, will inhibit light-induced oxygen uptake (Evans & Carr, 1979).

VII. New avenues for the future: *Chlamydomonas* as a chassis for engineering carbon fixation pathways

The studies discussed so far are based on established analytical approaches that have deepened our understanding of the CBC and its regulation, but this knowledge could be complemented by synthetic biology methods. Biology is indeed currently facing a revolution through its transition from analytic to synthetic biology approaches (Cameron, Bashor, & Collins, 2014). Synthesis is a forward biological engineering discipline, a powerful methodology to understand by building rather than by deconstruction (Endy, 2011). It relies on the capacity to design and build a biological system from standardized simple DNA bricks, to test it in a systematic way, and to gain new knowledge to allow optimization of the design. These DESIGN, BUILD, TEST and LEARN cycles, can then be iterated as many times as necessary to cumulate the improvements required for process optimization (Petzold, Chan, Nhan, & Adams, 2015). Synthetic biology offers new possibilities to answer fundamental questions using new approaches and concepts or to create artificial systems that have potential biotechnological applications (Képès, 2011).

The rise of green synthetic biology presents researchers with the potential to tackle the challenge of improving photosynthetic efficiency through engineering of microalgae, cyanobacteria and plants. With its photosynthetic apparatus very similar to that of land plants, its dispensable photosynthesis allowing growth of photosynthetic mutants by supplementation with organic carbon (acetate), and our long-term knowledge of its genetics and physiology, *Chlamydomonas* appears as an ideal chassis to enable and accelerate the green synthetic revolution. This will take advantage of standardized synthetic biology tools developed during recent years for engineering *Chlamydomonas* including a Modular Cloning (MoClo) toolkit comprising 119 bricks allowing fast and easy generation of any multigenic assembly (Crozet et al., 2018). New standardized MoClo parts, including new antibiotic

resistance modules (de Carpentier et al., 2020) and riboswitches (Mehrshahi et al., 2020), are regularly expanding engineering possibilities using *Chlamydomonas*.

Synthetic biology approaches aimed at improving carbon fixation fall into 4 major categories: (i) engineering synthetic photorespiration bypasses; (ii) improving the working conditions of Rubisco through carbon-concentrating mechanisms (CCM); (iii) engineering respiration; (iv) engineering redesigned or synthetic CO_2 fixation pathways (Erb & Zarzycki, 2016; Kubis & Bar-Even, 2019; S. P. Long, Marshall-Colon, & Zhu, 2015; Ort et al., 2015; Simkin, Lopez-Calcagno, & Raines, 2019). Numerous possibilities exist to rewire photorespiration, several of which have been implemented with great success in cyanobacteria, microalgae and plants (Bar-Even, 2018; Betti et al., 2016; Kubis & Bar-Even, 2019; Simkin et al., 2019; South et al., 2019; Trudeau et al., 2018; H. Yu, Li, Duchoud, Chuang, & Liao, 2018). Many organisms have developed carbon concentrating mechanisms (J. A. Raven, Cockell, & De La Rocha, 2008) that could be engineered in CCM-free crops to boost their yield, although the functions of many components associated with the CCM remain to be determined (Atkinson, Mao, Chan, & McCormick, 2020; Hibberd, Sheehy, & Langdale, 2008; B. M. Long, Rae, Rolland, Forster, & Price, 2016; Rae et al., 2017; Schuler, Mantegazza, & Weber, 2016) (see Vol 2, Chapter 7). Multiple engineering strategies have also been proposed to boost crop productivity by cutting respiratory carbon loss (Amthor et al., 2019; S. P. Long et al., 2015).

Major energy losses during photosynthesis, that reduce the overall light conversion efficiency, can be directly attributed to kinetic bottlenecks within the CBC (Raines, 2011; Stitt, Lunn, & Usadel, 2010). The limitation of photosynthesis is due to the slow turnover of the CBC compared to PET capacity at moderate to high light intensities (Marcus, Altman-Gueta, Wolff, & Gurevitz, 2011; Wobbe & Remacle, 2015). Under these conditions, the excess of excitation energy can be dissipated as heat through non-photochemical quenching, fluorescence or increased production of harmful ROS. Since the CBC bottlenecks lead to over-reduction of PET components and threatens cell survival, photosynthetic organisms have evolved sophisticated mechanisms to limit PET such as down-regulation of antenna size and inactivation of key photosynthetic complexes (Nawrocki et al., 2019; Pinnola & Bassi, 2018). For these reasons cell growth (biomass production) can sometimes be increased by lowering either light intensities or the size of antennae (Mussgnug et al., 2007; Ort & Melis, 2011). Engineering quenching pathways to accelerate relaxation during shading increased carbon fixation and plant dry matter by about 15% in tobacco under fluctuating light (Kromdijk et al., 2016). However, another way to optimize photosynthesis and increase production yields would be to enhance the efficiency of carbon fixation rather than to decrease light harvesting capacity.

As slow turnover of the CBC is the most important limiting factor in photosynthetic efficiency under optimal conditions, any improvement of this carbon fixation pathway will result directly in higher photosynthetic efficiency and increase the photoproduction of biomass and engineered products at moderate to high light intensities. At light saturation, the CBC is typically co-limited *in vivo* by the capacity for regeneration of the acceptor molecule for carboxylation, RuBP, and the capacity for carboxylation by the notoriously inefficient Rubisco (S. P. Long, Ainsworth, Rogers, & Ort, 2004; Zhu, de Sturler, & Long, 2007). The catalytic rate of Rubisco is indeed one of the slowest of any enzyme-catalyzed reaction and the enzyme's low specificity for CO_2 versus O_2 further detracts from carbon fixation (Bar-Even et al., 2011; Parry et al., 2013; G. Tcherkez, 2013; Zhu, Portis, & Long, 2004). Engineering strategies to improve Rubisco catalytic efficiency or specificity have generally failed (Kubis & Bar-Even, 2019). The enzyme appears trapped in a trade-off between catalytic rate and specificity. Several studies suggested that improvement of its CO_2 fixation rate comes at the expense of CO_2 affinity and that, despite its inefficiency, the enzyme might already be optimized through natural evolution (Erb & Zarzycki, 2016; Galmes et al., 2014; Savir, Noor, Milo, & Tlusty, 2010; G. G. Tcherkez, Farquhar, & Andrews, 2006), although several recent studies challenge this finding (Cummins, Kannappan, & Gready, 2018; Durao et al., 2015; Young et al., 2016) (see Vol 2, Chapter 7). For example, Synechocystis Rubisco was improved using directed evolution (3-fold increase of carboxylation efficiency) (Durao et al., 2015) and overproduction of Rubisco in cyanobacteria was shown to increase

production of biomass and carbon-based chemicals (Atsumi, Higashide, & Liao, 2009; Iwaki et al., 2006; Liang & Lindblad, 2016, 2017; Rosgaard, de Porcellinis, Jacobsen, Frigaard, & Sakuragi, 2012).

However, Rubisco is not the only enzyme limiting CBC turnover. Indeed, metabolic flux control analyses and modelling of the CBC suggested that more effective enzymatic partitioning/stoichiometry could significantly improve photosynthetic efficiency (Mettler et al., 2014; Raines, 2003, 2006, 2011; Simkin, McAusland, Headland, Lawson, & Raines, 2015; Stitt et al., 2010; Stitt & Schulze, 1994; Trudeau et al., 2018; Zhu et al., 2007). These studies predicted that SBPase could limit the CBC and, consistently, the overproduction of this enzyme increased CO_2 fixation and biomass production in several species (Ding, Wang, Zhang, & Ai, 2016; Driever et al., 2017; Fang et al., 2012; Lefebvre et al., 2005; Liang & Lindblad, 2016; Miyagawa, Tamoi, & Shigeoka, 2001; Ogawa et al., 2015; Rosenthal et al., 2011; Simkin et al., 2017; Suzuki, Kondo, & Makino, 2017; Tamoi, Nagaoka, Miyagawa, & Shigeoka, 2006). In *Chlamydomonas*, SBPase overexpression of up to 3-fold (0.3% of total cell protein) resulted in a significant increase of both the photosynthetic rate and growth under high-light and elevated CO_2 conditions (Hammel et al., 2020). Other enzymes such as FBPase, PGK, TRK or FBA are also potential targets for improvement (Liang, Englund, Lindberg, & Lindblad, 2018; Liang & Lindblad, 2016; Mettler et al., 2014; Simkin et al., 2017; Simkin et al., 2015; Uematsu, Suzuki, Iwamae, Inui, & Yukawa, 2012). Indeed, under low light or elevated CO_2 concentrations, the rate of Rubisco becomes less limiting and carbon fixation is mostly constrained by RuBP regeneration (Kubis & Bar-Even, 2019). Engineering in cyanobacteria to increase metabolic sinks has also proved efficient for improving photosynthetic capacity and photosystem I oxidation (Santos-Merino et al., 2021).

An alternative approach to improving natural CBC would be to build artificial CO_2-fixing synthetic cycles more efficient than naturally occurring ones, such as the MOG pathways (Malonyl-CoA-oxaloacetate-glyoxylate) (Bar-Even, Noor, Lewis, & Milo, 2010), the CETCH cycle (crotonyl–coenzyme A (CoA)/ethylmalonyl-CoA/hydroxybutyryl-CoA) (Schwander, Schada von Borzyskowski, Burgener, Cortina, & Erb, 2016) or the GED cycle (Gnd–Entner–Doudoroff) (Satanowski et al., 2020). New pathways using one carbon metabolism (Gleizer et al., 2019) or non-natural reactions (Bar-Even, 2018) have also been proposed but are hardly practically feasible since they would require challenging *de novo* enzyme design and complete metabolism rewiring, which are not possible with our current knowledge and technologies. Hence, many possibilities exist to improve the efficiency of the CBC, either through redesign of natural CBC or through replacement of CBC by more efficient synthetic CO_2 fixation pathways.

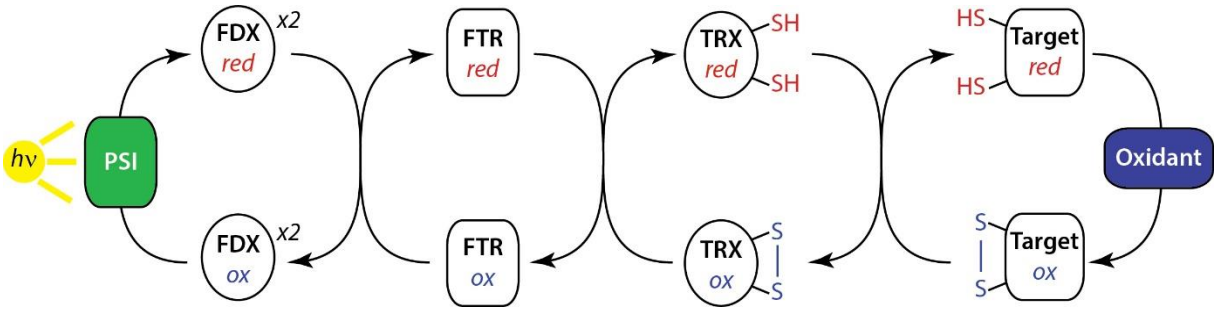

Figure 1. The Ferredoxin/Thioredoxin system.

FDX, ferredoxin; FTR, ferredoxin thioredoxin reductase; PSI, photosystem I; ox, oxidized; red, reduced

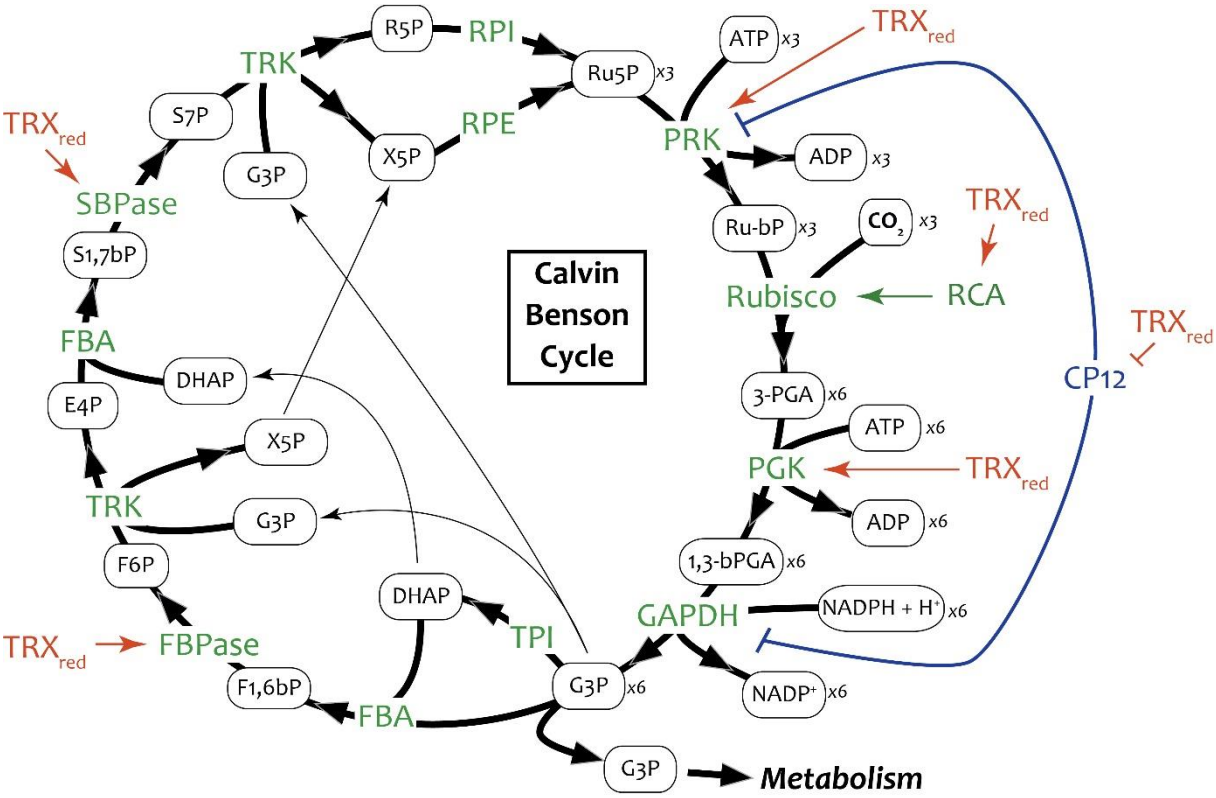

Figure 2. The Calvin-Benson Cycle in *Chlamydomonas reinhardtii*

The eleven enzymes of the CBC are indicated in green. Four enzymes are activated in the light by reduced thioredoxin (TRXred), bracketed by a blue line. Metabolites are indicated in black ellipses with their global stoichiometry. The carbon input (CO_2 in bold) and output (G3P) towards metabolism are indicated.

Enzymes: Rubisco, ribulose-1,5-bisphosphate Carboxylase/Oxygenase; PGK, phosphoglycerate kinase; GAPDH, glyceraldehyde-3-phosphate dehydrogenase; TPI, triose phosphate isomerase; FBA, fructose-1,6-bisphosphate aldolase; FBPase, fructose-1,6-bisphosphatase; TRK, transketolase; SBPase, sedoheptulose-1,7-bisphosphatase; RPE, ribulose-5-phosphate 3-epimerase; RPI, ribose-5-phosphate isomerase; PRK, phosphoribulokinase.

Metabolites: Ru-bP, ribulose-1,5-bisphosphate; 3-PGA, 3-phosphoglycerate; 1,3-bPGA, 1,3-bisphosphoglycerate; G3P, glyceraldehyde-3-phosphate; DHAP, dihydroxyacetone phosphate; F1,6bP, fructose-1,6-bisphosphate; F6P, fructose-6-phosphate; X5P, xylulose-5-phosphate; E4P, erythrose-4-phosphate; S1,7bP, sedoheptulose-1,7-bisphosphate; S7P, sedoheptulose-7-phosphate; R5P, ribose-5-phosphate; RuP, ribulose-5-phosphate.

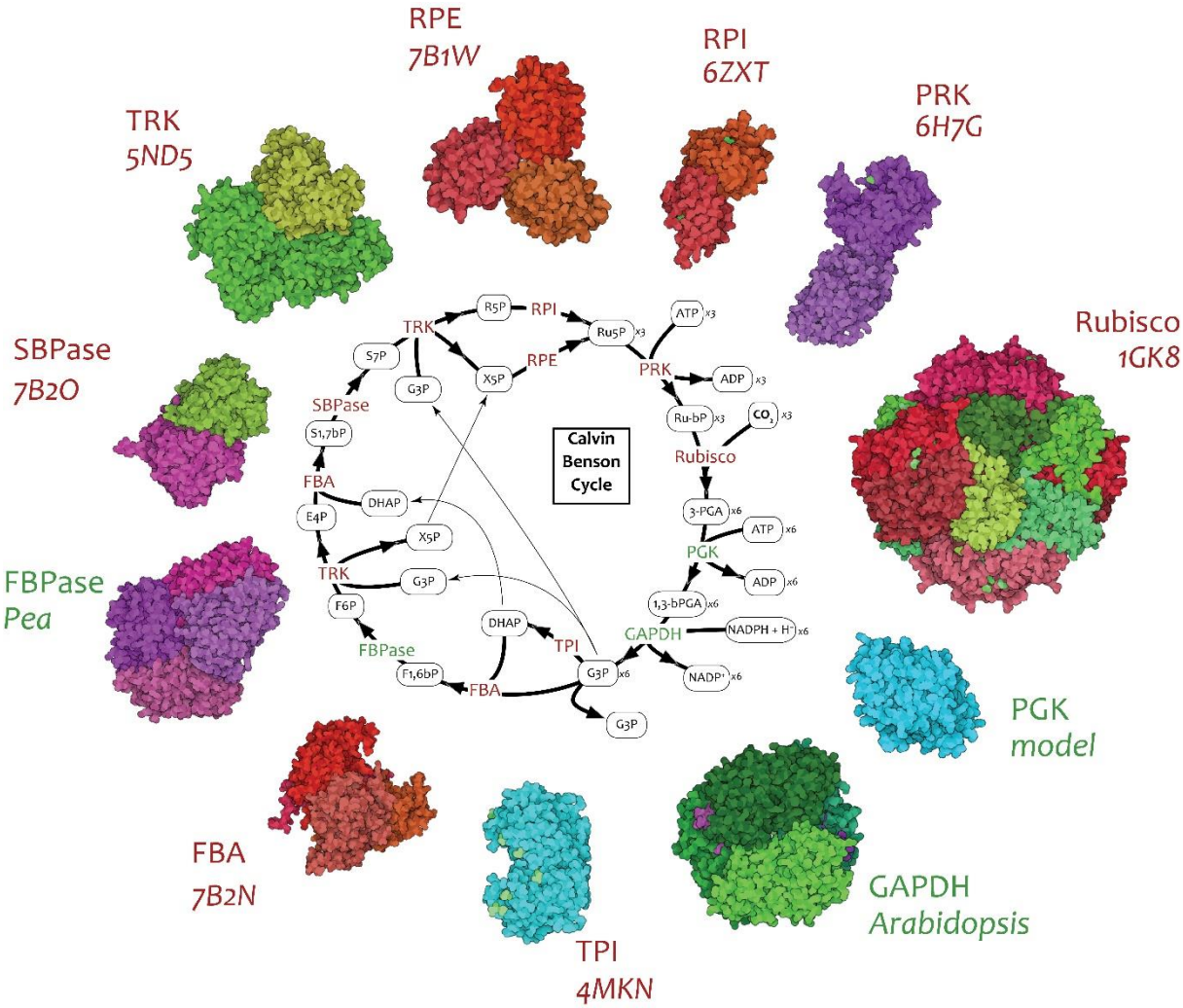

Figure 3. Structural components of the Calvin-Benson cycle

Metabolites are indicated in black with stoichiometric ratio for the fixation of $3xCO_2$ into 1xglyceraldehyde. Metabolites and enzymes are identified as in Figure 2. Known experimental structures (red) or models (green) of the Calvin-Benson enzymes in Chlamydomonas are represented with Illustrate software (Goodsell, Autin, & Olson, 2019). Protein Data Bank (PDB) identifiers 1GK8 (Rubisco), 4MKN (TPI), 7B2N (FBA), 5ND5 (TRK), 7B1W (RPE), 6H7G (PRK), 7B2O (SBPase), and 6ZXT (RPI) are indicated near their respective representation.

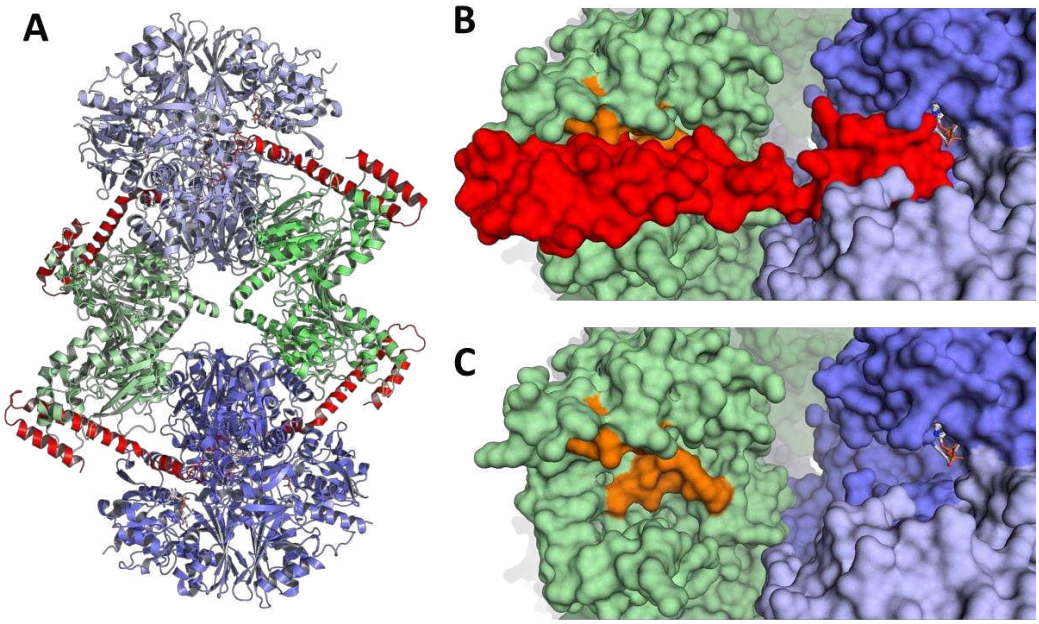

Figure 4: Crystal structure of GAPDH-CP12-PRK complex

A. Cartoon representation of the crystal structure of *Arabidopsis thaliana* GAPDH-CP12-PRK complex (PDB ID : 6KEZ (A. Yu et al., 2020)) with GAPDH tetramers colored in blue, CP12 in red, and PRK dimers in green. **B.** Surface representation of the insertion site of CP12 protein colored in red in the GAPDH and PRK active pockets. PRK is colored as in A. with residues involved in the fixation of phosphate and ATP in orange. Two GAPDH subunits are colored in shades of blue with NAD in white **C.** Same representation as in B. without CP12.

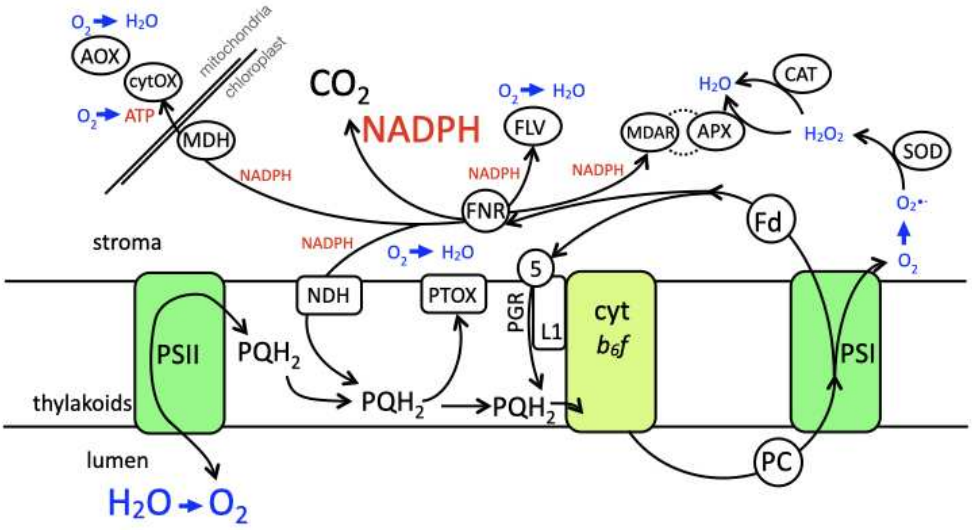

Figure 5. The photosynthetic electron transport chain and the pathways that consume and maintain NADPH homeostasis.

In the chloroplast, electrons are provided for the first charge separation through Photosystem II (PSII) by the water-splitting reaction giving rise to oxygen (O_2) as a side product. Plastoquinol (PQH_2), cytochrome *b*$_6$*f* complex (cyt*b*$_6$*f*) and plastocyanin (PC) are intersystem electron carriers that deliver electrons for a second charge separation through Photosystem I (PSI) in the thylakoid membrane. This linear electron flow passes to the stromal electron carriers, ferredoxins (Fd) and Ferredoxin NADP Reductase (FNR), to reduce the terminal electron acceptor $NADP^+$ and produce NADPH. The major consumer of NADPH is the CBC for CO_2 fixation. When NADPH:NADP+ ratios are high, Fd is redirected towards a recycling of electrons around cyt*b*$_6$*f* and PSI via the Proton Gradient Regulation (PGR5/PGRL1) pathway, referred to as cyclic electron flow. NADPH can also be directly recycled via the type 2 NADPH Reductase (NDH) and the PQ pool again by a cyclic electron flow around PSI. Plastid terminal oxidase (PTOX) is an oxygen valve that controls the equilibrium between the PQH_2 pool and NADPH (stromal redox poise) between dark and light. At the onset of light, the Flavodiiron (FLV) proteins catalyze a rapid O_2 valve for NADPH oxidation at the acceptor side of PSI that transfers electrons to make H_2O. The malate NADP dehydrogenase (MDH) can also rapidly metabolize NADPH in exchange for a transportable organic acid to transfer reducing power to the mitochondria for consumption of O_2 to drive ATP production (cytochrome oxidase pathway, cytOX) or, more likely during active photosynthesis, the alternative oxidase (AOX) pathway to complete a water-water cycle. When PSI and the PSI stromal carriers have no acceptors, the redox-active iron-centres spontaneously react with oxygen to produce superoxide anion radical ($O_2^{\bullet-}$). Superoxide dismutase detoxifies $O_2^{\bullet-}$ to H_2O_2 followed by further detoxification to water via catalase (CAT) and the ascorbate peroxidase (APX) / monodehydroascorbate reductase pathway (MDAR) that consumes NADPH. The size of the font represents the importance of the pathway, the black lines with arrows represent electron flows and the discontinuous lines represent multiple enzymatic reactions.

Table 1: Components of the chloroplast ferredoxin-thioredoxin system

Name	Gene Name	Genome Locus (Phytozome 12)	Uniprot	MW (kDa) Pre/mat*	Length (AA) Pre/mat*
Ferredoxin 1	*FDX1*	Cre14.g626700	A8IV40	13.2 / 9.9	126 / 94
Ferredoxin 2	*FDX2*	Cre16.g658400	A0A2K3CTD8	13.2 / ND	121 / ND
Ferredoxin 3	*FDX3*	Cre06.g306350	Q2HZ24	19.7 / ND	187 / ND
Ferredoxin 4	*FDX4*	Cre07.g334800	Q2HZ23	14.0 / ND	131 / ND
Ferredoxin 5	*FDX5*	Cre17.g700950	Q2HZ22	14.4 / ND	130 / ND
Ferredoxin 6	*FDX6*	Cre03.g183850	Q2HZ21	34.1 / ND	314 / ND
Ferredoxin 7	*FDX7*	Cre01.g006100	A8JFX3	13.7 / ND	133 / ND
Ferredoxin 8	*FDX8*	Cre01.g005600	A0A2K3E509	20.6 / ND	197 / ND
Ferredoxin 9	*FDX9*	Cre12.g487900	A0A2K3D298	10.7 / ND	101 / ND
Ferredoxin 10	*FDX10*	Cre04.g225450	A0A2K3DUL5	14.5 / ND	130 / ND
Ferredoxin 11	*FDX11*	Cre06.g291650	A8J2J6	12.1 / ND	117 / ND
Ferredoxin thioredoxin reductase Catalytic subunit	*FTRC*	Cre03.g193950	A8IWK2	16.0 / 13.1	145 / 116
Ferredoxin thioredoxin reductase Variable subunit	*FTRV*	Cre16.g687294	A8JA70	12.3 / 10.4	113 / 93
Thioredoxin f1	*TRXf1*	Cre01.g066552	Q84XR8	18.2 / 12.6	173 / 115
Thioredoxin f2	*TRXf2*	Cre05.g243050	A0A2K3DSC9	19.9 / 13.2	180 / 116
Thioredoxin m (*aka* CH2)	*TRXm*	Cre06.g269752	P23400	15.1 / 11.6	140 / 106
Thioredoxin x	*TRXx*	Cre01.g052250	Q84XR9	15.8 / 12.8	145 / 116
Thioredoxin y	*TRXy*	Cre10.g446100	Q84XS2	16.7 / 12.9	152 / 115
Thioredoxin z (*aka* CITRX)	*TRXz*	Cre02.g142800	A8J0Q8	19.5 / 13.9	183 / 128
NADPH-Dependent Thioredoxin reductase C	*NTRC1/NTR4*	Cre01.g054150	A0A2K3E888	58.9	536

Table 2: Enzymes of the Calvin Benson cycle and their regulators in *Chlamydomonas*

Protein Name	Gene Name	Cre	Uniprot	MW (kDa) Pre / mat	Length (aa) Pre / mat
Ribulose-1,5-bisphosphate carboxylase/oxygenase large subunit (RubisCO LSU)	*rbcL*	Cre.RbcL	P00877	52.47	475
Ribulose-1,5-bisphosphate carboxylase/oxygenase small subunit (RubisCO SSU)	*RBCS1* *RBCS2*	Cre02.g120100 Cre02.g120150	P00873 P08475	20.58 / 16.22 20.6 / 16.25	185 / 140 185 / 140
Phosphoglycerate kinase	*PGK1*	Cre11.g467770	Q548U3	48.96 / 42.58	462 / 402
Glyceraldehyde-3-phosphate dehydrogenase subunit A	*GAP3*	Cre01.g010900	P50362	40.24 / 36.82	374 /340
Triose phosphate isomerase	*TPIC1*	Cre01.g029300	Q5S7Y5	30.00 / 27.01	282 / 255
Fructose-1,6-bisphosphate aldolase	*ALDCHL*	Cre05.g234550	Q42690	40.92 / 38.11	377 / 350
Fructose-1,6-bisphosphatase	*FBP1*	Cre12.g510650	A8IKQ0	44.38 / 38.87	415 / 359
Transketolase	*TRK1*	Cre02.g080200	A8IAN1	77.55 / 73.85	718 / 683
Sedoheptulose-1,7-bisphosphatase	*SEBP1*	Cre03.g185550	P46284	41.38 / 35.00	385 / 323
Ribulose phosphate-3-epimerase	*RPE1*	Cre12.g511900	A8IKW6	28.35 / 25.54	265 / 238
Ribose-5-phosphate isomerase	*RPI1*	Cre03.g187450	A8IRQ1	28.77 / 26.58	269 / 248
Phosphoribulokinase	*PRK*	Cre12.g554800	P19824	48.96 / 42.58	462 / 402
Calvin cycle protein CP12	*CP12*	Cre08.g380250	A6Q0K5	11.40 / 8.44	107 / 80
RubisCO activase	*RCA1*	Cre04.g229300	P23489	44.97 / 41.58	408 / 376

Table 3: Main post-translational modifications of Calvin Benson cycle enzymes and their known sites

Protein Name	Targeted by thioredoxin[¶]		Regulatory Disulfide[¶]	S-Glutathionylation		S-Nitrosylation[¶]		Redox-modified cysteines[¶]	Phosphorylation sites[¶]
Rubisco (LSU)	yes[b, k]	C459[k]		yes[e]	C172[e]; C247[e]; C427[e]	yes[f]	C172[f]; C247[f]; C427[f]; C459[f]	C84[m]; C172[a, m,n]; C192[l, m, n]; C247[l, n]; C427[m, n]; C449[i, l, n, a, c]; C459[j, a,c, l, m]	T471[r]
Rubisco (SSU)	yes[b, k]	C110[k]; C128[k]; C141[k]		yes[e]		yes[f]	C110[f]	C86[l, m]; C110[i, l]; C128[i, l]; C141[i, l]	S98[r]; S107[r]
PGK	yes[g, k]	C159[k]; C412[k]	C278-C412[g]	yes[d, e]	C159[e]; C412[e]	yes[f]	C412[f]	C278[n]; C412[n]	S262[r]; S301[r]; S302[r]; T414[r]; S421[r]; T439[r]; S444[r]
GAPDH-A	yes[k]	C190[k]; C194[k]		yes[e]		yes[f]		C190[i, l, n]; C194[i, l, n]; C325[n]	T62[r]; S72[r]; S86[r, u]; T90[r]; S104[r]; S229[u]; T246[r]; T247[r]; S255[r]; S320[r, u]; S358[r]
TPI	yes[k]	C154[k]; C245[k]; C273[k]		yes[h]		yes[f, h]	C245[f]; C273[f]	C41[l, n]; C245[l, n]	S128[r, s]
FBA	yes[b, k]	C58[k]		yes[e]		yes[f]	C58[f]; C142[f]; C256[f]	C58[n]; C142[l, n]; C152[l, n]; C183[n]; C218[n]; C256[l, n]	S54[r]; T57[r]; S64[r, w]; S170[r]; S176[r]
FBPase	yes[k]	C109[k]; C228[k]; C233[k]; C362[k]		yes[e]	C109[e]	yes[f]	C233[f]	C109[l, n]; C152[l, n]; C156[l, n]; C228[l, n]; C233[l, n]; C362[l, n]	
TRK	yes[k]	C386[k]; C484[k]		yes[e]	C84[e]	yes[f]	C582[f]	C58[i]; C84[i, n]; C173[i]; C204[i]; C210[i]; C366[i]; C386[i, l, n]; C470[i, l, n]; C582[i, n]; C638[i]	S451[r]; S669[r]
SBPase	yes[b, k]	C218[k]; C227[k]; C351[k]; C358[k]		yes[e]		yes[f]	C351[f]; C358[f]	C111[l, n]; C116[l, n]; C218[l, n]; C227[l, n]; C351[l, n]; C358[l, n]	T108[v]; S110[r, v, w]; T114[p, r, v, w]; S119[r, u, v, w]; T306[r]; S307[r, v]; T309[r]
RPE	yes[k]			yes[e]		yes[f]		C68[l]	S50[r]; T220[r]; S239[r]

RPI	yes[b, k]	C149[k]; C175[k]		yes[d, e]		yes[f]		C149[l, n]; C175[l, n]	S87[r]
PRK	yes[b, k]	C274[k]; C280[k]	C47-C86[o] C274-C280[j]	yes[e]	C47[e]; C274[e]	yes[f]	C47[f]	C47[l, n]; C86[l, n]; C92[i, l, n]; C274[i, l, n]; C280[n]	T4[u]; T57[v]; S204[r]; S281[r, v]
CP12	yes[k]	C74[k;] C82[k]; C117[k]; C126[k]						C74[i, l, n]; C82[l, n]; C117[i, l, n]; C126[l, n]	S52[r]; T78[r]; S79[r, u, v]; T88[r, v, t]; T108[r, v]; T110[r, v]
RCA	yes[k]	C148[k]; C196[k]; C255[k]; C289[k]		yes[e]		yes[f]	C196[f]; C289[f]	C148[l, n]; C196[i, l, n]; C255[i, l, n]; C289[n]	S45[r, s, t ,u, v]; S53[q, r, s, t, u, v]; S85[r, u, v]; S86[r, u, v]; S96[r, u]; S163[r]; S390[r, u]; S400[r]; S401[r]; S407[r]

[¶] Amino acids numbering according to the full-length sequence of the v5.6 genome annotation. References are [a] (Moreno & Spreitzer, 1999) ; [b] (Lemaire et al., 2004) ; [c] (Marin-Navarro & Moreno, 2006) ; [d] (Michelet et al., 2008) ; [e] (Zaffagnini, Bedhomme, Groni, et al., 2012) ; [f] (Morisse, Zaffagnini, et al., 2014) ; [g] (Morisse, Michelet, et al., 2014) ; [h] (Zaffagnini et al., 2014) ; [i] (Slade, Werth, McConnell, Alvarez, & Hicks, 2015) ; [j] (Thieulin-Pardo et al., 2015) ; [k] (Perez-Perez et al., 2017) ; [l] (McConnell et al., 2018) ; [m] (Garcia-Murria et al., 2018) ; [n] (Ford et al., 2019) ; [o] (Gurrieri et al., 2019) ; [p] (Wagner et al., 2006) ; [q] (Lemeille, Turkina, Vener, & Rochaix, 2010) ; [r] (H. Wang et al., 2014) ; [s] (Werth et al., 2017); [t] (Roustan, Bakhtiari, Roustan, & Weckwerth, 2017) ; [u] (Roustan & Weckwerth, 2018) ; [v] (McConnell et al., 2018) ; [w] (Werth et al., 2019).

[Chapter References]

Aigner, H., Wilson, R. H., Bracher, A., Calisse, L., Bhat, J. Y., Hartl, F. U., & Hayer-Hartl, M. (2017). Plant RuBisCo assembly in E. coli with five chloroplast chaperones including BSD2. *Science, 358*(6368), 1272-1278. doi: 10.1126/science.aap9221

Allahverdiyeva, Y., Mustila, H., Ermakova, M., Bersanini, L., Richaud, P., Ajlani, G., . . . Aro, E. M. (2013). Flavodiiron proteins Flv1 and Flv3 enable cyanobacterial growth and photosynthesis under fluctuating light. *Proc Natl Acad Sci U S A, 110*(10), 4111-4116. doi: 10.1073/pnas.1221194110

Allen, J. F. (2003). Cyclic, pseudocyclic and noncyclic photophosphorylation: new links in the chain. *Trends Plant Sci, 8*(1), 15-19. doi: 10.1016/s1360-1385(02)00006-7

Allen, J. F., Bennett, J., Steinback, K. E., & Arntzen, C. J. (1981). Chloroplast protein phosphorylation couples plastoquinone redox state to distribution of excitation energy between photosystems. *Nature, 291*(5810), 25-29.

Alric, J. (2010). Cyclic electron flow around photosystem I in unicellular green algae. *Photosynth Res, 106*(1-2), 47-56. doi: 10.1007/s11120-010-9566-4

Alric, J., Lavergne, J., & Rappaport, F. (2010). Redox and ATP control of photosynthetic cyclic electron flow in Chlamydomonas reinhardtii (I) aerobic conditions. *Biochim Biophys Acta, 1797*(1), 44-51. doi: 10.1016/j.bbabio.2009.07.009

Amthor, J. S., Bar-Even, A., Hanson, A. D., Millar, A. H., Stitt, M., Sweetlove, L. J., & Tyerman, S. D. (2019). Engineering Strategies to Boost Crop Productivity by Cutting Respiratory Carbon Loss. *Plant Cell, 31*(2), 297-314. doi: 10.1105/tpc.18.00743

Anderson, L. E., Goldhaber-Gordon, I. M., Li, D., Tang, X. Y., Xiang, M., & Prakash, N. (1995). Enzyme-enzyme interaction in the chloroplast: glyceraldehyde-3-phosphate dehydrogenase, triose phosphate isomerase and aldolase. *Planta, 196*(2), 245-255. doi: 10.1007/BF00201381

Andersson, I., & Backlund, A. (2008). Structure and function of Rubisco. *Plant Physiol Biochem, 46*(3), 275-291. doi: 10.1016/j.plaphy.2008.01.001

Arsova, B., Hoja, U., Wimmelbacher, M., Greiner, E., Ustun, S., Melzer, M., . . . Bornke, F. (2010). Plastidial thioredoxin z interacts with two fructokinase-like proteins in a thiol-dependent manner: evidence for an essential role in chloroplast development in Arabidopsis and Nicotiana benthamiana. *Plant Cell, 22*(5), 1498-1515. doi: 10.1105/tpc.109.071001

Aslund, F., Berndt, K. D., & Holmgren, A. (1997). Redox potentials of glutaredoxins and other thiol-disulfide oxidoreductases of the thioredoxin superfamily determined by direct protein-protein redox equilibria. *J Biol Chem, 272*(49), 30780-30786. doi: 10.1074/jbc.272.49.30780

Atkinson, N., Mao, Y., Chan, K. X., & McCormick, A. J. (2020). Condensation of Rubisco into a proto-pyrenoid in higher plant chloroplasts. *Nat Commun, 11*(1), 6303. doi: 10.1038/s41467-020-20132-0

Atsumi, S., Higashide, W., & Liao, J. C. (2009). Direct photosynthetic recycling of carbon dioxide to isobutyraldehyde. *Nat Biotechnol, 27*(12), 1177-1180. doi: 10.1038/nbt.1586

Avilan, L., Gontero, B., Lebreton, S., & Ricard, J. (1997a). Information transfer in multienzyme complexes--2. The role of Arg64 of Chlamydomonas reinhardtii phosphoribulokinase in the information transfer between glyceraldehyde-3-phosphate dehydrogenase and phosphoribulokinase. *Eur J Biochem, 250*(2), 296-302. doi: 10.1111/j.1432-1033.1997.0296a.x

Avilan, L., Gontero, B., Lebreton, S., & Ricard, J. (1997b). Memory and imprinting effects in multienzyme complexes--I. Isolation, dissociation, and reassociation of a phosphoribulokinase-

glyceraldehyde-3-phosphate dehydrogenase complex from Chlamydomonas reinhardtii chloroplasts. *Eur J Biochem, 246*(1), 78-84. doi: 10.1111/j.1432-1033.1997.00078.x

Avilan, L., Puppo, C., Erales, J., Woudstra, M., Lebrun, R., & Gontero, B. (2012). CP12 residues involved in the formation and regulation of the glyceraldehyde-3-phosphate dehydrogenase-CP12-phosphoribulokinase complex in Chlamydomonas reinhardtii. *Mol Biosyst, 8*(11), 2994-3002. doi: 10.1039/c2mb25244a

Baalmann, E., Scheibe, R., Cerff, R., & Martin, W. (1996). Functional studies of chloroplast glyceraldehyde-3-phosphate dehydrogenase subunits A and B expressed in Escherichia coli: formation of highly active A4 and B4 homotetramers and evidence that aggregation of the B4 complex is mediated by the B subunit carboxy terminus. *Plant Mol Biol, 32*(3), 505-513. doi: 10.1007/BF00019102

Ballicora, M. A., Frueauf, J. B., Fu, Y., Schurmann, P., & Preiss, J. (2000). Activation of the potato tuber ADP-glucose pyrophosphorylase by thioredoxin. *J Biol Chem, 275*(2), 1315-1320. doi: 10.1074/jbc.275.2.1315

Balsera, M., Uberegui, E., Schurmann, P., & Buchanan, B. B. (2014). Evolutionary development of redox regulation in chloroplasts. *Antioxid Redox Signal, 21*(9), 1327-1355. doi: 10.1089/ars.2013.5817

Bar-Even, A. (2018). Daring metabolic designs for enhanced plant carbon fixation. *Plant Sci, 273*, 71-83. doi: 10.1016/j.plantsci.2017.12.007

Bar-Even, A., Noor, E., Lewis, N. E., & Milo, R. (2010). Design and analysis of synthetic carbon fixation pathways. *Proc Natl Acad Sci U S A, 107*(19), 8889-8894. doi: 10.1073/pnas.0907176107

Bar-Even, A., Noor, E., Savir, Y., Liebermeister, W., Davidi, D., Tawfik, D. S., & Milo, R. (2011). The moderately efficient enzyme: evolutionary and physicochemical trends shaping enzyme parameters. *Biochemistry, 50*(21), 4402-4410. doi: 10.1021/bi2002289

Bar-On, Y. M., & Milo, R. (2019). The global mass and average rate of rubisco. *Proc Natl Acad Sci U S A, 116*(10), 4738-4743. doi: 10.1073/pnas.1816654116

Bassham, J. A. (1971). Photosynthetic carbon metabolism. *Proc Natl Acad Sci U S A, 68*(11), 2877-2882. doi: 10.1073/pnas.68.11.2877

Bedhomme, M., Adamo, M., Marchand, C. H., Couturier, J., Rouhier, N., Lemaire, S. D., . . . Trost, P. (2012). Glutathionylation of cytosolic glyceraldehyde-3-phosphate dehydrogenase from the model plant Arabidopsis thaliana is reversed by both glutaredoxins and thioredoxins in vitro. *Biochem J, 445*(3), 337-347. doi: 10.1042/BJ20120505

Benhar, M., Forrester, M. T., & Stamler, J. S. (2009). Protein denitrosylation: enzymatic mechanisms and cellular functions. *Nat Rev Mol Cell Biol, 10*(10), 721-732. doi: 10.1038/nrm2764

Benson, A. A., Bassham, J. A., Calvin, M., Hall, A. G., Hirsch, H. E., Kawaguchi, S., . . . Tolbert, N. E. (1952). The path of carbon in photosynthesis. XV. Ribulose and sedoheptulose. *J Biol Chem, 196*(2), 703-716. doi: 10.2172/915054

Bergner, S. V., Scholz, M., Trompelt, K., Barth, J., Gabelein, P., Steinbeck, J., . . . Hippler, M. (2015). STATE TRANSITION7-Dependent Phosphorylation Is Modulated by Changing Environmental Conditions, and Its Absence Triggers Remodeling of Photosynthetic Protein Complexes. *Plant Physiol, 168*(2), 615-634. doi: 10.1104/pp.15.00072

Betti, M., Bauwe, H., Busch, F. A., Fernie, A. R., Keech, O., Levey, M., . . . Weber, A. P. (2016). Manipulating photorespiration to increase plant productivity: recent advances and perspectives for crop improvement. *J Exp Bot, 67*(10), 2977-2988. doi: 10.1093/jxb/erw076

Blaby, I. K., Blaby-Haas, C. E., Perez-Perez, M. E., Schmollinger, S., Fitz-Gibbon, S., Lemaire, S. D., & Merchant, S. S. (2015). Genome-wide analysis on Chlamydomonas reinhardtii reveals the impact of hydrogen peroxide on protein stress responses and overlap with other stress transcriptomes. *Plant J, 84*(5), 974-988. doi: 10.1111/tpj.13053

Blaby, I. K., Glaesener, A. G., Mettler, T., Fitz-Gibbon, S. T., Gallaher, S. D., Liu, B., . . . Merchant, S. S. (2013). Systems-level analysis of nitrogen starvation-induced modifications of carbon metabolism in a Chlamydomonas reinhardtii starchless mutant. *Plant Cell, 25*(11), 4305-4323. doi: 10.1105/tpc.113.117580

Boehm, M., Alahuhta, M., Mulder, D. W., Peden, E. A., Long, H., Brunecky, R., . . . Dubini, A. (2016). Crystal structure and biochemical characterization of Chlamydomonas FDX2 reveal two residues that, when mutated, partially confer FDX2 the redox potential and catalytic properties of FDX1. *Photosynth Res, 128*(1), 45-57. doi: 10.1007/s11120-015-0198-6

Bosco, M. B., Aleanzi, M. C., & Iglesias, A. A. (2012). Plastidic phosphoglycerate kinase from Phaeodactylum tricornutum: on the critical role of cysteine residues for the enzyme function. *Protist, 163*(2), 188-203. doi: 10.1016/j.protis.2011.07.001

Boyle, N. R., & Morgan, J. A. (2009). Flux balance analysis of primary metabolism in Chlamydomonas reinhardtii. *BMC Syst Biol, 3*(1), 4. doi: 10.1186/1752-0509-3-4

Brandes, H. K., Larimer, F. W., & Hartman, F. C. (1996). The molecular pathway for the regulation of phosphoribulokinase by thioredoxin f. *J Biol Chem, 271*(7), 3333-3335. doi: 10.1074/jbc.271.7.3333

Buchanan, B. B. (2016). The Path to Thioredoxin and Redox Regulation in Chloroplasts. *Annu Rev Plant Biol, 67*, 1-24. doi: 10.1146/annurev-arplant-043015-111949

Buchanan, B. B., Holmgren, A., Jacquot, J. P., & Scheibe, R. (2012). Fifty years in the thioredoxin field and a bountiful harvest. *Biochim Biophys Acta, 1820*(11), 1822-1829. doi: 10.1016/j.bbagen.2012.07.006

Buchert, F., Bailleul, B., & Hisabori, T. (2017). A gamma-subunit point mutation in Chlamydomonas reinhardtii chloroplast F1Fo-ATP synthase confers tolerance to reactive oxygen species. *Biochim Biophys Acta Bioenerg, 1858*(12), 966-974. doi: 10.1016/j.bbabio.2017.09.001

Bulté, Laurence, Gans, Pierre, Rebéillé, Fabrice, & Wollman, Francis-André. (1990). ATP control on state transitions in vivo in Chlamydomonas reinhardtii. *Biochimica et Biophysica Acta (BBA)-Bioenergetics, 1020*(1), 72-80.

Burlacot, A., Sawyer, A., Cuine, S., Auroy-Tarrago, P., Blangy, S., Happe, T., & Peltier, G. (2018). Flavodiiron-Mediated O2 Photoreduction Links H2 Production with CO2 Fixation during the Anaerobic Induction of Photosynthesis. *Plant Physiol, 177*(4), 1639-1649. doi: 10.1104/pp.18.00721

Calatrava, V., Chamizo-Ampudia, A., Sanz-Luque, E., Ocana-Calahorro, F., Llamas, A., Fernandez, E., & Galvan, A. (2017). How Chlamydomonas handles nitrate and the nitric oxide cycle. *J Exp Bot, 68*(10), 2593-2602. doi: 10.1093/jxb/erw507

Cameron, D. E., Bashor, C. J., & Collins, J. J. (2014). A brief history of synthetic biology. *Nat Rev Microbiol, 12*(5), 381-390. doi: 10.1038/nrmicro3239

Cardol, P., Alric, J., Girard-Bascou, J., Franck, F., Wollman, F. A., & Finazzi, G. (2009). Impaired respiration discloses the physiological significance of state transitions in Chlamydomonas. *Proc Natl Acad Sci U S A, 106*(37), 15979-15984. doi: 10.1073/pnas.0908111106

Carmo-Silva, A. E., & Salvucci, M. E. (2013). The regulatory properties of Rubisco activase differ among species and affect photosynthetic induction during light transitions. *Plant Physiol, 161*(4), 1645-1655. doi: 10.1104/pp.112.213348

Chapman, M. S., Suh, S. W., Curmi, P. M., Cascio, D., Smith, W. W., & Eisenberg, D. S. (1988). Tertiary structure of plant RuBisCO: domains and their contacts. *Science, 241*(4861), 71-74. doi: 10.1126/science.3133767

Chapman, S. P., Paget, C. M., Johnson, G. N., & Schwartz, J. M. (2015). Flux balance analysis reveals acetate metabolism modulates cyclic electron flow and alternative glycolytic pathways in Chlamydomonas reinhardtii. *Front Plant Sci, 6*, 474. doi: 10.3389/fpls.2015.00474

Charles, S. A., & Halliwell, B. (1981). Light activation of fructose bisphosphatase in isolated spinach chloroplasts and deactivation by hydrogen peroxide : A physiological role for the thioredoxin system. *Planta, 151*(3), 242-246. doi: 10.1007/BF00395175

Charoenwattanasatien, R., Zinzius, K., Scholz, M., Wicke, S., Tanaka, H., Brandenburg, J. S., . . . Kurisu, G. (2020). Calcium sensing via EF-hand 4 enables thioredoxin activity in the sensor-responder protein calredoxin in the green alga Chlamydomonas reinhardtii. *J Biol Chem, 295*(1), 170-180. doi: 10.1074/jbc.RA119.008735

Chaux, F., Burlacot, A., Mekhalfi, M., Auroy, P., Blangy, S., Richaud, P., & Peltier, G. (2017). Flavodiiron Proteins Promote Fast and Transient O2 Photoreduction in Chlamydomonas. *Plant Physiol, 174*(3), 1825-1836. doi: 10.1104/pp.17.00421

Chaux, F., Peltier, G., & Johnson, X. (2015). A security network in PSI photoprotection: regulation of photosynthetic control, NPQ and O2 photoreduction by cyclic electron flow. *Front Plant Sci, 6*, 875. doi: 10.3389/fpls.2015.00875

Chen, L., Wu, R., Feng, J., Feng, T., Wang, C., Hu, J., . . . Zuo, J. (2020). Transnitrosylation Mediated by the Non-canonical Catalase ROG1 Regulates Nitric Oxide Signaling in Plants. *Dev Cell, 53*(4), 444-457 e445. doi: 10.1016/j.devcel.2020.03.020

Chiadmi, M., Navaza, A., Miginiac-Maslow, M., Jacquot, J. P., & Cherfils, J. (1999). Redox signalling in the chloroplast: structure of oxidized pea fructose-1,6-bisphosphate phosphatase. *EMBO J, 18*(23), 6809-6815. doi: 10.1093/emboj/18.23.6809

Chibani, K., Couturier, J., Selles, B., Jacquot, J. P., & Rouhier, N. (2010). The chloroplastic thiol reducing systems: dual functions in the regulation of carbohydrate metabolism and regeneration of antioxidant enzymes, emphasis on the poplar redoxin equipment. *Photosynth Res, 104*(1), 75-99. doi: 10.1007/s11120-009-9501-8

Chibani, K., Tarrago, L., Schurmann, P., Jacquot, J. P., & Rouhier, N. (2011). Biochemical properties of poplar thioredoxin z. *FEBS Lett, 585*(7), 1077-1081. doi: 10.1016/j.febslet.2011.03.006

Chibani, K., Wingsle, G., Jacquot, J. P., Gelhaye, E., & Rouhier, N. (2009). Comparative genomic study of the thioredoxin family in photosynthetic organisms with emphasis on Populus trichocarpa. *Mol Plant, 2*(2), 308-322. doi: 10.1093/mp/ssn076

Cohen, I., Sapir, Y., & Shapira, M. (2006). A conserved mechanism controls translation of Rubisco large subunit in different photosynthetic organisms. *Plant Physiol, 141*(3), 1089-1097. doi: 10.1104/pp.106.079046

Collin, V., Issakidis-Bourguet, E., Marchand, C., Hirasawa, M., Lancelin, J. M., Knaff, D. B., & Miginiac-Maslow, M. (2003). The Arabidopsis plastidial thioredoxins: new functions and new insights into specificity. *J Biol Chem, 278*(26), 23747-23752. doi: 10.1074/jbc.M302077200

Collin, V., Lamkemeyer, P., Miginiac-Maslow, M., Hirasawa, M., Knaff, D. B., Dietz, K. J., & Issakidis-Bourguet, E. (2004). Characterization of plastidial thioredoxins from Arabidopsis belonging to the new y-type. *Plant Physiol, 136*(4), 4088-4095. doi: 10.1104/pp.104.052233

Courteille, A., Vesa, S., Sanz-Barrio, R., Cazale, A. C., Becuwe-Linka, N., Farran, I., . . . Rumeau, D. (2013). Thioredoxin m4 controls photosynthetic alternative electron pathways in Arabidopsis. *Plant Physiol, 161*(1), 508-520. doi: 10.1104/pp.112.207019

Crozet, P., Navarro, F. J., Willmund, F., Mehrshahi, P., Bakowski, K., Lauersen, K. J., . . . Lemaire, S. D. (2018). Birth of a Photosynthetic Chassis: A MoClo Toolkit Enabling Synthetic Biology in the Microalga Chlamydomonas reinhardtii. *ACS Synth Biol, 7*(9), 2074-2086. doi: 10.1021/acssynbio.8b00251

Cummins, P. L., Kannappan, B., & Gready, J. E. (2018). Directions for Optimization of Photosynthetic Carbon Fixation: RuBisCO's Efficiency May Not Be So Constrained After All. *Front Plant Sci, 9*, 183. doi: 10.3389/fpls.2018.00183

Dai, S., Friemann, R., Glauser, D. A., Bourquin, F., Manieri, W., Schurmann, P., & Eklund, H. (2007). Structural snapshots along the reaction pathway of ferredoxin-thioredoxin reductase. *Nature, 448*(7149), 92-96. doi: 10.1038/nature05937

Dai, S., Johansson, K., Miginiac-Maslow, M., Schurmann, P., & Eklund, H. (2004). Structural Basis of Redox Signaling in Photosynthesis: Structure and Function of Ferredoxin:thioredoxin Reductase and Target Enzymes. *Photosynth Res, 79*(3), 233-248. doi: 10.1023/B:PRES.0000017194.34167.6d

Dang, K. V., Plet, J., Tolleter, D., Jokel, M., Cuine, S., Carrier, P., . . . Peltier, G. (2014). Combined increases in mitochondrial cooperation and oxygen photoreduction compensate for deficiency in cyclic electron flow in Chlamydomonas reinhardtii. *Plant Cell, 26*(7), 3036-3050. doi: 10.1105/tpc.114.126375

Dayer, R., Fischer, B. B., Eggen, R. I., & Lemaire, S. D. (2008). The peroxiredoxin and glutathione peroxidase families in Chlamydomonas reinhardtii. *Genetics, 179*(1), 41-57. doi: 10.1534/genetics.107.086041

de Carpentier, F., Le Peillet, J., Boisset, N. D., Crozet, P., Lemaire, S. D., & Danon, A. (2020). Blasticidin S Deaminase: A New Efficient Selectable Marker for Chlamydomonas reinhardtii. *Front Plant Sci, 11*, 242. doi: 10.3389/fpls.2020.00242

De Mia, M., Lemaire, S. D., Choquet, Y., & Wollman, F. A. (2019). Nitric Oxide Remodels the Photosynthetic Apparatus upon S-Starvation in Chlamydomonas reinhardtii. *Plant Physiol, 179*(2), 718-731. doi: 10.1104/pp.18.01164

Decottignies, P., Schmitter, J. M., Dutka, S., Jacquot, J. P., & Miginiac-Maslow, M. (1991). Characterization and primary structure of a second thioredoxin from the green alga, Chlamydomonas reinhardtii. *Eur J Biochem, 198*(2), 505-512. doi: 10.1111/j.1432-1033.1991.tb16043.x

Decottignies, P., Schmitter, J. M., Jacquot, J. P., Dutka, S., Picaud, A., & Gadal, P. (1990). Purification, characterization, and complete amino acid sequence of a thioredoxin from a green alga, Chlamydomonas reinhardtii. *Arch Biochem Biophys, 280*(1), 112-121. doi: 10.1016/0003-9861(90)90525-4

Desplats, C., Mus, F., Cuine, S., Billon, E., Cournac, L., & Peltier, G. (2009). Characterization of Nda2, a plastoquinone-reducing type II NAD(P)H dehydrogenase in chlamydomonas chloroplasts. *J Biol Chem, 284*(7), 4148-4157. doi: 10.1074/jbc.M804546200

Diaz, M. G., Hernandez-Verdeja, T., Kremnev, D., Crawford, T., Dubreuil, C., & Strand, A. (2018). Redox regulation of PEP activity during seedling establishment in Arabidopsis thaliana. *Nat Commun, 9*(1), 50. doi: 10.1038/s41467-017-02468-2

Dietz, K. J. (2011). Peroxiredoxins in plants and cyanobacteria. *Antioxid Redox Signal, 15*(4), 1129-1159. doi: 10.1089/ars.2010.3657

Ding, F., Wang, M., Zhang, S., & Ai, X. (2016). Changes in SBPase activity influence photosynthetic capacity, growth, and tolerance to chilling stress in transgenic tomato plants. *Sci Rep, 6*, 32741. doi: 10.1038/srep32741

Driever, S. M., Simkin, A. J., Alotaibi, S., Fisk, S. J., Madgwick, P. J., Sparks, C. A., . . . Raines, C. A. (2017). Increased SBPase activity improves photosynthesis and grain yield in wheat grown in greenhouse conditions. *Philos Trans R Soc Lond B Biol Sci, 372*(1730). doi: 10.1098/rstb.2016.0384

Dunford, Roy P., Durrant, Marcus C., Catley, Merryn A., & Dyer, Tristan A. (1998). Location of the redox-active cysteines in chloroplast sedoheptulose-1,7-bisphosphatase indicates that its allosteric regulation is similar but not identical to that of fructose-1,6-bisphosphatase. *Photosynthesis Research, 58*(3), 221-230. doi: 10.1023/a:1006178826976

Durao, P., Aigner, H., Nagy, P., Mueller-Cajar, O., Hartl, F. U., & Hayer-Hartl, M. (2015). Opposing effects of folding and assembly chaperones on evolvability of Rubisco. *Nat Chem Biol, 11*(2), 148-155. doi: 10.1038/nchembio.1715

Endy, Drew. (2011). Building a new biology. *Comptes Rendus Chimie, 14*(4), 424-428. doi: 10.1016/j.crci.2010.11.013

Engel, B. D., Schaffer, M., Kuhn Cuellar, L., Villa, E., Plitzko, J. M., & Baumeister, W. (2015). Native architecture of the Chlamydomonas chloroplast revealed by in situ cryo-electron tomography. *Elife, 4*. doi: 10.7554/eLife.04889

Erales, J., Lignon, S., & Gontero, B. (2009). CP12 from Chlamydomonas reinhardtii, a permanent specific "chaperone-like" protein of glyceraldehyde-3-phosphate dehydrogenase. *J Biol Chem, 284*(19), 12735-12744. doi: 10.1074/jbc.M808254200

Erales, J., Mekhalfi, M., Woudstra, M., & Gontero, B. (2011). Molecular mechanism of NADPH-glyceraldehyde-3-phosphate dehydrogenase regulation through the C-terminus of CP12 in Chlamydomonas reinhardtii. *Biochemistry, 50*(14), 2881-2888. doi: 10.1021/bi1020259

Erb, T. J., & Zarzycki, J. (2016). Biochemical and synthetic biology approaches to improve photosynthetic CO2-fixation. *Curr Opin Chem Biol, 34*, 72-79. doi: 10.1016/j.cbpa.2016.06.026

Evans, E. H., & Carr, N. G. (1979). The Interaction of Respiration and Photosynthesis in Microalgae. In M. Gibbs & E. Latzko (Eds.), *Photosynthesis II* (pp. 163-173). Berlin, Heidelberg: Springer Berlin Heidelberg.

Fang, L., Lin, H. X., Low, C. S., Wu, M. H., Chow, Y., & Lee, Y. K. (2012). Expression of the Chlamydomonas reinhardtii sedoheptulose-1,7-bisphosphatase in Dunaliella bardawil leads to enhanced photosynthesis and increased glycerol production. *Plant Biotechnol J, 10*(9), 1129-1135. doi: 10.1111/pbi.12000

Farr, T. J., Huppe, H. C., & Turpin, D. H. (1994). Coordination of Chloroplastic Metabolism in N-Limited Chlamydomonas reinhardtii by Redox Modulation (I. The Activation of Phosphoribulosekinase and Glucose-6-Phosphate Dehydrogenase Is Relative to the Photosynthetic Supply of Electrons). *Plant Physiol, 105*(4), 1037-1042. doi: 10.1104/pp.105.4.1037

Fermani, S., Ripamonti, A., Sabatino, P., Zanotti, G., Scagliarini, S., Sparla, F., . . . Pupillo, P. (2001). Crystal structure of the non-regulatory A(4)isoform of spinach chloroplast glyceraldehyde-3-

phosphate dehydrogenase complexed with NADP. *J Mol Biol, 314*(3), 527-542. doi: 10.1006/jmbi.2001.5172

Fermani, S., Sparla, F., Falini, G., Martelli, P. L., Casadio, R., Pupillo, P., . . . Trost, P. (2007). Molecular mechanism of thioredoxin regulation in photosynthetic A2B2-glyceraldehyde-3-phosphate dehydrogenase. *Proc Natl Acad Sci U S A, 104*(26), 11109-11114. doi: 10.1073/pnas.0611636104

Fermani, S., Sparla, F., Marri, L., Thumiger, A., Pupillo, P., Falini, G., & Trost, P. (2010). Structure of photosynthetic glyceraldehyde-3-phosphate dehydrogenase (isoform A4) from Arabidopsis thaliana in complex with NAD. *Acta Crystallogr Sect F Struct Biol Cryst Commun, 66*(Pt 6), 621-626. doi: 10.1107/S1744309110013527

Fermani, S., Trivelli, X., Sparla, F., Thumiger, A., Calvaresi, M., Marri, L., . . . Trost, P. (2012). Conformational selection and folding-upon-binding of intrinsically disordered protein CP12 regulate photosynthetic enzymes assembly. *J Biol Chem, 287*(25), 21372-21383. doi: 10.1074/jbc.M112.350355

Ford, M. M., Smythers, A. L., McConnell, E. W., Lowery, S. C., Kolling, D. R. J., & Hicks, L. M. (2019). Inhibition of TOR in Chlamydomonas reinhardtii Leads to Rapid Cysteine Oxidation Reflecting Sustained Physiological Changes. *Cells, 8*(10). doi: 10.3390/cells8101171

Forti, G. (2008). The role of respiration in the activation of photosynthesis upon illumination of dark adapted Chlamydomonas reinhardtii. *Biochim Biophys Acta, 1777*(11), 1449-1454. doi: 10.1016/j.bbabio.2008.08.011

Forti, G., & Elli, G. (1996). Stimulation of Photophosphorylation by Ascorbate as a Function of Light Intensity. *Plant Physiol, 112*(4), 1509-1511. doi: 10.1104/pp.112.4.1509

Forti, G., Furia, A., Bombelli, P., & Finazzi, G. (2003). In vivo changes of the oxidation-reduction state of NADP and of the ATP/ADP cellular ratio linked to the photosynthetic activity in Chlamydomonas reinhardtii. *Plant Physiol, 132*(3), 1464-1474. doi: 10.1104/pp.102.018861

Foyer, C. H., Bloom, A. J., Queval, G., & Noctor, G. (2009). Photorespiratory metabolism: genes, mutants, energetics, and redox signaling. *Annu Rev Plant Biol, 60*, 455-484. doi: 10.1146/annurev.arplant.043008.091948

Foyer, C. H., & Noctor, G. (2005). Redox homeostasis and antioxidant signaling: a metabolic interface between stress perception and physiological responses. *Plant Cell, 17*(7), 1866-1875. doi: 10.1105/tpc.105.033589

Franck, Fabrice, Dinant, M, Cardol, Pierre, Remacle, Claire, & Matagne, René-Fernand. (2008). Importance of the alternative pathway of respiration for avoidance of ROS production and for optimisation of photosynthesis in Chlamydomonas.

Galmes, J., Kapralov, M. V., Andralojc, P. J., Conesa, M. A., Keys, A. J., Parry, M. A., & Flexas, J. (2014). Expanding knowledge of the Rubisco kinetics variability in plant species: environmental and evolutionary trends. *Plant Cell Environ, 37*(9), 1989-2001. doi: 10.1111/pce.12335

Gans, P., & Rebeille, F. (1990). Control in the dark of the plastoquinone redox state by mitochondrial activity in Chlamydomonas reinhardtii. *Biochimica et Biophysica Acta (BBA)-Bioenergetics, 1015*(1), 150-155.

Garcia-Murria, M. J., Karkehabadi, S., Marin-Navarro, J., Satagopan, S., Andersson, I., Spreitzer, R. J., & Moreno, J. (2008). Structural and functional consequences of the replacement of proximal residues Cys(172) and Cys(192) in the large subunit of ribulose-1,5-bisphosphate carboxylase/oxygenase from Chlamydomonas reinhardtii. *Biochem J, 411*(2), 241-247. doi: 10.1042/BJ20071422

Garcia-Murria, M. J., Sudhani, H. P. K., Marin-Navarro, J., Sanchez Del Pino, M. M., & Moreno, J. (2018). Dissecting the individual contribution of conserved cysteines to the redox regulation of RubisCO. *Photosynth Res, 137*(2), 251-262. doi: 10.1007/s11120-018-0497-9

Garcia-Sanchez, M. I., Gotor, C., Jacquot, J. P., Stein, M., Suzuki, A., & Vega, J. M. (1997). Critical residues of Chlamydomonas reinhardtii ferredoxin for interaction with nitrite reductase and glutamate synthase revealed by site-directed mutagenesis. *Eur J Biochem, 250*(2), 364-368. doi: 10.1111/j.1432-1033.1997.0364a.x

Gauthier, DA, & Turpin, DH. (1997). Interactions between inorganic phosphate (Pi) assimilation, photosynthesis and respiration in the Pi-limited green alga Selenastrum minutum. *Plant, Cell & Environment, 20*(1), 12-24.

Geigenberger, P., Kolbe, A., & Tiessen, A. (2005). Redox regulation of carbon storage and partitioning in response to light and sugars. *J Exp Bot, 56*(416), 1469-1479. doi: 10.1093/jxb/eri178

Gerotto, C., Alboresi, A., Meneghesso, A., Jokel, M., Suorsa, M., Aro, E. M., & Morosinotto, T. (2016). Flavodiiron proteins act as safety valve for electrons in Physcomitrella patens. *Proc Natl Acad Sci U S A, 113*(43), 12322-12327. doi: 10.1073/pnas.1606685113

Ghysels, B., Godaux, D., Matagne, R. F., Cardol, P., & Franck, F. (2013). Function of the chloroplast hydrogenase in the microalga Chlamydomonas: the role of hydrogenase and state transitions during photosynthetic activation in anaerobiosis. *PLoS One, 8*(5), e64161. doi: 10.1371/journal.pone.0064161

Gleizer, S., Ben-Nissan, R., Bar-On, Y. M., Antonovsky, N., Noor, E., Zohar, Y., . . . Milo, R. (2019). Conversion of Escherichia coli to Generate All Biomass Carbon from CO2. *Cell, 179*(6), 1255-1263 e1212. doi: 10.1016/j.cell.2019.11.009

Gontero, B., & Avilan, L. (2011). Creating order out of disorder: structural imprint of GAPDH on CP12. *Structure, 19*(12), 1728-1729. doi: 10.1016/j.str.2011.11.004

Gontero, B., Mulliert, G., Rault, M., Giudici-Orticoni, M. T., & Ricard, J. (1993). Structural and functional properties of a multi-enzyme complex from spinach chloroplasts. 2. Modulation of the kinetic properties of enzymes in the aggregated state. *Eur J Biochem, 217*(3), 1075-1082. doi: 10.1111/j.1432-1033.1993.tb18339.x

Goodenough, U., Blaby, I., Casero, D., Gallaher, S. D., Goodson, C., Johnson, S., . . . Wulan, T. (2014). The path to triacylglyceride obesity in the sta6 strain of Chlamydomonas reinhardtii. *Eukaryot Cell, 13*(5), 591-613. doi: 10.1128/EC.00013-14

Goodsell, D. S., Autin, L., & Olson, A. J. (2019). Illustrate: Software for Biomolecular Illustration. *Structure, 27*(11), 1716-1720 e1711. doi: 10.1016/j.str.2019.08.011

Gorman, D. S., & Levine, R. P. (1966). Photosynthetic Electron Transport Chain of Chlamydomonas reinhardi. V. Purification and Properties of Cytochrome 553 and Ferredoxin. *Plant Physiol, 41*(10), 1643-1647. doi: 10.1104/pp.41.10.1643

Goyer, A., Haslekas, C., Miginiac-Maslow, M., Klein, U., Le Marechal, P., Jacquot, J. P., & Decottignies, P. (2002). Isolation and characterization of a thioredoxin-dependent peroxidase from Chlamydomonas reinhardtii. *Eur J Biochem, 269*(1), 272-282. doi: 10.1046/j.0014-2956.2001.02648.x

Graciet, E., Gans, P., Wedel, N., Lebreton, S., Camadro, J. M., & Gontero, B. (2003). The small protein CP12: a protein linker for supramolecular complex assembly. *Biochemistry, 42*(27), 8163-8170. doi: 10.1021/bi034474x

Graciet, E., Lebreton, S., Camadro, J. M., & Gontero, B. (2002). Thermodynamic analysis of the emergence of new regulatory properties in a phosphoribulokinase-glyceraldehyde 3-

phosphate dehydrogenase complex. *J Biol Chem, 277*(15), 12697-12702. doi: 10.1074/jbc.M111121200

Graciet, E., Lebreton, S., & Gontero, B. (2004). Emergence of new regulatory mechanisms in the Benson-Calvin pathway via protein-protein interactions: a glyceraldehyde-3-phosphate dehydrogenase/CP12/phosphoribulokinase complex. *J Exp Bot, 55*(400), 1245-1254. doi: 10.1093/jxb/erh107

Gurrieri, L., Del Giudice, A., Demitri, N., Falini, G., Pavel, N. V., Zaffagnini, M., . . . Fermani, S. (2019). Arabidopsis and Chlamydomonas phosphoribulokinase crystal structures complete the redox structural proteome of the Calvin-Benson cycle. *Proc Natl Acad Sci U S A, 116*(16), 8048-8053. doi: 10.1073/pnas.1820639116

Gutle, D. D., Roret, T., Muller, S. J., Couturier, J., Lemaire, S. D., Hecker, A., . . . Jacquot, J. P. (2016). Chloroplast FBPase and SBPase are thioredoxin-linked enzymes with similar architecture but different evolutionary histories. *Proc Natl Acad Sci U S A, 113*(24), 6779-6784. doi: 10.1073/pnas.1606241113

Hammel, A., Sommer, F., Zimmer, D., Stitt, M., Muhlhaus, T., & Schroda, M. (2020). Overexpression of Sedoheptulose-1,7-Bisphosphatase Enhances Photosynthesis in Chlamydomonas reinhardtii and Has No Effect on the Abundance of Other Calvin-Benson Cycle Enzymes. *Front Plant Sci, 11*, 868. doi: 10.3389/fpls.2020.00868

Hanke, G., & Mulo, P. (2013). Plant type ferredoxins and ferredoxin-dependent metabolism. *Plant Cell Environ, 36*(6), 1071-1084. doi: 10.1111/pce.12046

Hanschmann, E. M., Godoy, J. R., Berndt, C., Hudemann, C., & Lillig, C. H. (2013). Thioredoxins, glutaredoxins, and peroxiredoxins--molecular mechanisms and health significance: from cofactors to antioxidants to redox signaling. *Antioxid Redox Signal, 19*(13), 1539-1605. doi: 10.1089/ars.2012.4599

Hazra, S., Henderson, J. N., Liles, K., Hilton, M. T., & Wachter, R. M. (2015). Regulation of ribulose-1,5-bisphosphate carboxylase/oxygenase (rubisco) activase: product inhibition, cooperativity, and magnesium activation. *J Biol Chem, 290*(40), 24222-24236. doi: 10.1074/jbc.M115.651745

He, S., Chou, H. T., Matthies, D., Wunder, T., Meyer, M. T., Atkinson, N., . . . Jonikas, M. C. (2020). The structural basis of Rubisco phase separation in the pyrenoid. *Nat Plants, 6*(12), 1480-1490. doi: 10.1038/s41477-020-00811-y

Healey, F. P., & Myers, J. (1971). The Kok Effect in Chlamydomonas reinhardi. *Plant Physiol, 47*(3), 373-379. doi: 10.1104/pp.47.3.373

Hertle, A. P., Blunder, T., Wunder, T., Pesaresi, P., Pribil, M., Armbruster, U., & Leister, D. (2013). PGRL1 is the elusive ferredoxin-plastoquinone reductase in photosynthetic cyclic electron flow. *Mol Cell, 49*(3), 511-523. doi: 10.1016/j.molcel.2012.11.030

Hess, D. T., Matsumoto, A., Kim, S. O., Marshall, H. E., & Stamler, J. S. (2005). Protein S-nitrosylation: purview and parameters. *Nat Rev Mol Cell Biol, 6*(2), 150-166. doi: 10.1038/nrm1569

Heyduk, T., Michalczyk, R., & Kochman, M. (1991). Long-range effects and conformational flexibility of aldolase. *J Biol Chem, 266*(24), 15650-15655. doi: 10.1016/S0021-9258(18)98456-5

Hibberd, J. M., Sheehy, J. E., & Langdale, J. A. (2008). Using C4 photosynthesis to increase the yield of rice-rationale and feasibility. *Curr Opin Plant Biol, 11*(2), 228-231. doi: 10.1016/j.pbi.2007.11.002

Hirasawa, M., Schurmann, P., Jacquot, J. P., Manieri, W., Jacquot, P., Keryer, E., . . . Knaff, D. B. (1999). Oxidation-reduction properties of chloroplast thioredoxins, ferredoxin:thioredoxin reductase,

and thioredoxin f-regulated enzymes. *Biochemistry, 38*(16), 5200-5205. doi: 10.1021/bi982783v

Hirasawa, M., Tripathy, J. N., Sommer, F., Somasundaram, R., Chung, J. S., Nestander, M., . . . Knaff, D. B. (2010). Enzymatic properties of the ferredoxin-dependent nitrite reductase from Chlamydomonas reinhardtii. Evidence for hydroxylamine as a late intermediate in ammonia production. *Photosynth Res, 103*(2), 67-77. doi: 10.1007/s11120-009-9512-5

Hoch, G., Owens, O. V., & Kok, B. (1963). Photosynthesis and respiration. *Arch Biochem Biophys, 101*, 171-180. doi: 10.1016/0003-9861(63)90547-2

Hochmal, A. K., Zinzius, K., Charoenwattanasatien, R., Gabelein, P., Mutoh, R., Tanaka, H., . . . Hippler, M. (2016). Calredoxin represents a novel type of calcium-dependent sensor-responder connected to redox regulation in the chloroplast. *Nat Commun, 7*, 11847. doi: 10.1038/ncomms11847

Hogg, N. (2002). The biochemistry and physiology of S-nitrosothiols. *Annu Rev Pharmacol Toxicol, 42*, 585-600. doi: 10.1146/annurev.pharmtox.42.092501.104328

Howard, T. P., Lloyd, J. C., & Raines, C. A. (2011). Inter-species variation in the oligomeric states of the higher plant Calvin cycle enzymes glyceraldehyde-3-phosphate dehydrogenase and phosphoribulokinase. *J Exp Bot, 62*(11), 3799-3805. doi: 10.1093/jxb/err057

Huang, C., Yu, Q. B., Lv, R. H., Yin, Q. Q., Chen, G. Y., Xu, L., & Yang, Z. N. (2013). The reduced plastid-encoded polymerase-dependent plastid gene expression leads to the delayed greening of the Arabidopsis fln2 mutant. *PLoS One, 8*(9), e73092. doi: 10.1371/journal.pone.0073092

Huppe, H. C., & Buchanan, B. B. (1989). Activation of a chloroplast type of fructose bisphosphatase from Chlamydomonas reinhardtii by light-mediated agents. *Z Naturforsch C J Biosci, 44*(5-6), 487-494. doi: 10.1515/znc-1989-5-624

Huppe, H. C., de Lamotte-Guery, F., Jacquot, J. P., & Buchanan, B. B. (1990). The ferredoxin-thioredoxin system of a green alga, Chlamydomonas reinhardtii: identification and characterization of thioredoxins and ferredoxin-thioredoxin reductase components. *Planta, 180*, 341-351. doi: 10.1007/BF00198785

Huppe, H. C., Farr, T. J., & Turpin, D. H. (1994). Coordination of Chloroplastic Metabolism in N-Limited Chlamydomonas reinhardtii by Redox Modulation (II. Redox Modulation Activates the Oxidative Pentose Phosphate Pathway during Photosynthetic Nitrate Assimilation). *Plant Physiol, 105*(4), 1043-1048. doi: 10.1104/pp.105.4.1043

Huppe, H. C., Picaud, A., Buchanan, B. B., & Miginiac-Maslow, M. (1991). Identification of an NADP/thioredoxin system in Chlamydomonas reinhardtii. *Planta, 186*, 115-121. doi: 10.1007/BF00201506

Hurwitz, J., Weissbach, A., Horecker, B. L., & Smyrniotis, P. Z. (1956). Spinach phosphoribulokinase. *J Biol Chem, 218*(2), 769-783. doi: 10.1016/S0021-9258(18)65841-7

Issakidis, E., Lemaire, M., Decottignies, P., Jacquot, J. P., & Miginiac-Maslow, M. (1996). Direct evidence for the different roles of the N- and C-terminal regulatory disulfides of sorghum leaf NADP-malate dehydrogenase in its activation by reduced thioredoxin. *FEBS Lett, 392*(2), 121-124. doi: 10.1016/0014-5793(96)00801-0

Iwaki, T., Haranoh, K., Inoue, N., Kojima, K., Satoh, R., Nishino, T., . . . Wadano, A. (2006). Expression of foreign type I ribulose-1,5-bisphosphate carboxylase/ oxygenase (EC 4.1.1.39) stimulates photosynthesis in cyanobacterium Synechococcus PCC7942 cells. *Photosynth Res, 88*(3), 287-297. doi: 10.1007/s11120-006-9048-x

Jacobs, J., Pudollek, S., Hemschemeier, A., & Happe, T. (2009). A novel, anaerobically induced ferredoxin in Chlamydomonas reinhardtii. *FEBS Lett, 583*(2), 325-329. doi: 10.1016/j.febslet.2008.12.018

Jacquot, J. P., Eklund, H., Rouhier, N., & Schurmann, P. (2009). Structural and evolutionary aspects of thioredoxin reductases in photosynthetic organisms. *Trends Plant Sci, 14*(6), 336-343. doi: 10.1016/j.tplants.2009.03.005

Jacquot, J. P., Lopez-Jaramillo, J., Chueca, A., Cherfils, J., Lemaire, S., Chedozeau, B., . . . Lopez-Gorge, J. (1995). High-level expression of recombinant pea chloroplast fructose-1,6-bisphosphatase and mutagenesis of its regulatory site. *Eur J Biochem, 229*(3), 675-681. doi: 10.1111/j.1432-1033.1995.tb20513.x

Jacquot, J. P., Lopez-Jaramillo, J., Miginiac-Maslow, M., Lemaire, S., Cherfils, J., Chueca, A., & Lopez-Gorge, J. (1997). Cysteine-153 is required for redox regulation of pea chloroplast fructose-1,6-bisphosphatase. *FEBS Lett, 401*(2-3), 143-147. doi: 10.1016/s0014-5793(96)01459-7

Jacquot, J. P., Stein, M., Hodges, M., & Miginiac-Maslow, M. (1992). PCR cloning of a nucleotidic sequence coding for the mature part of Chlamydomonas reinhardtii thioredoxin Ch2. *Nucleic Acids Res, 20*(3), 617. doi: 10.1093/nar/20.3.617

Jacquot, J. P., Stein, M., Suzuki, A., Liottet, S., Sandoz, G., & Miginiac-Maslow, M. (1997). Residue Glu-91 of Chlamydomonas reinhardtii ferredoxin is essential for electron transfer to ferredoxin-thioredoxin reductase. *FEBS Lett, 400*(3), 293-296. doi: 10.1016/s0014-5793(96)01407-x

Jans, F., Mignolet, E., Houyoux, P. A., Cardol, P., Ghysels, B., Cuine, S., . . . Franck, F. (2008). A type II NAD(P)H dehydrogenase mediates light-independent plastoquinone reduction in the chloroplast of Chlamydomonas. *Proc Natl Acad Sci U S A, 105*(51), 20546-20551. doi: 10.1073/pnas.0806896105

Jansen, R., & Gerstein, M. (2000). Analysis of the yeast transcriptome with structural and functional categories: characterizing highly expressed proteins. *Nucleic Acids Res, 28*(6), 1481-1488. doi: 10.1093/nar/28.6.1481

Jebanathirajah, J. A., & Coleman, J. R. (1998). Association of carbonic anhydrase with a Calvin cycle enzyme complex in Nicotiana tabacum. *Planta, 204*(2), 177-182. doi: 10.1007/s004250050244

Johnson, X., & Alric, J. (2012). Interaction between starch breakdown, acetate assimilation, and photosynthetic cyclic electron flow in Chlamydomonas reinhardtii. *Journal of Biological Chemistry, 287*(31), 26445-26452.

Johnson, X., Steinbeck, J., Dent, R. M., Takahashi, H., Richaud, P., Ozawa, S., . . . Alric, J. (2014). Proton gradient regulation 5-mediated cyclic electron flow under ATP- or redox-limited conditions: a study of DeltaATpase pgr5 and DeltarbcL pgr5 mutants in the green alga Chlamydomonas reinhardtii. *Plant Physiol, 165*(1), 438-452. doi: 10.1104/pp.113.233593

Jones, L. W., & Myers, J. (1963). A Common Link between Photosynthesis and Respiration in a Blue-Green Alga. *Nature, 199*, 670-672. doi: 10.1038/199670a0

Kaaki, W., Woudstra, M., Gontero, B., & Halgand, F. (2013). Exploration of CP12 conformational changes and of quaternary structural properties using electrospray ionization traveling wave ion mobility mass spectrometry. *Rapid Commun Mass Spectrom, 27*(1), 179-186. doi: 10.1002/rcm.6442

Kaye, Y., Huang, W., Clowez, S., Saroussi, S., Idoine, A., Sanz-Luque, E., & Grossman, A. R. (2019). The mitochondrial alternative oxidase from *Chlamydomonas reinhardtii* enables survival in high light. *J Biol Chem, 294*(4), 1380-1395. doi: 10.1074/jbc.RA118.004667

Képès, F. (2011). Biologie synthétique et intégrative. *Comptes Rendus Chimie, 14*(4), 420-423. doi: 10.1016/j.crci.2010.11.012

Kerfeld, C. A., & Melnicki, M. R. (2016). Assembly, function and evolution of cyanobacterial carboxysomes. *Curr Opin Plant Biol, 31*, 66-75. doi: 10.1016/j.pbi.2016.03.009

Keryer, E., Collin, V., Lavergne, D., Lemaire, S., & Issakidis-Bourguet, E. (2004). Characterization of Arabidopsis Mutants for the Variable Subunit of Ferredoxin:thioredoxin Reductase. *Photosynth Res, 79*(3), 265-274. doi: 10.1023/B:PRES.0000017173.46185.3e

Kessler, Erich. (1973). Effect of anaerobiosis on photosynthetic reactions and nitrogen metabolism of algae with and without hydrogenase. *Archiv Für Mikrobiologie, 93*(2), 91-100.

Kitayama, K., Kitayama, M., Osafune, T., & Togasaki, R. K. (1999). Subcellular localization of iron and manganese superoxide dismutase in Chlamydomonas reinhardtii (Chlorophyceae). *Journal of phycology, 35*(1), 136-142.

Klein, U. (1986). Compartmentation of glycolysis and of the oxidative pentose-phosphate pathway in Chlamydomonas reinhardii. *Planta, 167*(1), 81-86. doi: 10.1007/BF00446372

Knopf, J. A., & Shapira, M. (2005). Degradation of Rubisco SSU during oxidative stress triggers aggregation of Rubisco particles in Chlamydomonas reinhardtii. *Planta, 222*(5), 787-793. doi: 10.1007/s00425-005-0023-0

Kok, B. (1949). On the interrelation of respiration and photosynthesis in green plants. *Biochimica et Biophysica Acta, 3*, 625-631. doi: https://doi.org/10.1016/0006-3002(49)90136-5

Kong, F., Burlacot, A., Liang, Y., Légeret, B., Alseekh, S., Brotman, Y., . . . Peltier, G. (2018). Interorganelle communication: Peroxisomal MALATE DEHYDROGENASE2 connects lipid catabolism to photosynthesis through redox coupling in Chlamydomonas. *The Plant Cell, 30*(8), 1824-1847.

Krimm, I., Lemaire, S., Ruelland, E., Miginiac-Maslow, M., Jaquot, J. P., Hirasawa, M., . . . Lancelin, J. M. (1998). The single mutation Trp35-->Ala in the 35-40 redox site of Chlamydomonas reinhardtii thioredoxin h affects its biochemical activity and the pH dependence of C36-C39 1H-13C NMR. *Eur J Biochem, 255*(1), 185-195. doi: 10.1046/j.1432-1327.1998.2550185.x

Krishnan, A., Kumaraswamy, G. K., Vinyard, D. J., Gu, H., Ananyev, G., Posewitz, M. C., & Dismukes, G. C. (2015). Metabolic and photosynthetic consequences of blocking starch biosynthesis in the green alga C hlamydomonas reinhardtii sta6 mutant. *The Plant Journal, 81*(6), 947-960.

Kromdijk, J., Glowacka, K., Leonelli, L., Gabilly, S. T., Iwai, M., Niyogi, K. K., & Long, S. P. (2016). Improving photosynthesis and crop productivity by accelerating recovery from photoprotection. *Science, 354*(6314), 857-861. doi: 10.1126/science.aai8878

Kubis, A., & Bar-Even, A. (2019). Synthetic biology approaches for improving photosynthesis. *J Exp Bot, 70*(5), 1425-1433. doi: 10.1093/jxb/erz029

Kuken, A., Sommer, F., Yaneva-Roder, L., Mackinder, L. C., Hohne, M., Geimer, S., . . . Mettler-Altmann, T. (2018). Effects of microcompartmentation on flux distribution and metabolic pools in Chlamydomonas reinhardtii chloroplasts. *Elife, 7*. doi: 10.7554/eLife.37960

Kuo, E. Y., Cai, M. S., & Lee, T. M. (2020). Ascorbate peroxidase 4 plays a role in the tolerance of Chlamydomonas reinhardtii to photo-oxidative stress. *Sci Rep, 10*(1), 13287. doi: 10.1038/s41598-020-70247-z

Kuo, E. Y., Chang, H. L., Lin, S. T., & Lee, T. M. (2020). High Light-Induced Nitric Oxide Production Induces Autophagy and Cell Death in Chlamydomonas reinhardtii. *Front Plant Sci, 11*, 772. doi: 10.3389/fpls.2020.00772

Lancelin, J. M., Guilhaudis, L., Krimm, I., Blackledge, M. J., Marion, D., & Jacquot, J. P. (2000). NMR structures of thioredoxin m from the green alga Chlamydomonas reinhardtii. *Proteins, 41*(3), 334-349. doi: 10.1002/1097-0134(20001115)41:3<334::aid-prot60>3.3.co;2-d

Lancelin, J. M., Stein, M., & Jacquot, J. P. (1993). Secondary structure and protein folding of recombinant chloroplastic thioredoxin Ch2 from the green alga Chlamydomonas reinhardtii as determined by 1H NMR. *J Biochem, 114*(3), 421-431. doi: 10.1093/oxfordjournals.jbchem.a124192

Launay, H., Barre, P., Puppo, C., Manneville, S., Gontero, B., & Receveur-Brechot, V. (2016). Absence of residual structure in the intrinsically disordered regulatory protein CP12 in its reduced state. *Biochem Biophys Res Commun, 477*(1), 20-26. doi: 10.1016/j.bbrc.2016.06.014

Laurent, T. C., Moore, E. C., & Reichard, P. (1964). Enzymatic Synthesis of Deoxyribonucleotides. Iv. Isolation and Characterization of Thioredoxin, the Hydrogen Donor from Escherichia Coli B. *J Biol Chem, 239*, 3436-3444. doi: 10.1016/S0021-9258(18)97742-2

Le Moigne, T., Crozet, P., Lemaire, S. D., & Henri, J. (2020). High-Resolution Crystal Structure of Chloroplastic Ribose-5-Phosphate Isomerase from Chlamydomonas reinhardtii-An Enzyme Involved in the Photosynthetic Calvin-Benson Cycle. *Int J Mol Sci, 21*(20). doi: 10.3390/ijms21207787

Le Moigne, T., Gurrieri, L., Crozet, P., Marchand, C. H., Zaffagnini, M., Sparla, F., . . . Henri, J. (2021). Crystal structure of chloroplastic thioredoxin z defines a type-specific target recognition. *Plant J, 107*(2), 434-447. doi: 10.1111/tpj.15300

Le Moigne, T., Sarti, E., Nourisson, A., Carbone, A., Lemaire, S. D., & Henri, J. (2021). Crystal structure of chloroplast fructose-1,6-bisphosphate aldolase from the green alga Chlamydomonas reinhardtii. *bioRxiv*, 2021.2012.2028.474321. doi: 10.1101/2021.12.28.474321

Lebreton, S., Andreescu, S., Graciet, E., & Gontero, B. (2006). Mapping of the interaction site of CP12 with glyceraldehyde-3-phosphate dehydrogenase from Chlamydomonas reinhardtii. Functional consequences for glyceraldehyde-3-phosphate dehydrogenase. *FEBS J, 273*(14), 3358-3369. doi: 10.1111/j.1742-4658.2006.05342.x

Lebreton, S., Graciet, E., & Gontero, B. (2003). Modulation, via protein-protein interactions, of glyceraldehyde-3-phosphate dehydrogenase activity through redox phosphoribulokinase regulation. *J Biol Chem, 278*(14), 12078-12084. doi: 10.1074/jbc.M213096200

Lecler, R., Vigeolas, H., Emonds-Alt, B., Cardol, P., & Remacle, C. (2012). Characterization of an internal type-II NADH dehydrogenase from Chlamydomonas reinhardtii mitochondria. *Curr Genet, 58*(4), 205-216. doi: 10.1007/s00294-012-0378-2

Ledford, H. K., & Niyogi, K. K. (2005). Singlet oxygen and photo-oxidative stress management in plants and algae. *Plant, Cell & Environment, 28*(8), 1037-1045. doi: 10.1111/j.1365-3040.2005.01374.x

Lee, S., Kim, S. M., & Lee, R. T. (2013). Thioredoxin and thioredoxin target proteins: from molecular mechanisms to functional significance. *Antioxid Redox Signal, 18*(10), 1165-1207. doi: 10.1089/ars.2011.4322

Lefebvre, S., Lawson, T., Zakhleniuk, O. V., Lloyd, J. C., Raines, C. A., & Fryer, M. (2005). Increased sedoheptulose-1,7-bisphosphatase activity in transgenic tobacco plants stimulates photosynthesis and growth from an early stage in development. *Plant Physiol, 138*(1), 451-460. doi: 10.1104/pp.104.055046

Lemaire, S. D., Collin, V., Keryer, E., Issakidis-Bourguet, E., Lavergne, D., & Miginiac-Maslow, M. (2003). Chlamydomonas reinhardtii: a model organism for the study of the thioredoxin family. *Plant Physiology and Biochemistry, 41*(6-7), 513-521. doi: 10.1016/s0981-9428(03)00079-2

Lemaire, S. D., Collin, V., Keryer, E., Quesada, A., & Miginiac-Maslow, M. (2003). Characterization of thioredoxin y, a new type of thioredoxin identified in the genome of Chlamydomonas reinhardtii. *FEBS Lett, 543*(1-3), 87-92. doi: 10.1016/s0014-5793(03)00416-2

Lemaire, S. D., Guillon, B., Le Marechal, P., Keryer, E., Miginiac-Maslow, M., & Decottignies, P. (2004). New thioredoxin targets in the unicellular photosynthetic eukaryote Chlamydomonas reinhardtii. *Proc Natl Acad Sci U S A, 101*(19), 7475-7480. doi: 10.1073/pnas.0402221101

Lemaire, S. D., Michelet, L., Zaffagnini, M., Massot, V., & Issakidis-Bourguet, E. (2007). Thioredoxins in chloroplasts. *Curr Genet, 51*(6), 343-365. doi: 10.1007/s00294-007-0128-z

Lemaire, S. D., & Miginiac-Maslow, M. (2004). The thioredoxin superfamily in Chlamydomonas reinhardtii. *Photosynth Res, 82*(3), 203-220. doi: 10.1007/s11120-004-1091-x

Lemaire, S. D., Miginiac-Maslow, M., & Jacquot, J. P. (2002). Plant thioredoxin gene expression: control by light, circadian clock, and heavy metals. *Methods Enzymol, 347*, 412-421. doi: 10.1016/s0076-6879(02)47041-3

Lemaire, S. D., Quesada, A., Merchan, F., Corral, J. M., Igeno, M. I., Keryer, E., . . . Miginiac-Maslow, M. (2005). NADP-malate dehydrogenase from unicellular green alga Chlamydomonas reinhardtii. A first step toward redox regulation? *Plant Physiol, 137*(2), 514-521. doi: 10.1104/pp.104.052670

Lemaire, S. D., Richardson, J. M., Goyer, A., Keryer, E., Lancelin, J. M., Makhatadze, G. I., & Jacquot, J. P. (2000). Primary structure determinants of the pH- and temperature-dependent aggregation of thioredoxin. *Biochim Biophys Acta, 1476*(2), 311-323. doi: 10.1016/s0167-4838(99)00235-6

Lemaire, S. D., Stein, M., Issakidis-Bourguet, E., Keryer, E., Benoit, V. V., Pineau, B., . . . Jacquot, J. P. (1999). The complex regulation of ferredoxin/thioredoxin-related genes by light and the circadian clock. *Planta, 209*(2), 221-229. doi: 10.1007/s004250050626

Lemaire, S. D., Tedesco, D., Crozet, P., Michelet, L., Fermani, S., Zaffagnini, M., & Henri, J. (2018). Crystal Structure of Chloroplastic Thioredoxin f2 from Chlamydomonas reinhardtii Reveals Distinct Surface Properties. *Antioxidants (Basel), 7*(12). doi: 10.3390/antiox7120171

Lemaire, S., Keryer, E., Stein, M., Schepens, I. I., Issakidis-Bourguet, E., C, G. rard-Hirne, . . . Jacquot, J. P. (1999). Heavy-metal regulation of thioredoxin gene expression in chlamydomonas reinhardtii. *Plant Physiol, 120*(3), 773-778. doi: 10.1104/pp.120.3.773

Lemeille, S., Turkina, M. V., Vener, A. V., & Rochaix, J. D. (2010). Stt7-dependent phosphorylation during state transitions in the green alga Chlamydomonas reinhardtii. *Mol Cell Proteomics, 9*(6), 1281-1295. doi: 10.1074/mcp.M000020-MCP201

Lendzian, K., & Bassham, J. A. (1975). Regulation of glucose-6-phosphate dehydrogenase in spinach chloroplasts by ribulose 1,5-diphosphate and NADPH/NADP+ ratios. *Biochim Biophys Acta, 396*(2), 260-275. doi: 10.1016/0005-2728(75)90040-7

Levine, R. P. (1960). A screening technique for photosynthetic mutants in unicellular algae. *Nature, 188*(4747), 339-340. doi: 10.1038/188339b0

Li, Y., Han, D., Hu, G., Dauvillee, D., Sommerfeld, M., Ball, S., & Hu, Q. (2010). Chlamydomonas starchless mutant defective in ADP-glucose pyrophosphorylase hyper-accumulates triacylglycerol. *Metab Eng, 12*(4), 387-391. doi: 10.1016/j.ymben.2010.02.002

Liang, F., Englund, E., Lindberg, P., & Lindblad, P. (2018). Engineered cyanobacteria with enhanced growth show increased ethanol production and higher biofuel to biomass ratio. *Metab Eng, 46*, 51-59. doi: 10.1016/j.ymben.2018.02.006

Liang, F., & Lindblad, P. (2016). Effects of overexpressing photosynthetic carbon flux control enzymes in the cyanobacterium Synechocystis PCC 6803. *Metab Eng, 38*, 56-64. doi: 10.1016/j.ymben.2016.06.005

Liang, F., & Lindblad, P. (2017). Synechocystis PCC 6803 overexpressing RuBisCO grow faster with increased photosynthesis. *Metab Eng Commun, 4*, 29-36. doi: 10.1016/j.meteno.2017.02.002

Liaud, M. F., Brandt, U., Scherzinger, M., & Cerff, R. (1997). Evolutionary origin of cryptomonad microalgae: two novel chloroplast/cytosol-specific GAPDH genes as potential markers of ancestral endosymbiont and host cell components. *J Mol Evol, 44 Suppl 1*, S28-37. doi: 10.1007/pl00000050

Lin, M. T., Occhialini, A., Andralojc, P. J., Parry, M. A., & Hanson, M. R. (2014). A faster Rubisco with potential to increase photosynthesis in crops. *Nature, 513*(7519), 547-550. doi: 10.1038/nature13776

Liu, K., Yuan, C., Li, H., Chen, K., Lu, L., Shen, C., & Zheng, X. (2018). A qualitative proteome-wide lysine crotonylation profiling of papaya (Carica papaya L.). *Sci Rep, 8*(1), 8230. doi: 10.1038/s41598-018-26676-y

Lmoumene, C. E., Conte, D., Jacquot, J. P., & Houee-Levin, C. (2000). Redox properties of protein disulfide bond in oxidized thioredoxin and lysozyme: a pulse radiolysis study. *Biochemistry, 39*(31), 9295-9301. doi: 10.1021/bi000468e

Long, B. M., Rae, B. D., Rolland, V., Forster, B., & Price, G. D. (2016). Cyanobacterial CO2-concentrating mechanism components: function and prospects for plant metabolic engineering. *Curr Opin Plant Biol, 31*, 1-8. doi: 10.1016/j.pbi.2016.03.002

Long, S. P., Ainsworth, E. A., Rogers, A., & Ort, D. R. (2004). Rising atmospheric carbon dioxide: plants FACE the future. *Annu Rev Plant Biol, 55*, 591-628. doi: 10.1146/annurev.arplant.55.031903.141610

Long, S. P., Marshall-Colon, A., & Zhu, X. G. (2015). Meeting the global food demand of the future by engineering crop photosynthesis and yield potential. *Cell, 161*(1), 56-66. doi: 10.1016/j.cell.2015.03.019

Lucker, B., & Kramer, D. M. (2013). Regulation of cyclic electron flow in Chlamydomonas reinhardtii under fluctuating carbon availability. *Photosynth Res, 117*(1-3), 449-459. doi: 10.1007/s11120-013-9932-0

Mackinder, L. C. M., Chen, C., Leib, R. D., Patena, W., Blum, S. R., Rodman, M., . . . Jonikas, M. C. (2017). A Spatial Interactome Reveals the Protein Organization of the Algal CO2-Concentrating Mechanism. *Cell, 171*(1), 133-147 e114. doi: 10.1016/j.cell.2017.08.044

Mackinder, L. C., Meyer, M. T., Mettler-Altmann, T., Chen, V. K., Mitchell, M. C., Caspari, O., . . . Jonikas, M. C. (2016). A repeat protein links Rubisco to form the eukaryotic carbon-concentrating organelle. *Proc Natl Acad Sci U S A, 113*(21), 5958-5963. doi: 10.1073/pnas.1522866113

Marchand, C. H., Fermani, S., Rossi, J., Gurrieri, L., Tedesco, D., Henri, J., . . . Zaffagnini, M. (2019). Structural and Biochemical Insights into the Reactivity of Thioredoxin h1 from Chlamydomonas reinhardtii. *Antioxidants (Basel), 8*(1). doi: 10.3390/antiox8010010

Marco, P., Elman, T., & Yacoby, I. (2019). Binding of ferredoxin NADP(+) oxidoreductase (FNR) to plant photosystem I. *Biochim Biophys Acta Bioenerg, 1860*(9), 689-698. doi: 10.1016/j.bbabio.2019.07.007

Marco, P., Kozuleva, M., Eilenberg, H., Mazor, Y., Gimeson, P., Kanygin, A., . . . Yacoby, I. (2018). Binding of ferredoxin to algal photosystem I involves a single binding site and is composed of two

thermodynamically distinct events. *Biochim Biophys Acta Bioenerg, 1859*(4), 234-243. doi: 10.1016/j.bbabio.2018.01.001

Marcus, Y., Altman-Gueta, H., Wolff, Y., & Gurevitz, M. (2011). Rubisco mutagenesis provides new insight into limitations on photosynthesis and growth in Synechocystis PCC6803. *J Exp Bot, 62*(12), 4173-4182. doi: 10.1093/jxb/err116

Marin-Navarro, J., & Moreno, J. (2006). Cysteines 449 and 459 modulate the reduction-oxidation conformational changes of ribulose 1.5-bisphosphate carboxylase/oxygenase and the translocation of the enzyme to membranes during stress. *Plant Cell Environ, 29*(5), 898-908. doi: 10.1111/j.1365-3040.2005.01469.x

Marri, L., Pesaresi, A., Valerio, C., Lamba, D., Pupillo, P., Trost, P., & Sparla, F. (2010). In vitro characterization of Arabidopsis CP12 isoforms reveals common biochemical and molecular properties. *J Plant Physiol, 167*(12), 939-950. doi: 10.1016/j.jplph.2010.02.008

Marri, L., Trost, P., Pupillo, P., & Sparla, F. (2005). Reconstitution and properties of the recombinant glyceraldehyde-3-phosphate dehydrogenase/CP12/phosphoribulokinase supramolecular complex of Arabidopsis. *Plant Physiol, 139*(3), 1433-1443. doi: 10.1104/pp.105.068445

Marri, L., Trost, P., Trivelli, X., Gonnelli, L., Pupillo, P., & Sparla, F. (2008). Spontaneous assembly of photosynthetic supramolecular complexes as mediated by the intrinsically unstructured protein CP12. *J Biol Chem, 283*(4), 1831-1838. doi: 10.1074/jbc.M705650200

Marri, L., Zaffagnini, M., Collin, V., Issakidis-Bourguet, E., Lemaire, S. D., Pupillo, P., . . . Trost, P. (2009). Prompt and easy activation by specific thioredoxins of calvin cycle enzymes of Arabidopsis thaliana associated in the GAPDH/CP12/PRK supramolecular complex. *Mol Plant, 2*(2), 259-269. doi: 10.1093/mp/ssn061

Matagne, R. F., Michel-Wolwertz, M. R., Munaut, C., Duyckaerts, C., & Sluse, F. (1989). Induction and characterization of mitochondrial DNA mutants in Chlamydomonas reinhardtii. *J Cell Biol, 108*(4), 1221-1226. doi: 10.1083/jcb.108.4.1221

Mathy, G., Cardol, P., Dinant, M., Blomme, A., Gerin, S., Cloes, M., . . . Sluse, F. E. (2010). Proteomic and functional characterization of a Chlamydomonas reinhardtii mutant lacking the mitochondrial alternative oxidase 1. *J Proteome Res, 9*(6), 2825-2838. doi: 10.1021/pr900866e

McConnell, E. W., Werth, E. G., & Hicks, L. M. (2018). The phosphorylated redox proteome of Chlamydomonas reinhardtii: Revealing novel means for regulation of protein structure and function. *Redox Biol, 17*, 35-46. doi: 10.1016/j.redox.2018.04.003

McFarlane, C. R., Shah, N. R., Kabasakal, B. V., Echeverria, B., Cotton, C. A. R., Bubeck, D., & Murray, J. W. (2019). Structural basis of light-induced redox regulation in the Calvin-Benson cycle in cyanobacteria. *Proc Natl Acad Sci U S A, 116*(42), 20984-20990. doi: 10.1073/pnas.1906722116

Mehrshahi, P., Nguyen, Gtdt, Gorchs Rovira, A., Sayer, A., Llavero-Pasquina, M., Lim Huei Sin, M., . . . Smith, A. G. (2020). Development of Novel Riboswitches for Synthetic Biology in the Green Alga Chlamydomonas. *ACS Synth Biol, 9*(6), 1406-1417. doi: 10.1021/acssynbio.0c00082

Melandri, B. A., Baccarini, A., & Pupillo, P. (1968). Glyceraldehyde-3-phosphate dehydrogenase in photosynthetic tissues: kinetic evidence for competitivity between NADP and NAD. *Biochem Biophys Res Commun, 33*(1), 160-164. doi: 10.1016/0006-291x(68)90272-6

Menchise, V., Corbier, C., Didierjean, C., Jacquot, J. P., Benedetti, E., Saviano, M., & Aubry, A. (2000). Crystal structure of the W35A mutant thioredoxin h from Chlamydomonas reinhardtii: the substitution of the conserved active site Trp leads to modifications in the environment of the two catalytic cysteines. *Biopolymers, 56*(1), 1-7. doi: 10.1002/1097-0282(2000)56:1<1::AID-BIP1036>3.0.CO;2-5

Menchise, V., Corbier, C., Didierjean, C., Saviano, M., Benedetti, E., Jacquot, J. P., & Aubry, A. (2001). Crystal structure of the wild-type and D30A mutant thioredoxin h of Chlamydomonas reinhardtii and implications for the catalytic mechanism. *Biochem J, 359*(Pt 1), 65-75. doi: 10.1042/0264-6021:3590065

Mettler, T., Muhlhaus, T., Hemme, D., Schottler, M. A., Rupprecht, J., Idoine, A., . . . Stitt, M. (2014). Systems Analysis of the Response of Photosynthesis, Metabolism, and Growth to an Increase in Irradiance in the Photosynthetic Model Organism Chlamydomonas reinhardtii. *Plant Cell, 26*(6), 2310-2350. doi: 10.1105/tpc.114.124537

Meyer, Y., Belin, C., Delorme-Hinoux, V., Reichheld, J. P., & Riondet, C. (2012). Thioredoxin and glutaredoxin systems in plants: molecular mechanisms, crosstalks, and functional significance. *Antioxid Redox Signal, 17*(8), 1124-1160. doi: 10.1089/ars.2011.4327

Michelet, L., Zaffagnini, M., Morisse, S., Sparla, F., Perez-Perez, M. E., Francia, F., . . . Lemaire, S. D. (2013). Redox regulation of the Calvin-Benson cycle: something old, something new. *Front Plant Sci, 4*, 470. doi: 10.3389/fpls.2013.00470

Michelet, L., Zaffagnini, M., Vanacker, H., Le Marechal, P., Marchand, C., Schroda, M., . . . Decottignies, P. (2008). In vivo targets of S-thiolation in Chlamydomonas reinhardtii. *J Biol Chem, 283*(31), 21571-21578. doi: 10.1074/jbc.M802331200

Michelet, Laure, Roach, Thomas, Fischer, Beat B, Bedhomme, Mariette, Lemaire, Stephane D, & Krieger-Liszkay, ANJA. (2013). Down-regulation of catalase activity allows transient accumulation of a hydrogen peroxide signal in C hlamydomonas reinhardtii. *Plant, Cell & Environment, 36*(6), 1204-1213.

Mignolet, E., Lecler, R., Ghysels, B., Remacle, C., & Franck, F. (2012). Function of the chloroplastic NAD(P)H dehydrogenase Nda2 for H(2) photoproduction in sulphur-deprived Chlamydomonas reinhardtii. *J Biotechnol, 162*(1), 81-88. doi: 10.1016/j.jbiotec.2012.07.002

Mikkelsen, R., Mutenda, K. E., Mant, A., Schurmann, P., & Blennow, A. (2005). Alpha-glucan, water dikinase (GWD): a plastidic enzyme with redox-regulated and coordinated catalytic activity and binding affinity. *Proc Natl Acad Sci U S A, 102*(5), 1785-1790. doi: 10.1073/pnas.0406674102

Milanez, S., Mural, R. J., & Hartman, F. C. (1991). Roles of cysteinyl residues of phosphoribulokinase as examined by site-directed mutagenesis. *J Biol Chem, 266*(16), 10694-10699. doi: 10.1016/S0021-9258(18)99279-3

Mittard, V., Blackledge, M. J., Stein, M., Jacquot, J. P., Marion, D., & Lancelin, J. M. (1997). NMR solution structure of an oxidised thioredoxin h from the eukaryotic green alga Chlamydomonas reinhardtii. *Eur J Biochem, 243*(1-2), 374-383. doi: 10.1111/j.1432-1033.1997.0374a.x

Mittard, V., Morelle, N., Brutscher, B., Simorre, J. P., Marion, D., Stein, M., . . . Lancelin, J. M. (1995). 1H, 13C, 15N-NMR resonance assignments of oxidized thioredoxin h from the eukaryotic green alga Chlamydomonas reinhardtii using new methods based on two-dimensional triple-resonance NMR spectroscopy and computer-assisted backbone assignment. *Eur J Biochem, 229*(2), 473-485. doi: 10.1111/j.1432-1033.1995.tb20488.x

Miyagawa, Y., Tamoi, M., & Shigeoka, S. (2001). Overexpression of a cyanobacterial fructose-1,6-/sedoheptulose-1,7-bisphosphatase in tobacco enhances photosynthesis and growth. *Nat Biotechnol, 19*(10), 965-969. doi: 10.1038/nbt1001-965

Moll, B., & Levine, R. P. (1970). Characterization of a Photosynthetic Mutant Strain of Chlamydomonas reinhardi Deficient in Phosphoribulokinase Activity. *Plant Physiol, 46*(4), 576-580. doi: 10.1104/pp.46.4.576

Montrichard, F., Alkhalfioui, F., Yano, H., Vensel, W. H., Hurkman, W. J., & Buchanan, B. B. (2009). Thioredoxin targets in plants: the first 30 years. *J Proteomics, 72*(3), 452-474. doi: 10.1016/j.jprot.2008.12.002

Moreno, J., Garcia-Murria, M. J., & Marin-Navarro, J. (2008). Redox modulation of Rubisco conformation and activity through its cysteine residues. *J Exp Bot, 59*(7), 1605-1614. doi: 10.1093/jxb/erm310

Moreno, J., & Spreitzer, R. J. (1999). C172S substitution in the chloroplast-encoded large subunit affects stability and stress-induced turnover of ribulose-1,5-bisphosphate carboxylase/oxygenase. *J Biol Chem, 274*(38), 26789-26793. doi: 10.1074/jbc.274.38.26789

Morisse, S., Michelet, L., Bedhomme, M., Marchand, C. H., Calvaresi, M., Trost, P., . . . Lemaire, S. D. (2014). Thioredoxin-dependent redox regulation of chloroplastic phosphoglycerate kinase from Chlamydomonas reinhardtii. *J Biol Chem, 289*(43), 30012-30024. doi: 10.1074/jbc.M114.597997

Morisse, S., Zaffagnini, M., Gao, X. H., Lemaire, S. D., & Marchand, C. H. (2014). Insight into protein S-nitrosylation in Chlamydomonas reinhardtii. *Antioxid Redox Signal, 21*(9), 1271-1284. doi: 10.1089/ars.2013.5632

Mosebach, L., Heilmann, C., Mutoh, R., Gabelein, P., Steinbeck, J., Happe, T., . . . Hippler, M. (2017). Association of Ferredoxin:NADP(+) oxidoreductase with the photosynthetic apparatus modulates electron transfer in Chlamydomonas reinhardtii. *Photosynth Res, 134*(3), 291-306. doi: 10.1007/s11120-017-0408-5

Mussgnug, J. H., Thomas-Hall, S., Rupprecht, J., Foo, A., Klassen, V., McDowall, A., . . . Hankamer, B. (2007). Engineering photosynthetic light capture: impacts on improved solar energy to biomass conversion. *Plant Biotechnol J, 5*(6), 802-814. doi: 10.1111/j.1467-7652.2007.00285.x

Navrot, N., Gelhaye, E., Jacquot, J. P., & Rouhier, N. (2006). Identification of a new family of plant proteins loosely related to glutaredoxins with four CxxC motives. *Photosynth Res, 89*(2-3), 71-79. doi: 10.1007/s11120-006-9083-7

Nawrocki, W. J., Bailleul, B., Picot, D., Cardol, P., Rappaport, F., Wollman, F. A., & Joliot, P. (2019). The mechanism of cyclic electron flow. *Biochim Biophys Acta Bioenerg, 1860*(5), 433-438. doi: 10.1016/j.bbabio.2018.12.005

Nee, G., Zaffagnini, M., Trost, P., & Issakidis-Bourguet, E. (2009). Redox regulation of chloroplastic glucose-6-phosphate dehydrogenase: a new role for f-type thioredoxin. *FEBS Lett, 583*(17), 2827-2832. doi: 10.1016/j.febslet.2009.07.035

Nikolova, D., Heilmann, C., Hawat, S., Gabelein, P., & Hippler, M. (2018). Absolute quantification of selected photosynthetic electron transfer proteins in Chlamydomonas reinhardtii in the presence and absence of oxygen. *Photosynth Res, 137*(2), 281-293. doi: 10.1007/s11120-018-0502-3

Nishizawa, A. N., & Buchanan, B. B. (1981). Enzyme regulation in C4 photosynthesis. Purification and properties of thioredoxin-linked fructose bisphosphatase and sedoheptulose bisphosphatase from corn leaves. *J Biol Chem, 256*(12), 6119-6126. doi: 10.1016/S0021-9258(19)69136-2

Ogawa, T., Tamoi, M., Kimura, A., Mine, A., Sakuyama, H., Yoshida, E., . . . Shigeoka, S. (2015). Enhancement of photosynthetic capacity in Euglena gracilis by expression of cyanobacterial fructose-1,6-/sedoheptulose-1,7-bisphosphatase leads to increases in biomass and wax ester production. *Biotechnol Biofuels, 8*, 80. doi: 10.1186/s13068-015-0264-5

Ort, D. R., & Melis, A. (2011). Optimizing antenna size to maximize photosynthetic efficiency. *Plant Physiol, 155*(1), 79-85. doi: 10.1104/pp.110.165886

Ort, D. R., Merchant, S. S., Alric, J., Barkan, A., Blankenship, R. E., Bock, R., . . . Zhu, X. G. (2015). Redesigning photosynthesis to sustainably meet global food and bioenergy demand. *Proc Natl Acad Sci U S A, 112*(28), 8529-8536. doi: 10.1073/pnas.1424031112

Page, M. D., Allen, M. D., Kropat, J., Urzica, E. I., Karpowicz, S. J., Hsieh, S. I., . . . Merchant, S. S. (2012). Fe sparing and Fe recycling contribute to increased superoxide dismutase capacity in iron-starved Chlamydomonas reinhardtii. *Plant Cell, 24*(6), 2649-2665. doi: 10.1105/tpc.112.098962

Parry, M. A., Andralojc, P. J., Scales, J. C., Salvucci, M. E., Carmo-Silva, A. E., Alonso, H., & Whitney, S. M. (2013). Rubisco activity and regulation as targets for crop improvement. *J Exp Bot, 64*(3), 717-730. doi: 10.1093/jxb/ers336

Pasquini, M., Fermani, S., Tedesco, D., Sciabolini, C., Crozet, P., Naldi, M., . . . Francia, F. (2017). Structural basis for the magnesium-dependent activation of transketolase from Chlamydomonas reinhardtii. *Biochim Biophys Acta Gen Subj, 1861*(8), 2132-2145. doi: 10.1016/j.bbagen.2017.05.021

Peden, E. A., Boehm, M., Mulder, D. W., Davis, R., Old, W. M., King, P. W., . . . Dubini, A. (2013). Identification of global ferredoxin interaction networks in Chlamydomonas reinhardtii. *J Biol Chem, 288*(49), 35192-35209. doi: 10.1074/jbc.M113.483727

Pedersen, T. A., Kirk, Martha, & Bassham, J. A. (1966). Light-Dark Transients in Levels of Intermediate Compounds during Photosynthesis in Air-Adapted Chlorella. *Physiologia Plantarum, 19*(1), 219-231. doi: 10.1111/j.1399-3054.1966.tb09094.x

Peltier, G., Aro, E. M., & Shikanai, T. (2016). NDH-1 and NDH-2 Plastoquinone Reductases in Oxygenic Photosynthesis. *Annu Rev Plant Biol, 67*, 55-80. doi: 10.1146/annurev-arplant-043014-114752

Peltier, G., & Thibault, P. (1985). O(2) uptake in the light in chlamydomonas: evidence for persistent mitochondrial respiration. *Plant Physiol, 79*(1), 225-230. doi: 10.1104/pp.79.1.225

Perez-Perez, M. E., Lemaire, S. D., & Crespo, J. L. (2016). Control of Autophagy in Chlamydomonas Is Mediated through Redox-Dependent Inactivation of the ATG4 Protease. *Plant Physiol, 172*(4), 2219-2234. doi: 10.1104/pp.16.01582

Perez-Perez, M. E., Martin-Figueroa, E., & Florencio, F. J. (2009). Photosynthetic regulation of the cyanobacterium Synechocystis sp. PCC 6803 thioredoxin system and functional analysis of TrxB (Trx x) and TrxQ (Trx y) thioredoxins. *Mol Plant, 2*(2), 270-283. doi: 10.1093/mp/ssn070

Perez-Perez, M. E., Mauries, A., Maes, A., Tourasse, N. J., Hamon, M., Lemaire, S. D., & Marchand, C. H. (2017). The Deep Thioredoxome in Chlamydomonas reinhardtii: New Insights into Redox Regulation. *Mol Plant, 10*(8), 1107-1125. doi: 10.1016/j.molp.2017.07.009

Perez-Perez, M. E., Zaffagnini, M., Marchand, C. H., Crespo, J. L., & Lemaire, S. D. (2014). The yeast autophagy protease Atg4 is regulated by thioredoxin. *Autophagy, 10*(11), 1953-1964. doi: 10.4161/auto.34396

Perez-Ruiz, J. M., Naranjo, B., Ojeda, V., Guinea, M., & Cejudo, F. J. (2017). NTRC-dependent redox balance of 2-Cys peroxiredoxins is needed for optimal function of the photosynthetic apparatus. *Proc Natl Acad Sci U S A, 114*(45), 12069-12074. doi: 10.1073/pnas.1706003114

Petersen, J., Teich, R., Becker, B., Cerff, R., & Brinkmann, H. (2006). The GapA/B gene duplication marks the origin of Streptophyta (charophytes and land plants). *Mol Biol Evol, 23*(6), 1109-1118. doi: 10.1093/molbev/msj123

Petzold, C. J., Chan, L. J., Nhan, M., & Adams, P. D. (2015). Analytics for Metabolic Engineering. *Front Bioeng Biotechnol, 3*, 135. doi: 10.3389/fbioe.2015.00135

Pinnola, A., & Bassi, R. (2018). Molecular mechanisms involved in plant photoprotection. *Biochem Soc Trans, 46*(2), 467-482. doi: 10.1042/BST20170307

Porter, M. A., & Hartman, F. C. (1990). Exploration of the function of a regulatory sulfhydryl of phosphoribulokinase from spinach. *Arch Biochem Biophys, 281*(2), 330-334. doi: 10.1016/0003-9861(90)90452-5

Porter, M. A., Milanez, S., Stringer, C. D., & Hartman, F. C. (1986). Purification and characterization of ribulose-5-phosphate kinase from spinach. *Arch Biochem Biophys, 245*(1), 14-23. doi: 10.1016/0003-9861(86)90185-2

Portis, A. R., Jr. (2003). Rubisco activase - Rubisco's catalytic chaperone. *Photosynth Res, 75*(1), 11-27. doi: 10.1023/A:1022458108678

Portis, A. R., Jr., & Heldt, H. W. (1976). Light-dependent changes of the Mg2+ concentration in the stroma in relation to the Mg2+ dependency of CO2 fixation in intact chloroplasts. *Biochim Biophys Acta, 449*(3), 434-436. doi: 10.1016/0005-2728(76)90154-7

Portis, A. R., Jr., Li, C., Wang, D., & Salvucci, M. E. (2008). Regulation of Rubisco activase and its interaction with Rubisco. *J Exp Bot, 59*(7), 1597-1604. doi: 10.1093/jxb/erm240

Puzanskiy, R. K., Romanyuk, D. A., Kirpichnikova, A. A., & Shishova, M. F. (2020). [Alteration in the Expression of Genes Encoding Primary Metabolism Enzymes and Plastid Transporters during the Culture Growth of Chlamydomonas reinhardtii]. *Mol Biol (Mosk), 54*(4), 562-579. doi: 10.31857/S0026898420040151

Rae, B. D., Long, B. M., Forster, B., Nguyen, N. D., Velanis, C. N., Atkinson, N., . . . McCormick, A. J. (2017). Progress and challenges of engineering a biophysical CO2-concentrating mechanism into higher plants. *J Exp Bot, 68*(14), 3717-3737. doi: 10.1093/jxb/erx133

Rae, B. D., Long, B. M., Whitehead, L. F., Forster, B., Badger, M. R., & Price, G. D. (2013). Cyanobacterial carboxysomes: microcompartments that facilitate CO2 fixation. *J Mol Microbiol Biotechnol, 23*(4-5), 300-307. doi: 10.1159/000351342

Raines, C. A. (2003). The Calvin cycle revisited. *Photosynth Res, 75*(1), 1-10. doi: 10.1023/A:1022421515027

Raines, C. A. (2006). Transgenic approaches to manipulate the environmental responses of the C3 carbon fixation cycle. *Plant Cell Environ, 29*(3), 331-339. doi: 10.1111/j.1365-3040.2005.01488.x

Raines, C. A. (2011). Increasing photosynthetic carbon assimilation in C3 plants to improve crop yield: current and future strategies. *Plant Physiol, 155*(1), 36-42. doi: 10.1104/pp.110.168559

Rault, M., Giudici-Orticoni, M. T., Gontero, B., & Ricard, J. (1993). Structural and functional properties of a multi-enzyme complex from spinach chloroplasts. 1. Stoichiometry of the polypeptide chains. *Eur J Biochem, 217*(3), 1065-1073. doi: 10.1111/j.1432-1033.1993.tb18338.x

Raven, J. A., Beardall, J., & Sanchez-Baracaldo, P. (2017). The possible evolution and future of CO2-concentrating mechanisms. *J Exp Bot, 68*(14), 3701-3716. doi: 10.1093/jxb/erx110

Raven, J. A., Cockell, C. S., & De La Rocha, C. L. (2008). The evolution of inorganic carbon concentrating mechanisms in photosynthesis. *Philos Trans R Soc Lond B Biol Sci, 363*(1504), 2641-2650. doi: 10.1098/rstb.2008.0020

Raven, J. A., Giordano, M., Beardall, J., & Maberly, S. C. (2012). Algal evolution in relation to atmospheric CO2: carboxylases, carbon-concentrating mechanisms and carbon oxidation cycles. *Philos Trans R Soc Lond B Biol Sci, 367*(1588), 493-507. doi: 10.1098/rstb.2011.0212

Raven, John A., & Beardall, John. (2003). Carbohydrate Metabolism and Respiration in Algae. In Larkum A.W.D., Douglas S.E. & R. J.A. (Eds.), *Photosynthesis in Algae* (Vol. 14, pp. 205-224). Springer, Dordrecht.

Rebeille, Fabrice, & Gans, Pierre. (1988). Interaction between chloroplasts and mitochondria in microalgae: role of glycolysis. *Plant physiology, 88*(4), 973-975.

Ricard, J., Giudici-Orticoni, M. T., & Buc, J. (1990). Thermodynamics of information transfer between subunits in oligomeric enzymes and kinetic cooperativity. 1. Thermodynamics of subunit interactions, partition functions and enzyme reaction rate. *Eur J Biochem, 194*(2), 463-473. doi: 10.1111/j.1432-1033.1990.tb15640.x

Ricard, J., Giudici-Orticoni, M. T., & Gontero, B. (1994). The modulation of enzyme reaction rates within multi-enzyme complexes. 1. Statistical thermodynamics of information transfer through multi-enzyme complexes. *Eur J Biochem, 226*(3), 993-998. doi: 10.1111/j.1432-1033.1994.00993.x

Richardson, J. M., 3rd, Lemaire, S. D., Jacquot, J. P., & Makhatadze, G. I. (2000). Difference in the mechanisms of the cold and heat induced unfolding of thioredoxin h from Chlamydomonas reinhardtii: spectroscopic and calorimetric studies. *Biochemistry, 39*(36), 11154-11162. doi: 10.1021/bi000610b

Robbens, S., Petersen, J., Brinkmann, H., Rouze, P., & Van de Peer, Y. (2007). Unique regulation of the Calvin cycle in the ultrasmall green alga Ostreococcus. *J Mol Evol, 64*(5), 601-604. doi: 10.1007/s00239-006-0159-y

Rodriguez-Suarez, R. J., Mora-Garcia, S., & Wolosiuk, R. A. (1997). Characterization of cysteine residues involved in the reductive activation and the structural stability of rapeseed (Brassica napus) chloroplast fructose-1,6-bisphosphatase. *Biochem Biophys Res Commun, 232*(2), 388-393. doi: 10.1006/bbrc.1997.6242

Rolland, N., Atteia, A., Decottignies, P., Garin, J., Hippler, M., Kreimer, G., . . . Wagner, V. (2009). Chlamydomonas proteomics. *Curr Opin Microbiol, 12*(3), 285-291. doi: 10.1016/j.mib.2009.04.001

Romanova, A. K., Semenova, G. A., Ignat'ev, A. R., Novichkova, N. S., & Fomina, I. R. (2016). Biochemistry and cell ultrastructure changes during senescence of Beta vulgaris L. leaf. *Protoplasma, 253*(3), 719-727. doi: 10.1007/s00709-015-0923-1

Rosenthal, D. M., Locke, A. M., Khozaei, M., Raines, C. A., Long, S. P., & Ort, D. R. (2011). Over-expressing the C(3) photosynthesis cycle enzyme Sedoheptulose-1-7 Bisphosphatase improves photosynthetic carbon gain and yield under fully open air CO(2) fumigation (FACE). *BMC Plant Biol, 11*, 123. doi: 10.1186/1471-2229-11-123

Rosgaard, L., de Porcellinis, A. J., Jacobsen, J. H., Frigaard, N. U., & Sakuragi, Y. (2012). Bioengineering of carbon fixation, biofuels, and biochemicals in cyanobacteria and plants. *J Biotechnol, 162*(1), 134-147. doi: 10.1016/j.jbiotec.2012.05.006

Rouhier, N., Lemaire, S. D., & Jacquot, J. P. (2008). The role of glutathione in photosynthetic organisms: emerging functions for glutaredoxins and glutathionylation. *Annu Rev Plant Biol, 59*, 143-166. doi: 10.1146/annurev.arplant.59.032607.092811

Roustan, V., Bakhtiari, S., Roustan, P. J., & Weckwerth, W. (2017). Quantitative in vivo phosphoproteomics reveals reversible signaling processes during nitrogen starvation and recovery in the biofuel model organism Chlamydomonas reinhardtii. *Biotechnol Biofuels, 10*, 280. doi: 10.1186/s13068-017-0949-z

Roustan, V., & Weckwerth, W. (2018). Quantitative Phosphoproteomic and System-Level Analysis of TOR Inhibition Unravel Distinct Organellar Acclimation in Chlamydomonas reinhardtii. *Front Plant Sci, 9*, 1590. doi: 10.3389/fpls.2018.01590

Ruelland, E., & Miginiac-Maslow, M. (1999). Regulation of chloroplast enzyme activities by thioredoxins: activation or relief from inhibition? *Trends Plant Sci, 4*(4), 136-141. doi: 10.1016/s1360-1385(99)01391-6

Sainis, J. K., & Harris, G. C. (1986). The association of ribulose-1,5-bisphosphate carboxylase with phosphoriboisomerase and phosphoribulokinase. *Biochem Biophys Res Commun, 139*(3), 947-954. doi: 10.1016/s0006-291x(86)80269-8

Salvucci, M. E., Werneke, J. M., Ogren, W. L., & Portis, A. R. (1987). Purification and species distribution of rubisco activase. *Plant Physiol, 84*(3), 930-936. doi: 10.1104/pp.84.3.930

Santos-Merino, M., Torrado, A., Davis, G. A., Rottig, A., Bibby, T. S., Kramer, D. M., & Ducat, D. C. (2021). Improved photosynthetic capacity and photosystem I oxidation via heterologous metabolism engineering in cyanobacteria. *Proc Natl Acad Sci U S A, 118*(11). doi: 10.1073/pnas.2021523118

Sanz-Luque, E., Ocana-Calahorro, F., Llamas, A., Galvan, A., & Fernandez, E. (2013). Nitric oxide controls nitrate and ammonium assimilation in Chlamydomonas reinhardtii. *J Exp Bot, 64*(11), 3373-3383. doi: 10.1093/jxb/ert175

Saroussi, S. I., Wittkopp, T. M., & Grossman, A. R. (2016). The Type II NADPH Dehydrogenase Facilitates Cyclic Electron Flow, Energy-Dependent Quenching, and Chlororespiratory Metabolism during Acclimation of Chlamydomonas reinhardtii to Nitrogen Deprivation. *Plant Physiol, 170*(4), 1975-1988. doi: 10.1104/pp.15.02014

Sasaki, Y., Kozaki, A., & Hatano, M. (1997). Link between light and fatty acid synthesis: thioredoxin-linked reductive activation of plastidic acetyl-CoA carboxylase. *Proc Natl Acad Sci U S A, 94*(20), 11096-11101. doi: 10.1073/pnas.94.20.11096

Satanowski, A., Dronsella, B., Noor, E., Vogeli, B., He, H., Wichmann, P., . . . Bar-Even, A. (2020). Awakening a latent carbon fixation cycle in Escherichia coli. *Nat Commun, 11*(1), 5812. doi: 10.1038/s41467-020-19564-5

Savir, Y., Noor, E., Milo, R., & Tlusty, T. (2010). Cross-species analysis traces adaptation of Rubisco toward optimality in a low-dimensional landscape. *Proc Natl Acad Sci U S A, 107*(8), 3475-3480. doi: 10.1073/pnas.0911663107

Sawyer, A., & Winkler, M. (2017). Evolution of Chlamydomonas reinhardtii ferredoxins and their interactions with [FeFe]-hydrogenases. *Photosynth Res, 134*(3), 307-316. doi: 10.1007/s11120-017-0409-4

Scagliarini, Sandra, Trost, Paolo, Pupillo, Paolo, & Valenti, Vincenzo. (1993). Light activation and molecular-mass changes of NAD(P)-glyceraldehyde 3-phosphate dehydrogenase of spinach and maize leaves. *Planta, 190*(3), 313-319. doi: 10.1007/bf00196959

Schmollinger, S., Muhlhaus, T., Boyle, N. R., Blaby, I. K., Casero, D., Mettler, T., . . . Merchant, S. S. (2014). Nitrogen-Sparing Mechanisms in Chlamydomonas Affect the Transcriptome, the Proteome, and Photosynthetic Metabolism. *Plant Cell, 26*(4), 1410-1435. doi: 10.1105/tpc.113.122523

Schroda, M., Hemme, D., & Muhlhaus, T. (2015). The Chlamydomonas heat stress response. *Plant J, 82*(3), 466-480. doi: 10.1111/tpj.12816

Schroter, Y., Steiner, S., Matthai, K., & Pfannschmidt, T. (2010). Analysis of oligomeric protein complexes in the chloroplast sub-proteome of nucleic acid-binding proteins from mustard reveals potential redox regulators of plastid gene expression. *Proteomics, 10*(11), 2191-2204. doi: 10.1002/pmic.200900678

Schuler, M. L., Mantegazza, O., & Weber, A. P. (2016). Engineering C4 photosynthesis into C3 chassis in the synthetic biology age. *Plant J, 87*(1), 51-65. doi: 10.1111/tpj.13155

Schurmann, P. (2002). Ferredoxin-dependent thioredoxin reductase: a unique iron-sulfur protein. *Methods Enzymol, 347*, 403-411. doi: 10.1016/s0076-6879(02)47040-1

Schurmann, P., & Buchanan, B. B. (2008). The ferredoxin/thioredoxin system of oxygenic photosynthesis. *Antioxid Redox Signal, 10*(7), 1235-1274. doi: 10.1089/ars.2007.1931

Schwander, T., Schada von Borzyskowski, L., Burgener, S., Cortina, N. S., & Erb, T. J. (2016). A synthetic pathway for the fixation of carbon dioxide in vitro. *Science, 354*(6314), 900-904. doi: 10.1126/science.aah5237

Sekiguchi, T., Yoshida, K., Okegawa, Y., Motohashi, K., Wakabayashi, K. I., & Hisabori, T. (2020). Chloroplast ATP synthase is reduced by both f-type and m-type thioredoxins. *Biochim Biophys Acta Bioenerg, 1861*(11), 148261. doi: 10.1016/j.bbabio.2020.148261

Selinski, J., & Scheibe, R. (2019). Malate valves: old shuttles with new perspectives. *Plant Biol (Stuttg), 21 Suppl 1*, 21-30. doi: 10.1111/plb.12869

Sengupta, R., & Holmgren, A. (2014). Thioredoxin and glutaredoxin-mediated redox regulation of ribonucleotide reductase. *World J Biol Chem, 5*(1), 68-74. doi: 10.4331/wjbc.v5.i1.68

Serrato, A. J., Fernandez-Trijueque, J., Barajas-Lopez, J. D., Chueca, A., & Sahrawy, M. (2013). Plastid thioredoxins: a "one-for-all" redox-signaling system in plants. *Front Plant Sci, 4*, 463. doi: 10.3389/fpls.2013.00463

Setlik, I., Ried, A., & Berkova, E. (1973). *Czech. Acad. Sci. Inst. Microbiol. Annu. Rep. Lab. Algol.*

Setterdahl, A. T., Chivers, P. T., Hirasawa, M., Lemaire, S. D., Keryer, E., Miginiac-Maslow, M., . . . Knaff, D. B. (2003). Effect of pH on the oxidation-reduction properties of thioredoxins. *Biochemistry, 42*(50), 14877-14884. doi: 10.1021/bi0302088

Shao, N., Beck, C. F., Lemaire, S. D., & Krieger-Liszkay, A. (2008). Photosynthetic electron flow affects H2O2 signaling by inactivation of catalase in Chlamydomonas reinhardtii. *Planta, 228*(6), 1055-1066. doi: 10.1007/s00425-008-0807-0

Shimakawa, G., Ishizaki, K., Tsukamoto, S., Tanaka, M., Sejima, T., & Miyake, C. (2017). The Liverwort, Marchantia, Drives Alternative Electron Flow Using a Flavodiiron Protein to Protect PSI. *Plant Physiol, 173*(3), 1636-1647. doi: 10.1104/pp.16.01038

Sicard-Roselli, C., Lemaire, S., Jacquot, J. P., Favaudon, V., Marchand, C., & Houee-Levin, C. (2004). Thioredoxin Ch1 of Chlamydomonas reinhardtii displays an unusual resistance toward one-electron oxidation. *Eur J Biochem, 271*(17), 3481-3487. doi: 10.1111/j.1432-1033.2004.04279.x

Simkin, A. J., Lopez-Calcagno, P. E., Davey, P. A., Headland, L. R., Lawson, T., Timm, S., . . . Raines, C. A. (2017). Simultaneous stimulation of sedoheptulose 1,7-bisphosphatase, fructose 1,6-bisphophate aldolase and the photorespiratory glycine decarboxylase-H protein increases CO2 assimilation, vegetative biomass and seed yield in Arabidopsis. *Plant Biotechnol J, 15*(7), 805-816. doi: 10.1111/pbi.12676

Simkin, A. J., Lopez-Calcagno, P. E., & Raines, C. A. (2019). Feeding the world: improving photosynthetic efficiency for sustainable crop production. *J Exp Bot, 70*(4), 1119-1140. doi: 10.1093/jxb/ery445

Simkin, A. J., McAusland, L., Headland, L. R., Lawson, T., & Raines, C. A. (2015). Multigene manipulation of photosynthetic carbon assimilation increases CO2 fixation and biomass yield in tobacco. *J Exp Bot, 66*(13), 4075-4090. doi: 10.1093/jxb/erv204

Slade, W. O., Werth, E. G., McConnell, E. W., Alvarez, S., & Hicks, L. M. (2015). Quantifying reversible oxidation of protein thiols in photosynthetic organisms. *J Am Soc Mass Spectrom, 26*(4), 631-640. doi: 10.1007/s13361-014-1073-y

South, P. F., Cavanagh, A. P., Liu, H. W., & Ort, D. R. (2019). Synthetic glycolate metabolism pathways stimulate crop growth and productivity in the field. *Science, 363*(6422). doi: 10.1126/science.aat9077

Sparla, F., Costa, A., Lo Schiavo, F., Pupillo, P., & Trost, P. (2006). Redox regulation of a novel plastid-targeted beta-amylase of Arabidopsis. *Plant Physiol, 141*(3), 840-850. doi: 10.1104/pp.106.079186

Sparla, F., Fermani, S., Falini, G., Zaffagnini, M., Ripamonti, A., Sabatino, P., . . . Trost, P. (2004). Coenzyme site-directed mutants of photosynthetic A4-GAPDH show selectively reduced NADPH-dependent catalysis, similar to regulatory AB-GAPDH inhibited by oxidized thioredoxin. *J Mol Biol, 340*(5), 1025-1037. doi: 10.1016/j.jmb.2004.06.005

Sparla, F., Pupillo, P., & Trost, P. (2002). The C-terminal extension of glyceraldehyde-3-phosphate dehydrogenase subunit B acts as an autoinhibitory domain regulated by thioredoxins and nicotinamide adenine dinucleotide. *J Biol Chem, 277*(47), 44946-44952. doi: 10.1074/jbc.M206873200

Sparla, F., Zaffagnini, M., Wedel, N., Scheibe, R., Pupillo, P., & Trost, P. (2005). Regulation of photosynthetic GAPDH dissected by mutants. *Plant Physiol, 138*(4), 2210-2219. doi: 10.1104/pp.105.062117

Spreitzer, R. J., & Salvucci, M. E. (2002). Rubisco: structure, regulatory interactions, and possibilities for a better enzyme. *Annu Rev Plant Biol, 53*, 449-475. doi: 10.1146/annurev.arplant.53.100301.135233

Stein, M., Jacquot, J. P., Jeannette, E., Decottignies, P., Hodges, M., Lancelin, J. M., . . . Miginiac-Maslow, M. (1995). *Chlamydomonas reinhardtii* thioredoxins: structure of the genes coding for the chloroplastic m and cytosolic h isoforms; expression in Escherichia coli of the recombinant proteins, purification and biochemical properties. *Plant Mol Biol, 28*(3), 487-503. doi: 10.1007/BF00020396

Stitt, M., Lunn, J., & Usadel, B. (2010). Arabidopsis and primary photosynthetic metabolism - more than the icing on the cake. *Plant J, 61*(6), 1067-1091. doi: 10.1111/j.1365-313X.2010.04142.x

Stitt, M., & Schulze, D. (1994). Does Rubisco control the rate of photosynthesis and plant growth? An exercise in molecular ecophysiology. *Plant, Cell and Environment, 17*(5), 465-487. doi: 10.1111/j.1365-3040.1994.tb00144.x

Strenkert, D., Schmollinger, S., Gallaher, S. D., Salome, P. A., Purvine, S. O., Nicora, C. D., . . . Merchant, S. S. (2019). Multiomics resolution of molecular events during a day in the life of Chlamydomonas. *Proc Natl Acad Sci U S A, 116*(6), 2374-2383. doi: 10.1073/pnas.1815238116

Subramanian, V., Wecker, M. S. A., Gerritsen, A., Boehm, M., Xiong, W., Wachter, B., . . . Ghirardi, M. L. (2019). Ferredoxin5 Deletion Affects Metabolism of Algae during the Different Phases of Sulfur Deprivation. *Plant Physiol, 181*(2), 426-441. doi: 10.1104/pp.19.00457

Sun, H., Liu, X., Li, F., Li, W., Zhang, J., Xiao, Z., . . . Yang, J. (2017). First comprehensive proteome analysis of lysine crotonylation in seedling leaves of Nicotiana tabacum. *Sci Rep, 7*(1), 3013. doi: 10.1038/s41598-017-03369-6

Sun, J., Qiu, C., Qian, W., Wang, Y., Sun, L., Li, Y., & Ding, Z. (2019). Ammonium triggered the response mechanism of lysine crotonylome in tea plants. *BMC Genomics, 20*(1), 340. doi: 10.1186/s12864-019-5716-z

Sun, Y., Valente-Paterno, M., Bakhtiari, S., Law, C., Zhan, Y., & Zerges, W. (2019). Photosystem Biogenesis Is Localized to the Translation Zone in the Chloroplast of Chlamydomonas. *Plant Cell, 31*(12), 3057-3072. doi: 10.1105/tpc.19.00263

Suss, K. H., Arkona, C., Manteuffel, R., & Adler, K. (1993). Calvin cycle multienzyme complexes are bound to chloroplast thylakoid membranes of higher plants in situ. *Proc Natl Acad Sci U S A, 90*(12), 5514-5518. doi: 10.1073/pnas.90.12.5514

Suzuki, Y., Kondo, E., & Makino, A. (2017). Effects of co-overexpression of the genes of Rubisco and transketolase on photosynthesis in rice. *Photosynth Res, 131*(3), 281-289. doi: 10.1007/s11120-016-0320-4

Syeda, R., Xu, J., Dubin, A. E., Coste, B., Mathur, J., Huynh, T., . . . Patapoutian, A. (2015). Chemical activation of the mechanotransduction channel Piezo1. *Elife, 4*. doi: 10.7554/eLife.07369

Tagliani, A., Rossi, J., Marchand, C. H., De Mia, M., Tedesco, D., Gurrieri, L., . . . Zaffagnini, M. (2021). Structural and functional insights into nitrosoglutathione reductase from Chlamydomonas reinhardtii. *Redox Biol, 38*, 101806. doi: 10.1016/j.redox.2020.101806

Tamoi, M., Murakami, A., Takeda, T., & Shigeoka, S. (1998). Lack of Light/Dark Regulation of Enzymes Involved in the Photosynthetic Carbon Reduction Cycle in Cyanobacteria, Synechococcus PCC 7942 and Synechocystis PCC 6803. *Biosci Biotechnol Biochem, 62*(2), 374-376. doi: 10.1271/bbb.62.374

Tamoi, M., Nagaoka, M., Miyagawa, Y., & Shigeoka, S. (2006). Contribution of fructose-1,6-bisphosphatase and sedoheptulose-1,7-bisphosphatase to the photosynthetic rate and carbon flow in the Calvin cycle in transgenic plants. *Plant Cell Physiol, 47*(3), 380-390. doi: 10.1093/pcp/pcj004

Tarrago, L., Laugier, E., Zaffagnini, M., Marchand, C., Le Marechal, P., Rouhier, N., . . . Rey, P. (2009). Regeneration mechanisms of *Arabidopsis thaliana* methionine sulfoxide reductases B by glutaredoxins and thioredoxins. *J Biol Chem, 284*(28), 18963-18971. doi: 10.1074/jbc.M109.015487

Taylor, T. C., Backlund, A., Bjorhall, K., Spreitzer, R. J., & Andersson, I. (2001). First crystal structure of Rubisco from a green alga, Chlamydomonas reinhardtii. *J Biol Chem, 276*(51), 48159-48164. doi: 10.1074/jbc.M107765200

Tcherkez, G. (2013). Modelling the reaction mechanism of ribulose-1,5-bisphosphate carboxylase/oxygenase and consequences for kinetic parameters. *Plant Cell Environ, 36*(9), 1586-1596. doi: 10.1111/pce.12066

Tcherkez, G. G., Farquhar, G. D., & Andrews, T. J. (2006). Despite slow catalysis and confused substrate specificity, all ribulose bisphosphate carboxylases may be nearly perfectly optimized. *Proc Natl Acad Sci U S A, 103*(19), 7246-7251. doi: 10.1073/pnas.0600605103

Teige, M., Melzer, M., & Suss, K. H. (1998). Purification, properties and in situ localization of the amphibolic enzymes D-ribulose 5-phosphate 3-epimerase and transketolase from spinach chloroplasts. *Eur J Biochem, 252*(2), 237-244. doi: 10.1046/j.1432-1327.1998.2520237.x

Terashima, M., Specht, M., & Hippler, M. (2011). The chloroplast proteome: a survey from the Chlamydomonas reinhardtii perspective with a focus on distinctive features. *Curr Genet, 57*(3), 151-168. doi: 10.1007/s00294-011-0339-1

Terauchi, A. M., Lu, S. F., Zaffagnini, M., Tappa, S., Hirasawa, M., Tripathy, J. N., . . . Merchant, S. S. (2009). Pattern of expression and substrate specificity of chloroplast ferredoxins from Chlamydomonas reinhardtii. *J Biol Chem, 284*(38), 25867-25878. doi: 10.1074/jbc.M109.023622

Thieulin-Pardo, G., Remy, T., Lignon, S., Lebrun, R., & Gontero, B. (2015). Phosphoribulokinase from Chlamydomonas reinhardtii: a Benson-Calvin cycle enzyme enslaved to its cysteine residues. *Mol Biosyst, 11*(4), 1134-1145. doi: 10.1039/c5mb00035a

Toledano, M. B., Delaunay-Moisan, A., Outten, C. E., & Igbaria, A. (2013). Functions and cellular compartmentation of the thioredoxin and glutathione pathways in yeast. *Antioxid Redox Signal, 18*(13), 1699-1711. doi: 10.1089/ars.2012.5033

Trost, P., Fermani, S., Marri, L., Zaffagnini, M., Falini, G., Scagliarini, S., . . . Sparla, F. (2006). Thioredoxin-dependent regulation of photosynthetic glyceraldehyde-3-phosphate dehydrogenase: autonomous vs. CP12-dependent mechanisms. *Photosynth Res, 89*(2-3), 263-275. doi: 10.1007/s11120-006-9099-z

Trudeau, D. L., Edlich-Muth, C., Zarzycki, J., Scheffen, M., Goldsmith, M., Khersonsky, O., . . . Bar-Even, A. (2018). Design and in vitro realization of carbon-conserving photorespiration. *Proc Natl Acad Sci U S A, 115*(49), E11455-E11464. doi: 10.1073/pnas.1812605115

Tsukamoto, Y., Fukushima, Y., Hara, S., & Hisabori, T. (2013). Redox control of the activity of phosphoglycerate kinase in Synechocystis sp. PCC6803. *Plant Cell Physiol, 54*(4), 484-491. doi: 10.1093/pcp/pct002

Turpin, David H. (1991). Effects of Inorganic N Availability on Algal Photosynthesis and Carbon Metabolism. *Journal of phycology, 27*(1), 14-20. doi: 10.1111/j.0022-3646.1991.00014.x

Uematsu, K., Suzuki, N., Iwamae, T., Inui, M., & Yukawa, H. (2012). Increased fructose 1,6-bisphosphate aldolase in plastids enhances growth and photosynthesis of tobacco plants. *J Exp Bot, 63*(8), 3001-3009. doi: 10.1093/jxb/ers004

Uniacke, J., & Zerges, W. (2008). Stress induces the assembly of RNA granules in the chloroplast of Chlamydomonas reinhardtii. *J Cell Biol, 182*(4), 641-646. doi: 10.1083/jcb.200805125

van der Linde, K., Gutsche, N., Leffers, H. M., Lindermayr, C., Muller, B., Holtgrefe, S., & Scheibe, R. (2011). Regulation of plant cytosolic aldolase functions by redox-modifications. *Plant Physiol Biochem, 49*(9), 946-957. doi: 10.1016/j.plaphy.2011.06.009

Villeret, V., Huang, S., Zhang, Y., Xue, Y., & Lipscomb, W. N. (1995). Crystal structure of spinach chloroplast fructose-1,6-bisphosphatase at 2.8 A resolution. *Biochemistry, 34*(13), 4299-4306. doi: 10.1021/bi00013a019

Wagner, V., Gessner, G., Heiland, I., Kaminski, M., Hawat, S., Scheffler, K., & Mittag, M. (2006). Analysis of the phosphoproteome of Chlamydomonas reinhardtii provides new insights into various cellular pathways. *Eukaryot Cell, 5*(3), 457-468. doi: 10.1128/EC.5.3.457-468.2006

Walker, D. (1992). *Energy, plants and man*: Univ Science Books.

Wang, D., & Portis, A. R., Jr. (2006). Increased sensitivity of oxidized large isoform of ribulose-1,5-bisphosphate carboxylase/oxygenase (rubisco) activase to ADP inhibition is due to an interaction between its carboxyl extension and nucleotide-binding pocket. *J Biol Chem, 281*(35), 25241-25249. doi: 10.1074/jbc.M604756200

Wang, H., Gau, B., Slade, W. O., Juergens, M., Li, P., & Hicks, L. M. (2014). The global phosphoproteome of Chlamydomonas reinhardtii reveals complex organellar phosphorylation in the flagella and thylakoid membrane. *Mol Cell Proteomics, 13*(9), 2337-2353. doi: 10.1074/mcp.M114.038281

Wang, H., Yan, X., Aigner, H., Bracher, A., Nguyen, N. D., Hee, W. Y., . . . Hayer-Hartl, M. (2019). Rubisco condensate formation by CcmM in beta-carboxysome biogenesis. *Nature, 566*(7742), 131-135. doi: 10.1038/s41586-019-0880-5

Wang, Y., Stessman, D. J., & Spalding, M. H. (2015). The CO2 concentrating mechanism and photosynthetic carbon assimilation in limiting CO2 : how Chlamydomonas works against the gradient. *Plant J, 82*(3), 429-448. doi: 10.1111/tpj.12829

Wang, Z. T., Ullrich, N., Joo, S., Waffenschmidt, S., & Goodenough, U. (2009). Algal lipid bodies: stress induction, purification, and biochemical characterization in wild-type and starchless Chlamydomonas reinhardtii. *Eukaryot Cell, 8*(12), 1856-1868. doi: 10.1128/EC.00272-09

Weber, A., Menzlaff, E., Arbinger, B., Gutensohn, M., Eckerskorn, C., & Flugge, U. I. (1995). The 2-oxoglutarate/malate translocator of chloroplast envelope membranes: molecular cloning of a transporter containing a 12-helix motif and expression of the functional protein in yeast cells. *Biochemistry, 34*(8), 2621-2627. doi: 10.1021/bi00008a028

Wedel, N., & Soll, J. (1998). Evolutionary conserved light regulation of Calvin cycle activity by NADPH-mediated reversible phosphoribulokinase/CP12/ glyceraldehyde-3-phosphate dehydrogenase complex dissociation. *Proc Natl Acad Sci U S A, 95*(16), 9699-9704. doi: 10.1073/pnas.95.16.9699

Weger, H. G., Guy, R. D., & Turpin, D. H. (1990). Cytochrome and alternative pathway respiration in green algae : measurements using inhibitors and o(2) discrimination. *Plant Physiol, 93*(1), 356-360. doi: 10.1104/pp.93.1.356

Wei, L., Derrien, B., Gautier, A., Houille-Vernes, L., Boulouis, A., Saint-Marcoux, D., . . . Wollman, F. A. (2014). Nitric oxide-triggered remodeling of chloroplast bioenergetics and thylakoid proteins upon nitrogen starvation in Chlamydomonas reinhardtii. *Plant Cell, 26*(1), 353-372. doi: 10.1105/tpc.113.120121

Wenderoth, I., Scheibe, R., & von Schaewen, A. (1997). Identification of the cysteine residues involved in redox modification of plant plastidic glucose-6-phosphate dehydrogenase. *J Biol Chem, 272*(43), 26985-26990. doi: 10.1074/jbc.272.43.26985

Werth, E. G., McConnell, E. W., Couso Lianez, I., Perrine, Z., Crespo, J. L., Umen, J. G., & Hicks, L. M. (2019). Investigating the effect of target of rapamycin kinase inhibition on the Chlamydomonas reinhardtii phosphoproteome: from known homologs to new targets. *New Phytol, 221*(1), 247-260. doi: 10.1111/nph.15339

Werth, E. G., McConnell, E. W., Gilbert, T. S., Couso Lianez, I., Perez, C. A., Manley, C. K., . . . Hicks, L. M. (2017). Probing the global kinome and phosphoproteome in Chlamydomonas reinhardtii via sequential enrichment and quantitative proteomics. *Plant J, 89*(2), 416-426. doi: 10.1111/tpj.13384

Wienkoop, S., Weiss, J., May, P., Kempa, S., Irgang, S., Recuenco-Munoz, L., . . . Weckwerth, W. (2010). Targeted proteomics for Chlamydomonas reinhardtii combined with rapid subcellular protein fractionation, metabolomics and metabolic flux analyses. *Mol Biosyst, 6*(6), 1018-1031. doi: 10.1039/b920913a

Wilson, R. H., Hayer-Hartl, M., & Bracher, A. (2019). Crystal structure of phosphoribulokinase from Synechococcus sp. strain PCC 6301. *Acta Crystallogr F Struct Biol Commun, 75*(Pt 4), 278-289. doi: 10.1107/S2053230X19002693

Winkler, M., Hemschemeier, A., Jacobs, J., Stripp, S., & Happe, T. (2010). Multiple ferredoxin isoforms in Chlamydomonas reinhardtii - their role under stress conditions and biotechnological implications. *Eur J Cell Biol, 89*(12), 998-1004. doi: 10.1016/j.ejcb.2010.06.018

Wobbe, L., & Remacle, C. (2015). Improving the sunlight-to-biomass conversion efficiency in microalgal biofactories. *J Biotechnol, 201*, 28-42. doi: 10.1016/j.jbiotec.2014.08.021

Wunder, T., Cheng, S. L. H., Lai, S. K., Li, H. Y., & Mueller-Cajar, O. (2018). The phase separation underlying the pyrenoid-based microalgal Rubisco supercharger. *Nat Commun, 9*(1), 5076. doi: 10.1038/s41467-018-07624-w

Xu, M., Luo, J., Li, Y., Shen, L., Zhang, X., Yu, J., . . . Yang, J. (2021). First comprehensive proteomics analysis of lysine crotonylation in leaves of peanut (Arachis hypogaea L.). *Proteomics, 21*(5), e2000156. doi: 10.1002/pmic.202000156

Xue, X., Gauthier, D. A., Turpin, D. H., & Weger, H. G. (1996). Interactions between Photosynthesis and Respiration in the Green Alga Chlamydomonas reinhardtii (Characterization of Light-Enhanced Dark Respiration). *Plant Physiol, 112*(3), 1005-1014. doi: 10.1104/pp.112.3.1005

Yacoby, I., Pochekailov, S., Toporik, H., Ghirardi, M. L., King, P. W., & Zhang, S. (2011). Photosynthetic electron partitioning between [FeFe]-hydrogenase and ferredoxin:NADP+-oxidoreductase (FNR) enzymes in vitro. *Proc Natl Acad Sci U S A, 108*(23), 9396-9401. doi: 10.1073/pnas.1103659108

Yamamoto, H., Takahashi, S., Badger, M. R., & Shikanai, T. (2016). Artificial remodelling of alternative electron flow by flavodiiron proteins in Arabidopsis. *Nat Plants, 2*, 16012. doi: 10.1038/nplants.2016.12

Yang, W., Wittkopp, T. M., Li, X., Warakanont, J., Dubini, A., Catalanotti, C., . . . Grossman, A. R. (2015). Critical role of Chlamydomonas reinhardtii ferredoxin-5 in maintaining membrane structure and dark metabolism. *Proc Natl Acad Sci U S A, 112*(48), 14978-14983. doi: 10.1073/pnas.1515240112

Yeh, H. L., Lin, T. H., Chen, C. C., Cheng, T. X., Chang, H. Y., & Lee, T. M. (2019). Monodehydroascorbate Reductase Plays a Role in the Tolerance of Chlamydomonas reinhardtii to Photooxidative Stress. *Plant Cell Physiol, 60*(10), 2167-2179. doi: 10.1093/pcp/pcz110

Yosef, I., Irihimovitch, V., Knopf, J. A., Cohen, I., Orr-Dahan, I., Nahum, E., . . . Shapira, M. (2004). RNA binding activity of the ribulose-1,5-bisphosphate carboxylase/oxygenase large subunit from Chlamydomonas reinhardtii. *J Biol Chem, 279*(11), 10148-10156. doi: 10.1074/jbc.M308602200

Yoshida, K., & Hisabori, T. (2016). Two distinct redox cascades cooperatively regulate chloroplast functions and sustain plant viability. *Proc Natl Acad Sci U S A, 113*(27), E3967-3976. doi: 10.1073/pnas.1604101113

Yoshida, K., & Hisabori, T. (2017). Distinct electron transfer from ferredoxin-thioredoxin reductase to multiple thioredoxin isoforms in chloroplasts. *Biochem J, 474*(8), 1347-1360. doi: 10.1042/BCJ20161089

Young, J. N., Heureux, A. M., Sharwood, R. E., Rickaby, R. E., Morel, F. M., & Whitney, S. M. (2016). Large variation in the Rubisco kinetics of diatoms reveals diversity among their carbon-concentrating mechanisms. *J Exp Bot, 67*(11), 3445-3456. doi: 10.1093/jxb/erw163

Yu, A., Xie, Y., Pan, X., Zhang, H., Cao, P., Su, X., . . . Li, M. (2020). Photosynthetic Phosphoribulokinase Structures: Enzymatic Mechanisms and the Redox Regulation of the Calvin-Benson-Bassham Cycle. *Plant Cell, 32*(5), 1556-1573. doi: 10.1105/tpc.19.00642

Yu, H., Li, X., Duchoud, F., Chuang, D. S., & Liao, J. C. (2018). Augmenting the Calvin-Benson-Bassham cycle by a synthetic malyl-CoA-glycerate carbon fixation pathway. *Nat Commun, 9*(1), 2008. doi: 10.1038/s41467-018-04417-z

Zaffagnini, M., Bedhomme, M., Groni, H., Marchand, C. H., Puppo, C., Gontero, B., . . . Lemaire, S. D. (2012). Glutathionylation in the photosynthetic model organism Chlamydomonas reinhardtii: a proteomic survey. *Mol Cell Proteomics, 11*(2), M111 014142. doi: 10.1074/mcp.M111.014142

Zaffagnini, M., Bedhomme, M., Marchand, C. H., Morisse, S., Trost, P., & Lemaire, S. D. (2012). Redox regulation in photosynthetic organisms: focus on glutathionylation. *Antioxid Redox Signal, 16*(6), 567-586. doi: 10.1089/ars.2011.4255

Zaffagnini, M., De Mia, M., Morisse, S., Di Giacinto, N., Marchand, C. H., Maes, A., . . . Trost, P. (2016). Protein S-nitrosylation in photosynthetic organisms: A comprehensive overview with future perspectives. *Biochim Biophys Acta, 1864*(8), 952-966. doi: 10.1016/j.bbapap.2016.02.006

Zaffagnini, M., Fermani, S., Costa, A., Lemaire, S. D., & Trost, P. (2013). Plant cytoplasmic GAPDH: redox post-translational modifications and moonlighting properties. *Front Plant Sci, 4*, 450. doi: 10.3389/fpls.2013.00450

Zaffagnini, M., Fermani, S., Marchand, C. H., Costa, A., Sparla, F., Rouhier, N., . . . Trost, P. (2019). Redox Homeostasis in Photosynthetic Organisms: Novel and Established Thiol-Based Molecular Mechanisms. *Antioxid Redox Signal, 31*(3), 155-210. doi: 10.1089/ars.2018.7617

Zaffagnini, M., Michelet, L., Marchand, C., Sparla, F., Decottignies, P., Le Marechal, P., . . . Lemaire, S. D. (2007). The thioredoxin-independent isoform of chloroplastic glyceraldehyde-3-phosphate dehydrogenase is selectively regulated by glutathionylation. *FEBS J, 274*(1), 212-226. doi: 10.1111/j.1742-4658.2006.05577.x

Zaffagnini, M., Michelet, L., Sciabolini, C., Di Giacinto, N., Morisse, S., Marchand, C. H., . . . Lemaire, S. D. (2014). High-resolution crystal structure and redox properties of chloroplastic triosephosphate isomerase from Chlamydomonas reinhardtii. *Mol Plant, 7*(1), 101-120. doi: 10.1093/mp/sst139

Zaffagnini, M., Morisse, S., Bedhomme, M., Marchand, C. H., Festa, M., Rouhier, N., . . . Trost, P. (2013). Mechanisms of nitrosylation and denitrosylation of cytoplasmic glyceraldehyde-3-phosphate dehydrogenase from Arabidopsis thaliana. *J Biol Chem, 288*(31), 22777-22789. doi: 10.1074/jbc.M113.475467

Zalutskaya, Z., Kochemasova, L., & Ermilova, E. (2018). Dual positive and negative control of Chlamydomonas PII signal transduction protein expression by nitrate/nitrite and NO via the components of nitric oxide cycle. *BMC Plant Biol, 18*(1), 305. doi: 10.1186/s12870-018-1540-x

Zerges, W., Wang, S., & Rochaix, J. D. (2002). Light activates binding of membrane proteins to chloroplast RNAs in Chlamydomonas reinhardtii. *Plant Mol Biol, 50*(3), 573-585. doi: 10.1023/a:1020246007858

Zhan, Y., Dhaliwal, J. S., Adjibade, P., Uniacke, J., Mazroui, R., & Zerges, W. (2015). Localized control of oxidized RNA. *J Cell Sci, 128*(22), 4210-4219. doi: 10.1242/jcs.175232

Zhan, Y., Marchand, C. H., Maes, A., Mauries, A., Sun, Y., Dhaliwal, J. S., . . . Zerges, W. (2018). Pyrenoid functions revealed by proteomics in Chlamydomonas reinhardtii. *PLoS One, 13*(2), e0185039. doi: 10.1371/journal.pone.0185039

Zhang, N., Schurmann, P., & Portis, A. R., Jr. (2001). Characterization of the regulatory function of the 46-kDa isoform of Rubisco activase from Arabidopsis. *Photosynth Res, 68*(1), 29-37. doi: 10.1023/A:1011845506196

Zhu, X. G., de Sturler, E., & Long, S. P. (2007). Optimizing the distribution of resources between enzymes of carbon metabolism can dramatically increase photosynthetic rate: a numerical simulation using an evolutionary algorithm. *Plant Physiol, 145*(2), 513-526. doi: 10.1104/pp.107.103713

Zhu, X. G., Portis, A. R., & Long, S. P. (2004). Would transformation of C3 crop plants with foreign Rubisco increase productivity? A computational analysis extrapolating from kinetic properties to canopy photosynthesis. *Plant, Cell and Environment, 27*(2), 155-165. doi: 10.1046/j.1365-3040.2004.01142.x

1.6 OBJECTIFS DU DOCTORAT

De nombreuses informations, études et articles scientifiques sont disponibles à propos du CBBC et des onze enzymes qui le composent, particulièrement chez l'organisme unicellulaire modèle *Chlamydomonas reinhardtii*. Néanmoins, des lacunes dans ces connaissances sont encore présentes.

S'il existe plusieurs structures tridimensionnelles de TRK issues d'organismes photosynthétique ou bien plusieurs structures de Rubisco dans plusieurs conditions différentes, le CBBC ne possède pas encore une description exhaustive de toutes les enzymes le composant dans un organisme unique. Chez Chlamydomonas, la structure de la Rubisco a été la première à être déterminée, suivie de TPI, TRK et PRK, tandis que la GAPDH fait l'objet d'un article publié en juin 2022. Un manque d'informations structurales sur les autres enzymes photosynthétiques du CBBC persistait encore alors que j'ai entrepris ces recherches : les structures expérimentales des paralogues photosynthétiques de RPI, FBA, PGK et les structures de SBPase et FBPase chloroplastiques de Chlamydomonas.

La description systématique des structures de ces enzymes chez Chlamydomonas serait un ajout considérable à la compréhension des mécanismes catalytiques spécifiques à la photosynthèse et de la régulation globale et coordonnée du CBBC. Une description précise de la position dans l'espace des acides aminés potentiellement impliqués dans ces mécanismes de régulations et dans les mécanismes catalytiques de ces enzymes, par exemple leur exposition au solvant, est un point important dans la compréhension de ceux-ci. L'analyse des surfaces d'interactions, potentielles ou démontrés, sont également des informations non négligeables dans la compréhension du cycle de Calvin-Benson-Bassham.

Un deuxième axe d'étude de ce cycle et de ces enzymes cible les interactions des enzymes entres elles. Les protéines du CBBC peuvent s'associer dans des assemblages supramoléculaires influant sur la fonction de ces enzymes. Si de nombreuses informations sont publiées sur certains de ces complexes hétéro-multimériques, chez Chlamydomonas la littérature se concentre surtout sur les deux

complexes Rubisco-EPYC1 et GAPDH-CP12-PRK évoqués précédemment. Le second axe de ma thèse a donc été d'essayer d'identifier au moins un de ces potentiels nouveaux complexes activateurs.

Ainsi, les différentes problématiques que je me suis posées au début de ce doctorat ont été les suivantes :

- La complétion de l'étude de génomique structurale du CBBC entamée par mon équipe et leurs collaborateurs.

- L'analyse des propriétés structurales particulières des enzymes photosynthétiques, notamment leurs régulations par modifications post-traductionnelles.

- L'identification et la caractérisation de complexes activateurs hétéro-multimériques d'enzymes du CBBC chez Chlamydomonas.

2 RESULTATS

Dans ce chapitre je décrirai les différents résultats de mes travaux de détermination et d'analyse de quatre structures tridimensionnelles d'enzymes du cycle de Calvin-Benson-Bassham (section 2.1) puis de la recherche des états supramoléculaires que des enzymes du cycle établissent par leurs interactions hétéro-multimériques (section 2.2). L'analyse structure-fonction de la RPI et de la FBA sont le sujet de deux articles publiés. L'étude de la SBPase est en cours de rédaction sous la forme du manuscrit rapporté ici. La structure de PGK est en cours d'analyse mais sera présentée. Enfin, la détermination d'une structure de FBPase sera entreprise par microscopie électronique à la suite de résultats préliminaires que j'ai obtenus et qui sont présentés ici.

2.1 STRUCTURES TRIDIMENSIONNELLES

2.1.1 Ribose-5-phosphate isomérase 1

2.1.1.1 Résumé de l'article

L'article qui suit a été publié le 21 octobre 2020 dans le numéro spécial « *Structural/Functional Characterization of Plant Proteins* » de la revue *International Journal of Molecular Sciences* (IJMS). Il traite de la structure de la Ribose-5-Phosphate Isomérase 1 (RPI1) chloroplastique de *Chlamydomonas (Le Moigne et al. 2020)*. RPI1 participe aux étapes tardives de la régénération du RuBP en catalysant l'isomérisation du ribose-5-phosphate en ribulose-5-phosphate (Zhang et al. 2003; Benson et al. 1952). Si la structure de RPI avait auparavant fait l'objet de nombreuses études chez divers organismes (Chen et al. 2020), RPI1 de Chlamydomonas apporte la première description d'une structure de RPI chloroplastique.

La structure de RPI1 a été déterminée à une haute résolution de 1,40 Å ce qui nous a permis de positionner deux sous-unités de RPI1 dans l'unité asymétrique, mais également 511 molécules d'eau, deux ions sodium et huit ions sulfates. RPI1 se replie en deux domaines constitués de six hélices α et douze brins β (Figure 1 de Le Moigne et

al. (2020)). Dans l'unité asymétrique, RPI1 est un homo-dimère, de même qu'en solution. Le domaine amino-terminal adopte un pli de Rossmann (CATH classification : 3.40.50.1360) et le domaine carboxy-terminal est un domaine ACT (CATH classification : 3.30.70.260). RPI est décrite comme un homo-tétramère chez certains taxons comme les archées, elle est également décrite comme un dimère chez d'autres comme les bactéries ou les protozoaires (Chen et al. 2020). Chez les *Viridiplantae*, aucune information n'était disponible sur l'organisation quaternaire de RPI1. Cette étude a permis d'éclairer la question en classant l'enzyme de *Chlamydomonas* et la taxonomie associée à un homo-dimère, révélé par l'empilement cristallin et par chromatographie d'exclusion de taille. Cette interface dimérique de 1165 $Å^2$ est stabilisée par des liaisons faibles établies par 33 acides aminés (Figure 3 de Le Moigne et al. (2020)). La masse moléculaire apparente en chromatographie d'exclusion stérique (SEC) et les dimensions calculées d'après la diffusion des rayons X aux petits angles (SAXS) valident l'état homo-dimérique en solution (Figure 2 de Le Moigne et al. (2020)).

Le site catalytique de l'enzyme se situe à l'opposé de l'interface de dimérisation. La poche de liaison du substrat est chargée positivement, facilitant l'interaction avec le phosphate du substrat R5P et du produit Ru5P. Les résidus K37, G59, S60, T61, A62, I150 et K155 sont les principaux composants de la poche catalytique (Figure 4 de Le Moigne et al. (2020)). Ils sont conservés à travers les trois grands domaines du vivant d'après les alignements de séquences paralogues et l'analyse du score de conservation des résidus exposés au solvant via la méthode Consurf (Landau et al. 2005). Il est possible de coupler les données de la structure de Chlamydomonas, où un ion sulfate et des molécules d'eau permettent d'aligner le ribulose-5-phosphate à la position qu'il occupe probablement dans le complexe de Michaelis, comme dans la co-structure de RPI de *Legionella pneumophila* complexée au Ru5P (Code PDB : 6MC0). Nous validons ainsi l'hypothèse selon laquelle le mécanisme catalytique de la RPI photosynthétique ne diffère pas d'une espèce à l'autre ou d'un type métabolique (la voie des pentoses phosphates) à l'autre (le CBBC) (Figure 5 de Le Moigne et al. (2020)).

CrRPI est la cible de modifications post-traductionnelles dont les échanges redox et les phosphorylations de résidus sérine ou thréonine. Le modèle cristallographique nous permet de cartographier ces sites de modification, par exemple les cystéines 149 et 250 distantes de 4,4 Å sont susceptibles de se lier en un pont disulfure, ou la cystéine 175 accessible au solvant pour une possible S-nitrosylation, S-glutathionylation ou la formation d'un pont disulfure avec une autre chaîne polypeptidique. Les deux résidus retrouvés dans les études de phosphoprotéomique se trouvent proches ou à l'intérieur du site actif et leur modification pourrait donc avoir un impact sur l'activité catalytique de l'enzyme : l'ajout d'un groupement phosphate causerait un encombrement stérique doublé de l'insertion de plusieurs charges négatives défavorisant l'interaction avec les ligands phosphorylés.

2.1.1.2 High-resolution crystal structure of chloroplastic ribose-5-phosphate isomerase from Chlamydomonas reinhardtii – an enzyme involved in the photosynthetic Calvin-Benson Cycle

International Journal of
Molecular Sciences

MDPI

Article

High-Resolution Crystal Structure of Chloroplastic Ribose-5-Phosphate Isomerase from *Chlamydomonas reinhardtii*—An Enzyme Involved in the Photosynthetic Calvin-Benson Cycle

Théo Le Moigne [1,2], Pierre Crozet [1,3], Stéphane D. Lemaire [1,4] and Julien Henri [1,*]

1 Laboratoire de Biologie Moléculaire et Cellulaire des Eucaryotes, UMR8226, Institut de Biologie Physico-Chimique, Sorbonne Université, CNRS, 75005 Paris, France; lemoigne@ibpc.fr (T.L.M.); pierre.crozet@sorbonne-universite.fr (P.C.); lemaire@ibpc.fr (S.D.L.)
2 Faculty of Sciences, Doctoral School of Plant Sciences, Université Paris-Saclay, 91190 Saint-Aubin, France
3 Polytech Sorbonne, Sorbonne Université, 4 place Jussieu, 75005 Paris, France
4 Laboratoire de Biologie Computationnelle et Quantitative, UMR7238, Institut de Biologie Paris-Seine, Sorbonne Université, CNRS, 4 place Jussieu, 75005 Paris, France
* Correspondence: julien.henri@sorbonne-universite.fr

Received: 31 August 2020; Accepted: 19 October 2020; Published: 21 October 2020

Abstract: The Calvin–Benson cycle is the key metabolic pathway of photosynthesis responsible for carbon fixation and relies on eleven conserved enzymes. Ribose-5-phosphate isomerase (RPI) isomerizes ribose-5-phosphate into ribulose-5-phosphate and contributes to the regeneration of the Rubisco substrate. Plant RPI is the target of diverse post-translational modifications including phosphorylation and thiol-based modifications to presumably adjust its activity to the photosynthetic electron flow. Here, we describe the first experimental structure of a photosynthetic RPI at 1.4 Å resolution. Our structure confirms the composition of the catalytic pocket of the enzyme. We describe the homo-dimeric state of the protein that we observed in the crystal and in solution. We also map the positions of previously reported post-translational modifications and propose mechanisms by which they may impact the catalytic parameters. The structural data will inform the biochemical modeling of photosynthesis.

Keywords: photosynthesis; chloroplast; Calvin–Benson cycle; protein structure; X-ray crystallography; ribose isomerase; post-translational modification; redox; oligomerization; protein complexes

1. Introduction

Photosynthesis is the biological process allowing the conversion of light energy into chemical energy through fixation of atmospheric carbon [1]. Fixation of carbon dioxide occurs through the Calvin–Benson cycle (CBC) by carboxylation of the acceptor pentose ribulose-1,5-bisphosphate (RubP) by Rubisco [2]. RubP is generated by phosphorylation of ribulose-5-phosphate (Ru5P) by phosphoribulokinase (PRK). Prior to this phosphorylation step, ribose-5-phosphate (R5P) carbonyl group is transferred from carbon 1 to carbon 2. This reaction is catalyzed by the metabolic enzyme ribose-5-phosphate isomerase (RPI) [3]. Two forms of RPI have been classified: type A (RPI_A) and type B (RPI_B). RPI_A is ubiquitous in all species while RPI_B is only present in some bacteria and protozoans [4]. Beside its critical role in the CBC, RPI_A is implicated in the non-oxidative branch of the pentose phosphate pathway (PPP) [5]. RPI_A function in the PPP makes it an attractive target for drug development in the treatment of trypanosomatid-caused diseases [4]. RPI_A structures and catalytic

mechanism (EC 5.3.1.6) have been described in several organisms, but the structure of photosynthetic chloroplast localized RPI_A has never been reported to date. Analysis of RPI enzymatic kinetics has been principally performed on RPI_B in several species, and research on RPI_A enzymology is comparatively scarcer. The catalytic mechanism of RPI_A has nonetheless been established in several species and summarized in a recent review [4].

Chlamydomonas reinhardtii is a model unicellular photosynthetic green alga [6]. Its nuclear genome encodes two RPI at loci Cre03.g187450.t1.2 and Cre07.g314600.t1.2 [7], the protein products of which are respectively named RPI1 and RPI2. Both proteins are predicted to be addressed to the chloroplast according to the Predalgo tool [8] and in agreement with the chloroplast localization of the CBC and PPP in *C. reinhardtii* [9,10]. Among RPI1 and RPI2, RPI1 was selected as the most probable contributor to the CBC because its transcripts are 16 to 199 times more abundant than that of RPI2 in *C. reinhardtii* [11] and because accumulation of RPI1 transcript varies according to a night/day cycle, mirroring luminous flux.

In *C. reinhardtii*, the estimated CrRPI1 protein quantity is 0.34 amol per cell and 2.5 $\mu mol.L^{-1}$ in the chloroplast [12]. Considering the cellular concentration of metabolites [12,13], the approximate molar ratio of substrate or product to CrRPI1 is respectively estimated at 80 and 50. In order to adapt to the variations of metabolites concentration in the chloroplast stroma, CBC enzymatic activities are generally regulated according to the environmental light [14,15]. These regulations occur through several signaling pathways, e.g., dithiol-disulfide exchanges, S-thiolations, S-glutathionylations, and S-nitrosylations [15–17]. The stroma magnesium concentration is also known to influence the catalytic activity of CBC enzymes [18,19]. Post-translational redox modifications of RPI were detected from *C. reinhardtii* proteomic studies [20]. Phosphorylated peptides of CBC enzymes were also identified from *C. reinhardtii* extracts [21], suggesting a catalytic post-translational regulation by reversible phosphorylation.

Here, we present the first experimental structure of a chloroplastic RPI. We describe the structural characteristics that classifies CrRPI1 in the RPI_A family. We map the positions of previously reported post-translational modifications and propose mechanisms by which they may impact the catalytic parameters.

2. Results

2.1. CrRPI1 Structural Folds

We solved the crystal structure of CrRPI1 in the $P2_1$ space group at 1.40 Å resolution (Table 1). Model building of the two subunits of the asymmetric unit achieved the placement of 235 amino acid residues in the first subunit and 237 in the second (Figure 1A). The residues of each subunit were numbered according to uniProtKB entry A8IRQ1. The high resolution of the dataset further allowed us to position eight sulfates, two sodiums, and 511 water molecules in the crystal asymmetric unit.

Table 1. Crystallographic data collection and refinement statistics.

	CrRPI1
Wavelength (Å)	0.979
Resolution range (Å)	40.22–1.40 (1.45–1.40)
Space group	P 2_1
Unit cell	45.15 63.95 80.91 90 96.13 90
Total reflections	613,155 (55,349)
Unique reflections	89,012 (8611)
Multiplicity	6.9 (6.4)
Completeness (%)	99.6 (96.5)
Mean I/sigma(I)	20.58 (1.24)
Wilson B-factor (Å^2)	21.45
R-merge	0.0519 (1.272)
R-meas	0.05611 (1.382)
R-pim	0.02114 (0.5327)
CC1/2	0.999 (0.382)
CC*	1 (0.744)
Reflections used in refinement	88,983 (8601)
Reflections used for R-free	2000 (194)
R-work	0.1594 (0.3457)
R-free	0.1774 (0.3813)
CC (work)	0.972 (0.730)
CC (free)	0.967 (0.836)
Number of non-hydrogen atoms	4206
macromolecules	3648
ligands	47
solvent	511
Protein residues	474
RMS (bonds) (Å)	0.011
RMS (angles) (deg)	1.18
Ramachandran favored (%)	99.79
Ramachandran allowed (%)	0.21
Ramachandran outliers (%)	0.00
Rotamer outliers (%)	1.00
Clashscore	2.69
Average B-factor (Å^2)	25.46
macromolecules	23.78
ligands	47.04
Solvent	35.49

Statistics for the highest-resolution shell are shown in parentheses.

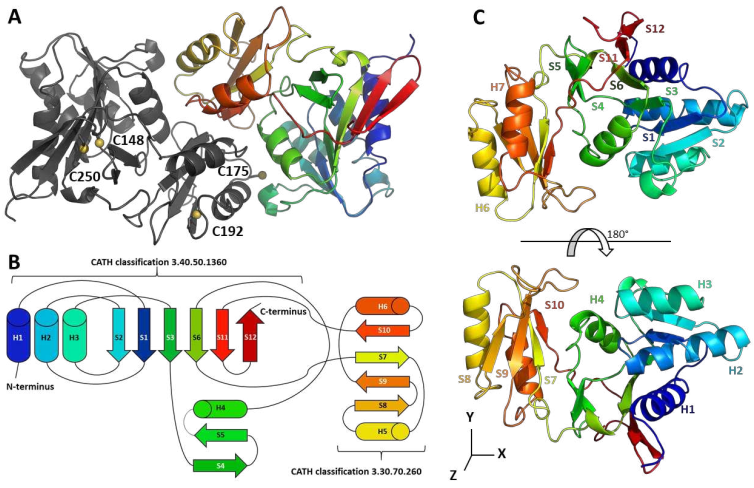

Figure 1. Crystal structure of CrRPI1. (**A**) Cartoon representation of the CrRPI1 crystallographic dimer colored in grey for the first subunit and from blue (N-terminus) to red (C-terminus) for the second subunit. (**B**) Two-dimensional representation of secondary structures of CrRPI1 colored as the second subunit in (**A**). (**C**) Cartoon representation of a CrRPI1 monomer. Two views of the protein are represented as in (**A**) and rotated by 180° on the *x*-axis. Secondary structures are annotated as in (**A**).

Each monomer is composed of six alpha helices and twelve beta strands distributed into two domains. Domain 1 spans residues 29 to 160 and 246 to 264, folds according to the Rossmann topology, and is part of an unnamed structural superfamily (CATH classification 3.40.50.1360). Domain 2 is inserted in between the two parts of domain 1, spans residues 161 to 245, and is classified as an ACT domain (CATH classification 3.30.70.260) (Figure 1B).

Our model aligns with 62 entries of the Protein data bank with an average RMSD lower than 1.8 Å. The closest similarity is with the Ribose 5-phosphate isomerase from *Plasmodium falciparum* (PDB 2F8M, RMSD = 0.852 Å over 229 aligned Cα). CrRPI1 secondary structure content is distributed as follows: α helix h1 (residues 33–45), β strand s1 (52–56), h2 (60–75), s2 (81–85), h3 (88–97), s3 (112–115), s4 (118–121), s5 (124–127), h4 (135–143), s6 (146–152), s7 (167–171), h5 (176–185), s8 (193–196), s9 (211–216), h6 (225–233), s10 (238–240), s11 (249–254) and s12 (257–262) (Figure 1C). In addition, residues 104, 105, 106 and residues 152, 153, 154 form two 3_{10} helices. Residues 22 to 28 and 265 to 269 at amino- and carboxy-termini were not modelled because of a lack of interpretable electron density. The secondary structure content and organization is the same as a canonical RPI previously reported (PfRPI, PDB 2F8M, [22]) except for the presence of CrRPI1 3_{10} helix formed by residues 104–106 that is absent from PfRPI.

Domain 1 is composed of helices 1, 2, 3, and 4, with strands 4 and 5 forming a small antiparallel sheet and strands 1, 2, 3, 6, and 12 that arrange in a parallel sheet completed by strand 11 in antiparallel orientation. These secondary structures are organized in a three-layer sandwich composed of helices 1, 2, 3 for the first layer, the parallel sheet in the second layer and by strand 4, 5, helix 4 and the two 3_{10} helices for the third layer. Domain 2 is relatively smaller with helices 5 and 6 forming the first stratum of a two-layer sandwich and strands 7, 8, 9, and 10 organized as an antiparallel sheet forming the second layer. The first domain contains the catalytic pocket, while the second was proposed to play a role in the oligomerization of RPI_A [4].

2.2. CrRPI1 is a Homodimer

RPI_A has been described as a functional dimer in solution [3,23,24] in bacteria and protozoa or as a functional tetramer in species from archaea and fungi taxa [4]. However, nothing was described for *Viridiplantae* enzymes. In our study, CrRPI1 elutes with the apparent molecular weight of a homodimer in solution over two different gel filtration matrices (Figure 2A). Small angle X-rays scattering (SAXS) curves obtained after size-exclusion chromatography of the purified protein (SEC-SAXS, Figure 2B) compute a molecular weight between 49.25 kDa and 56.2 kDa, fitting with two monomers of 27.55 kDa each. The homodimeric state is also observed in the crystal asymmetric unit (Figure 1A) with α helices h4, h5 and h6 and β strands s10 contributing to the interface. CrRPI1 dimer was aligned with *Plasmodium falciparum* RPI dimer (PDB entry 2F8M) with an RMSD = 2.115 Å over 438 equivalent atoms. Both dimers have the same quaternary organization, with corresponding subunits positioned in virtually identical positions. The only significant difference lies in the 3_{10} helix formed by residues 104–106 of CrRPI1 that is structured as a loop in PfRPI. The interface between two subunits of CrRPI1 is calculated from the arrangement of the two subunits forming the asymmetric unit (Figure 3A) by the PDBe-PISA server v1.52 [25]. The subunit A-to-subunit B interface is 1165 $Å^2$ wide and has a computed Δ^iG = −19.3 kcal/mol (*p*-value = 0.027). In comparison, PfRPI dimer interface is more extended with a surface of 1340.8 $Å^2$ and an equivalent computed Δ^iG = −19.4 kcal/mol (*p*-value = 0.048). CrRPI1 interface is composed by the 33 following residues: P85, T103, L104, D105, P108, K109, L135, R136, K138, M139, V140, M142, A143, V172, Q173, F174, C175, H176, K177, Y178, T179, R82, D207, N208, S209, N210, L232, G233, D235, G236, V237, V238, D239. It is stabilized by three hydrogen bonds between residues $Y178_A$ (α helix h5) and $D105_B$ (3_{10} helix 104–106), $F174_A$ and $N208_B$, $D105_A$ and $Y178_B$, and one salt bridge between $K177_A$ and $D105_B$ (Figure 3C). PfRPI possesses similar pairs $Y145_A$–$E74_B$, $N177_A$–$F143_B$, and $E74_A$–$K146_B$ (main chain carbonyl) in bonding distance, but no salt bridge and additional hydrogen bonds that are absent in CrRPI1 homodimer. While CrRPI1

dimerization interface residues are strictly conserved in the algae taxon, they are relatively poorly conserved throughout evolution (Figure 3B and Figure S1) [26].

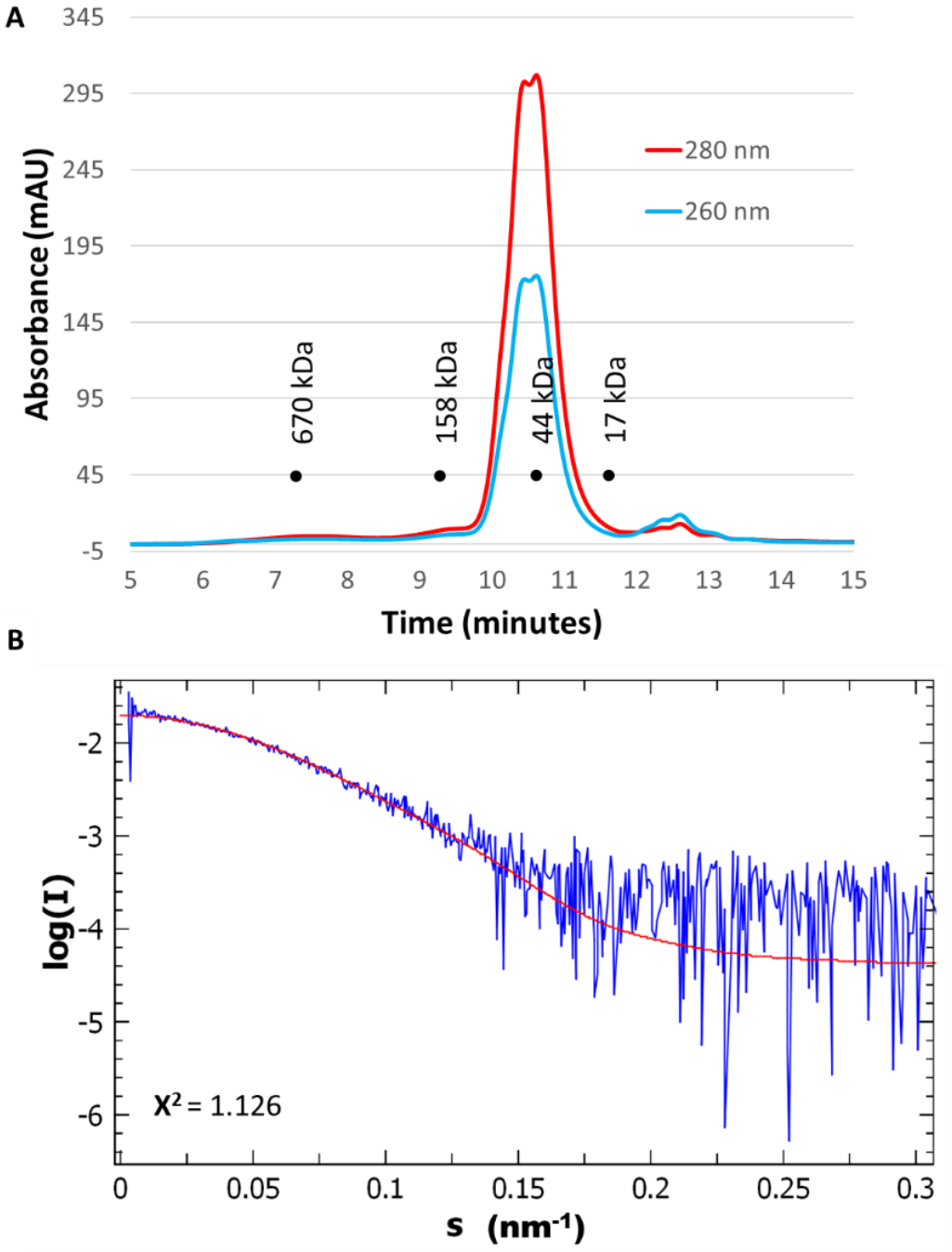

Figure 2. Size-exclusion chromatography coupled to small angle X-rays scattering (SEC-SAXS) analysis of CrRPI1. (**A**) High performance liquid chromatography (HPLC) chromatogram of CrRPI1 with absorption at 280 nm in red and at 260 nm in blue. (**B**) SAXS scattering curve log(I) = f(s) in blue was fitted to the crystallographic dimeric model of CrRPI1 in red.

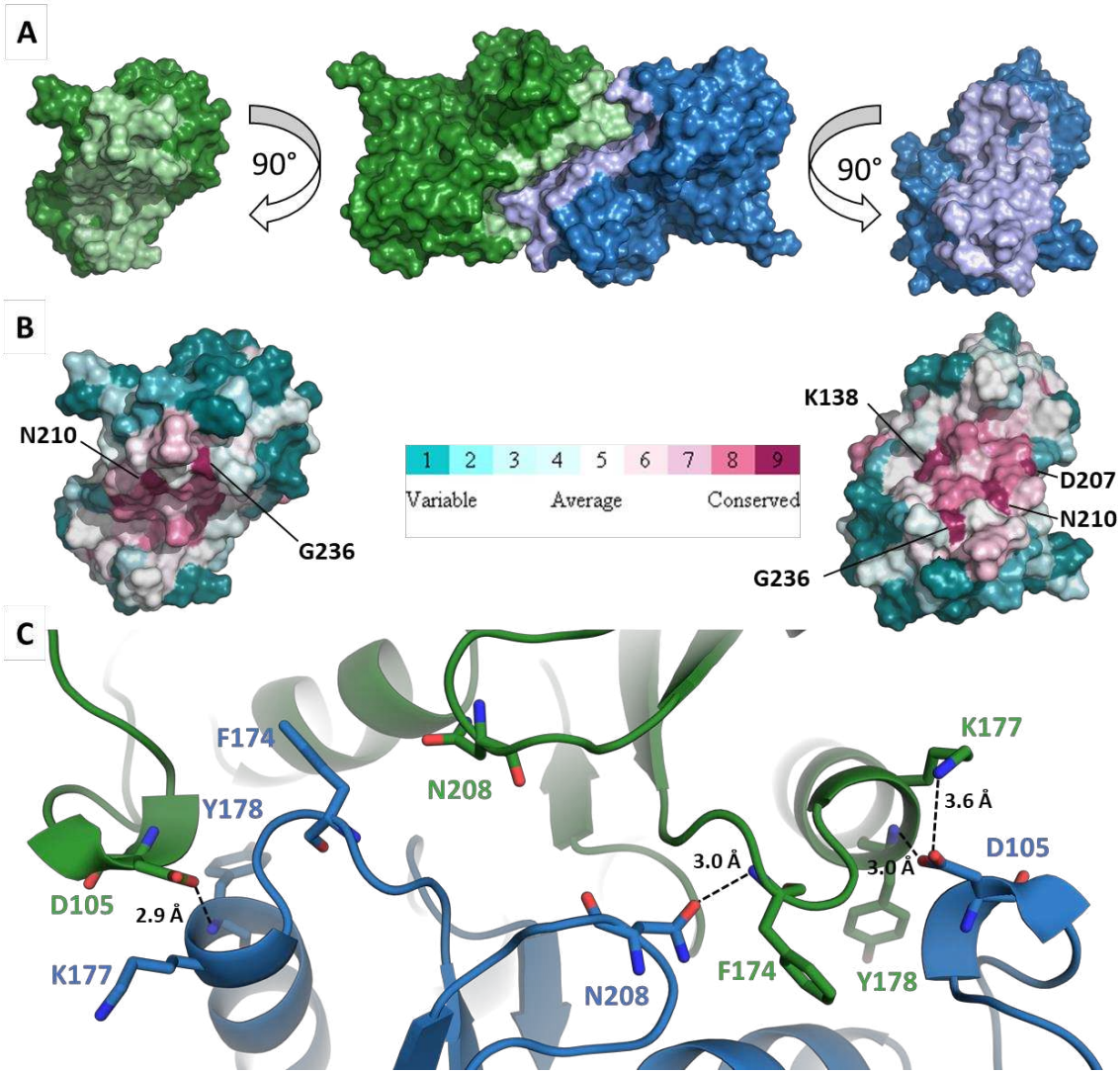

Figure 3. CrRPI1 homodimerization. (**A**) From left to right, Connolly solvent exclusion surface representation of subunit A, dimer and subunit B of CrRPI1. Subunit A is colored in green, and subunit B in blue. Residues composing the interface between the two subunits are colored in light green and light blue for subunits A and B respectively. (**B**) Surface residues conservation of subunits A and B as calculated with CONSURF colored from teal (least conserved) to purple (most conserved). Most conserved residues of the interface are annotated. (**C**) Cartoon representation of the dimer interface. Residues in bonding distances are represented in stick and annotated. Polar contacts are traced with black dashed lines with interatomic distances indicated in Ångström (Å).

2.3. RPI1 Catalytic Site

CrRPI1 crystallographic model includes a sulfate ion, a sodium ion and water molecules located in a shallow pocket exposed to solvent (Figure 4A). Structural superposition of CrRPI1 with RpiA from *Legionella pneumophila* (LpRPI, PDB: 6MC0, RMSD = 0.734 Å), which is co-crystalized with ribose-5-phosphate bound to the active site, reveals extended similarities (Figure S2). Surface charges were calculated on Pymol using the APBS electrostatics plugin [27,28]. For both enzymes, the active site is an analog cavity with an electronegative charge at the center, surrounded by electropositive charges at the rims (Figure 5A,B). Electrostatic surface potentials are similarly distributed on both active sites, suggesting an identical electrostatic complementarity toward the substrate. Indeed, an electropositive patch just outside the cavity is ideally positioned to accommodate the phosphate moiety of R5P in LpRPI (Figure 5B) and was found to anchor the co-crystallized sulfate ion in CrRPI1 (Figure 5A).

The sulfate ion in CrRPI1 hence occupies the location of the phosphate of the ribose-5-phosphate (Figure 5A,B) supporting a conserved mode of substrate recognition. This sulfate ion is coordinated by polar contacts with the side chains of S60, T61, and K155 and the main chain amine of T61. Residues K37, G59, S60, T61, A62, I150, and K155 principally contribute to the rest of the pocket surface in CrRPI1 (Figure 4B). All these residues are highly conserved in all species from the three kingdoms of life (Figure S1). Water molecules in CrRPI1 are placed where R5P carbon skeleton binds LpRPI. The sodium ion co-crystallized with CrRPI1 lies where the aldehyde function of R5P binds LpRPI. Residues D115 and E137 have been proposed to play a critical role in the catalytic mechanism [3,29]. In our model of CrRPI1, their side chains are positioned at, respectively, 3.1 Å and 6.4 Å away from the sodium ion, allowing their interaction with the carbonyl function of the substrate. Side chains rearrangements and water displacements are expected for the formation of the Michaelis complex and the subsequent catalytic isomerization.

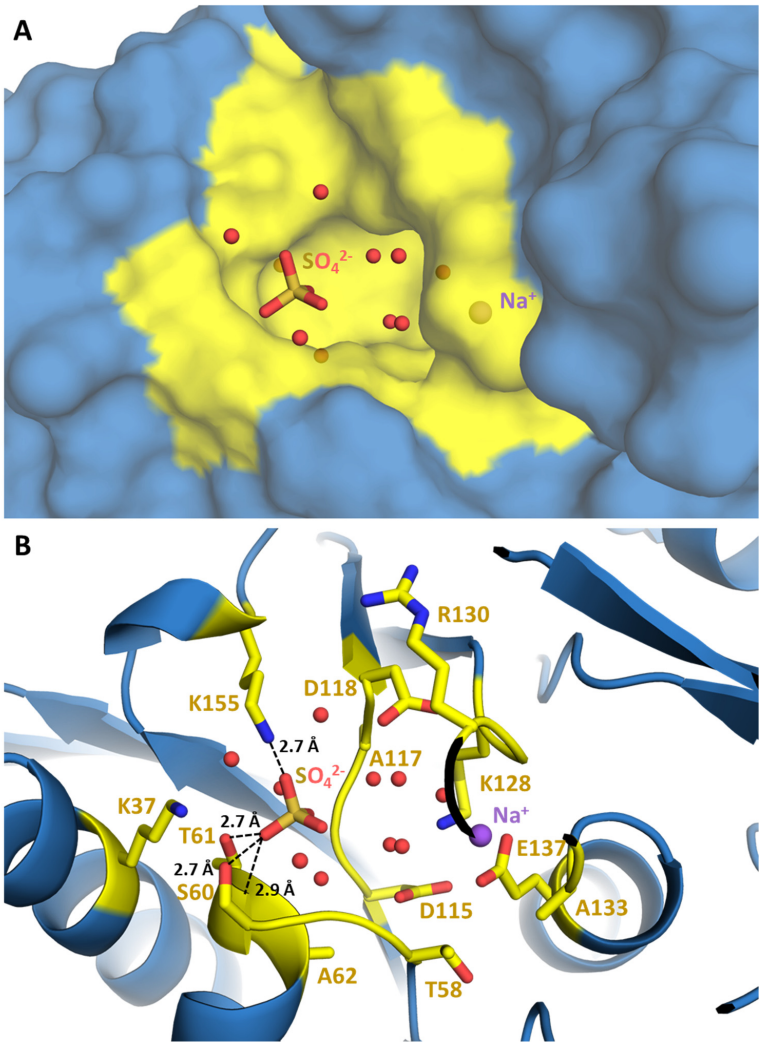

Figure 4. CrRPI1 catalytic pocket. (**A**) The Connolly solvent exclusion surface of the catalytic cleft of CrRPI1 with ligands in it (sulfate ion, water, sodium ion). Residues contributing to the cavity are colored in yellow, other residues are colored in blue. (**B**) The same view of the catalytic cleft as in (**A**). The protein is colored in blue and represented in cartoon. Residues contributing to the catalytic cleft are colored in yellow and their side chains are represented in sticks. Polar contacts between ligand and residues are represented in black dashed lines with corresponding interatomic distances indicated in Ångströms (Å).

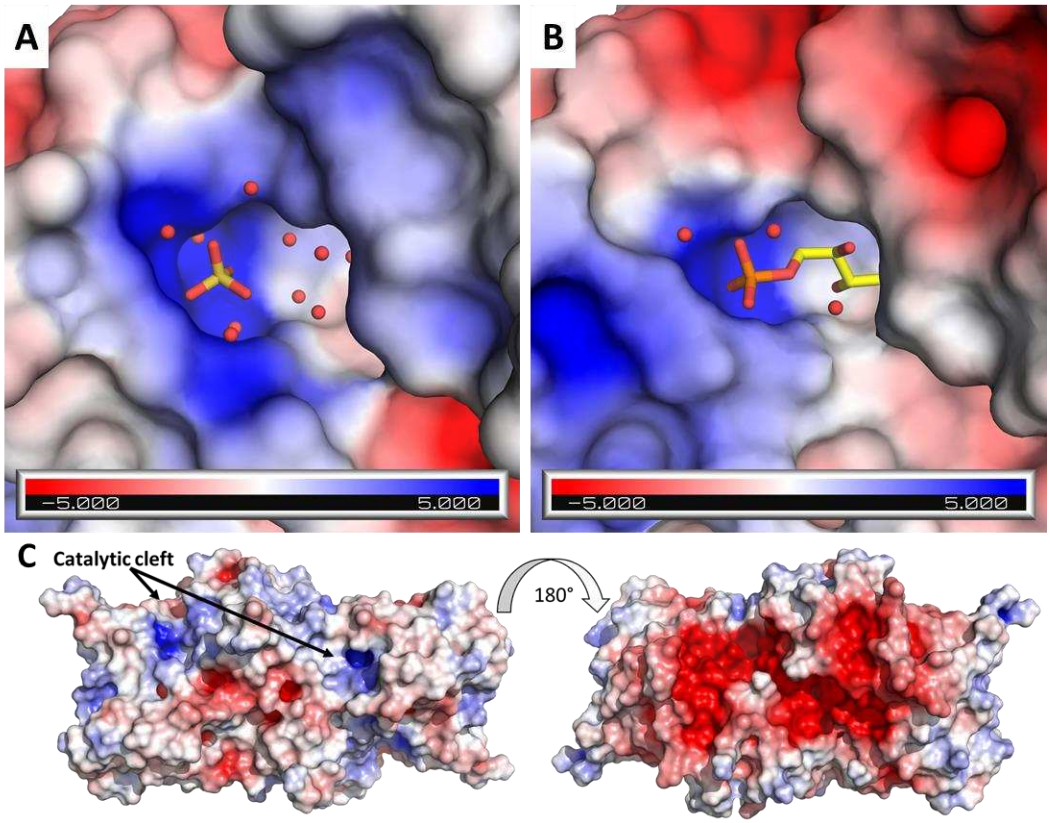

Figure 5. Electrostatic potential of RPI surface. (**A**) View of the catalytic cleft of CrRPI1 electrostatic surface calculated by PyMOL APBS and represented in a gradient from blue (electropositive) to red (electronegative). The sulfate ion is represented in sticks and water molecules as spheres. (**B**) View of the catalytic cleft of *Legionella pneumophila* RpiA of PDB model 6MC0, superposed to CrRPI1 model and colored as in A. Co-crystallized ribose-5-phosphate is represented in sticks. (**C**) Electronegative patch of CrRPI1 dimer. Electrostatic surface of CrRPI1 dimer facing the catalytic cleft up and with a 180° rotation from this position was calculated by PyMOL APBS.

2.4. CrRPI1 Sites of Post-Translational Modifications

All CBC enzymes undergo diverse types of redox post-translational modifications including disulfide bond formation, glutathionylation or nitrosylation, under the control of thioredoxins (TRX) and glutaredoxins (GRX) [15,20]. CrRPI1 contains four cysteines: C149, C250 and C192 are conserved in green microalgae, while C175 is present in algae and land plants (Figure S1). Two cysteines (C149 and C175) were identified as reactive in vivo through a high-throughput screen, and C149 was further identified as a putative TRX target [20]. CrRPI1 was also identified as a target of S-nitrosylation or S-glutathionylation in proteomic studies [16,30]. In our CrRPI1 crystal structure, C149 and C250 position their sulfur atoms 4.4 Å apart, a distance compatible with the formation of a disulfide bridge. C149 and C250 side chains are modelled as free thiols (Figure 1A and Figure S3). Both side chains are buried in the protein hydrophobic core where TRX or GRX should be excluded once RPI1 is folded. The two other cysteines of CrRPI1 are closer to the surface but separated by 20 Å, precluding the formation of an intramolecular disulfide bridge. C192 has a solvent exposed backbone and its sidechain points toward the hydrophobic core. C175 has its sulfur atom exposed to solvent and is the most likely to be the target of redox post translational modifications, such as the formation of an intermolecular disulfide bridge with another dimer of CrRPI1 or with a partner protein. Indeed, CrRPI1 is predicted to interact with ten other proteins in *Chlamydomonas reinhardtii* by the STRING database [31] and a disulfide bridge may stabilize or condition these interactions. Phosphoglycerate kinase 1 (PGK1), transketolase 1 (TRK1), ribulose-5-phosphate 3-epimerase 1 (RPE1)

and 2 (RPE2), and phosphoribulokinase (PRK) are predicted to belong to this interaction network and are also part of the CBC and proven targets of redox regulation [20,32,33]. Protein interactions may hence contribute to the redox regulation of the CBC under varying physiological and environmental conditions. Furthermore TRK, RPI, RPE, and PRK activities are consecutive in the cycle, which may allow them to constitute an enzymatic metabolon.

A large electronegative patch is present at the back side of the dimer, 20 Å away from the catalytic pocket (Figure 5C). It spans both subunits and forms a continuous ellipsoid of approximately 55 Å in length and 30 Å in width. This extended surface patch is a candidate docking zone for additional partner or regulatory proteins. For instance, photosynthetic redox activator CrTRXf2 was reported to expose an electropositive crown of residues around its active site [34] and a large electropositive crescent surrounds CrPRK active site [35]. Such putative interactants or others bearing similar electropositive surfaces would favorably interact on the back side of CrRPI1 by electrostatic complementarity.

Phosphoproteomic studies [21] identified two phosphorylated amino acids on CrRPI1: T61 and S87 (Figure S3). Both are localized on the same surface as the catalytic cavity, T61 hydroxyl group being at 2.7 Å of one of the oxygens of aforementioned active site sulfate. S87 is positioned 13.2 Å away from T61, at the opposite side of the catalytic cleft at 7.1 Å of E137. Phosphorylation of T61 would insert a bulky negatively charged group, which would probably preclude the binding of phosphate from the R5P substrate. Phosphorylation of T61 would thus outcompete the binding of R5P. S87 phosphorylation may play a less direct role in the regulation of R5P binding. Both T61 and S87 are fully conserved from bacteria to plants and metazoans (Figure S1).

3. Discussion

We describe the first structure of a ribose-5-phosphate isomerase from a *Viridiplanta*, the model microalga *Chlamydomonas reinhardtii*. The structural fold of CrRPI1 (Figure 1B) is similar to previously described structures of canonical RPI_A [29] even though plastidial RPI participates in both the Calvin-Benson cycle and the pentose phosphate pathway. CrRPI1 catalytic site is described free from substrate and product, representing the apo state of the enzyme. Six water molecules, a sulfate ion and a sodium ion are however present and therefore allow to predict the coordination and placement of its substrate R5P in this pocket through structural superposition and sequence analysis. Most of the residues shaping the catalytic pocket are strictly conserved (Figure S1), supporting a conserved catalytic mechanism for all RPI_A described to date [4].

CrRPI1 is a homodimer in solution and in the crystal packing (Figure 1A, Figure 2A,B, and Figure 3A–C). This homodimeric organization was previously observed (*L. pneumophila* PDB 6MC0). RPI was alternatively reported to form homotetramers in other species such as *Saccharomyces cerevisiae* or archaea [36,37]. The oligomerization appears to depend on the length of the 197–204 loop and the interaction network of the conserved residue R197, as suggested based on the *S. cerevisiae* structure [36]. In CrRPI1 homodimer, the distance between catalytic residues $D115_A$ and $D115_B$ is 40 Å. Whether homodimerization induces cooperativity between the active sites will be tested in future studies.

By contributing to the Calvin-Benson cycle and to the pentose phosphate pathway [2,38], CrRPI1 activity should be subject to several, maybe mutually exclusive, regulations of its catalytic parameters. Structural analysis suggests several possible, mutually permissive regulation mechanisms. First, CrRPI1 was identified in *C. reinhardtii* thioredoxome [20], as a consequence of its affinity with the dithiol-disulfide exchanger thioredoxin. Hence, RPI1 is likely to be activated in concert with other CBC enzymes, such as PRK [35]. The presence of only cysteines 149 and 250 at disulfide bonding distance, but not accessible to solvent, argues in favor of irreversible redox states of the cysteine pair once the protein is folded. The two other cysteines 175 and 192 side chains are close to or exposed to solvent. They are modelled in CrRPI1 at a distance of 20 Å which precludes the formation of an intramolecular disulfide bridge. Alternatively, other redox post translational modifications of these cysteines, such as intermolecular disulfide bridges, S-glutathionylation, S-nitrosylation may occur as suggested by

proteomic studies [16,20,30]. Interestingly, RPI1 could also interact with partner proteins, including through intermolecular disulfide bridges. The formation of multienzymatic complexes with following and preceding enzymes from the CBC may allow channeling of substrates as suggested by a study on flux distribution and metabolic pools in *Chlamydomonas reinhardtii* chloroplast [39]. This hypothesis has to be tested by isolation of such complexes from cellular extracts.

Regulation of the isomerase activity could also be achieved by phosphorylation of residues T61 and S87. Addition of a phosphate group onto T61 hydroxyl would block the entrance of the catalytic pocket with a negatively charged steric hindrance at the R5P and Ru5P binding site. This hypothesis seems attractive as, most importantly, these two residues are highly conserved throughout all analyzed species. This might indicate a ubiquitous, ancestral regulation rather than a CBC-specific control. The identity of the kinase/phosphatase couple that specifically targets CrRPI1 will be addressed during future research.

In spite of its long evolution in the photosynthetic lineage, chloroplastic CrRPI1 seems to have no major structural difference with previously described RPI of the A-type. Some putative regulatory elements are diverging from other studied RPI_A and will need further functional characterizations. The co-regulations exerted by multiples signaling pathways on RPI, the coordinated regulations on RPI, and the rest of the metabolic pathways it belongs to should be further computed in a systems biology perspective. For this purpose, our high-resolution crystal structure of the first chloroplastic ribose-phosphate isomerase serves as a general blueprint for the analytic and synthetic biochemistry of an essential step of photosynthesis.

4. Materials and Methods

4.1. Cloning

The amino acid sequence of *Chlamydomonas reinhardtii* ribose-5-phosphate isomerase (Cre03.g187450, UniRef100 entry A8IRQ1) was analyzed with TargetP2.0 [40], ChloroP [41] and Predalgo [8] to predict the transit peptide cleavage site. The subsequent mature sequence of chloroplastic protein coding for amino acids 23 to 269 was amplified by PCR using a forward primer introducing an NcoI restriction site (bolded) at the start codon: 5′-CGCA**CCATGG**CCGCGCCGGTCTCAA-3′ and a reverse primer introducing a BamHI restriction site (bolded) downstream of the stop codon: 5′-GCACG**GGATCC**TTAGTGCTTCTTGGGGTTGGG-3′ as previously reported [30]. The PCR was performed using the *Chlamydomonas reinhardtii* EST index [42] database plasmid AV390085 obtained from the Kazusa DNA Research Institute (Chiba, Japan). After purification, the PCR product was digested by NcoI and BamHI and cloned into the NdeI and BamHI restriction sites of a modified pET-3d-His vector allowing expression of the protein with a polyhistidine-tag at the N-terminus. The resulting plasmid, pET3d-His-CrRPI1 was then validated by Sanger sequencing.

4.2. Protein Expression and Purification

Recombinant CrRPI1 was produced using the *Escherichia coli* strain BL21(DE3) Rosetta-2 pLysS (Novagen Merck, Darmstadt, Germany) transformed with the pET3d-His6-CrRPI1 plasmid. Bacteria were grown in LB medium supplemented with ampicillin (100 μg/mL) at 37 °C until the culture reached exponential phase at an optical density at 600 nm of 0.4. The expression of RPI was then induced by addition of 0.2 mmol/L of IPTG and incubation at 27 °C for three hours. Cells were harvested by centrifugation 5000 rcf for 10 min at 4 °C, resuspended in 30 mmol/L Tris-HCL pH = 7.9, 0.5 mmol/L EDTA (buffer A), and lysed by 2 min sonication with 0.4 sec pulses at output 5 on W-375 sonicator equipped with microtip (Qsonica, Newtown, CT, USA). The total extract was then centrifuged at 20,000 rcf for 20 min and the soluble fraction loaded on an affinity chromatography with 2 mL of NiNTA resin (Sigma-Aldrich Merck, Darmstad, Germany). The resin was washed with Buffer A supplemented with increasing concentrations of imidazole (10 mmol/L, 20 mmol/L, and 30 mmol/L). CrRPI1 was then eluted in with buffer A supplemented with 100 mmol/L, 200 mmol/L

and 300 mmol/L of imidazole. Fractions were then analyzed by SDS-PAGE on a 12% acrylamide gel revealed by Coomassie blue staining. Fractions containing purified CrRPI1 were pooled, and buffer exchanged against buffer A prior to being concentrated by ultrafiltration on 3000 MWCO filter units (Millipore Merck, Darmstadt, Germany). A final concentration of 9 $mg.mL^{-1}$ was measured by NanoDrop 2000 spectrophotometer (Thermo Fisher Scientific, Waltham, MA, USA) with theoretical Mw = 27,551 $g.mol^{-1}$ and ε = 14,565 $mol^{-1}.L.cm^{-1}$. Proteins were then analyzed by injection on a Superose 6 increase size exclusion chromatography column in buffer C (20 mM Tris-HCl pH 7.9, 100 mmol/L NaCl).

4.3. Protein Crystallization and Structure Determination

Purified CrRPI1 was tested for crystallization on commercial sparse-screening conditions (Qiagen, Hilden Germany) of the Joint Center for Structural Genomics screens [43] and JBScreen classic 1–8 (Jena Bioscience, Jena, Germany) with a mixture of 50 nL of protein and 50 nL of precipitant solution equilibrated against 30 µL of reservoir solution at 20 °C. Two monocrystal grew after one year in conditions JBScreen 6-C8 (3 $mmol.L^{-1}$ ammonium sulfate) and JBScreen 6-D9 (3 $mmol.L^{-1}$ ammonium sulfate, 20% glycerol). Crystals were flash frozen in liquid nitrogen for diffraction experiments at Proxima-1 beamline of SOLEIL synchrotron (Gif sur Yvette, France) [44]. A 99.63% complete dataset at 1.40 Å resolution was obtained from 3600 images over 360° of phi rotation and indexed in the $P2_1$ space group, integrated, scaled and converted with XDSME [45]. Structure was phased by molecular replacement with PHENIX [46,47], PHASER-MR [48] using a search model obtained from the Robetta server [49]. Two CrRPI1 monomers were found in the asymmetric unit. Model was then refined by iterative cycle of manual building in WinCOOT [50,51], followed by refinement with PHENIX.REFINE [52] until completion of a structure passing MOLPROBITY [53] evaluation with 100% residues in Ramachandran restrains, RMS(bond) = 0.011, RMS(angles) = 1.18 and final Rwork = 0.1594, Rfree = 0.1774 (Table 1). Structure representations were drawn with PYMOL (Schrodinger, New York, NY, USA).

4.4. SEC-SAXS Analysis

Here, 50 µL of pure CrRPI1 at a concentration of 10 $mg.mL^{-1}$ were injected on BioSEC-3 300 size-exclusion chromatography column (Agilent Technologies, Santa Clara, CA, USA) equilibrated in buffer C, in series with the small-angle X-rays scattering (SAXS) exposure capillary at the synchrotron beamline SWING (SOLEIL, Gif sur Yvette, France). Collected scattering images were analyzed on the application Foxtrot 3.3.4 (Xenocs, Sassenage, France) and the ATSAS 2.8.3 suite [54,55]. PrimusQT calculated a radius of gyration of 28.16 ± 0.18 Å and estimated SAXS CrRPI1 molecular weight at 52,781 Da (Qp), 53,991 Da (MoW), 49,221 (Vc), and 55,257 Da (size and shape). This molecular weight allows us to fit between 1.78 and 2.00 times the molecular weight of monomeric recombinant CrRPI1 estimated with Expasy ProtParam at 27,551 Da.

4.5. Structural Data

Crystallographic data are registered at the Protein Data Bank under accession code 6ZXT.

Supplementary Materials: Supplementary materials can be found at http://www.mdpi.com/1422-0067/21/20/7787/s1. Figure S1. Sequence alignment made by Clustal Omega of RPI_A from different species. Residues with more than 50 % conservation are colored in red, strictly conserved residues are in white with a red background. Numbering is according to *Chlamydomonas reinhardtii*. RPI sequences were retrieved from uniprotKB database for the following species: *Chlamydomonas reinhardtii* (A8IRQ1), *Glycine Max* (I1NC83), *Arabidopsis thaliana* (Q9S726), *Plasmodium falciparum* (Q8I3W2), *Deinococcus radiodurans* (Q9RW24), *Streptococcus pneumoniae* (B2INU5), *Mus musculus* (P47968), *Homo sapiens* (P49247), *Gonium pectorale* (A0A150H4N9), *Volvox carteri f. nagariensis* (D8TV46), *Chlorella sorokiniana* (A0A2P6TRF5), *Raphidocelis subcapitata* (A0A2V0PB57), *Chlorella variabilis* (E1Z7C4), *Chlamydomonas eustigma* (A0A250XAH6), *Polytomella sp. Pringsheim 198.80* (K0J8U0), *Thermus thermophilus* (Q72J47), *Synechocystis sp. PCC6803* (Q55766), *Burkholderia thailandensis* (A0A2Z4SMZ7), *Legionella pneumophila* (A5I9R2). Figure S2. Comparison of the catalytic clefts of CrRPI1 and LpRPI (PDB entry 6MC0). (A) Structures are aligned (RMSD = 0.701 Å) and represented in cartoon with side chains of catalytic pocket colored in magenta and

represented as sticks. Other residues of CrRPI1 and LpRPI are respectively colored in blue and green. Sulfate ion and Ribose-5-phosphate are represented in sticks, water molecules and Na ion are represented in spheres. (B) Structure of CrRPI1. (C) Structure of LpRPI. Figure S3. (A) CrRPI1 post-translational modifications sites. Residues of the catalytic cleft are colored in orange. Cysteines and residues found phosphorylated in Wang, Gau et al. are represented in sticks and respectively colored in red and blue. (B) Connolly solvent exclusion surface of the same view as A. and same color code.

Author Contributions: Conceptualization, S.D.L. and J.H.; investigation, T.L.M. and J.H.; resources, S.D.L. and J.H.; writing—original draft preparation, T.L.M. and J.H.; writing—review and editing, T.L.M., P.C., S.D.L., and J.H.; supervision, J.H.; funding acquisition, S.D.L. and J.H. All authors have read and agreed to the published version of the manuscript.

Funding: This research was funded by CNRS, Sorbonne Université and Agence Nationale de la Recherche Grants LABEX DYNAMO 11-LABX-0011 and JCJC CALVINTERACT ANR-19-CE11-0009.

Acknowledgments: We thank the FR 550 Institut de Biologie Physico-Chimique for the access to the crystallization platform and to the data visualization wall. We acknowledge SOLEIL beamlines Proxima-1 and Proxima-2a for providing the setup of X-ray diffraction experiments and beamline SWING for SAXS experiments. We thank Laure Michelet, Fernanda Borrega, and Sandrine Hoang for help with the preparation and characterization of the recombinant protein.

Conflicts of Interest: The authors declare no conflict of interest. The funders had no role in the design of the study; in the collection, analyses, or interpretation of data; in the writing of the manuscript, or in the decision to publish the results.

References

1. Pfannschmidt, T.; Yang, C. The hidden function of photosynthesis: A sensing system for environmental conditions that regulates plant acclimation responses. *Protoplasma* **2012**, *249* (Suppl 2), S125–S136. [CrossRef]
2. Benson, A.A.; Bassham, J.A.; Calvin, M.; Hall, A.G.; Hirsch, H.E.; Kawaguchi, S.; Lynch, V.; Tolbert, N.E. The path of carbon in photosynthesis. XV. Ribulose and sedoheptulose. *J. Biol. Chem.* **1952**, *196*, 703–716. [PubMed]
3. Zhang, R.; Andersson, C.E.; Savchenko, A.; Skarina, T.; Evdokimova, E.; Beasley, S.; Arrowsmith, C.H.; Edwards, A.M.; Joachimiak, A.; Mowbray, S.L. Structure of Escherichia coli ribose-5-phosphate isomerase: A ubiquitous enzyme of the pentose phosphate pathway and the Calvin cycle. *Structure* **2003**, *11*, 31–42. [CrossRef]
4. Chen, J.; Wu, H.; Zhang, W.; Mu, W. Ribose-5-phosphate isomerases: Characteristics, structural features, and applications. *Appl. Microbiol. Biotechnol.* **2020**, *104*, 6429–6441. [CrossRef] [PubMed]
5. Stincone, A.; Prigione, A.; Cramer, T.; Wamelink, M.M.; Campbell, K.; Cheung, E.; Olin-Sandoval, V.; Gruning, N.M.; Kruger, A.; Tauqeer Alam, M.; et al. The return of metabolism: Biochemistry and physiology of the pentose phosphate pathway. *Biol. Rev. Camb. Philos. Soc.* **2015**, *90*, 927–963. [CrossRef]
6. Sasso, S.; Stibor, H.; Mittag, M.; Grossman, A.R. From molecular manipulation of domesticated Chlamydomonas reinhardtii to survival in nature. *eLife* **2018**, *7*, e39233. [CrossRef] [PubMed]
7. Merchant, S.S.; Prochnik, S.E.; Vallon, O.; Harris, E.H.; Karpowicz, S.J.; Witman, G.B.; Terry, A.; Salamov, A.; Fritz-Laylin, L.K.; Marechal-Drouard, L.; et al. The Chlamydomonas genome reveals the evolution of key animal and plant functions. *Science* **2007**, *318*, 245–250. [CrossRef] [PubMed]
8. Tardif, M.; Atteia, A.; Specht, M.; Cogne, G.; Rolland, N.; Brugiere, S.; Hippler, M.; Ferro, M.; Bruley, C.; Peltier, G.; et al. PredAlgo: A new subcellular localization prediction tool dedicated to green algae. *Mol. Biol. Evol.* **2012**, *29*, 3625–3639. [CrossRef] [PubMed]
9. Johnson, X.; Alric, J. Central carbon metabolism and electron transport in Chlamydomonas reinhardtii: Metabolic constraints for carbon partitioning between oil and starch. *Eukaryot. Cell* **2013**, *12*, 776–793. [CrossRef]
10. Klein, U. Compartmentation of glycolysis and of the oxidative pentose-phosphate pathway in Chlamydomonas reinhardii. *Planta* **1986**, *167*, 81–86. [CrossRef]
11. Strenkert, D.; Schmollinger, S.; Gallaher, S.D.; Salome, P.A.; Purvine, S.O.; Nicora, C.D.; Mettler-Altmann, T.; Soubeyrand, E.; Weber, A.P.M.; Lipton, M.S.; et al. Multiomics resolution of molecular events during a day in the life of Chlamydomonas. *Proc. Natl. Acad. Sci. USA* **2019**, *116*, 2374–2383. [CrossRef] [PubMed]

12. Hammel, A.; Sommer, F.; Zimmer, D.; Stitt, M.; Mühlhaus, T.; Schroda, M. Overexpression of sedoheptulose-1,7-bisphosphatase enhances photosynthesis in *Chlamydomonas reinhardtii* and has no effect on the abundance of other Calvin-Benson cycle enzymes. *bioRxiv* **2020**. [CrossRef]
13. Mettler, T.; Muhlhaus, T.; Hemme, D.; Schottler, M.A.; Rupprecht, J.; Idoine, A.; Veyel, D.; Pal, S.K.; Yaneva-Roder, L.; Winck, F.V.; et al. Systems Analysis of the Response of Photosynthesis, Metabolism, and Growth to an Increase in Irradiance in the Photosynthetic Model Organism Chlamydomonas reinhardtii. *Plant Cell* **2014**, *26*, 2310–2350. [CrossRef] [PubMed]
14. Scheibe, R. Redox-modulation of chloroplast enzymes: A common principle for individual control. *Plant Physiol.* **1991**, *96*, 1–3. [CrossRef] [PubMed]
15. Michelet, L.; Zaffagnini, M.; Morisse, S.; Sparla, F.; Perez-Perez, M.E.; Francia, F.; Danon, A.; Marchand, C.H.; Fermani, S.; Trost, P.; et al. Redox regulation of the Calvin-Benson cycle: Something old, something new. *Front. Plant Sci.* **2013**, *4*, 470. [CrossRef]
16. Morisse, S.; Zaffagnini, M.; Gao, X.H.; Lemaire, S.D.; Marchand, C.H. Insight into protein S-nitrosylation in Chlamydomonas reinhardtii. *Antioxid. Redox. Signal.* **2014**, *21*, 1271–1284. [CrossRef]
17. Michelet, L.; Zaffagnini, M.; Vanacker, H.; Le Marechal, P.; Marchand, C.; Schroda, M.; Lemaire, S.D.; Decottignies, P. In vivo targets of S-thiolation in Chlamydomonas reinhardtii. *J. Biol. Chem.* **2008**, *283*, 21571–21578. [CrossRef]
18. Huppe, H.C.; Buchanan, B.B. Activation of a chloroplast type of fructose bisphosphatase from Chlamydomonas reinhardtii by light-mediated agents. *Z. Naturforsch. C J. Biosci.* **1989**, *44*, 487–494. [CrossRef]
19. Pasquini, M.; Fermani, S.; Tedesco, D.; Sciabolini, C.; Crozet, P.; Naldi, M.; Henri, J.; Vothknecht, U.; Bertucci, C.; Lemaire, S.D.; et al. Structural basis for the magnesium-dependent activation of transketolase from Chlamydomonas reinhardtii. *Biochim. Biophys. Acta Gen. Subj.* **2017**, *1861*, 2132–2145. [CrossRef]
20. Perez-Perez, M.E.; Mauries, A.; Maes, A.; Tourasse, N.J.; Hamon, M.; Lemaire, S.D.; Marchand, C.H. The Deep Thioredoxome in Chlamydomonas reinhardtii: New Insights into Redox Regulation. *Mol. Plant* **2017**, *10*, 1107–1125. [CrossRef]
21. Wang, H.; Gau, B.; Slade, W.O.; Juergens, M.; Li, P.; Hicks, L.M. The global phosphoproteome of Chlamydomonas reinhardtii reveals complex organellar phosphorylation in the flagella and thylakoid membrane. *Mol. Cell. Proteom.* **2014**, *13*, 2337–2353. [CrossRef] [PubMed]
22. Holmes, M.A.; Buckner, F.S.; Van Voorhis, W.C.; Verlinde, C.L.; Mehlin, C.; Boni, E.; DeTitta, G.; Luft, J.; Lauricella, A.; Anderson, L.; et al. Structure of ribose 5-phosphate isomerase from Plasmodium falciparum. *Acta Crystallogr. Sect. F Struct. Biol. Cryst. Commun.* **2006**, *62*, 427–431. [CrossRef] [PubMed]
23. Essenberg, M.K.; Cooper, R.A. Two ribose-5-phosphate isomerases from Escherichia coli K12: Partial characterisation of the enzymes and consideration of their possible physiological roles. *Eur. J. Biochem.* **1975**, *55*, 323–332. [CrossRef] [PubMed]
24. Rutner, A.C. Spinach 5-phosphoribose isomerase. Purification and properties of the enzyme. *Biochemistry* **1970**, *9*, 178–184. [CrossRef] [PubMed]
25. Krissinel, E.; Henrick, K. Inference of macromolecular assemblies from crystalline state. *J. Mol. Biol.* **2007**, *372*, 774–797. [CrossRef]
26. Landau, M.; Mayrose, I.; Rosenberg, Y.; Glaser, F.; Martz, E.; Pupko, T.; Ben-Tal, N. ConSurf 2005: The projection of evolutionary conservation scores of residues on protein structures. *Nucleic Acids Res.* **2005**, *33*, W299–W302. [CrossRef]
27. Jurrus, E.; Engel, D.; Star, K.; Monson, K.; Brandi, J.; Felberg, L.E.; Brookes, D.H.; Wilson, L.; Chen, J.; Liles, K.; et al. Improvements to the APBS biomolecular solvation software suite. *Protein Sci. Publ. Protein Soc.* **2018**, *27*, 112–128. [CrossRef]
28. Dolinsky, T.J.; Czodrowski, P.; Li, H.; Nielsen, J.E.; Jensen, J.H.; Klebe, G.; Baker, N.A. PDB2PQR: Expanding and upgrading automated preparation of biomolecular structures for molecular simulations. *Nucleic Acids Res.* **2007**, *35*, W522–W525. [CrossRef]
29. Hamada, K.; Ago, H.; Sugahara, M.; Nodake, Y.; Kuramitsu, S.; Miyano, M. Oxyanion hole-stabilized stereospecific isomerization in ribose-5-phosphate isomerase (Rpi). *J. Biol. Chem.* **2003**, *278*, 49183–49190. [CrossRef]

30. Zaffagnini, M.; Bedhomme, M.; Groni, H.; Marchand, C.H.; Puppo, C.; Gontero, B.; Cassier-Chauvat, C.; Decottignies, P.; Lemaire, S.D. Glutathionylation in the photosynthetic model organism Chlamydomonas reinhardtii: A proteomic survey. *Mol. Cell. Proteom.* **2012**, *11*, M111.014142. [CrossRef]
31. Szklarczyk, D.; Gable, A.L.; Lyon, D.; Junge, A.; Wyder, S.; Huerta-Cepas, J.; Simonovic, M.; Doncheva, N.T.; Morris, J.H.; Bork, P.; et al. STRING v11: Protein-protein association networks with increased coverage, supporting functional discovery in genome-wide experimental datasets. *Nucleic Acids Res.* **2019**, *47*, D607–D613. [CrossRef]
32. Morisse, S.; Michelet, L.; Bedhomme, M.; Marchand, C.H.; Calvaresi, M.; Trost, P.; Fermani, S.; Zaffagnini, M.; Lemaire, S.D. Thioredoxin-dependent redox regulation of chloroplastic phosphoglycerate kinase from Chlamydomonas reinhardtii. *J. Biol. Chem.* **2014**, *289*, 30012–30024. [CrossRef] [PubMed]
33. Marri, L.; Zaffagnini, M.; Collin, V.; Issakidis-Bourguet, E.; Lemaire, S.D.; Pupillo, P.; Sparla, F.; Miginiac-Maslow, M.; Trost, P. Prompt and easy activation by specific thioredoxins of calvin cycle enzymes of Arabidopsis thaliana associated in the GAPDH/CP12/PRK supramolecular complex. *Mol. Plant* **2009**, *2*, 259–269. [CrossRef] [PubMed]
34. Lemaire, S.D.; Tedesco, D.; Crozet, P.; Michelet, L.; Fermani, S.; Zaffagnini, M.; Henri, J. Crystal Structure of Chloroplastic Thioredoxin f2 from Chlamydomonas reinhardtii Reveals Distinct Surface Properties. *Antioxidants* **2018**, *7*, 171. [CrossRef] [PubMed]
35. Gurrieri, L.; Del Giudice, A.; Demitri, N.; Falini, G.; Pavel, N.V.; Zaffagnini, M.; Polentarutti, M.; Crozet, P.; Marchand, C.H.; Henri, J.; et al. Arabidopsis and Chlamydomonas phosphoribulokinase crystal structures complete the redox structural proteome of the Calvin-Benson cycle. *Proc. Natl. Acad. Sci. USA* **2019**, *116*, 8048–8053. [CrossRef]
36. Graille, M.; Meyer, P.; Leulliot, N.; Sorel, I.; Janin, J.; Van Tilbeurgh, H.; Quevillon-Cheruel, S. Crystal structure of the S. cerevisiae D-ribose-5-phosphate isomerase: Comparison with the archaeal and bacterial enzymes. *Biochimie* **2005**, *87*, 763–769. [CrossRef]
37. Ishikawa, K.; Matsui, I.; Payan, F.; Cambillau, C.; Ishida, H.; Kawarabayasi, Y.; Kikuchi, H.; Roussel, A. A hyperthermostable D-ribose-5-phosphate isomerase from Pyrococcus horikoshii characterization and three-dimensional structure. *Structure* **2002**, *10*, 877–886. [CrossRef]
38. Dickens, F. Recent advances in knowledge of the hexose monophosphate shunt. *Ann. N. Y. Acad. Sci.* **1958**, *75*, 71–94. [CrossRef]
39. Kuken, A.; Sommer, F.; Yaneva-Roder, L.; Mackinder, L.C.; Hohne, M.; Geimer, S.; Jonikas, M.C.; Schroda, M.; Stitt, M.; Nikoloski, Z.; et al. Effects of microcompartmentation on flux distribution and metabolic pools in Chlamydomonas reinhardtii chloroplasts. *eLife* **2018**, *7*, e37960. [CrossRef]
40. Emanuelsson, O.; Brunak, S.; von Heijne, G.; Nielsen, H. Locating proteins in the cell using TargetP, SignalP and related tools. *Nat. Protoc.* **2007**, *2*, 953–971. [CrossRef]
41. Emanuelsson, O.; Nielsen, H.; von Heijne, G. ChloroP, a neural network-based method for predicting chloroplast transit peptides and their cleavage sites. *Protein Sci. Publ. Protein Soc.* **1999**, *8*, 978–984. [CrossRef]
42. Asamizu, E.; Nakamura, Y.; Miura, K.; Fukuzawa, H.; Fujiwara, S.; Hirono, M.; Iwamoto, K.; Matsuda, Y.; Minagawa, J.; Shimogawara, K.; et al. Establishment of publicly available cDNA material and information resource of Chlamydomonas reinhardtii (Chlorophyta) to facilitate gene function analysis. *Phycologia* **2004**, *43*, 722–726. [CrossRef]
43. Lesley, S.A.; Wilson, I.A. Protein production and crystallization at the joint center for structural genomics. *J. Struct. Funct. Genom.* **2005**, *6*, 71–79. [CrossRef] [PubMed]
44. Coati, A.; Chavas, L.M.G.; Fontaine, P.; Foos, N.; Guimaraes, B.; Gourhant, P.; Legrand, P.; Itie, J.P.; Fertey, P.; Shepard, W.; et al. Status of the crystallography beamlines at synchrotron SOLEIL. *Eur. Phys. J. Plus* **2017**, *132*, 174. [CrossRef]
45. Legrand, P. XDSME: XDS Made Easier. 2017. Available online: https://github.com/legrandp/xdsme (accessed on 20 October 2020).
46. Adams, P.D.; Afonine, P.V.; Bunkoczi, G.; Chen, V.B.; Davis, I.W.; Echols, N.; Headd, J.J.; Hung, L.W.; Kapral, G.J.; Grosse-Kunstleve, R.W.; et al. PHENIX: A comprehensive Python-based system for macromolecular structure solution. *Acta Crystallogr. D Biol. Crystallogr.* **2010**, *66*, 213–221. [CrossRef] [PubMed]

47. Adams, P.D.; Afonine, P.V.; Bunkoczi, G.; Chen, V.B.; Echols, N.; Headd, J.J.; Hung, L.W.; Jain, S.; Kapral, G.J.; Grosse Kunstleve, R.W.; et al. The Phenix software for automated determination of macromolecular structures. *Methods* **2011**, *55*, 94–106. [CrossRef] [PubMed]
48. McCoy, A.J.; Grosse-Kunstleve, R.W.; Adams, P.D.; Winn, M.D.; Storoni, L.C.; Read, R.J. Phaser crystallographic software. *J. Appl. Crystallogr.* **2007**, *40*, 658–674. [CrossRef] [PubMed]
49. Raman, S.; Vernon, R.; Thompson, J.; Tyka, M.; Sadreyev, R.; Pei, J.; Kim, D.; Kellogg, E.; DiMaio, F.; Lange, O.; et al. Structure prediction for CASP8 with all-atom refinement using Rosetta. *Proteins* **2009**, *77* (Suppl. 9), 89–99. [CrossRef]
50. Emsley, P.; Cowtan, K. Coot: Model-building tools for molecular graphics. *Acta Crystallogr. D Biol. Crystallogr.* **2004**, *60*, 2126–2132. [CrossRef]
51. Emsley, P.; Lohkamp, B.; Scott, W.G.; Cowtan, K. Features and development of Coot. *Acta Crystallogr. Sect. D Biol. Crystallogr.* **2010**, *66*, 486–501. [CrossRef]
52. Afonine, P.V.; Grosse-Kunstleve, R.W.; Echols, N.; Headd, J.J.; Moriarty, N.W.; Mustyakimov, M.; Terwilliger, T.C.; Urzhumtsev, A.; Zwart, P.H.; Adams, P.D. Towards automated crystallographic structure refinement with phenix.refine. *Acta Crystallogr. Sect. D Biol. Crystallogr.* **2012**, *68*, 352–367. [CrossRef]
53. Chen, V.B.; Arendall, W.B., 3rd; Headd, J.J.; Keedy, D.A.; Immormino, R.M.; Kapral, G.J.; Murray, L.W.; Richardson, J.S.; Richardson, D.C. MolProbity: All-atom structure validation for macromolecular crystallography. *Acta Crystallogr. D Biol. Crystallogr.* **2010**, *66*, 12–21. [CrossRef] [PubMed]
54. Petoukhov, M.V.; Franke, D.; Shkumatov, A.V.; Tria, G.; Kikhney, A.G.; Gajda, M.; Gorba, C.; Mertens, H.D.; Konarev, P.V.; Svergun, D.I. New developments in the ATSAS program package for small-angle scattering data analysis. *J. Appl. Crystallogr.* **2012**, *45*, 342–350. [CrossRef] [PubMed]
55. Franke, D.; Petoukhov, M.V.; Konarev, P.V.; Panjkovich, A.; Tuukkanen, A.; Mertens, H.D.T.; Kikhney, A.G.; Hajizadeh, N.R.; Franklin, J.M.; Jeffries, C.M.; et al. ATSAS 2.8: A comprehensive data analysis suite for small-angle scattering from macromolecular solutions. *J. Appl. Crystallogr.* **2017**, *50*, 1212–1225. [CrossRef]

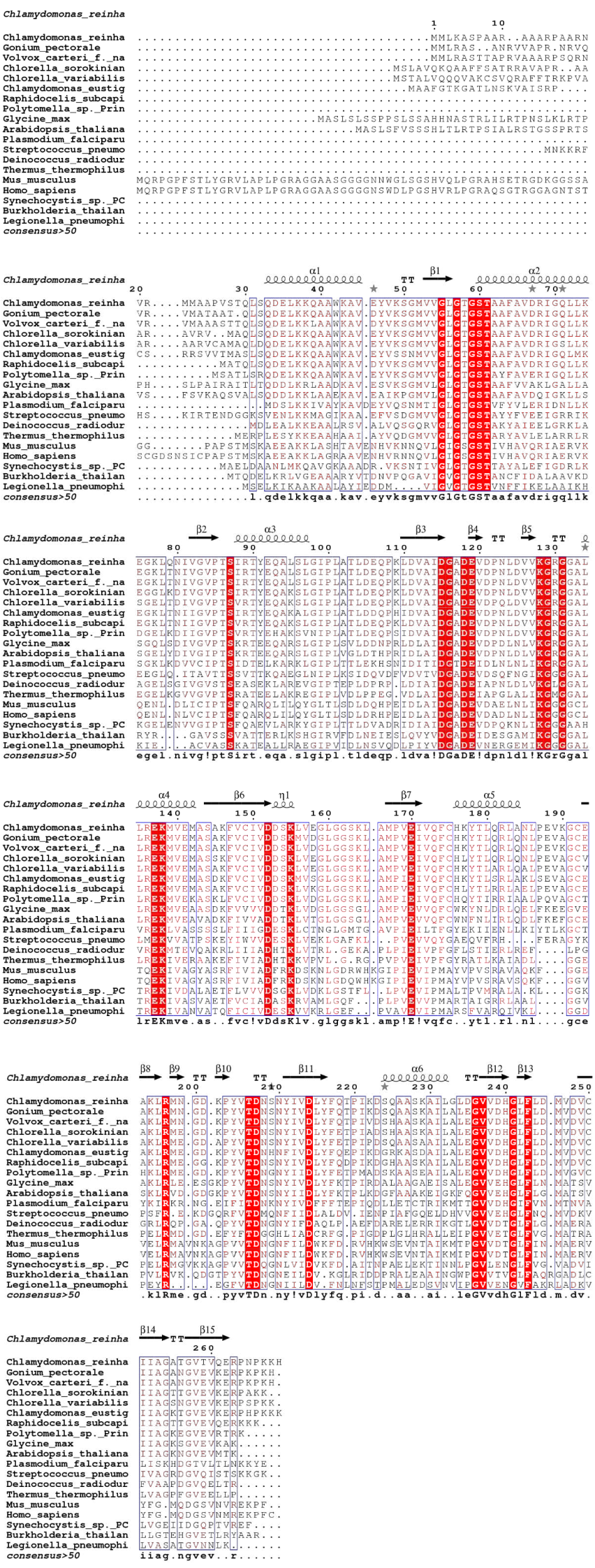

Supplementary figure S1: Sequence alignment made by Clustal Omega of RPI_A from different species. Residues with more than 50 % conservation are colored in red, strictly conserved residues are in white with a red background. Numbering is according to *Chlamydomonas reinhardtii*. RPI sequences were retrieved from uniprotKB database for the following species : *Chlamydomonas reinhardtii* (A8IRQ1), *Glycine Max* (I1NC83), *Arabidopsis thaliana* (Q9S726), *Plasmodium falciparum* (Q8I3W2), *Deinococcus radiodurans* (Q9RW24), *Streptococcus pneumoniae* (B2INU5), *Mus musculus* (P47968), *Homo sapiens* (P49247), *Gonium pectorale* (A0A150H4N9), *Volvox carteri f. nagariensis* (D8TV46), *Chlorella sorokiniana* (A0A2P6TRF5), *Raphidocelis subcapitata* (A0A2V0PB57), *Chlorella variabilis* (E1Z7C4), *Chlamydomonas eustigma* (A0A250XAH6), *Polytomella sp. Pringsheim 198.80* (K0J8U0), *Thermus thermophilus* (Q72J47), *Synechocystis sp. PCC6803* (Q55766), *Burkholderia thailandensis* (A0A2Z4SMZ7), *Legionella pneumophila* (A5I9R2).

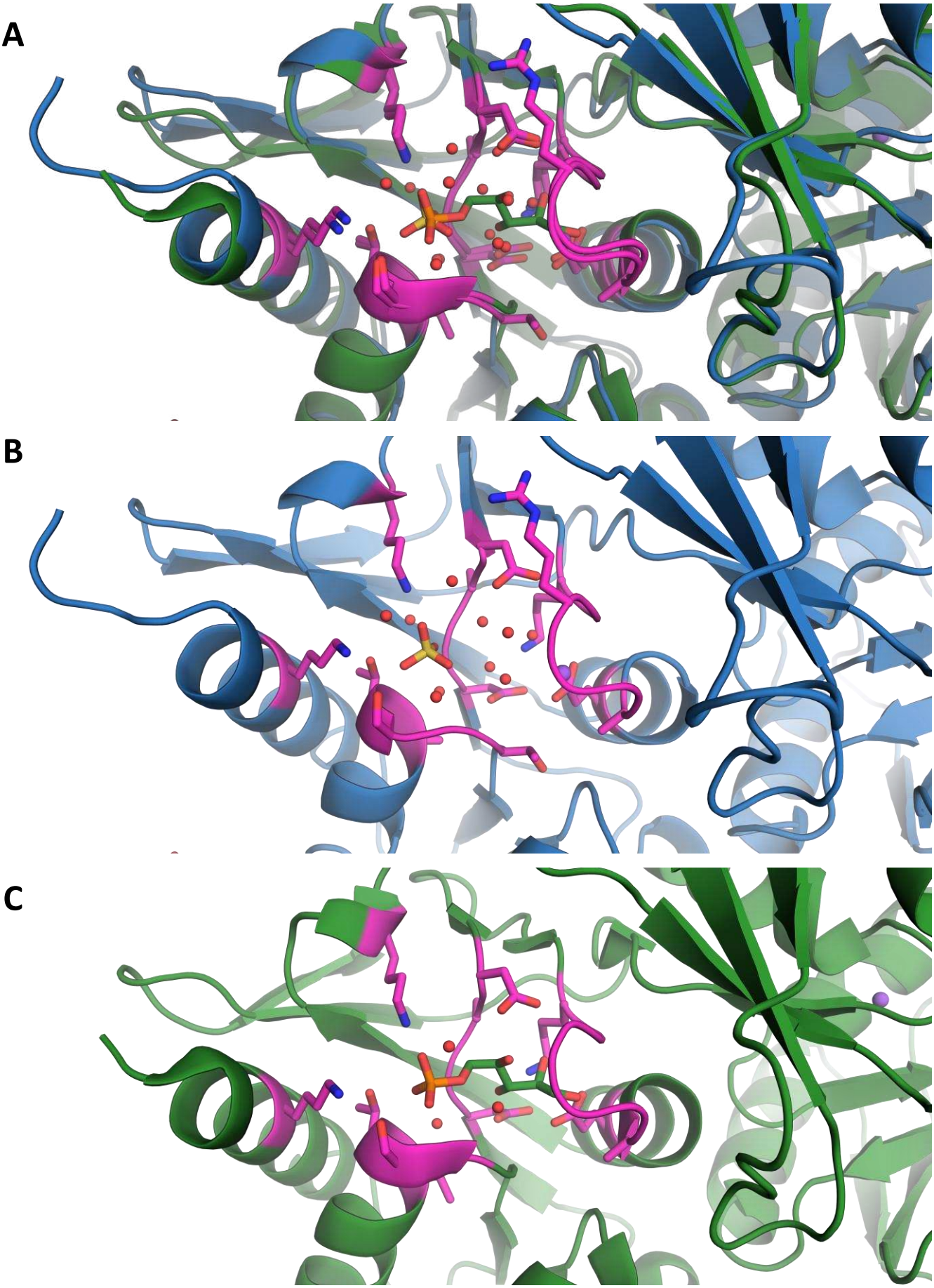

Supplementary figure S2: Comparison of the catalytic clefts of CrRPI1 and LpRPI (PDB entry 6MC0). (**A**) Structures are aligned (RMSD= 0.701 Å) and represented in cartoon with side chains of catalytic pocket colored in magenta and represented as sticks. Other residues of CrRPI1 and LpRPI are respectively colored in blue and green. Sulfate ion and Ribose-5-phosphate are represented in sticks, water molecules and Na ion are represented in spheres. (**B**) Structure of CrRPI1. (**C**) Structure of LpRPI.

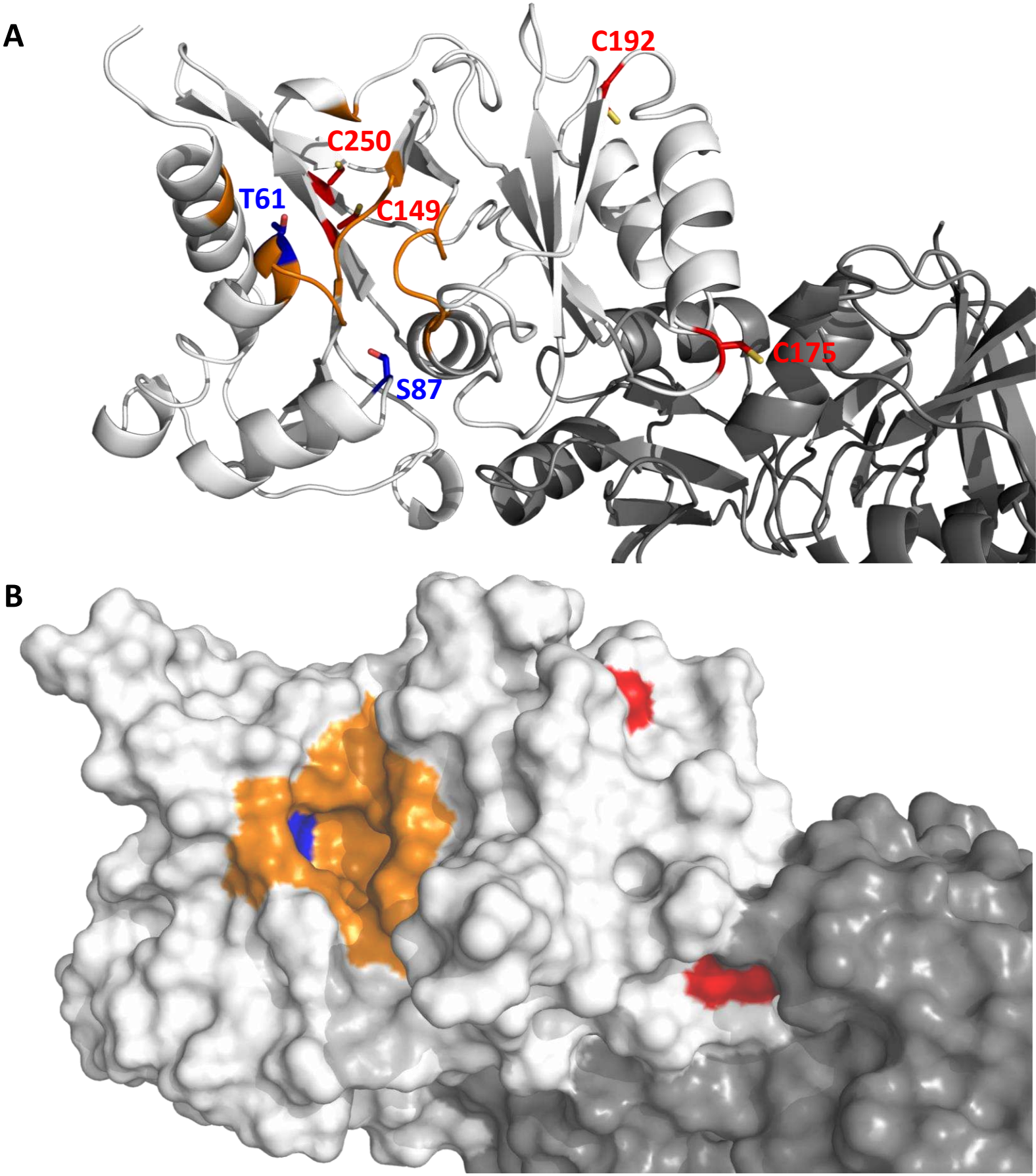

Supplementary figure S3: (**A**) CrRPI1 post-translational modifications sites. Residues of the catalytic cleft are colored in orange. Cysteines and residues found phosphorylated in Wang, Gau *et al.* are represented in sticks and respectively colored in red and blue. (**B**) Connolly solvent exclusion surface of the same view as A. and same color code.

2.1.1.3 Conclusion

La description de cette première structure cristallographique de RPI1 chloroplastique nous a permis de confirmer que celle-ci possédait un repliement similaire à celles précédemment décrites dans les voies cataboliques. Le mécanisme catalytique est probablement le même entre les RPI des différentes voies. Au contraire, la présence de plusieurs résidus ciblés par différentes modifications post-traductionnelles à proximité du site catalytique semble évoquer une régulation complexe et différenciée selon la voie dans laquelle l'enzyme est engagée. Les modifications redox en aval de l'activité des photosystèmes pourraient contribuer à une activation allostérique de RPI1, par des changements conformationnels à distance du site catalytique. La modification redox pourrait contribuer à la stabilisation de complexes hétéro-multimériques incluant RPI1 auparavant proposés (Küken et al. 2018; Suss et al. 1993; Skrukrud et al. 1991).

2.1.2 Fructose-1,6-bisphosphate aldolase 3

2.1.2.1 Résumé de l'article

CrFBA3 a été l'objet d'une publication le 6 juin 2022 dans la revue *Journal of Structural Biology*. Notre étude a été menée en deux parties, d'une part la description de la structure cristallographique de CrFBA3 déterminée à une résolution de 2,36 Å (Code PDB : 7B2N), d'autre part, le tri parmi les séquences paralogues de FBA de celles dont la fonction est affectée au CBBC. L'analyse de séquences par le logiciel ProfileView a été conduite par nos collaborateurs au Laboratoire de Biologie Computationnelle et Quantitative : Pr. Alessandra Carbone et Dr. Edoardo Sarti. L'étude démontre la capacité de ProfileView à discriminer les paralogues selon leurs fonctions cellulaires, permettant une classification fonctionnelle des enzymes à partir de leurs séquences. En pratique, ProfileView nous a permis de valider FBA3 comme l'aldolase du CBBC, par opposition aux FBA1, 2, et 4 qui sont classées non-photosynthétiques.

Comme CrRPI1, CrFBA3 participe à la régénération du substrat de la Rubisco dans le CBBC. FBA3 catalyse deux réactions distinctes, l'association du dihydroxyacétone phosphate (DHAP) avec le

glyceraldéhyde-3-phosphate (G3P) ou l'érythrose-4-phosphate (E4P) pour former respectivement du fructose-1,6-bisphosphate (FBP) ou du sédoheptulose-1,7-bisphosphate (SBP) (Benson et al. 1952). Dans la glycolyse, l'aldolase assure la catalyse de la rupture du FBP en DHAP et G3P. Comme RPI, de nombreuses études structurales et enzymatiques existent sur des FBA cytoplasmiques de la glycolyse. La détermination de la structure de FBA3 en fait néanmoins la première représentante d'une structure de FBA chloroplastique du CBBC.

La structure de CrFBA3, des expériences de SAXS et des analyses de chromatographie d'exclusion de taille s'accordent pour conclure que CrFBA3 est un homo-tétramère composé de quatre sous-unités de FBA3 virtuellement identiques, ayant un repliement centré sur un tonneau α8/β8 TIM (CATH classification 3.20.20) et composé de onze hélices α et neuf brins β (Figure 1 de Le Moigne et al. (2022b)).

L'identification du site actif de la protéine a été faite en vérifiant la conservation des onze résidus identifiés comme faisant partie du site actif dans les FBA glycolytiques (Gardberg et al. 2011b; Gardberg et al. 2011a; Lafrance-Vanasse and Sygusch 2007; St-Jean et al. 2005; Dalby et al. 1999) et également par la présence d'un ou deux ions sulfates coordonnés par ces résidus dans les différentes sous-unités modélisées dans l'unité asymétrique de CrFBA3. En superposant ces onze acides aminés aux onze même acides aminés d'autres structures de FBA (D52, S54, T57, K125, K164, R166, E204, K246, S288, R318), on peut supposer que le mécanisme catalytique est identique parmi les FBA paralogues (Figure 3 de Le Moigne et al. (2022b)).

FBA3 est également retrouvée comme la cible de plusieurs modifications post-traductionnelles (Wang et al. 2014; Zaffagnini et al. 2012a). Les cystéines 58, 142 et 256 sont ainsi identifiées comme cibles de S-nitrosylation et les cystéines 58 et 142, cibles de S-glutathionylation (Zaffagnini et al. 2012a). Pour les résidus phosphorylés, quatre sérines et une thréonine sont connues. La sérine 54 et la thréonine 57 font partie de ces acides aminés retrouvés phosphorylés, mais ils font aussi partie des résidus permettant la fixation du substrat au site actif (Figure 5 de Le Moigne et al. (2022b)). Ces phosphorylations pourraient donc provoquer un problème d'encombrement stérique couplé à une répulsion de charges négatives

avec le substrat dans son site de liaison. Comme proposé pour RPI, ces phosphorylations pourraient avoir une fonction inhibitrice sur le site catalytique.

L'analyse de séquences par la méthode ProfileView a quant à elle permis de confirmer la fonction photosynthétique de CrFBA3, la distinguant effectivement des autres FBA (CrFBA1, CrFBA2, et CrFBA4 codées par le même organisme). Le tri de paralogues amène des prédictions de fonction photosynthétiques ou non photosynthétiques pour 3886 séquences de FBA de la banque Pfam, facilitant l'identification future des FBA photosynthétiques chez d'autres organismes (Figure 6 de Le Moigne et al. (2022b)).

2.1.2.2 Crystal structure of chloroplast fructose-1,6-bisphosphate aldolase from the green alga Chlamydomonas reinhardtii

Journal of Structural Biology 214 (2022) 107873

Contents lists available at ScienceDirect

Journal of Structural Biology

journal homepage: www.elsevier.com/locate/yjsbi

Research Article

Crystal structure of chloroplast fructose-1,6-bisphosphate aldolase from the green alga *Chlamydomonas reinhardtii*

Théo Le Moigne [a,b,c], Edoardo Sarti [a], Antonin Nourisson [d,e], Mirko Zaffagnini [f], Alessandra Carbone [a], Stéphane D. Lemaire [a,b], Julien Henri [a,b,*]

[a] Sorbonne Université, CNRS, UMR 7238, Institut de Biologie Paris-Seine, Laboratoire de Biologie Computationnelle et Quantitative, 4 place Jussieu, F-75005 Paris, France
[b] Sorbonne Université, CNRS, UMR 8226, Institut de Biologie Physico-Chimique, Laboratoire de Biologie Moléculaire et Cellulaire des Eucaryotes, 13 rue Pierre et Marie Curie, 75005 Paris, France
[c] Faculty of Sciences, Doctoral School of Plant Sciences, Université Paris-Saclay, 91190 Saint-Aubin, France
[d] Institut Pasteur, Université de Paris, CNRS UMR3528, Unité Architecture et Dynamique des Macromolécules Biologiques, F-75015 Paris, France
[e] Sorbonne Université, ED515 Complexité du Vivant, F-75005 Paris, France
[f] Department of Pharmacy and Biotechnology, University of Bologna, 40126, Bologna, Italy

ARTICLE INFO

Edited by Bauke W. Dijkstra

Keywords:
Photosynthesis
Calvin-Benson-Bassham cycle
Carbon fixation
Aldolase
Enzyme
Structure
Functional classification
Post-translational modifications
Redox

ABSTRACT

The Calvin-Benson cycle fixes carbon dioxide into organic triosephosphates through the collective action of eleven conserved enzymes. Regeneration of ribulose-1,5-bisphosphate, the substrate of Rubisco-mediated carboxylation, requires two lyase reactions catalyzed by fructose-1,6-bisphosphate aldolase (FBA). While cytoplasmic FBA has been extensively studied in non-photosynthetic organisms, functional and structural details are limited for chloroplast FBA encoded by oxygenic phototrophs. Here we determined the crystal structure of plastidial FBA from the unicellular green alga *Chlamydomonas reinhardtii* (Cr). We confirm that *Cr*FBA folds as a TIM barrel, describe its catalytic pocket and homo-tetrameric state. Multiple sequence profiling classified the photosynthetic paralogs of FBA in a distinct group from non-photosynthetic paralogs. We mapped the sites of thiol- and phospho-based post-translational modifications known from photosynthetic organisms and predict their effects on enzyme catalysis.

1. Introduction

Photosynthesis is a paramount biological chain reaction sustaining life on Earth through the conversion of light energy into chemical energy and the subsequent fixation of atmospheric carbon into triosephosphates (Pfannschmidt and Yang 2012). The Calvin-Benson cycle (CBC) is an eleven enzymes cycle resulting in the production of six molecules of glyceraldehyde-3-phosphate (G3P) from three ribulose-1,5-bisphosphate (RuBP) and three carbon dioxides (Bassham et al., 1950). In order to regenerate RuBP and sustain the cycle, five G3P are recycled into three RuBP by a series of reactions involving eight out of eleven CBC enzymes. Two G3P are converted to dihydroxyacetone phosphate (DHAP), one is reacted with G3P to form fructose-1,6-bisphosphate (FBP) and the other is ligated with erythrose-4-phosphate (E4P) to form sedoheptulose-1,7-bisphosphate (SBP) (Sharkey 2019). Both reactions are catalyzed by fructose-bisphosphate aldolase (FBA, E.C. 4.1.2.13), which therefore acts in two distinct steps of the CBC. Indeed, it can use two different couples of substrates and provides substrates to downstream fructose-1,6-bisphosphatase (FBPase) and sedoheptulose-1,7-bisphosphatase (SBPase). *Pisum sativum* FBAs were isolated from plant, and their enzymatic activity assayed (Anderson and Pacold 1972; Razdan et al., 1992). Change in FBA abundance are correlated with the activity of the CBC, supporting a potential control of FBA over photosynthetic carbon fixation (Haake et al., 1998; Simkin et al., 2015).

FBA is ubiquitous in the three phylogenetic kingdoms because it acts in the fourth step of glycolysis preparatory phase where it splits FBP into DHAP and G3P (Anderson and Advani, 1970; Fothergill-Gilmore and

* Corresponding author at: Sorbonne Université, CNRS, UMR 7238, Institut de Biologie Paris-Seine, Laboratoire de Biologie Computationnelle et Quantitative, 4 place Jussieu, F-75005 Paris, France.
E-mail address: julien.henri@sorbonne-universite.fr (J. Henri).

https://doi.org/10.1016/j.jsb.2022.107873
Received 21 February 2022; Received in revised form 31 May 2022; Accepted 2 June 2022
Available online 6 June 2022

Michels, 1993). The nuclear genome of the green alga *Chlamydomonas reinhardtii* codes for at least four aldolases paralogs: FBA1 (Uniprot entry A8JCY4, Ensembl gene CHLRE_01g006950v5), FBA2 (Uniprot entry A8I9H5, Ensembl gene CHLRE_02g093450v5), ALDCHL/FBA3 (Uniprot entry Q42690, Ensembl gene CHLRE_05g234550v5), and FBA4 (Uniprot entry A8I2Q9, Ensembl gene CHLRE_02g115650v5). ALDCHL/FBA3 is predicted to be localized in the chloroplast by its amino-terminal 17-residue (Tardif et al., 2012) or 27-residue transit peptide (Almagro Armenteros et al., 2019). Mature proteins containing 333/323 residues was quantified as the 9th most abundant protein in Chlamydomonas proteome (Schroda et al., 2015), the third most abundant CBC enzyme after Rubisco large and small subunits (Hammel et al., 2020). The estimated concentration of FBA3 is 4.2–10.1 amol/cell (Wienkoop et al., 2010; Hammel et al., 2020), or 75.1–658.5 μmol/L in the chloroplast stroma (Mettler et al., 2014; Hammel et al., 2020). DHAP and G3P substrates are respectively concentrated at 0.2 mmol/L and 0.01 mmol/L in Chlamydomonas illuminated by 41 μmol photons/m^2/s, and their concentrations increase at 0.7 mmol/L and 0.03 mmol/L under 145 μmol photons/m^2/s. Substrate over enzyme ratios are low (0.4 G3P:FBA, 9 DHAP:FBA at 145 μmol photons/m^2/s and 75.1 μmol/L enzyme, the lowest estimate of FBA3 concentration), indicating that FBA functions far from substrates saturation. This undersaturation of the active site is further confirmed by the relatively high K_M values reported for a bacterial FBA, which has Michaelis-Menten constants (K_M) for DHAP and G3P of 0.095 mmol/L and 1.17 mmol/L, respectively (Rozova et al., 2010). Moderate turnover numbers (k_{cat}) were observed ranging from 0.2 to 65 sec^{-1}. Although there is a lack of knowledge about the kinetic properties of the chloroplast isoforms, we can hypothesize that the catalytic capacity of FBA in the plastidial context is likely to exert a kinetic control over CBC metabolic flow.

FBA structures are classified into two groups, differentiated by their catalytic mechanism (Fothergill-Gilmore and Michels 1993; Reyes-Prieto and Bhattacharya 2007). Class I aldolases form a Schiff-base intermediate with the substrate DHAP while class II aldolases are metal-dependent enzymes using divalent cations (Flechner et al., 1999). The two classes have been described as evolutionary independent (Marsh and Lebherz 1992). Despite folding as a similar α/β TIM barrel (SCOPe lineage c.1.10), class I and II aldolases have dissimilar quaternary structures, class I aldolases being homotetrameric and class II aldolase homodimeric.

Mounting evidence supports that CBC enzymes are target of multiple post-translational modifications by means of reversible oxidation of cysteine thiols (reviewed in (Michelet et al., 2013; Zaffagnini et al., 2019; Müller-Schüssele et al., 2021)) or threonine/serine phosphorylation (Wang et al., 2014; Werth et al., 2019). *Cr*FBA3 has been retrieved in the thioredoxome of *Chlamydomonas reinhardtii* supporting the relative affinity of FBA3 for thioredoxin through residue Cys58 (Lemaire et al., 2004; Perez-Perez et al., 2017). *Cr*FBA3 was identified as a putative target of GSSG-mediated S-glutathionylation (Zaffagnini et al., 2012a), and it was also found undergoing S-nitrosylation on three cysteine sites (Cys58, Cys142, and Cys256 (Morisse et al., 2014)), and phosphorylation on Ser54, Thr57, Ser64, Ser170, Ser176 (Wang et al., 2014; Werth et al., 2019). Moreover, FBA was reported to be modified by lysine crotonylation in *Carica papaya* (Liu et al., 2018). FBA is subjected to lysine acetylation in *Arabidopsis* (Finkemeier et al., 2011), while *Chlamydomonas* FBA was found to interact with CP12, a small intrinsically disordered protein specifically involved in the formation of inhibitory supercomplex with two CBC enzymes, namely phosphoribulokinase and glyceraldehyde-3-phosphate dehydrogenase (PRK and GAPDH, respectively) (Erales et al., 2008; Yu et al., 2020). Post-translational modifications and protein-protein interactions may support reversible regulatory mechanisms of protein catalysis but their interpretation requires a precise mapping of modified groups in the context of the protein structure.

A functional classification of the *Cr*FBA paralogs among their homologs could support the unique role of *Cr*FBA3 in the carbon fixation pathway. The sequence-based computational method ProfileView (Vicedomini et al., 2019) has been recently designed to address the functional classification of the great diversity of homologous sequences hiding, in many cases, a variety of functional activities that cannot be anticipated. ProfileView relies on two main ideas: the use of multiple probabilistic models whose construction explores evolutionary information in large datasets of sequences (Bernardes et al., 2016; Ugarte et al., 2018; Vicedomini et al., 2021; Fortunato et al., 2016; Amato et al., 2017), and a new definition of a representation space where to look at sequences from the point of view of probabilistic models combined together. ProfileView has been previously applied to classify families of proteins for which functions should be discovered or characterized within known groups (Vicedomini et al., 2021). It was proven very successful in identifying functional differences between otherwise phylogenetically similar sequences. Here, we meet a new challenge and use ProfileView to distinguish paralogs by their function in the FBA family.

In order to determine the structure-function-regulation relationships of photosynthetic FBA, we solved the high-resolution structure of the recombinant protein from Chlamydomonas, and performed a computational analysis that confirms functional segregation of *Cr*FBA3 relative to the other FBA paralogs present in *Chlamydomonas*.

2. Results

2.1. CrFBA3 general structure

The recombinant FBA3 from *Chlamydomonas reinhardtii* was purified to homogeneity and the crystal structure was solved at 2.36 Å resolution. The protein crystallized in the C2 space group (Table 1) and the crystallographic model includes eight polypeptide chains of 329–332 residues numbered according to the UniProtKB entry Q42690. Residual electron density at 1 σ additionally allowed us to place 29 sulfate ions, one chloride ion, and 989 water molecules in the crystal asymmetric unit. Amino acids prior to Met27 and after Thr360 have not been modelled because of a lack of electron density, as expected for peptidic extensions of low complexity. Alignment of the eight chains onto each

Table 1
X-ray diffraction and crystallographic model statistics.

	Fructose bisphosphate aldolase
Wavelength (Å)	0.9840
Resolution range (Å)	46.67–2.36 (2.44–2.36)
Space group	C2
Unit cell (Å, °)	109.49–251.07–126.411–90–90.11–90
Total reflections	988,770 (90,253)
Unique reflexions	138,497 (13,155)
Multiplicity	7.1 (6.9)
Completeness (%)	99.42 (94.42)
Mean I/sigma(I)	13.34 (1.46)
Wilson B-factor ($Å^2$)	40.19
R-merge	0.2 (1.495)
R-meas	0.2159 (1.617)
R-pim	0.08067 (0.6089)
CC1/2	0.995 (0.566)
CC*	0.999 (0.85)
Reflections used in refinement	138,424 (13,104)
Reflections used for R-free	1984 (189)
R-work	0.2025 (0.3002)
R-free	0.2500 (0.3513)
CC (work)	0.954 (0.775)
CC (free)	0.921 (0.643)
RMS (bonds) (Å)	0.004
RMS (angles) (°)	0.63
Ramachandran favoured (%)	96.28
Ramachandran allowed (%)	3.34
Ramachandran outliers (%)	0.38
Rotamer outliers (%)	0.43
Clashscore	6.97
Average B-factor ($Å^2$)	46.74

other showed carbon alpha RMSD values comprised between 0.177 Å and 0.295 Å. All chains are therefore virtually identical except for some amino acid positions at N-terminal and/or C-terminal extremities, so we will focus on chain C for the following description, this chain being the most complete among the eight different chains of the asymmetric unit. Structural alignment of *Cr*FBA3 to the protein data bank archive returned 470 matches, with highest similarities towards *Arabidopsis thaliana* glycolytic FBA (PDB ID: 6RS1, Q-score = 0.88; RMSD = 0.93 Å), with *Plasmodium falciparum* FBA (PDB ID: 4TR9, Q-score = 0.87; RMSD = 0.89 Å), and with *Toxoplasma gondii* FBA (PDB ID: 4D2J, Q-score = 0.87; RMSD = 0.95 Å). *Cr*FBA3 is an α/β protein composed of eleven α-helices and nine β-strands folded as a TIM barrel (CATH classification: 3.20.20) and numerated from H1 to H11 and S1 to S9, respectively (Fig. 1). Regions of the protein with the largest chain-to-chain differences are otherwise highlighted by the highest B-factors, and are mainly localized on the H2, H3, H4, H5 and H10 and H11 α-helices and the loops that connect them (Fig. 2). These regions are located close to the active site of the protein and may allow rearrangements of its accessibility, in order to potentially accommodate substrates and products according to an induced fit mechanism.

2.2. *CrFBA3 active site*

Active site of *Cr*FBA3 is localized in the center of the TIM barrel at the C-terminal pole of the β-strands. This site is a strongly electropositive pocket, containing one or two sulfate ions captured in the crystallization solution and several water molecules (Fig. 3). Active site of class I aldolase have already been described structurally and chemically in various organisms (Dalby et al., 1999; St-Jean et al., 2005; Lafrance-Vanasse and Sygusch 2007; Gardberg et al., 2011a; Gardberg et al., 2011b). Eleven catalytic residues described in these articles are present in *Chlamydomonas reinhardtii* FBA3 at the following positions: Asp52, Ser54, Thr57, Lys125, Lys164, Arg166, Glu204, Glu206, Lys246, Ser288, and Arg318. Side chains of all catalytic residues are identically oriented placed in *Chlamydomonas reinhardtii* and mammals orthologs taken as references (Fig. 3). Human FBA has been described to perform its lyase activity by forming a Schiff base between the substrate and the lysine in position 229 while being stabilized by the two positively charged amino acids (Arg148 and Lys146; Gamblin et al., 1991). The hypothesis of a similar catalytic mechanism between *Cr*FBA3 and other FBA is comforted by superposing *Cr*FBA3 structure to two FBA structures co-crystallized with their substrate in which amino acids from *Cr*FBA3 are well superposed with those found in homologs from *Homo sapiens* FBA (*Hs*FBA) (PDB ID: 4ALD) and *Oryctolagus cuniculus* FBA (*Oc*FBA) (PDB ID: 1ZAI) with RMSD of 0.813 Å and 0.886 Å, respectively (Fig. 3). Residues K229, R148, and K146 of human FBA align with residues K246, R166, and K164 of *Cr*FBA3 (Fig. 3A-B). The residues side chains are positioned in highly similar conformations (Fig. 3D).

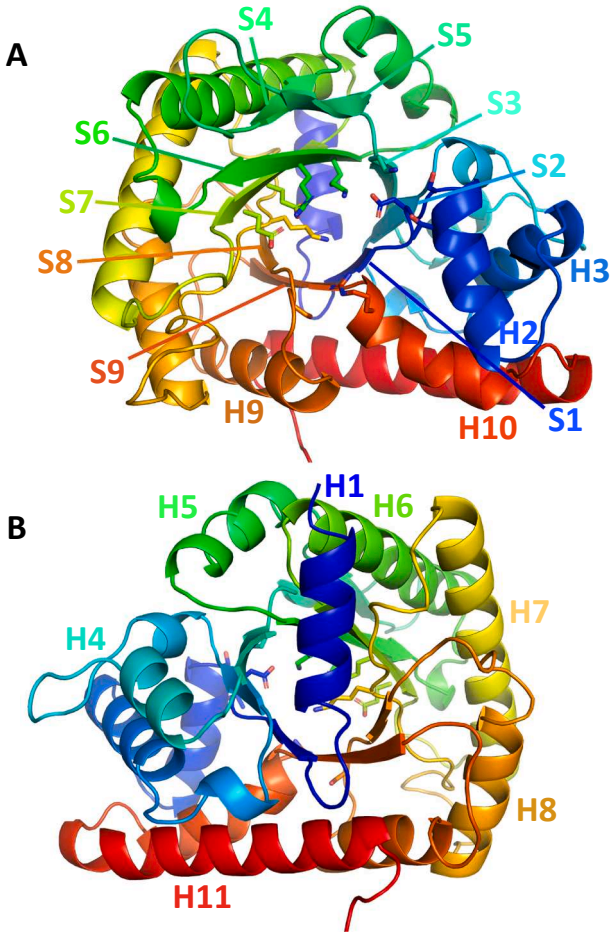

Fig. 1. A. Front view of *Cr*FBA3 represented as cartoon and colored from N-terminal to C-terminal from blue to red. Alpha helices and beta strands are named from H1 to H11 and from S1 to S9. Active site residues side chains are represented in sticks. **B.** Back view (180° rotation).

2.3. *CrFBA3 is a homo-tetramer*

*Cr*FBA3 crystal has an asymmetric unit containing eight quasi-identical protein chain. The analysis of the quaternary structure of recombinant *CrFBA3* protein indicated a homo-tetrameric state in solution, as the principal peak of protein elute at an approximative mass of 160 kDa closely matching the mass of four monomers of 39 kDa each (supplementary Fig. 2A). Analytical size exclusion chromatography coupled to small angle X-ray scattering (SEC-SAXS) experiments confirmed the tetrameric state in solution (supplementary Fig. 2B). Alteration of the redox state of *Cr*FBA3 induced by oxidizing or reducing treatments prior to SEC-SAXS slightly impacted the estimated mass of the protein in solution being 151–176 kDa and 142–162 kDa for oxidized and reduced protein, respectively, and may suggest a more compact state for reduced FBA. Altogether, these results agree for a homo-tetrameric state of *Cr*FBA3 in solution, which is also described in other structures of class I FBA in other species (Marsh and Lebherz 1992). In order to evaluate the physiological oligomeric state of FBA3, we fractionated soluble extracts of *Chlamydomonas* cultures over a calibrated size-exclusion column and the presence of FBA3 in the eluted fractions was monitored by western blot using anti-FBA3 antibodies (Fig. 4C). FBA3 eluted in one principal species with an apparent molecular weight of 170 kDa, consistent with that of a homotetramer.

2.4. *CrFBA3 sites of post-translational modifications*

*Cr*FBA3 possesses six cysteines in its mature sequence. At least three cysteines may be targeted for redox post-translational modifications mediated by thioredoxins (Perez-Perez et al., 2017). The two couples of cysteines Cys142-Cys183 and Cys218-Cys256 are close enough, with respectively 8.3 Å and 10.2 Å between the two sulphur atoms, to form disulphide bonds. Recent redox-based proteomic studies identified Cys58, Cys142, and Cys256 as targets of S-nitrosylation while Cys58 and Cys142 were shown to be S-glutathionylated (Zaffagnini et al., 2012b). Despite being identified as putative redox target, Cys58 lateral chain is oriented toward the core of the protein and is not exposed to solvent (Fig. 5), raising the hypothesis that redox alteration of the thiol group of this residue demands local conformational changes or alternatively occurs in a later unfolded state of the protein. Also, Cys58 redox modification could be a co-translational modification rather than a post-translational modification occurring during the protein folding process. Cys142 is close to the catalytic cleft and to the external shell of the protein but is still poorly accessible to the solvent on our structure unless

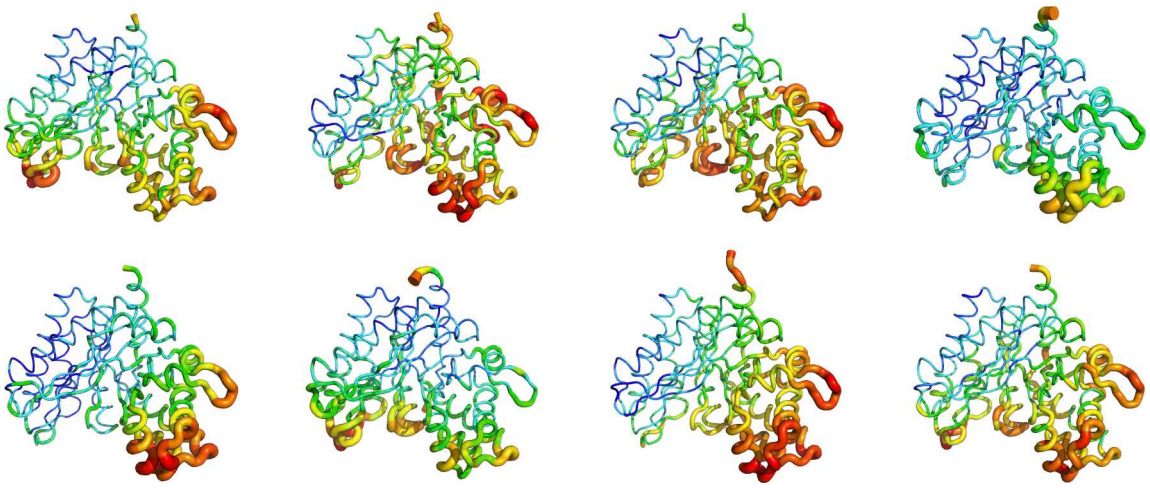

Fig. 2. Representation of the eight monomeric chains of *Cr*FBA3 of the asymmetric unit. Each amino acids is colored from blue to red and is thicker in function of their B-factor value, respectively with the lower B-factor blue and small and the higher thick and red.

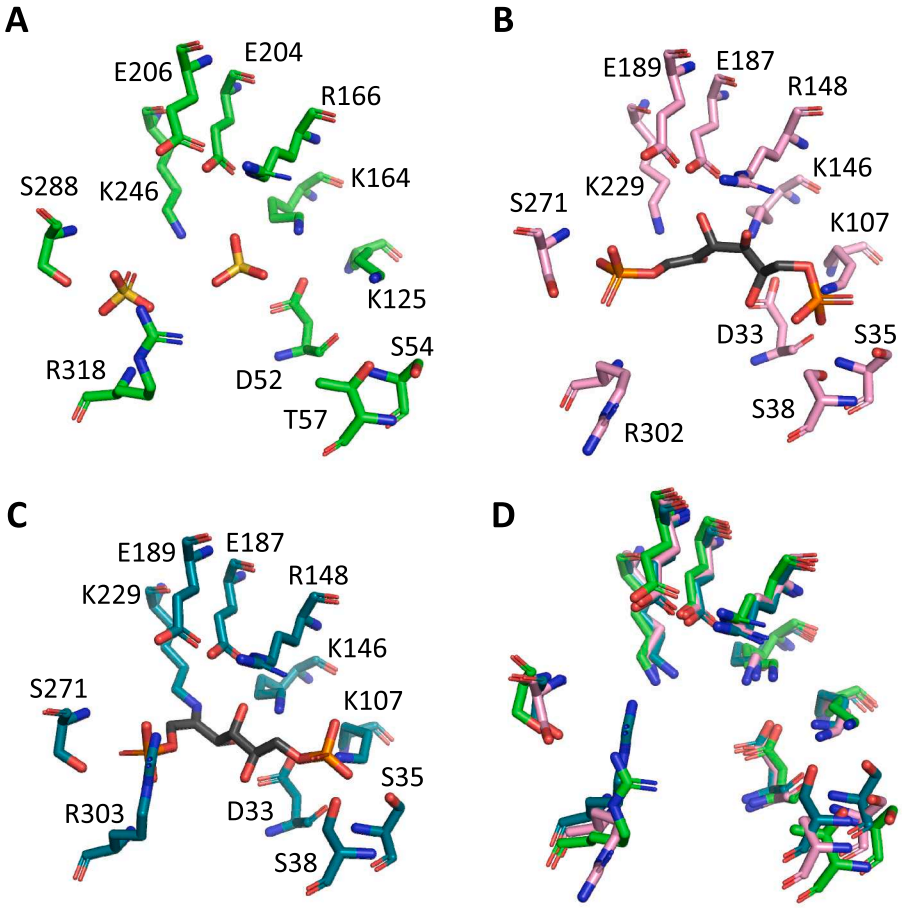

Fig. 3. A. Stick representation of amino acids of the catalytic site of *Cr*FBA3. Atoms are colored with the CPK colouring code with an exception of carbons which are colored in green. Two sulphate ions inside the pocket are also represented. **B.** Stick representation of amino acids of the catalytic site of *Hs*FBA and a fructose-1,6-bisphosphate molecule from the PDB structure 4ALD aligned on the *Cr*FBA3 structure. Atoms are colored as in A. with carbons in light pink. **C.** Stick representation of amino acids of the catalytic site of *Oc*FBA and a fructose-1,6-bisphosphate molecule from the PDB structure 1ZAI aligned on the *Cr*FBA3 structure. Atoms are colored as in A. with carbons in teal. **D.** Superposition of the amino acids from A. B. and C.

*Cr*FBA3 undergoes to a dynamic remodelling of β-strands 4 and 5 (Fig. 1). These β-strands are actually the ones with the highest B-factors (Fig. 2), supporting the hypothesis of a rearrangement of this part of the protein in function of the redox conditions. Cys256 is actually the most exposed thiol of *Cr*FBA3, making it the best candidate for a redox control of the enzyme. However, this residue is located at 19.6 Å from the catalytic Arg166 (Fig. 5). Such a distance prevents a direct effect of redox modification on protein catalysis but could induce local structural shifts that could alter substrate binding and/or substrate processing. Rabbit muscle aldolase is actually subject to a dithio-disulfide exchange at Cys72 and Cys338 that induces a conformational change propagating towards Cys239 at a 28-Å distance (PDB: 1ado and (Heyduk et al., 1991)).

Phosphoproteomic studies found five amino acids that are phosphorylated in *Cr*FBA3 (Wang et al., 2014; Werth et al., 2019). These amino acids are dispersed in the primary structure, namely Ser54, Thr57, Ser64, Ser170, and Ser176. All corresponding sidechains are solvent exposed in *Cr*FBA3 crystal structure (Fig. 5). Ser54, Thr57, and

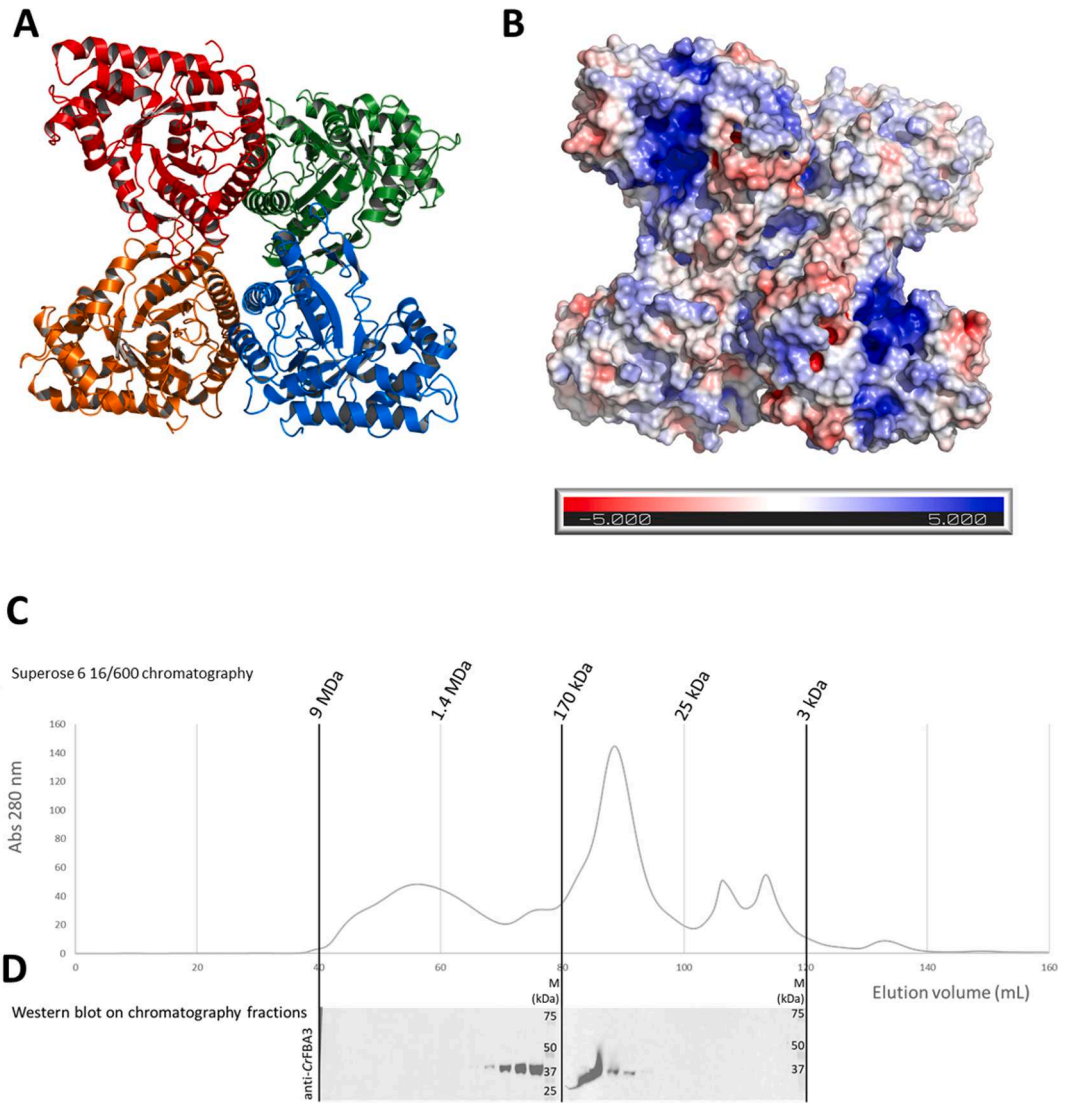

Fig. 4. **A.** Cartoon representation of the homotetramer of *Cr*FBA3. The different subunits are represented in red, green, orange and blue. **B.** Electrostatic surface of *Cr*FBA3 calculated by PyMOL APBS and represented in a gradient from blue (electropositive) to red (electronegative). *Cr*FBA3 is in the same orientation as in A. **C.** Size-exclusion chromatogram of *Chlamydomonas reinhardtii* cellular extracts separated on superose 6 16/600 column. Theoretical molecular masses from column calibration are indicated in MDa, kDa. **D.** Western blot with anti-*Cr*FBA3 antibody on chromatography fractions.

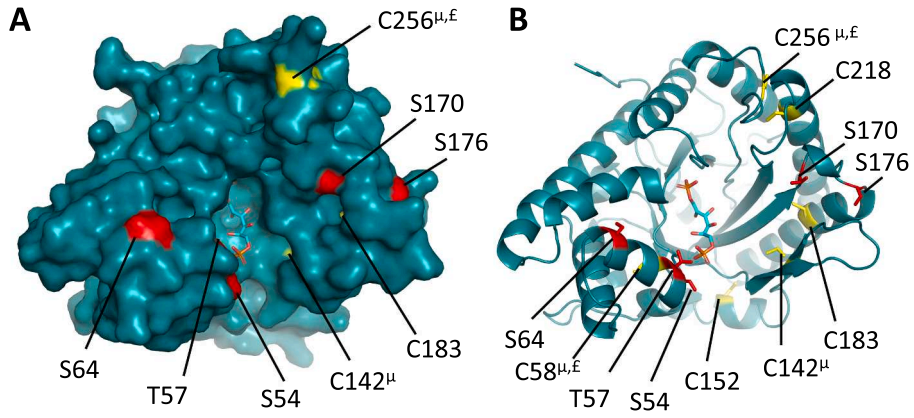

Fig. 5. Redox post-translational modification sites colored in gold and phosphorylation sites colored in red on *Cr*FBA3. Fructose-1,6-bisphosphate is modelled in cyan sticks, by alignment with the co-crystal structure of human FBA complexed with FBP (PDB entry 4ALD). **A.** Surface representation of the FBA monomer. **B.** Cartoon representation of the FBA monomer, same orientation as in A. μ=nitrosylation, £=gluthationylation.

Ser64 are localized on the α-helix 2 which is a key element of the catalytic pocket. In fact, Ser54 and Thr57 are part of the amino acids needed to accommodate the substrate in the active site (Dalby et al., 1999; St-Jean et al., 2005; Gardberg et al., 2011a). Phosphorylation of these residues could interfere with the fixation of the substrate both via steric and charge obstructions, supporting a negative regulatory mechanism widely conserved as these residues are conserved from photosynthetic organisms to animals, archaea, and bacteria (supplementary Fig. 3). Residues Ser170 and Ser176 are localized on the loop between β-strand 6 and α-helix 6 separated by a 3^{10} helix. This loop is on the other side of the catalytic site, bordering it. While Ser176 is conserved in FBA from all living organisms, Ser170 is only conserved in photosynthetic organisms.

Diverse post-translational modifications were reported on homologous class I aldolases, such as carbonylation (Lazarus et al., 2015), and lysine methylations (Mininno et al., 2012) or acetylation (Kim et al., 2006, Barbosa Leite et al., 2020). *Homo sapiens* ALDOA is glycated by methylglyoxal at residues Arg42, Lys146, Lys229, and Lys41 (Donnellan et al., 2022), as well as acetylated at Lys12, Lys41, and Lys146 (Kim et al., 2006). Arg42, Lys146 and Lys229 directly contribute to substrate binding (PDB entry 4ALD), while Lys12 is located 29.1 Å away from the catalytic site and Lys41 side chain points 8.7 Å away from the substrate, suggesting that an effect of post-translational modifications on activity require conformational changes. Strikingly, Lys41, Arg42 belong to α-helix H2 (54-SNATCGKRLDS-64) where Ser54, Thr57, and S64 are phosphorylated while Cys58 is nitrosylated or glutathionylated. Helix 2 appears as a putative hotspot for multiple post-translational modifications, at an appropriate distance for allosteric control of FBA catalytic activity.

2.5. *CrFBA3 is recognized as the Calvin-Benson paralog in Chlamydomonas reinhardtii*

In order to demonstrate the implication of the paralog FBA3 in the CBC, we classified paralogous sequences from different photosynthetic species (Figure S5), whether belonging to the CBC or not, to find the subset of sequences involved in the CBC and verified that FBA3 belongs to it.

Note that phylogeny-based algorithms are not suitable for this classification because FBA paralogous sequences share higher sequence identity than homologous sequences in different species and are clustered together by these computational methods despite their functional differences (Figure S6). Function-based clustering is known to be a difficult problem.

Here, we use ProfileView (Vicedomini et al., 2022), a sequence-based computational method designed to functionally classify sets of homologous sequences and based on multiple profile Hidden Markov Models (pHMM; (Eddy, 1998; Bernardes et al., 2016; Ugarte et al., 2018). We demonstrate that ProfileView distinguishes paralogous sequences in the *C. reinhardtii* genome with respect to their function.

Starting from a set of 1244 FBA sequences (PF00247) covering a large diversity of species, ProfileView builds a library of 1244 pHMMs. After filtering them it uses 40 of them to define a multidimensional space of 2x40 dimensions where the FBA homologous sequences to be classified are represented. This set comprises 2601 homologous FBA sequences, from both prokaryotic and eukaryotic photosynthetic organisms. Among these sequences, there are the four *C. reinhardtii* FBA paralogs that constitute the object of our enquiry. Within the set, we also find FBA paralogs from other species that have been classified as CBC-related and non-CBC-related. ProfileView constructs a functional tree (Fig. 6) organizing the input sequences by function (see Methods), where, intuitively, distinguished subtrees of sequences correspond to distinguished functions. In order to functionally interpret ProfileView distinguished subtrees, we used available functional knowledge on FBA homologous sequences included in the tree and belonging to other species (*Volvox carteri*, *Arabidopsis thaliana*, *Synechocystis* sp. PCC 6803, see Table 2). We checked whether CBC-related paralogs were grouped under a common subtree or not. As shown in Fig. 6A, ProfileView reconstructs three different subtrees, colored green, yellow and red. CBC and non-CBC-related sequences are located in different subtrees: the green one collects all known CBC sequences, whereas the yellow and red ones collect all known non-CBC ones. The two, yellow and red, subtrees

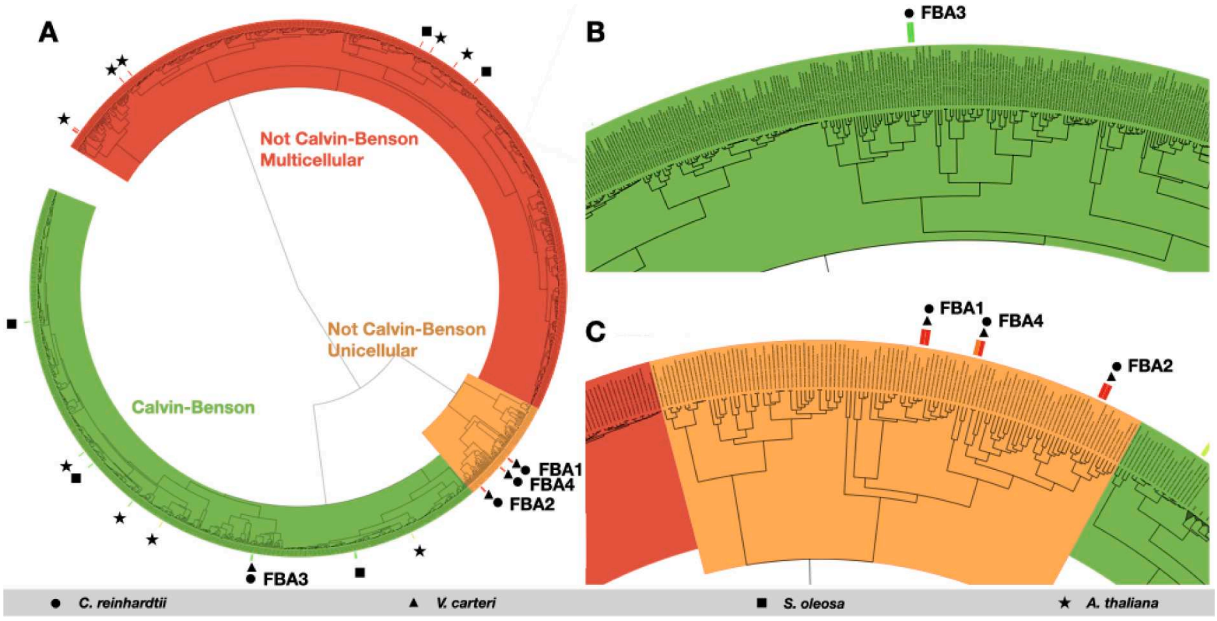

Fig. 6. FBA functional tree. ProfileView tree showing functional relationship between FBA sequences of photosynthetic organisms: **A.** The tree separates FBA paralogs participating in Calvin-Benson (green subtree) and not participating in Calvin-Benson (orange and red subtrees, for unicellular and multicellular organisms respectively). For *C. reinhardtii*, the paralog FBA3 is localized in the Calvin-Benson subtree, whereas the other three paralogs FBA1, FBA2, FBA4 are grouped together in a different subtree. **B.** Zoom on the Calvin-Benson subtree containing the *C. reinhardtii* FBA3 sequence. **C.** Detail of the Unicellular Non-Calvin-Benson subtree, where the other *C. reinhardtii* FBA paralogs are found. In all panels, circles correspond to *C. reinhardtii* sequences, triangles to *V. carteri*, squares to *S. oleosa*, and stars to *A. thaliana*.

Table 2
Uniprot codes and the corresponding classification found by crossreferencing online databases. Classification was manually conducted by considering that Calvin-Benson FBA bear a chloroplast-addressing peptide, as predicted by ChloroP (Emanuelsson Nielsen et al. 1999) and Predalgo (Tardif et al., 2012), and present a circadian expression available for *Chlamydomonas* (Strenkert Merchant et al. PNAS 2019) and *Arabidopsis* (Romanowski et al. 2020).

Uniprot code	Uniprot accession numbers	Classification
Q42690_CHLRE	Q42690, A8JE10, Q36725	*C. reinhardtii* FBA3 (positive test)
A8JCY4_CHLRE	A8JCY4	*C. reinhardtii* FBA1 (negative test)
A8I9H5_CHLRE	A8I9H5	*C. reinhardtii* FBA2 (negative test)
A8I2Q9_CHLRE	A8I2Q9	*C. reinhardtii* FBA4 (negative test)
A0A0K9Q9C0_SPIOL	A0A0K9Q9C0	Non-Calvin-Benson
A0A1P8B8S7_ARATH	A0A1P8B8S7	Non-Calvin-Benson
ALFP2_ARATH	Q944G9, Q5XEU6, Q9SVJ6	Non-circadian chloroplastic
A0A1P8B8Q8_ARATH	A0A1P8B8Q8	Non-Calvin-Benson
ALFC5_ARATH	O65581	Non-Calvin-Benson
ALFC8_ARATH	Q9LF98	Non-Calvin-Benson
A0A0K9QNV9_SPIOL	A0A0K9QNV9	Non-Calvin-Benson
D8TKY4_VOLCA	D8TKY4	Circadian chloroplastic
ALFC7_ARATH	P22197, O65582, Q53YH0	Non-Calvin-Benson
D8UAC8_VOLCA	D8UAC8	Non-Calvin-Benson
ALFP1_ARATH	Q9SJU4, Q2V473, Q93WF5, Q94C97	Circadian chloroplastic
F4IGL5_ARATH	F4IGL5	Circadian chloroplastic
F4IGL7_ARATH	F4IGL7	Circadian chloroplastic
ALFP3_ARATH	Q9ZU52	Non-circadian chloroplastic
A0A0K9R8B2_SPIOL	A0A0K9R8B2	Chloroplastic
D8U593_VOLCA	D8U593	Non-Calvin-Benson
ALFC4_ARATH	F4KGQ0, Q8LET3, Q8W4G8, Q9LZR9	Non-Calvin-Benson
D8UIJ0_VOLCA	D8UIJ0	Non-Calvin-Benson
A0A0K9QFF9_SPIOL	A0A0K9QFF9	Chloroplastic
F4JUJ5_ARATH	F4JUJ5	Non-circadian chloroplastic
A0A0K9QU20_SPIOL	A0A0K9QU20	Chloroplastic
ALFC6_ARATH	Q9SJQ9	Non-Calvin-Benson
B3H6D7_ARATH	B3H6D7	Non-Calvin-Benson
A0A1P8BBB5_ARATH	A0A1P8BBB5	Non-Calvin-Benson
A0A0K9R0B2_SPIOL	A0A0K9R0B2	Chloroplastic

contain almost exclusively sequences from unicellular and multicellular organisms, respectively. This means that the *Cr*FBA3 sequence is neatly separated from its paralogs *Cr*FBA1, *Cr*FBA2 and *Cr*FBA4: FBA3 appears in the Calvin-Benson subtree (Fig. 6B), whereas the others appear in the unicellular non-Calvin-Benson subtree (Fig. 6C).

3. Conclusion

We describe here the structure of chloroplastic FBA3 from *Chlamydomonas reinhardtii*. If nothing seems different in the catalytic mechanism of *Cr*FBA3 in comparison with already described class I FBA from other species, post-translational regulatory target sites of *Cr*FBA3 appear original and chloroplast-specific. The two Cys58 and Cys142, both target of S-glutathionylation and S-nitrosylation, are only conserved in photosynthetic organisms and therefore could be specific targets of a distinct and stress-related regulation of CBC. The amino acid Ser170, target of phosphorylation events, is in the same case as it is conserved only in photosynthetic organism. Alpha helix 2 contain residues Ser54, Thr57, Cys58, and Ser64 that are subject to post-translational modifications, it also has high B-factor in comparison to the other secondary elements and is close to the active site. These characteristics making it a probable regulation cluster and an important area in the activity of *Cr*FBA3 (Seoane and Carbone 2021).

This work also provides a computational analysis that allows a functional classification of the *Cr*FBA paralogs among their homologs. This classification supports the unique role of *Cr*FBA3 in the Calvin-Benson cycle.

The computational approach addressing the functional classification of FBA paralogous proteins is presented in this work for the first time. Indeed, the ProfileView method (Vicedomini et al., 2019) has similarly been used for functional classification of other protein sequences across species. Here, we demonstrate that, based on it, one can classify paralogous sequences within a species by function, a problem which might be considered different from the classification problem formulated on homology. The results obtained on the FBA protein family open the door to new applications in protein sequence classification and their putative physiological role.

4. Experimental procedures

4.1. Cloning

Nuclear encoded amino acids sequence of *Chlamydomonas reinhardtii* Fructose-bisphosphate aldolase 3 (Cre05.g234550, UniRef100 entry Q42690) was analyzed by TargetP2.0 (Emanuelsson et al., 2007; Almagro Armenteros et al., 2019), ChloroP (Emanuelsson et al., 1999) and Predalgo (Tardif et al., 2012) to predict the transit peptide. The subsequent mature sequence of chloroplastic protein coding for amino acid 28 to 377 has been amplified by PCR from the *Chlamydomonas reinhardtii* EST index (Asamizu and Nakamura 2004). PCR product was then inserted into pET3d-His6 by restriction and ligation at 5′-Nde1 and 3′-BamH1 sites to obtain a pET3d-His6-*Cr*FBA3 expression plasmid. Plasmid sequences were validated by Sanger sequencing.

4.2. Protein expression and purification

Transformation of *Escherichia coli* strain BL21(DE3) Rosetta-2 pLysS (Novagen Merck, Darmstadt Germany) were made with a pET3d-His6-*Cr*FBA3 plasmid. This strain was grown in 2YT medium supplemented with ampicillin (100 μg/mL) at 37 °C until the culture reached exponential phase at an optical density at 600 nm of 0.8. The culture medium was supplemented with 0.2 mmol/L of IPTG and a temperature shift to 15 °C for 19 h was made. Culture was next centrifugated at 4,000 *g* for 10 min at 4 °C. The cell pellet was resuspended in a buffer composed of 20 mmol/L Tris-HCl (pH7.9), 100 mmol/L NaCl, 5% glycerol and lyzed at a pressure of 2400 bar in a CF high-pressure homogenizer (Constant Systems Ltd., Daventry United Kingdom). The total extract of proteins was then centrifuged for 20 min at 20,000 *g* and the soluble fraction loaded on an affinity chromatography with 2 ml of NiNTA resin (Sigma-Aldrich Merck, Darmstad Germany). The resin was washed with 20 ml of 20 mmol/L Tris-HCl (pH7.9) supplemented with 100 mmol/L NaCl (buffer A) complemented with respectively 10 mmol/L and 20 mmol/L of imidazole. *Cr*FBA3 was then eluted in 2 consecutive steps with buffer A complemented with 100 mmol/L, 200 mmol/L and 500 mmol/L of imidazole. Fractions were then analyzed by SDS-PAGE on a 12% acrylamide gel revealed by Coomassie blue staining. Fractions containing pure *Cr*FBA3 were pooled, concentrated by ultrafiltration on 5,000 MWCO filter units (Millipore Merck, Darmstadt Germany) until a final volume of 10 ml prior to be injected on a size exclusion column HiLoad 26/600 Superdex 200 pg (Cityva life sciences) in buffer A. Fractions containing pure *Cr*FBA were pooled, concentrated by ultrafiltration on 5,000 MWCO filter units (Millipore Merck, Darmstadt Germany) to a final concentration of 9 $mg.mL^{-1}$ that was measured by NanoDrop 2000 spectrophotometer (Thermo Fisher Scientific, Waltham MA USA) with theoretical Mw = 39,390 $g.mol^{-1}$ and ε_{280} = 50,037 $mol^{-1}.L.cm^{-1}$.

4.3. Protein crystallization and structure determination

Purified *Cr*FBA3 was tested for crystallization at two concentration of 9 mg/mL and 4.5 mg/mL on commercial sparse-screening conditions

(Qiagen, Hilden Germany) based on the work of Jancarik and Kim (Jancarik et al., 1991) with a mixture of 50 nL of protein and 50 nL of precipitant solution equilibrated against 40 μL of reservoir solution at 20 °C. Several conditions showed small crystals in presence of ammonium sulfate. Condition A4 of Qiagen "the classics" kit (5% (v/v) isopropanol, 2 mol/L ammonium sulfate) was selected to be optimized in a 2D gradient from 0% to 10% isopropanol and from 2 mol/L to 2.5 mol/L of ammonium sulfate with 2 μL drops of protein/precipitant solution ratio 1/1 equilibrated against 1 mL of reservoir solution. Protein concentration was brought to 2.6 mg/mL to avoid formation of clustered crystals and monocrystals were grown in a solution of 5 % isopropanol and 2 mol/L ammonium sulfate. Crystals were flash frozen in liquid nitrogen for diffraction experiment at Proxima-2A beamline of SOLEIL synchrotron (Saint-Aubin, France). A 99.41 % complete dataset at 2.36 Å resolution was obtained from 3600 images and indexed in the C2 space group, integrated, scaled and converted with XDSME (Legrand, 2017). Structure was phased by molecular replacement with PHENIX (Adams et al., 2010; Adams et al., 2011) PHASER-MR (McCoy et al., 2007) using a search model obtained from the Phyre2 server (Kelley et al., 2015). Eight *Cr*FBA monomers were found in the asymmetric unit. Model was then refined by iterative cycle of manual building in WinCOOT (Emsley and Cowtan, 2004); Emsley et al. 2010) followed by refinement with PHENIX.REFINE (Afonine et al., 2012) until completion of a structure passing MOLPROBITY (Chen et al., 2010) evaluation with 99.5% residues in Ramachandran restrains RMS(bond) = 0.008, RMS (angles) = 0.93 and final Rwork = 0.2002, Rfree = 0.2429 (Table 1). Structure representations were drawn with PYMOL 2.4 (Schrodinger, New York USA).

4.4. Structural data

Reflections and coordinates files of the final model are registered in the protein data bank under accession code 7B2N.

4.5. Computational analysis

Generation of functional trees.

ProfileView (Vicedomini et al., 2019) takes as input a set of homologous sequences and a protein domain, and returns a classification of the sequences in functional subgroups together with functional motifs characterising the subgroups. The first main idea of ProfileView is to extract conserved patterns from the space of available sequences through the construction of many probabilistic models for a protein family that should sample the diversity of the available homologous sequences and reflect shared structural and functional characteristics. These models are built as conservation profiles (Eddy, 1998).

A pHMM can either generate new sequences, which are similar to the sequences used for its construction, or it can evaluate how likely it would be for a given query sequence to be generated by that model. To do so, it associates the query with an absolute likelihood score, which allows scores associated with different queries to be meaningfully compared.

ProfileView exploits this feature of pHMM for functionally describing an arbitrary set of query sequences. Indeed, the second main idea of ProfileView is to use its library of probabilistic models to embed input sequences into a multidimensional representation space, where each dimension is associated with a distinguished probabilistic model. Namely, each input sequence to be classified receives a score from each pHMM expressing how close the pHMM is to the sequence. All the scores are recorded as a vector entry for the sequence. Protein sequences are thus represented as points on this space, and distances can be calculated between each pair. These distances do not reflect mere sequence identities, but rather capture functional aspects that would have been overlooked by simpler, sequence-related metrics. Lastly, the distances are used to generate a tree that functionally relates all the query sequences. The internal nodes of the tree are, whenever possible, annotated by representative pHMM and by functional motifs. We expect this tree to discriminate paralogs taking part in Calvin-Benson cycle, such as *C. reinhardtii* FBA3, from paralogs involved in other chemical pathways (FBA1, FBA2, FBA4).

The *C. reinhardtii* FBA3 protein sequence (UniProt code Q42690) contains only one protein domain which encompasses the most conserved part of the protein. It is the large Pfam domain Glycolytic PF00274. In order to generate ProfileView functional tree for the 2601 homologous FBA sequences and including all *C. reinhardtii* FBA paralogous sequences, we devised the following pipeline:

(1) Selection of the sequences for the construction of the probabilistic models

To generate the ProfileView library of probabilistic models for the Glycolytic PF00274 domain, we downloaded the Pfam "full" alignment (Pfam version 34 - https://pfam.xfam.org/family/Glycolytic). We favored this set of sequences because of their relatively limited number of gaps (high sequence length homogeneity), hand curation and uniform sampling of homologous sequences on their phylogenetic tree. Of the 3886 sequences, 29% and 22% of them come from Proteobacteria and Metazoa respectively, and thus are not related to the Calvin-Benson cycle. Only 16% of sequences come from Viridiplantae. Nonetheless, it is important to select sequences covering most diversity as possible, in order to construct the most diversified model space for functional discrimination. No filter based on taxonomic classification was used in this step of the construction.

(2) Clustering of the selected sequences

Sequences having more than 20% gaps associated with amino acids of the query sequence were removed from the set, in order to filter out sequences with missing domains. The remaining 2356 sequences were clustered using MMseqs2 with parameters –min-seq-id 0.65 -c 0.8. The parameters were chosen as in (Ugarte et al. 2018) and on its observation that optimal performances are obtained with 1000–1500 sequences. The resulting set contains 1244 sequences and spans the original diversity of taxa (supplementary Fig. 5).

(3) Generation of the pHMM library

We used the ProfileView-build routine to generate a library composed of 1244 pHMM models. These models are compiled from an equal amount of automatically-generated alignments, containing a variable number of sequences gathered in Uniprot (Uniclust30 08/2018).

(4) Generating the functional tree

To determine the functional differences between FBA paralogs in photosynthetic species, we considered the complete Pfam "uniprot" dataset (15967 sequences) and selected sequences to be classified in the ProfileView tree based on taxonomy: we selected taxa with Uniprot classification Cryptophyceae, Glaucocystophyceae, Rhodophyta, and Viridiplantae. In order to have the maximum number of available sequences in the tree, no length- nor sequence identity-based filtering was applied. We identified 2601 sequences (of which 96% are Viridiplantae, 3% Cryptophyceae, 2% Rhodophyta, and only 2 Glaucocystophyceae). Note that the overlap between the 1244 sequences which are "seed" for the model construction and the 2601 classified sequences amounts to 252 sequences.

CRediT authorship contribution statement

Théo Le Moigne: Data curation, Formal analysis, Investigation, Methodology, Validation, Writing – original draft, Writing – review &

editing. **Edoardo Sarti:** Data curation, Formal analysis, Investigation, Methodology, Software, Validation, Writing – original draft, Writing – review & editing. **Antonin Nourisson:** Investigation, Methodology, Writing – review & editing. **Mirko Zaffagnini:** Writing – review & editing. **Alessandra Carbone:** Conceptualization, Data curation, Formal analysis, Funding acquisition, Investigation, Project administration, Resources, Software, Supervision, Validation, Writing – original draft, Writing – review & editing. **Stéphane D. Lemaire:** Investigation, Project administration, Resources, Writing – review & editing. **Julien Henri:** Conceptualization, Data curation, Funding acquisition, Investigation, Project administration, Resources, Supervision, Validation, Writing – original draft, Writing – review & editing.

Declaration of Competing Interest

The authors declare that they have no known competing financial interests or personal relationships that could have appeared to influence the work reported in this paper.

Acknowledgements

This work was funded by ANR grants CALVINDESIGN (ANR-17-CE05-0001), CALVINTERACT (ANR-19-CE11-0009) and LABEX DYNAMO (ProjetIA-11-LABX-0011). We thank the *Institut de Biologie Physico-Chimique* (CNRS FR 550) for access to crystallization facility. We acknowledge SOLEIL for provision of synchrotron radiation facilities at beamlines Proxima-1, Proxima-2A, and SWING. We thank Dr. Olivier Vallon for helpful discussions.

Appendix A. Supplementary data

Supplementary data to this article can be found online at https://doi.org/10.1016/j.jsb.2022.107873.

References

Adams, P.D., Afonine, P.V., Bunkoczi, G., Chen, V.B., Davis, I.W., Echols, N., Headd, J.J., Hung, L.W., Kapral, G.J., Grosse-Kunstleve, R.W., McCoy, A.J., Moriarty, N.W., Oeffner, R., Read, R.J., Richardson, D.C., Richardson, J.S., Terwilliger, T.C., Zwart, P.H., 2010. PHENIX: a comprehensive Python-based system for macromolecular structure solution. Acta Crystallogr. D Biol. Crystallogr. 66 (Pt 2), 213–221.

Adams, P.D., Afonine, P.V., Bunkóczi, G., Chen, V.B., Echols, N., Headd, J.J., Hung, L.-W., Jain, S., Kapral, G.J., Grosse Kunstleve, R.W., McCoy, A.J., Moriarty, N.W., Oeffner, R.D., Read, R.J., Richardson, D.C., Richardson, J.S., Terwilliger, T.C., Zwart, P.H., 2011. The Phenix software for automated determination of macromolecular structures. Methods 55 (1), 94–106.

Afonine, P.V., Grosse-Kunstleve, R.W., Echols, N., Headd, J.J., Moriarty, N.W., Mustyakimov, M., Terwilliger, T.C., Urzhumtsev, A., Zwart, P.H., Adams, P.D., 2012. Towards automated crystallographic structure refinement with phenix.refine. Acta Crystallogr. D Biol. Crystallogr. 68 (Pt 4), 352–367.

Almagro Armenteros, J.J., Salvatore, M., Emanuelsson, O., Winther, O., von Heijne, G., Elofsson, A., Nielsen, H., 2019. Detecting sequence signals in targeting peptides using deep learning. Life Sci. Alliance 2 (5), e201900429. https://doi.org/10.26508/lsa:201900429.

Amato, A., Dell'Aquila, G., Musacchia, F., Annunziata, R., Ugarte, A., Maillet, N., Carbone, A., Ribera d'Alcalà, M., Sanges, R., Iudicone, D., Ferrante, M.I., 2017. Marine diatoms change their gene expression profile when exposed to microscale turbulence under nutrient replete conditions. Sci. Rep. 7 (1), 3826.

Anderson, L.E., Advani, V.R., 1970. Chloroplast and cytoplasmic enzymes: three distinct isoenzymes associated with the reductive pentose phosphate cycle. Plant Physiol. 45 (5), 583–585.

Anderson, L.E., Pacold, I., 1972. Chloroplast and Cytoplasmic Enzymes: IV. Pea Leaf Fructose 1,6-Diphosphate Aldolases. Plant Physiol. 49 (3), 393–397.

Asamizu, E., Nakamura, Y., 2004. System for expressed sequence tags (EST) analysis. Tanpakushitsu Kakusan Koso 49 (11 Suppl), 1847–1852.

Barbosa Leite, A., Severo Gomes, A.A., de Castro Nascimento Sousa, A.C., Roberto de Mattos Fontes, M., Schenkman, S., Silvio Moretti, N., 2020. Effect of lysine acetylation on the regulation of Trypanosoma brucei glycosomal aldolase activity. Biochem. J. 477(9), 1733-1744.

Bassham, J.A., Benson, A.A., Calvin, M., 1950. The path of carbon in photosynthesis. J. Biol. Chem. 185 (2), 781–787.

Bernardes, J., Zaverucha, G., Vaquero, C., Carbone, A., 2016. Improvement in Protein Domain Identification Is Reached by Breaking Consensus, with the Agreement of Many Profiles and Domain Co-occurrence. PLoS Comput. Biol. 12 (7), e1005038.

Chen, V.B., Arendall 3rd, W.B., Headd, J.J., Keedy, D.A., Immormino, R.M., Kapral, G.J., Murray, L.W., Richardson, J.S., Richardson, D.C., 2010. MolProbity: all-atom structure validation for macromolecular crystallography. Acta Crystallogr. D Biol. Crystallogr. 66 (Pt 1), 12–21.

Dalby, A., Dauter, Z., Littlechild, J.A., 1999. Crystal structure of human muscle aldolase complexed with fructose 1,6-bisphosphate: mechanistic implications. Protein Sci. 8 (2), 291–297.

Donnellan, L., Young, C., Simpson, B.S., Acland, M., Dhillon, V.S., Costabile, M., Fenech, M., Hoffmann, P., Deo, P., 2022. Proteomic Analysis of Methylglyoxal Modifications Reveals Susceptibility of Glycolytic Enzymes to Dicarbonyl Stress. Int. J. Mol. Sci. 23 (7), 3689. https://doi.org/10.3390/ijms23073689.

Eddy, S.R., 1998. Profile hidden Markov models. Bioinformatics 14 (9), 755–763. https://doi.org/10.1093/bioinformatics/14.9.755. PMID: 9918945.

Emanuelsson, O., Brunak, S., von Heijne, G., Nielsen, H., 2007. Locating proteins in the cell using TargetP, SignalP and related tools. Nat. Protoc. 2 (4), 953–971.

Emanuelsson, O., Nielsen, H., Heijne, G.V., 1999. ChloroP, a neural network-based method for predicting chloroplast transit peptides and their cleavage sites. Protein Sci. 8 (5), 978–984.

Emsley, P., Cowtan, K., 2004. Coot: model-building tools for molecular graphics. Acta Crystallogr. D Biol. Crystallogr. 60 (Pt 12 Pt 1), 2126–2132.

Emsley, P., Lohkamp, B., Scott, W.G., Cowtan, K., 2010. Features and development of Coot. Acta Crystallogr. D Biol. Crystallogr. 66 (Pt 4), 486–501.

Erales, J., Avilan, L., Lebreton, S., Gontero, B., 2008. Exploring CP12 binding proteins revealed aldolase as a new partner for the phosphoribulokinase/glyceraldehyde 3-phosphate dehydrogenase/CP12 complex–purification and kinetic characterization of this enzyme from Chlamydomonas reinhardtii. FEBS J. 275 (6), 1248–1259.

Finkemeier, I., Laxa, M., Miguet, L., Howden, A.J., Sweetlove, L.J., 2011. Proteins of diverse function and subcellular location are lysine acetylated in Arabidopsis. Plant Physiol. 155 (4), 1779–1790.

Flechner, A., Gross, W., Martin, W.F., Schnarrenberger, C., 1999. Chloroplast class I and class II aldolases are bifunctional for fructose-1,6-biphosphate and sedoheptulose-1,7-biphosphate cleavage in the Calvin cycle. FEBS Lett. 447 (2–3), 200–202.

Fortunato, A.E., Jaubert, M., Enomoto, G., Bouly, J.-P., Raniello, R., Thaler, M., Malviya, S., Bernardes, J.S., Rappaport, F., Gentili, B., Huysman, M.J.J., Carbone, A., Bowler, C., d'Alcalà, M.R., Ikeuchi, M., Falciatore, A., 2016. Diatom Phytochromes Reveal the Existence of Far-Red-Light-Based Sensing in the Ocean. Plant Cell 28 (3), 616–628.

Fothergill-Gilmore, L.A., Michels, P.A.M., 1993. Evolution of glycolysis. Prog. Biophys. Mol. Biol. 59 (2), 105–235.

Gamblin, S.J., Davies, G.J., Grimes, J.M., Jackson, R.M., Littlechild, J.A., Watson, H.C., 1991. Activity and specificity of human aldolases. J. Mol. Biol. 219 (4), 573–576.

Gardberg, A., Abendroth, J., Bhandari, J., Sankaran, B., Staker, B., 2011a. Structure of fructose bisphosphate aldolase from Bartonella henselae bound to fructose 1,6-bisphosphate. Acta Crystallogr., Sect. F: Struct. Biol. Cryst. Commun. 67 (Pt 9), 1051–1054.

Gardberg, A., Sankaran, B., Davies, D., Bhandari, J., Staker, B., Stewart, L., 2011b. Structure of fructose bisphosphate aldolase from Encephalitozoon cuniculi. Acta Crystallogr., Sect. F: Struct. Biol. Cryst. Commun. 67 (Pt 9), 1055–1059.

Haake, V., Zrenner, R., Sonnewald, U., Stitt, M., 1998. A moderate decrease of plastid aldolase activity inhibits photosynthesis, alters the levels of sugars and starch, and inhibits growth of potato plants. Plant J. 14 (2), 147–157.

Hammel, A., Sommer, F., Zimmer, D., Stitt, M., Muhlhaus, T., Schroda, M., 2020. Overexpression of Sedoheptulose-1,7-Bisphosphatase Enhances Photosynthesis in Chlamydomonas reinhardtii and Has No Effect on the Abundance of Other Calvin-Benson Cycle Enzymes. Front. Plant Sci. 11, 868.

Heyduk, T., Michalczyk, R., Kochman, M., 1991. Long-range effects and conformational flexibility of aldolase. J. Biol. Chem. 266 (24), 15650–15655.

Jancarik, J., Scott, W.G., Milligan, D.L., Koshland, D.E., Kim, S.-H., 1991. Crystallization and preliminary X-ray diffraction study of the ligand-binding domain of the bacterial chemotaxis-mediating aspartate receptor of Salmonella typhimurium. J. Mol. Biol. 221 (1), 31–34.

Kelley, L.A., Mezulis, S., Yates, C.M., Wass, M.N., Sternberg, M.J.E., 2015. The Phyre2 web portal for protein modeling, prediction and analysis. Nat. Protoc. 10 (6), 845–858.

Kim, S.C., Sprung, R., Chen, Y., Xu, Y., Ball, H., Pei, J., Cheng, T., Kho, Y., Xiao, H., Xiao, L., Grishin, N.V., White, M., Yang, X.-J., Zhao, Y., 2006. Substrate and Functional Diversity of Lysine Acetylation Revealed by a Proteomics Survey. Mol. Cell 23 (4), 607–618.

Lafrance-Vanasse, J., Sygusch, J., 2007. Carboxy-terminus recruitment induced by substrate binding in eukaryotic fructose bis-phosphate aldolases. Biochemistry 46 (33), 9533–9540.

Lazarus, R.C., Buonora, J.E., Jacobowitz, D.M., Mueller, G.P., 2015. Protein carbonylation after traumatic brain injury: cell specificity, regional susceptibility, and gender differences. Free Radic Biol Med 78, 89–100.

Legrand, P. (2017). "XDSME: XDS Made Easier." GitHub repository.

Lemaire, S.D., Guillon, B., Le Maréchal, P., Keryer, E., Miginiac-Maslow, M., Decottignies, P., 2004. New thioredoxin targets in the unicellular photosynthetic eukaryote Chlamydomonas reinhardtii. Proc Natl Acad Sci U S A 101 (19), 7475–7480.

Liu, K., Yuan, C., Li, H., Chen, K., Lu, L., Shen, C., Zheng, X., 2018. A qualitative proteome-wide lysine crotonylation profiling of papaya (Carica papaya L.). Sci. Rep. 8 (1), 8230.

Marsh, J.J., Lebherz, H.G., 1992. Fructose-bisphosphate aldolases: an evolutionary history. Trends Biochem. Sci. 17 (3), 110–113.

McCoy, A.J., Grosse-Kunstleve, R.W., Adams, P.D., Winn, M.D., Storoni, L.C., Read, R.J., 2007. Phaser crystallographic software. J. Appl. Crystallogr. 40 (Pt 4), 658–674.

Mettler, T., Muhlhaus, T., Hemme, D., Schottler, M.A., Rupprecht, J., Idoine, A., Veyel, D., Pal, S.K., Yaneva-Roder, L., Winck, F.V., Sommer, F., Vosloh, D., Seiwert, B., Erban, A., Burgos, A., Arvidsson, S., Schonfelder, S., Arnold, A., Gunther, M., Krause, U., Lohse, M., Kopka, J., Nikoloski, Z., Mueller-Roeber, B., Willmitzer, L., Bock, R., Schroda, M., Stitt, M., 2014. Systems Analysis of the Response of Photosynthesis, Metabolism, and Growth to an Increase in Irradiance in the Photosynthetic Model Organism Chlamydomonas reinhardtii. Plant Cell 26 (6), 2310–2350.

Michelet, L., Zaffagnini, M., Morisse, S., Sparla, F., Perez-Perez, M.E., Francia, F., Danon, A., Marchand, C.H., Fermani, S., Trost, P., Lemaire, S.D., 2013. Redox regulation of the Calvin-Benson cycle: something old, something new. Front. Plant Sci. 4, 470.

Mininno, M., Brugière, S., Pautre, V., Gilgen, A., Ma, S., Ferro, M., Tardif, M., Alban, C., Ravanel, S., 2012. Characterization of chloroplastic fructose 1,6-bisphosphate aldolases as lysine-methylated proteins in plants. J. Biol. Chem. 287 (25), 21034–21044.

Morisse, S., Zaffagnini, M., Gao, X.-H., Lemaire, S.D., Marchand, C.H., 2014. Insight into protein S-nitrosylation in Chlamydomonas reinhardtii. Antioxid. Redox Signal. 21 (9), 1271–1284.

Müller-Schüssele, S.J., Bohle, F., Rossi, J., Trost, P., Meyer, A.J., Zaffagnini, M., 2021. Plasticity in plastid redox networks: evolution of glutathione-dependent redox cascades and glutathionylation sites. BMC Plant Biol. 21 (1), 322.

Pérez-Pérez, M.E., Mauriès, A., Maes, A., Tourasse, N.J., Hamon, M., Lemaire, S.D., Marchand, C.H., 2017. The Deep Thioredoxome in Chlamydomonas reinhardtii: New Insights into Redox Regulation. Mol Plant 10 (8), 1107–1125.

Pfannschmidt, T., Yang, C., 2012. The hidden function of photosynthesis: a sensing system for environmental conditions that regulates plant acclimation responses. Protoplasma 249 (Suppl 2), S125–S136.

Razdan, K., Heinrikson, R.L., Zurcher-Neely, H., Morris, P.W., Anderson, L.E., 1992. Chloroplast and cytoplasmic enzymes: isolation and sequencing of cDNAs coding for two distinct pea chloroplast aldolases. Arch. Biochem. Biophys. 298 (1), 192–197.

Reyes-Prieto, A., Bhattacharya, D., 2007. Phylogeny of Calvin cycle enzymes supports Plantae monophyly. Mol. Phylogenet. Evol. 45 (1), 384–391.

Rozova, O.N., Khmelenina, V.N., Mustakhimov, I.I., Reshetnikov, A.S., Trotsenko, Y.A., 2010. Characterization of recombinant fructose-1,6-bisphosphate aldolase from Methylococcus capsulatus Bath. Biochemistry (Mosc) 75 (7), 892–898.

Schroda, M., Hemme, D., Mühlhaus, T., 2015. The Chlamydomonas heat stress response. Plant J. 82 (3), 466–480.

Seoane, B., Carbone, A., 2021. The complexity of protein interactions unravelled from structural disorder. PLoS Comput. Biol. 17 (1), e1008546.

Sharkey, T.D., 2019. Discovery of the canonical Calvin-Benson cycle. Photosynth. Res. 140 (2), 235–252.

Simkin, A.J., McAusland, L., Headland, L.R., Lawson, T., Raines, C.A., 2015. Multigene manipulation of photosynthetic carbon assimilation increases CO2 fixation and biomass yield in tobacco. J. Exp. Bot. 66 (13), 4075–4090.

St-Jean, M., Lafrance-Vanasse, J., Liotard, B., Sygusch, J., 2005. High resolution reaction intermediates of rabbit muscle fructose-1,6-bisphosphate aldolase: substrate cleavage and induced fit. J. Biol. Chem. 280 (29), 27262–27270.

Tardif, M., Atteia, A., Specht, M., Cogne, G., Rolland, N., Brugiere, S., Hippler, M., Ferro, M., Bruley, C., Peltier, G., Vallon, O., Cournac, L., 2012. PredAlgo: a new subcellular localization prediction tool dedicated to green algae. Mol. Biol. Evol. 29 (12), 3625–3639.

Ugarte, A., Vicedomini, R., Bernardes, J., Carbone, A., 2018. A multi-source domain annotation pipeline for quantitative metagenomic and metatranscriptomic functional profiling. Microbiome 6 (1), 149.

Vicedomini, R., Blachon, C., Oteri, F., Carbone, A., 2021. MyCLADE: a multi-source domain annotation server for sequence functional exploration. Nucleic Acids Res. 49 (W1), W452–W458.

Vicedomini, R., J. P. Bouly, E. Laine, A. Falciatore and A. Carbone (2019). "ProfileView: multiple probabilistic models resolve protein families functional diversity." bioRxiv: 717249.

Vicedomini, R., J. P. Bouly, E. Laine, A. Falciatore and A. Carbone (2022). "Multiple Profile Models Extract Features from Protein Sequence Data and Resolve Functional Diversity of Very Different Protein Families." Molecular Biology and Evolution **39** (4).

Wang, H., Gau, B., Slade, W.O., Juergens, M., Li, P., Hicks, L.M., 2014. The global phosphoproteome of Chlamydomonas reinhardtii reveals complex organellar phosphorylation in the flagella and thylakoid membrane. Mol. Cell. Proteomics 13 (9), 2337–2353.

Werth, E.G., McConnell, E.W., Couso Lianez, I., Perrine, Z., Crespo, J.L., Umen, J.G., Hicks, L.M., 2019. Investigating the effect of target of rapamycin kinase inhibition on the Chlamydomonas reinhardtii phosphoproteome: from known homologs to new targets. New Phytol. 221 (1), 247–260.

Wienkoop, S., Weiss, J., May, P., Kempa, S., Irgang, S., Recuenco-Munoz, L., Pietzke, M., Schwemmer, T., Rupprecht, J., Egelhofer, V., Weckwerth, W., 2010. Targeted proteomics for Chlamydomonas reinhardtii combined with rapid subcellular protein fractionation, metabolomics and metabolic flux analyses. Mol. BioSyst. 6 (6), 1018–1031.

Yu, A., Xie, Y., Pan, X., Zhang, H., Cao, P., Su, X., Chang, W., Li, M., 2020. Photosynthetic Phosphoribulokinase Structures: Enzymatic Mechanisms and the Redox Regulation of the Calvin-Benson-Bassham Cycle. Plant Cell 32 (5), 1556–1573.

Zaffagnini, M., M. Bedhomme, H. Groni, C. H. Marchand, C. Puppo, B. Gontero, C. Cassier-Chauvat, P. Decottignies and S. D. Lemaire (2012). "Glutathionylation in the photosynthetic model organism Chlamydomonas reinhardtii: a proteomic survey." Mol Cell Proteomics **11**(2): M111 014142.

Zaffagnini, M., M. Bedhomme, H. Groni, C. H. Marchand, C. Puppo, B. Gontero, C. Cassier-Chauvat, P. Decottignies and S. D. Lemaire (2012). "Glutathionylation in the photosynthetic model organism Chlamydomonas reinhardtii: a proteomic survey." Mol Cell Proteomics **11**(2): M111.014142.

Zaffagnini, M., Fermani, S., Marchand, C.H., Costa, A., Sparla, F., Rouhier, N., Geigenberger, P., Lemaire, S.D., Trost, P., 2019. Redox Homeostasis in Photosynthetic Organisms: Novel and Established Thiol-Based Molecular Mechanisms. Antioxid. Redox Signal. 31 (3), 155–210.

Supplementary figure 1. Purification of recombinant *Cr*FBA3.

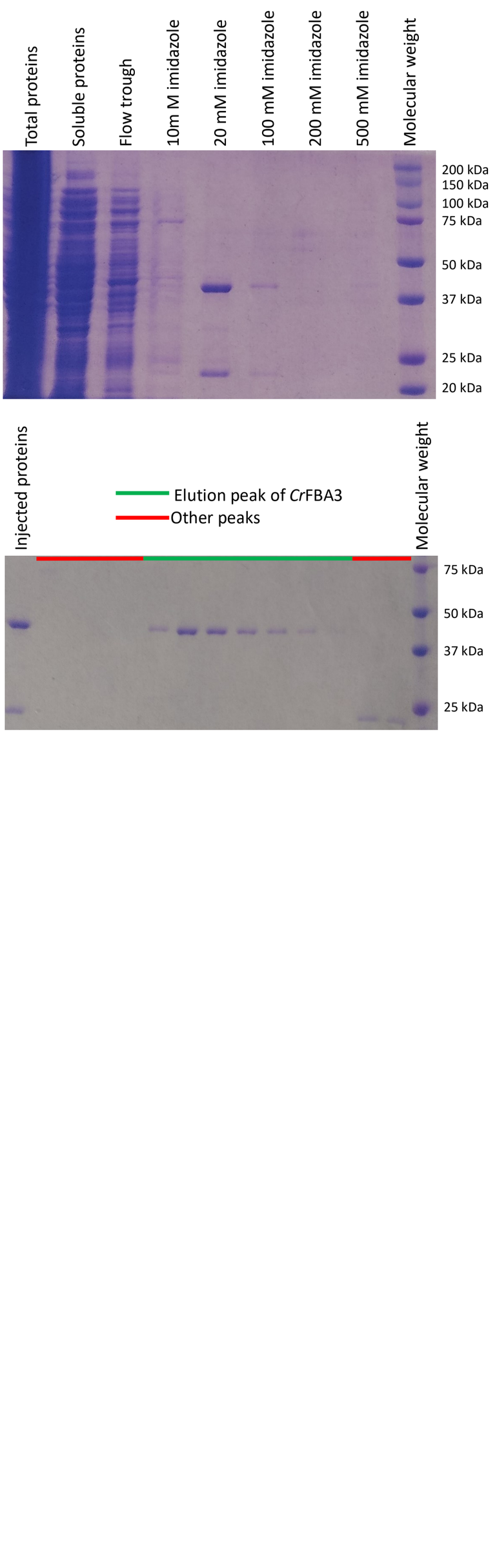

Supplementary figure 2.
Size-exclusion chromatography coupled to small angle X-rays scattering (SEC-SAXS) analysis of *Cr*FBA3. A. Chromatogram of *Cr*FBA3 with absorption at 280 nm in blue and elution volume of calibration proteins arrowed in black. B. SAXS scattering curve log (I)=f(s) in blue fitted with the crystallographic tetrameric model of *Cr*FBA3 in red. C. SAXS scattering curve log(I)=f(s) of data from a sample of *Cr*FBA3 without any treatment (black dots), CrFBA3 with 10 mM DTTox (blue dots), and CrFBA3 with 10 mM DTT (red dots).

A

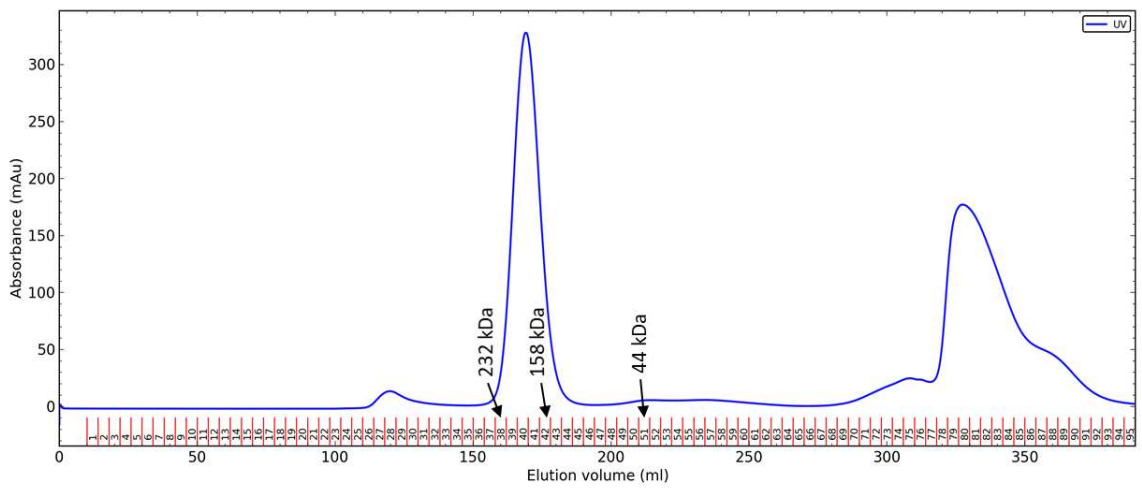

B

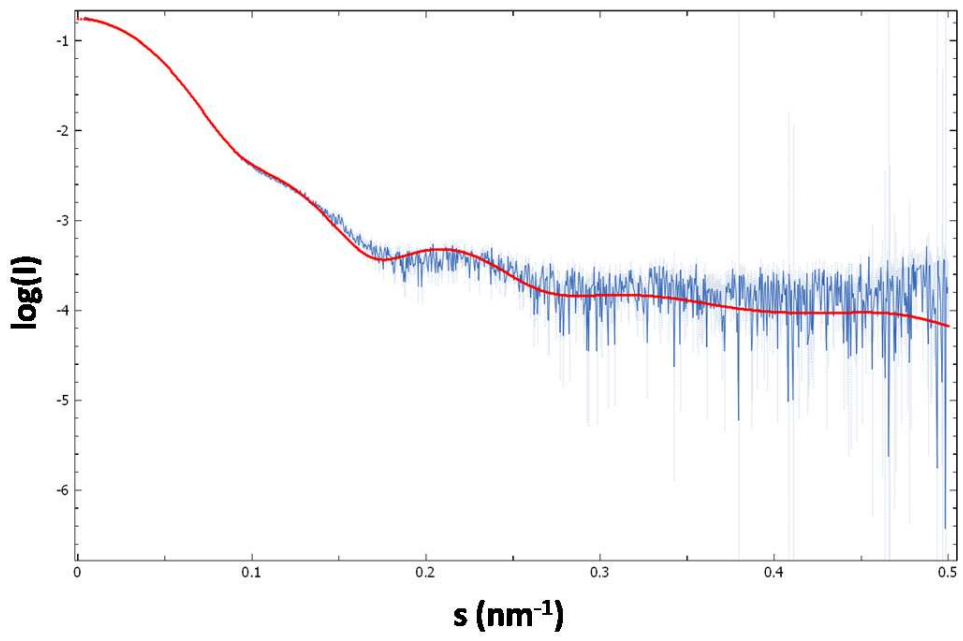

C

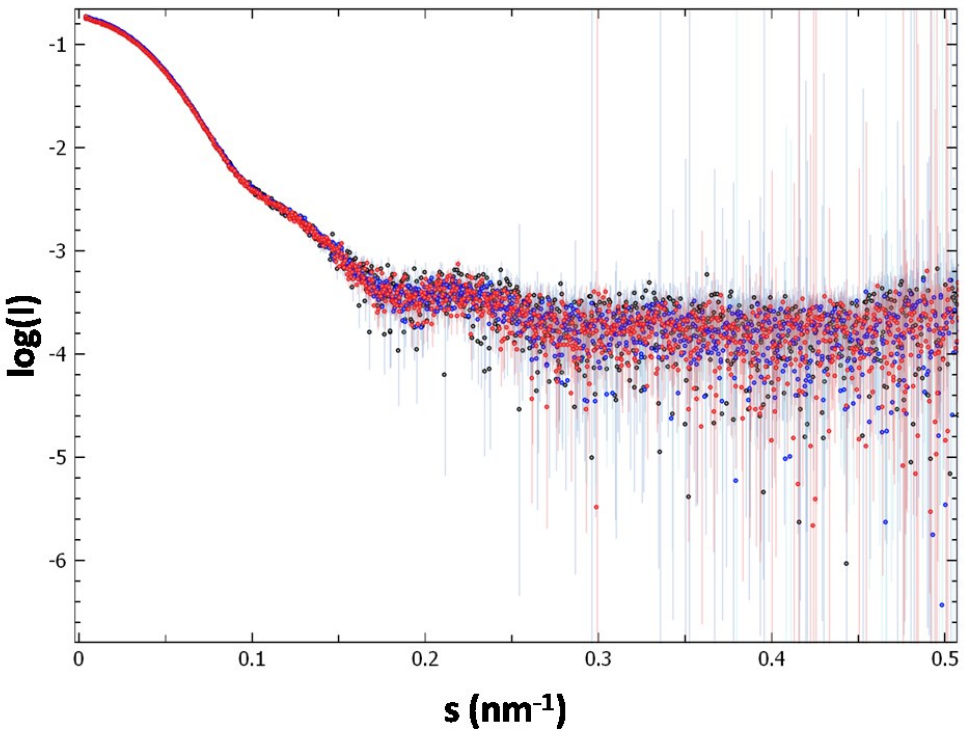

Supplementary figure 3. Multiple sequence alignment of FBA. Active site residues are indicated with a green triangle.

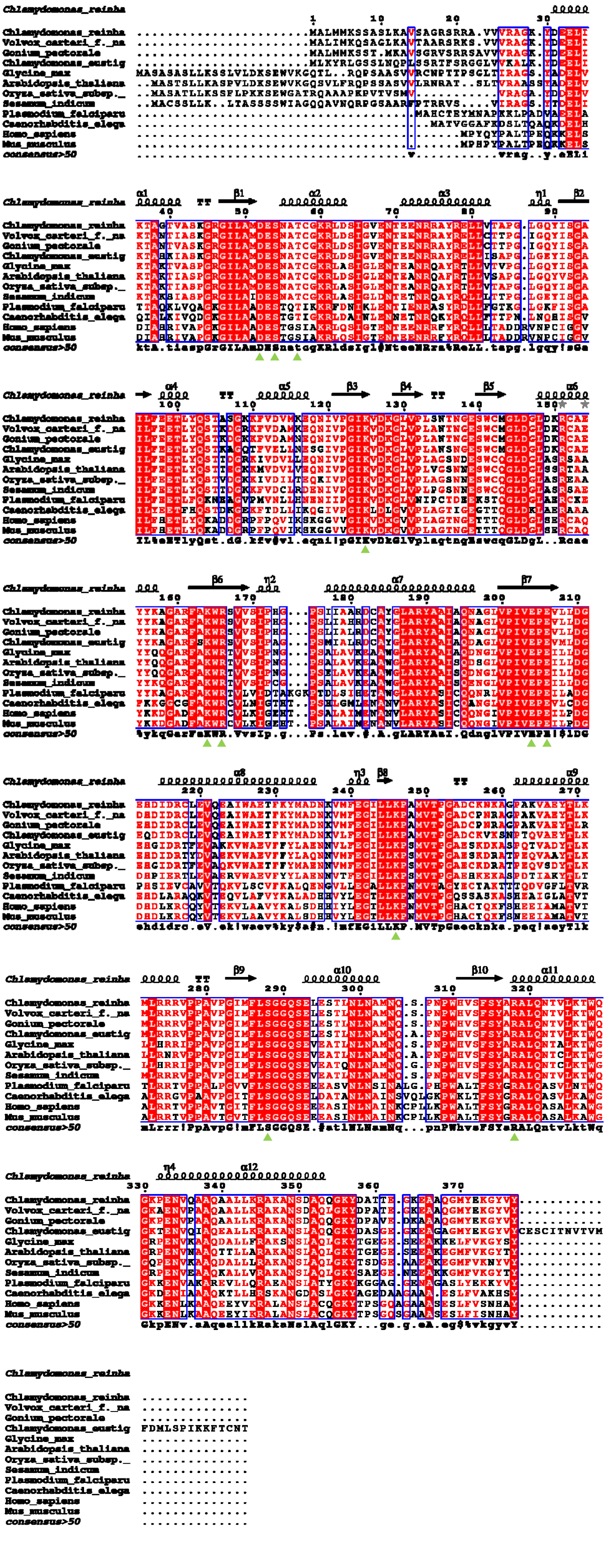

Supplementary figure 4. High-resolution tree of FBA sequences. See Supplementary Figure 5 for the description of taxa represented in the tree.

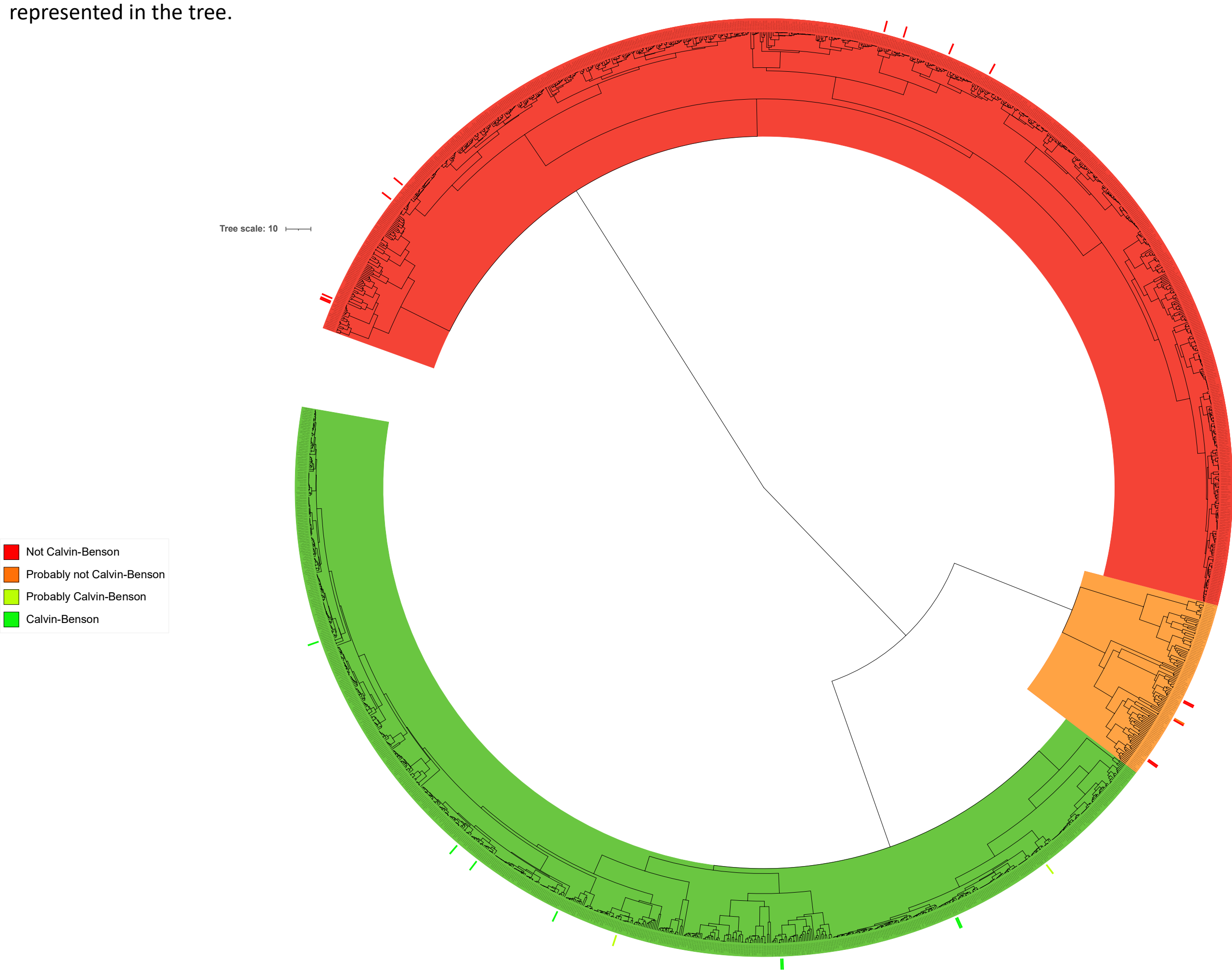

Supplementary Figure 5. Proportion of taxa represented in the FBA tree of Figure 6A and Supplementary figure 4. The 1244 sequences used to construct the profile models belong to a very large spectrum of species as reported in the pie diagram.

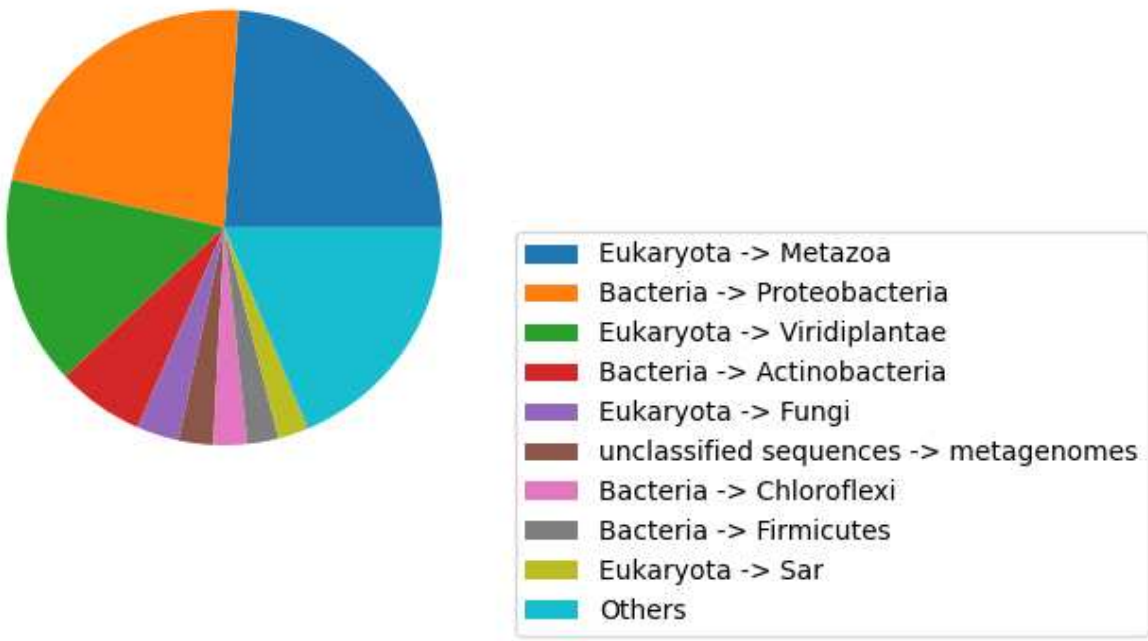

Supplementary figure 6. Tree of sequences classified with ProfileView in this manuscript. The tree has been constructed with the phylogenetic reconstruction method BioNJ (Gascuel 1997). The topology of the tree presents a cascade of sequences whose functional role cannot be distinguished.

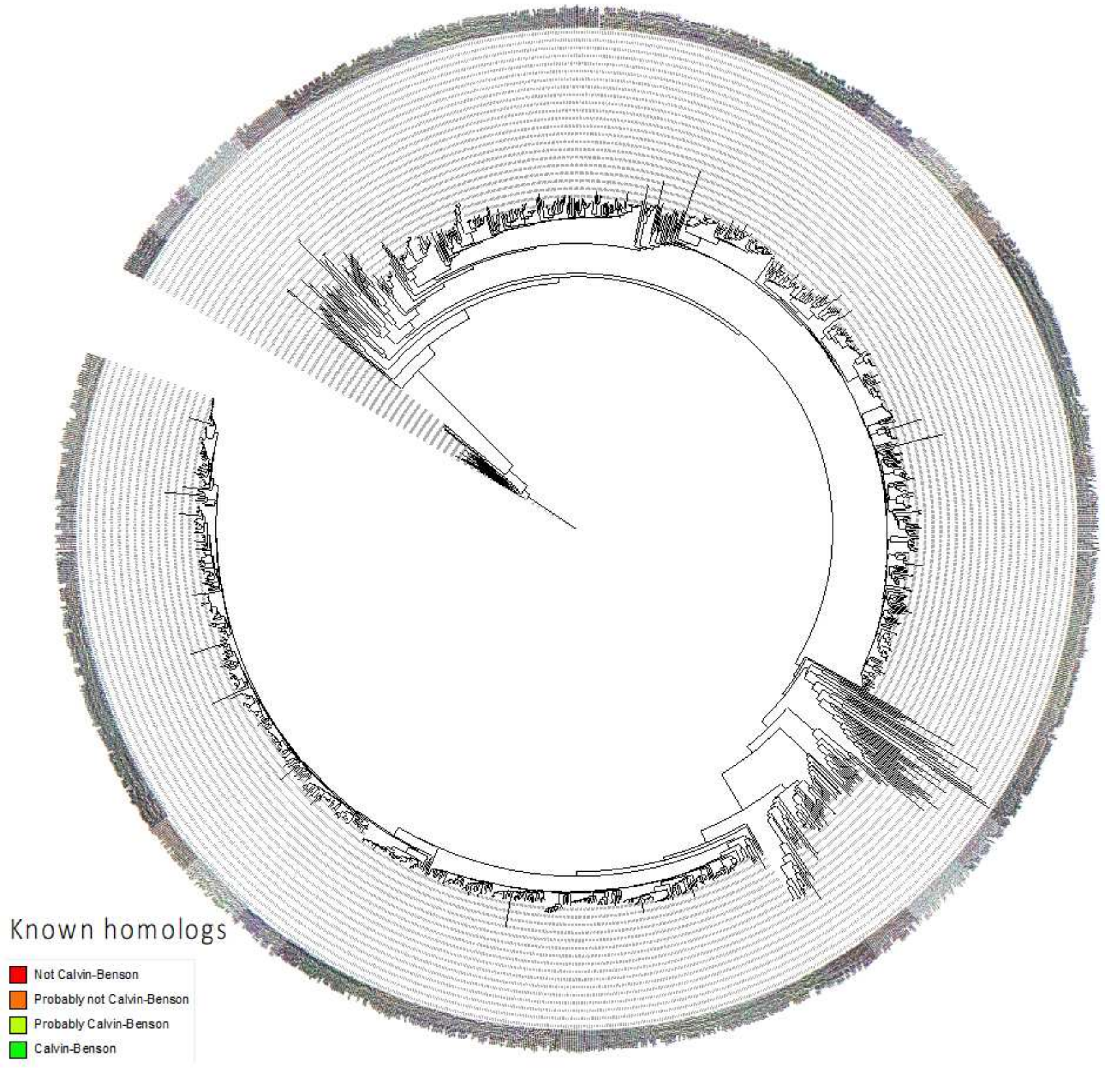

2.1.2.3 Conclusion

Si le décryptage des propriétés structurales de CrFBA3 indique que son site catalytique est commun à ceux décrits auparavant dans d'autres voies métaboliques, tout comme CrRPI1, la collaboration avec une équipe de bio-informaticiens nous a permis de confirmer qu'en utilisant une classification fonctionnelle des enzymes, celles du CBBC se distinguent de leurs paralogues cytoplasmique et sont ségrégées dans une branche spécifique de l'arbre de fonctions (*cf.* figure 6 de Le Moigne et al. (2022b)). La signature de séquence ou de structure ségrégant les FBA photosynthétiques est encore à définir par une analyse plus poussée de l'arbre de fonction. En revanche, la non conservation de certains acides aminés ciblés par des modifications post-traductionnelles vis-à-vis de paralogues cytoplasmiques, ainsi que la nécessité de régulation des enzymes du CBBC lors des phases d'obscurité ou de la disponibilité de leurs cosubstrats soulève l'hypothèse qu'une spécificité des enzymes du CBBC se trouve dans ses modes de régulation. Cette spécificité pourrait peut-être se trouver dans les potentielles interactions de FBA3 avec d'autres protéines, celle-ci interagissant avec CP12, la protéine régulatrice du complexe GAPDH-CP12-PRK (Erales et al. 2008) ou bien dans les différentes modifications des acides aminées de FBA3. La régulation par des modifications redox a notamment été étudiée sur les enzymes qui succèdent à CrFBA3 dans le CBBC et qui sont la fructose-1,6-bisphosphatase (FBPase) et la sedoheptulose-1,7-bisphosphatase (SBPase), comme nous le verront dans la section suivante traitant de la SBPase.

2.1.3 Sédoheptulose-1,7-bisphosphatase

2.1.3.1 Résumé du manuscrit

La sédoheptulose-1,7-bisphosphatase 1 de Chlamydomonas (CrSBPase1) est l'une des deux bisphosphatases du CBBC impliquées dans la régénération du substrat de la Rubisco. C'est l'une des trois enzymes exclusives au CBBC, ne faisant pas partie d'autres voies métaboliques non photosynthétiques.

La purification de CrSBPase montre que durant l'étape de chromatographie d'exclusion de taille, celle-ci est principalement éluée à un volume correspondant à un poids moléculaire de 79 kDa d'après la fonction de calibration de la colonne. Cette masse apparente est proche de celle d'un homo-dimère de SBPase. Ce pic d'élution est asymétrique et présente un épaulement dont le volume d'élution correspond à une masse de 49 kDa. Cette espèce supplémentaire, indistincte de celle formant le dimère en électrophorèse sur gel de polyacrylamide dénaturant, laisse supposer des états hétérogènes de la SBPase et non pas une contamination, que nous interprétons comme un mélange entre dimère et monomère.

Malgré cet état hétérogène, la protéine cristallise dans plusieurs conditions testées des cribles standards utilisés au laboratoire. Les cristaux les plus gros ont permis l'obtention d'un jeu de données de diffraction des rayons X de qualité suffisante pour la résolution de la structure cristallographique à 3,09 Å de résolution dans un groupe d'espace $P2_12_12$ (Code PDB : 7B2O). Le phasage de ces données a été fait par remplacement moléculaire en utilisant comme modèle la structure de la SBPase de *Physcomitrella patens* (code PDB 5IZ3) partageant 72 % d'identité de séquence avec CrSBPase (Gütle et al. 2016). L'affinement des cartes de densité électronique et du modèle de CrSBPase ont permis d'obtenir une unité asymétrique contenant 6 monomères de SBPase. L'analyse du modèle cristallographique de cette première forme cristallisée de CrSBPase montre une conservation des acides aminés du site actif. Par comparaison avec la structure de FBPase de muscle humaine (code PDB : 5L0A) co-cristallisée avec son substrat il est possible d'identifier les acides aminés potentiellement impliqués dans la fixation du SBP chez CrSBPase (Figure C et D du manuscrit). La structure de CrSBPase révèle que parmi les 10 cystéines positionnées, deux forment un pont disulfure intra-chaîne dans chaque copie (Figure 1E du manuscrit). Ce pont est localisé sur un motif peptidique exposé au solvant, à proximité immédiate d'une courte épingle à cheveux β constituée d'un feuillet à deux brins β antiparallèles reliés par un coude (Figure 3A du manuscrit). Localisée à 18 Å des résidus attribués au site catalytique, cette paire de cystéines pourrait moduler indirectement, par effet allostérique, les propriétés de catalyse après la réduction du pont disulfure. En effet, en présence

d'un agent réducteur DTT, d'ion Mg^{2+} ou de thiorédoxine de type f2 une modification de l'activité est observée.

Afin d'identifier les changements de conformation suivant la réduction du pont disulfure, des cristaux de CrSBPase co-incubée avec 10 $mmol.L^{-1}$ de l'agent réducteur Tris-carboxyéthyl phosphine (TCEP) ont été obtenus et ont permis l'obtention d'une nouvelle structure de CrSBPase (code PDB 7ZUV). L'unité asymétrique inclut huit chaînes de SBPase. Six chaînes présentent le pont disulfure comme la structure obtenue en conditions non réductrice, confirmant indépendamment la validité de ce modèle ; les deux autres chaînes ont quant à elle un état de la paire de cystéines 115-120 différent, avec le pont disulfure absent et plusieurs état de la boucle localement réarrangée en une forme partiellement ou totalement désordonnée (Figure 3 du manuscrit). Ce réarrangement de la boucle en différentes conformations a été confirmé par des simulations de dynamique moléculaire menées en collaboration avec le Dr. Nicolas Chéron du département de chimie de l'Ecole Normale Supérieure. La réduction du pont disulfure permet donc une plus grande mobilité de la chaîne autour des cystéines, notamment la réorganisation de l'épingle à cheveux β en un élément mobile. Or, le peptide ordonné autour du pont disulfure se positionne à courte distance de l'interface d'homo-dimérisation. Ainsi, la réduction du pont disulfure C115-C120 cause un désordre local qui pourrait induire une déstabilisation de la structure homo-dimérique de SBPase. Des mutants ponctuels de CrSBPase dont les C115 ou C120 sont substituées en sérines inaptes à la formation du pont montrent tous deux des différences de profils d'élution en chromatographie d'exclusion stérique. Les mutants CrSBPase C115S ou C120S présentent des quantités d'homodimères nettement moins importante que celles de CrSBPase *WT* au profit d'une augmentation des états monomériques et tétramériques.

2.1.3.2 *Structure of the photosynthetic Calvin-Benson-Bassham sedoheptulose-1,7-bisphosphatase SBPase from the model microalga* Chlamydomonas reinhardtii

Structure of the photosynthetic Calvin-Benson-Bassham sedoheptulose-1,7-bisphosphatase SBPase from the model microalga *Chlamydomonas reinhardtii*

Théo Le Moigne[1,2], Martina Santoni[1,3], Lucile Jomat[1], Stéphane D. Lemaire[1], Mirko Zaffagnini[3], Nicolas Chéron[4], Julien Henri[1,*]

1. Sorbonne Université, CNRS, Laboratoire de Biologie Computationnelle et Quantitative UMR 7238, Institut de Biologie Paris-Seine, 4 Place Jussieu, Paris F-75005, France
2. Faculty of Sciences, Doctoral School of Plant Sciences, Université Paris-Saclay, Saint-Aubin F-91190, France
3. Department of Pharmacy and Biotechnology, University of Bologna, Via Irnerio 42, Bologna I-40126, Italy
4. Ecole Normale Supérieure, CNRS, Sorbonne Université, Laboratoire Pasteur UMR 8640, Département de Chimie de l'Ecole Normale Supérieure rue d'Ulm, F-Paris 75005, France

*corresponding author
e-mail: julien.henri@sorbonne-universite.fr
Phone: +33144276606

Abstract

The Calvin-Benson-Bassham cycle (CBBC) performs carbon fixation in photosynthetic organisms. Among the eleven enzymes that participate in the pathway, sedoheptulose-1,7-bisphosphatase (SBPase) is expressed in photo-autotrophs and contributes to the regeneration of ribulose-1,5-bisphosphate, the carbon fixation co-substrate used by ribulose-1,5-bisphosphate carboxylase/oxygenase (Rubisco). While SBPase is structurally similar to fructose-1,6-bisphosphatase

(FBPase) involved in both neoglucogenesis and the CBBC, its function is indispensable to build a productive cycle. In this study we report the first structure of an SBPase from a chlorophyte, the model unicellular green microalga *Chlamydomonas reinhardtii*. By combining experimental and computational structural analyses, we describe the topology, conformations and quaternary structure of *Cr*SBPase. We identify active site residues and locate sites of redox- and phospho- post-translational modifications that contribute to enzymatic functions. *Cr*SBPase adopts distinct oligomeric states that appear to dynamically contribute to the control of its activity.

Introduction

Photosynthetic carbon fixation is performed by eleven enzyme that collectively operate the Calvin-Benson-Bassham cycle (CBBC) (Calvin 1962, Johnson 2016), wherein ribulose-1,5-bisphosphate carboxylase/oxygenase (Rubisco) plays the prominent role of catalyzing fixation of inorganic carbon onto a pentose acceptor: ribulose-1,5-bisphosphate (RuBP). The net gain of the CBBC is one triose in the form of a glyceraldehyde-3-phosphate (G3P) for every three Rubisco catalyzed carboxylations (Johnson and Alric 2013). Regeneration of RuBP is ensured by the other ten enzymes of the CBBC, among which phosphoribulokinase (PRK) catalyzes the phosphorylation of ribulose-5-phosphate (R5P) and sedoheptulose-1,7-bisphosphatase (SEBP, SBPase) catalyzes the hydrolysis of sedoheptulose-1,7-bisphosphate (SBP) into sedoheptulose-7-phosphate (S7P). Remaining CBC enzymes are paralogs of those involved in cytosolic glycolysis, neoglucogenesis or the pentose-phosphate pathway. Hence, Rubisco, PRK and SBPase are expressed in photosynthetic organisms and represent biochemical functions so far uniquely attributed to the photosynthetic CBBC. Meanwhile, the CBBC is considered conserved in plants and cyanobacteria since its enzymes are expressed in cyanobacteria and chloroplasts, that evolved from ancestral endosymbiosis. For instance, the analysis of PRK from *Synechocystis* PCC 6301, *Arabidopsis thaliana*, and *Chlamydomonas reinhardtii* display high structural similarities (Gurrieri, Del Giudice et al. 2019, Wilson, Hayer-Hartl et al. 2019).

Native SBPase was purified from wheat chloroplasts (Woodrow 1982) and corn leaves (Nishizawa and Buchanan 1981), allowing quantitative assays of its catalytic function and the in vitro confirmation of its activation by magnesium, pH, and the redox potential (Anderson 1974, Woodrow and Walker 1980, Cadet and Meunier 1988). Redox control is exerted through a ferredoxin-thioredoxin cascade arising from the activity of the illuminated photosystems (Schürmann and Buchanan 1975). In *Nicotiana* leaves extracts, SBPase reaches its maximal activity after 10 minutes illumination (Zimmer, Swart et al. 2021). This delayed activation kinetics is consistent with the slow reduction pattern of *Arabidopsis* SBPase in vitro (Yoshida and Hisabori 2018).

The crystal structure of SBPase from the moss *Physcomitrella patens* (*Pp*SBPase) has been solved at a resolution of 1.3 Å (Protein Data Bank entry : 5iz3)(Gütle, Roret et al. 2016). *Pp*SBPase fold is highly similar to that of fructose-1,6-bisphosphatase (FBPase), yet the protein was shown to distinctively oligomerize as a homodimer and to form a disulfide bridge in a different motif than that previously described for FBPase (Chiadmi, Navaza et al. 1999). In spite of their homology, the sequences of FBPase and SBPase seem to have evolved different regulatory properties that allow different contributions to the CBBC. Recently, it was proposed that the CBBC can bypass fructose-1,6-bisphosphate (FBP) altogether, by only relying on SBP, glycolysis and the oxidative pentose-phosphate pathway paralogs to regenerate the substrate of Rubisco (Ohta 2022). Engineered SBPase overexpression enhances photosynthesis and growth in plants (Lefebvre, Lawson et al. 2005, Feng, Han et al. 2007, Feng, Wang et al. 2007, Rosenthal, Locke et al. 2011, Simkin, Lopez-Calcagno et al. 2017) and in microalga (Hammel, Sommer et al. 2020). SBPase appears as a metabolic bottleneck for CBC along with Rubisco, making it a target for improvement of photosynthetic capacity by synthetic biology (Kubis and Bar-Even 2019), especially in the experimentally convenient multi-omic model *Chlamydomonas reinhardtii* (Mettler, Mühlhaus et al. 2014, Schmollinger, Mühlhaus et al. 2014).

SBPase is encoded by *Chlamydomonas reinhardtii* gene Cre03.g185550 (Uniprot entry P46284). The protein is expressed by a nuclear gene and addressed to the chloroplast by a 54-residue amino-terminal peptide (Emanuelsson, Brunak et al. 2007, Almagro Armenteros, Salvatore et al. 2019).

SBPase abundance in the cell was quantified by mass spectrometric proteomics as 1.1-1.3 ± 0.3 amol/cell, representing 0.15 % of total cell proteins (Hammel, Sommer et al. 2020). In *Chlamydomonas* extracts, SBPase was shown to undergo post-translational modifications by phosphorylation of serines and threonines (Werth, McConnell et al. 2017), and redox modifications of cysteines (Zaffagnini, Bedhomme et al. 2012, Morisse, Zaffagnini et al. 2014, Pérez-Pérez, Mauriès et al. 2017). However, the mechanisms by which post-translational modifications affect the catalytic activity of SBPase is still lacking. Here, we describe the crystal structures of *Cr*SBPase in two redox states, assay its functions in vitro, and investigate the correlations between dithiol/disulfide exchanges and the oligomerization of the protein. Our results suggest that a redox control over oligomer equilibrium could represent a novel mechanism to regulate enzymatic activities in the CBBC.

Material and methods

Chemical reagents were purchased from Merck (Darmstadt, Germany), chromatography material was provided by Cytiva (Vélizy-Villacoublay, France), crystallization solutions and consumable were purchased from Qiagen (Hilden, Germany), Hampton Research (Aliso Viejo, CA USA), and SPT Labtech (Melbourn, UK).

Cloning and mutagenesis of *Cr*SBPase expression plasmids

The sequence coding for full-length mature SBPase was amplified by polymerase chain reaction (PCR) from *Chlamydomonas reinhardtii* total ribonucleic acids extract and inserted at sites 5'-NdeI and BamHI-3' into expression vector pET3c modified for the fusion of an amino-terminal hexa-histidine tag in the recombinant protein, yielding plasmid pSL-175-His6-*Cr*SBPase-WT. PCR primers were 5'-TCTCGCCATATGGCCGTTCTGACCCAGGCC-3' (forward, NdeI site underlined) and 5'-CGGGTGGGATCCTTAGGCAGCCACCTTCTC-3' (reverse, BamHI site underlined). The encoded protein encompasses 331 amino acids, with a molar mass of 36176.7 $g.mol^{-1}$ and a theoretical extinction coefficient of 24722.5 $mol^{-1}.L.cm^{-1}$. Unless otherwise stated, amino acids residues numbering is that of

GenBank entry DAA79954.1. Point mutants of cysteines 115, 120, 149, and 153 singly substituted for serines were generated by site-directed PCR mutagenesis with primers listed in supplementary table 1, producing plasmids pSL-181-His6-*Cr*SBPase-mC115S, pSL-182-His6-*Cr*SBPase-mC120S, pSL-183-His6-*Cr*SBPase-mC149S, pSL-184-His6-*Cr*SBPase-mC153S.

Recombinant *Cr*SBPase purification

Plasmids pSL-175, -181, -182, -183, -184 were used to transform *Escherichia coli* BL21(DE3). The transformants were grown at 37°C in 2YT supplemented with 150 µg/mL ampicillin. When cultures reached an OD600≈0.6, T7-dependent *Cr*SBPase overexpression was induced by the addition of isopropyl-β-D-thiogalactopyranoside (IPTG) at 0.2 mmol.L^{-1} for 3 h.

Harvested cell pellets were resuspended in 20 mmol.L^{-1} Tris pH 7.9, 100 mmol.L^{-1} NaCl (buffer A) and lyzed by 1 sec / 1 sec pulsed sonication for 3 min. The soluble fraction of the lysate was separated by 20 min centrifugation at 20 000 rcf and loaded on 2 mL Ni-NTA resin for His-tag mediated affinity chromatography. Resin was washed in four steps with 25 mL buffer A, 25 mL buffer A supplemented with 10, 20, and 30 mmol.L^{-1} imidazole, and *Cr*SBPase was eluted with 10 mL buffer A supplemented with 100, 200, and 300 mmol.L^{-1} imidazole. Pooled eluates containing *Cr*SBPase were loaded on HiLoad Superdex 200 26/600 size-exclusion chromatography column and eluted in buffer A. Protein purity was assessed by electrophoresis on 12 % acrylamide gel in denaturing and reducing conditions (supplementary figure 1). Peak fractions were assembled and concentrated by ultrafiltration on Amicon units of MWCO 30000. Final proteins concentrations were in the 1-10 mg.mL^{-1} range as measured by nanodrop spectrophotometer.

Western blot

Polyclonal antibodies were generated by immunization of rabbits with pure recombinant *Cr*SBPase (Genecust, Boynes France). Analyzed fractions were separated by denaturing polyacrylamide electrophoresis and transferred to nitrocellulose membrane for detection with primary antibody

subsequently detected by secondary anti-rabbit antibodies coupled to horseradish peroxidase. Detection was done with commercial ECL peroxidase assay (GE Healthcare, Chicago IL USA) with a Chemidoc (Bio-Rad, Hercules CA USA).

Crystallization and structure determination

Pure recombinant His6-*Cr*SBPase-WT concentrated at 3-6 mg/mL was tested for crystallization on screens JCSG I-IV in 200 nL sitting drops. Single crystals were obtained and optimized with mother liquor 0.1 mol.L^{-1} sodium HEPES pH=7.5, 2 % (v/v) polyethylene glycol 400, 2.0 mol.L^{-1} ammonium sulfate, flash-frozen in mother liquor supplemented with 25 % glycerol and tested for X-ray diffraction. Complete X-ray diffraction datasets were collected at SOLEIL beamline Proxima-2A and allowed the determination of the crystal structure by model replacement with 5iz3, the structure of ortholog SBPase from the moss *Physcomitrella patens.* Model building in COOT and refinement in the PHENIX software suite yielded structure 7b2o (Emsley, Lohkamp et al. 2010) (Adams, Afonine et al. 2011) (Liebschner, Afonine et al. 2019). After we obtained our experimental structure, the European Bioinformatics Institute (Hinxton, UK) communicated high-accuracy prediction models computed by Deepmind ALPHAFOLD2 (Jumper, Evans et al. 2021), including a prediction of *Cr*SBPase structure (https://alphafold.ebi.ac.uk/entry/P46284) that matches 7b2o crystal structure with RMSD=0.453 Å. Hence, X-ray crystallography and ALPHAFOLD independently contribute to the proposed structural analysis.

In order to determine the structure of *Cr*SBPase in a reduced state, crystals were grown in the presence of 10 mmol.L^{-1} of the reducing agent tris-(2-carboxyethyl)phosphine (TCEP) in condition JCSG IV E8/56 0.2 mol.L^{-1} lithium sulfate, 0.1 mol.L^{-1} Tris pH 7.0, 1.0 mol.L^{-1} sodium/potassium tartrate. Crystals were cryo-protected in mother liquor supplemented with 25 % ethylene glycol, flash-frozen and tested for X-ray diffraction at SOLEIL beamline Proxima-2A. A complete dataset was collected that allowed the determination of the structure by molecular replacement with 7b2o as a template. Among the eight *Cr*SBPase copies of the asymmetric unit, two had their disulfides absent as a consequence of the TCEP

155 treatment while the others six subunits were essentially identical to untreated structures in entry
156 7b2o.
157
158 **Enzymatic assays**
159 The catalytic activity of 10-200 nmol.L^{-1} pure recombinant *Cr*SBPase was assayed in buffer A, by
160 absorbance spectrophotometry by coupling the hydrolysis of 0.6-6 mmol.L^{-1} fructose-1,6-bisphosphate
161 (FBP) into fructose-6-phosphate (F6P) to the reduction of 0.2-0.5 mmol.L^{-1} $NADP^+$ into NADPH through
162 isomerization of F6P into glucose-6-phosphate (G6P) by 0.1-0.5 U.mL^{-1} phosphoglucose isomerase
163 (PGI) and the oxidation of G6P into 6-phosphogluconolactone (6PGL) by 0.1-0.5 U.mL^{-1} glucose-6-
164 phosphate dehydrogenase (G6PDH) (figure 2A). Reporter assay is coupled in a molar ratio
165 FBP:F6P:G6P:6PGL of 1:1:1:1 to the oxidation of one molar equivalent of $NADP^+$ into NADPH that we
166 recorded over 0-20 minutes by measuring the absorbance at 340 nm with a UVIKON
167 spectrophotometer. Pre-treatment with 0-100 mmol.L^{-1} DTT, 0-30 mmol.L^{-1} $MgSO_4$, and 0-15 µmol.L^{-1}
168 recombinant *Cr*TRXf2 (Lemaire, Tedesco et al. 2018) was done for 30 min at room temperature before
169 adding the enzyme in the reporter solution.
170
171 **Titration of reactive cysteines**
172 Quantification of free reactive cysteines on recombinant CrSBPase was done with 5,5'-dithio-bis-(2-
173 nitrobenzoic Acid) (DTNB, Ellman's reagent) mixed with the purified recombinant protein in a 50:1
174 molar ratio in a 1 mL reaction volume that included 100 mmol/L Tris-HCl pH 7.9. Reaction of DTNB with
175 free thiols like those of solvent-exposed cysteines produces 2-nitro-5-thiobenzoate (TNB^-) that we
176 quantified by monitoring the absorbance at 412 nm and a molar extinction coefficient of TNB^- of 14.15
177 $mmol^{-1}$.L.cm^{-1}. We calculated the number of free reactive cysteines per *Cr*SBPase monomer by dividing
178 the molar concentration of TNB^- by that of the protein at equilibrium (t >60 min). The titration was
179 replicated five times.

Molecular dynamics

Molecular dynamics (MD) simulations were performed with the Gromacs package (v2021.4) (Pronk, Páll et al. 2013, Abraham, Murtola et al. 2015). A dimer of SBPase was solvated in a rhombic dodecahedron box with at least 8 Å between the protein atoms and the box edges, which corresponds to ~64000 atoms in total (~18000 water molecules) and a triclinic box of 97x97x68 $Å^3$. The box was neutralized with 18 sodium atoms to make it neutral. The starting conformation was the crystallized structure of oxidized SBPase, and we protonated C115 and C120 to manually create the reduced state. The protein was described with the Amber14SB force field (Maier, Martinez et al. 2015) and water with the TIP3P model (Jorgensen 1981). Non-bonding interactions were described with standard parameters: van der Waals interactions had a cutoff of 8 Å, and electrostatic interactions were computed with PME with default parameters with a separation between spaces at 8 Å. Bonds containing a hydrogen atom were restrained with the LINCS algorithm with default parameters. After an energy minimization, the system was equilibrated under the NPT conditions with a δt=1 fs timestep, the velocity-rescale thermostat and the Berendsen barostat. Velocities were generated at 100 K and the system was heated up to 300 K in 400 ps before performing 100 ps at 300 K. We then ran simulations of 20 µs under the NPT conditions with a δt=2 fs timestep, the velocity-rescale thermostat and the Parrinello-Rahman barostat.

Small-angle X-ray scattering

Pure recombinant *Cr*SBPase was injected on Agilent HPLC BioSEC-3 300 column in buffer A, in line with the X-ray beam capillary at SOLEIL beamline SWING. *Cr*SBPase was untreated or pre-treated with 10 $mmol.L^{-1}$ of reducing agent dithiothreitol (DTTred) or oxidizing agent trans-1,2-dithiane-4,5-diol (DTTox). Diffusion curves were analyzed with ATSAS software to determine the molecular mass and oligomeric state of the protein.

Results

Crystal structure of *Cr*SBPase

Pure recombinant *Cr*SBPase crystallized in space group $P2_12_12$ and provided a complete X-ray diffraction dataset at a resolution of 3.09 Å. The asymmetric unit is composed of six polypeptide chains and four water molecules. All chains align within a root mean square deviation (RMSD) <0.25 Å and can be considered identical. 309 of the 331 amino acid residues could be built in the electron density, the unmodelled sequences are in the disordered extensions at the amino- and carboxy-termini of the model. Crystallographic data and model coordinates were registered at the protein data bank under accession code 7b2o. *Cr*SBPase folds into two domains (figure 1A-B), an amino-terminal domain composed of a mixed β-sheet formed by strands 3-9 and a carboxy-terminal domain composed of a mixed β-sheet formed by strands 10-13. α-helices 1-3 pack on the amino-terminal end of the seven-strand sheet, while α-helices 4,5, and 8 pack on the carboxy-terminal end of the four-strand sheet. α-helices 6 and 7 are sandwiched in between the two sheets. A short antiparallel β-sheet constituted of 4-residue long strands 1 and 2 separated by a β-turn and preceded by loop 113-ASCAGTAC-120 is inserted between α-helices 2 and 3. Residues 113-130 forming the loop and β-hairpin (LBH) motif are positioned away from the core of the protein and will be further discussed in the next sections.

SBPase catalytic pocket

*Cr*SBPase is structurally similar to its ortholog from the moss *Physcomitrella patens* (Gütle, Roret et al. 2016). SBPase is a homolog of fructose-1,6-bisphosphatase (FBPase), another enzyme of the Calvin-Benson-Bassham cycle in photosynthetic organisms and an enzyme ubiquituously involved in neoglucogenesis. Cytosolic isoforms of FBPase have been extensively studied. For instance, the crystal structure of human muscle FBPase complexed with its substrate fructose-1,6-bisphosphate (FBP) was determined (PDB entry: 5l0a). We aligned the structure *Cr*SBPase onto that of human FBPase:FBP, confirming their similarity (RMSD = 0.824 Å) with the notable exception of the LBH motif which is absent in the neoglucogenic enzyme. In a 4-Å distance to FBPase co-crystallized FBP we aligned 12

residues that are likely available for FBP or SBP binding by *Cr*SBPase (figure 1C): E155, D173, D176, G177, Y287, G289, G290, M291, K317, L318, R319, and E323. These residues are exposed to solvent in a continuous surface (figure 1D). Water molecule H_2O 401 could be modelled at the center of the putative SBPase catalytic pocket, in the vicinity of E155, D173, D176, R319, and E323.

Sites of redox post-translational modifications

Ten cysteines could be located in the model. Previous proteomic studies established that SBPase cysteines 115, 120, 222, 231, 355, and 362 are redox-modified by thioredoxin dithiol/disulfide exchange (Lemaire, Guillon et al. 2004, Pérez-Pérez, Mauriès et al. 2017), gluthationylation (Zaffagnini, Bedhomme et al. 2012), or nitrosylation at C355 and C362 (Morisse, Zaffagnini et al. 2014). C222, C231, C355, and C362 are targets of thioredoxin. DTNB titration on the native purified SBPase indicates that 4,0 ±0,6 cysteines are reactive owing to their relative exposure to solvent in a free reactive form. Accessible surface area and accessibility (ASA) calculation is consistent with DTNB titration, with the four cysteines C149, C153, C231, and C357 exposed to solvent, and the six others either shielded from solvent or engaged in a disulfide bridge (Ahmad, Gromiha et al. 2004). In *Cr*SBPase crystal structure C222 and C231 are positioned on neighbouring strands of the amino-terminal domain, exposing their thiol 3.5 Å away from each other (Figure 1E). The formation of an intramolecular disulfide bridge at this cysteines pair is possible if local main chain rearrangements allow a closer contact. C362 thiol is positioned 10.5 Å away from the nearest thiol, of C340. Additionally, both are exposed on an opposite side of the carboxy-terminal β-sheet, disfavouring the formation of an internal disulfide bridge. C355 points its side chain towards C153, with a thiol-thiol distance of 4.6 Å. A third thiol is exposed by C169 at 10.1 Å, on the same side of the amino-terminal β-sheet. A C355-C153/C169 thiol-disulfide exchange is plausible, as was described for plant FBPase (Jacquot, Lopez-Jaramillo et al. 1997), but has not been observed in *Cr*SBPase. Local rearrangements that occur upon FBPase disulfide reduction causes a larger scale relaxation of the active site required to reach maximal catalytic potential (Chiadmi, Navaza et al. 1999) as kinetically characterized in *Arabidopsis* (Yoshida and Hisabori 2018) and *Nicotiana* (Zimmer,

Swart et al. 2021). In SBPase, the FBPase-type regulatory disulfide is not observed but the C115-C120 bridge in the LBH motif may regulate the enzyme by alternative means. Indeed, the disulfide-bonded cysteines constrain loop 113-ASCAGTAC-120 into a compact lasso conformation that could open into a relaxed conformation hypothetically activating catalysis.

Sites of post-translational phosphorylations

*Cr*SBPase was reported to be phosphorylated from algae extracts at residues T112, S114, T118, S123, T310, S311, T313 (Wagner, Gessner et al. 2006, Werth, McConnell et al. 2017, McConnell, Werth et al. 2018). Consistently with the proximity of these residues in two sectors of the sequence (supplementary figure 2), the candidate modification sites are located in two contiguous regions in the three-dimensional model (figure 1F). T112, S114, T118, and S123 are exposed to solvent of amino-terminal domain at the surface. The residues belong to or are located nearby the 113-ASCAGTAC-120 motif where phosphorylations may cross-signal with redox modifications on cysteines 115 and 120. T310, S311, and T313 are located on the other edge of *Cr*SBPase, at solvent exposed tip of the carboxy-terminal domain. Their co-localization at the 310-TSPT-313 motif facilitate a coordinated phosphorylation of the three residues by the same kinase. Because both groups of potential phospho-sites are located at 17-18 Å from the catalytic pocket (H_2O 401 taken as a reference point), there is no straightforward mechanism by which such modifications would exert a control over *Cr*SBPase activity. The identification of the actual kinases/phosphatases couples that control SBPase phosphorylation would facilitate the study of this mechanism.

***Cr*SBPase enzymatic activity**

Recombinant *Cr*SBPase was assayed for its capacity to catalyze FBP hydrolysis into F6P (Figure 2A), a proxi for the hydrolysis of SBP into S7P that we could not test by lack of available substrate and kinetic reporter method. In vitro, we measured a specific activity of 10.5 ±3.3 $\mu mol.min^{-1}mg^{-1}$ that compares to previously published values gathered from *Chlamydomonas* recombinant SBPase with a

283 discontinuous inorganic phosphate titration assay and SBP as a substrate: 7.15 µmol.min^{-1}mg^{-1} (Tamoi,
284 Nagaoka et al. 2005). Chemical reduction of recombinant *Cr*SBPase by 10 mmol.L^{-1} DTT increased its
285 specific activity by a factor of 2.3 (figure 2C) with an unexpected decrease of activity at higher
286 concentration of the reducing agent, presumably caused by denaturation or aggregation of the
287 enzyme. Magnesium addition activated the enzyme activity by 8.9-fold, and an optimal magnesium
288 concentration of 10 mmol.L^{-1} (figure 2D). The chloroplast thioredoxin *Cr*TRXf2 was tested and validated
289 for its capacity to activate SBPase by reduction with a 4.7-fold factor and an optimal TRX concentration
290 of 1 µmol.L^{-1} (figure 2E).
291
292 **Redox controlled dynamics of *Cr*SBPase**
293 *Cr*SBPase crystallized under the reducing treatment of 10 mmol.L^{-1} TCEP. Among the eight subunits in
294 the asymmetric unit, C155-C120 disulfide is absent in two chains (subunits C colored in magenta and E
295 colored in salmon, figure 3D and 3F), while the other six subunits still have the C155-C120 disulfide
296 bridge (figure 3B,C,E,G,H,I). These six subunits present mildly variable conformations of the 113-
297 ASCAGTAC-120 lasso conformation that compare to the untreated oxidized structure of *Cr*SBPase
298 (figure 3A). Reduction of the C155-C120 disulfide increases local disorder (supplementary figure 3),
299 and the main chain electron density became uninterpretable over a few residues for subunits C and E.
300 Molecular dynamics (MD) simulations of the reduced structure were performed by starting from a
301 dimer of the crystallized oxidized form and forcing residues C115 and C120 to be reduced in a -SH state.
302 We then ran two independent replicas of 20 µs of classical MD. In addition, we also ran two
303 independent replicas of 2 µs of MD in the oxidized form. In one of the replicas of the reduced form
304 (MD1), the protein structure barely changed as can be seen in the SG(C115)/SG(C120) distance that
305 plateaued at ~7 Å, as well as in the RMSD with respect to the starting conformation that stayed around
306 2 Å (see supplementary figures 7-8 for plots and 12 for images of the structures). However, in the other
307 replica of the reduced form (MD2), significant changes of conformation appeared: the
308 SG(C115)/SG(C120) distance ended up at ~10 Å with peaks at 20 Å and the RMSD ended up at 3.7 and

2.8 Å (supplementary figures 7-8). The difference between MD1 and MD2 is stronger when one focuses on the RMSD of the mobile motif (residues 112 to 131, supplementary figure 9). We observed that after 17 µs of MD all chains adopted an equilibrated conformation and then fluctuated around that conformation (supplementary figure 9); representative structures extracted from MD were thus obtained from a clustering on the time bloc 17-20 µs.

The two chains A and B from MD2 adopt a different final conformation (see figure 4A for the overlap with the crystallized oxidized structure and figure 4B for the overlap with the crystallized reduced structure), and we cannot directly conclude on which one is the most stable. Moreover, the residues 115 to 128 of each chain from MD do not overlap well with the crystallized reduced structure which means that neither of the two chains conformations from MD has converged towards the crystallized state. However, we can observe in the reduced crystallized structure that residues 134 to 148 form an α-helix which is also present in chain B from MD2 whereas this structure is not kept in chain A from MD2 (see green chain on the right of figures 4A-B). In addition, mobile motif from chain B seems to open towards the solvent in a similar way that what FBPase does in the reduced state. Thus, we conclude that chain B from MD2 is more representative of the true reduced conformation than chain A from MD2. If we compare the mobility of chain B from MD2 in the reduced state with one chain in the oxidized state (also chain B from the second simulation), we can see that on overall the mobile motif is more flexible in the reduced state, which is especially true for residues around C120 (residues 118 to 123, supplementary figure 10). We then analyzed the RMSD of residues 112 to 131 from chain B during MD2 (supplementary figure 11): residues 112, 130 and 131 barely moves which is expected since they belong or are directly connected to the two α-helixes flanking the mobile motif. At $\sim$6 µs of the trajectory almost all other residues (with the exception of C120) display an abrupt change of conformation, with a different magnitude though: starting from $\sim$2 Å, the RMSD jumped to 3 Å for some residues and to 15 Å for other residues. At $\sim$13.5 µs, another change occurs which involves C120 but not all the other residues. Thus, we conclude that the opening of the motif happens in a concerted way and not sequentially residue per residue.

Oligomeric states of *Cr*SBPase

Size-exclusion profile of the purified protein is polydisperse with at least three distinct species of *Cr*SBPase (supplementary figure 1A,C). Wild-type recombinant protein elutes as a main peak of 79 kDa, close to the mass of a homodimer (theoretical mass from sequence: 36 kDa). This peak is broadened by a later-eluting shoulder, with the apparent molecular mass of the tailing species at 48 kDa that suggests the presence of a monomeric state of *Cr*SBPase. The third species elutes at an apparent molecular mass of 145 kDa, that fits with that of a homotetramer. According to the absorbance of each peak and considering that they represent all states of purified *Cr*SBPase in solution, we estimate a repartition of species of 10:53:37 for the tetramer:dimer:monomer mixture (total=100). Re-injection of the dimer peak fraction over size-exclusion chromatography yielded a similar mixed profile, supporting a dynamic equilibrium over the time of the experiment (>2 h).

*Cr*SBPase was crystallized in space groups $P2_12_12$ or $P12_11$ with respectively 6 and 8 protomers in the asymmetric unit. Proteins Interfaces Structures and Assemblies (PISA) analysis reveals that protomers of both crystals pack as homodimers of up 4 200 Å² in a similar manner (figure 4A) (Krissinel and Henrick 2007). In the asymmetric unit of 7zuv or within crystallographic neighbouring units of 7b2o, *Cr*SBPase further packs into a homotetramer, a dimer of dimers (figure 4B).The apparent molecular mass of SBPase extracted from *Chlamydomonas* cultures cultivated in TAP medium under 40 $\mu E.m^{-2}.s^{-1}$ illumination is comprised between 130 and 40 kDa (supplementary figure 4) with the homodimer representing the predominant state.

Small-angle X-ray scattering (SAXS) of *Cr*SBPase untreated or reduced by 10 $mmol.L^{-1}$ dithiothreitol (DTT) reveals an increase in the protein radius of gyration from 39 to 62 Å upon reduction (supplementary figure 5) indicative of a change in the oligomeric state of SBPase correlated with redox modifications. Besides, after a week at 4°C, the purified protein partially precipitates into an amorphous aggregate that treatment with 10 $mmol.L^{-1}$ TCEP turns into liquid-liquid phase separations (supplementary figure 6). Since the LBH redox module is positioned at the homodimer interface (figure

5C), we postulated that the reduction of the C115-C120 disulfide and the subsequent local conformation changes depicted by MD affect the oligomer equilibrium of the enzyme. As a matter of fact, we observed that point mutants C115S or C120S that are unable to form the C115-C120 disulfide elute in a different oligomer ratio than wild-type SBPase (supplementary figure 1C), with an relative accumulation of monomer and tetramer species at the expense of the dimer state in both mutants. Meanwhile, the in vitro specific activity of the disulfide bridge mutants still appeared responsive to DTT-activation: SBPase mutant C115S specific activity increases by 33- or 35-fold and SBPase mutant C120S by 39- or 110-fold upon DTT treatment. We conclude that C115-C120 disulfide is not the single redox regulator of SBPase active site. SBPase mutant C153S targeting a cysteine of the FBPase-type redox module is still responsive to DTT activation as well. The identity of all the cysteines that contribute to SBPase catalytic modulation is thus yet to be established.

Conclusions and perspectives

We report the first crystal structure of an SBPase from the microalga *Chlamydomonas reinhardtii*, a model for the molecular and cell biology of plants. SBPase is a photosynthetic enzyme involved in the regenerative phase of the Calvin-Benson-Bassham cycle proved to be the target of multiple regulations that we map onto our structural model, highly similar to that of SBPase from the moss *Physcomitrella patens* and to FBPase from chloroplast or cytosolic origins. Notwithstanding its propensity to form crystals, recombinant SBPase populates a range of oligomeric states, dominated by a homodimeric form susceptible to exchange for monomers, tetramers and higher-order assemblies. This oligomer equilibrium is dynamic and is correlated with the presence of a disulfide bridge at the vicinity of the monomer-monomer interface, in the SBPase-specific LBH motif. We postulate that the reversible reduction/oxidation of C115-C120 modulates the oligomerization of SBPase, through the induction of a local disorder that we observed in the crystal of the protein under reducing condition and that correlates with computations of molecular dynamics.

How this oligomeric exchange impacts the actual activity of the enzyme is an open question but should be aligned with previous reports on the allosteric character of the structurally apparented enzyme FBPase that follow a dimer/tetramer exchanges (Barciszewski, Wisniewski et al. 2016) with a Hill cooperativity coefficient close to 2 (Giudici-Orticoni, Buc et al. 1990). Lastly, systematic proteome mapping in the chloroplast of *Chlamydomonas* localized SBPase in a region surrounding the Rubisco pyrenoid nearby five other CBBC enzymes: phosphoglycerate kinase 1 (PGK), glyceraldehyde-3-phosphate dehydrogenases (GAP1, GAP3), fructose-bisphosphate aldolase (FBA3), ribulose-5-phosphate 3-epimerase (RPE1), and phosphoribulokinase (PRK) (Wang, Patena et al. 2022). Based on our structure-function study on recombinant SBPase we propose that upon reductive activation SBPase is co-addressed to this liquid partition of the stroma where it contributes to Calvin-Benson-Bassham reactions at optimized rates.

Tables.

Table 1. Crystallographic data collections and models building statistics.

	7b2o (oxidized)	7zuv (partially reduced)
Wavelength (Å)	0.9801	0.9801
Resolution range (Å)	46.62 - 3.095 (3.206 - 3.095)	48.54 - 3.11 (3.221 - 3.11)
Space group	P 2_1 2_1 2	P 1 2_1 1
Unit cell (Å, °)	178.224 183.652 75.196 90 90 90	53.774 163.462 172.765 90 91.939 90
Total reflections	615155 (55989)	376091 (32376)
Unique reflections	45740 (4245)	53456 (5213)
Multiplicity	13.4 (12.9)	7.0 (6.2)
Completeness (%)	99.34 (94.20)	99.65 (97.17)
Mean I/sigma(I)	12.02 (1.72)	8.54 (1.30)
Wilson B-factor (Å²)	64.82	68.45
R-merge	0.495 (1.877)	0.2492 (1.502)
R-meas	0.5144 (1.954)	0.2691 (1.64)
R-pim	0.1386 (0.5343)	0.1009 (0.6477)
CC1/2	0.983 (0.623)	0.988 (0.479)
CC*	0.996 (0.876)	0.997 (0.805)
Reflections used in refinement	45607 (4242)	53417 (5193)
Reflections used for R-free	1986 (183)	1983 (191)
R-work	0.1942 (0.3071)	0.1963 (0.3239)
R-free	0.2390 (0.3482)	0.2328 (0.3740)
CC(work)	0.944 (0.788)	0.956 (0.726)
CC(free)	0.912 (0.649)	0.949 (0.596)
Number of non-hydrogen atoms	14194	18714
Macromolecules	14190	18704
Solvent	4	10
Protein residues	1859	2451
RMS(bonds) (Å)	0.005	0.004
RMS(angles) (°)	0.75	0.73
Ramachandran favored (%)	94.26	94.80
Ramachandran allowed (%)	5.52	4.70
Ramachandran outliers (%)	0.22	0.50
Rotamer outliers (%)	0.13	0.55
Clashscore	4.88	6.60
Average B-factor (Å²)	67.00	68.41
macromolecules (Å²)	67.01	68.40
solvent (Å²)	49.59	94.37

Statistics for the highest-resolution shell are shown in parentheses.

Figures legends

Figure 1. Crystal structure of CrSBPase.

A. Topology is displayed as cartoon with main chain colored from blue (amino-terminus) to red (carboxy-terminus). B. Rotated view of A. by x-axis over -90°. C. Putative active site residues inferred from alignment with FBPase bound to FBP (5l0a, human muscle fructose-1,6-bisphosphatase E69Q mutant in active R-state in complex with fructose-1,6-bisphosphate) are represented in sticks. D. Surface representation in the B. orientation with putative active site residues colored in cyan. Water molecule H_2O 401 oxygen is represented as a red sphere. E. Cysteines site chains are represented in spheres. F. Threonines and serines side chains reported to be the target of phosphorylations are represented in spheres.

Figure 2. Functional characterization of CrSBPase *in vitro*.

A. Schematic reporter assay set to detect FBPase activity of recombinant *CrS*BPase in vitro. F1,6bP fructose-1,6-bisphosphate, F6P fructose-6-phosphate, Pi inorganic phosphate, G6P glucose-6-phosphate, G6PDH glucose-6-phosphate dehydrogenase, 6PG 6-phosphogluconolactone, $NADP^+$/NADPH nicotinamide adenine dinucleotide phosphate in oxidized/reduced form. B. Linear response of the assay in the enzyme concentration range. C.D.E. Effect of reduction by dithiothreitol (DTT), Magnesium ($MgSO_4$), and recombinant thioredoxin (*Cr*TRXf2).

Figure 3. Crystallographic structures of *Cr*SBPase under reducing treatment.

A-I. Aligned structures of *Cr*SBPase protomers without redox treatment (A, 7b2o chain A) or in the presence of 10 $mmol.L^{-1}$ TCEP reducing agent (B-I, 7zuv chains A-H).

Figure 4. Molecular dynamics simulation of *Cr*SBPase after reduction.

A. Overlap of the crystallographic structure of oxidized SBPase and representative structures of equilibrated reduced SBPase during molecular dynamics simulation 2 (MD2). For structures extracted

from MD, only residues 109 to 148 are displayed since most of the other residues are closely overlapping those of the crystallographic structure. B. Overlap of the crystallographic structure of reduced SBPase and representative structures of equilibrated reduced SBPase during MD2. For structures extracted from MD, only residues 109 to 148 are displayed.

Figure 5. Oligomeric structure of CrSBPase.

A. Asymmetric unit dimer of untreated *Cr*SBPase (7b2o). Chains are represented in cartoon and colored cyan (chain B) and salmon (chain E). B. Asymmetric unit homotetramer under reducing treatment (7zuv). Chains A (cyan), C (magenta), F (white), and H (orange) belong to the same asymmetric unit. C. Close-up view on figure A homodimer interface. Loop 113-ASCAGTAC-120 from chain B (in cyan) is in 5-Å distance of neighbouring chain E (in salmon). C115 and C120 are bonded by a disulfide bridge. D. Surface representation of 7b2o homodimer, colored according to conservation score from teal (lowest conservation) to purple (highest conservation) among 150 aligned homologs.

Supplementary information

Supplementary table 1. Primers used for point mutagenesis.

5'-forward C115S	CCGCACCGCCTCGAGCGCCGGTACCGCCTGCGTG
3'-reverse C115S	CACGCAGGCGGTACCGGCGCTCGAGGCGGTGCGG
5'-forward C120S	GCGCCGGTACCGCCAGCGTGAACAGCTTCGGCG
3'-reverse C120S	CGCCGAAGCTGTTCACGCTGGCGGTACCGGCGC
5'-forward C149S	GAAGTACTCGCACGTGAGCAAGCTGGCCTGCTCCG
3'-reverse C149S	CGGAGCAGGCCAGCTTGCTCACGTGCGAGTACTTC
5'-forward C153S	GTGCAAGCTGGCCAGCTCCGAGGAGGTGCCCG
3'-reverse C153S	CGGGCACCTCCTCGGAGCTGGCCAGCTTGCAC

Supplementary figure 1. Purification of recombinant *Cr*SBPase. A. Size-exclusion chromatography profile recorded at absorbance λ= 280 nm on Superdex 200 26/600 GL column. B. Electrophoresis of affinity-chromatography fractions on 12% acrylamide gel in denaturing and reducing condition. Gel was stained with Coomassie blue. Mw: molecular mass standards ladder. C. Size-exclusion chromatograms of *Cr*SBPase wild-type (green), mutant C115S (blue), mutant C120S (orange), and C153S (purple). Mutant C149S failed to express in detectable amounts.

Supplementary figure 2. SBPase multiple sequences alignment.

*Cr*SBPase mature sequence was used for a BLAST search. Retrieved homolog sequences were aligned and colored-coded according to residue conservation. Illustration made with EndScript (Robert and Gouet 2014).

Supplementary figure 3. Related to figure 3. Local disorder of the 113-ASCAGTAC-120 loop.

Main chain was traced according to crystallographic b-factor, with large orange sections representing high b-factor values and thin blue sections representing low b-factors. A-I. Aligned structures of *Cr*SBPase protomers without redox treatment (A, 7b2o chain A) or in the presence of 10 mmol.L^{-1} TCEP reducing agent (B-I, 7zuv chains A-H).

Supplementary figure 4. Size-exclusion fractionation of *Chlamydomonas* cell extracts.

A. *Chlamydomonas* cell culture was harvested, lyzed and the soluble fraction of the lysate was loaded on Superose6 16/600 size-exclusion column. Chromatography fractions were analyzed by western blot with anti-*Cr*SBPase primary antibodies. First membrane was loaded with fractions eluted from 40 to 80 mL. Second membrane was loaded with fractions eluted from 80 to 120 mL. M lane is loaded with molecular mass standards ladder. Recombinant *Cr*SBPase was loaded on last lane.

Supplementary figure 5. Size-exclusion chromatography coupled to small angle X-rays scattering (SEC-SAXS) of *Cr*SBPase.

A. X-ray scattering curve log(I) = f(s) for pure *Cr*SBPase untreated (dark blue) or treated (light blue) by 10 mmol.L^{-1} dithiothréitol (DTT). B. Radius of gyration of untreated protein was computed by ATSAS Primus Guinier Wizard as Rg= 39.14 ±0.06 Å (Franke, Petoukhov et al. 2017). C. Radius of gyration of DTT-treated protein was computed as Rg= 62.47 ±0.38 Å.

Supplementary figure 6. Phase separation of reduced *Cr*SBPase precipitates.

*Cr*SBPase at 2 mg/mL formed amorphous precipitates after storage at 4°C for a week. The suspension was sedimented by centrifugation at 20 000 rcf for 20 minutes and a microliter drop of the supernatant or of the pellet were treated with 10 mmol.L^{-1} reducing agent TCEP and visualized by binocular optical microscope. A. Untreated precipitate. B. TCEP-treated precipitate. C. Untreated supernatant. D. TCEP-treated supernatant.

Supplementary figure 7.

SG(Cys115)/SG(Cys120) distances along the MD trajectories for each chain (left: oxidized state, right: reduced state). Light colors: raw data saved every 100ps, dark colors: moving average on 20ns blocs.

Supplementary figure 8.

RMSD of main chain along the MD trajectories for each chain (left: oxidized state, right: reduced state). Light colors: raw data saved every 100ps, dark colors: moving average on 20ns blocs.

Supplementary figure 9.

RMSD of main chain of the mobile motif in the reduced state (residues 112 to 131) along the MD trajectories for each chain (left: RMSD with respect to the starting conformation of MD, right: RMSD

with respect to the conformation at 20µs). Light colors: raw data saved every 100ps, dark colors: moving average on 20ns blocs.

Supplementary figure 10.

RMSF per residue for each chain (top row: full sequence, bottom row: zoom on residues 110 to 170; left column: oxidized state, middle column: reduced state, right column: comparison of one chain from each state).

Supplementary figure 11.

RMSD of main chain of each residue from the mobile motif along the trajectory of chain B from MD2. Data are moving average on 200ns blocs.

Supplementary figure 12. Structure of SBPase in MD1 and MD2.

A. Overlap of the crystallographic structure of oxidized SBPase and representative structures of equilibrated reduced SBPase during MD1 (based on clustering the last 3µs). For structures extracted from MD, only residues 111 to 132 are displayed since the other residues are closely overlapping those of the crystallographic structure. B. Overlap of the crystallographic structure of oxidized SBPase and representative structures of equilibrated reduced SBPase during MD2. For structures extracted from MD, only residues 109 to 148 are displayed since most of the other residues are closely overlapping those of the crystallographic structure.

Structural data

Crystal structures of recombinant *Cr*SBPase untreated or treated with reducing agent were deposited in the protein data bank under respective accession codes 7b2o and 7zuv.

Authors contributions

JH, NC: Conceptualization; JH, NC, MS, TLM: Data curation; JH, NC, MZ: Formal analysis; JH: Funding acquisition; JH, NC, MZ, SDL, MS, TLM: Investigation; JH, NC, MZ, MS, TLM: Methodology; JH, SDL: Project administration; JH, NC, SDL: Resources; NC: Software; JH, MZ: Supervision; JH, NC, MZ, SDL, MS, TLM: Writing - original draft; JH, NC, MZ, SDL, MS, TLM: Writing - review & editing.

Acknowlegdements

We acknowledge the Institut de Biologie Physico-Chimique (CNRS, FR 505) for access to the crystallization facility. We acknowledge SOLEIL for provision of synchrotron radiation facilities at beamlines SWING, PROXIMA-1, and PROXIMA-2A. We thank Guillaume Q. Robert for his contribution to protein purification, crystallization under reducing treatment, and model building. Plasmids pSL-175, -181, -182, 183, and -184 were cloned by Dr. Laure Michelet. This work was funded by the grant CALVINTERACT from the Agence Nationale de la Recherche (ANR-19-CE11-0009). Martina Santoni received funding from the Bologna University and Sorbonne University exchange program ERASMUS+. The authors express their gratitude to the financial support of the AAP AIN INSB CNRS.

Conflicts of interest statement

The authors report no conflict of interest relevant to the conduct or report of this research.

Figures

Figure 1.

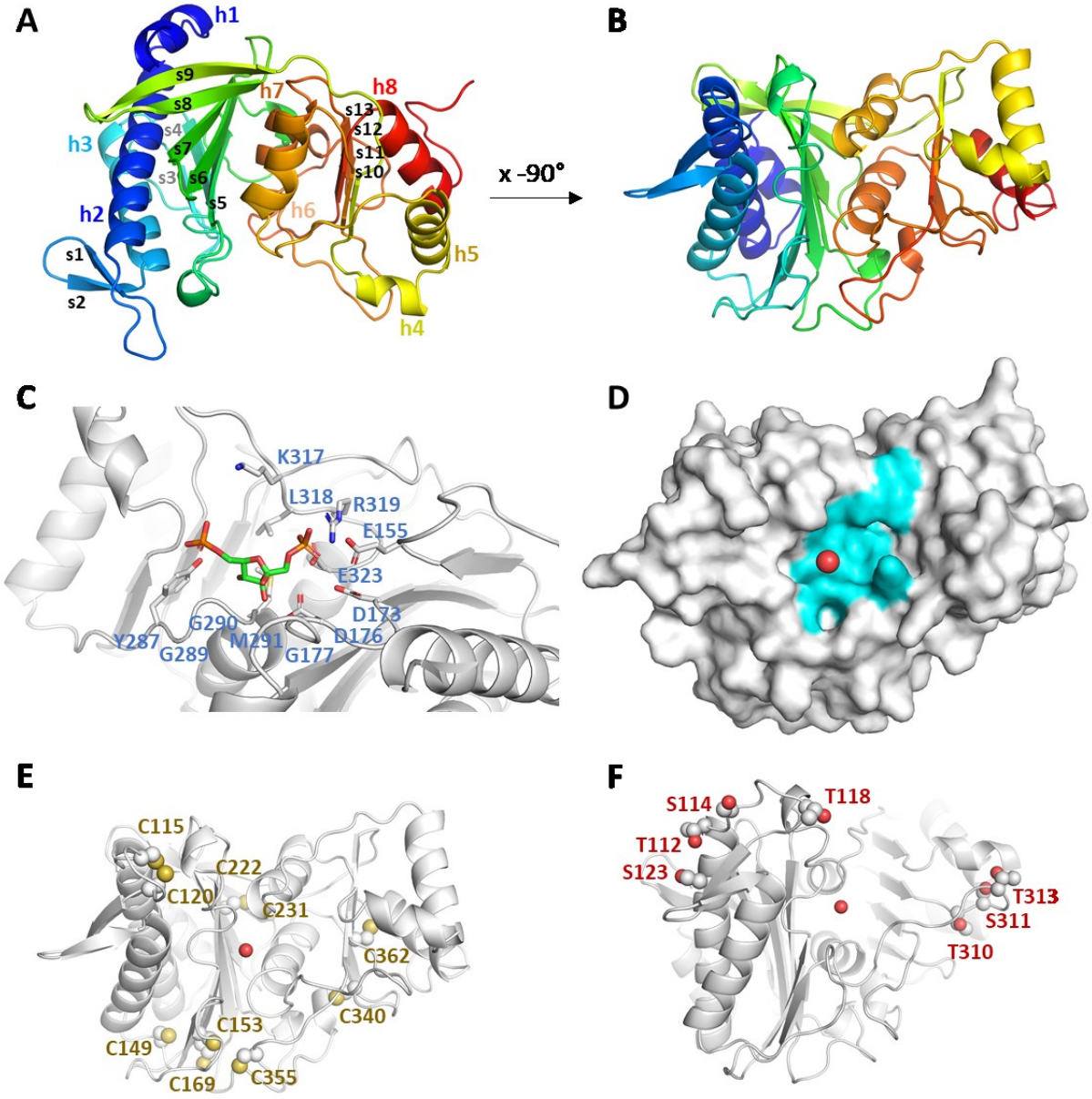

542

543

Figure 2.

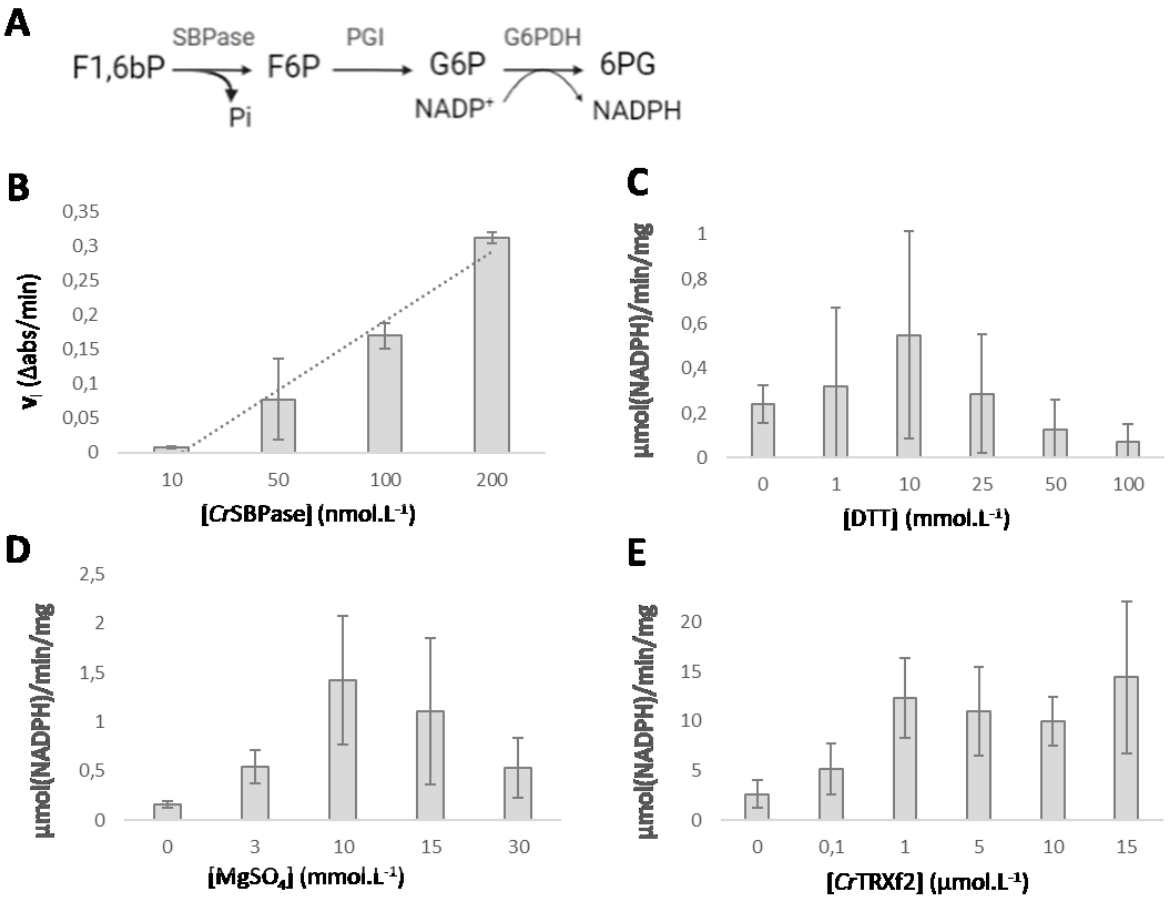
A
SBPase
PGI
G6PDH
F1,6bP
F6P
G6P
6PG
Pi
NADP+
NADPH
B
v0 (Δabs/min)
0,35
0,3
0,25
0,2
0,15
0,1
0,05
0
10
50
100
200
[CrSBPase] (nmol.L-1)
C
µmol(NADPH)/min/mg
1
0,8
0,6
0,4
0,2
0
0
1
10
25
50
100
[DTT] (mmol.L-1)
D
µmol(NADPH)/min/mg
2,5
2
1,5
1
0,5
0
0
3
10
15
30
[MgSO4] (mmol.L-1)
E
µmol(NADPH)/min/mg
20
15
10
5
0
0
0,1
1
5
10
15
[CrTRXf2] (µmol.L-1)

544

Figure 3.

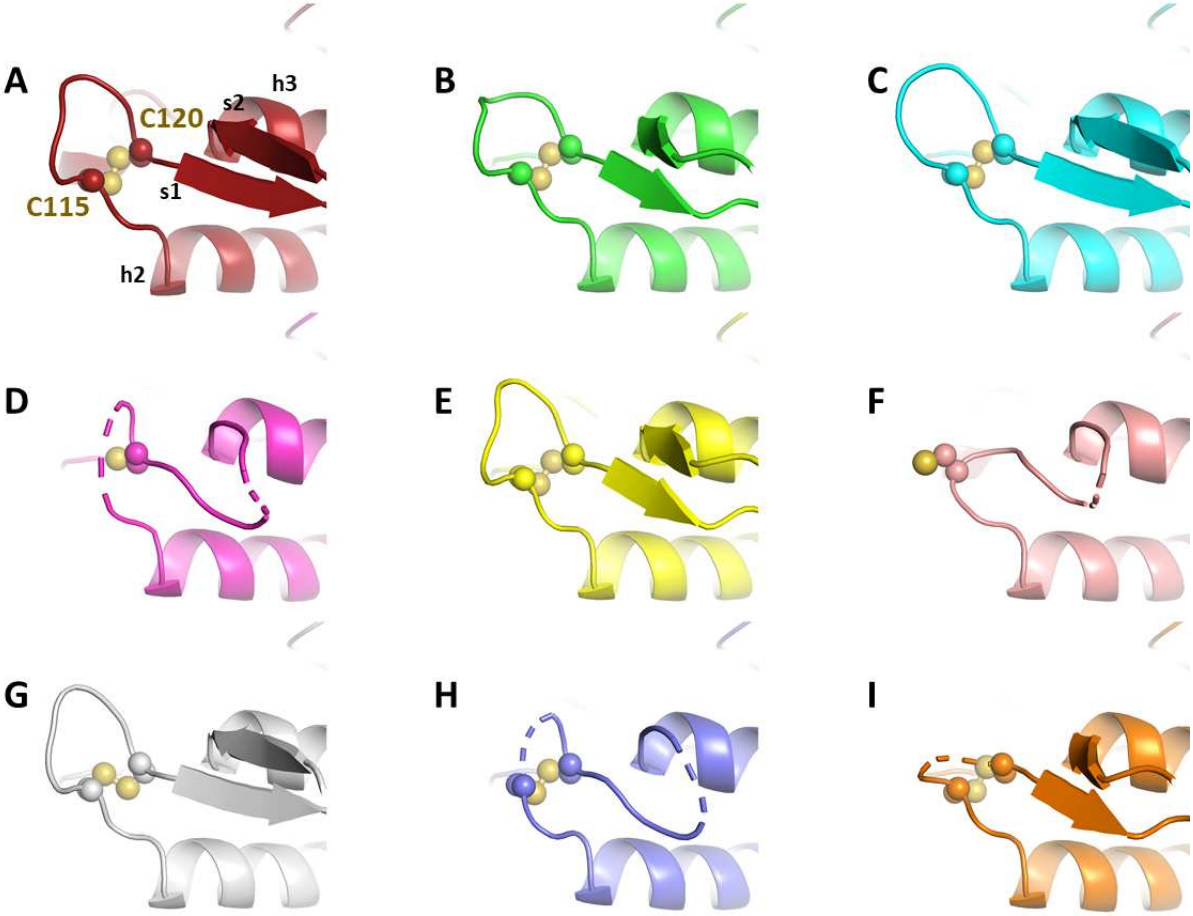

545

546

Figure 4.

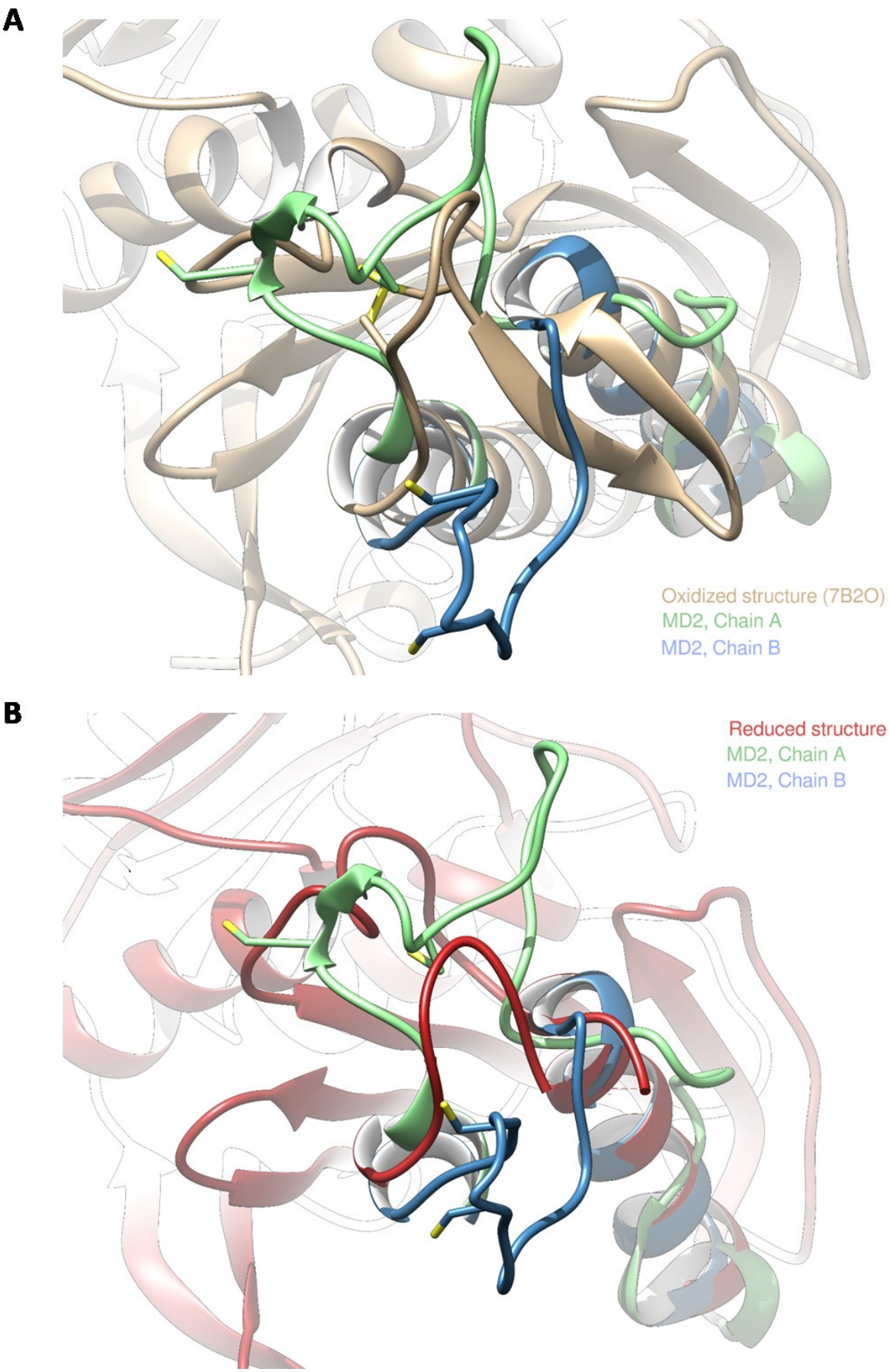
A
Oxidized structure (7B2O)
MD2, Chain A
MD2, Chain B
B
Reduced structure
MD2, Chain A
MD2, Chain B

547

Figure 5.

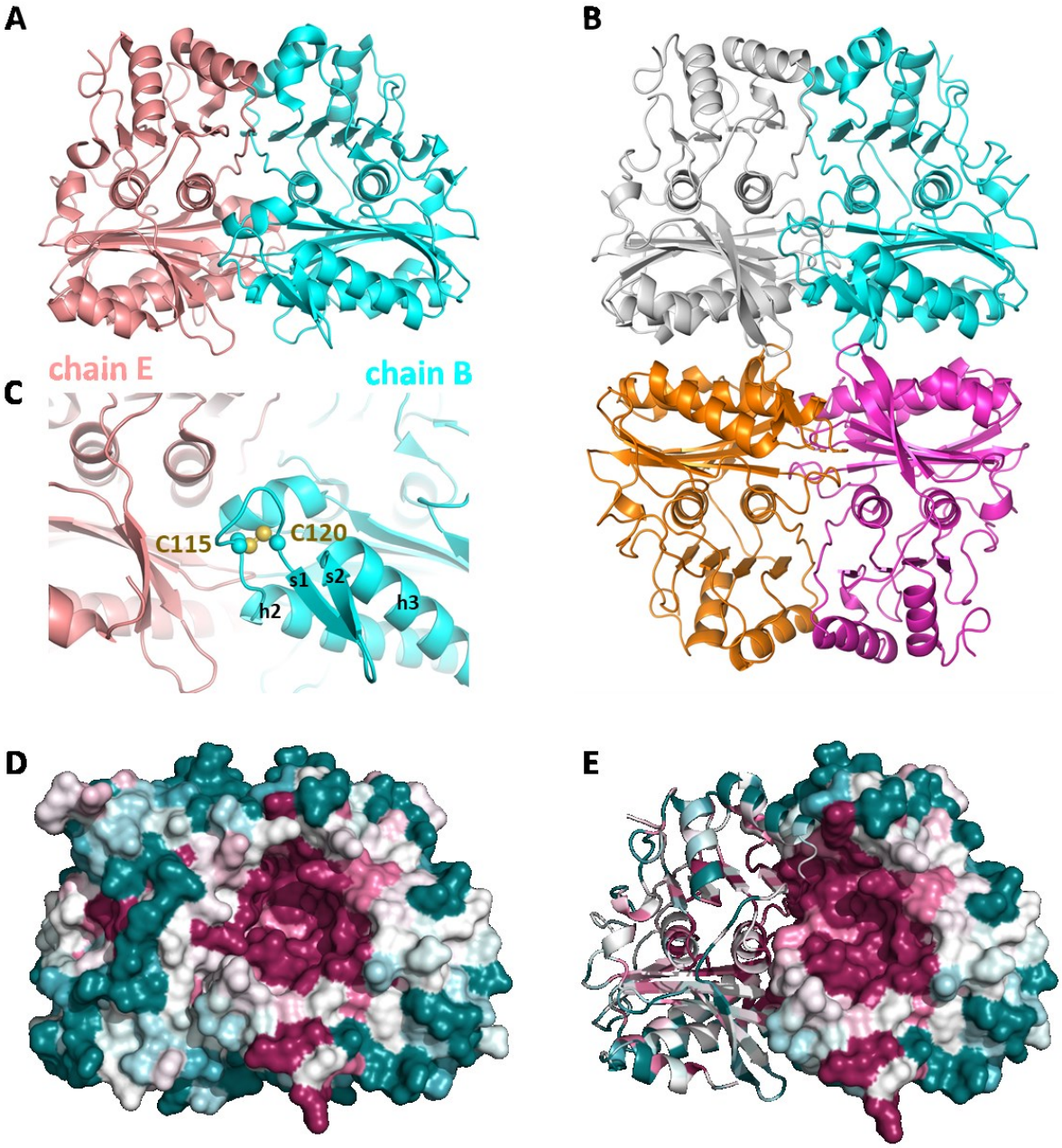

548

Supplementary figures

Supplementary figure 1.

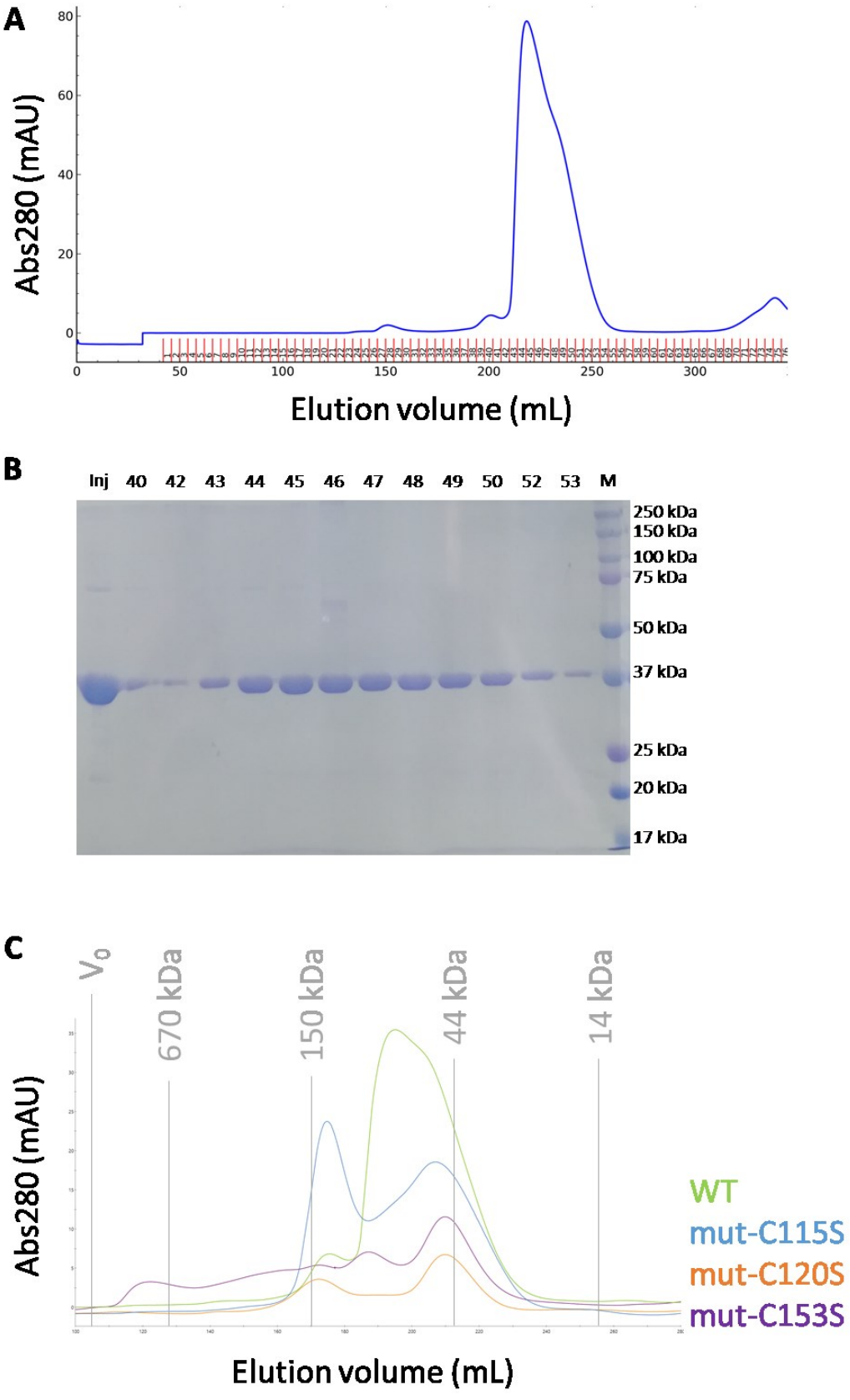

Supplementary figure 2.

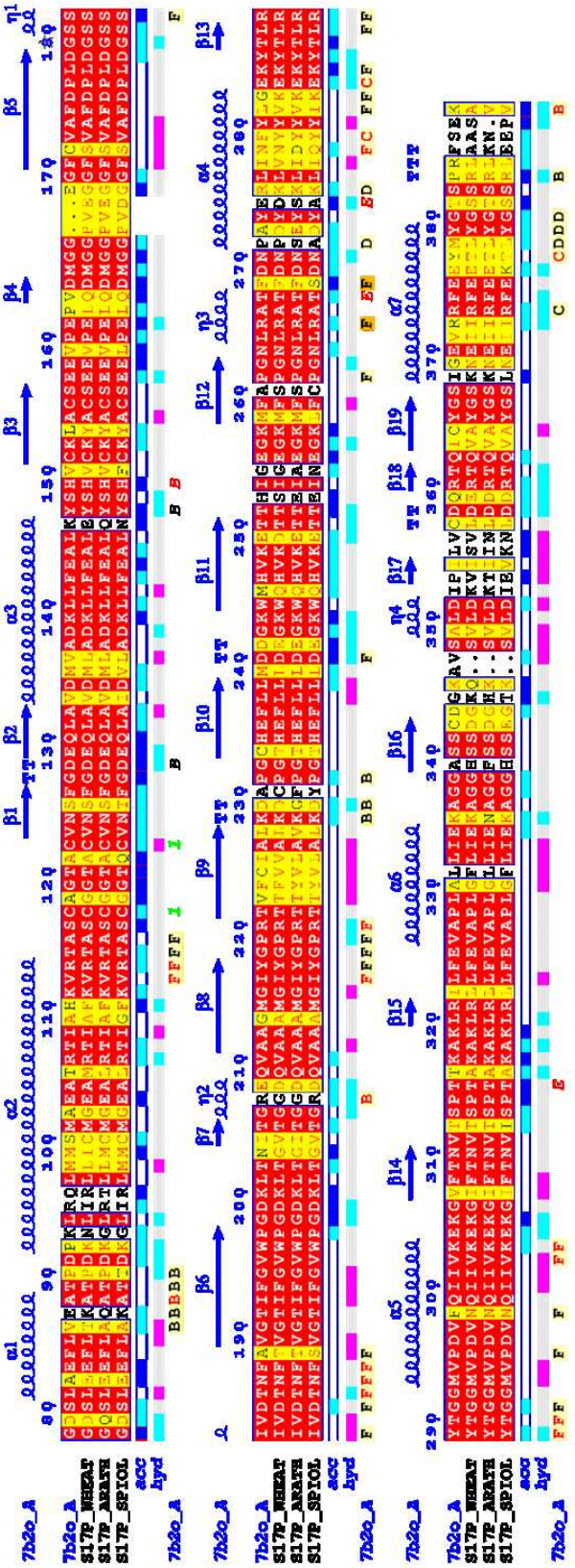

550

Supplementary figure 3.

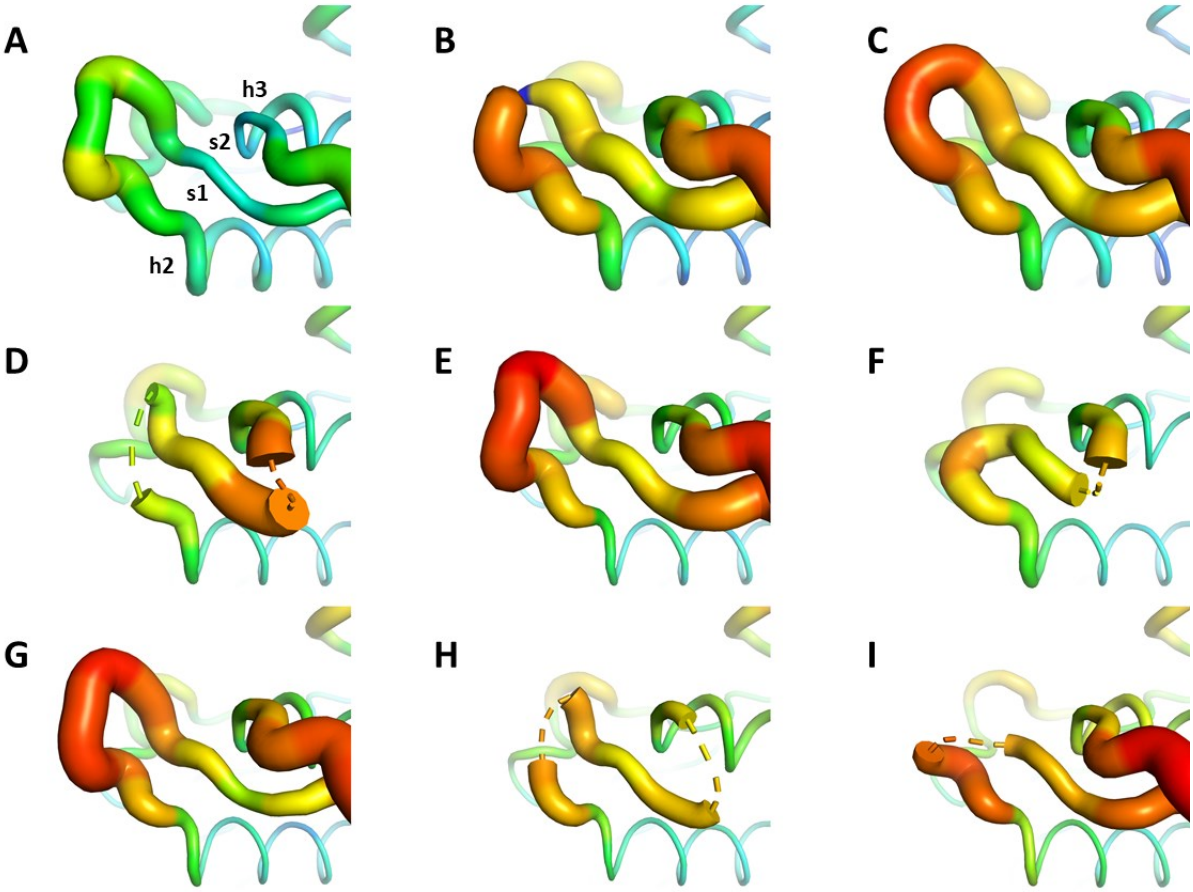

551

Supplementary figure 4.

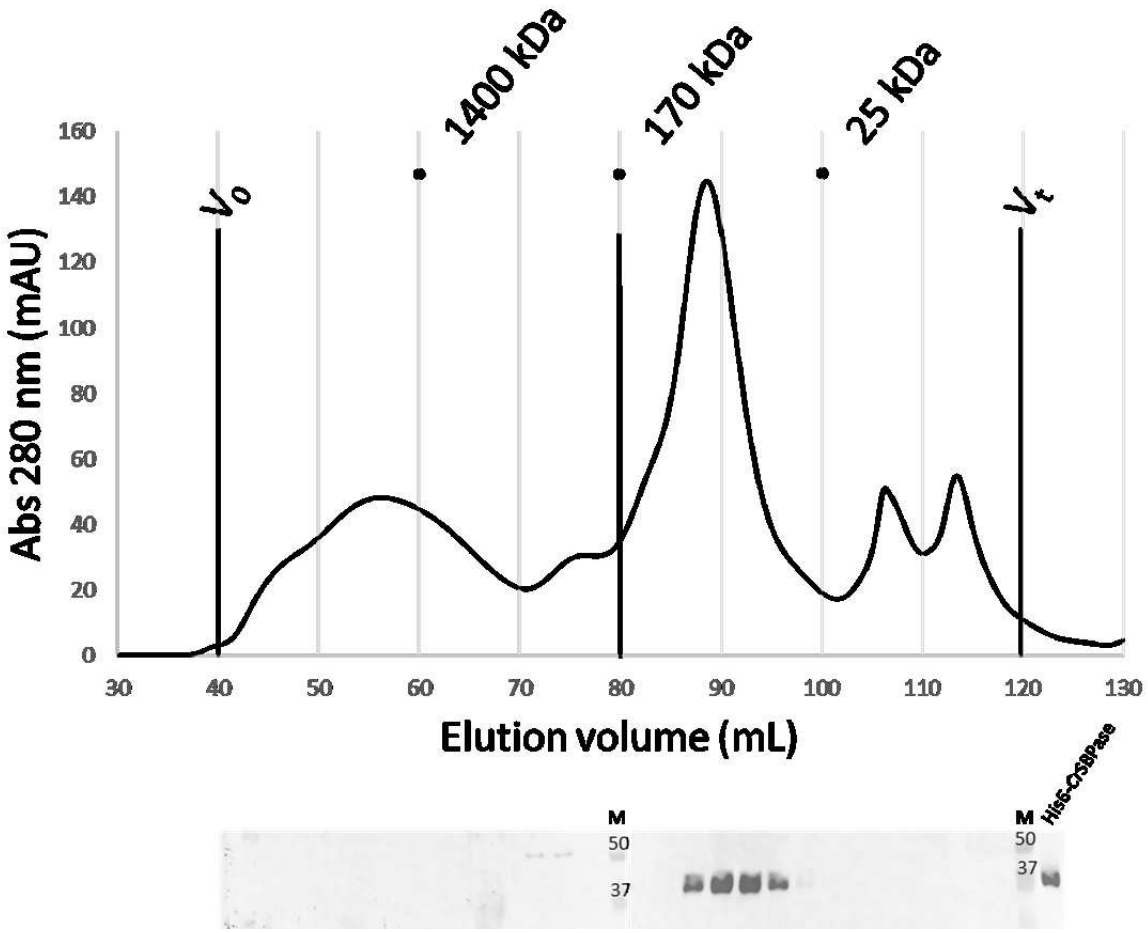

552

553

Supplementary figure 5.

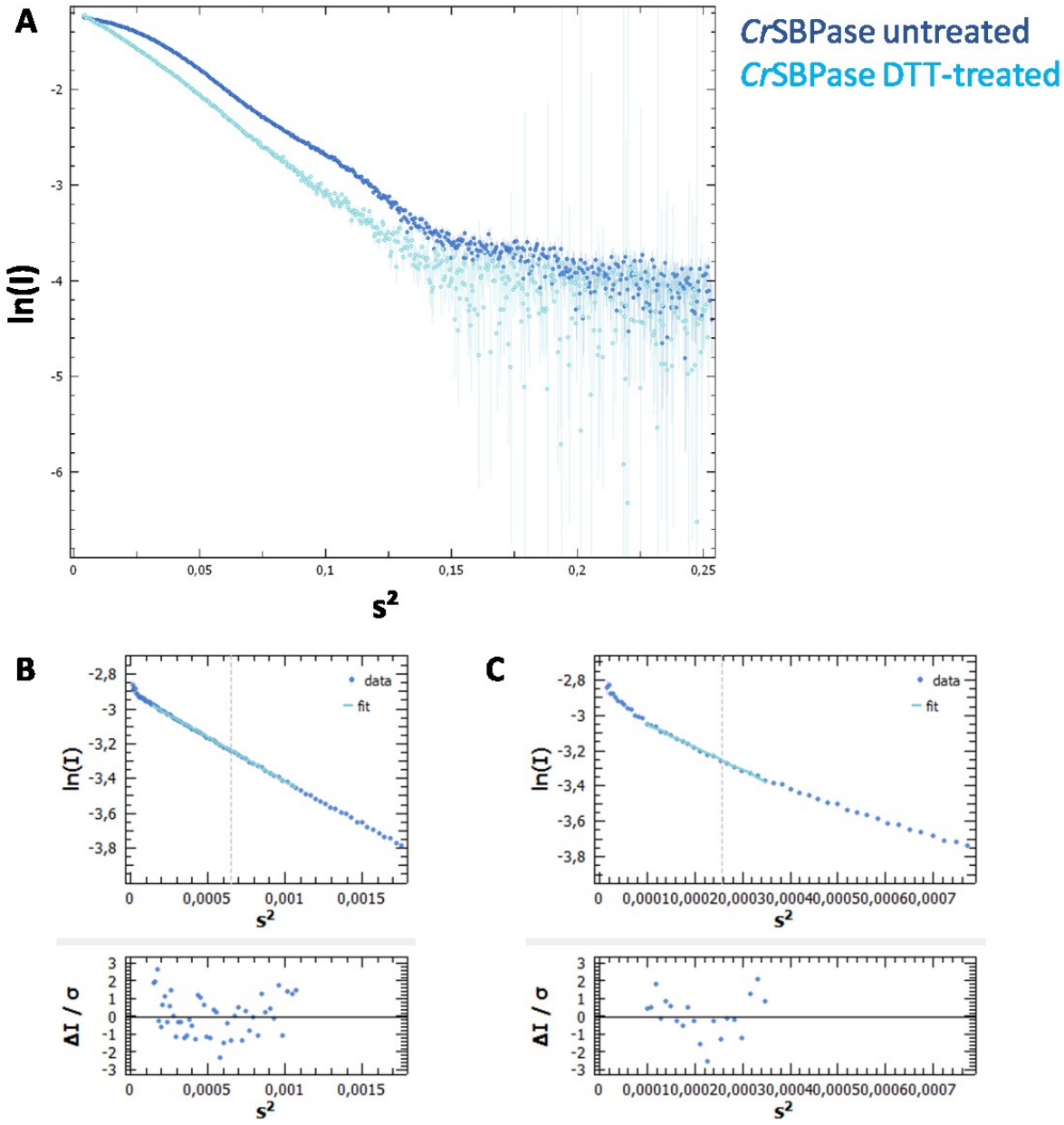

554

555

Supplementary figure 6.

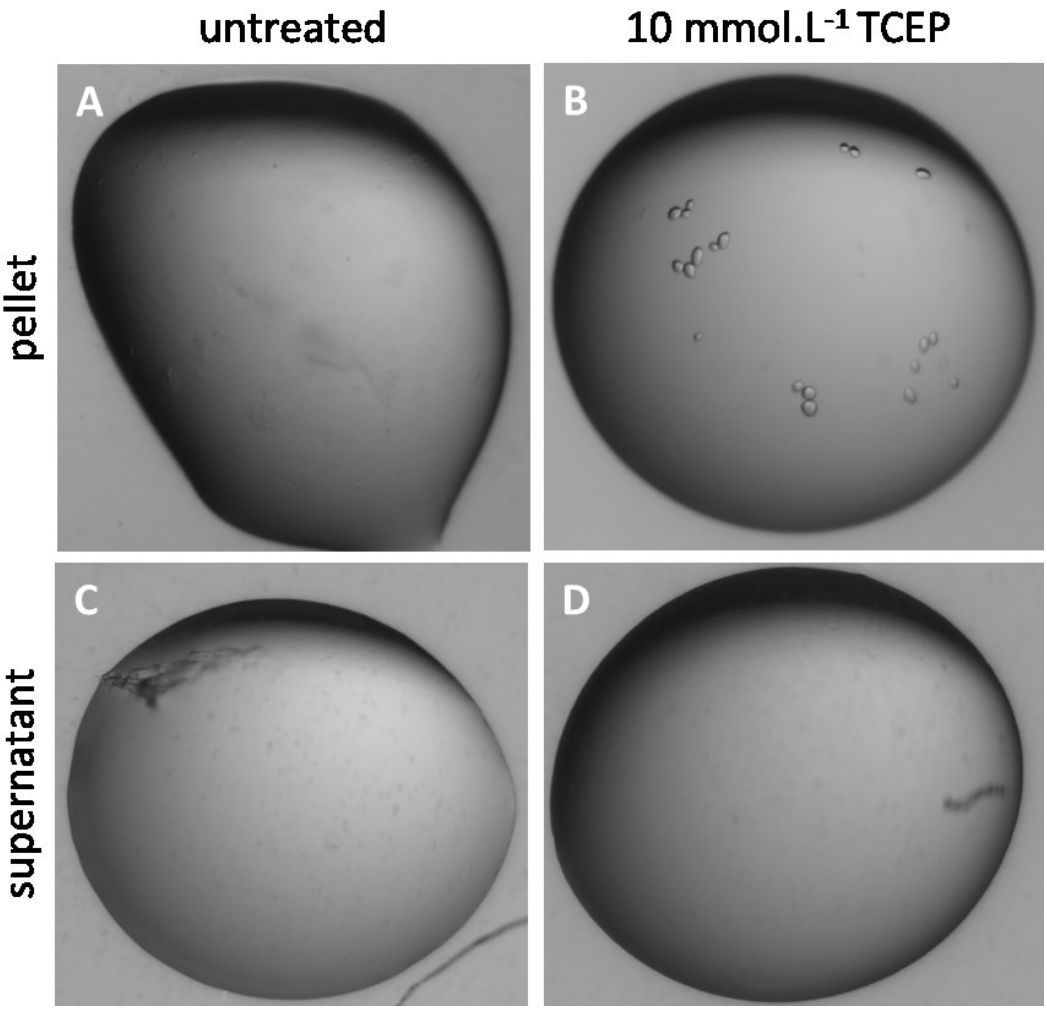

556

557

Supplementary figure 7.

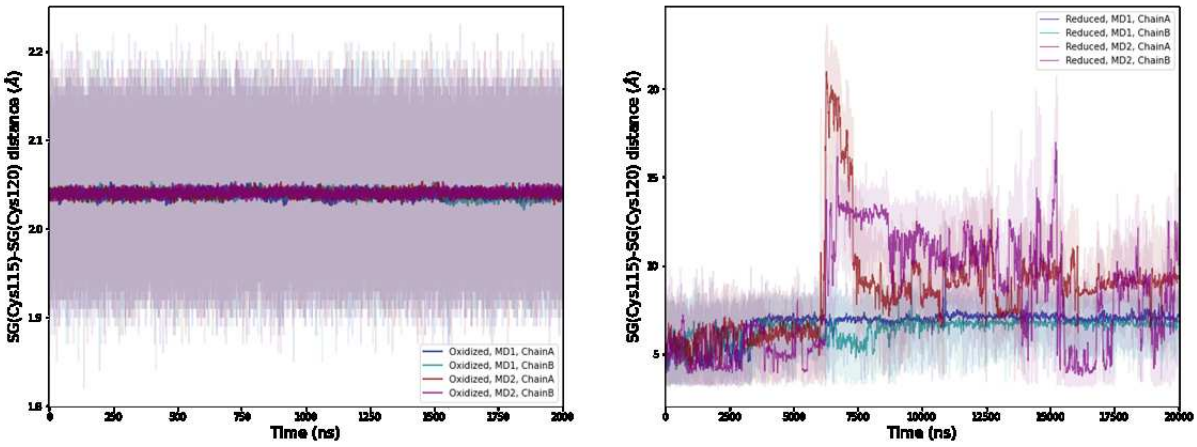

Supplementary figure 8.

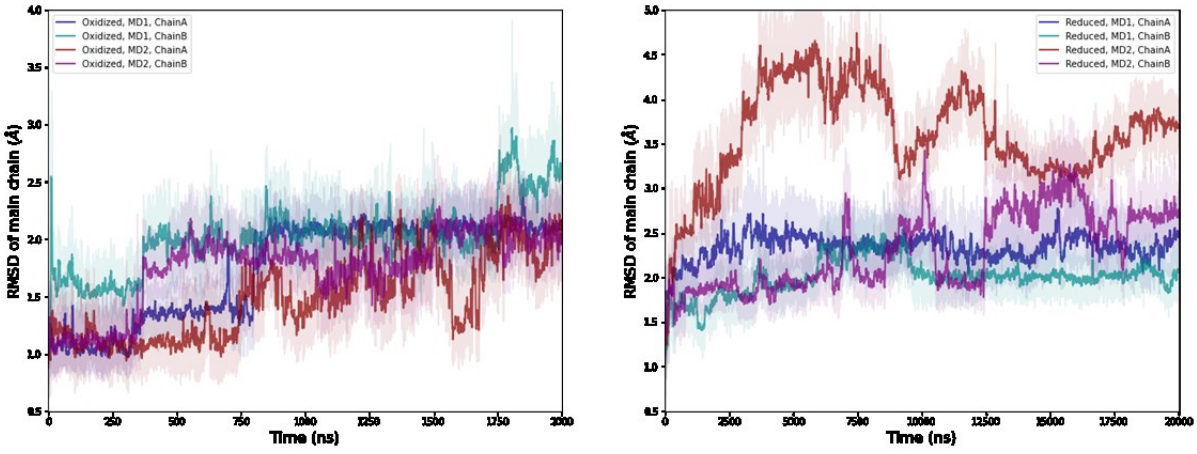

Supplementary figure 9.

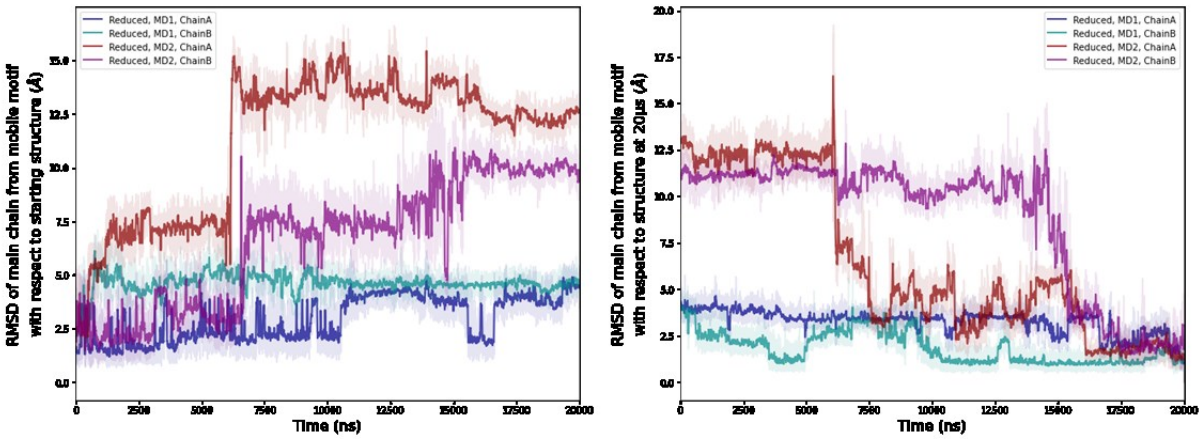

562

563

Supplementary figure 10.

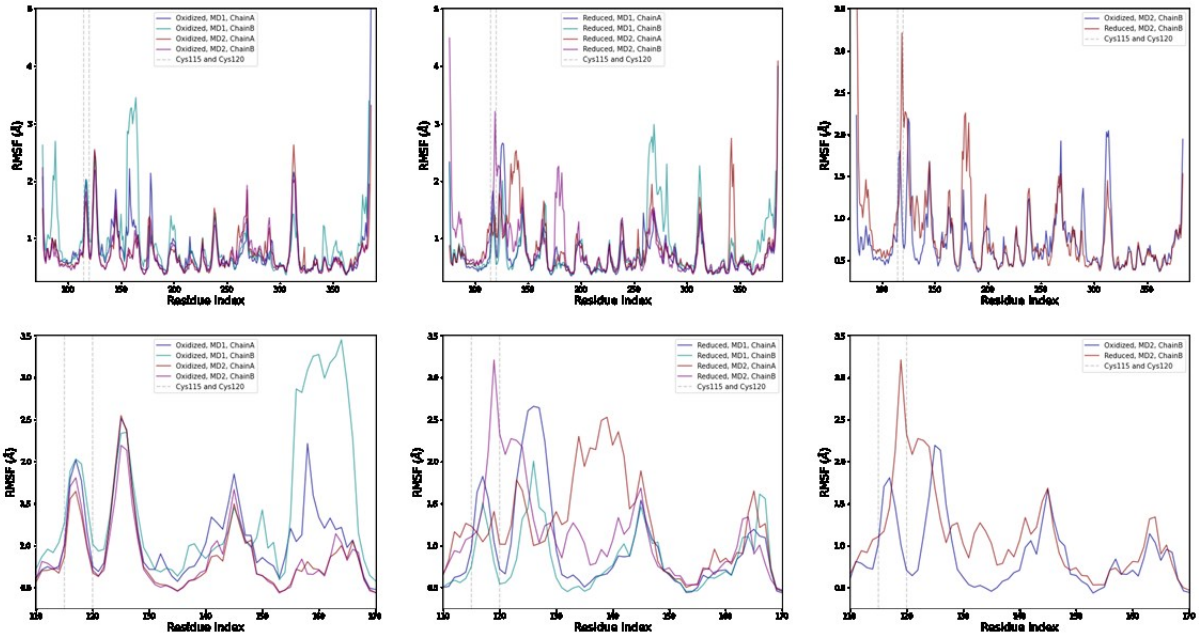

Supplementary figure 11.

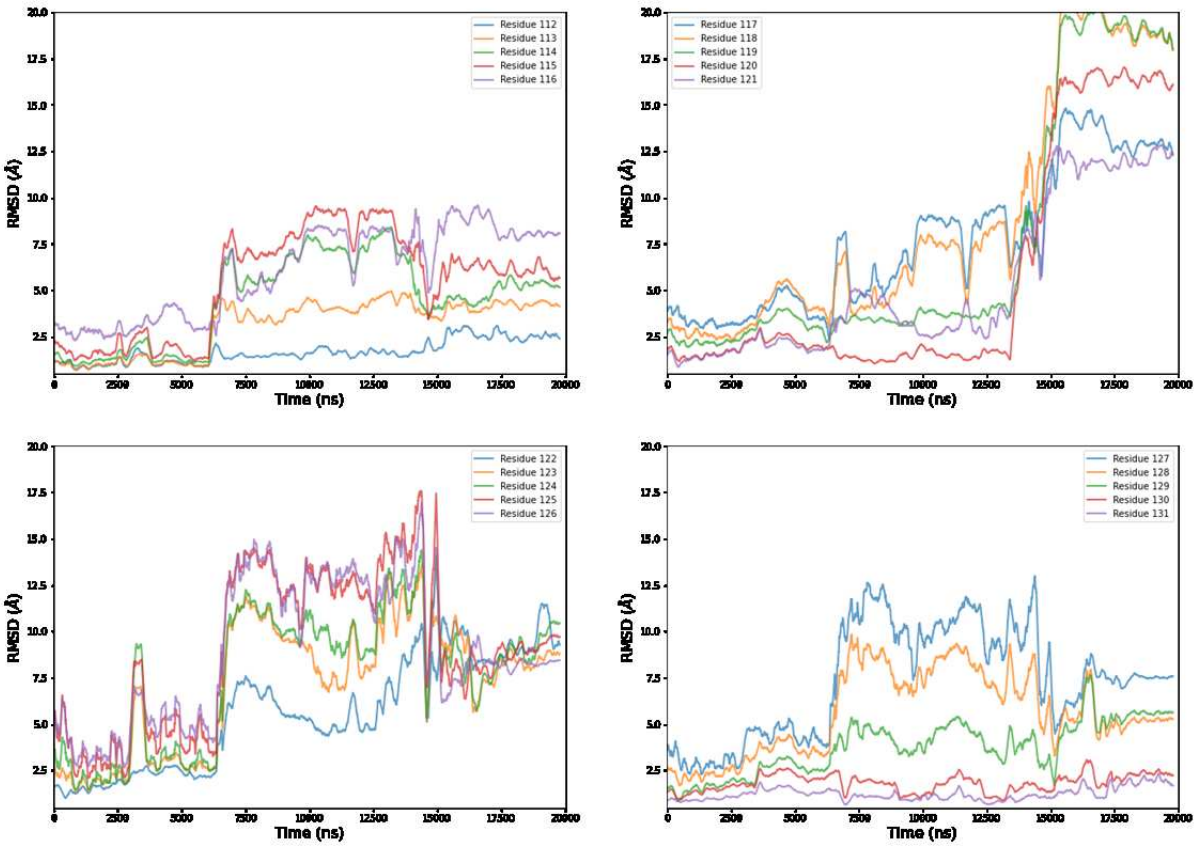

Supplementary figure 12.

A

B

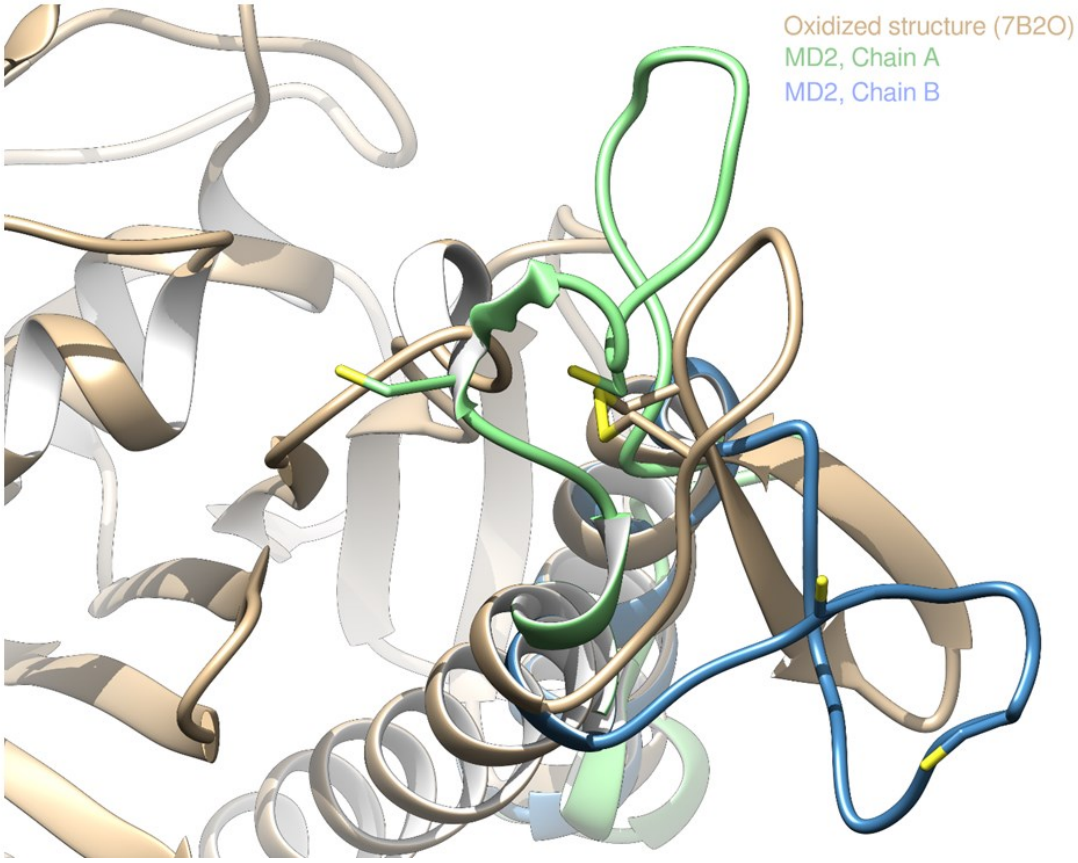

568

Bibliography

Abraham, M. J., T. Murtola, R. Schulz, S. Páll, J. C. Smith, B. Hess and E. Lindahl (2015). "GROMACS: High performance molecular simulations through multi-level parallelism from laptops to supercomputers." SoftwareX **1-2**: 19-25.

Adams, P. D., P. V. Afonine, G. Bunkóczi, V. B. Chen, N. Echols, J. J. Headd, L. W. Hung, S. Jain, G. J. Kapral, R. W. Grosse Kunstleve, A. J. McCoy, N. W. Moriarty, R. D. Oeffner, R. J. Read, D. C. Richardson, J. S. Richardson, T. C. Terwilliger and P. H. Zwart (2011). "The Phenix software for automated determination of macromolecular structures." Methods **55**(1): 94-106.

Ahmad, S., M. Gromiha, H. Fawareh and A. Sarai (2004). "ASAView: database and tool for solvent accessibility representation in proteins." BMC Bioinformatics **5**: 51.

Almagro Armenteros, J. J., M. Salvatore, O. Emanuelsson, O. Winther, G. von Heijne, A. Elofsson and H. Nielsen (2019). "Detecting sequence signals in targeting peptides using deep learning." Life Sci Alliance **2**(5).

Anderson, L. E. (1974). "Activation of pea leaf chloroplast sedoheptulose 1,7-diphosphate phosphatase by light and dithiothreitol." Biochem Biophys Res Commun **59**(3): 907-913.

Barciszewski, J., J. Wisniewski, R. Kolodziejczyk, M. Jaskolski, D. Rakus and A. Dzugaj (2016). "T-to-R switch of muscle fructose-1,6-bisphosphatase involves fundamental changes of secondary and quaternary structure." Acta Crystallogr D Struct Biol **72**(Pt 4): 536-550.

Cadet, F. and J. C. Meunier (1988). "pH and kinetic studies of chloroplast sedoheptulose-1,7-bisphosphatase from spinach (Spinacia oleracea)." Biochem J **253**(1): 249-254.

Calvin, M. (1962). "The path of carbon in photosynthesis." Science **135**(3507): 879-889.

Chiadmi, M., A. Navaza, M. Miginiac-Maslow, J. P. Jacquot and J. Cherfils (1999). "Redox signalling in the chloroplast: structure of oxidized pea fructose-1,6-bisphosphate phosphatase." EMBO J **18**(23): 6809-6815.

Emanuelsson, O., S. Brunak, G. von Heijne and H. Nielsen (2007). "Locating proteins in the cell using TargetP, SignalP and related tools." Nat Protoc **2**(4): 953-971.

Emsley, P., B. Lohkamp, W. G. Scott and K. Cowtan (2010). "Features and development of Coot." Acta Crystallogr D Biol Crystallogr **66**(Pt 4): 486-501.

Feng, L., Y. Han, G. Liu, B. An, J. Yang, G. Yang, Y. Li and Y. Zhu (2007). "Overexpression of sedoheptulose-1,7-bisphosphatase enhances photosynthesis and growth under salt stress in transgenic rice plants." Funct Plant Biol **34**(9): 822-834.

Feng, L., K. Wang, Y. Li, Y. Tan, J. Kong, H. Li, Y. Li and Y. Zhu (2007). "Overexpression of SBPase enhances photosynthesis against high temperature stress in transgenic rice plants." Plant Cell Rep **26**(9): 1635-1646.

Franke, D., M. V. Petoukhov, P. V. Konarev, A. Panjkovich, A. Tuukkanen, H. D. T. Mertens, A. G. Kikhney, N. R. Hajizadeh, J. M. Franklin, C. M. Jeffries and D. I. Svergun (2017). "ATSAS 2.8: a comprehensive data analysis suite for small-angle scattering from macromolecular solutions." J Appl Crystallogr **50**(Pt 4): 1212-1225.

Giudici-Orticoni, M. T., J. Buc, M. Bidaud and J. Ricard (1990). "Thermodynamics of information transfer between subunits in oligomeric enzymes and kinetic cooperativity. 3. Information transfer between the subunits of chloroplast fructose bisphosphatase." Eur J Biochem **194**(2): 483-490.

Gurrieri, L., A. Del Giudice, N. Demitri, G. Falini, N. V. Pavel, M. Zaffagnini, M. Polentarutti, P. Crozet, C. H. Marchand, J. Henri, P. Trost, S. D. Lemaire, F. Sparla and S. Fermani (2019). "Arabidopsis and Chlamydomonas phosphoribulokinase crystal structures complete the redox structural proteome of the Calvin-Benson cycle." Proc Natl Acad Sci U S A **116**(16): 8048-8053.

Gütle, D. D., T. Roret, S. J. Müller, J. Couturier, S. D. Lemaire, A. Hecker, T. Dhalleine, B. B. Buchanan, R. Reski, O. Einsle and J. P. Jacquot (2016). "Chloroplast FBPase and SBPase are thioredoxin-linked enzymes with similar architecture but different evolutionary histories." Proc Natl Acad Sci U S A **113**(24): 6779-6784.

Hammel, A., F. Sommer, D. Zimmer, M. Stitt, T. Mühlhaus and M. Schroda (2020). "Overexpression of Sedoheptulose-1,7-Bisphosphatase Enhances Photosynthesis in Chlamydomonas reinhardtii and Has No Effect on the Abundance of Other Calvin-Benson Cycle Enzymes." Front Plant Sci **11**: 868.
Jacquot, J. P., J. Lopez-Jaramillo, M. Miginiac-Maslow, S. Lemaire, J. Cherfils, A. Chueca and J. Lopez-Gorge (1997). "Cysteine-153 is required for redox regulation of pea chloroplast fructose-1,6-bisphosphatase." FEBS Lett **401**(2-3): 143-147.
Johnson, M. P. (2016). "Photosynthesis." Essays Biochem **60**(3): 255-273.
Johnson, X. and J. Alric (2013). "Central carbon metabolism and electron transport in Chlamydomonas reinhardtii: metabolic constraints for carbon partitioning between oil and starch." Eukaryot Cell **12**(6): 776-793.
Jorgensen, W. L. (1981). "Quantum and statistical mechanical studies of liquids. 10. Transferable intermolecular potential functions for water, alcohols, and ethers. Application to liquid water." Journal of the American Chemical Society **103**(2): 335-340.
Jumper, J., R. Evans, A. Pritzel, T. Green, M. Figurnov, O. Ronneberger, K. Tunyasuvunakool, R. Bates, A. Zidek, A. Potapenko, A. Bridgland, C. Meyer, S. A. A. Kohl, A. J. Ballard, A. Cowie, B. Romera-Paredes, S. Nikolov, R. Jain, J. Adler, T. Back, S. Petersen, D. Reiman, E. Clancy, M. Zielinski, M. Steinegger, M. Pacholska, T. Berghammer, S. Bodenstein, D. Silver, O. Vinyals, A. W. Senior, K. Kavukcuoglu, P. Kohli and D. Hassabis (2021). "Highly accurate protein structure prediction with AlphaFold." Nature **596**(7873): 583-589.
Krissinel, E. and K. Henrick (2007). "Inference of macromolecular assemblies from crystalline state." J Mol Biol **372**(3): 774-797.
Kubis, A. and A. Bar-Even (2019). "Synthetic biology approaches for improving photosynthesis." J Exp Bot **70**(5): 1425-1433.
Lefebvre, S., T. Lawson, O. V. Zakhleniuk, J. C. Lloyd, C. A. Raines and M. Fryer (2005). "Increased sedoheptulose-1,7-bisphosphatase activity in transgenic tobacco plants stimulates photosynthesis and growth from an early stage in development." Plant Physiol **138**(1): 451-460.
Lemaire, S. D., B. Guillon, P. Le Maréchal, E. Keryer, M. Miginiac-Maslow and P. Decottignies (2004). "New thioredoxin targets in the unicellular photosynthetic eukaryote Chlamydomonas reinhardtii." Proc Natl Acad Sci U S A **101**(19): 7475-7480.
Lemaire, S. D., D. Tedesco, P. Crozet, L. Michelet, S. Fermani, M. Zaffagnini and J. Henri (2018). "Crystal Structure of Chloroplastic Thioredoxin f2 from Chlamydomonas reinhardtii Reveals Distinct Surface Properties." Antioxidants (Basel) **7**(12).
Liebschner, D., P. V. Afonine, M. L. Baker, G. Bunkóczi, V. B. Chen, T. I. Croll, B. Hintze, L. W. Hung, S. Jain, A. J. McCoy, N. W. Moriarty, R. D. Oeffner, B. K. Poon, M. G. Prisant, R. J. Read, J. S. Richardson, D. C. Richardson, M. D. Sammito, O. V. Sobolev, D. H. Stockwell, T. C. Terwilliger, A. G. Urzhumtsev, L. L. Videau, C. J. Williams and P. D. Adams (2019). "Macromolecular structure determination using X-rays, neutrons and electrons: recent developments in Phenix." Acta Crystallogr D Struct Biol **75**(Pt 10): 861-877.
Maier, J. A., C. Martinez, K. Kasavajhala, L. Wickstrom, K. E. Hauser and C. Simmerling (2015). "ff14SB: Improving the Accuracy of Protein Side Chain and Backbone Parameters from ff99SB." Journal of Chemical Theory and Computation **11**(8): 3696-3713.
McConnell, E. W., E. G. Werth and L. M. Hicks (2018). "The phosphorylated redox proteome of Chlamydomonas reinhardtii: Revealing novel means for regulation of protein structure and function." Redox Biol **17**: 35-46.
Mettler, T., T. Mühlhaus, D. Hemme, M. A. Schöttler, J. Rupprecht, A. Idoine, D. Veyel, S. K. Pal, L. Yaneva-Roder, F. V. Winck, F. Sommer, D. Vosloh, B. Seiwert, A. Erban, A. Burgos, S. Arvidsson, S. Schönfelder, A. Arnold, M. Günther, U. Krause, M. Lohse, J. Kopka, Z. Nikoloski, B. Mueller-Roeber, L. Willmitzer, R. Bock, M. Schroda and M. Stitt (2014). "Systems Analysis of the Response of Photosynthesis, Metabolism, and Growth to an Increase in Irradiance in the Photosynthetic Model Organism Chlamydomonas reinhardtii." Plant Cell **26**(6): 2310-2350.
Morisse, S., M. Zaffagnini, X. H. Gao, S. D. Lemaire and C. H. Marchand (2014). "Insight into protein S-nitrosylation in Chlamydomonas reinhardtii." Antioxid Redox Signal **21**(9): 1271-1284.

Nishizawa, A. N. and B. B. Buchanan (1981). "Enzyme regulation in C4 photosynthesis. Purification and properties of thioredoxin-linked fructose bisphosphatase and sedoheptulose bisphosphatase from corn leaves." J Biol Chem **256**(12): 6119-6126.
Ohta, J. (2022). "A novel variant of the Calvin-Benson cycle bypassing fructose bisphosphate." Sci Rep **12**(1): 3984.
Pérez-Pérez, M. E., A. Mauriès, A. Maes, N. J. Tourasse, M. Hamon, S. D. Lemaire and C. H. Marchand (2017). "The Deep Thioredoxome in Chlamydomonas reinhardtii: New Insights into Redox Regulation." Mol Plant **10**(8): 1107-1125.
Pronk, S., S. Páll, R. Schulz, P. Larsson, P. Bjelkmar, R. Apostolov, M. R. Shirts, J. C. Smith, P. M. Kasson, D. van der Spoel, B. Hess and E. Lindahl (2013). "GROMACS 4.5: a high-throughput and highly parallel open source molecular simulation toolkit." Bioinformatics **29**(7): 845-854.
Robert, X. and P. Gouet (2014). "Deciphering key features in protein structures with the new ENDscript server." Nucleic Acids Research **42**(W1): W320-W324.
Rosenthal, D. M., A. M. Locke, M. Khozaei, C. A. Raines, S. P. Long and D. R. Ort (2011). "Over-expressing the C(3) photosynthesis cycle enzyme Sedoheptulose-1-7 Bisphosphatase improves photosynthetic carbon gain and yield under fully open air CO(2) fumigation (FACE)." BMC Plant Biol **11**: 123.
Schmollinger, S., T. Mühlhaus, N. R. Boyle, I. K. Blaby, D. Casero, T. Mettler, J. L. Moseley, J. Kropat, F. Sommer, D. Strenkert, D. Hemme, M. Pellegrini, A. R. Grossman, M. Stitt, M. Schroda and S. S. Merchant (2014). "Nitrogen-Sparing Mechanisms in Chlamydomonas Affect the Transcriptome, the Proteome, and Photosynthetic Metabolism." Plant Cell **26**(4): 1410-1435.
Schürmann, P. and B. B. Buchanan (1975). "Role of ferredoxin in the activation of sedoheptulose diphosphatase in isolated chloroplasts." Biochim Biophys Acta **376**(1): 189-192.
Simkin, A. J., P. E. Lopez-Calcagno, P. A. Davey, L. R. Headland, T. Lawson, S. Timm, H. Bauwe and C. A. Raines (2017). "Simultaneous stimulation of sedoheptulose 1,7-bisphosphatase, fructose 1,6-bisphophate aldolase and the photorespiratory glycine decarboxylase-H protein increases CO(2) assimilation, vegetative biomass and seed yield in Arabidopsis." Plant Biotechnol J **15**(7): 805-816.
Tamoi, M., M. Nagaoka and S. Shigeoka (2005). "Immunological properties of sedoheptulose-1,7-bisphosphatase from Chlamydomonas sp. W80." Biosci Biotechnol Biochem **69**(4): 848-851.
Wagner, V., G. Gessner, I. Heiland, M. Kaminski, S. Hawat, K. Scheffler and M. Mittag (2006). "Analysis of the phosphoproteome of Chlamydomonas reinhardtii provides new insights into various cellular pathways." Eukaryot Cell **5**(3): 457-468.
Wang, L., W. Patena, K. A. Van Baalen, Y. Xie, E. R. Singer, S. Gavrilenko, M. Warren-Williams, L. Han, H. R. Harrigan, V. Chen, V. T. N. P. Ton, S. Kyin, H. H. Shwe, M. H. Cahn, A. T. Wilson, J. Hu, D. J. Schnell, C. D. McWhite and M. Jonikas (2022). "A Chloroplast Protein Atlas Reveals Novel Structures and Spatial Organization of Biosynthetic Pathways." bioRxiv: 2022.2005.2031.493820.
Werth, E. G., E. W. McConnell, T. S. Gilbert, I. Couso Lianez, C. A. Perez, C. K. Manley, L. M. Graves, J. G. Umen and L. M. Hicks (2017). "Probing the global kinome and phosphoproteome in Chlamydomonas reinhardtii via sequential enrichment and quantitative proteomics." Plant J **89**(2): 416-426.
Wilson, R. H., M. Hayer-Hartl and A. Bracher (2019). "Crystal structure of phosphoribulokinase from Synechococcus sp. strain PCC 6301." Acta Crystallogr F Struct Biol Commun **75**(Pt 4): 278-289.
Woodrow, I. E. (1982). "Sedoheptulose-1,7-bisphosphatase from wheat chloroplasts." Methods Enzymol **90 Pt E**: 392-396.
Woodrow, I. E. and D. A. Walker (1980). "Light-mediated activation of stromal sedoheptulose bisphosphatase." Biochem J **191**(3): 845-849.
Yoshida, K. and T. Hisabori (2018). "Determining the Rate-Limiting Step for Light-Responsive Redox Regulation in Chloroplasts." Antioxidants (Basel) **7**(11).
Zaffagnini, M., M. Bedhomme, C. H. Marchand, S. Morisse, P. Trost and S. D. Lemaire (2012). "Redox regulation in photosynthetic organisms: focus on glutathionylation." Antioxid Redox Signal **16**(6): 567-586.
Zimmer, D., C. Swart, A. Graf, S. Arrivault, M. Tillich, S. Proost, Z. Nikoloski, M. Stitt, R. Bock, T. Mühlhaus and A. Boulouis (2021). "Topology of the redox network during induction of photosynthesis as revealed by time-resolved proteomics in tobacco." Sci Adv **7**(51): eabi8307.

2.1.3.3 Conclusion

L'obtention de deux structures de SBPase de Chlamydomonas permet la confirmation du repliement global de cette enzyme précédemment décrit chez la mousse *Physcomitrella patens*. La localisation d'un pont disulfure décrit comme régulateur dans cette espèce (Gütle et al. 2016) est également observée par cette nouvelle structure de SBPase. La conformation réduite de ce pont disulfure montre une augmentation de la mobilité et des réarrangements structuraux de la boucle contenant les deux cystéines 115 et 120 confirmée par des simulations de dynamiques moléculaires. Cette région de la protéine contient également plusieurs résidus susceptibles d'être phosphorylés et qui soulèvent la question d'une double régulation de l'enzyme. De même, les changements d'état redox semblent provoquer des changements dans les assemblages homo-oligomériques de SBPase. L'activation de l'enzyme en présence d'agent réducteur, d'une certaine concentration de magnésium ou de la présence de thiorédoxine est observé chez CrSBPase. Un contrôle de l'activité SBPase par le changement d'état homo-oligomérique est à présent à l'étude, distinguant la dynamique redox de SBPase des mécanismes attribués à FBPase.

2.1.4 Phosphoglycérate Kinase

Intervenant à la suite de la Rubisco dans le cycle de Calvin-Benson-Bassham, la PGK est une enzyme indispensable à la synthèse de G3P. Elle catalyse la phosphorylation de 3-PGA en 1,3-bPGA. C'est également l'une des deux enzymes du CBBC qui nécessitent la présence d'ATP comme co-substrat, avec la PRK. Impliquée dans la glycolyse, le mécanisme catalytique de cette enzyme a été étudié pour des isoformes non chloroplastiques (Zerrad et al. 2011).

Cette enzyme est composée de deux domaines liés par une hélice α, le premier en N-terminal correspond au domaine de liaison au 3-PGA, tandis que le second correspond au domaine de liaison à l'ATP. Ces deux domaines ont un repliement de Rossmann (CATH 3.40.50.1260), ils sont principalement dans une conformation ouverte et subissent un changement de cette conformation vers une conformation fermée en présence de leurs substrat et cosubstrat

(Zerrad et al. 2011). Chez Chlamydomonas, la régulation de l'activité de l'isoforme chloroplastique de PGK a été précédemment étudiée. Elle est retrouvée comme étant la cible de plusieurs modifications post-traductionnelles (Morisse et al. 2014b; Michelet et al. 2013; Zaffagnini et al. 2012a) et est décrite comme ayant une activité enzymatique régulée par la réduction via la thiorédoxine de type f d'un pont disulfure entre les cystéines 227 et 361 (Morisse et al. 2014a). Dans cette même publication, des modèles d'homologie se basant sur les structures tridimensionnelles de PGK glycolytiques sont utilisés pour expliquer le changement de conformation de PGK lors de la réduction du pont disulfure. Cependant ces simulations sont limitées par la fiabilité de modèles basés seulement sur l'homologie de séquence.

Pour pallier ce manque d'informations structurales et confirmer ou infirmer les hypothèses décrites, j'ai résolu la structure de la PGK1 chloroplastique de Chlamydomonas. CrPGK1 est éluée à une masse d'environ 43 kDa d'après la fonction de calibration de la colonne d'exclusion stérique. Cette masse est très proche des 43,8 kDa théoriques calculés à partir de la séquence de la protéine recombinante et semble admettre un état monomérique en solution de CrPGK1. Des cristaux ont été obtenus dans un tampon de cristallisation composé de 100 mmol.L^{-1} MES pH 5, 20% polyéthylène glycol 6000. Ces cristaux ont un groupe d'espace C 1 2 1 contenant deux monomères de PGK par unité asymétrique. Après un remplacement moléculaire en utilisant un modèle de la « *AlphaFold Protein Structure Database* » et affinement, un jeu de données d'une résolution de 1.98 Å a permis l'obtention d'une structure nouvelle (Code PDB : 7ZY7).

La structure de PGK chloroplastique de Chlamydomonas a confirmé la prédiction du repliement de l'enzyme en deux domaines liés par une hélice α (Figure 11 A). Les acides aminés intervenant dans la fixation du 3-PGA et de l'ATP et formant le site actif entre les deux domaines sont très conservés (figure 11 B) et n'amènent pas à émettre l'hypothèse d'une différence dans le mécanisme précédemment décrit. Au contraire, de même que pour RPI et FBA nous proposons que le mécanisme catalytique de PGK soit identique pour les paralogues du CBBC ou de la glycolyse. De plus, les cystéines 227 et 361 auparavant décrites comme régulatrices de l'activité de CrPGK sont proches des cystéines du modèle d'homologie de CrPGK sous forme oxydée et renforcent les conclusions de celui-ci.

La présence de densités électroniques additionnelles dans le jeu de données obtenu m'a permis de modéliser trois ions phosphates dans l'unité asymétrique. Ceux-ci proviennent des conditions d'expression de l'enzyme. Dans le modèle de l'enzyme ils sont situés dans les poches de fixation de l'ATP. Le monomère 1 lie deux phosphates, le monomère 2 n'en lie qu'un. En superposant la structure du monomère 1 à la structure de PGK de souris (*Mus musculus*) (code PDB : 2PAA) ayant co-cristallisé avec une molécule d'ATP, on observe une superposition des deux ions phosphates avec les phosphates α et γ de la molécule d'ATP. Ces deux ions phosphates sont à une distance de 3.6 Å et 3.8 Å des sérines 261 et 420 de CrPGK. Ces deux sérines font également partie d'une étude de phosphoprotéomique les décrivant comme phosphorylées chez Chlamydomonas, soulevant pour la troisième fois la question d'un potentiel encombrement stérique entre ces phosphorylations et le substrat d'une enzyme du CBBC comme pour RPI et FBA. La phosphorylation de ces deux résidus pourrait alors être un mécanisme d'inhibition de la PGK chloroplastique réduisant fortement l'affinité de l'enzyme pour son cosubstrat ATP de manière réversible.

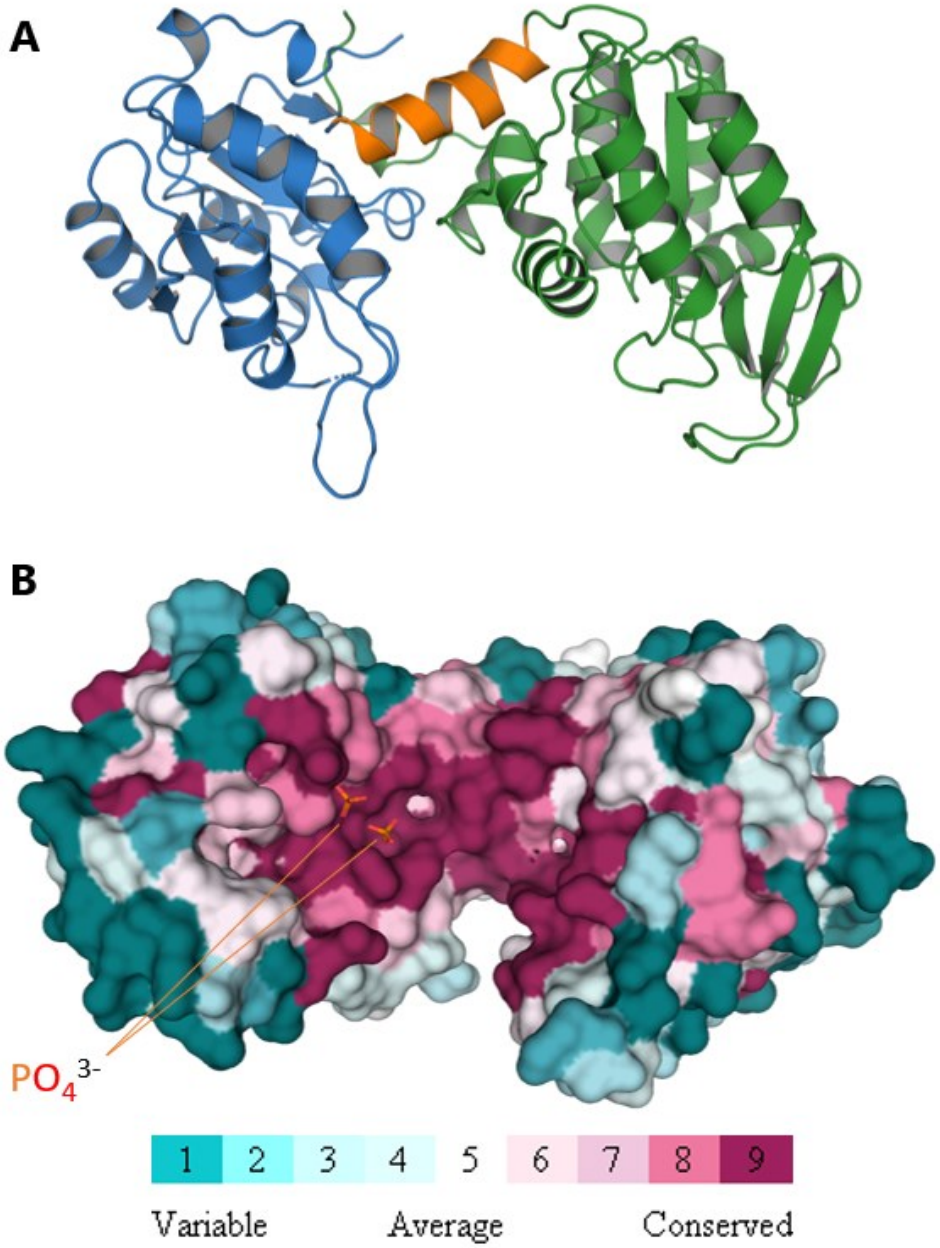

Figure 11 : A. Monomère de PGK représenté en ruban avec la sous-unité N-terminale colorée en bleu, la sous-unité C-terminale colorée en vert et l'hélice α de liaison colorée en orange. **B.** Surface d'exclusion du solvant de Connolly du monomère de PGK, les acides aminés sont colorés en fonction de leurs conservations du cyan au violet, des moins conservés aux plus conservés. Les deux ions phosphates de la structure sont représentés en batônnets.

Cette structure de PGK photosynthétique fera l'objet d'analyse plus détaillée dans l'équipe, en collaboration avec nos partenaires de l'Université de Bologne. La régulation redox de cette enzyme ayant été démontrée *in vitro*, il serait intéressant de se pencher sur la relation entre les modifications et les changements de conformation, particulièrement sur l'interaction entre les deux domaines de PGK.

2.1.5 Fructose-1,6-bisphosphatase

La FBPase est à présent la dernière enzyme du CBBC dont la structure demeure inconnue chez Chlamydomonas. Afin d'obtenir et d'analyser l'ensemble des structures du CBBC chez un organisme unique, CrFBPase1 a donc fait l'objet de mes recherches.

2.1.5.1 Essais de cristallographie

CrFBPase1 recombinante se produit de manière hétérologue chez *Escherichia coli* DE3 en relativement grandes quantités (23 mg par litre de culture). Ces quantités sont suffisantes pour réaliser les nombreux essais de cristallisation en conditions réductrices ou oxydantes, sur de multiples cribles de référence (cribles commerciaux Nextal Qiagen ou Molecular Dimensions : JCSGI-II-III-IV, Classics I-II, PEGs, PEG-Ions, Ammonium Sulfate, MPD, ProComplex, JBS 1-8, Wizard). Cependant, ces cribles n'ont jamais permis l'obtention de cristaux. Dans un deuxième temps, j'ai employé le cristallophore Xo4 (Polyvalan) comme agent de nucléation sur ces mêmes cribles (Engilberge et al. 2017). J'ai enfin testé la co-cristallisation avec le substrat FBP. Aucun de ces essais de cristallisation n'a donné de résultat exploitable pour FBPase en dépit de la pureté élevée de la protéine sur chromatographie d'exclusion de taille et sur électrophorèse sur gel de polyacrylamide en conditions dénaturantes.

2.1.5.2 Microscopie électronique

Au vu des récents progrès de la cryo-microscopie électronique sur particules uniques dans le domaine de la résolution de structures tridimensionnelles et après les tentatives infructueuses de cristallisation de la FBPase, une collaboration avec Dr. Manuela Dezi de l'équipe Microscopie Moléculaire des Membranes (MMM, Institut Curie) a été entamée. Cette collaboration à premièrement consisté en

une réalisation d'images de microscopie électronique à température ambiante pour vérifier le comportement de FBPase et déterminer les meilleurs paramètres susceptibles de mener à une résolution de la structure de la protéine par cette méthodologie.

Une production de FBPase recombinante en suivant les paramètres de culture précédemment mis au point a été réalisée. La FBPase a ensuite été purifiée en deux étapes (*cf.* matériels et méthodes section 4.2). Les premiers tests ont été faits en coloration négative à l'acétate d'uranyle à trois concentrations différentes de protéine et deux temps de dépôts différents sur un microscope Tecnai Spirit 80 keV (FEI, Hillsboro, Etats-Unis). Les images obtenues permettent la détection des particules de CrFBPase régulièrement réparties (Figure 12 A). J'ai observé plusieurs états homo-oligomériques de ces particules, notamment ce qui semble être des homo-tétramères (Figure 12 B), des homo-dimères (Figure 12 C) ou des homo-trimères (Figure 12 D).

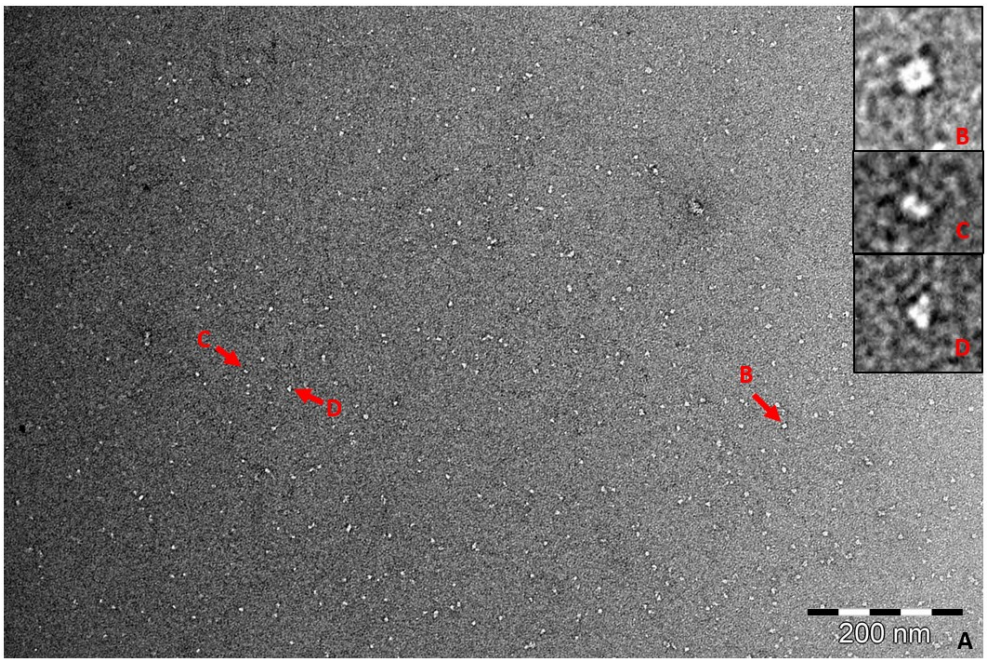

Figure 12 : A. Image de microscopie électronique en coloration négative de CrFBPase à 2,5 ng.mL^{-1}. **B. C.** et **D.** Zooms de cette même image sur des assemblages homo-oligomériques de CrFBPase.

L'hétérogénéité visible des états oligomériques de la CrFBPase après purification pourrait en partie expliquer les difficultés de cristallisation de cette protéine car des échanges entre espèces oligomériques de symétries distinctes empoisonneraient la croissance de cristaux réguliers, prérequis à une diffraction interprétable. La poursuite des études en microscopie électronique passera par le dépôt de la protéine sur des grilles de congélation pour la détermination de la structure par cryo-microscopie sur particules uniques. Les dimensions de complexes oligomériques de CrFBPase (88 kDa pour un homo-dimère, 166 kDa pour un homo-tétramère) sont à la limite de masse pour l'obtention de données à résolution inférieure à 3 Å en l'état actuel de la méthode.

2.2 ISOLEMENT DE COMPLEXES D'ENZYMES DU CYCLE DE CALVIN-BENSON-BASSHAM

Les enzymes du CBBC peuvent s'associer en complexes hétéro-multimériques de hautes masses moléculaires. Si cette association est connue et bien documentée pour deux de ces complexes qui sont ceux de GAPDH-CP12-PRK et Rubisco-EPYC1 (*Cf.* section 1.4.3.2), ce n'est pas le cas de tous les assemblages proposés dans la littérature. J'ai donc mis au point plusieurs méthodes de détection d'états complexés de protéines à partir d'extraits cellulaires de Chlamydomonas. L'objectif de ces expérimentations étant l'isolement et la caractérisation d'un ou plusieurs complexes d'enzymes du CBBC. Ces informations permettront potentiellement la reconstitution *in vitro* d'un complexe à partir de protéines recombinantes pour une caractérisation biochimique.

2.2.1 Détection d'assemblages de hautes masses moléculaires

Des extraits protéiques de Chlamydomonas souche D66 ont été réalisés, et injectés sur une colonne de chromatographie d'exclusion de taille (SEC) ayant une gamme de séparation couvrant théoriquement des masses de 5000 kDa à 5 kDa. Les différentes fractions obtenues en sortie de cette colonne ont été analysées en western blot avec des anticorps polyclonaux dirigés contre chaque protéine du CBBC. Si la présence de protéines du CBBC est détectée dans des fractions éluées à des volumes correspondant à des hautes masses moléculaires, alors ces protéines sont retenues comme candidates à la participation à des complexes.

La majorité de la Rubisco de Chlamydomonas étant séparée dans le pyrénoïde et les autres enzymes du CBBC étant colocalisées autour du pyrénoïde (Wang et al. 2022; Küken et al. 2018), il a été décidé d'exclure dans un premier temps la Rubisco de l'analyse. La séparation des protéines sur SEC a permis d'obtenir vingt-six fractions dont les masses moléculaires s'étalent de 8600 kDa à 3 kDa d'après la calibration de la colonne par des marqueurs de masses. Le chromatogramme obtenu présente plusieurs pics d'intensités et largeurs variables, le pic principal étant élué à un volume de 88 ml correspondant à une masse apparente de 80 kDa (Figure 13). L'extrait cellulaire de Chlamydomonas ayant été chargé directement sur la colonne, c'est le protéome soluble total de l'ensemble des protéines exprimées dans les conditions de culture utilisées qui compose ce profil.

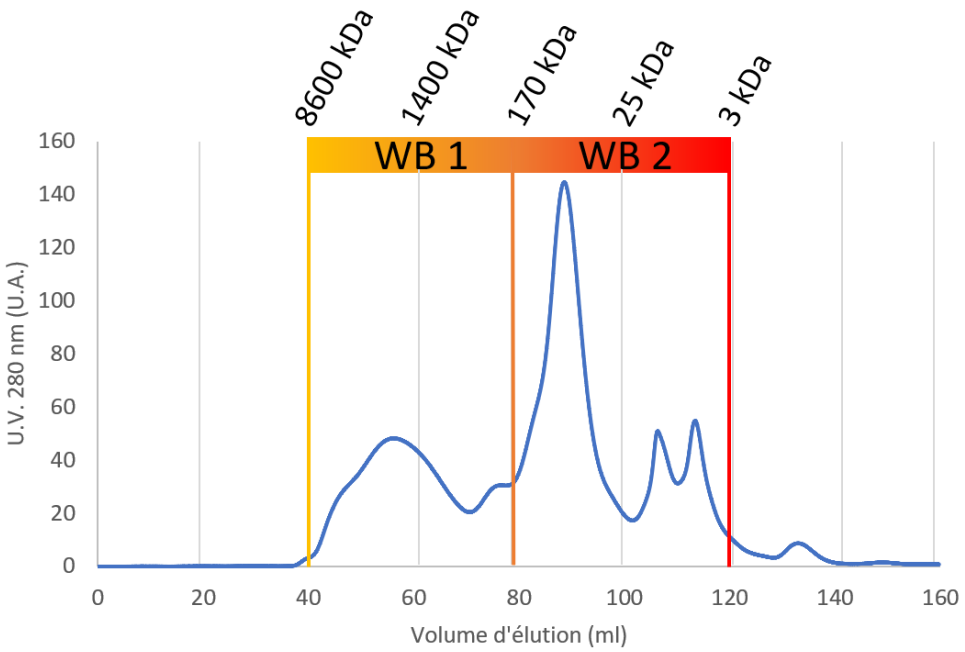

Figure 13 : Chromatogramme lu en absorbance à 280 nm en fonction du volume d'élution d'extraits protéiques de Chlamydomonas injectés sur une colonne Superose 6 16/600. Les masses moléculaires indiquées correspondent à des estimations du volume d'élution de celles-ci par rapport à des marqueurs de calibration injectés dans les mêmes conditions. Les annotations WB1 et WB2 et les barres colorées correspondent aux fractions déposées sur deux gels d'électrophorèse avant transfert sur membranes de western blot (WB) (*Cf.* figure 14).

Les détections de CrFBPase1, CrTRK1, CrPRK, CrPGK1, CrSBPase1, CrTPI1, CrRPI1, CrRPE1 et CrFBA3 ont été systématiquement réalisées par WB avec l'un des deux anticorps polyclonaux dont je disposais pour chaque protéine (Figure 14). Les détections de CrGAPA seront à réaliser lorsque nous disposerons des anticorps appropriés.

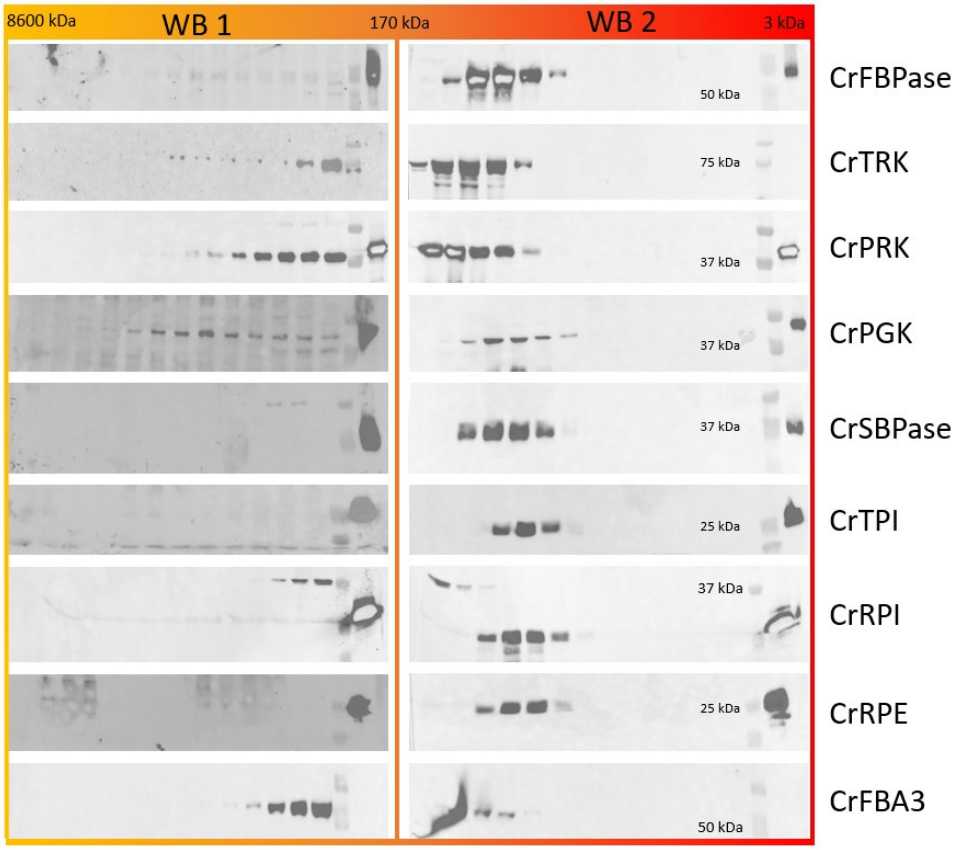

Figure 14 : Western blot avec des anticorps dirigés sur 9 des 11 protéines du CBBC indiquées dans la colonne de droite. Une migration sur gel d'électrophorèse dénaturant réducteur de 26 fractions obtenues par SEC est faite sur deux membranes contenant chacune 13 fractions dans leur ordre chronologique d'élution. Sur chacune des membrane la dernière piste à droite correspond à la protéine recombinante ciblée par l'anticorps. L'anticorps primaire produit chez des lapins est détecté par un anticorps secondaire couplé à la peroxydase HRP, dont l'activité est révélée par chimioluminescence selon le kit ECL sur un appareil ChemiDoc (GE Healthcare). L'avant dernière piste de chaque membrane correspond aux marqueurs de masses moléculaires. La concentration en anticorps et les temps d'exposition des membranes ont été préalablement optimisés pour chaque détection.

Comme précisé précédemment la Rubisco ne fait pas partie de cette analyse. La CrGAPDH n'a pas pu être analysée faute d'anticorps suffisamment spécifique. Deux contrôles de protéines recombinantes

sont également manquant pour les protéines CrTRK et CrFBA3, ces résultats ont tout de même été considérés comme valides, les bandes détectées étant à un volume d'élution en SEC correspondant à leurs états oligomériques connus et proches de leurs masses moléculaires attendues sur SDS-PAGE.

Si la plupart des protéines (CrRPE, CrRPI, CrTPI, CrSBPase, CrFBA3) sont éluées et détectées à des volumes et distances de migrations correspondant respectivement à leurs assemblages homo-oligomérique indépendamment observés en SEC des protéines pures, quatre protéines (CrPRK, CrFBPase, CrTRK, CrPGK) présentent des bandes dans des fractions éluées à des hautes masses moléculaires, entre 8600 et 170 kDa (WB1). Ces élutions à masses moléculaires anormalement élevées en font donc des candidates pour des assemblages en complexes hétéro-multimériques, potentiellement entre elles, ou avec d'autres protéines non sondées. C'est donc sur ces quatre candidates que la suite de mon travail sur ces potentiels complexes du CBBC s'est concentré.

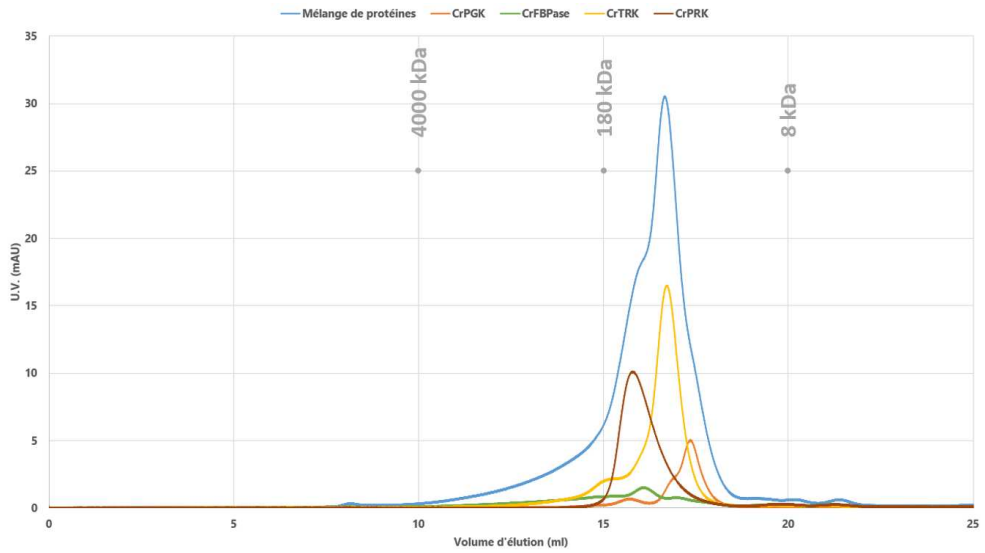

Figure 15 : Superposition des chromatogrammes d'injection des quatre protéines recombinantes CrPRK, CrTRK, CrPGK, CrFBPase et du mélange de celles-ci sur colonne Superose 6 10/300.

2.2.2 Co-élutions des enzymes du cycle de Calvin-Benson-Bassham

En me focalisant sur les quatre enzymes précédemment citées, j'ai réalisé des tests de co-élutions sur chromatographie d'exclusion de taille. Ces tests consistent à injecter sur une colonne de résine Superose 6 une quantité fixe des protéines produites de manière recombinantes chez *Escherichia coli* séparément, puis de co-injecter ces mêmes quantités de protéines mélangées et de rechercher leur présence dans des pics élués à des volumes précoces révélateurs de masses d'assemblages supramoléculaires. La figure 15 montre la superposition des chromatogrammes obtenus. Le chromatogramme du mélange des protéines présente deux pics définis se superposant à environs 16 et 17 ml d'élution. Le premier de ces pics correspond au pic de PRK homo-dimérique, et le second à une superposition des pics des associations homo-multimériques des trois autres protéines. Une absorbance plus importante dans le chromatogramme du mélange de protéines de 10 ml à 14 ml suggère des associations entres protéines hétérogènes mais pas de complexes définis de manière monodisperse. On remarque également un pic de petite taille autour de 8 ml qui correspond au volume mort de la colonne, indiquant la présence d'agrégats ou de complexes de masses supérieures à 8000 kDa.

Les conditions de formation des potentiels complexes du CBBC n'étant pas connues, nous avons toutefois supposé que des interactions entre enzymes pourraient contribuer à augmenter leur activité par rapport à leur état dissocié, individuel. Alors, ces assemblages activateurs pourraient s'établir dans les conditions où les enzymes du CBBC sont les plus actives (*cf.* partie 1.4) : à l'état réduit, en présence de magnésium, ainsi qu'à pH 7,9, en absence de calcium et non phosphorylées. Les essais de co-élution des mélanges ont donc été répétés en présence de DTT et de magnésium (Figure 16). Si la présence de complexes hétéro-multimériques de hautes masses ne semble toujours pas se révéler en présence d'un agent réducteur, de magnésium ou des deux en même temps, ces adjuvants semblent en revanche favoriser la dissociation d'homo-multimères des enzymes. Ainsi l'épaulement autour de 16 ml correspondant au pic de l'homo-dimère de CrPRK (80 kDa) visible dans le chromatogramme du mélange de protéines sans traitement n'apparaît plus dans les trois autres conditions testées qui présentent un pic correspondant au

volume d'élution de 18 ml d'un monomère de CrPRK (40 kDa) de plus grande intensité. Au contraire de notre hypothèse de travail, les conditions physico-chimiques d'activation montrent un effet de dissociation des états complexés pour ces homo-oligomères. Ce résultat fait écho à la dissociation induite par le DTT décrite sur CrSBPase (section 2.1.3).

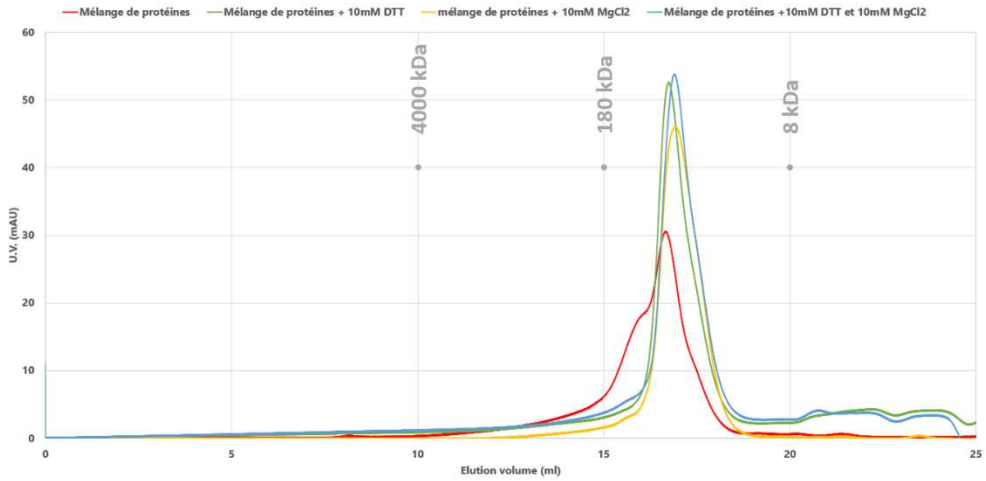

Figure 16 : Superposition des chromatogrammes des mélange des quatre protéines (CrPRK, CrTRK, CrPGK, CrFBPase) en rouge sur Superose 6 10/300 dans un tampon additionné de 10 mmol.L^{-1} DTT en vert, 10 mmol.L^{-1} $MgCl_2$ en jaune ou de la combinaison des deux en bleu.

Ces tentatives de co-élutions de protéines recombinantes n'ont toutefois pas permis de mettre en évidence une association de ces protéines malgré les résultats prédits par les extraits cellulaires séparés sur superose 6 et détection par western blots. Ce résultat négatif pourrait être dû à l'absence de modifications post-traductionnelles des protéines produites de manière recombinante ou bien à l'absence d'un facteur de complexation comme une autre protéine partenaire d'assemblage, un métabolite, un cofacteur redox, absents du tampon de chromatographie. Pour réviser l'hypothèse de l'interaction en présence d'un facteur d'assemblage présent *in vivo*, un autre protocole d'isolement de complexes a été appliqué pour la détection d'interactions entre enzymes.

2.2.3 Isolement de complexes sur colonne CNBr-sépharose

Suite aux expériences précédentes, la fixation covalente d'une des protéines cibles, CrPGK, sur une résine CNBr-sépharose a été réalisée dans le but de tester la rétention dans des extraits protéiques de Chlamydomonas sur cette résine et identifier des protéines candidates à la formation d'états supramoléculaires.

La protéine choisie pour être fixée de manière covalente à la résine est CrPGK car sa production à grande échelle est facile, la protéine pure est stable sur plusieurs jours, elle est monomérique donc ne forme aucun complexe avec elle-même en solution et elle est la plus abondante dans les hautes masses moléculaires observées en SEC (Figure 13). Après fixation covalente de CrPGK dans des conditions non dénaturantes sur la résine et passage de l'extrait protéique de Chlamydomonas, et après lavage avec le tampon d'extraction de cette résine, deux choix d'élutions ont été réalisés. La première élution contenait un agent réducteur pour essayer de détacher les potentiels complexes dépendant de ponts disulfures, à la manière du complexe inhibiteur GAPDH-CP12-PRK. La seconde élution contenait une haute concentration de sels afin de déstabiliser les interactions polaires responsables de certaines interactions fortes entres protéines. Ces deux traitements sont compatibles avec un état natif (non dénaturé) de la PGK liée à la résine et de ses interactants. Un aliquote de la résine après ces deux élutions a également été solubilisé pour vérifier la conservation de PGK non protéolysée sur cette résine, ainsi que pour évaluer la rétention éventuelle des trois autres protéines dans le cas d'une interaction médiée par un autre paramètre que ceux testés par les deux méthodes d'élution (Figure 17). Des contrôles négatifs de passage du même extrait protéique sur une résine identique non liée à CrPGK montrent une rétention aspécifique des quatre protéines négligeable et non comparable à la quantité retenue par la résine avec fixation de CrPGK (Annexe 2).

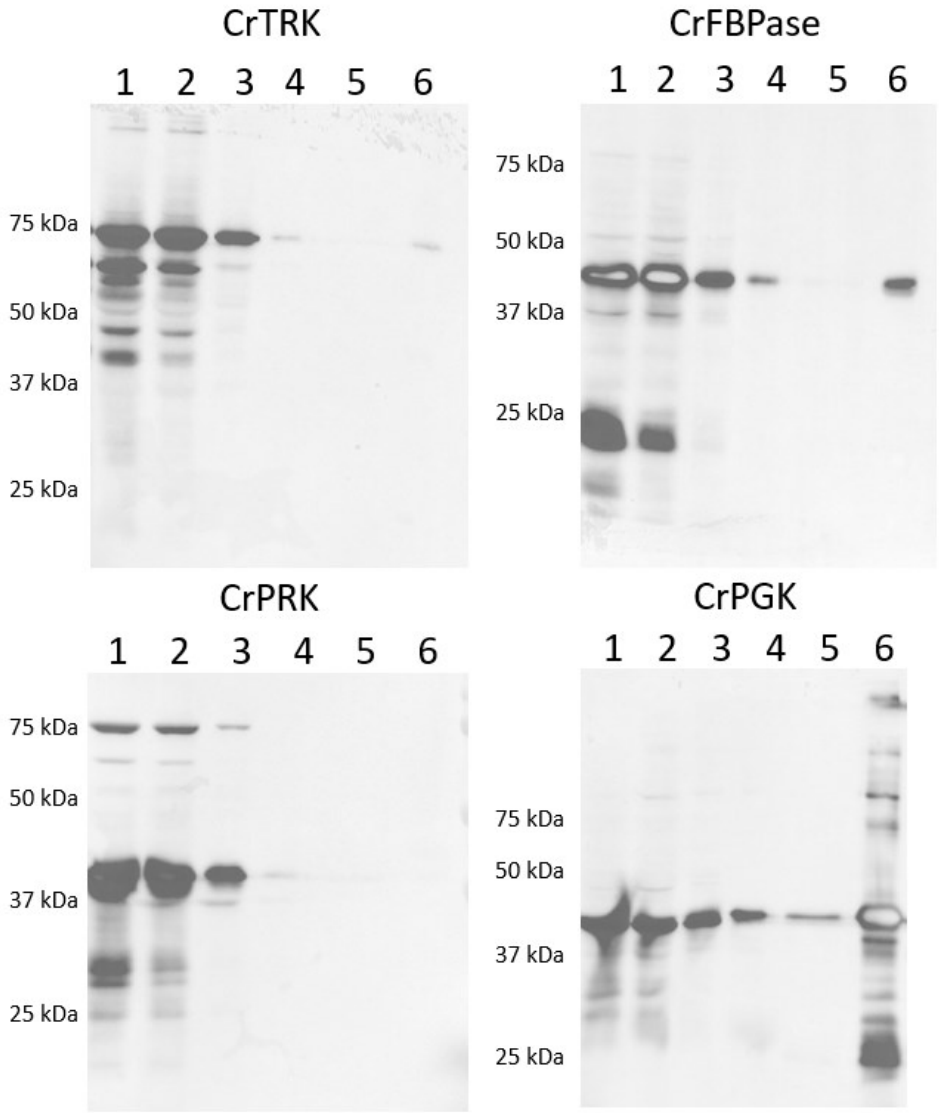

Figure 17 : Western Blot avec anticorps dirigé contre CrTRK, CrFBPase, CrPRK et CrPGK. Les différents numéros au-dessus des membranes indiquent les pistes de migration des différents aliquotes de la résine CNBr-sépharose liée covalement avec CrPGK recombinante. Piste 1 : extrait protéique soluble avant dépôt sur la résine, piste 2 : non retenu, piste 3 : lavage avec tampon 20 mM Tris-HCl pH 7,9 ; 100 mM NaCl, piste 4 : élution dans le tampon précédent additionné de 10 mM DTT, piste 5 : élution dans un tampon 20 mM Tris-HCl pH 7,9 ; 2 M NaCl, piste 6 : résine solubilisée après élutions.

Nous observons d'abord sur le Western-Blot dirigé contre CrPGK des bandes correspondant à CrPGK dans toutes les pistes. Ces bandes sont dues soit à la PGK des extraits protéiques soit à celle fixée à la résine qui se désorbe progressivement. On peut également observer la présence de bandes de protéines aspécifiques à des distances de migration ne pouvant pas correspondre aux protéines cibles intègres, essentiellement sur les pistes 1 et 2 non retenues par CrPGK. Les protéines cibles sont détectées aux bandes les plus intenses et migrent autour de leurs poids moléculaires attendus ce qui permet une interprétation fiable des résultats. CrPRK est la protéine dont le western blot est le plus difficile à interpréter, en raison d'une piste contrôle présentant des bandes mal définies. Il est tout de même possible d'observer des bandes distinctes dans les pistes 3 et 4, indiquant une rétention partielle de CrPRK sur la résine, la piste 4 étant une élution par réduction au DTT. Il est en revanche possible de détecter CrTRK dans les deux pistes 3 et 4 ainsi que sur la piste 6. La bande peu intense de cette piste montre donc une interaction possible avec CrPGK, ou une autre protéine elle-même interagissant avec CrPGK, suffisamment forte pour résister aux élutions. CrFBPase présente le même profil que CrTRK avec des intensités plus fortes, aux pistes 3, 4 et 6.

Ces différentes expériences ne permettent pas de déterminer précisément la composition et la stœchiométrie d'un complexe d'enzymes du CBBC, mais elles renforcent l'hypothèse d'interactions supramoléculaires entre ces quatre enzymes du CBBC. De la même manière, même si les expériences de co-élution n'ont pas permis de déterminer les conditions exactes d'interaction de ces protéines, les informations apportées par ces expériences permettent un rétrécissement des cibles à étudier pour la continuation de ce projet de recherche. Les facteurs cellulaires médiant l'interaction dans les extraits pourront être révélés par des expériences de spectrométrie de masse sur les éluats de colonnes CNBr-sépharose ou des résines IgG-sépharoses chargées des anticorps polyclonaux de ces protéines (immuno *pull-downs*).

3 DISCUSSION

3.1 CONCLUSIONS

Durant mes trois ans de doctorat j'ai pu répondre en partie aux problématiques posées au début de celui-ci. L'étude structurale des enzymes du cycle de Calvin-Benson-Bassham chez *Chlamydomonas reinhardtii* a pu bénéficier de quatre structures supplémentaires, permettant de monter le nombre de structures connue à dix sur les onze composant le cycle (Figure 18). Deux de ces structures ont fait l'objet de publications dans des journaux à comité de lecture. Une autre analyse structurale fait l'un l'objet d'un manuscrit qui sera soumis à un journal pour publication. J'ai déterminé la structure d'une thiorédoxine z chloroplastique, la première représentante de ce type se distinguant par sa surface de reconnaissance des cibles, et qui a fait l'objet d'une publication (*Cf.* annexe 1)

La résolution des structures de RPI1, FBA3, SBPase1 et PGK1 chloroplastiques de l'organisme modèle *Chlamydomonas reinhardtii* permet une analyse moléculaire des mécanismes catalytiques de celles-ci. D'après la conservation des résidus des sites actifs, nous confirmons l'absence de différences entre les mécanismes catalytiques de RPI, FBA et PGK par rapport à leurs homologues non photosynthétiques. Les résultats obtenus par l'apport de ma structure de CrSBPase et les analyses d'activités enzymatiques effectuées en parallèle ont montré une similarité entre les sites actifs de différentes espèces photosynthétiques mais une disparité dans la régulation de l'activité de l'enzyme. Ces différences, bien que ne pouvant pas encore faire l'objet d'une hypothèse fonctionnelle montre que la régulation des enzymes du cycle de Calvin-Benson-Bassham s'effectuerait selon plusieurs modes pouvant se combiner.

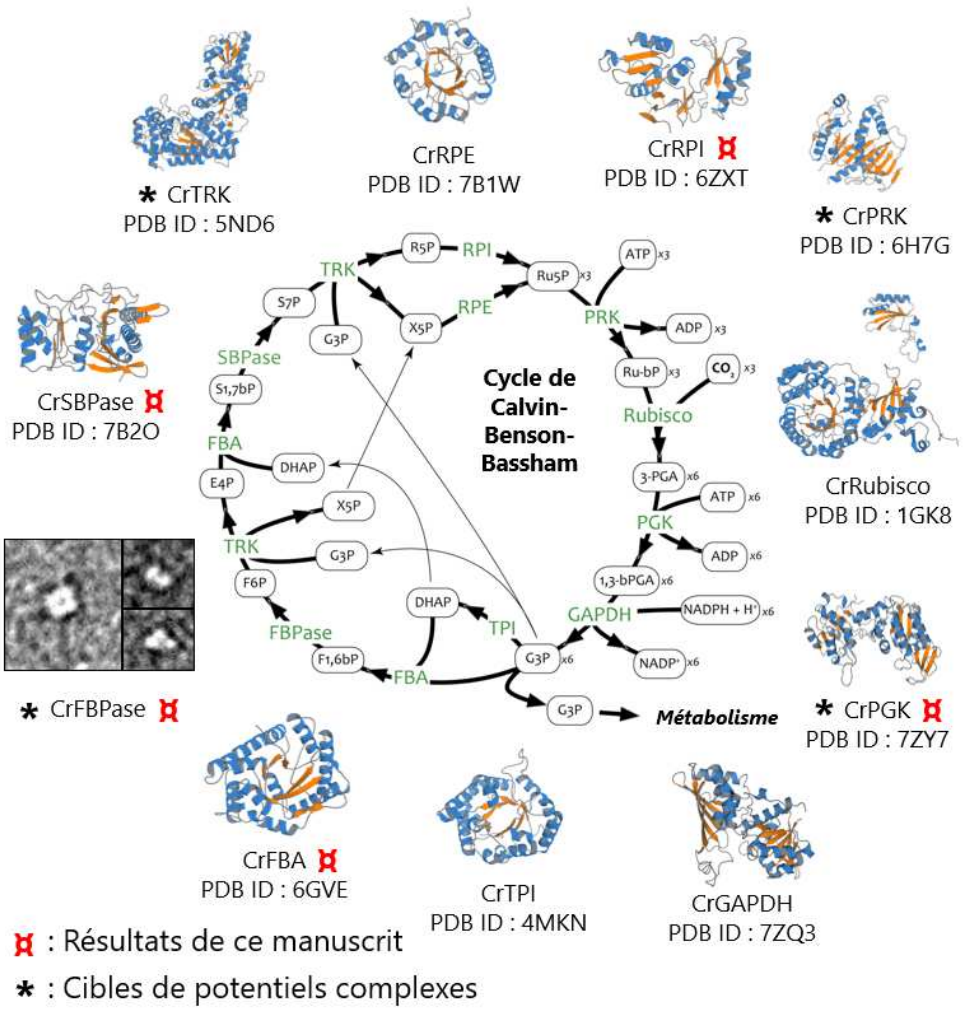

Figure 18 : Résumé visuel des résultats présentés. Les abréviations des noms des protéines et métabolites sont détaillés dans la section abréviations. Les protéines isolées comme candidates à la formation de complexes sont indiquées par une astérisque. Les protéines ayant fait l'objet d'analyses structurale durant ma thèse sont indiquées par un symbole « ¤ » rouge.

Ces éléments de régulation peuvent appartenir au domaine des modifications redox sur cystéines, des modifications par phosphorylations sur sérines ou thréonines, mais peuvent également être d'autre nature, comme la concentration en certains ions (magnésium, calcium), métabolites ou cofacteurs. Ces sites de phosphorylations auxquelles plusieurs équipes se sont intéressées semblent devoir jouer un rôle important pour les enzymes du CBBC

dont j'ai résolu la structures, sur des sites de liaison à proximité ou faisant partie des sites actifs des enzymes. La fonction physiologique de ces phosphorylations reste une question ouverte jusqu'à l'identification des kinases et phosphatases qui les contrôlent suivant des signaux à définir. Il est probable que les phosphorylations inhibent les mécanismes catalytiques de ces enzymes. Les mécanismes de régulations redox en revanche font l'objet de plusieurs publications et l'obtention de ces structures a permis de confirmer l'emplacement de cystéines régulatrices de CrPGK, précédemment seulement modélisées. De même, la structure de CrSBPase a permis de localiser le pont disulfure décrit comme régulateur à la même position dans l'espace que celui de PpSBPase. La suite de l'analyse de CrSBPase montre néanmoins une nouveauté quant au mécanisme de régulation exercé par ce pont.

L'apport de ces nouveautés sous la forme d'analyses structurales montre bien l'intérêt de l'étude au cas par cas des enzymes du CBBC et renforce encore l'attrait pour l'obtention de la structure tri-dimensionnelle de CrFBPase pour finaliser la disponibilité de l'entièreté des structures du cycle chez un organisme unique. Cette disponibilité des structures du CBBC pourra entre autres aider la reconstitution des potentiels complexes de la section 2.2, en étant utilisé comme base pour l'étude des surfaces d'interactions compatibles ou pour des simulations d'amarrage protéines-protéines.

La bibliographies des complexes du cycle de Calvin-Benson-Bassham est composée d'un certain nombre d'articles communiqués depuis les années 1970. Cette bibliographie peut être divisée en deux parties, la première traitant du complexe inhibiteur GAPDH-CP12-PRK, la seconde traitant de l'association des autres protéines du cycle. Si la première partie est consensuelle, la seconde diverge sur la composition de ces autres potentiels complexes, sur l'espèce chez laquelle ces complexes sont étudiés et ne permet pas d'émettre d'hypothèse claire sur la fonction de ceux-ci. J'ai essayé d'isoler l'un de ces complexes chez *Chlamydomonas reinhardtii*. Si la présence d'assemblages de masses supérieures à celles des protéines seules à bien été confirmée dans des extraits protéiques de Chlamydomonas, la composition de ces assemblages reste encore sujette à discussion. Les quatre protéines candidates que j'ai pu retrouver à des masses

moléculaires supérieures à 200 kDa, sont PGK, PRK, TRK et FBPase. L'utilisation de deux méthodes différentes s'accorde sur une possible interaction de ces protéines mais il semble également que ces interactions sont faibles, transitoires et nécessitent des facteurs additionnels. Les tentatives de reconstruction de ce potentiel complexe dans plusieurs conditions n'ayant pas donné satisfaction, elles permettent néanmoins d'émettre certaines hypothèses sur le ou les éléments indispensables à la stabilisation de ces complexes.

Ces études structurales et d'interactions ont permis de confirmer et d'ajouter des connaissances au cycle de Calvin-Benson-Bassham qui, malgré sa première description entre les années 1952 et 1954, conserve des zones d'ombres. Le premier objectif de ce travail de doctorat qui était d'avancer dans la description des structures du CBBC chez Chlamydomonas à fait l'objet de l'essentiel de mes efforts du fait de résultats très encourageants durant les étapes initiales de cristallisation, exception faite de CrFBPase. Ces différentes analyses structurales permettent ainsi au nombre de structures d'enzymes du CBBC de Chlamydomonas inconnues de descendre à une seule. La seconde partie de mon travail de doctorat a subi le contrecoup de cette concentration des efforts et a fait l'objet de moins de temps de travail. J'ai néanmoins apporté des éclaircissements sur la composition des complexes du CBBC chez Chlamydomonas. Ces deux parties complémentaires ont donc permis de résoudre des interrogations mais soulèvent aussi des questions sur les régulations et les interactions de ces enzymes entres-elles ou avec d'autres partenaires qui devront être traitées à l'avenir.

3.2 PERSPECTIVES

L'impossibilité de cristalliser certaines protéines est l'un des goulot d'étranglement de la résolution de structures tri-dimensionnelles de protéines par cristallographie. De ce fait, CrFBPase n'a pu faire l'objet d'une analyse structurale moléculaire, sa structure n'ayant pas pu être obtenue. Pour résoudre cet inconvénient la résolution de sa structure par cryo-microscopie électronique a été envisagée en collaboration. Une autre solution que nous avons envisagée et commencé à tester en même temps que cette collaboration a été l'utilisation d'algorithmes de résolution de

structures tri-dimensionnelles à partir de séquences d'acides aminés. Des algorithmes semblent depuis 2021 prédire avec suffisamment de fiabilité les structures de monomères protéiques non membranaires ayant des repliements similaires à ceux déjà décrit dans la PDB. Le programme Alphafold 2 a ainsi durant le concours CASP14 (Critical Assessment of Protein Structure Prediction) pu prédire de manière précise des structures de protéines inconnues. L'utilisation de ce prédicteur de structure a déjà été utile dans le cadre de ce travail de doctorat, le jeu de données de la structure de CrPGK ayant été phasé en utilisant un modèle d'Alphafold 2. L'utilisation de ces algorithmes de prédiction permet donc de simplifier certaines étapes ou d'obtenir des modèles pour des comparaisons de structures de manière simple et il semble que ceux-ci vont prendre une importance croissante dans le domaine de la biologie structurale.

L'utilisation de méthodes informatiques en association avec des sciences expérimentales est donc un axe de développement de la suite de ce projet, comme a pu le montrer l'article concernant CrFBA3 (Le Moigne et al. 2022b). De même la collaboration actuelle avec le Dr. Nicolas Chéron pour étudier la dynamique moléculaire des motifs portant le pont disulfure de CrSBPase est un autre exemple de l'interconnexion entre biologie structurale et biologie computationnelle. La résolution de la structure de SBPase a permis d'introduire un possible mécanisme de régulation par changements d'état multimérique de cette protéine qui ne font pour l'instant pas l'objet d'une hypothèse explicative. Nous proposons une régulation redox de CrSBPase plus indirecte que celle décrite précédemment sur FBPase, impliquant des échanges d'états homo-oligomériques et des effets allostériques.

Si les structures des enzymes de ce cycle sont, à l'exception de CrFBPase, identifiées et connues chez *Chlamydomonas reinhardtii*, l'analyse de leurs caractéristiques enzymatiques reste encore manquante pour certaines d'entre elles. L'études de ces activités enzymatiques couplées à celle de leurs modifications redox et post-traductionnelles mènerait à une meilleure compréhension des mécanismes de régulations des organismes photosynthétiques (Raines 2022). Cette meilleure compréhension de ces mécanismes pourrait alors aider à la compréhension fine des passages de la lumière à

l'obscurité et inversement. La modulation des activités enzymatiques du CBBC en fonction de l'intensité lumineuse relié à l'état redox intracellulaire ou à d'autres paramètres reste donc un champ d'étude intéressant.

Les différences physiologiques entre les phases lumineuses et d'obscurité sont importantes chez *Chlamydomonas reinhardtii*. La concentration en ions (Mg^{2+}, pH, etc.), la régulation redox des enzymes, la formation du complexe GAPDH-CP12-PRK sont des éléments variants entre ces deux phases. Ce dernier point est notamment à mettre en perspective avec les tentatives d'isolement d'autres complexes du cycle de Calvin-Benson-Bassham. En effet, les extraits protéiques utilisés pour cet isolement de complexes ont été obtenus depuis des cultures de Chlamydomonas en milieu contenant de l'acétate et en présence d'une lumière de 40 $\mu E.m^{-2}.s^{-1}$. Tester la présence à hautes masses moléculaires des enzymes détectées ici à partir d'extraits protéiques obtenus depuis des culture en milieu minimum, forçant Chlamydomonas à la photosynthèse, ou encore à l'obscurité dans la situation inverse pourrait donner des indices sur la stabilité, la fonction ou les conditions de formation de ces assemblages. De même, une manière d'étudier ces complexes serait d'envisager la liaison covalente des protéines les composant via des expériences de pontage covalent (*cross-linking*) pour stabiliser les interactions de ceux-ci.

A plus long terme, la possibilité d'utiliser Chlamydomonas comme un châssis de biologie synthétique pour mettre au point un cycle de Calvin-Benson-Bassham amélioré est une option. Ce cycle étant limité dans son efficacité globale par l'activité de certaines enzymes, il est possible d'imaginer une augmentation de celle-ci. L'association en complexes artificiels d'enzymes contigües dans le cycle pour avoir un effet de « *channeling* » serait une piste à envisager. Pour mieux comprendre ces possibilités d'assemblages enzymatiques, la connaissance de leurs structures tri-dimensionnelle pour connaître leurs acides aminés de surface et l'étude d'assemblages préexistants semble être un bon début.

4 MATERIELS ET METHODES

4.1 CLONAGES

Les différents gènes utilisés codant pour les protéines du CBBC de *Chlamydomonas reinhardtii* ont été précédemment clonés au laboratoire dans différents plasmides de surexpression inductible en *Escherichia coli* BL21 DE3 (c*f.* Tableau 1). Les constructions comportent toutes une étiquette 6 histidines à l'extrémité amino-terminale permettant une purification d'affinité sur résine de nickel. Les séquences des protéines ont été obtenues dans la banque de données UniProtKB et sont listées ci-après :

CrPGK : code UniProtKB : Q548U3

```
        10         20         30         40         50
MALSMKMRAN ARVSGRRVAA VAPRVVPFSS ASSSVLRSGF ALRCLWTSAA
        60         70         80         90        100
WAALASVVEA VKKSVGDLHK ADLEGKRVFV RADLNVPLDK ATLAITDDTR
       110        120        130        140        150
IRAAVPTLKY LLDNGAKVLL TSHLGRPKGG PEDKYRLTPV VARLSELLGK
       160        170        180        190        200
PVTKVDDCIG PEVEKAVGAM KNGELLLLEN CRFYKEEEKN EPEFAKKLAA
       210        220        230        240        250
NADLYVNDAF GTAHRAHAST EGVTKFLKPS VAGFLLQKEL DYLDGAVSNP
       260        270        280        290        300
KRPFVAIVGG SKVSSKITVI EALMEKCDKI IIGGGMIFTF YKARALKVGS
       310        320        330        340        350
SLVEDDKIEL AKKLEEMAKA KGVQLLLPTD VVVADKFDAN ANTQTVPITA
       360        370        380        390        400
IPDGWMGLDI GPDSVKTFND ALADAKTVVW NGPMGVFEFP QVRQRTVSIA
       410        420        430        440        450
NTLAGLTPKG CITIIGGGDS VAAVEQAGVA EKMSHISTGG GASLELLEGK
       460
VLPGVAALDE K
```

CrSBPase : code UniProtKB : P46284

```
        10         20         30         40         50
MAAMMMRQKV AGAIAGERRS AVAPKMGRAA TAPVVVASAN ASAFKGAAVT
        60         70         80         90        100
ARVKASTRAA RVQSRRTAVL TQAKIGDSLA EFLVEATPDP KLRHVMMSMA
       110        120        130        140        150
EATRTIAHKV RTASCAGTAC VNSFGDEQLA VDMVADKLLF EALKYSHVCK
       160        170        180        190        200
LACSEEVPEP VDMGGEGFCV AFDPLDGSSS SDTNFAVGTI FGVWPGDKLT
       210        220        230        240        250
NITGREQVAA GMGIYGPRTV FCIALKDAPG CHEFLLMDDG KWMHVKETTH
       260        270        280        290        300
IGEGKMFAPG NLRATFDNPA YERLINFYLG EKYTLRYTGG IVPDLFQIIV
       310        320        330        340        350
KEKGVFTNLT SPTTKAKLRI LFEVAPLALL IEKAGGASSC DGKAVSALDI
       360        370        380
PILVCDQRTQ ICYGSIGEVR RFEEYMYGTS PRFSEKVVA
```

CrRPI1 : code UniProtKB : A8IRQ1

```
        10         20         30         40         50
MMLKASPAAR AAARPAARNV RMMAAPVSTQ LSQDELKKQA AWKAVEYVKS
        60         70         80         90        100
GMVVGLGTGS TAAFAVDRIG QLLKEGKLQN IVGVPTSIRT YEQALSLGIP
       110        120        130        140        150
LATLDEQPKL DVAIDGADEV DPNLDVVKGR GGALLREKMV EMASAKFVCI
       160        170        180        190        200
VDDSKLVEGL GGSKLAMPVE IVQFCHKYTL QRLANLPEVK GCEAKLRMNG
       210        220        230        240        250
DKPYVTDNSN YIVDLYFQTP IKDSQAASKA ILGLDGVVDH GLFLDMVDVC
       260
IIAGATGVTV QERPNPKKH
```

CrFBA3 : code UniProtKB : Q42690

```
        10         20         30         40         50
MALMMKSSAS LKAVSAGRSR RAVVVRAGKY DEELIKTAGT VASKGRGILA
        60         70         80         90        100
MDESNATCGK RLDSIGVENT EENRRAYREL LVTAPGLGQY ISGAILFEET
       110        120        130        140        150
LYQSTASGKK FVDVMKEQNI VPGIKVDKGL VPLSNTNGES WCMGLDGLDK
       160        170        180        190        200
RCAEYYKAGA RFAKWRSVVS IPHGPSIIAA RDCAYGLARY AAIAQNAGLV
       210        220        230        240        250
PIVEPEVLLD GEHDIDRCLE VQEAIWAETF KYMADNKVMF EGILLKPAMV
       260        270        280        290        300
TPGADCKNKA GPAKVAEYTL KMLRRRVPPA VPGIMFLSGG QSELESTLNL
       310        320        330        340        350
NAMNQSPNPW HVSFSYARAL QNTVLKTWQG KPENVQAAQA ALLKRAKANS
       360        370
DAQQGKYDAT TEGKEAAQGM YEKGYVY
```

CrFBPase : code UniProtKB : A8IKQ0

```
        10         20         30         40         50
MAATMLRSST QSGIAAKAGR KEAVSVRAVA QPQRQAGAAS VFSSSSSGAA
        60         70         80         90        100
ARRGVVAQAT AVATPAAKPA AKTSQYELFT LTTWLLKEEM KGTIDGELAT
       110        120        130        140        150
VISSVSLACK QIASLVNRAG ISNLTGVAGN QNVQGEDQKK LDVVSNEVFK
       160        170        180        190        200
NCLASCGRTG VIASEEEDQP VAVEETYSGN YIVVFDPLDG SSNIDAGISV
       210        220        230        240        250
GSIFGIYEPS EECPIDAMDD PQKMMEQCVM NVCQPGSRLK CAGYCLYSSS
       260        270        280        290        300
TIMVLTIGNG VFGFTLDPLV GEFVLTHPNV QIPEVGKIYS FNEGNYGLWD
       310        320        330        340        350
DSVKAYMDSL KDPKKWDGKP YSARYIGSLV GDFHRTLLYG GIYGYPGDAK
       360        370        380        390        400
NKNGKLRLLY ECAPMSFIAE QAGGLGSTGQ ERVLDVNPEK VHQRVPLFIG
       410
SKKEVEYLES FTKKH
```

Les séquences précédentes sont les séquences comprenant le peptide d'adressage au chloroplaste qui est retiré lors du clonage pour l'expression d'une protéine recombinante correspondant à la protéine mature présente dans le chloroplaste. La prédiction de la longueur du peptide d'adressage est réalisée *in silico* par ChloroP, TargetP et PredAlgo (Almagro Armenteros et al. 2019; Tardif et al. 2012).

4.2 EXPRESSION ET PURIFICATION DES PROTEINES RECOMBINANTES

Les différentes protéines recombinantes ont été exprimées dans les souches *Escherichia coli* BL21(DE3) ou *Escherichia coli* BL21(DE3) Rosetta-2 pLysS (Novagen Merck, Damstadt, Germany) (*cf.* Tableau 1). Ces souches ont été transformées en utilisant les différents plasmides listés en Tableau 1 et cultivées à 37°C dans les milieux LB ou 2YT (*cf.* Tableau 1) en présence de 150 $\mu g.ml^{-1}$ d'ampicilline jusqu'à atteindre une densité optique à 580 nm entre 0,4 et 0,6 correspondant à la phase de croissance exponentielle. La production de protéines recombinantes de ces cultures est induite par l'ajout de 0,2 $mmol.L^{-1}$ d'isopropyl-β-D-thiogalactopyranoside (IPTG) et une incubation à des températures de 15°C durant une nuit ou 27°C, 30°C et 37 °C durant 3 à 4 h en fonction de la protéine surexprimée (*cf.* Tableau 1). A la fin de la période d'induction, les cultures sont centrifugées à 4000 g pendant 20 minutes, le surnageant éliminé, les culots re-suspendus dans 30 ml de tampon A (20 $mmol.L^{-1}$ Tris-HCl pH=7,9, 100 $mmol.L^{-1}$ NaCl) par litre de culture et congelé à -20°C.

La lyse des cellules a été réalisée par deux méthodes différentes en fonction de la disponibilité des matériels : par sonication ou par pression avec un « *one shot cell disrupter* » (CellD, Daventry, Royaume-Uni), les différentes méthodes de lyse n'ayant pas montré de différences significatives pour deux lots de cultures de la même protéine pris pour comparaison. La lyse par sonication est réalisée par un cycle de trois fois 1 min de lyse à 10 % d'intensité et pulse de 1 sec / 1sec entrecoupée d'une minute de repos sur la glace. La lyse sous pression est réalisée à 20 kPSI. Une fois les cellules lysées, le reste des étapes de purification s'effectue à 4°C ou sur la glace sauf indications contraires. Un aliquote de 40 µl du lysat total est prélevé et conservé dans le but de vérifier sa composition via migration sur SDS-PAGE après ajout de 10 µl de tampon Laemmli 5X.

	CrRPI1	CrFBA3	CrSBPase	CrPGK	CrFBPase
Construction plasmidique	pET-3d-HIS-CrRPI	pET-3c-HIS-CrFBA3	pET-3c-HIS-CrSBPase	pET-3c-HIS-CrPGK1	pET-3c-HIS-CrFBPase
Souche de production	*E. coli* Rosetta-2 pLysS	*E. coli* Rosetta-2 pLysS	*E. coli* Rosetta-2 pLysS ou *E. coli* BL21 (DE3)	*E. coli* BL21 (DE3)	*E. coli* Rosetta-2 pLysS
Milieu	LB	2YT	2YT ou LB	LB	2YT
Température et durée d'induction	37°C 3-4h	15°C overnight	37°C 3-4h	37°C 3-4h	30°C 3-4h
Masse moléculaire théorique (kDa)	27,55	39,39	36,18	43,87	40,15
Coefficient d'extinction molaire ($M^{-1}.cm^{-1}$)	14 565	50 035	24 722	20 000	40 590
Durée et température de cristallisation	autour d'un an à 20°C	autour d'une semaine à 20°C	autour d'une semaine à 20°C	autour d'une semaine à 20°C	Pas de cristallisation
Conditions de cristallisation	3 mM Sulfate d'ammonium 20% glycérol	5% isopropanol 2 M Sulfate d'ammonium	100 mM Sodium HEPES pH 7.5, 2% PEG 400, 2 M sulfate d'ammonium	100 mM MES pH 5 20% PEG 6000	ø

Tableau 1 : Paramètres de production et de cristallisation des protéines CrRPI1, CrFBA3, CrSBPase, CrPGK, CrFBPase.

Le lysat cellulaire ainsi obtenu est ensuite centrifugé 20 min à 20000 g. Le surnageant est déposé, après prélèvement d'un aliquote de 40 µL, sur 2 mL en volume sec d'une résine NiNTA (Merck, Darmstadt, Allemagne) d'affinité pour les étiquettes hexahistidine. L'élution des protéines d'intérêt de cette colonne se fait par étapes à différentes concentrations d'imidazole dans des tampons composés du tampon A (20 $mmol.L^{-1}$ Tris-HCl pH=7,9, 100 $mmol.L^{-1}$ NaCl) complété par une concentration d'imidazole croissante. Les différentes étapes de lavage de la résine se composent de 10 mL de tampon A, 10 mL de tampon A + 10 $mmol.L^{-1}$ imidazole, 5 mL de tampon A + 50 $mmol.L^{-1}$ imidazole, 5 mL tampon A + 100 $mmol.L^{-1}$ imidazole, 5 mL tampon A + 200 $mmol.L^{-1}$ imidazole et 5 mL de tampon A + 500 $mmol.L^{-1}$ imidazole. A chaque étape de sortie de la résine, un aliquote de 40 µL est prélevé. La détermination des fractions dans lesquelles se trouve la protéine d'intérêt se fait par électrophorèse sur gel de 12% de polyacrylamide en conditions dénaturantes (SDS-PAGE), durant une

migration à 200 V pendant 45 à 60 min et coloration au bleu de Coomassie.

Après détermination des fractions contenant la protéine d'intérêt, et concentration par ultrafiltration sur amicon (Merck, Darmstadt, Allemagne) à un volume de 10 mL, les éluats sont injectés sur une colonne de chromatographie d'exclusion de taille Superdex 200 26/600 (Cytiva, Danaher, Washington D.C., USA) dans du tampon A. Après sélection des fractions susceptibles de contenir notre protéine d'intérêt en regardant le chromatogramme à d'absorbance à 280 nm en fonction du volume d'élution, des aliquotes de 40 µL de ces fractions sont prélevé et complété par 10 µL de tampon Laemmli 5x pour vérifier la présence et la pureté de la protéine sur SDS-PAGE. Les fractions sélectionnées sont concentrées par ultrafiltration sur amicon à 4000 g, jusqu'à obtention de la concentration désirée, généralement de 3 à 30 mg/mL. La concentration est calculée d'après l'absorbance à 280 nm sur un spectrophotomètre Nanodrop (ThermoFisher, Waltham, Etats-Unis) en utilisant le coefficient d'absorption molaire théorique de la protéine (ε) et sa masse molaire, calculé par l'outil ProtParam (Gasteiger et al. 2005) à partir de la séquence primaire de la protéine.

4.3 CRISTALLISATION DES PROTEINES

L'obtention de cristaux pour la détermination de structures par diffraction des rayons X a été réalisée en une ou deux étapes. Dans la première étape le criblage de conditions de cristallisation se fait sur des kits de cristallisation commerciaux (Qiagen, Venlo, Pays-Bas), les principaux kits utilisés sont les kits JCSG I, II, III et IV ainsi que les kits Classics 1 et 2. Chaque kit est composé de 96 conditions indépendantes de pH, force ionique, agent de précipitation, et additifs. Ces cribles ont été réalisés par la méthode de la goutte assise en utilisant le robot de pipetage Mosquito (STP Labtech, Melbourne, Royaume-Uni) sur des plaques 96 puits TTP IQ. Le volume des gouttes obtenues est de 200 nL avec un ratio 1/1 de solution de cristallisation issue du crible et de solution de protéines. Les gouttes de chaque condition sont scellées dans une enceinte à atmosphère isolée, avec un puits contenant 30 µL de la solution de cristallisation. Par diffusion de vapeur, le système tend à un équilibre où le volume de la goutte se

réduit, augmentant la concentration des protéines et de précipitants jusqu'à une éventuelle nucléation-croissance de monocristaux micrométriques. Si les cristaux obtenus avec cette méthode sont de qualité suffisante (taille, isolement, cristal non maclé, etc.) ceux-ci sont directement congelés dans l'azote liquide en solution cryo-protectante de 25 % de glycérol ou éthylène glycol, et testés sur les lignes de lumière du synchrotron SOLEIL.

Dans le cas où les cristaux obtenus durant les cribles ne sont pas de qualité suffisante, des étapes d'optimisation des cristaux ont été réalisées. Ces optimisations ont été réalisées avec un pipetage manuel, en utilisant la méthode de la goutte suspendue sur des plaques 24 puits. Les réservoirs des puits sont remplis avec 500 µL de solution de cristallisation identique à celle des conditions du crible ayant données les meilleurs cristaux ou s'approchant de celle-ci en modifiant les concentrations de précipitants ou le pH de la solution. Des gouttes d'un volume de 1 µL ou 2 µL, et d'un ratio 1/1 entre la solution de cristallisation et la solution contenant la protéine sont réalisées sur des lames en verre qui viennent refermer le puits scellé par de la graisse.

Toutes les plaques de cristallisation, cribles ou optimisations, ont été incubé à 20°C. Les durées de cristallisation diffèrent entres les protéines allant de 2-3 jours à 2-3 semaines voire plusieurs mois pour CrRPI1.

4.4 DETERMINATION DES MODELES DE STRUCTURES DES PROTEINES

Les cristaux sont soumis à des essais de diffraction sur les lignes PROXIMA 1 ou 2. Si le cristal est de qualité suffisante et diffracte les rayons X de manière satisfaisante, une collecte sur 360° des taches de diffraction est effectuée en prenant une image pour une rotation de 0.1° du cristal. Les 3600 images ainsi obtenues constituent un jeu de données qui est traité avec le logiciel XDSme pour l'indexation et l'intégration des donnés et l'attribution d'un groupe d'espace. Ces jeux de données ont été phasés avec PHASER, un logiciel de la suite PHENIX (Liebschner et al. 2019) par remplacement moléculaire en utilisant les modèles listés dans la table 2 de données cristallographiques.

Une fois les jeux de données phasés, les cartes de densité électronique sont utilisées pour affiner le modèle moléculaire par une série de va-et-vient entre affinage automatique via le logiciel REFINE de la suite PHENIX et un affinage manuel sur la version adaptée pour le système d'exploitation Windows du logiciel COOT (Emsley et al. 2010). Ces itérations successives ont pour but de déterminer un modèle de la protéine en accord avec la carte de densité électronique tout en respectant les paramètres stéréochimiques standards des liaisons (Figure 19).

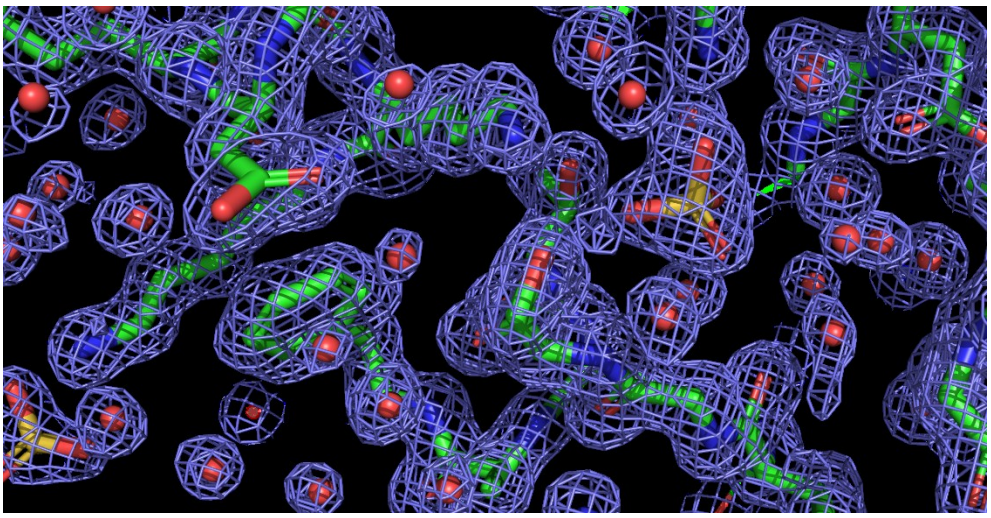

Figure 19 : Carte de densité électronique de CrRPI1, contourée à 1σ. La protéine est représentée en bâtonnet avec une coloration des atomes selon le code CPK à l'exception des atomes de carbone en verts.

Cet équilibre entre données théoriquement possible et données réelles peut prendre un certain temps, par exemple la résolution de SBPase la résolution de 3,1 Å a posé des problèmes par manque d'informations sur la position de certaines chaînes latérales de densité ininterprétable. L'inverse étant également vrai, pour RPI la haute résolution de 1,4 Å a permis le placement de centaines de molécules d'eau dans et autour de la protéine ce qui allonge considérablement le temps de traitement des données. L'évaluation de la qualité de ces modèles a ensuite été réalisée par les outils de validation de la base de données de structures des protéines (Protein Data Bank, PDB) (Berman et al. 2003). Ces outils m'ont permis de vérifier les paramètres stéréochimiques des liaisons (distance interatomique, contraintes

d’angles, etc.) présentes dans les modèles de protéines et les différentes caractéristiques théoriques des acides aminés du modèle (angles de Ramachandran, rotamères des chaînes latérales). A la fin de la modélisation, on obtient donc une série de statistiques évaluant la qualité du modèle, rapportées dans le tableau 2. Les représentations de structures dans les figures ont été faite avec le logiciel PYMOL (Schrödinger, New York, USA).

	CrRPI	CrFBA3	CrSBPase	CrSBPase red	CrPGK
Code PDB de déposition	7ZXT	7B2N	7B2O	7ZUV	7ZY7
Résolution (Å)	40.22-1.404 (1.454-1.404)	46.67-2.361 (2.445-2.361)	46.62-3.095 (3.206-3.095)	48.54-3.11 (3.221-3.11)	41.16-1.98 (2.051-1.98)
Groupe d'espace	P 1 2_1 1	C 1 2 1	P 2_1 2_1 2	P 1 2_1 1	C 1 2 1
Unité asymétrique (Å, °)	45.152 63.952 80.909 90-96.132-90	109.493 251.068 126.411 90-90.111-90	178.224 183.652 75.196 90-90-90	53.774 163.462 172.765 90-91.939-90	207.851 53.138 66.406 90-90.697-90
Nombre de réflexions totales	613155 (55349)	988770 (90253)	615155 (55989)	376091 (32376)	351724 (32656)
Nombre de réflexions uniques	89012 (8611)	138497 (13155)	45740 (4245)	53456 (5213)	50808 (4999)
Multiplicité	6.9 (6.4)	7.1 (6.9)	13.4 (12.9)	7.0 (6.2)	6.9 (6.5)
Complétion (%)	99.62 (96.48)	99.42 (94.42)	99.34 (94.20)	99.65 (97.17)	99.86 (98.94)
I/sigma(I) moyen	20.58 (1.24)	13.34 (1.46)	12.02 (1.72)	8.54 (1.30)	10.00 (1.23)
Wilson B-factor ($Å^2$)	21.45	40.19	64.82	68.45	31.59
R-merge	0.0519 (1.272)	0.2 (1.495)	0.495 (1.877)	0.2492 (1.502)	0.2101 (1.702)
R-meas	0.05611 (1.382)	0.2159 (1.617)	0.5144 (1.954)	0.2691 (1.64)	0.2273 (1.85)
R-pim	0.02114 (0.5327)	0.08067 (0.6089)	0.1386 (0.5343)	0.1009 (0.6477)	0.08589 (0.7164)
CC1/2	0.999 (0.382)	0.995 (0.566)	0.983 (0.623)	0.988 (0.479)	0.994 (0.368)
CC*	1 (0.744)	0.999 (0.85)	0.996 (0.876)	0.997 (0.805)	0.998 (0.733)
Réflexions usées dans l'affinement	88983 (8601)	138424 (13104)	45607 (4242)	53417 (5193)	50762 (4964)
Réflexions usées pour le R-free	2000 (194)	1984 (189)	1986 (183)	1983 (191)	1998 (199)
R-work	0.1594 (0.3457)	0.2025 (0.3002)	0.1942 (0.3071)	0.1963 (0.3239)	0.1800 (0.3274)
R-free	0.1774 (0.3813)	0.2500 (0.3513)	0.2390 (0.3482)	0.2328 (0.3740)	0.2250 (0.3629)
CC (work)	0.972 (0.730)	0.954 (0.775)	0.944 (0.788)	0.956 (0.726)	0.967 (0.746)
CC (free)	0.967 (0.836)	0.921 (0.643)	0.912 (0.649)	0.949 (0.596)	0.937 (0.617)
Nombre d'atomes non-hydrogène	4206	21451	14194	18714	6419
Macromolécules	3648	20317	14190	18704	5948
Ligands	47	146	Ø	10	15
Solvant	511	988	4	Ø	456
Acides aminés	474	2649	1859	2451	788
RMS (liaisons) (Å)	0.011	0.004	0.005	0.004	0.008
RMS (angles) (°)	1.18	0.63	0.75	0.73	0.87
Ramachandran favorisés (%)	99.79	96.28	94.26	94.80	97.69
Ramachandran autorisés (%)	0.21	3.34	5.52	4.70	2.31

Ramachandran aberrants (%)	0.00	0.38	0.22	0.50	0.00
Rotamères aberrants (%)	1.00	0.43	0.13	0.55	0.00
Clashscore	2.69	6.97	4.88	6.60	3.30
B-factor moyen (Å^2)	25.46	46.74	67	68.41	34.06
Macromolécules	23.78	46.76	67.01	68.40	33.60
Ligands	47.04	68.59	Ø	94.37	60.74
Solvant	35.49	43.19	49.59	Ø	39.16
Modèle de remplacement moléculaire	Modèle du serveur Robetta	Modèle du serveur Phyre2	Modèle du serveur Phyre2	7ZY7 (CrSBPase)	Modèle du serveur Alphafold

Tableau 2 : Statistiques de diffractions cristallographiques et d'affinement des modèles de CrRPI, CrFBA3, CrSBPase, CrSBPase partiellement réduite et CrPGK.

4.5 ANALYSES DE DIFFUSION DES RAYONS X AUX PETITS ANGLES

Afin d'estimer la masse des protéines en solution et calculer des enveloppes moléculaires de ces protéines, des mesures de diffusion des rayons X aux petits angles (SAXS pour *Small Angle X-rays Scattering*) couplées à une chromatographie d'exclusion de taille ont été réalisé sur CrRPI, CrFBA3, CrSBPase et CrPGK. Ces expériences ont toutes été réalisées sur la ligne de lumière SWING du synchrotron SOLEIL (Saint-Aubin, France). Le dispositif utilisé consiste en un injecteur automatique relié à une colonne BioSEC-3 300 (Agilent technologies, Santa Clara, CA, USA), les échantillons séparés dans la colonne sont alors élués dans le capillaire passant devant le faisceau de rayons X. Les rayons X diffusés au contact de la protéine vont frapper un détecteur Eiger X4M (Baden, Suisse) qui collecte l'intensité des rayons X à de petits angles de diffusion. Les données sont traitées avec la suite de logiciels ATSAS (Franke et al. 2017; Petoukhov et al. 2012) afin d'établir des courbes moyennes de l'intensité diffusée en fonction du vecteur de diffusion « s ». Ces courbes servent au calcul de rayons de gyration, de volumes, et de dimensions de l'objet. Les données étaient de qualité insuffisantes pour la modélisation d'enveloppes.

Des mesures de SEC-SAXS ont été effectuées sur des échantillons de 500 ng de CrRPI1 purifiée dans son tampon de purification (*cf.* partie précédente).

Pour CrFBA3, trois types d'essais ont été réalisés, une injection de 6,6 mg/ml de protéine pure puis des injections de la même quantité de protéine incubée préalablement au moins une demi-heure avec 10 $mmol.L^{-1}$ de DTT ou 10 $mmol.L^{-1}$ de DTTox.

Pour SBPase, neuf échantillons ont été injectés : 2,5 mg/ml de SBPase, la même quantité incubée avec 20 $mmol.L^{-1}$ de DTT et la même quantité incubée avec 20 $mmol.L^{-1}$ de DTT et 3 $mmol.L^{-1}$ de $MgCl_2$. Ces trois conditions étant triplées par trois lots différents de SBPase, des lots A, B et C représentant respectivement le début, le milieu et la fin du pic d'élution de SBPase sur Superose 200 après purification.

4.6 ISOLEMENT ET CARACTERISATION DES COMPLEXES DU CYCLE DE CALVIN-BENSON-BASSHAM PAR CHROMATOGRAPHIE ET WESTERN BLOT

Afin de déterminer la présence et la composition des potentiels complexes du cycle de Calvin-Benson-Bassham, des cultures de Chlamydomonas souche D66 ont été effectuées dans un milieu TAP (Tris Acétate Phosphate), avec agitation et une exposition lumineuse de 2000 lux jusqu'à atteindre une densité de cellules égale à $5*10^4$ cellules/mL. Ces cultures ont ensuite été centrifugées 10 minutes à 3000 g, le culot congelé à -20°C jusqu'à utilisation.

La lyse des cellules est effectuée par une re-suspension du culot dans un tampon contenant 20 $mmol.L^{-1}$ Tris-HCl pH=7,9, 100 $mmol.L^{-1}$ NaCl, 5 $mmol.L^{-1}$ L-cystéine, 500 $\mu mol.L^{-1}$ NADH, 1 $mmol.L^{-1}$ EDTA utilisé pour l'isolement du complexe GAPDH-CP12-PRK (communication personnelle du Dr. Sandrine Lanfranchi), suivi par 3 cycles de décongélation/congélation dans l'eau chaude et l'azote liquide. Toutes les étapes suivantes se déroulent à une température de 4°C ou dans la glace. Les extraits cellulaires totaux sont centrifugés à 100 000 g pendant 20 minutes. Le surnageant est injecté sur une colonne Superose 6 (Cytiva, Danaher, Washington DC, USA) sur appareil de chromatographie liquide rapide de protéine (FPLC, Äkta

Cytiva) dans le tampon de lyse. Les protéines éluées de la colonne sont réparties en fractions soit de 500 µl lors de l'utilisation de la colonne Superose 6 10/300 soit de 2 ml lors de l'utilisation de la colonne Superose 6 16/600. Des aliquotes de 40 µL ces fractions sont ensuite prélevés, adjoint de 10 µL tampon Laemmli 5X. 25 µL du mélange est ensuite déposé pour électrophorèse SDS-PAGE en vue de réalisation de western blots ciblant les différentes protéines du CBBC. Après SDS-PAGE, les protéines sont transférées sur membranes de nitrocellulose (GE healthcare, Chicago, IL, USA) dans un appareil de transfert semi-sec (GE healthcare, Chicago, IL, USA) et dans un tampon de transfert (100 $mmol.L^{-1}$ Tris, 192 $mmol.L^{-1}$ glycine, 0.1 % sodium dodécyl sulfate (SDS), 20 % éthanol) durant 45 min à un voltage de 15 V. La membrane est ensuite colorée au rouge Ponceau afin de vérifier le transfert des protéines. Un premier bain de blocage est réalisé dans un tampon TBS-Tween adjoint de 5 % de lait en poudre durant 2 h à température ambiante. Un second bain est réalisé dans un tampon TBS-tween adjoint d'un anticorps primaire ciblant la protéine du CBBC voulu à une dilution de 1/10000 durant 1 h à température ambiante ou sur la nuit à 4°C. Les anticorps utilisés ont été produits à partir de CrFBA3 recombinante dans des lapins par la société Genecust (Genecust, Boynes, France). Cette incubation est suivie de quatre lavages de 5 min dans du TBS-tween à température ambiante, puis d'un bain de TBS-tween contenant l'anticorps secondaire couplé à une péroxydase. Quatre lavages en TBS-tween de 5 min sont ensuite effectués avant la révélation de la membrane avec un kit de révélation « ECL prime western blotting detection reagent » (GE healthcare, Chicago, IL, USA) et une exposition dans un système de détection Chemidoc (Biorad, Hercules, Etats-Unis) durant une durée d'exposition optimale.

4.7 RESINE PHOSPHOGLYCERATE KINASE-CNBR-SEPHAROSE

Suite aux résultats obtenues par SEC et WB, une fixation de CrPGK sur résine de bromure de cyanogène (CNBr) couplé à une matrice solide sépharose (CNBr-sépharose, Sigma-Aldrich) suivi d'un chargement d'extraits de Chlamydomonas ont été réalisés. La résine va permettre la formation de liens covalents entre le bromure de cyanogène et les groupement amine des protéines pour les fixer à la phase stationnaire.

La première étape est l'activation de la résine selon le protocole suivant : ajout d'une quantité de résine déshydratée suffisante pour obtenir 1 mL de résine réhydratée avec une solution de 1 $mmol.L^{-1}$ HCl ; après réhydratation, la suite des étapes ainsi que les différents tampon sont à 4°C. La résine est lavée 15 fois par 1 mL de solution 1 $mmol.L^{-1}$ HCl pour laver la résine. Une fois la résine lavée, la solution de protéine à lier est déposée et incubée sur la nuit. Cette solution de protéines (ici 15 mg de CrPGK recombinante) a préalablement subi un traitement de protection des cystéines consistant en trente minutes d'incubation avec 10 $mmol.L^{-1}$ de DTNB puis une dialyse sur la nuit dans un tampon de couplage (100 $mmol.L^{-1}$ $NaHCO_3$ pH=8,3, 500 $mmol.L^{-1}$ NaCl). L'excès de protéine est lavé avec 5 fois 1 mL de tampon de couplage. Des aliquotes de tampon en sortie de colonne sont collectés pour vérification par l'absorbance à 280 nm la présence de protéines. Les groupements CNBr n'ayant pas réagi sont bloqués deux heures dans un tampon 100 $mmol.L^{-1}$ Tris HCl pH=7.9. Quatre lavages sont réalisés en alternant haut et bas pH avec, 3 fois 1 mL de tampon 100 $mmol.L^{-1}$ Tris HCl pH=7,9, 500 $mmol.L^{-1}$ NaCl et 3 fois 1 mL de tampon 10 $mmol.L^{-1}$ acétate pH=3, 500 $mmol.L^{-1}$ NaCl. Les cystéines sont déprotégées avec passage de 5 fois 1 mL de tampon 20 $mmol.L^{-1}$ Tris HCl pH=7,9, 100 $mmol.L^{-1}$ NaCl, 10 $mmol.L^{-1}$ DTT puis 5 fois 1 mL du même tampon sans DTT. La résine est ensuite prête pour le dépôt des extraits protéiques de Chlamydomonas.

Les extraits protéiques de Chlamydomonas sont préparés selon le même protocole que pour la caractérisation des complexes par SEC et western blot (*cf.* matériels et méthodes 4.6). Ces extraits sont incubés sur la résine pendant 2 heures avec agitation. Puis cette résine subit 5 lavages de 1 mL de tampon 20 $mmol.L^{-1}$ Tris HCl pH=7,9, 100 $mmol.L^{-1}$ NaCl, suivi de 5 élutions de 1 mL du même tampon supplémenté de 10 $mmol.L^{-1}$ DTT, puis 5 élutions d'un tampon 20 $mmol.L^{-1}$ Tris HCl pH=7,9, 2 $mol.L^{-1}$ NaCl. Pour chaque lavages et élutions un aliquote est prélevé et mélangé à du tampon Laemmli pour analyse par électrophorèse et western blots.

4.8 MICROSCOPIE ELECTRONIQUE

Les deux essais de microscopie électronique en coloration négative ont été réalisés en partenariat avec l'équipe Microscopie Moléculaire des Membranes de l'Institut Curie. Les grilles utilisées ont été fournies par l'ingénieure Aurélie Di Cicco, spécialiste den microscopie électronique. Ces grilles ont été chargés négativement sous vide avec un courant de 1 mA.

Le dépôt des protéines sur ces grilles chargées s'est déroulé de la manière suivante : dépôt de 3 µl de solution de protéines, 30 sec de séchage sur papier filtre Whatman, ajout d'une goutte de colorant (acétate d'uranyle), séchage immédiat sur papier filtre Whatman, ajout d'une goutte de colorant, attente une minute, sécher sur papier filtre Whatman puis à l'air libre. Les grilles sont ensuite prêtes pour la microscopie. L'appareil utilisé a été un Tecnai Spirit 80 kV (FEI, Hillsboro, OR, USA).

Trois concentrations de protéines ont été utilisées : 50, 25 et 2,5 µg/ml de CrFBPase recombinante purifiée. Deux temps de dépôt ont été fait pour la concentration de 2,5 µg/ml : 15 et 30 sec. Les conditions ayant données les meilleurs images pour envisager une résolution de structure en utilisant la cryo-microscopie électronique sur particules uniques sont un dépôt de 2,5 µg/ml de FBPase avec un temps de dépôt de 30 sec.

5 BIBLIOGRAPHIE

Almagro Armenteros JJ, Salvatore M, Emanuelsson O, Winther O, von Heijne G, Elofsson A, Nielsen H (2019) Detecting sequence signals in targeting peptides using deep learning. Life Sci Alliance 2 (5):e201900429. doi:10.26508/lsa.201900429

Andersson I, Backlund A (2008) Structure and function of Rubisco. Plant Physiology and Biochemistry 46 (3):275-291. doi:10.1016/j.plaphy.2008.01.001

Avilan L, Gontero B, Lebreton S, Ricard J (1997) Information Transfer in Multienzyme Complexes. 2. The Role of Arg64 of *Chlamydomonas reinhardtii* Phosphoribulokinase in the Information Transfer Between Glyceraldehydes-3-Phosphate Dehydrogenase and Phosphoribulokinase. European Journal of Biochemistry 250 (2):296-302. doi:10.1111/j.1432-1033.1997.0296a.x

Balsera M, Buchanan BB (2019) Evolution of the thioredoxin system as a step enabling adaptation to oxidative stress. Free Radic Biol Med 140:28-35. doi:10.1016/j.freeradbiomed.2019.03.003

Balsera M, Uberegui E, Schürmann P, Buchanan BB (2014) Evolutionary development of redox regulation in chloroplasts. Antioxid Redox Signal 21 (9):1327-1355. doi:10.1089/ars.2013.5817

Bar-On YM, Milo R (2019) The global mass and average rate of rubisco. Proceedings of the National Academy of Sciences of the United States of America 116 (10):4738-4743. doi:10.1073/pnas.1816654116

Barrett J, Girr P, Mackinder LCM (2021) Pyrenoids: CO(2)-fixing phase separated liquid organelles. Biochim Biophys Acta Mol Cell Res 1868 (5):118949. doi:10.1016/j.bbamcr.2021.118949

Bassham JA, Benson AA, Kay LD, Harris AZ, Wilson AT, Calvin M (1954) The Path of Carbon in Photosynthesis. XXI. The Cyclic Regeneration of Carbon Dioxide Acceptor 1 Journal of the American Chemical Society 76 (7):1760-1770. doi:10.1021/ja01636a012

Benson AA, Bassham JA, Calvin M, Hall AG, Hirsch H, Kawaguchi S, Lynch V, Tolbert NE (1952) The Path of Carbon in

Photosynthesis, XV. Ribulose andSedoheptulose. Office of Scientific and Technical Information (OSTI). doi:10.2172/915054
Berman H, Henrick K, Nakamura H (2003) Announcing the worldwide Protein Data Bank. Nature Structural & Molecular Biology 10 (12):980-980. doi:10.1038/nsb1203-980
Bracher A, Whitney SM, Hartl FU, Hayer-Hartl M (2017) Biogenesis and Metabolic Maintenance of Rubisco. Annual Review of Plant Biology 68 (1):29-60. doi:10.1146/annurev-arplant-043015-111633
Buchanan BB, Holmgren A, Jacquot JP, Scheibe R (2012) Fifty years in the thioredoxin field and a bountiful harvest. Biochim Biophys Acta 1820 (11):1822-1829. doi:10.1016/j.bbagen.2012.07.006
Burgess SJ, Tamburic B, Zemichael F, Hellgardt K, Nixon PJ (2011) Solar-driven hydrogen production in green algae. Adv Appl Microbiol 75:71-110. doi:10.1016/b978-0-12-387046-9.00004-9
Cejudo FJ, Ojeda V, Delgado-Requerey V, González M, Pérez-Ruiz JM (2019) Chloroplast Redox Regulatory Mechanisms in Plant Adaptation to Light and Darkness. Front Plant Sci 10:380. doi:10.3389/fpls.2019.00380
Chardot T, Meunier JC (1991) Properties of oxidized and reduced spinach (*Spinacia oleracea*) chloroplast fructose-1,6-bisphosphatase activated by various agents. Biochemical Journal 278 (3):787-791. doi:10.1042/bj2780787
Chen J, Wu H, Zhang W, Mu W (2020) Ribose-5-phosphate isomerases: characteristics, structural features, and applications. Appl Microbiol Biotechnol 104 (15):6429-6441. doi:10.1007/s00253-020-10735-4
Chiadmi M (1999) Redox signalling in the chloroplast: structure of oxidized pea fructose-1,6-bisphosphate phosphatase. The EMBO Journal 18 (23):6809-6815. doi:10.1093/emboj/18.23.6809
Clasper S, Easterby JS, Powls R (1991) Properties to two high-molecular-mass forms of glyceraldehyde-3-phosphate dehydrogenase from spinach leaf, one of which also possesses latent phosphoribulokinase activity. European Journal of Biochemistry 202 (3):1239-1246. doi:10.1111/j.1432-

1033.1991.tb16496.x
Craig RJ, Gallaher SD, Shu S, Salomé P, Jenkins JW, Blaby-Haas CE, Purvine SO, O'Donnell S, Barry K, Grimwood J, Strenkert D, Kropat J, Daum C, Yoshinaga Y, Goodstein DM, Vallon O, Schmutz J, Merchant SS (2022) The Chlamydomonas Genome Project, version 6: reference assemblies for mating type plus and minus strains reveal extensive structural mutation in the laboratory. bioRxiv:2022.2006.2016.496473. doi:10.1101/2022.06.16.496473
Dalby A, Dauter Z, Littlechild JA (1999) Crystal structure of human muscle aldolase complexed with fructose 1,6-bisphosphate: mechanistic implications. Protein Sci 8 (2):291-297. doi:10.1110/ps.8.2.291
Emsley P, Lohkamp B, Scott WG, Cowtan K (2010) Features and development of Coot. Acta Crystallogr D Biol Crystallogr 66 (Pt 4):486-501. doi:10.1107/s0907444910007493
Engilberge S, Riobé F, Di Pietro S, Lassalle L, Coquelle N, Arnaud CA, Pitrat D, Mulatier JC, Madern D, Breyton C, Maury O, Girard E (2017) Crystallophore: a versatile lanthanide complex for protein crystallography combining nucleating effects, phasing properties, and luminescence. Chem Sci 8 (9):5909-5917. doi:10.1039/c7sc00758b
Erales J, Avilan L, Lebreton S, Gontero B (2008) Exploring CP12 binding proteins revealed aldolase as a new partner for the phosphoribulokinase/glyceraldehyde 3-phosphate dehydrogenase/CP12 complex - purification and kinetic characterization of this enzyme from *Chlamydomonas reinhardtii*. FEBS Journal 275 (6):1248-1259. doi:10.1111/j.1742-4658.2008.06284.x
Erales J, Mekhalfi M, Woudstra M, Gontero B (2011) Molecular Mechanism of NADPH-Glyceraldehyde-3-phosphate Dehydrogenase Regulation through the C-Terminus of CP12 in *Chlamydomonas reinhardtii*. Biochemistry 50 (14):2881-2888. doi:10.1021/bi1020259
Fermani S, Trivelli X, Sparla F, Thumiger A, Calvaresi M, Marri L, Falini G, Zerbetto F, Trost P (2012) Conformational Selection and Folding-upon-binding of Intrinsically Disordered Protein CP12 Regulate Photosynthetic Enzymes Assembly*. Journal of

Biological Chemistry 287 (25):21372-21383. doi:https://doi.org/10.1074/jbc.M112.350355
Field CB, Behrenfeld MJ, Randerson JT, Falkowski P (1998) Primary Production of the Biosphere: Integrating Terrestrial and Oceanic Components. Science 281 (5374):237-240. doi:10.1126/science.281.5374.237
Finkemeier I, Laxa M, Miguet L, Howden AJM, Sweetlove LJ (2011) Proteins of Diverse Function and Subcellular Location Are Lysine Acetylated in Arabidopsis. Plant Physiology 155 (4):1779-1790. doi:10.1104/pp.110.171595
Franke D, Petoukhov MV, Konarev PV, Panjkovich A, Tuukkanen A, Mertens HDT, Kikhney AG, Hajizadeh NR, Franklin JM, Jeffries CM, Svergun DI (2017) ATSAS 2.8: a comprehensive data analysis suite for small-angle scattering from macromolecular solutions. Journal of Applied Crystallography 50 (4):1212-1225. doi:10.1107/s1600576717007786
García-Murria MJ, Sudhani HPK, Marín-Navarro J, Sánchez Del Pino MM, Moreno J (2018) Dissecting the individual contribution of conserved cysteines to the redox regulation of RubisCO. Photosynth Res 137 (2):251-262. doi:10.1007/s11120-018-0497-9
Gardberg A, Abendroth J, Bhandari J, Sankaran B, Staker B (2011a) Structure of fructose bisphosphate aldolase from *Bartonella henselae* bound to fructose 1,6-bisphosphate. Acta Crystallogr Sect F Struct Biol Cryst Commun 67 (Pt 9):1051-1054. doi:10.1107/s174430911101894x
Gardberg A, Sankaran B, Davies D, Bhandari J, Staker B, Stewart L (2011b) Structure of fructose bisphosphate aldolase from *Encephalitozoon cuniculi*. Acta Crystallogr Sect F Struct Biol Cryst Commun 67 (Pt 9):1055-1059. doi:10.1107/s1744309111021841
Gasteiger E, Hoogland C, Gattiker A, Durand S, Wilkins MR, Appel RD, Bairoch A (2005) Protein identification and analysis tools on the ExPASy server. The Proteomics Protocols Handbook, Humana Press:571-607
Genkov T, Spreitzer RJ (2009) Highly Conserved Small Subunit Residues Influence Rubisco Large Subunit Catalysis. Journal of Biological Chemistry 284 (44):30105-30112.

doi:10.1074/jbc.m109.044081
Giudici-Orticoni M-T, Buc J, Bidaud M, Ricard J (1990) Thermodynamics of information transfer between subunits in oligomeric enzymes and kinetic cooperativity. 3. Information transfer between the subunits of chloroplast fructose bisphosphatase. European Journal of Biochemistry 194 (2):483-490. doi:10.1111/j.1432-1033.1990.tb15642.x
Gontero B, Cardenas ML, Ricard J (1988) A functional five-enzyme complex of chloroplasts involved in the Calvin cycle. European Journal of Biochemistry 173 (2):437-443. doi:10.1111/j.1432-1033.1988.tb14018.x
Gontero B, Mulliert G, Rault M, Giudici-Orticoni M-T, Ricard J (1993) Structural and functional properties of a multi-enzyme complex from spinach chloroplasts. 2. Modulation of the kinetic properties of enzymes in the aggregated state. European Journal of Biochemistry 217 (3):1075-1082. doi:10.1111/j.1432-1033.1993.tb18339.x
González-Mondragón E, Zubillaga RA, Saavedra E, Chánez-Cárdenas ME, Pérez-Montfort R, Hernández-Arana A (2004) Conserved cysteine 126 in triosephosphate isomerase is required not for enzymatic activity but for proper folding and stability. Biochemistry 43 (11):3255-3263. doi:10.1021/bi036077s
Groben R, Kaloudas D, Raines CA, Offmann B, Maberly SC, Gontero B (2010) Comparative sequence analysis of CP12, a small protein involved in the formation of a Calvin cycle complex in photosynthetic organisms. Photosynth Res 103 (3):183-194. doi:10.1007/s11120-010-9542-z
Gurrieri L, Del Giudice A, Demitri N, Falini G, Pavel NV, Zaffagnini M, Polentarutti M, Crozet P, Marchand CH, Henri J, Trost P, Lemaire SD, Sparla F, Fermani S (2019) Arabidopsis and Chlamydomonas phosphoribulokinase crystal structures complete the redox structural proteome of the Calvin-Benson cycle. Proc Natl Acad Sci U S A 116 (16):8048-8053. doi:10.1073/pnas.1820639116
Gurrieri L, Fermani S, Zaffagnini M, Sparla F, Trost P (2021) Calvin–Benson cycle regulation is getting complex. Trends in Plant Science 26 (9):898-912. doi:https://doi.org/10.1016/j.tplants.2021.03.008

Gütle DD, Roret T, Müller SJ, Couturier J, Lemaire SD, Hecker A, Dhalleine T, Buchanan BB, Reski R, Einsle O, Jacquot J-P (2016) Chloroplast FBPase and SBPase are thioredoxin-linked enzymes with similar architecture but different evolutionary histories. Proceedings of the National Academy of Sciences 113 (24):6779-6784. doi:10.1073/pnas.1606241113

He S, Chou HT, Matthies D, Wunder T, Meyer MT, Atkinson N, Martinez-Sanchez A, Jeffrey PD, Port SA, Patena W, He G, Chen VK, Hughson FM, McCormick AJ, Mueller-Cajar O, Engel BD, Yu Z, Jonikas MC (2020) The structural basis of Rubisco phase separation in the pyrenoid. Nat Plants 6 (12):1480-1490. doi:10.1038/s41477-020-00811-y

Holmgren A (1968) Thioredoxin. 6. The amino acid sequence of the protein from *escherichia coli* B. Eur J Biochem 6 (4):475-484. doi:10.1111/j.1432-1033.1968.tb00470.x

Holmgren A, Buchanan BB, Wolosiuk RA (1977) Photosynthetic regulatory protein from rabbit liver is identical with thioredoxin. FEBS Lett 82 (2):351-354. doi:10.1016/0014-5793(77)80619-4

Hosur MV, Sainis JK, Kannan KK (1993) Crystallization and X-ray analysis of a multienzyme complex containing RUBISCO and RuBP. J Mol Biol 234 (4):1274-1278. doi:10.1006/jmbi.1993.1681

Houtz RL, Magnani R, Nayak NR, Dirk LMA (2007) Co- and post-translational modifications in Rubisco: unanswered questions. Journal of Experimental Botany 59 (7):1635-1645. doi:10.1093/jxb/erm360

Huppe HC, Buchanan BB (1989) Activation of a Chloroplast Type of Fructose Bisphosphatase from *Chlamydomonas reinhardtii* by Light-Mediated Agents. Zeitschrift für Naturforschung C 44 (5-6):487-494. doi:10.1515/znc-1989-5-624

Ishijima S, Uchibori A, Takagi H, Maki R, Ohnishi M (2003) Light-induced increase in free Mg2+ concentration in spinach chloroplasts: measurement of free Mg2+ by using a fluorescent probe and necessity of stromal alkalinization. Arch Biochem Biophys 412 (1):126-132. doi:10.1016/s0003-9861(03)00038-9

Jacquot JP, Lopez-Jaramillo J, Chueca A, Cherfils J, Lemaire S,

Chedozeau B, Miginiac-Maslow M, Decottignies P, Wolosiuk R, Lopez-Gorge J (1995) High-level expression of recombinant pea chloroplast fructose-1,6-bisphosphatase and mutagenesis of its regulatory site. Eur J Biochem 229 (3):675-681. doi:10.1111/j.1432-1033.1995.tb20513.x

Jacquot JP, Lopez-Jaramillo J, Miginiac-Maslow M, Lemaire S, Cherfils J, Chueca A, Lopez-Gorge J (1997) Cysteine-153 is required for redox regulation of pea chloroplast fructose-1,6-bisphosphatase. FEBS Lett 401 (2-3):143-147. doi:10.1016/s0014-5793(96)01459-7

Jelakovic S, Kopriva S, Süss KH, Schulz GE (2003) Structure and catalytic mechanism of the cytosolic D-ribulose-5-phosphate 3-epimerase from rice. J Mol Biol 326 (1):127-135. doi:10.1016/s0022-2836(02)01374-8

Johnson MP (2016) Photosynthesis. Essays in Biochemistry 60 (3):255-273. doi:10.1042/ebc20160016

Johnson X, Alric J (2013) Central Carbon Metabolism and Electron Transport in *Chlamydomonas reinhardtii*: Metabolic Constraints for Carbon Partitioning between Oil and Starch. Eukaryotic Cell 12 (6):776-793. doi:10.1128/ec.00318-12

Joint IR, Morris I, Fuller RC (1972a) Possible regulatory characteristics of the fructose diphosphatase--phosphoribulokinase complex from *Rhodospirillum rubrum*. Biochim Biophys Acta 276 (1):333-337. doi:10.1016/0005-2744(72)90037-x

Joint IR, Morris I, Fuller RC (1972b) Purification of a complex of alkaline fructose 1,6-bisphosphatase and phosphoribulokinase from *Rhodospirillum rubrum*. J Biol Chem 247 (15):4833-4838

Jordan DB, Ogren WL (1981) Species variation in the specificity of ribulose biphosphate carboxylase/oxygenase. Nature 291 (5815):513-515. doi:10.1038/291513a0

Keech O, Gardeström P, Kleczkowski LA, Rouhier N (2017) The redox control of photorespiration: from biochemical and physiological aspects to biotechnological considerations. Plant, Cell & Environment 40 (4):553-569. doi:10.1111/pce.12713

Kitano K, Maeda N, Fukui T, Atomi H, Imanaka T, Miki K (2001) Crystal structure of a novel-type archaeal rubisco with pentagonal symmetry. Structure 9 (6):473-481. doi:10.1016/s0969-

2126(01)00608-6
Klein U (1986) Compartmentation of glycolysis and of the oxidative pentose-phosphate pathway in *Chlamydomonas reinhardii*. Planta 167 (1):81-86. doi:10.1007/BF00446372
Kornberg MD, Sen N, Hara MR, Juluri KR, Nguyen JVK, Snowman AM, Law L, Hester LD, Snyder SH (2010) GAPDH mediates nitrosylation of nuclear proteins. Nature Cell Biology 12 (11):1094-1100. doi:10.1038/ncb2114
Kruger NJ, von Schaewen A (2003) The oxidative pentose phosphate pathway: structure and organisation. Current Opinion in Plant Biology 6 (3):236-246. doi:https://doi.org/10.1016/S1369-5266(03)00039-6
Küken A, Sommer F, Yaneva-Roder L, Mackinder LC, Höhne M, Geimer S, Jonikas MC, Schroda M, Stitt M, Nikoloski Z, Mettler-Altmann T (2018) Effects of microcompartmentation on flux distribution and metabolic pools in *Chlamydomonas reinhardtii* chloroplasts. eLife 7. doi:10.7554/elife.37960
Lafrance-Vanasse J, Sygusch J (2007) Carboxy-terminus recruitment induced by substrate binding in eukaryotic fructose bis-phosphate aldolases. Biochemistry 46 (33):9533-9540. doi:10.1021/bi700615r
Lam GP, Vermuë MH, Eppink MHM, Wijffels RH, van den Berg C (2018) Multi-Product Microalgae Biorefineries: From Concept Towards Reality. Trends Biotechnol 36 (2):216-227. doi:10.1016/j.tibtech.2017.10.011
Landau M, Mayrose I, Rosenberg Y, Glaser F, Martz E, Pupko T, Ben-Tal N (2005) ConSurf 2005: the projection of evolutionary conservation scores of residues on protein structures. Nucleic Acids Research 33 (suppl_2):W299-W302. doi:10.1093/nar/gki370
Launay H, Barré P, Puppo C, Manneville S, Gontero B, Receveur-Bréchot V (2016) Absence of residual structure in the intrinsically disordered regulatory protein CP12 in its reduced state. Biochemical and Biophysical Research Communications 477 (1):20-26. doi:https://doi.org/10.1016/j.bbrc.2016.06.014
Launay H, Barré P, Puppo C, Zhang Y, Maneville S, Gontero B, Receveur-Bréchot V (2018) Cryptic Disorder Out of Disorder: Encounter between Conditionally Disordered CP12 and

Glyceraldehyde-3-Phosphate Dehydrogenase. J Mol Biol 430 (8):1218-1234. doi:10.1016/j.jmb.2018.02.020
Le Moigne T, Boisset ND, de Carpentier F, Crozet P, Danon A, Henri J, Marchand CH, Lemaire SD, Johnson X (2022a) Photoproduction of reducing power and the Calvin-Benson Cycle. In: Grossman A, Wollman F-A (eds) The Chlamydomonas Sourcebook Volume 2: Organellar and Metabolic Processes, vol 2. 3rd edition edn. ELSEVIER,
Le Moigne T, Crozet P, Lemaire SD, Henri J (2020) High-Resolution Crystal Structure of Chloroplastic Ribose-5-Phosphate Isomerase from *Chlamydomonas reinhardtii*-An Enzyme Involved in the Photosynthetic Calvin-Benson Cycle. Int J Mol Sci 21 (20). doi:10.3390/ijms21207787
Le Moigne T, Sarti E, Nourisson A, Zaffagnini M, Carbone A, Lemaire SD, Henri J (2022b) Crystal structure of chloroplast fructose-1,6-bisphosphate aldolase from the green alga *Chlamydomonas reinhardtii*. Journal of Structural Biology 214 (3):107873. doi:https://doi.org/10.1016/j.jsb.2022.107873
Lemaire SD, Guillon B, Le Maréchal P, Keryer E, Miginiac-Maslow M, Decottignies P (2004) New thioredoxin targets in the unicellular photosynthetic eukaryote *Chlamydomonas reinhardtii*. Proc Natl Acad Sci U S A 101 (19):7475-7480. doi:10.1073/pnas.0402221101
Levine RP (1960) GENETIC CONTROL OF PHOTOSYNTHESIS IN *CHLAMYDOMONAS REINHARDI*. Proceedings of the National Academy of Sciences 46 (7):972-978. doi:10.1073/pnas.46.7.972
Liebschner D, Afonine PV, Baker ML, Bunkóczi G, Chen VB, Croll TI, Hintze B, Hung LW, Jain S, McCoy AJ, Moriarty NW, Oeffner RD, Poon BK, Prisant MG, Read RJ, Richardson JS, Richardson DC, Sammito MD, Sobolev OV, Stockwell DH, Terwilliger TC, Urzhumtsev AG, Videau LL, Williams CJ, Adams PD (2019) Macromolecular structure determination using X-rays, neutrons and electrons: recent developments in Phenix. Acta Crystallogr D Struct Biol 75 (Pt 10):861-877. doi:10.1107/s2059798319011471
López-Castillo LM, Jiménez-Sandoval P, Baruch-Torres N, Trasviña-Arenas CH, Díaz-Quezada C, Lara-González S, Winkler R,

Brieba LG (2016) Structural Basis for Redox Regulation of Cytoplasmic and Chloroplastic Triosephosphate Isomerases from *Arabidopsis thaliana*. Front Plant Sci 7:1817. doi:10.3389/fpls.2016.01817

Mackinder LC, Meyer MT, Mettler-Altmann T, Chen VK, Mitchell MC, Caspari O, Freeman Rosenzweig ES, Pallesen L, Reeves G, Itakura A, Roth R, Sommer F, Geimer S, Mühlhaus T, Schroda M, Goodenough U, Stitt M, Griffiths H, Jonikas MC (2016) A repeat protein links Rubisco to form the eukaryotic carbon-concentrating organelle. Proc Natl Acad Sci U S A 113 (21):5958-5963. doi:10.1073/pnas.1522866113

Mackinder LCM, Chen C, Leib RD, Patena W, Blum SR, Rodman M, Ramundo S, Adams CM, Jonikas MC (2017) A Spatial Interactome Reveals the Protein Organization of the Algal CO(2)-Concentrating Mechanism. Cell 171 (1):133-147.e114. doi:10.1016/j.cell.2017.08.044

Maes D, Zeelen JP, Thanki N, Beaucamp N, Alvarez M, Thi MH, Backmann J, Martial JA, Wyns L, Jaenicke R, Wierenga RK (1999) The crystal structure of triosephosphate isomerase (TIM) from *Thermotoga maritima*: a comparative thermostability structural analysis of ten different TIM structures. Proteins 37 (3):441-453

Marri L, Zaffagnini M, Collin V, Issakidis-Bourguet E, Lemaire SD, Pupillo P, Sparla F, Miginiac-Maslow M, Trost P (2009) Prompt and Easy Activation by Specific Thioredoxins of Calvin Cycle Enzymes of *Arabidopsis thaliana* Associated in the GAPDH/CP12/PRK Supramolecular Complex. Molecular Plant 2 (2):259-269. doi:10.1093/mp/ssn061

Mattioli EJ, Rossi J, Meloni M, De Mia M, Marchand CH, Tagliani A, Fanti S, Falini G, Trost P, Lemaire SD, Fermani S, Calvaresi M, Zaffagnini M (2022) Structural snapshots of nitrosoglutathione binding and reactivity underlying S-nitrosylation of photosynthetic GAPDH. Redox Biology 54:102387. doi:https://doi.org/10.1016/j.redox.2022.102387

McConnell EW, Werth EG, Hicks LM (2018) The phosphorylated redox proteome of *Chlamydomonas reinhardtii*: Revealing novel means for regulation of protein structure and function. Redox Biol 17:35-46. doi:10.1016/j.redox.2018.04.003

McFarlane CR, Shah NR, Kabasakal BV, Echeverria B, Cotton CAR, Bubeck D, Murray JW (2019) Structural basis of light-induced redox regulation in the Calvin-Benson cycle in cyanobacteria. Proceedings of the National Academy of Sciences 116 (42):20984-20990. doi:doi:10.1073/pnas.1906722116

Mendiola L, Akazawa T (1964) Partial Purification and the Enzymatic Nature of Fraction I Protein of Rice Leaves*. Biochemistry 3 (2):174-179. doi:10.1021/bi00890a006

Merchant SS, Prochnik SE, Vallon O, Harris EH, Karpowicz SJ, Witman GB, Terry A, Salamov A, Fritz-Laylin LK, Maréchal-Drouard L, Marshall WF, Qu LH, Nelson DR, Sanderfoot AA, Spalding MH, Kapitonov VV, Ren Q, Ferris P, Lindquist E, Shapiro H, Lucas SM, Grimwood J, Schmutz J, Cardol P, Cerutti H, Chanfreau G, Chen CL, Cognat V, Croft MT, Dent R, Dutcher S, Fernández E, Fukuzawa H, González-Ballester D, González-Halphen D, Hallmann A, Hanikenne M, Hippler M, Inwood W, Jabbari K, Kalanon M, Kuras R, Lefebvre PA, Lemaire SD, Lobanov AV, Lohr M, Manuell A, Meier I, Mets L, Mittag M, Mittelmeier T, Moroney JV, Moseley J, Napoli C, Nedelcu AM, Niyogi K, Novoselov SV, Paulsen IT, Pazour G, Purton S, Ral JP, Riaño-Pachón DM, Riekhof W, Rymarquis L, Schroda M, Stern D, Umen J, Willows R, Wilson N, Zimmer SL, Allmer J, Balk J, Bisova K, Chen CJ, Elias M, Gendler K, Hauser C, Lamb MR, Ledford H, Long JC, Minagawa J, Page MD, Pan J, Pootakham W, Roje S, Rose A, Stahlberg E, Terauchi AM, Yang P, Ball S, Bowler C, Dieckmann CL, Gladyshev VN, Green P, Jorgensen R, Mayfield S, Mueller-Roeber B, Rajamani S, Sayre RT, Brokstein P, Dubchak I, Goodstein D, Hornick L, Huang YW, Jhaveri J, Luo Y, Martínez D, Ngau WC, Otillar B, Poliakov A, Porter A, Szajkowski L, Werner G, Zhou K, Grigoriev IV, Rokhsar DS, Grossman AR (2007) The Chlamydomonas genome reveals the evolution of key animal and plant functions. Science 318 (5848):245-250. doi:10.1126/science.1143609

Mettler T, Mühlhaus T, Hemme D, Schöttler MA, Rupprecht J, Idoine A, Veyel D, Pal SK, Yaneva-Roder L, Winck FV, Sommer F, Vosloh D, Seiwert B, Erban A, Burgos A, Arvidsson S, Schönfelder S, Arnold A, Günther M, Krause U, Lohse M, Kopka J, Nikoloski Z, Mueller-Roeber B, Willmitzer L, Bock R, Schroda

M, Stitt M (2014) Systems Analysis of the Response of Photosynthesis, Metabolism, and Growth to an Increase in Irradiance in the Photosynthetic Model Organism *Chlamydomonas reinhardtii*. Plant Cell 26 (6):2310-2350. doi:10.1105/tpc.114.124537

Meyer MT, Whittaker C, Griffiths H (2017) The algal pyrenoid: key unanswered questions. Journal of Experimental Botany 68 (14):3739-3749. doi:10.1093/jxb/erx178

Michelet L, Zaffagnini M, Massot V, Keryer E, Vanacker H, Miginiac-Maslow M, Issakidis-Bourguet E, Lemaire SD (2006) Thioredoxins, glutaredoxins, and glutathionylation: new crosstalks to explore. Photosynth Res 89 (2-3):225-245. doi:10.1007/s11120-006-9096-2

Michelet L, Zaffagnini M, Morisse S, Sparla F, Pérez-Pérez ME, Francia F, Danon A, Marchand CH, Fermani S, Trost P, Lemaire SD (2013) Redox regulation of the Calvin-Benson cycle: something old, something new. Frontiers in plant science 4:470-470. doi:10.3389/fpls.2013.00470

Michelet L, Zaffagnini M, Vanacker H, Le Maréchal P, Marchand C, Schroda M, Lemaire SD, Decottignies P (2008) In Vivo Targets of S-Thiolation in *Chlamydomonas reinhardtii*. Journal of Biological Chemistry 283 (31):21571-21578. doi:10.1074/jbc.m802331200

Mininno M, Brugière S, Pautre V, Gilgen A, Ma S, Ferro M, Tardif M, Alban C, Ravanel S (2012) Characterization of Chloroplastic Fructose 1,6-Bisphosphate Aldolases as Lysine-methylated Proteins in Plants. Journal of Biological Chemistry 287 (25):21034-21044. doi:10.1074/jbc.m112.359976

Morisse S, Michelet L, Bedhomme M, Marchand CH, Calvaresi M, Trost P, Fermani S, Zaffagnini M, Lemaire SD (2014a) Thioredoxin-dependent Redox Regulation of Chloroplastic Phosphoglycerate Kinase from *Chlamydomonas reinhardtii*. Journal of Biological Chemistry 289 (43):30012-30024. doi:10.1074/jbc.m114.597997

Morisse S, Zaffagnini M, Gao X-H, Lemaire SD, Marchand CH (2014b) Insight into protein S-nitrosylation in *Chlamydomonas reinhardtii*. Antioxid Redox Signal 21 (9):1271-1284. doi:10.1089/ars.2013.5632

Nicholson S, Easterby JS, Powls R (1987) Properties of a multimeric protein complex from chloroplasts possessing potential activities of NADPH-dependent glyceraldehyde-3-phosphate dehydrogenase and phosphoribulokinase. European Journal of Biochemistry 162 (2):423-431. doi:10.1111/j.1432-1033.1987.tb10619.x

Nishizawa AN, Buchanan BB (1981) Enzyme regulation in C4 photosynthesis. Purification and properties of thioredoxin-linked fructose bisphosphatase and sedoheptulose bisphosphatase from corn leaves. J Biol Chem 256 (12):6119-6126

Okegawa Y, Motohashi K (2015) Chloroplastic thioredoxin *m* functions as a major regulator of Calvin cycle enzymes during photosynthesis *in vivo*. The Plant Journal 84 (5):900-913. doi:10.1111/tpj.13049

Pasquini M, Fermani S, Tedesco D, Sciabolini C, Crozet P, Naldi M, Henri J, Vothknecht U, Bertucci C, Lemaire SD, Zaffagnini M, Francia F (2017) Structural basis for the magnesium-dependent activation of transketolase from *Chlamydomonas reinhardtii*. Biochimica et Biophysica Acta (BBA) - General Subjects 1861 (8):2132-2145. doi:10.1016/j.bbagen.2017.05.021

Pérez-Pérez ME, Mauriès A, Maes A, Tourasse NJ, Hamon M, Lemaire SD, Marchand CH (2017) The Deep Thioredoxome in *Chlamydomonas reinhardtii*: New Insights into Redox Regulation. Molecular Plant 10 (8):1107-1125. doi:10.1016/j.molp.2017.07.009

Petoukhov MV, Franke D, Shkumatov AV, Tria G, Kikhney AG, Gajda M, Gorba C, Mertens HDT, Konarev PV, Svergun DI (2012) New developments in theATSASprogram package for small-angle scattering data analysis. Journal of Applied Crystallography 45 (2):342-350. doi:10.1107/s0021889812007662

Pfannschmidt T, Yang C (2012) The hidden function of photosynthesis: a sensing system for environmental conditions that regulates plant acclimation responses. Protoplasma 249 Suppl 2:S125-136. doi:10.1007/s00709-012-0398-2

Portis AR, Heldt HW (1976) Light-dependent changes of the Mg2+ concentration in the stroma in relation to the Mg2+

dependency of CO2 fixation in intact chloroplasts. Biochimica et Biophysica Acta (BBA) - Bioenergetics 449 (3):434-446. doi:https://doi.org/10.1016/0005-2728(76)90154-7
Raines CA (2022) Improving plant productivity by re-tuning the regeneration of RuBP in the Calvin Benson Bassham Cycle. New Phytologist. doi:10.1111/nph.18394
Rault M, Giudici-Orticoni M-T, Gontero B, Ricard J (1993) Structural and functional properties of a multi-enzyme complex from spinach chloroplasts. 1. Stoichiometry of the polypeptide chains. European Journal of Biochemistry 217 (3):1065-1073. doi:10.1111/j.1432-1033.1993.tb18338.x
Ricard J, Giudici-Orticoni M-T, Gontero B (1994) The Modulation of Enzyme Reaction Rates within Multi-Enzyme Complexes. 1. Statistical Thermodynamics of Information Transfer Through Multi-Enzyme Complexes. European Journal of Biochemistry 226 (3):993-998. doi:10.1111/j.1432-1033.1994.00993.x
Rouhier N, Cerveau D, Couturier J, Reichheld JP, Rey P (2015) Involvement of thiol-based mechanisms in plant development. Biochim Biophys Acta 1850 (8):1479-1496. doi:10.1016/j.bbagen.2015.01.023
Roustan V, Bakhtiari S, Roustan PJ, Weckwerth W (2017) Quantitative in vivo phosphoproteomics reveals reversible signaling processes during nitrogen starvation and recovery in the biofuel model organism *Chlamydomonas reinhardtii*. Biotechnol Biofuels 10:280. doi:10.1186/s13068-017-0949-z
Roustan V, Weckwerth W (2018) Quantitative Phosphoproteomic and System-Level Analysis of TOR Inhibition Unravel Distinct Organellar Acclimation in *Chlamydomonas reinhardtii*. Front Plant Sci 9:1590. doi:10.3389/fpls.2018.01590
Sainis JK, Jawali N (1994) Channeling of the intermediates and catalytic facilitation to Rubisco in a multienzyme complex of Calvin cycle enzymes. Indian J Biochem Biophys 31 (4):215-220
Sainis JK, Merriam K, Harris GC (1989) The Association of d-Ribulose-1,5-Bisphosphate Carboxylase/Oxygenase with Phosphoribulokinase. Plant Physiology 89 (1):368-374. doi:10.1104/pp.89.1.368
Salomé PA, Merchant SS (2019) A Series of Fortunate Events: Introducing Chlamydomonas as a Reference Organism. The

Plant Cell 31 (8):1682-1707. doi:10.1105/tpc.18.00952
Samanta M, Banerjee M, Murthy MR, Balaram H, Balaram P (2011) Probing the role of the fully conserved Cys126 in triosephosphate isomerase by site-specific mutagenesis--distal effects on dimer stability. Febs j 278 (11):1932-1943. doi:10.1111/j.1742-4658.2011.08110.x
Schneider G, Lindqvist Y, Brändén CI, Lorimer G (1986) Three-dimensional structure of ribulose-1,5-bisphosphate carboxylase/oxygenase from *Rhodospirillum rubrum* at 2.9 A resolution. Embo j 5 (13):3409-3415. doi:10.1002/j.1460-2075.1986.tb04662.x
Schürmann P, Buchanan BB (2008) The Ferredoxin/Thioredoxin System of Oxygenic Photosynthesis. Antioxidants & Redox Signaling 10 (7):1235-1274. doi:10.1089/ars.2007.1931
Schürmann P, Jacquot JP (2000) PLANT THIOREDOXIN SYSTEMS REVISITED. Annual Review of Plant Physiology and Plant Molecular Biology 51 (1):371-400. doi:10.1146/annurev.arplant.51.1.371
Shin S-E, Lim J-M, Koh HG, Kim EK, Kang NK, Jeon S, Kwon S, Shin W-S, Lee B, Hwangbo K, Kim J, Ye SH, Yun J-Y, Seo H, Oh H-M, Kim K-J, Kim J-S, Jeong W-J, Chang YK, Jeong B-R (2016) CRISPR/Cas9-induced knockout and knock-in mutations in *Chlamydomonas reinhardtii*. Scientific Reports 6 (1):27810. doi:10.1038/srep27810
Skrukrud CL, Gordon IM, Dorwin S, Yuan X-H, Johansson G, Anderson LE (1991) Purification and Characterization of Pea Chloroplastic Phosphoriboisomerase. Plant Physiology 97 (2):730-735. doi:10.1104/pp.97.2.730
Sobota JM, Imlay JA (2011) Iron enzyme ribulose-5-phosphate 3-epimerase in *Escherichia coli* is rapidly damaged by hydrogen peroxide but can be protected by manganese. Proc Natl Acad Sci U S A 108 (13):5402-5407. doi:10.1073/pnas.1100410108
St-Jean M, Lafrance-Vanasse J, Liotard B, Sygusch J (2005) High resolution reaction intermediates of rabbit muscle fructose-1,6-bisphosphate aldolase: substrate cleavage and induced fit. J Biol Chem 280 (29):27262-27270. doi:10.1074/jbc.M502413200
Strenkert D, Schmollinger S, Gallaher SD, Salomé PA, Purvine SO,

Nicora CD, Mettler-Altmann T, Soubeyrand E, Weber APM, Lipton MS, Basset GJ, Merchant SS (2019) Multiomics resolution of molecular events during a day in the life of Chlamydomonas. Proceedings of the National Academy of Sciences 116 (6):2374-2383. doi:10.1073/pnas.1815238116

Suss KH, Arkona C, Manteuffel R, Adler K (1993) Calvin cycle multienzyme complexes are bound to chloroplast thylakoid membranes of higher plants in situ. Proceedings of the National Academy of Sciences 90 (12):5514-5518. doi:10.1073/pnas.90.12.5514

Suss KH, Prokhorenko I, Adler K (1995) In Situ Association of Calvin Cycle Enzymes, Ribulose-1,5-Bisphosphate Carboxylase/Oxygenase Activase, Ferredoxin-NADP+ Reductase, and Nitrite Reductase with Thylakoid and Pyrenoid Membranes of *Chlamydomonas reinhardtii* Chloroplasts as Revealed by Immunoe. Plant Physiology 107 (4):1387-1397. doi:10.1104/pp.107.4.1387

Tamoi M, Ishikawa T, Takeda T, Shigeoka S (1996) Molecular Characterization and Resistance to Hydrogen Peroxide of Two Fructose-1,6-bisphosphatases from *Synechococcus* PCC 7942. Archives of Biochemistry and Biophysics 334 (1):27-36. doi:https://doi.org/10.1006/abbi.1996.0425

Tang GL, Wang YF, Bao JS, Chen HB (1999) Overexpression in *Escherichia coli* and characterization of the chloroplast triosephosphate isomerase from spinach. Protein Expr Purif 16 (3):432-439. doi:10.1006/prep.1999.1087

Tardif M, Atteia A, Specht M, Cogne G, Rolland N, Brugière S, Hippler M, Ferro M, Bruley C, Peltier G, Vallon O, Cournac L (2012) PredAlgo: A New Subcellular Localization Prediction Tool Dedicated to Green Algae. Molecular Biology and Evolution 29 (12):3625-3639. doi:10.1093/molbev/mss178

Taylor TC, Backlund A, Bjorhall K, Spreitzer RJ, Andersson I (2001) First Crystal Structure of Rubisco from a Green Alga,*Chlamydomonas reinhardtii*. Journal of Biological Chemistry 276 (51):48159-48164. doi:10.1074/jbc.m107765200

Tcherkez GGB, Farquhar GD, Andrews TJ (2006) Despite slow catalysis and confused substrate specificity, all ribulose bisphosphate carboxylases may be nearly perfectly optimized. Proceedings

of the National Academy of Sciences 103 (19):7246-7251. doi:10.1073/pnas.0600605103
Thieulin-Pardo G, Remy T, Lignon S, Lebrun R, Gontero B (2015) Phosphoribulokinase from *Chlamydomonas reinhardtii*: a Benson–Calvin cycle enzyme enslaved to its cysteine residues. Molecular BioSystems 11 (4):1134-1145. doi:10.1039/c5mb00035a
Trinh MDL, Masuda S (2022) Chloroplast pH Homeostasis for the Regulation of Photosynthesis. Frontiers in Plant Science 13. doi:10.3389/fpls.2022.919896
Udvardy J, Godeh MM, Farkas GL (1982) Regulatory properties of a fructose 1,6-bisphosphatase from the cyanobacterium *Anacystis nidulans*. Journal of Bacteriology 151 (1):203-208. doi:10.1128/jb.151.1.203-208.1982
Van Noort G, Wildman SG (1964) Proteins of green leaves: IX. Enzymatic properties of fraction-1 protein isolated by a specific antibody. Biochimica et Biophysica Acta (BBA) - General Subjects 90 (2):309-317. doi:https://doi.org/10.1016/0304-4165(64)90194-1
Vavitsas K, Crozet P, Vinde MH, Davies F, Lemaire SD, Vickers CE (2019) The Synthetic Biology Toolkit for Photosynthetic Microorganisms. Plant Physiology 181 (1):14-27. doi:10.1104/pp.19.00345
Walden H, Bell GS, Russell RJ, Siebers B, Hensel R, Taylor GL (2001) Tiny TIM: a small, tetrameric, hyperthermostable triosephosphate isomerase. J Mol Biol 306 (4):745-757. doi:10.1006/jmbi.2000.4433
Wang H, Gau B, Slade WO, Juergens M, Li P, Hicks LM (2014) The global phosphoproteome of *Chlamydomonas reinhardtii* reveals complex organellar phosphorylation in the flagella and thylakoid membrane. Mol Cell Proteomics 13 (9):2337-2353. doi:10.1074/mcp.M114.038281
Wang L, Jonikas MC (2020) The pyrenoid. Current Biology 30 (10):R456-R458. doi:10.1016/j.cub.2020.02.051
Wang L, Patena W, Van Baalen KA, Xie Y, Singer ER, Gavrilenko S, Warren-Williams M, Han L, Harrigan HR, Chen V, Ton VTNP, Kyin S, Shwe HH, Cahn MH, Wilson AT, Hu J, Schnell DJ, McWhite CD, Jonikas M (2022) A Chloroplast Protein Atlas

Reveals Novel Structures and Spatial Organization of Biosynthetic Pathways. Cold Spring Harbor Laboratory. doi:10.1101/2022.05.31.493820
Wang Q, Yang S, Wan S, Li X (2019) The Significance of Calcium in Photosynthesis. Int J Mol Sci 20 (6). doi:10.3390/ijms20061353
Wolosiuk RA, Buchanan BB (1978a) Activation of Chloroplast NADP-linked Glyceraldehyde-3-Phosphate Dehydrogenase by the Ferredoxin/Thioredoxin System. Plant Physiol 61 (4):669-671. doi:10.1104/pp.61.4.669
Wolosiuk RA, Buchanan BB (1978b) Regulation of chloroplast phosphoribulokinase by the ferredoxin/thioredoxin system. Arch Biochem Biophys 189 (1):97-101. doi:10.1016/0003-9861(78)90119-4
Wunder T, Oh ZG, Mueller-Cajar O (2019) CO(2) -fixing liquid droplets: Towards a dissection of the microalgal pyrenoid. Traffic 20 (6):380-389. doi:10.1111/tra.12650
Yu A, Xie Y, Pan X, Zhang H, Cao P, Su X, Chang W, Li M (2020) Photosynthetic Phosphoribulokinase Structures: Enzymatic Mechanisms and the Redox Regulation of the Calvin-Benson-Bassham Cycle[OPEN]. The Plant Cell 32 (5):1556-1573. doi:10.1105/tpc.19.00642
Zaffagnini M, Bedhomme M, Groni H, Marchand CH, Puppo C, Gontero B, Cassier-Chauvat C, Decottignies P, Lemaire SD (2012a) Glutathionylation in the photosynthetic model organism *Chlamydomonas reinhardtii*: a proteomic survey. Mol Cell Proteomics 11 (2):M111.014142. doi:10.1074/mcp.M111.014142
Zaffagnini M, Bedhomme M, Marchand CH, Morisse S, Trost P, Lemaire SD (2012b) Redox regulation in photosynthetic organisms: focus on glutathionylation. Antioxid Redox Signal 16 (6):567-586. doi:10.1089/ars.2011.4255
Zaffagnini M, Fermani S, Marchand CH, Costa A, Sparla F, Rouhier N, Geigenberger P, Lemaire SD, Trost P (2019) Redox Homeostasis in Photosynthetic Organisms: Novel and Established Thiol-Based Molecular Mechanisms. Antioxid Redox Signal 31 (3):155-210. doi:10.1089/ars.2018.7617
Zaffagnini M, Michelet L, Marchand C, Sparla F, Decottignies P, Le Maréchal P, Miginiac-Maslow M, Noctor G, Trost P, Lemaire SD

(2007) The thioredoxin-independent isoform of chloroplastic glyceraldehyde-3-phosphate dehydrogenase is selectively regulated by glutathionylation. Febs j 274 (1):212-226. doi:10.1111/j.1742-4658.2006.05577.x

Zaffagnini M, Michelet L, Sciabolini C, Di Giacinto N, Morisse S, Marchand CH, Trost P, Fermani S, Lemaire SD (2014) High-Resolution Crystal Structure and Redox Properties of Chloroplastic Triosephosphate Isomerase from *Chlamydomonas reinhardtii*. Molecular Plant 7 (1):101-120. doi:10.1093/mp/sst139

Zerrad L, Merli A, Schröder GF, Varga A, Gráczer É, Pernot P, Round A, Vas M, Bowler MW (2011) A Spring-loaded Release Mechanism Regulates Domain Movement and Catalysis in Phosphoglycerate Kinase. Journal of Biological Chemistry 286 (16):14040-14048. doi:10.1074/jbc.m110.206813

Zhan Y, Marchand CH, Maes A, Mauries A, Sun Y, Dhaliwal JS, Uniacke J, Arragain S, Jiang H, Gold ND, Martin VJJ, Lemaire SD, Zerges W (2018) Pyrenoid functions revealed by proteomics in *Chlamydomonas reinhardtii*. PLOS ONE 13 (2):e0185039. doi:10.1371/journal.pone.0185039

Zhang R-G, Andersson CE, Savchenko A, Skarina T, Evdokimova E, Beasley S, Arrowsmith CH, Edwards AM, Joachimiak A, Mowbray SL (2003) Structure of *Escherichia coli* Ribose-5-Phosphate Isomerase. Structure 11 (1):31-42. doi:10.1016/s0969-2126(02)00933-4

6 ANNEXES

6.1 ANNEXE 1 : CRYSTAL STRUCTURE OF CHLOROPLASTIC THIOREDOXIN Z DEFINES A TYPE-SPECIFIC TARGET RECOGNITION

6.1.1 Résumé de l'article

Les thiorédoxines sont de petites protéines capables de réduire les ponts disulfures d'autres protéines. Elles sont composées d'un repliement centré sur un feuillet β mixte entouré d'hélices α et possèdant un motif peptidique de type WC(G/P)PC permettant la réduction de ponts disulfures (Buchanan et al. 2012; Holmgren 1968). Ces thiorédoxines sont également capable de catalyser des réactions de dé-nitrosylation, dé-glutathionylation ou dé-persulfidation. Il existe plusieurs gènes codant pour des thiorédoxines dans les cellules, notamment chez les organismes photosynthétique ou l'on retrouve 21 isoformes chez *Arabidopsis thaliana* et 10 chez *Chlamydomonas reinhardtii*. Ces 10 isoformes peuvent se regrouper en 7 types, le type h localisé dans le cytosol et la mitochondrie, le type o dans la mitochondrie et les type f, m, x, y et z dans le chloroplaste (Balsera et al. 2014; Michelet et al. 2006). L'existence de ces différents types de thiorédoxines ayant la même fonction suppose l'existence de cibles différentes associées à un type de thiorédoxine. La reconnaissance de ces cibles est médiée via la charge électrostatique de surface des thiorédoxines. Ainsi, la thiorédoxine f (TRXf) est décrite comme contribuant aux cascades de régulation redox et aux changements métaboliques médiés par ceux-ci dans le cycle de Calvin-Benson-Bassham (Nishizawa and Buchanan 1981; Wolosiuk and Buchanan 1978b, a; Holmgren et al. 1977). Cette thiorédoxine est d'abord réduite par le système ferrrédoxine/ferrédoxine thiorédoxine réductase permettant un lien entre pouvoir réducteur et intensité lumineuse chez les organismes photosynthétiques (Pérez-Pérez et al. 2017). La thiorédoxine z (TRXz) à été décrite comme ayant des cibles différentes de celles du type f, mais la liste de ces interactions reste encore à ce jour incomplète.

La description dans cet article de la première structure de TRXz de Chlamydomonas reinhardtii nous à permis de confirmer que celle-ci possède bien le repliement caractéristique des thiorédoxines et une similarité structurale avec les autres type de thiorédoxines. Elle possède également le motif caractéristique WCGPC lui donnant sa réactivité. Malgré un doute initial sur l'assemblage homomultimérique de cette protéine apparaissant autour de 30±5 kDa en chromatographie d'exclusion de taille et sous la forme d'un homodimère dans l'unité asymétrique du cristal ayant permis la résolution de la structure, des expériences de diffusion des rayons X aux petits angle et de spéctrométrie de masse confirment un état monomérique en solution. La surface de la TRXz présente une charge de surface électronégative atypique pour les thiorédoxines ce qui pourrait en faire sa spécificité puisqu'également présente autour du motif WCGPG. La thiorédoxine f2 (TRXf2) est décrite comme pouvant réduire la PRK et ainsi augmenter son activité, vraisemblablement en ciblant la cystéine C55 à proximité d'une surface éléctronégative compatible avec la charge de surface électropositive de la TRXf2. Cette même cystéine possédant également une large surface chargée positivement à proximité, l'activation de cette protéine par TRXz à été testée. TRXz peut en effet augmenter l'activité de PRK à hauteur de 60% de son activité maximale activée par TRXf2. Ce résultat n'était pas égalé en présence d'un même ratio de thiorédoxine m. L'activation de PRK par réduction de pont disulfure peut se faire alternativement avec les deux thiorédoxines f et z.

6.1.2 Crystal structure of chloroplastic thioredoxin z defines a type-specific target recognition

the plant journal

The Plant Journal (2021) 107, 434–447 doi: 10.1111/tpj.15300

Crystal structure of chloroplastic thioredoxin z defines a type-specific target recognition

Théo Le Moigne[1,2,3], Libero Gurrieri[4], Pierre Crozet[1,3,5], Christophe H. Marchand[1,3,6], Mirko Zaffagnini[4], Francesca Sparla[4], Stéphane D. Lemaire[1,3] and Julien Henri[1,3,*]

[1]Laboratoire de Biologie Computationnelle et Quantitative, Institut de Biologie Paris-Seine, UMR 7238, CNRS, Sorbonne Université, 4 Place Jussieu, Paris 75005, France,

[2]Faculty of Sciences, Doctoral School of Plant Sciences, Université Paris-Saclay, Saint-Aubin 91190, France,

[3]Laboratoire de Biologie Moléculaire et Cellulaire des Eucaryotes, Institut de Biologie Physico-Chimique, UMR 8226, CNRS, Sorbonne Université, 13 Rue Pierre et Marie Curie, Paris 75005, France,

[4]Department of Pharmacy and Biotechnology, University of Bologna, Via Irnerio 42, Bologna 40126, Italy,

[5]Sorbonne Université, Polytech Sorbonne, Paris 75005, France, and

[6]Plateforme de Protéomique, Institut de Biologie Physico-Chimique, FR 550, CNRS, 13 Rue Pierre et Marie Curie, Paris 75005, France

Received 18 December 2020; revised 13 April 2021; accepted 22 April 2021; published online 30 April 2021.
*For correspondence (e-mail julien.henri@sorbonne-universite.fr).

SUMMARY

Thioredoxins (TRXs) are ubiquitous disulfide oxidoreductases structured according to a highly conserved fold. TRXs are involved in a myriad of different processes through a common chemical mechanism. Plant TRXs evolved into seven types with diverse subcellular localization and distinct protein target selectivity. Five TRX types coexist in the chloroplast, with yet scarcely described specificities. We solved the crystal structure of a chloroplastic z-type TRX, revealing a conserved TRX fold with an original electrostatic surface potential surrounding the redox site. This recognition surface is distinct from all other known TRX types from plant and non-plant sources and is exclusively conserved in plant z-type TRXs. We show that this electronegative surface endows thioredoxin z (TRXz) with a capacity to activate the photosynthetic Calvin–Benson cycle enzyme phosphoribulokinase. The distinct electronegative surface of TRXz thereby extends the repertoire of TRX–target recognitions.

Keywords: Calvin–Benson cycle, Photosynthesis, protein structure, protein–protein interactions, redox post-translational modifications, thioredoxins.

INTRODUCTION

Thioredoxins (TRXs) are small ubiquitous disulfide oxidoreductases (Buchanan *et al.*, 2012; Gleason and Holmgren, 1981; Hall *et al.*, 1971; Holmgren, 1968; Lillig and Holmgren, 2007). TRXs fold into a highly conserved and thermostable domain composed of a mixed β-sheet closely surrounded by α-helices and exposing a WC(G/P)PC pentapeptidic motif (Holmgren, 1968; Pan and Bardwell, 2006). Phylogenetic analyses described the history of the TRX fold through 4 billion years of evolution into the contemporary proteins (Ingles-Prieto *et al.*, 2013; Napolitano *et al.*, 2019). TRXs modify the ternary or quaternary structures of proteins by reducing target disulfide bonds into separate thiols (Blomback *et al.*, 1974; Holmgren and Morgan, 1976). TRXs have also been proposed to be involved in other redox modifications of cysteines by catalyzing denitrosylation, deglutathionylation, or depersulfidation reactions, contributing therefore to redox signaling cascades and metabolic remodeling (Bedhomme *et al.*, 2012; Benhar *et al.*, 2008; Berger *et al.*, 2016; Greetham *et al.*, 2010; Wedmann *et al.*, 2016), as recently reviewed in Zaffagnini *et al.* (2016, 2019). The midpoint redox potential of TRXs lies between −310 and −230 mV at pH 7 (Collin *et al.*, 2003; Gonzalez Porque *et al.*, 1970; Hirasawa *et al.*, 1999; Setterdahl *et al.*, 2003; Watson *et al.*, 2003) with a nucleophilic active site cysteine reacting in the thiolate state ($-S^-$), favored at physiological pH by a local environment determining a cysteine pK_a in the 6.5–7.5 range (Ferrer-Sueta *et al.*, 2011; Marchand *et al.*, 2019; Roos *et al.*, 2013).

The TRX system is recognized as having multiple roles in a myriad of cellular processes and numerous human

diseases (Buchanan *et al.*, 2012; Hanschmann *et al.*, 2013; Lee *et al.*, 2013; Toledano *et al.*, 2013). Non-photosynthetic organisms contain a limited number of TRXs reduced by NADPH:thioredoxin reductase (NTR). By contrast, TRXs are encoded by a larger multigene family in photosynthetic organisms (21 isoforms in the model plant *Arabidopsis thaliana* and 10 in the unicellular green alga *Chlamydomonas reinhardtii*). Phylogenetic analyses grouped TRXs in the cytosolic/mitochondrial h-type, the mitochondrial o-type, and five chloroplastic types (f-, m-, x-, y-, and z-types) (Balsera *et al.*, 2014; Michelet *et al.*, 2006). Cytosolic and mitochondrial TRXs are reduced by NTR but chloroplastic TRXs are specifically reduced in the light by ferredoxin: thioredoxin reductase (FTR), which derives electrons from ferredoxin and the photosynthetic electron transfer chain (Balsera *et al.*, 2014; Jacquot *et al.*, 2009; Kang *et al.*, 2019; Michelet *et al.*, 2013; Schurmann and Buchanan, 2008; Zaffagnini *et al.*, 2019). This unique reduction mechanism allows to couple the redox state of TRX to light intensity and to use the chloroplast TRX system as a light-dependent signaling pathway for regulation of cellular metabolism and processes (Perez-Perez *et al.*, 2017). In photoautotrophic organisms, TRXs were originally identified as light-dependent regulators of the Calvin–Benson cycle (CBC), responsible for fixation of atmospheric CO_2 into triose phosphates using energy (ATP) and reducing power (NADPH) produced in the light by the photosynthetic electron transfer chain. Early studies identified four key enzymes of the CBC as TRX targets: phosphoribulokinase (PRK) (Wolosiuk and Buchanan, 1978b), glyceraldehyde-3-phosphate dehydrogenase (GAPDH) (Wolosiuk and Buchanan, 1978a), fructose-1,6-bisphosphatase (FBPase) (Holmgren *et al.*, 1977), and sedoheptulose-1,7-bisphosphatase (SBPase) (Nishizawa and Buchanan, 1981). These enzymes have a low activity in the dark and are activated upon illumination by the ferredoxin/TRX system because reduction of specific regulatory disulfides by TRX triggers conformational changes that shift the enzyme to a high-activity conformation. Besides the CBC, chloroplast TRXs were later recognized as regulators of multiple targets involved in numerous pathways and processes (Lemaire *et al.*, 2007; Zaffagnini *et al.*, 2019). TRXs were especially recognized to provide electrons for the regeneration of major antioxidant enzymes such as peroxiredoxins (Collin *et al.*, 2003; Liebthal *et al.*, 2018; Navrot *et al.*, 2006; Perez-Perez *et al.*, 2009; Sevilla *et al.*, 2015; Tarrago *et al.*, 2009; Yoshida *et al.*, 2019b).

In the microalga *C. reinhardtii*, 10 TRX isoforms have been identified, including six nuclear-encoded chloroplastic TRXs (CrTRXf1, CrTRXf2, CrTRXm, CrTRXx, CrTRXy, and CrTRXz) (Balsera *et al.*, 2014; Lemaire *et al.*, 2007; Zaffagnini *et al.*, 2019). Proteomic analyses based on affinity purification chromatography and *in vitro* reconstitution of the cytosolic TRX system allowed the identification of 1053 TRX targets and 1052 putative regulatory sites in *Chlamydomonas* (Lemaire *et al.*, 2004; Perez-Perez *et al.*, 2017). Among these, all CBC enzymes were identified, indicating that they are potential TRX interactors, and direct TRX-dependent activation of CBC enzymes was only demonstrated for PRK (Gurrieri *et al.*, 2019), FBPase (Huppe and Buchanan, 1989), SBPase (Gutle *et al.*, 2016), and phosphoglycerate kinase (PGK) (Morisse *et al.*, 2014). By contrast with land plants, photosynthetic GAPDH from *C. reinhardtii* (CrGAPDH) is not directly regulated by TRX but only indirectly through formation of the $(A_4\text{-GAPDH})_2$–$CP12_4$–PRK_2 complex (Avilan *et al.*, 2012; Marri *et al.*, 2009; Trost *et al.*, 2006). Among the five TRX types present in chloroplasts, only TRXf has been systematically compared to other types and demonstrated to target FBPase (Collin *et al.*, 2003; Michelet *et al.*, 2013), PRK (Gurrieri *et al.*, 2019; Marri *et al.*, 2009), GAPDH in land plants (Marri *et al.*, 2009), and PGK in *Chlamydomonas* (Morisse *et al.*, 2014). Structural analysis revealed that electrostatic complementarity is the principal driver of TRXf–target recognition (Balmer *et al.*, 2004; Bunik *et al.*, 1999; De Lamotte-Guery *et al.*, 1991; Lemaire *et al.*, 2018; Mora-Garcia *et al.*, 1998). Besides, TRXs were recently attributed a reciprocal redox function for the oxidation of targets upon light-to-dark transitions through the action of TRXL2 and 2-Cys peroxiredoxins (Cejudo *et al.*, 2019; Ojeda *et al.*, 2018; Vaseghi *et al.*, 2018; Yoshida *et al.*, 2018, 2019a, 2019b). Finally, TRXs are involved in a multiplicity of other plastid functions either through their redox capacities (Kang *et al.*, 2019), in the complex redox cellular network (Konig *et al.*, 2012; Yoshida and Hisabori, 2016), or through participation in large supramolecular assemblies (Kulczyk *et al.*, 2017; Schroter *et al.*, 2010).

In *Populus trichocarpa* and in *A. thaliana*, TRXz was reported to be reduced by FTR (Chibani *et al.*, 2011; Yoshida and Hisabori, 2017). TRXz can also act as a potential electron acceptor for a special type of chloroplastic TRX named NADPH:thioredoxin reductase C (NTRC) (Yoshida and Hisabori, 2016), TRXf, m, x, and y (Bohrer *et al.*, 2012), and interacts with fructokinase-like proteins (FLN1 and FLN2) in *A. thaliana* and *Nicotiana benthamiana* (Arsova *et al.*, 2010). TRXz–FLN interaction regulates plastid-encoded polymerase (PEP) (Arsova *et al.*, 2010; Huang *et al.*, 2013). Notably, TRXz reduces plastid redox-insensitive protein 2 (PRIN2) cysteine 68 (C68) heteromolecular disulfides bridges within a homodimer in *A. thaliana*, releasing monomeric PRIN2, which activates PEP transcription (Diaz *et al.*, 2018). TRXz redox activity may however be dispensable and TRXz–FLN1 are proposed to be essential components of the PEP complex (Wimmelbacher and Bornke, 2014). TRXz also interacts with *A. thaliana* thioredoxin-like MRL7 (Yua *et al.*, 2014) and temperature-sensitive virescent protein mediates the TRXz interaction with PEP in rice (*Oryza sativa*) (Sun *et al.*, 2017). In rice, TRXz was also found to interact with chloroplastic

RNA-editing enzymes (Wang *et al.*, 2020). Yet, the full set of TRXz targets or interaction partners has not yet been elucidated and the corresponding molecular basis for TRXz specificity towards its targets remains to be deciphered.

Altogether, it is striking that the very ancient and simple 12–15-kDa TRX fold has evolved into this plethora of functions, suggesting a fine selection of redox properties and specific surface recognitions. In order to gain insights into the molecular functions of chloroplastic z-type TRXz and the physico-chemical basis for its specificity, we solved the high-resolution crystal structure of TRXz from *C. reinhardtii*. This structure is representative of a z-type TRX and unravels a conserved native folding compared to other structurally solved TRXs. Model analysis mapped its redox site and identified the surfaces it exposes for selective protein recognition. TRXz displays electro-complementary surfaces with *C. reinhardtii* PRK (CrPRK). We show that PRK is indeed activated by TRXz reduction *in vitro*.

RESULTS

CrTRXz folds as a canonical TRX

Recombinant TRXz from *C. reinhardtii* (CrTRXz) was heterologously expressed in *Escherichia coli* as a 149-amino acid polypeptide (predicted mature protein including residues 56–183 plus the N-terminal affinity tag) and purified to homogeneity by metal-affinity chromatography. Purified CrTRXz was crystallized, and the crystals were cryoprotected, submitted to X-ray diffraction for the collection of a complete dataset indexed in space group $P3_221$, and solved by molecular replacement with CrTRXf2 (Protein Data Bank [PDB] ID: 6I1C) as a search model. Model correction and completion up to 116 amino acid residues and one water molecule was refined to $R = 0.2296$ and $R_{free} = 0.2335$ at a resolution of 2.4 Å (Table 1). CrTRXz folds according to the canonical TRX topology (SCOPe entry c.47), that is, a central mixed β-sheet of four strands sandwiched between two pairs of α-helices (Figure 1(a,b)). The strand order is 2–1–3–4, with strand 3 antiparallel to strands 1, 2, and 4. The succession of secondary structures is as follows: residues 67–76 form helix 1, residues 80–86 strand 1, residues 91–107 helix 2, residues 111–117 strand 2, residues 122–128 helix 3, residues 135–139 strand 3, residues 148–151 strand 4, and residues 156–167 helix 4 (Figure S1). The length of helix 1 is conserved in the eukaryotic branch of TRX evolution since the last eukaryotic common ancestor (Ingles-Prieto *et al.*, 2013). Residues 118–120 were modeled as one turn of a helix 3_{10} with D119 hydrogen-bonding with W89 and the unique water molecule of the model. Residues ^{54}HMVI^{57} and ^{61}KVEKIS^{66} of recombinant CrTRXz form an unfolded extension at the N-terminus of the model, deforming it from an ideal sphere. Residues 58–60 and 170–183 were not built because of a lack of interpretable electron density. Pairwise alignments of equivalent C_α of CrTRXf2 and CrTRXm onto CrTRXz yielded a root mean square deviation (RMSD) of 0.838 Å and 1.356 Å, respectively, confirming the close structural similarity between the experimentally solved *Chlamydomonas* TRX structures (Figure S2). Further alignments with experimentally determined structures from the PDB revealed also high similarities with *Plasmodium falciparum* TRX2 (PDB ID: 3UL3, RMSD = 1.16 Å), resurrected ancestral TRX from the inferred last bacterial common ancestor (PDB ID: 4BA7, RMSD = 1.18 Å), *Bacteroides fragilis* TRXP (PDB ID: 3HXS, RMSD = 1.19 Å), and 20 other TRXs with RMSD ≤ 1.30 Å. CrTRXz topology is classical among TRXs.

CrTRXz redox site and environment

Disulfide oxidoreductase activity of TRX relies on a pair of cysteines located at the N-terminal tip of helix 2 in a conserved motif composed of the WCGPC peptide. The

Table 1 Crystallographic diffraction data and model statistics

	CrTRXz
Resolution range	40.34–2.444 (2.532–2.444)
Space group	P 32 2 1
Unit cell	61.985 61.985 61.138 90 90 120
Total reflections	210 020 (19 582)
Unique reflections	5300 (485)
Multiplicity	39.6 (38.0)
Completeness (%)	99.40 (94.17)
Mean I/sigma (I)	17.68 (1.29)
Wilson B-factor	65.65
R-merge	0.6065 (1.461)
R-meas	0.6145 (1.48)
R-pim	0.09769 (0.2389)
CC1/2	0.909 (0.792)
CC*	0.976 (0.94)
Reflections used in refinement	5269 (485)
Reflections used for R-free	525 (36)
R-work	0.2296 (0.3471)
R-free	0.2335 (0.3213)
CC (work)	0.462 (0.009)
CC (free)	0.38 (0.246)
Number of non-hydrogen atoms	865
Macromolecules	864
Solvent	1
Protein residues	113
RMS (bonds)	0.010
RMS (angles)	1.44
Ramachandran favored (%)	99.08
Ramachandran allowed (%)	0.92
Ramachandran outliers (%)	0.00
Rotamer outliers (%)	7.37
Clashscore	6.82
Average B-factor	70.15
Macromolecules	70.19
Solvent	30

Statistics for the highest-resolution shell are reported in parentheses.
RMS, root mean square; TRXz, thioredoxin z.

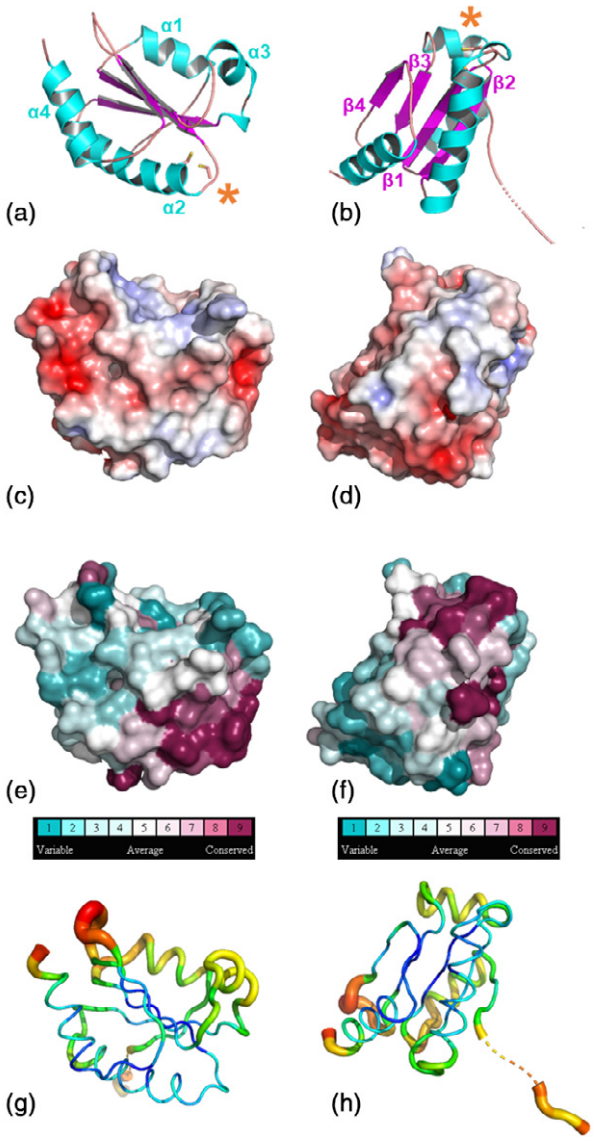

Figure 1. Crystallographic structure of chloroplastic CrTRXz.
(a) Cartoon representation with helices 1–4 colored in cyan and strands 1–4 colored in magenta. Cysteine side chains are represented in sticks and highlighted with an asterisk. Residue numbering is in accordance with UniProt entry A8J0Q8-1.
(b) 90° rotation around the *y*-axis of (a).
(c) Electrostatic surface potential calculated with APBS (Baker *et al.*, 2001). Electronegative surface is colored in red while electropositive surface is colored in blue.
(d) 90° rotation around the *y*-axis of (c).
(e) Conservation of surface residues as calculated with CONSURF colored from purple (most conserved) to blue (least conserved).
(f) 90° rotation around the *y*-axis of (e).
(g) B-factor representation. High B-factors are colored in red and low B-factors are colored in blue. APBS, Adaptive Poisson-Boltzman Solver; TRXz, thioredoxin z.

N-terminal active site cysteine (Cys_N) attacks the disulfide bond on a target protein while the second active site cysteine (Cys_C) resolves the intermolecular disulfide bridge to free the reduced target protein and the oxidized TRX. The mature CrTRXz sequence possesses two cysteines: Cys_N (C90) and Cys_C (C93) (Figure S1). Both are located at the tip of helix 2 (Figure 2(a)). Side chain thiols are modeled at 3.1 Å distance in what appears as a reduced state. The nucleophilic C90 displays a 13.56-$Å^2$ solvent-accessible area, making it available for redox exchange with a target protein disulfide. The orientation of its thiol group is however unfavorable to thiol electron exchange because it points inwards in the direction of the TRX core. A local rearrangement of loop 88–91 would be required to tumble the C90 thiol towards the solvent. Such a local rearrangement of the TRX redox site would partly account for the entropy dependence of target disulfide binding (Palde and Carroll, 2015). In *E. coli* TRX, D26 is buried in the core of the protein, where it acts as a base catalyst in the thiol–disulfide interchange reaction (Chivers and Raines, 1997; LeMaster *et al.*, 1997). D31 was confirmed to play the same role in CrTRXh1, and this requires a water molecule for proton exchange (Menchise *et al.*, 2001). CrTRXz also buries D84 at the equivalent position and its carboxyl side chain points in the direction of resolving C93 at a distance of 6.4 Å (Figure 2(b)). An intermediate water molecule, though not visible at the resolution of our structure, would fit in between at distances favoring hydrogen bonds with D84 and C93 (Figure 2(b)). P134 at the N-terminal side of strand 3 faces the redox site at 3.5 Å and 4.6 Å from C93 and C90, respectively. P134 is built in the *cis* conformation. As reported earlier, this *cis*-proline is an important kinetic bottleneck for protein folding (Kelley and Richards, 1987) and is already observed in inferred pre-Cambrian TRXs (Gamiz-Arco *et al.*, 2019). Altogether, the redox site microenvironment and structural-dependent functional features of TRXs are present and canonical in CrTRXz.

CrTRXz is monomeric

We unexpectedly observed early elution of purified CrTRXz during size-exclusion chromatography (SEC), showing an apparent higher molecular weight of the protein when compared to CrTRXf2. The experiment was repeated over two analytical gel filtration matrices (BioSEC3-300 and S6Increase) and the results were confirmed by comparison of distribution coefficients (Kav): $Kav(CrTRXz)_{BioSEC3\text{-}300} = 0.625 \pm 0.005$, $Kav(CrTRXf2)_{BioSEC3\text{-}300} = 0.89$; and $Kav(CrTRXz)_{S6Increase} = 0.611$, $Kav(CrTRXf2)_{S6Increase} = 0.723$ (Figure S3). According to BioSEC3-300 gel filtration calibrated with globular standards, the apparent molecular weight of CrTRXz is 30 ± 5 kDa, approximating twice the molecular weight of a 16-kDa subunit. Consequently, CrTRXz appears as a possible globular homodimer according to SEC analysis.

Analysis of protein interfaces in the crystal packing with PISA (EMBL-EBI) indeed uncovers six direct contact surfaces of 22.4, 98.9, 286.5, 322.1, 437.3, and 812.1 $Å^2$ of the

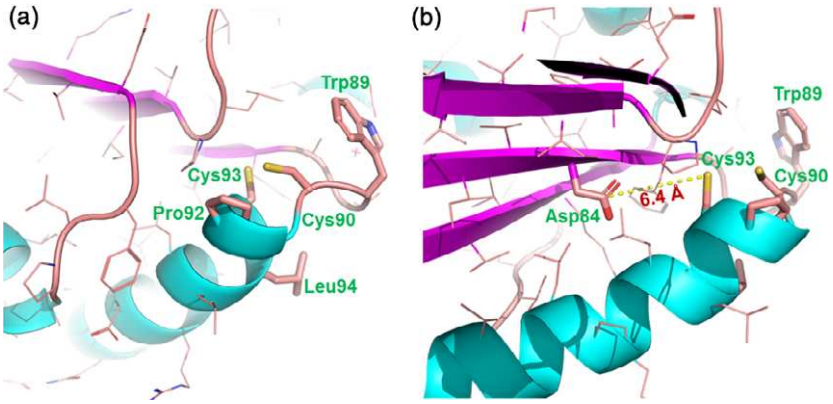

Figure 2. Redox site of CrTRXz. The main chain is represented as a cartoon. Side chains are represented as lines and colored according to atom type (blue = nitrogen, red = oxygen, yellow = sulfur).
(a) Redox site ^{89}WCPGCL^{94} side chains are highlighted in sticks and labeled as three-letter codes. C90 is located at the conserved nucleophile position.
(b) The nucleophile D84 side chain is shown as sticks. The carboxylate–thiol distance to C93 of 6.4 Å is drawn in a broken line.

asymmetric unit monomer and its closest neighbors. The available surface of a monomer is 6848 Å^2; hence, the largest 812.1-Å^2 interface covers 12% of the CrTRXz surface. This crystallographic A:B dimer is formed by subunit A at positions *x*, *y*, *z* and subunit B at positions $-x + 2$, $-x + y + 1$, $-z + 2/3$ in a neighboring unit cell (Figure 3(a)). PISA computes a solvation free energy gain ($\Delta^i G$) of -11.3 kcal mol^{-1} upon formation of the interface. Twenty-one residues are located at the interface. Ten residues form hydrogen bonds between $R77_A$:$E71_B$, $R149_A$:$M127_B$, $E71_A$:$R77_B$, $M127_A$:$R149_B$, and at equivalent yet non-symmetrical positions $R129_A$:$R129_B$. Four residues form multiple salt bridges between $R77_A$:$E71_B$ and equivalent $E71_A$:$R77_B$. Overall, PISA scores this interface with a complexation significance of 1 (stable assembly), while the other five detected interfaces score at 0 (no stable assembly).

To try and probe the quaternary structure of CrTRXz in solution, we subjected two independent SEC-purified preparations of pure CrTRXz to small-angle X-ray scattering (SEC-SAXS) (Figure 3(b,c)). Guinier analysis radii of gyration of 20.16 ± 0.25 Å (protein preparation 1) and 23.34 ± 0.43 Å (preparation 2) allowed computation of respective molecular weight intervals of 15.80–17.75 kDa and 18.35–20.85 kDa at 95% credibility. The oligomeric state of CrTRXz detected by SAXS is consequently that of a monomer of 16.2 kDa. MS analysis of CrTRXz under native or denaturing conditions showed only the presence of monomeric species in our experimental conditions, suggesting that in solution CrTRXz is mainly monomeric.

In conclusion, the dimerization observed in crystal packing is too weak or too transitory to represent the principal protein population *in vitro* in the SAXS and MS experimental setups, while the higher apparent molecular weight on SEC may be due to non-globularity. The monomeric state is the most probable form expected in the diluted, non-crystalline physiological context.

CrTRXz reactive surface displays a unique electronegative potential

Multiplicity of TRX types in the chloroplast stroma raises the question of their specificity and the underlying physico-chemical determinants for selective and non-overlapping disulfide bond recognition in different targets (Lemaire *et al.*, 2007). In order to identify z-type specificities, we analyzed the high-resolution crystal structure of CrTRXz. The secondary structure topology is almost identical to those of other known TRXs (Figure S2). The redox residues are also positioned at the canonical sites and they form the most conserved surface of the protein among homologs (Figure 1(e,f)) (Ashkenazy *et al.*, 2016). The dynamics of the main chain are approximated by the crystallographic b-factors, the highest values of which are grouped at the N- and C-terminal ends and at the loop connecting strands 3 and 4 (Figure 1(g,h)). Helices 3 and 1 also group higher than average b-factors, albeit to a lower extent than the aforementioned loop and N/C-termini. This local flexibility may predict functional deformations of the CrTRXz structure upon folding, upon binding of protein partners, or during allosteric controls. All dynamic elements are however located far from the redox site and they are unlikely to contribute alone to the selectivity of CrTRXz towards targets.

The principal determinant of CrTRXf2 selectivity was described as an electropositive crown of residues exposed at the surface surrounding the redox site (Balmer *et al.*, 2004; Bunik *et al.*, 1999; Lemaire *et al.*, 2018; Yokochi *et al.*, 2019). We compared the electrostatic surface of CrTRXz and observed large electronegative patches and a general lack of electropositive elements (Figure 1(c,d)). Notably, CrTRXz presents the z-type conserved apolar L94 immediately after the redox site WCGPC, while all other plastidial TRX possess in this position either a positively charged

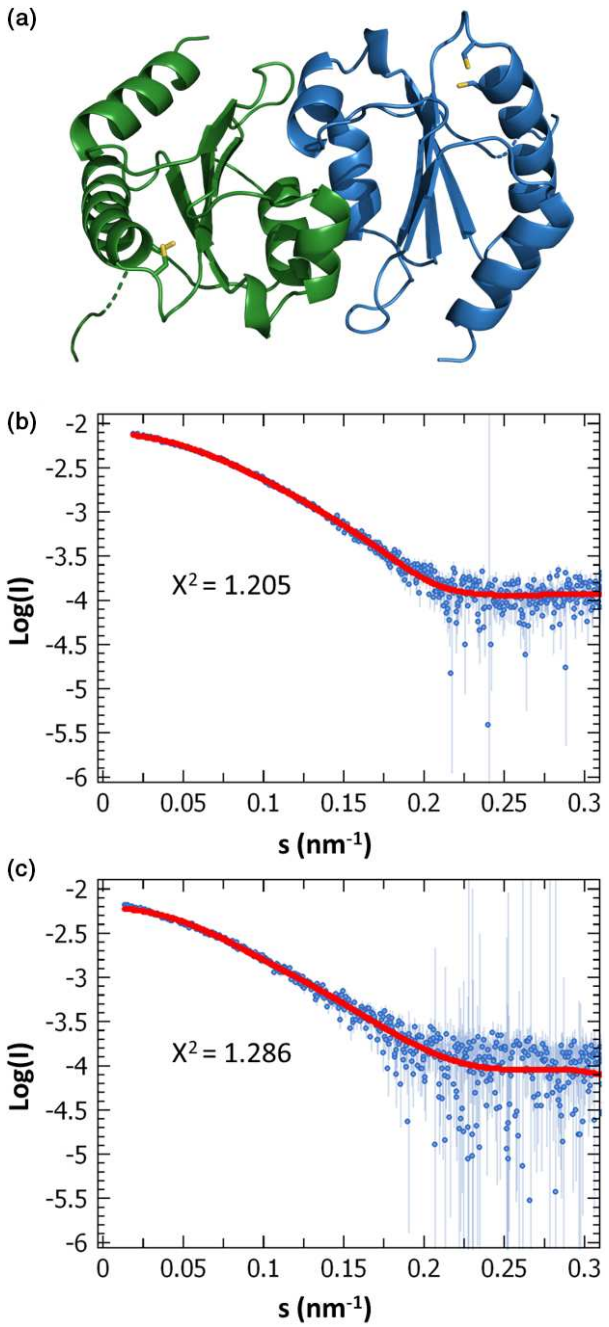

Figure 3. TRXz quaternary structure.
(a) Crystallographic dimer of CrTRXz represented in cartoon format with reactive cysteine side chains shown as sticks. Chain A is colored in blue, chain B in green.
(b) Small-angle X-ray scattering (SAXS) curve log(*I*) = *f*(*s*) of batch 1 of CrTRXz in blue was fitted to the crystallographic monomeric model of CrTRXz in red. (c) Same experiment as (b) with batch 2 of CrTRXz.

residue (R/K for m-, x-, and f-types) or a hydrogen bond donor residue (Q for y-type). Differential electrostatic repartition is particularly marked in the vicinity of the redox site and represents a significant qualitative difference with CrTRXf2 and CrTRXm equivalent surfaces (Figure 4(b,d,f)). The principal determinants of CrTRXf2 selectivity were proposed to be K78, K114, N130, K131, N133, K134, K143, and K164 (PDB ID: 6I1C) (Lemaire *et al.*, 2018). Equivalent positions on structurally aligned CrTRXz are occupied by E63, Q102, D119, E120, N121, P122, Q131, and E151. Seven out of these eight residues are conserved in TRXz homologs (Figure S1) and the electronegative surface is predicted to be conserved in a land plant ortholog (Figure S4), supporting an important function for type-z physiological functions in plants. In both CrTRXf2 and CrTRXz crystal structures, the aforementioned side chains are located at the protein surfaces and point their polar groups to the solvent. If the amino groups of lysines expose a +1 charge while the carboxyl groups of aspartates and glutamates expose a −1 charge at physiological pH, the aforementioned CrTRXf2 selectivity surface will accumulate a net charge of +6 while corresponding positions on CrTRXz sum a net charge of −4. The contributions of asparagine and glutamine residues to each selectivity surface are less explicit since they potentially behave as hydrogen bond donors or acceptors.

Overall, TRXz and TRXf2 recognition modes probably rely on distinct surface properties of targets because they present opposite electrostatic profiles. According to their mature sequence, CrTRXz presents an acidic isoelectric point while that of CrTRXf2 is basic (4.55 and 8.45, respectively). CrTRXm also presents an acidic isoelectric point (5.09), but important surface differences with CrTRXz stem from the charge repartition around the redox surface (Figures 4(b,d)).

TRXz is electro-complementary to known protein interactants

Four candidate proteins have been described as TRXz interactants in *A. thaliana*: FLN1, FLN2, PRIN2, and MRL7 (Arsova *et al.*, 2010; Diaz *et al.*, 2018; Yua *et al.*, 2014). The molecular structure of these proteins is not experimentally determined but their structures were predicted by homology using PHYRE software (Kelley *et al.*, 2015) (Figure 5). AtFLN1 possesses five cysteines and based on the protein model, adjacent C105 and C106 residues are buried within the structure and seem to be affected by TRX only in a solvent-exposed unfolded state. C204, C398, and C418 are predicted to be solvent-exposed and available for TRX redox interaction (Figure 5(a)) even though they probably do not form intramolecular disulfide bridges as they appear too distant. C398 is surrounded by an electropositive surface complementary to the CrTRXz recognition surface (Figure 5(b)). Homology-modeled AtFLN2 includes nine cysteines, where (i) the consecutive C208 and C209 are also located under the surface and probably not accessible in the folded state (Figure 5(c)), (ii) C290, C307, C322, C326, and C419 are present at the predicted surface, while (iii) C529 is hidden to solvent and C253 is at the bottom of

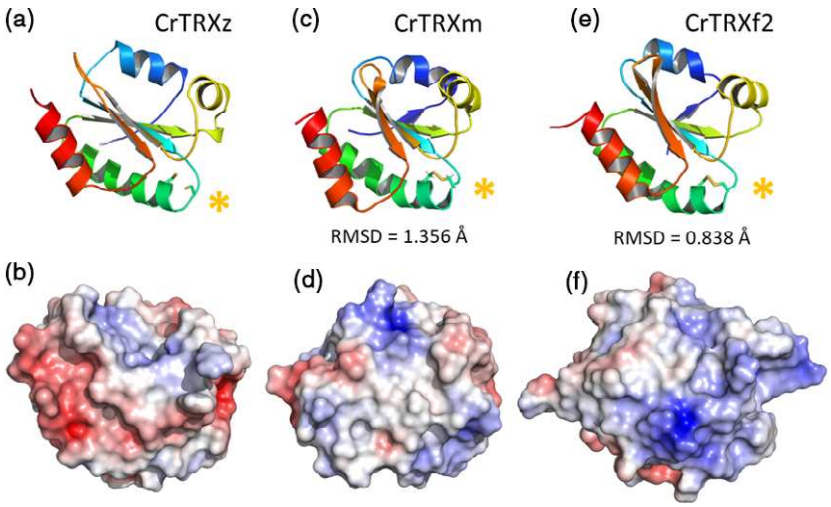

Figure 4. Structural comparison of plastidial TRX experimental structures. Root mean square deviations (RMSDs) between equivalent alpha carbons were calculated with PyMOL.
(a) CrTRXz crystal structure (this study) represented in cartoon format and colored from blue (N-terminus) to red (C-terminus). Cysteine side chains are shown as sticks and highlighted with an asterisk.
(b) Electrostatic surface potential of CrTRXz calculated with APBS (Baker *et al.*, 2001). Electronegative surface is colored in red while electropositive surface is colored in blue.
(c) CrTRXm nuclear magnetic resonance structure (Lancelin *et al.*, 2000) (PDB ID: 1DBY) represented and colored as in (a).
(d) Electrostatic surface potential of CrTRXm calculated with APBS and colored as in (b).
(e) CrTRXf2 crystal structure (PDB ID: 6I1C) represented and colored as in (a).
(f) Electrostatic surface potential calculated with APBS of CrTRXf2 and colored as in (b). APBS, Adaptive Poisson-Boltzman Solver.

a deep and narrow cleft. C290, C322, C326, and C327 are surrounded by electropositive surfaces that qualify them as potential targets of TRXz redox interaction (Figure 5(d)). The three latter would make good candidates for intramolecular dithiol/disulfide exchange since their thiols are predicted to be located at distances of 7.7, 8.5, and 9.2 Å. The AtMRL7 model encompasses two cysteines, both predicted at the solvent-exposed surface of the protein (Figure 5(e)). C281 is surrounded by marked electropositive potentials and may hence be targeted by the electrocomplementary TRXz redox surface (Figure 5(f)). AtPRIN2 could not be modeled by PHYRE as a globular structure, because of the lack of close homology with experimental models (best sequence identity 27% for 32% residue coverage, or 22% identity for 49% coverage). However, the 20-residue peptide NH_3^+-LSSLSRRGFVCRAAEYKFPDP-COO^- centered on redox target C68 (underlined) contains three arginines and one lysine and even though the mature protein sequence confers an acidic pI (4.43), the local environment of the cysteine in this peptide presents a basic pI of 9.31, which would make it a reasonable target for interaction with the TRXz electronegative surface.

CrTRXz can activate CrPRK *in vitro*

While CrPRK is a well-known CrTRXf2 target, presumably because of its partially negative surface around C55, another large positive patch is also present near C55 at the enzymatic pocket (Gurrieri *et al.*, 2019; Marri *et al.*, 2009). The mixed environment of CrPRK C55 suggests an independent, alternative mechanism of redox activation by TRXz. We probed the activation efficiency of CrTRXf2, CrTRXz, and CrTRXm on PRK activity. The ability of CrTRXs to reductively activate oxidized CrPRK was measured using different TRX:PRK ratios and assaying enzyme activity after 1 h of incubation (Figure 6). In every incubation, the concentration of CrPRK was 5 μM and the concentration of TRX varied from 0.5 μM (TRX:PRK ratio, 1:10) to 50 μM (TRX:PRK ratio, 10:1). At the lowest ratio (1:10), no TRX significantly activated PRK, while at higher ratios both CrTRXz and CrTRXf2 activated the enzyme. The CrTRXz activation plateaued at twofold excess, reaching 60% of maximal activity. No further activation was observed at higher TRX:PRK ratios. PRK activity in the presence of CrTRXf2 increased until sixfold excess, where 100% of maximal activity was obtained. CrTRXm was able to partially activate PRK only at the highest molar ratios (i.e., TRX:PRK ratios of 6:1 and 10:1). These results demonstrate that CrTRXf2 is the main activator for PRK *in vitro*, whereas CrTRXz is able to activate CrPRK to a lower extent.

DISCUSSION

Here, we report the experimental structure of TRXz from the model alga *C. reinhardtii* (PDB ID: 7ASW). Structural analysis reveals that chloroplastic CrTRXz is a classical

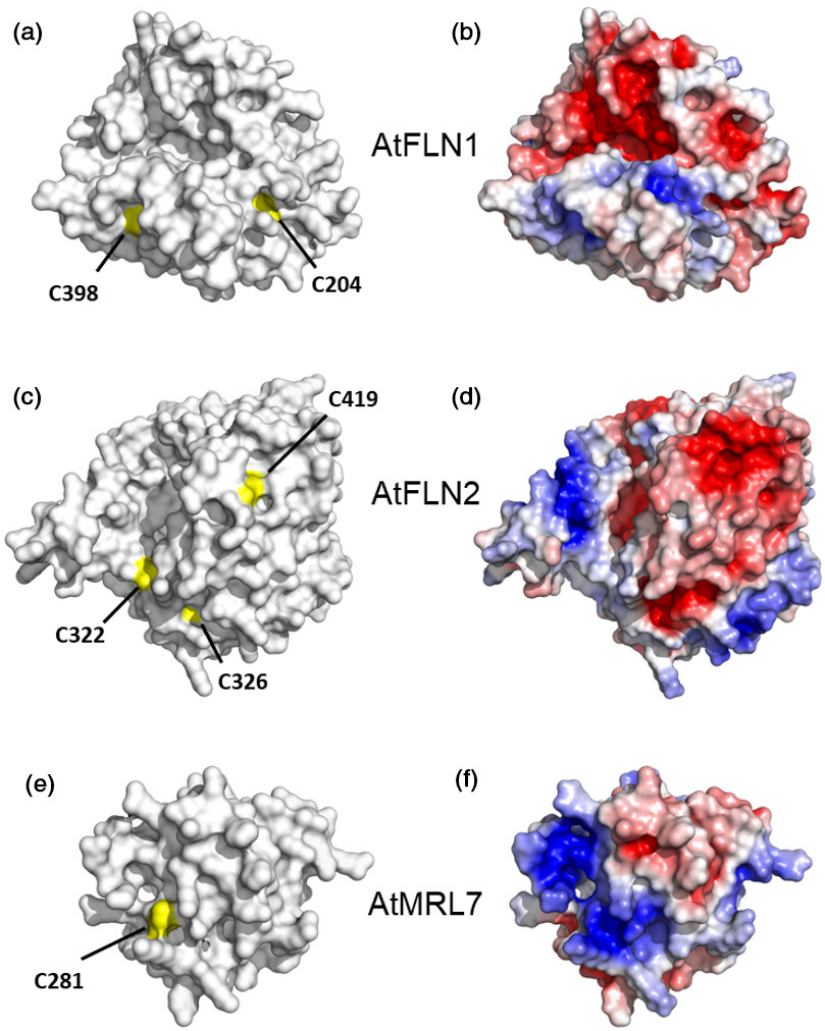

Figure 5. Electrostatic surface of PHYRE2 (Kelley *et al.*, 2015) homology-modeled TRXz protein partners.
(a) Connolly solvent exclusion surface of AtFLN1 residues 90–464 from the sequence of UniProt entry Q9M394 with cysteines in yellow.
(b) Electrostatic surface potential calculated with APBS. Electronegative surface is colored in red while electropositive surface is colored in blue (c). Connolly solvent exclusion surface of AtFLN2 205–557 from the sequence of UniProt entry F4I0K2 with cysteines in yellow.
(d) Electrostatic surface potential calculated with APBS and colored as in (b).
(e) Connolly solvent exclusion surface of AtMRL7 residues 195–312 from the sequence of UniProt entry F4JLC1 with cysteines in yellow.
(f) Electrostatic surface potential calculated with APBS and colored as in (a). APBS, Adaptive Poisson-Boltzman Solver.

TRX with an atypical electronegative surface conserved in plant homologs. We dissected TRXz surface properties to assess its putative specificity over known target proteins of AtTRXz. Moreover, based on structural features, we proposed the Calvin–Benson enzyme CrPRK as being recognized by CrTRXz, which was confirmed by our *in vitro* activity assays.

CrTRXz maintains the canonical fold of TRX

The determination of the crystal structure of chloroplastic TRXz from the green alga *C. reinhardtii* confirmed that it folds as a canonical αβα compact domain exposing the conserved WCGPC redox pentapeptide at nucleophile-attacking distance of incoming target disulfide bonds. Other signatures of reactivity and folding were observed in our structure, for example the base catalyst aspartate at a water-bridging distance to the resolving Cys_C, the 10-residue helix 1 of eukaryotic TRXs, and the folding bottleneck *cis*-P134. The reactive Cys redox pair appears dissociated in a dithiol state available for the reduction of a target disulfide bond.

CrTRXz evolved distinct features

Although conforming to the TRX standard, our crystal structure reveals distinct features of CrTRXz. The peptide connecting strand 2 and helix 3 is folded as a short helix

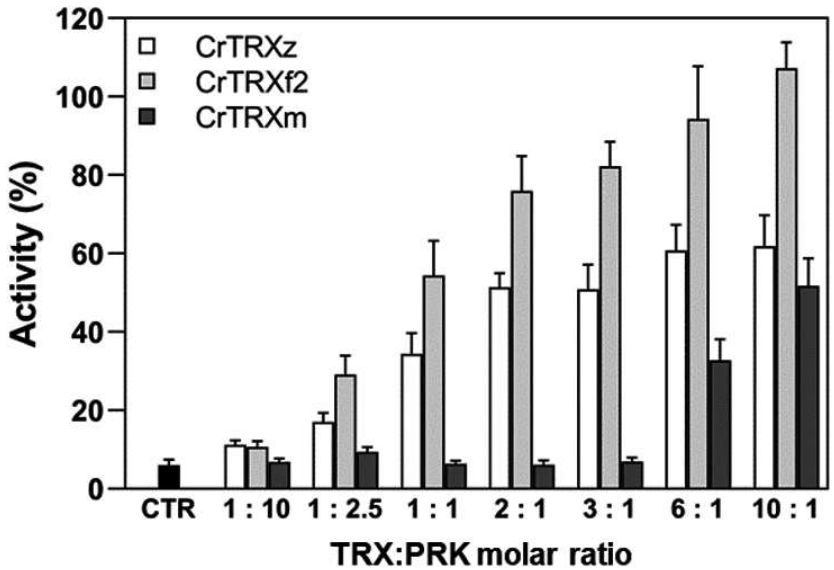

Figure 6. Activation efficiency of CrTRXz, CrTRXf2, and CrTRXm on CrPRK. Activation of oxidized CrPRK (5 μM) after 1 h incubation with increasing concentrations (0.5–50 μM) of CrTRXz (white bars), CrTRXf2 (light gray bars), and CrTRXm (dark gray bars) in the presence of 0.2 mM DTT. TRX:PRK ratios are indicated for each tested condition. Control sample (CTR, black bar) shows the activity after incubation with 0.2 mM DTT without TRXs. All activities were normalized to fully activated PRK obtained after 4 h of reduction with 40 mM DTT. Data are reported as mean ± standard deviation (n = 3). DTT, dithiothreitol; PRK, phosphoribulokinase.

3_{10} that is stabilized by hydrogen-bonding interaction of D119 with W89, adjacent to Cys_N in the redox site. This particular state may modify the reactivity of the TRXz active site or rather a functional conformation of TRX since D119 is conserved in CrTRXx, y, h1, h2, and o while it is substituted by an isosteric asparagine in CrTRXf2 and m. C126 of AtTRXf1 was shown to be glutathionylated and the glutathionylation demonstrated to subsequently affect the redox capacity of this TRX (Michelet *et al.*, 2005). CrTRXf1 and f2 but not the other TRX types possess this regulatory cysteine, at the first position after the aforementioned D119 or its equivalents. Hence, regulation of TRX by redox signaling may be caused by distal effects on the redox site through a bonding network similar to CrTRXz D119–W89. Interestingly, selective inactivation of TRXf by glutathionylation would leave TRXz as an alternative to perform photosynthetic functions such as light- and TRX-dependent activations of PRK.

CrTRXz crystallizes as a homodimer and elutes as larger than globular monomer objects as judged by SEC. SAXS and native mass spectrometry however unequivocally contradicted the dimer hypothesis in solution, with the measured gyration radii and diffusion curves revealing a monomeric state of globular CrTRXz *in vitro*. Dimerization is either a pure crystallization artifact or a transitory interaction in restricted conditions of high local concentration, like those of a liquid–liquid phase separation or of a multiprotein complex. The interaction surface is distant from the redox site and may rather serve to scaffold TRXz-containing complexes with internal twofold symmetries. Other TRX quaternary states were tested in the past and TRX proved monomeric (Capitani and Schurmann, 2004; Gronenborn *et al.*, 1999) in the reduced state (Weichsel *et al.*, 1996).

Electronegativity as a driver of CrTRXz-specific complexation

Western blot protein quantification of *A. thaliana* leaf extracts indicated relative abundances of 69.1% TRXm, 22.2% TRXf, 6.3% TRXx, 1.3% TRXy, and 1.1% TRXz, representing a TRXz concentration of 1–5 pmol mg^{-1} stromal protein (Okegawa and Motohashi, 2015). Notwithstanding its relative scarcity, TRXz still makes significant contributions to chloroplast functions, as demonstrated by the lethality of its deletion mutant. We propose that TRXz loss cannot be compensated by other TRXs because of the irreplaceable specialization of its electronegative surface. Described determinants of TRXf2 selectivity present an opposite, electropositive character compared to TRXz. Reported targets of TRXz in *A. thaliana* present exposed cysteines on electropositive surfaces that match the TRXz redox site (Figure 5). One interesting candidate for interaction is TRXf itself, since the electropositive environment of its active site is an ideal electro-complementary platform for TRXz docking. Consistently, TRXz was reported to be reduced *in vitro* by FTR (Chibani *et al.*, 2011) but also by other TRX types (Bohrer *et al.*, 2012), suggesting that it could play a specific role in reductive or oxidant signaling (Bohrer *et al.*, 2012; Yoshida and Hisabori, 2016).

We report here that CrTRXz is able to activate CrPRK, a known target of the main CBC activator TRXf2. CrTRXz activation is slightly weaker than that of CrTRXf2 but stronger than CrTRXm activation. It relies on the ratio between TRX and target, so TRXz could efficiently activate PRK or other targets when it reaches a certain concentration in the chloroplast. Interestingly, the cell has at its disposal two different TRXs to activate PRK and tune the CBC flux according to environmental conditions. In conditions when TRXf2 is inactivated by glutathionylation (Michelet *et al.*, 2005), one can hypothesize that TRXz becomes the replacement activator of PRK.

TRX complementarities should now be confirmed by the description of the actual complexes between TRX and targets, ideally from experimental structures at atomic resolution. TRXm, x, and y in the chloroplast still await a comprehensive description of the molecular basis for specific disulfide targeting, as well as TRXh/TRXo and bacterial TRX in their respective compartments. Later on, a global simulation of electron transfers in the proteome will require knowledge on the concentrations of all TRXs, reductant sources, and targets, their mutual binding affinities, interaction turnovers, and their cysteine redox potentials.

EXPERIMENTAL PROCEDURES

Cloning

The amino acid sequence of the nuclear-encoded *C. reinhardtii* TRXz (UniRef100 entry A8J0Q8, TRX-related protein CITRX) was analyzed by TargetP2.0 (Almagro Armenteros *et al.*, 2019; Emanuelsson *et al.*, 2007), ChloroP (Emanuelsson *et al.*, 1999), and Predalgo (Tardif *et al.*, 2012) to predict the transit peptide cutting site and the subsequent mature sequence of chloroplastic protein. The sequence coding for amino acids 56–183 was PCR-amplified from *C. reinhardtii* expressed sequence tags database plasmid AV642845 with DNA primers 5′-TGTCGC**CATATG**GTCATTAGCCATGGAAAG-3′ and 5′-CTCCTT**AAGCTT**CTACTGCTGCGGCGCCTCGGG-3′. The PCR product was inserted into pET28a by restriction with *Nde*I and *Hin*dIII and subsequent ligation, yielding pET28a-His_6-CrTRXz. Recombinant protein is a fusion of Met-HHHHHH-SSFLVPRGSHM- and TRXz residues 56–183, as validated by plasmid Sanger sequencing. Residue numbering is in accordance with UniProt sequence A8J0Q8-1 throughout the text.

Expression and purification

Escherichia coli strain BL21(DE3) Rosetta-2 pLysS (Novagen Merck, Darmstadt, Germany) was transformed with pET28a-His6-CrTRXz and grown in 1 L of 2YT medium supplemented with kanamycin (50 μg ml^{-1}) and chloramphenicol (34 μg ml^{-1}) to the exponential phase at an optical density of 0.6 before induction of overexpression with 200 μM isopropyl β-D-1-thiogalactopyranoside for 3.5 h at 37°C. Cell pellet (4.1 g) was resuspended in 20 ml buffer A (20 mM Tris-Cl pH 7.9, 200 mM NaCl) and lysed by 2 min sonication with 0.4-sec pulses at output 5 on a W-375 sonicator equipped with a microtip (Qsonica, Newtown, CT, USA) on ice. Total extract was clarified by 20 min centrifugation at 30 000 *g* at 4°C and the soluble fraction was loaded on an affinity chromatograph over 5 ml of NiNTA resin (Sigma-Aldrich Merck, Darmstadt, Germany). Resin was step-washed with 10 ml of buffer A supplemented with 10, 20, 30, 40, or 50 mM imidazole. Elution was executed with steps of 10 ml of buffer A supplemented with 100, 150, 200, or 250 mM imidazole. Collected fractions were analyzed by SDS-PAGE and Coomassie staining, revealing the presence of >99% pure TRXz in wash fractions 20, 30, 40, and 50 and elution fractions 100 and 200. Pooled fractions were buffer-exchanged to buffer A and concentrated by ultrafiltration on 3000 MWCO Amicon filter units (Millipore Merck, Darmstadt, Germany). A final concentration of 10.2 mg ml^{-1} was measured by a NanoDrop 2000 spectrophotometer (Thermo Fisher Scientific, Waltham, MA, USA) with theoretical Mw = 16 191.5 g mol^{-1} and ε_{280} = 5567.5 mol^{-1} L cm^{-1}.

Size-exclusion chromatography

Affinity-purified recombinant CrTRXz (0.1 mg) was loaded on a Superose6 10/300 Increase column or a BioSEC3-300 column in 20 mM Tris-Cl pH 7.9, 100 mM NaCl. Isocratic elution was recorded at 280 nm.

Small-angle X-ray scattering. Diffusion curves were collected from a BioSEC3-300 SEC in line with an X-ray exposure capillary at the beamline SWING of Synchrotron SOLEIL (Saint-Aubin, France). Data were processed with FOXTROT (Xenocs, Grenoble France) using CLEVERAVG algorithms and interpreted with ATSAS (Petoukhov *et al.*, 2012; Franke *et al.*, 2017).

Crystallization and structure determination

Purified CrTRXz was tested for crystallization in commercial sparse-screening conditions (Qiagen, Hilden, Germany) of the Joint Center for Structural Genomics screens (Lesley and Wilson, 2005) with a mixture of 30 nl protein and 30 nl precipitant equilibrated against a reservoir volume of 30 μl mother liquor. Monocrystals sized 30 μm grew in 1 week in condition 38 at position D2 of screen IV (0.1 M HEPES pH 7.5, 1.26 M ammonium sulfate). Crystals were transferred in mother liquor supplemented with 12.5% glycerol and flash-frozen in liquid nitrogen for diffraction experiments at a micro-focused beamline PROXIMA-2A at a SOLEIL synchrotron (Saint-Aubin, France). A 99.36% complete dataset was collected at 2.444 Å resolution. Data were indexed in space group $P3_221$, integrated, scaled, and converted with XDSME (Legrand, 2017). The structure was phased by molecular replacement with PHENIX (Adams *et al.*, 2010, 2011) and PHASER-MR (McCoy *et al.*, 2007) using CrTRXf2 (PDB ID: 6I1C) (Lemaire *et al.*, 2018) as a search model and a single protein in the asymmetric unit. The model was refined by iterative cycles of manual building in COOT (Emsley and Cowtan, 2004; Emsley *et al.*, 2010) followed by refinement with PHENIX.REFINE (Afonine *et al.*, 2012) until completion of a structure passing MOLPROBITY (Chen *et al.*, 2010) evaluation with 100% residues for Ramachandran restrains RMS (bonds) = 0.010, RMS (angles) = 1.44 and final R_{work} = 0.2296, R_{free} = 0.2335 (Table 1). Structure representations were drawn with PyMOL (Schrodinger, New York, NY, USA).

TRX activation assay

CrPRK was recombinantly expressed as published earlier (Gurrieri *et al.*, 2019). Pure CrPRK was oxidized in the presence of 0.2 mM 5,5′-dithiobis(2-nitrobenzoic acid) (Sigma-Aldrich, Darmstadt, Germany) for 45 min at room temperature. CrPRK was desalted to stop the oxidation and used to assay TRX activation efficiency. Oxidized CrPRK at 5 μM was incubated in the presence of 0.2 mM dithiothreitol (DTT) and 0.5–50 μM CrTRXz, CrTRXf2, and CrTRXm

for 60 min. PRK activity was assayed as in Gurrieri *et al.* (2019). Control activity was obtained incubating CrPRK with 0.2 mM DTT for 60 min. Activities were normalized on fully reduced PRK obtained after 4 h incubation at room temperature in the presence of 40 mM DTT.

ACKNOWLEDGMENTS

This work was funded by CNRS, Sorbonne Université, and Agence Nationale de la Recherche grants LABEX DYNAMO 11-LABX-0011, CALVINDESIGN (ANR-17-CE05-001), and CALVINTERACT (ANR-19-CE11-0009). Libero Gurrieri was supported by grant PON ARS01 00881 'ORIGAMI' (Italian Ministry of University and Research). Fernanda Pires Borrega and Sandrine Hoang contributed to the preparation of recombinant thioredoxin z. The Institut de Biologie Physico-Chimique (FR 550 CNRS) provided access to crystallization facilities. We acknowledge SOLEIL for provision of synchrotron radiation facilities. We thank Martin Savko, Serena Sirigu, and William Shepard for assistance in using the beamline PROXIMA-2a and Aurélien Thureau and Javier Perez for assistance in using the beamline SWING.

AUTHOR CONTRIBUTIONS

Conception, MZ, FS, SDL, and JH; acquisition and analysis of data, TLM, LG, CHM, and JH; manuscript writing, reviewing, and editing, TLM, LG, PC, CHM, MZ, FS, SDL, and JH; funding and resource acquisition, FS, SDL, and JH. All authors have read and agreed to the final version of the manuscript.

CONFLICT OF INTEREST

The authors have no conflicts of interest to declare.

DATA AVAILABILITY STATEMENT

Validated crystallographic reflection data and the model are deposited in the Protein Data Bank under identifier 7ASW.

SUPPORTING INFORMATION

Additional Supporting Information may be found in the online version of this article.

Figure S1. Sequence alignment of CrTRXz homologs. Sequence alignment was performed by Clustal Omega with homologs from different species. Residues with more than 50% conservation are colored in red, and strictly conserved residues are shown in white with a red background. Numbering is in accordance with the sequence of thioredoxin z (TRXz) from *Chlamydomonas reinhardtii*. TRX sequences were retrieved from the UniProtKB database for the following species: *C. reinhardtii* (A8J0Q8), *Gonium pectorale* (A0A150FZQ6), *Tetrabaena socialis* (A0A2J7ZQ73), *Volvox carteri* f. *nagariensis* (D8TVT1), *Ostreococcus tauri* (A0A1Y5IIS5), *Arabidopsis thaliana* (Q9M7X9), *Synechocystis* sp. *PCC 6714* (A0A068MSG5), and *Glycine max* (I1JW39).

Figure S2. CrTRX experimental structures. (a) Side and top views of the CrTRXz structure. CrTRXz is represented in cartoon format and colored in rainbow colors from the N-terminus (blue) to the C-terminus (red). Reactive cysteine side chains are represented in sticks. (b) CrTRXm in the same orientation, representation, and coloration as in (a). (c) CrTRXf2 in the same orientation, representation, and coloration as in (a). (d) Structural alignment of CrTRXf2, CrTRXm, and CrTRXh structures colored in white on the CrTRXz structure colored in green, realized by PyMOL. Root mean square deviation (RMSD) values of alignments are 1.357, 0.838, and 1.123 Å for CrTRXm, CrTRXf2, and CrTRXh, respectively.

Figure S3. CrTRXz size-exclusion chromatography. High-pressure liquid chromatography profile over a BioSEC3-300 column of (a) preparation 1 and (b) preparation 2 of CrTRXz. Globular calibration standards are eluted at 7.2 ml (670 kDa), 9.2 ml (158 kDa), 10.6 ml (44 kDa), and 11.7 ml (17 kDa). Dead column volume is 6.5 ml and total column volume is 13.4 ml. TRXz peaks are indicated by green arrows.

Figure S4. Comparison of homology models of *A. thaliana* TRXz computed from the sequence in UniProt entry Q9M7X9 isoform 1 with the experimental structure of *C. reinhardtii* TRXz. Structures align with RMSD values of 1.1–1.4 Å. Nucleophilic cysteine side chains are displayed as spheres with sulfur in gold. (a) *Arabidopsis thaliana* TRXz SWISS-MODEL analysis by homology with 50 template thioredoxins. (b) Experimental crystal structure of *C. reinhardtii* TRXz (this study). (c) Comparison of an *A. thaliana* TRXz model to an ortholog with 24% sequence identity using Phyre2 with a confidence score of 99/100. (d) Electrostatic potential of AtTRXz, as determined using SWISS-MODEL. (e) Electrostatic potential of the CrTRXz crystal structure. (f) Electrostatic potential of the AtTRXz Phyre2 model. Potential is colored from red (negative) to blue (positive).

REFERENCES

Adams, P.D., Afonine, P.V., Bunkoczi, G., Chen, V.B., Davis, I.W., Echols, N. *et al.* (2010) PHENIX: A comprehensive Python-based system for macromolecular structure solution. *Acta Crystallographica Section D: Biological Crystallography*, **66**, 213–221.

Adams, P.D., Afonine, P.V., Bunkoczi, G., Chen, V.B., Echols, N., Headd, J.J. *et al.* (2011) The Phenix software for automated determination of macromolecular structures. *Methods*, **55**, 94–106.

Afonine, P.V., Grosse-Kunstleve, R.W., Echols, N., Headd, J.J., Moriarty, N.W., Mustyakimov, M. *et al.* (2012) Towards automated crystallographic structure refinement with phenix.refine. *Acta Crystallographica Section D: Biological Crystallography*, **68**, 352–367.

Almagro Armenteros, J.J., Salvatore, M., Emanuelsson, O., Winther, O., Von Heijne, G., Elofsson, A. *et al.* (2019) Detecting sequence signals in targeting peptides using deep learning. *Life Science Alliance*, **2**.

Arsova, B., Hoja, U., Wimmelbacher, M., Greiner, E., Ustun, S., Melzer, M. *et al.* (2010) Plastidial thioredoxin z interacts with two fructokinase-like proteins in a thiol-dependent manner: Evidence for an essential role in chloroplast development in *Arabidopsis* and *Nicotiana benthamiana*. *The Plant Cell*, **22**, 1498–1515.

Ashkenazy, H., Abadi, S., Martz, E., Chay, O., Mayrose, I., Pupko, T. *et al.* (2016) ConSurf 2016: An improved methodology to estimate and visualize evolutionary conservation in macromolecules. *Nucleic Acids Research*, **44**, W344–W350.

Avilan, L., Puppo, C., Erales, J., Woudstra, M., Lebrun, R. & Gontero, B. (2012) CP12 residues involved in the formation and regulation of the glyceraldehyde-3-phosphate dehydrogenase-CP12-phosphoribulokinase complex in *Chlamydomonas reinhardtii*. *Molecular Biosystems*, **8**, 2994–3002.

Baker, N.A., Sept, D., Joseph, S., Holst, M.J. & Mccammon, J.A. (2001) Electrostatics of nanosystems: Application to microtubules and the ribosome. *Proceedings of the National Academy of Sciences of the United States of America*, **98**, 10037–10041.

Balmer, Y., Koller, A., Val, G.D., Schurmann, P. & Buchanan, B.B. (2004) Proteomics uncovers proteins interacting electrostatically with thioredoxin in chloroplasts. *Photosynthetic Research*, **79**, 275–280.

Balsera, M., Uberegui, E., Schurmann, P. & Buchanan, B.B. (2014) Evolutionary development of redox regulation in chloroplasts. *Antioxidants and Redox Signaling*, **21**, 1327–1355.

Bedhomme, M., Adamo, M., Marchand, C.H., Couturier, J., Rouhier, N., Lemaire, S.D. *et al.* (2012) Glutathionylation of cytosolic glyceraldehyde-3-phosphate dehydrogenase from the model plant *Arabidopsis thaliana*

is reversed by both glutaredoxins and thioredoxins in vitro. *Biochemical Journal*, **445**, 337–347.

Benhar, M., Forrester, M.T., Hess, D.T. & Stamler, J.S. (2008) Regulated protein denitrosylation by cytosolic and mitochondrial thioredoxins. *Science*, **320**, 1050–1054.

Berger, H., De Mia, M., Morisse, S., Marchand, C.H., Lemaire, S.D., Wobbe, L. *et al.* (2016) A light switch based on protein S-nitrosylation fine-tunes photosynthetic light harvesting in *Chlamydomonas*. *Plant Physiology*, **171**, 821–832.

Blomback, B., Blomback, M., Finkbeiner, W., Holmgren, A., Kowalska-Loth, B. & Olovson, G. (1974) Enzymatic reduction of disulfide bonds in fibrinogen by the thioredoxin system. I. Identification of reduced bonds and studies on reoxidation process. *Thrombosis Research*, **4**, 55–75.

Bohrer, A.S., Massot, V., Innocenti, G., Reichheld, J.P., Issakidis-Bourguet, E. & Vanacker, H. (2012) New insights into the reduction systems of plastidial thioredoxins point out the unique properties of thioredoxin z from *Arabidopsis*. *Journal of Experimental Botany*, **63**, 6315–6323.

Buchanan, B.B., Holmgren, A., Jacquot, J.P. & Scheibe, R. (2012) Fifty years in the thioredoxin field and a bountiful harvest. *Biochimica et Biophysica Acta*, **1820**, 1822–1829.

Bunik, V., Raddatz, G., Lemaire, S., Meyer, Y., Jacquot, J.P. & Bisswanger, H. (1999) Interaction of thioredoxins with target proteins: Role of particular structural elements and electrostatic properties of thioredoxins in their interplay with 2-oxoacid dehydrogenase complexes. *Protein Science*, **8**, 65–74.

Capitani, G. & Schurmann, P. (2004) On the quaternary assembly of spinach chloroplast thioredoxin m. *Photosynthetic Research*, **79**, 281–285.

Cejudo, F.J., Ojeda, V., Delgado-Requerey, V., Gonzalez, M. & Perez-Ruiz, J.M. (2019) Chloroplast redox regulatory mechanisms in plant adaptation to light and darkness. *Frontiers in Plant Science*, **10**, 380.

Chen, V.B., Arendall, W.B. 3rd, Headd, J.J., Keedy, D.A., Immormino, R.M., Kapral, G.J. *et al.* (2010) MolProbity: All-atom structure validation for macromolecular crystallography. *Acta Crystallogrophica Section D: Biological Crystallography*, **66**, 12–21.

Chibani, K., Tarrago, L., Schürmann, P., Jacquot, J.P. & Rouhier, N. (2011) Biochemical properties of poplar thioredoxin z. *FEBS Letters*, **585**.

Chivers, P.T. & Raines, R.T. (1997) General acid/base catalysis in the active site of *Escherichia coli* thioredoxin. *Biochemistry*, **36**, 15810–15816.

Collin, V., Issakidis-Bourguet, E., Marchand, C., Hirasawa, M., Lancelin, J.M., Knaff, D.B. *et al.* (2003) The *Arabidopsis* plastidial thioredoxins: New functions and new insights into specificity. *Journal of Biological Chemistry*, **278**, 23747–23752.

De Lamotte-Guery, F., Miginiac-Maslow, M., Decottignies, P., Stein, M., Minard, P. & Jacquot, J.P. (1991) Mutation of a negatively charged amino acid in thioredoxin modifies its reactivity with chloroplastic enzymes. *European Journal of Biochemistry*, **196**, 287–294.

Diaz, M.G., Hernandez-Verdeja, T., Kremnev, D., Crawford, T., Dubreuil, C. & Strand, A. (2018) Redox regulation of PEP activity during seedling establishment in *Arabidopsis thaliana*. *Nature Communications*, **9**, 50.

Emanuelsson, O., Brunak, S., Von Heijne, G. & Nielsen, H. (2007) Locating proteins in the cell using TargetP, SignalP and related tools. *Nature Protocols*, **2**, 953–971.

Emanuelsson, O., Nielsen, H. & Von Heijne, G. (1999) ChloroP, a neural network-based method for predicting chloroplast transit peptides and their cleavage sites. *Protein Science*, **8**, 978–984.

Emsley, P. & Cowtan, K. (2004) Coot: Model-building tools for molecular graphics. *Acta Crystallographica Section D: Biological Crystallography*, **60**, 2126–2132.

Emsley, P., Lohkamp, B., Scott, W.G. & Cowtan, K. (2010) Features and development of Coot. *Acta Crystallographica Section D: Biological Crystallography*, **66**, 486–501.

Ferrer-Sueta, G., Manta, B., Botti, H., Radi, R., Trujillo, M. & Denicola, A. (2011) Factors affecting protein thiol reactivity and specificity in peroxide reduction. *Chemical Research in Toxicology*, **24**, 434–450.

Franke, D., Petoukhov, M.V., Konarev, P.V., Panjkovich, A., Tuukkanen, A., Mertens, H.D.T. *et al.* (2017) ATSAS 2.8: A comprehensive data analysis suite for small-angle scattering from macromolecular solutions. *Journal of Applied Crystallography*, **50**, 1212–1225.

Gamiz-Arco, G., Risso, V.A., Candel, A.M., Ingles-Prieto, A., Romero-Romero, M.L., Gaucher, E.A. *et al.* (2019) Non-conservation of folding rates in the thioredoxin family reveals degradation of ancestral unassisted-folding. *Biochemical Journal*.

Gleason, F.K. & Holmgren, A. (1981) Isolation and characterization of thioredoxin from the cyanobacterium, *Anabaena* sp. *Journal of Biological Chemistry*, **256**, 8306–8309.

Gonzalez Porque, P., Baldesten, A. & Reichard, P. (1970) Purification of a thioredoxin system from yeast. *Journal of Biological Chemistry*, **245**, 2363–2370.

Greetham, D., Vickerstaff, J., Shenton, D., Perrone, G.G., Dawes, I.W. & Grant, C.M. (2010) Thioredoxins function as deglutathionylase enzymes in the yeast *Saccharomyces cerevisiae*. *BMC Biochemistry*, **11**, 3.

Gronenborn, A.M., Clore, G.M., Louis, J.M. & Wingfield, P.T. (1999) Is human thioredoxin monomeric or dimeric? *Protein Science*, **8**, 426–429.

Gurrieri, L., Del Giudice, A., Demitri, N., Falini, G., Pavel, N.V., Zaffagnini, M. *et al.* (2019) *Arabidopsis* and *Chlamydomonas* phosphoribulokinase crystal structures complete the redox structural proteome of the Calvin-Benson cycle. *Proceedings of the National Academy of Sciences of the United States of America*, **116**, 8048–8053.

Gutle, D.D., Roret, T., Muller, S.J., Couturier, J., Lemaire, S.D., Hecker, A. *et al.* (2016) Chloroplast FBPase and SBPase are thioredoxin-linked enzymes with similar architecture but different evolutionary histories. *Proceedings of the National Academy of Sciences of the United States of America*, **113**, 6779–6784.

Hall, D.E., Baldesten, A., Holmgren, A. & Reichard, P. (1971) Yeast thioredoxin. Amino-acid sequence around the active-center disulfide of thioredoxin I and II. *European Journal of Biochemistry*, **23**, 328–335.

Hanschmann, E.M., Godoy, J.R., Berndt, C., Hudemann, C. & Lillig, C.H. (2013) Thioredoxins, glutaredoxins, and peroxiredoxins-molecular mechanisms and health significance: From cofactors to antioxidants to redox signaling. *Antioxidants and Redox Signaling*, **19**, 1539–1605.

Hirasawa, M., Schurmann, P., Jacquot, J.P., Manieri, W., Jacquot, P., Keryer, E. *et al.* (1999) Oxidation-reduction properties of chloroplast thioredoxins, ferredoxin:thioredoxin reductase, and thioredoxin f-regulated enzymes. *Biochemistry*, **38**, 5200–5205.

Holmgren, A. (1968) Thioredoxin. 6. The amino acid sequence of the protein from *Escherichia coli* B. *European Journal of Biochemistry*, **6**, 475–484.

Holmgren, A., Buchanan, B.B. & Wolosiuk, R.A. (1977) Photosynthetic regulatory protein from rabbit liver is identical with thioredoxin. *FEBS Letters*, **82**, 351–354.

Holmgren, A. & Morgan, F.J. (1976) Enzyme reduction of disulfide bonds by thioredoxin. The reactivity of disulfide bonds in human choriogonadotropin and its subunits. *European Journal of Biochemistry*, **70**, 377–383.

Huang, C., Yu, Q.B., Lv, R.H., Yin, Q.Q., Chen, G.Y., Xu, L. *et al.* (2013) The reduced plastid-encoded polymerase-dependent plastid gene expression leads to the delayed greening of the *Arabidopsis* fln2 mutant. *PLoS One*, **8**, e73092.

Huppe, H.C. & Buchanan, B.B. (1989) Activation of a chloroplast type of fructose bisphosphatase from *Chlamydomonas reinhardtii* by light-mediated agents. *Zeitschrift für Naturforschung C: A Journal of Biosciences*, **44**, 487–494.

Ingles-Prieto, A., Ibarra-Molero, B., Delgado-Delgado, A., Perez-Jimenez, R., Fernandez, J.M., Gaucher, E.A. *et al.* (2013) Conservation of protein structure over four billion years. *Structure*, **21**, 1690–1697.

Jacquot, J.P., Eklund, H., Rouhier, N. & Schurmann, P. (2009) Structural and evolutionary aspects of thioredoxin reductases in photosynthetic organisms. *Trends in Plant Science*, **14**, 336–343.

Kang, Z., Qin, T. & Zhao, Z. (2019) Thioredoxins and thioredoxin reductase in chloroplasts: A review. *Gene*, **706**, 32–42.

Kelley, L.A. Mezulis, S., Yates, C.M., Wass, M.N. & Sternberg, M.J.(2015) The Phyre2 web portal for protein modeling, prediction and analysis. *Nature Protocols*, **10**, 845–858.

Kelley, R.F. & Richards, F.M. (1987) Replacement of proline-76 with alanine eliminates the slowest kinetic phase in thioredoxin folding. *Biochemistry*, **26**, 6765–6774.

Konig, J., Muthuramalingam, M. & Dietz, K.J. (2012) Mechanisms and dynamics in the thiol/disulfide redox regulatory network: Transmitters, sensors and targets. *Current Opinions in Plant Biology*, **15**, 261–268.

Kulczyk, A.W., Moeller, A., Meyer, P., Sliz, P. & Richardson, C.C. (2017) Cryo-EM structure of the replisome reveals multiple interactions

coordinating DNA synthesis. *Proceedings of the National Academy of Sciences of the United States of America*, **114**, E1848–E1856.

Lancelin, J.M., Guilhaudis, L., Krimm, I., Blackledge, M.J., Marion, D. & Jacquot, J.P. (2000) NMR structures of thioredoxin m from the green alga *Chlamydomonas reinhardtii*. *Proteins*, **41**, 334–349.

Lee, S., Kim, S.M. & Lee, R.T. (2013) Thioredoxin and thioredoxin target proteins: From molecular mechanisms to functional significance. *Antioxidants and Redox Signaling*, **18**, 1165–1207.

Legrand, P. (2017) XDSME: XDS Made Easier.

Lemaire, S.D., Guillon, B., Le Marechal, P., Keryer, E., Miginiac-Maslow, M. & Decottignies, P. (2004) New thioredoxin targets in the unicellular photosynthetic eukaryote *Chlamydomonas reinhardtii*. *Proceedings of the National Academy of Sciences of the United States of America*, **101**, 7475–7480.

Lemaire, S.D., Michelet, L., Zaffagnini, M., Massot, V. & Issakidis-Bourguet, E. (2007) Thioredoxins in chloroplasts. *Current Genetics*, **51**, 343–365.

Lemaire, S.D., Tedesco, D., Crozet, P., Michelet, L., Fermani, S., Zaffagnini, M. *et al.* (2018) Crystal structure of chloroplastic thioredoxin f2 from *Chlamydomonas reinhardtii* reveals distinct surface properties. *Antioxidants (Basel)*, **7**.

Lemaster, D.M., Springer, P.A. & Unkefer, C.J. (1997) The role of the buried aspartate of *Escherichia coli* thioredoxin in the activation of the mixed disulfide intermediate. *Journal of Biological Chemistry*, **272**, 29998–30001.

Lesley, S.A. & Wilson, I.A. (2005) Protein production and crystallization at the joint center for structural genomics. *Journal of Structural and Functional Genomics*, **6**, 71–79.

Liebthal, M., Maynard, D. & Dietz, K.J. (2018) Peroxiredoxins and redox signaling in plants. *Antioxidants and Redox Signaling*, **28**, 609–624.

Lillig, C.H. & Holmgren, A. (2007) Thioredoxin and related molecules—from biology to health and disease. *Antioxidants and Redox Signaling*, **9**, 25–47.

Marchand, C.H., Fermani, S., Rossi, J., Gurrieri, L., Tedesco, D., Henri, J. *et al.* (2019) Structural and biochemical insights into the reactivity of thioredoxin h1 from *Chlamydomonas reinhardtii*. *Antioxidants (Basel)*, **8**.

Marri, L., Zaffagnini, M., Collin, V., Issakidis-Bourguet, E., Lemaire, S.D., Pupillo, P. *et al.* (2009) Prompt and easy activation by specific thioredoxins of calvin cycle enzymes of *Arabidopsis thaliana* associated in the GAPDH/CP12/PRK supramolecular complex. *Molecular Plant*, **2**, 259–269.

Mccoy, A.J., Grosse-Kunstleve, R.W., Adams, P.D., Winn, M.D., Storoni, L.C. & Read, R.J. (2007) Phaser crystallographic software. *Journal of Applied Crystallography*, **40**, 658–674.

Menchise, V., Corbier, C., Didierjean, C., Saviano, M., Benedetti, E., Jacquot, J.P. *et al.* (2001) Crystal structure of the wild-type and D30A mutant thioredoxin h of *Chlamydomonas reinhardtii* and implications for the catalytic mechanism. *Biochemical Journal*, **359**, 65–75.

Michelet, L., Zaffagnini, M., Marchand, C., Collin, V., Decottignies, P., Tsan, P. *et al.* (2005) Glutathionylation of chloroplast thioredoxin f is a redox signaling mechanism in plants. *Proceedings of the National Academy of Sciences of the United States of America*, **102**, 16478–16483.

Michelet, L., Zaffagnini, M., Massot, V., Keryer, E., Vanacker, H., Miginiac-Maslow, M. *et al.* (2006) Thioredoxins, glutaredoxins, and glutathionylation: New crosstalks to explore. *Photosynthetic Research*, **89**, 225–245.

Michelet, L., Zaffagnini, M., Morisse, S., Sparla, F., Perez-Perez, M.E., Francia, F. *et al.* (2013) Redox regulation of the Calvin-Benson cycle: Something old, something new. *Frontiers in Plant Science*, **4**, 470.

Mora-Garcia, S., Rodriguez-Suarez, R. & Wolosiuk, R.A. (1998) Role of electrostatic interactions on the affinity of thioredoxin for target proteins. Recognition of chloroplast fructose-1, 6-bisphosphatase by mutant *Escherichia coli* thioredoxins. *Journal of Biological Chemistry*, **273**, 16273–16280.

Morisse, S., Michelet, L., Bedhomme, M., Marchand, C.H., Calvaresi, M., Trost, P. *et al.* (2014) Thioredoxin-dependent redox regulation of chloroplastic phosphoglycerate kinase from *Chlamydomonas reinhardtii*. *Journal of Biological Chemistry*, **289**, 30012–30024.

Napolitano, S., Reber, R.J., Rubini, M. & Glockshuber, R. (2019) Functional analyses of ancestral thioredoxins provide insights into their evolutionary history. *Journal of Biological Chemistry*, **294**, 14105–14118.

Navrot, N., Gelhaye, E., Jacquot, J.P. & Rouhier, N. (2006) Identification of a new family of plant proteins loosely related to glutaredoxins with four CxxC motives. *Photosynthetic Research*, **89**, 71–79.

Nishizawa, A.N. & Buchanan, B.B. (1981) Enzyme regulation in C4 photosynthesis. Purification and properties of thioredoxin-linked fructose bisphosphatase and sedoheptulose bisphosphatase from corn leaves. *Journal of Biological Chemistry*, **256**, 6119–6126.

Ojeda, V., Perez-Ruiz, J.M. & Cejudo, F.J. (2018) 2-Cys peroxiredoxins participate in the oxidation of chloroplast enzymes in the dark. *Molecular Plant*, **11**, 1377–1388.

Okegawa, Y. & Motohashi, K. (2015) Chloroplastic thioredoxin m functions as a major regulator of Calvin cycle enzymes during photosynthesis in vivo. *Plant Journal*, **84**, 900–913.

Palde, P.B. & Carroll, K.S. (2015) A universal entropy-driven mechanism for thioredoxin-target recognition. *Proceedings of the National Academy of Sciences of the United States of America*, **112**, 7960–7965.

Pan, J.L. & Bardwell, J.C. (2006) The origami of thioredoxin-like folds. *Protein Science*, **15**, 2217–2227.

Perez-Perez, M.E., Mata-Cabana, A., Sanchez-Riego, A.M., Lindahl, M. & Florencio, F.J. (2009) A comprehensive analysis of the peroxiredoxin reduction system in the *Cyanobacterium synechocystis* sp. strain PCC 6803 reveals that all five peroxiredoxins are thioredoxin dependent. *Journal of Bacteriology*, **191**, 7477–7489.

Perez-Perez, M.E., Mauries, A., Maes, A., Tourasse, N.J., Hamon, M., Lemaire, S.D. *et al.* (2017) The deep thioredoxome in *Chlamydomonas reinhardtii*: New insights into redox regulation. *Molecular Plant*, **10**, 1107–1125.

Petoukhov, M.V., Franke, D., Shkumatov, A.V., Tria, G., Kikhney, A.G., Gajda, M. *et al.* (2012) New developments in the ATSAS program package for small-angle scattering data analysis. *Journal of Applied Crystallography*, **45**, 342–350.

Roos, G., Foloppe, N. & Messens, J. (2013) Understanding the pK(a) of redox cysteines: The key role of hydrogen bonding. *Antioxidants and Redox Signaling*, **18**, 94–127.

Schroter, Y., Steiner, S., Matthai, K. & Pfannschmidt, T. (2010) Analysis of oligomeric protein complexes in the chloroplast sub-proteome of nucleic acid-binding proteins from mustard reveals potential redox regulators of plastid gene expression. *Proteomics*, **10**, 2191–2204.

Schurmann, P. & Buchanan, B.B. (2008) The ferredoxin/thioredoxin system of oxygenic photosynthesis. *Antioxidants and Redox Signaling*, **10**, 1235–1274.

Setterdahl, A.T., Chivers, P.T., Hirasawa, M., Lemaire, S.D., Keryer, E., Miginiac-Maslow, M. *et al.* (2003) Effect of pH on the oxidation-reduction properties of thioredoxins. *Biochemistry*, **42**, 14877–14884.

Sevilla, F., Camejo, D., Ortiz-Espin, A., Calderon, A., Lazaro, J.J. & Jimenez, A. (2015) The thioredoxin/peroxiredoxin/sulfiredoxin system: Current overview on its redox function in plants and regulation by reactive oxygen and nitrogen species. *Journal of Experimental Botany*, **66**, 2945–2955.

Sun, J., Zheng, T., Yu, J., Wu, T., Wang, X., Chen, G. *et al.* (2017) TSV, a putative plastidic oxidoreductase, protects rice chloroplasts from cold stress during development by interacting with plastidic thioredoxin Z. *New Phytologist*, **215**, 240–255.

Tardif, M., Atteia, A., Specht, M., Cogne, G., Rolland, N., Brugiere, S. *et al.* (2012) PredAlgo: A new subcellular localization prediction tool dedicated to green algae. *Molecular Biology and Evolution*, **29**, 3625–3639.

Tarrago, L., Laugier, E., Zaffagnini, M., Marchand, C., Le Marechal, P., Rouhier, N. *et al.* (2009) Regeneration mechanisms of *Arabidopsis thaliana* methionine sulfoxide reductases B by glutaredoxins and thioredoxins. *Journal of Biological Chemistry*, **284**, 18963–18971.

Toledano, M.B., Delaunay-Moisan, A., Outten, C.E. & Igbaria, A. (2013) Functions and cellular compartmentation of the thioredoxin and glutathione pathways in yeast. *Antioxidants and Redox Signaling*, **18**, 1699–1711.

Trost, P., Fermani, S., Marri, L., Zaffagnini, M., Falini, G., Scagliarini, S. *et al.* (2006) Thioredoxin-dependent regulation of photosynthetic glyceraldehyde-3-phosphate dehydrogenase: Autonomous vs. CP12-dependent mechanisms. *Photosynthetic Research*, **89**, 263–275.

Vaseghi, M.J., Chibani, K., Telman, W., Liebthal, M.F., Gerken, M., Schnitzer, H. *et al.* (2018) The chloroplast 2-cysteine peroxiredoxin functions

as thioredoxin oxidase in redox regulation of chloroplast metabolism. *Elife*, **7**.

Wang, Y., Wang, Y., Ren, Y., Duan, E., Zhu, X., Hao, Y. *et al.* (2020) White Panicle2 encoding thioredoxin z, regulates plastid RNA editing by interacting with multiple organellar RNA editing factors in rice. *New Phytologist*.

Watson, W.H., Pohl, J., Montfort, W.R., Stuchlik, O., Reed, M.S., Powis, G. *et al.* (2003) Redox potential of human thioredoxin 1 and identification of a second dithiol/disulfide motif. *Journal of Biological Chemistry*, **278**, 33408–33415.

Wedmann, R., Onderka, C., Wei, S., Szijarto, I.A., Miljkovic, J.L., Mitrovic, A. *et al.* (2016) Improved tag-switch method reveals that thioredoxin acts as depersulfidase and controls the intracellular levels of protein persulfidation. *Chemical Science*, **7**, 3414–3426.

Weichsel, A., Gasdaska, J.R., Powis, G. & Montfort, W.R. (1996) Crystal structures of reduced, oxidized, and mutated human thioredoxins: Evidence for a regulatory homodimer. *Structure*, **4**, 735–751.

Wimmelbacher, M. & Bornke, F. (2014) Redox activity of thioredoxin z and fructokinase-like protein 1 is dispensable for autotrophic growth of *Arabidopsis thaliana*. *Jouranl of Experimental Botany*, **65**, 2405–2413.

Wolosiuk, R.A. & Buchanan, B.B. (1978a) Activation of chloroplast NADP-linked glyceraldehyde-3-phosphate dehydrogenase by the ferredoxin/thioredoxin system. *Plant Physiology*, **61**, 669–671.

Wolosiuk, R.A. & Buchanan, B.B. (1978b) Regulation of chloroplast phosphoribulokinase by the ferredoxin/thioredoxin system. *Archives of Biochemistry and Biophysics*, **189**, 97–101.

Yokochi, Y., Sugiura, K., Takemura, K., Yoshida, K., Hara, S., Wakabayashi, K.I. *et al.* (2019) Impact of key residues within chloroplast thioredoxin-f on recognition for reduction and oxidation of target proteins. *Journal of Biological Chemistry*, **294**, 17437–17450.

Yoshida, K., Hara, A., Sugiura, K., Fukaya, Y. & Hisabori, T. (2018) Thioredoxin-like2/2-Cys peroxiredoxin redox cascade supports oxidative thiol modulation in chloroplasts. *Proceedings of the National Academy of Sciences of the United States of America*, **115**, E8296–E8304.

Yoshida, K. & Hisabori, T. (2016) Two distinct redox cascades cooperatively regulate chloroplast functions and sustain plant viability. *Proceedings of the National Academy of Sciences of the United States of America*, **113**, E3967–E3976.

Yoshida, K. & Hisabori, T. (2017) Distinct electron transfer from ferredoxin-thioredoxin reductase to multiple thioredoxin isoforms in chloroplasts. *Biochemical Journal*, **474**, 1347–1360.

Yoshida, K., Uchikoshi, E., Hara, S. & Hisabori, T. (2019a) Thioredoxin-like2/2-Cys peroxiredoxin redox cascade acts as oxidative activator of glucose-6-phosphate dehydrogenase in chloroplasts. *Biochemical Journal*, **476**, 1781–1790.

Yoshida, K., Yokochi, Y. & Hisabori, T. (2019b) New light on chloroplast redox regulation: Molecular mechanism of protein thiol oxidation. *Frontiers in Plant Science*, **10**, 1534.

Yua, Q.B., Ma, Q., Kong, M.M., Zhao, T.T., Zhang, X.L., Zhou, Q. *et al.* (2014) AtECB1/MRL7, a thioredoxin-like fold protein with disulfide reductase activity, regulates chloroplast gene expression and chloroplast biogenesis in *Arabidopsis thaliana*. *Molecular Plant*, **7**, 206–217.

Zaffagnini, M., De Mia, M., Morisse, S., Di Giacinto, N., Marchand, C.H., Maes, A. *et al.* (2016) Protein S-nitrosylation in photosynthetic organisms: A comprehensive overview with future perspectives. *Biochimica et Biophysica Acta*, **1864**, 952–966.

Zaffagnini, M., Fermani, S., Marchand, C.H., Costa, A., Sparla, F., Rouhier, N. *et al.* (2019) Redox homeostasis in photosynthetic organisms: Novel and established thiol-based molecular mechanisms. *Antioxidants and Redox Signaling*, **31**, 155–210.

6.1.3 Conclusion

L'obtention de cette première structure de TRXz a permis de confirmer le repliement canonique de ce type de thiorédoxine, ainsi que la conservation du motif WCGPC. Ces éléments permettent de confirmer que la TRXz conserve bien sa fonction de réduction des ponts disulfures. Un élément nouveau est la présence de cette TRXz en tant que dimère apparent en chromatographie d'exclusion de taille et dans le cristal. Ceci n'a jamais été décrit, mais pourrait être simplement dû à l'imprécision de la chromatographie et à la stabilisation artéfactuelle de dimères dans l'empilement cristallin. En effet, après des expériences complémentaires de SAXS et de spectrométrie de masse native, TRXz apparait comme monomérique en solution. La structure de TRXz permet d'observer une charge de surface de la protéine principalement négative, ce qui doit contribuer à la reconnaissance de ses cibles, de la même manière que la charge principalement positive de TRXf2.

Malgré sa relative faible abondance parmi les thiorédoxines d'Arabidopsis (1.1% des thiorédoxines totales (Okegawa and Motohashi 2015)), les mutants de délétion de TRXz sont létaux. Ceci, indique des fonctions chloroplastiques indispensables peuvent être liées à ses interactions avec la polymérase chloroplastique. La TRXz est également capable d'activer la CrPRK à des niveaux inférieurs à TRXf, ce qui n'est pas le cas de la thiorédoxine cytoplasmique prise pour contrôle. La cellule possède donc deux systèmes d'activation de PRK, ce qui pourrait être un mécanisme de secours.

6.2 ANNEXE 2 : WESTERN BLOT CONTROLE AVEC ANTICORPS DIRIGE CONTRE CRTRK, CRFBPASE, CRPRK ET CRPGK.

Les différents numéros au-dessus des membranes indiquent les pistes de migration des différents aliquotes de la résine CNBr-sépharose bloquée. Piste 1 : extrait protéique soluble avant dépôt sur la résine, piste 2 : non retenu, piste 3 : lavage avec tampon 20 mM Tris-HCl pH 7,9 ; 100 mM NaCl, piste 4 : élution dans le tampon précédent additionné de 10 mM DTT, piste 5 : élution dans un tampon 20 mM Tris-HCl pH 7,9 ; 2 M NaCl, piste 6 : résine solubilisée après élutions.

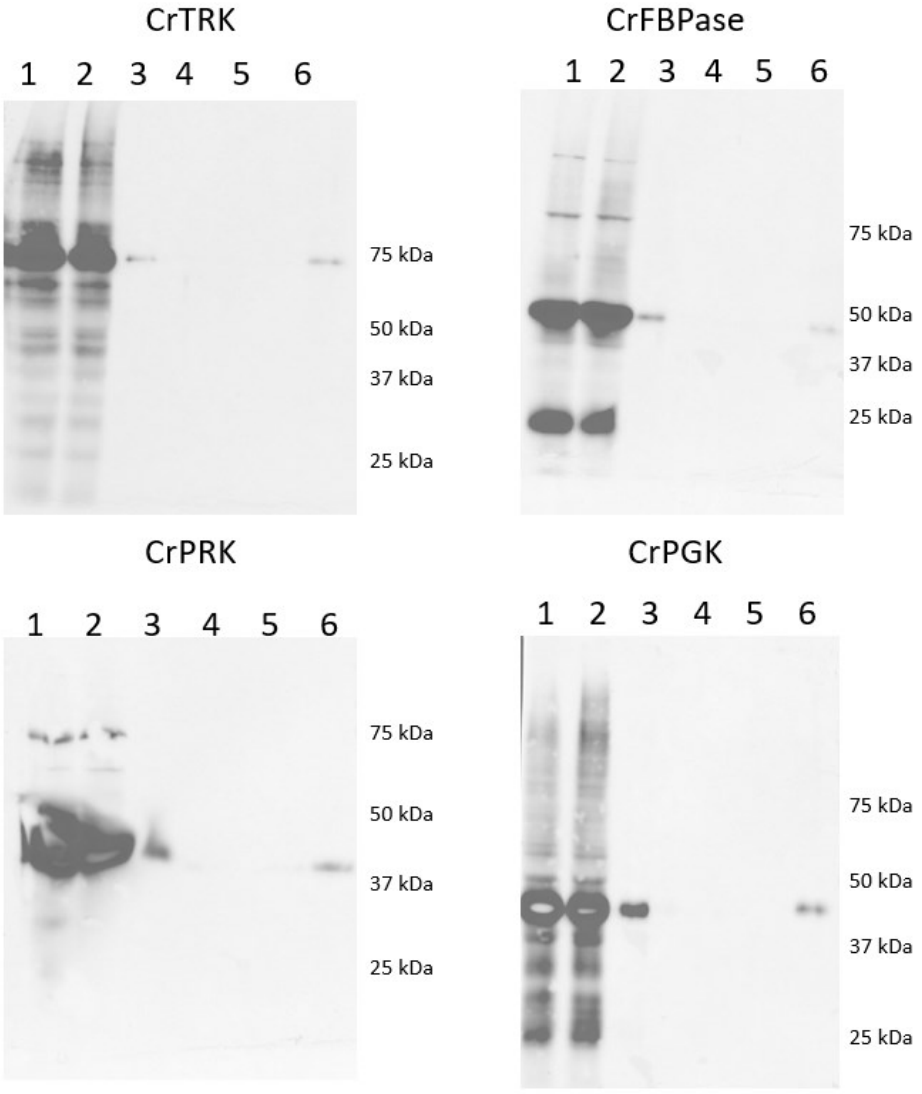

université PARIS-SACLAY | ÉCOLE DOCTORALE Sciences du végétal : du gène à l'écosystème (SEVE)

Titre : Structures et interactions des enzymes du cycle de Calvin-Benson-Bassham

Mots clés : photosynthèse, fixation de carbone, microalgue, biologie structurale

Résumé : La photosynthèse est l'un des principaux processus permettant la vie sur Terre. Elle se déroule en deux phases, la conversion de l'énergie lumineuse et de l'eau en pouvoir réducteur et en énergie chimique et le cycle de Calvin-Benson-Bassham (CBBC) qui fixe le CO_2 atmosphérique en molécules organiques.

Le CBBC est catalysé par onze enzymes, essentielles à la photosynthèse et conservées dans la lignée verte des plantes et des microalgues. Les enzymes du CBBC sont régulées par de multiples modes, dont des modifications post-traductionnelles et des interactions protéine-protéine.

Afin de décrire le système CBBC au niveau moléculaire, nous avons cherché à déterminer la structure tridimensionnelle de ces enzymes à haute résolution.

J'ai purifié, cristallisé, résolu et analysé les structures cristallines de la ribose-5-phosphate isomérase (RPI), de la fructose bisphosphate aldolase (FBA), de la sédoheptulose-1,7-bisphosphatase (SBPase) et de la phosphoglycérate kinase (PGK) de la microalgue verte modèle *Chlamydomonas reinhardtii*. J'ai également recherché des complexes multi-enzymatiques entre les enzymes du CBBC *in vitro*.

Title : Structures and interactions of Calvin-Benson-Bassham cycle enzymes

Keywords : photosynthesis, carbon fixation, microalgae, structural biology

Abstract : Photosynthesis is one of the main processes supporting life. It is composed of two phases, the conversion of light energy and water into reductive power and chemical energy, and the Calvin-Benson-Bassham cycle (CBBC) that fixes atmospheric CO_2 into organic molecules.

The CBBC is catalyzed by eleven enzymes, essential for photosynthesis and conserved in the green lineage of plants and microalgae. CBBC enzymes are regulated by multiple modes, including post-translational modifications and protein-protein interactions.

In order to describe the CBBC system at the molecular level, we aimed at determining the tridimensional structure of these enzymes at high resolution.

I purified, crystallized, solved and analyzed the crystal structures of the ribose-5-phosphate isomerase (RPI), the fructose bisphosphate aldolase (FBA), the sedoheptulose-1,7-bisphosphatase (SBPase), and the phosphoglycerate kinase (PGK) from the model green microalga *Chlamydomonas reinhardtii*, and searched for multi-enzymatic complexes formed by CBBC enzymes *in vitro*.